UILU-ENG-99-2009

CIVIL ENGINEERING STUDIES
Structural Research Series No. 627

ISSN: 0069-4274

COMPRESSIVE MEMBRANE CAPACITY ESTIMATES IN LATERALLY EDGE RESTRAINED REINFORCED CONCRETE ONE-WAY SLABS

By

Ronald W. Welch
and
William J. Hall
William L. Gamble

A Report on Research Sponsored by

THE UNITED STATES ARMY,

DEPARTMENT OF CIVIL AND MECHANICAL ENGINEERING
UNITED STATES MILITARY ACADEMY

and

DEPARTMENT OF CIVIL AND ENVIRONMENTAL ENGINEERING
UNIVERSITY OF ILLINOIS AT URBANA-CHAMPAIGN

MAY 1999

50272-101

REPORT DOCUMENTATION PAGE	1. REPORT NO. UILU-ENG-99-2009	2.	3. Recipient's Accession No.

4. Title and Subtitle
COMPRESSIVE MEMBRANE CAPACITY ESTIMATES IN LATERALLY EDGE RESTRAINED REINFORCED CONCRETE ONE-WAY SLABS

5. Report Date
May 1999

6.

7. Author(s)
R.W. Welch, W.J. Hall and W.L. Gamble

8. Performing Organization Rept. No.
SRS 627

9. Performing Organization Name and Address
University of Illinois at Urbana-Champaign
Department of Civil and Environmental Engineering
205 N. Mathews Avenue
Urbana, Illinois 61801

10. Project/Task/Work Unit No.

11. Contract(C) or Grant(G) No.
(C)
(G)

12. Sponsoring Organization Name and Address
The United States Army, Department of Civil and Environmental Engineering, The United States Military Academy
Department of Civil and Environmental Engineering, University of Illinois at Urbana-Champaign

13. Type of Report & Period Covered

14.

15. Supplementary Notes

16. Abstract (Limit: 200 words)

The load capacity of laterally restrained reinforced concrete one-way slabs is estimated in compressive membrane theory with use of a midspan deflection. However, the midspan deflection estimates exhibit large variability. The point of peak thrust leads to a more accurate index of the peak load capacity than midspan deflection. The calculation of the thrust within the compressive membrane theory is a maximum when the slab's axial shortening and the outward support movement are a maximum. The use of the peak thrust to select the peak capacity, when combined with a modification to Park and Gamble's (1980) compressive membrane theory, provides an improved overall correlation to the experimental data for a large range of span-to-thickness ratios ($2.7 < L/h < 28.3$).

In this study, peak midspan deflection estimates were developed to define the peak point of the load-deflection curve. The slab's axial concrete compressive strength and the peak concrete compressive strain are used within a curvature and geometrically based deflection equation, to predict the midspan deflection. The post-peak trough and ultimate points are related empirically to the tensile membrane curve, and the generated load-deflection curve compares well with the experimental data.

A simple compressive membrane load capacity estimate for laterally restrained reinforced concrete one-way slabs is developed for field use. The estimate uses the axial force-moment interaction equations and a ratio for the peak thrust to the slab's axial capacity, and results in an accurate estimate of the peak compressive membrane capacity using yield line theory.

17. Document Analysis a. Descriptors

Compressive Membrane Capacity, One-Way Slabs, Reinforced Concrete, Edge Restrained, In-Plane Strength Enhancement

b. Identifiers/Open-Ended Terms

c. COSATI Field/Group

18. Availability Statement	19. Security Class (This Report)	21. No. of Pages
Release Unlimited	Unclassified	448
	20. Security Class (This Page) Unclassified	22. Price

COMPRESSIVE MEMBRANE CAPACITY ESTIMATES IN LATERALLY EDGE RESTRAINED REINFORCED CONCRETE ONE-WAY SLABS

By

Ronald W. Welch
and
William J. Hall and **William L. Gamble**

A Technical Report of Research Supported by the

UNITED STATES MILITARY ACADEMY,

THE UNITED STATES ARMY

and

THE DEPARTMENT OF CIVIL AND ENVIRONMENTAL ENGINEERING

Department of Civil and Environmental Engineering
University of Illinois at Urbana-Champaign, 1999
Urbana, Illinois
May 1999

ABSTRACT

COMPRESSIVE MEMBRANE CAPACITY ESTIMATES IN LATERALLY EDGE RESTRAINED REINFORCED CONCRETE ONE-WAY SLABS

Ronald Wayne Welch, Ph.D.
Department of Civil and Environmental Engineering
University of Illinois at Urbana-Champaign, 1999
Professor William J. Hall, Advisor

The load capacity of laterally restrained reinforced concrete one-way slabs currently is estimated by entering the compressive membrane theory with a midspan deflection. However, the midspan deflection estimates exhibit large variability. The point of peak thrust is a more accurate index of the peak load capacity, than midspan deflection estimates and even experimentally measured midspan deflections. The calculation of the thrust within the compressive membrane theory is a maximum when the slab's axial shortening and the outward support movement are a maximum. The use of the peak thrust to select the peak capacity, when combined with a modification to Park and Gamble's (1980) compressive membrane theory, provides an improved overall correlation to the experimental data for a large range of span-to-thickness ratios ($2.7 < L/h < 28.3$).

Peak midspan deflection estimates were developed to define the peak point of the load-deflection curve. A relationship exists between the slab's axial concrete compressive strength and the peak concrete compressive strain used within a curvature and geometrically based deflection equation to predict the midspan deflection. The post-peak trough and ultimate points are related empirically to the tensile membrane curve such that the generated load-deflection curve compares extremely well with the experimental data.

A simple compressive membrane load capacity estimate for laterally restrained reinforced concrete one-way slabs is developed for field use. The estimate uses the axial force-moment interaction equations and a ratio for the peak thrust to the slab's axial capacity. The resulting thrust enhanced moment capacities at the support and midspan hinge lines allow for a simple, and extremely accurate, estimate of the peak compressive membrane capacity using yield line theory.

ACKNOWLEDGMENTS

This report was prepared as a doctoral dissertation by Lieutenant Colonel Ronald W. Welch, U.S. Army Corps of Engineers, and submitted to the Graduate College of the University of Illinois at Urbana-Champaign in partial fulfillment of the requirements for the degree of Doctor of Philosophy in Civil Engineering. The thesis was completed under the supervision of Professor William J. Hall.

This research study was made possible through the funding of the United States Army in support of faculty development for the Department of Civil and Mechanical Engineering at the United States Military Academy. The financial support was greatly appreciated. Any findings or recommendations in this report are those of the authors and do not necessarily reflect the views of the sponsor.

The authors wish to express sincere gratitude to Professors John D. Haltiwanger and Mark A. Aschheim for their continuous interest, constructive assistance, suggestions and comments. LTC Welch is indebted to Colonels Terry D. Hand and Thomas A. Lenox for supporting his selection to attend graduate school and return to the West Point faculty of the Department of Civil and Mechanical Engineering.

This dissertation would have been extremely difficult to complete without the general support of the U.S. Army Engineer Waterways Experiment Station and the technical support of the Department of Civil and Environmental Engineering Staff at the University of Illinois.

TABLE OF CONTENTS

LIST OF TABLES

TABLE **PAGE**

LIST OF FIGURES

FIGURE **PAGE**

LIST OF SYMBOLS AND ABBREVIATIONS

ABAQUS	Finite Element Computer Program
ACI	American Concrete Institute
a	Average Capacity Between Considering All or Half of the Reinforcement at Midspan in the Tensile Membrane Resistance Calculation (psi)
a_1	Vertical Distance (in)
AFESC	Air Force Engineering and Services Center
ASCE	American Society of Civil Engineers
A-M	Axial Force-Moment Interaction
b	Width (in)
c, c'	Neutral Axis Depth at Positive, Negative Moment (in)
C	Compressive Thrust (lb) in Concrete or Reinforcement Usually Followed by a Subscript to Denote Midspan, Support, Concrete or Steel
CICR	Conservative Incipient Collapse Ratio
CMC	Compressive Membrane Curve
d	Effective Depth to Tension Reinforcement (in) or Representing the use of all Reinforcement at Midspan in Tensile Membrane Resistance Calculations
d '	Effective Depth to Compression Reinforcement (in)
DIF	Dynamic Increase Factor
DNA	Defense Nuclear Agency
DSM	Direct Stiffness Method
E	Modulus of Elasticity (ksi)
EC	Empirically Based Curves
Exp	Experimental Data
E_c	Concrete Modulus of Elasticity (ksi)

E_s	Steel Modulus of Elasticity (ksi)
f	Fixed-Supported Edge Condition
f'_c	Concrete Compressive Strength (psi)
f''_c	$(0.85)(f'_c)$
f_c	Earlier Representation of Concrete Compressive Strength (psi)
f_y	Steel Yield Strength - No Strain Hardening (ksi)
f_s	Steel Stress (ksi)
f_u	Steel Ultimate Strength (ksi)
FE	Finite Element
FEMA	Federal Emergency Management Agency
h	Slab Thickness (in)
inc	Increment
ICR	Incipient Collapse Ratio
ksi	Kips per Square Inch (1 kip = 1000 pounds)
k_1	Compressive Stress Block Parameter
K(P)	Keenan's Deflection Estimate Within Park and Gamble's Compressive Membrane Theory
K(W)	Keenan's Deflection Estimate Within the Author's Compressive Membrane Theory
lb	pound
L	Span Length (in)
LCICR	Load Capacity at the Conservative Incipient Collapse Ratio (psi)
L/h	Span-to-Thickness Ratio
m	Average Between Fixed-Supported and Simply-Supported Yield Line Capacities (psi)
M	Moment (lb-in) or Mattock's Deflection Estimate (in)

m_u, m'_u ..... Resisting Moment When Summed About Mid-Depth: Positive, Negative

n ..... E_s/E_c or Algebraic Factor in EQN 4.28

NCEL ..... Naval Civil Engineering Laboratory

NCSA ..... National Center for Super-Computing Applications

NLGEOM ..... Term in ABAQUS Which Prepares the Program to Track Structures That May Experience Geometric Instability

n_u, n'_u ..... Compressive Membrane Force at Midspan, Support (lb)

N_u ..... Axial Thrust (lb)

N_{ub} ..... Axial Thrust at the Balanced Point (lb)

OCE ..... Office, Chief of Engineers

psf ..... Pounds per Square Foot

psi ..... Pounds per Square Inch

P ..... Uniform Pressure (psi) or Axial Force in a Column (lb)

P_{bal} ..... Axial Force at Balanced Conditions (lb)

P_o ..... Pure Axial Capacity (lb)

P-Δ ..... The Increased Lateral Deflection in a Column from the Increased End Moments (P*Δ) (lb-in)

PP ..... Graphical Peak Capacity in Park and Gamble's Compressive Membrane Theory (psi) or the Incremented Deflection Associated with the Graphical Peak Capacity (in)

PDI ..... Deflection Indexed Capacity within Park and Gamble's Compressive Membrane Theory (psi)

PTI ..... Peak Thrust Indexed Capacity in Park and Gamble's Compressive Membrane Theory (psi) or the Incremented Deflection Associated with the Peak Thrust (in)

P_{avg} ..... Average Capacity Between the Graphical Peak Capacity (PP) and the Peak Thrust Indexed Capacity (PTI) (psi)

q	Reinforcement Index, $\rho f_y/f'_c$
q_b	Reinforcement Index at Balanced Conditions, $\rho_{bal} f_y/f'_c$
q_y	Yield Flexural Resistance (psi)
q_u	Ultimate Flexural Resistance (psi)
r	Reinforcement Rupture Stress (ksi)
R	Rupture
s	Principal Reinforcement Spacing (in) or Keenan's representation of the Outward Movement of the Supports or the Simply-Supported Edge Conditions or Representing Only Half of the Midspan Reinforcement in the Tensile Membrane Resistance Calculation
s_s	Shear Stirrup Spacing (in)
S	Support Restraint (lb/in)
SP(tt)	Simple Peak Capacity Estimate Using the T/P_o Ratios for the Thick and All Thin Slabs
SP(ttvt)	Simple Peak Capacity Estimate Using the T/P_o Ratios for the Thick, Thin and Very Thin Slabs
SS	Simply-Supported
STATIC RIKS	Term in ABAQUS Which Prepares the Program to Use Controlled Incremental Loading While Expecting a Decrease in Loading with an Increase in Deflections
t	Thickness (in) or Support Movement (in)
T	Peak Compressive Thrust (lb) or Tensile Force in Reinforcement Usually Followed by a Subscript to Denote Midspan or Support Location
T_y	Tension Force Carried by the Steel Reinforcement at Yield Capacity
u	Deflection (in)
V_c	Plain Concrete Shear Strength (lb)
w	Uniform Distributed Load (psi)

w_c ..... Density of Concrete

w_o ..... Midspan Deflection (in)

w/c ..... Water-Cement Ratio

W ..... Peak Compressive Membrane Capacity (psi)

W_{avg} ..... Average Capacity Between the Graphical Peak Capacity (WP) and the Peak Thrust Indexed Capacity (WTI) (psi)

W(P) ..... Author's Deflection Estimate With Park and Gamble's Compressive Membrane Theory (in)

W(W) ..... Author's Deflection Estimate With His Compressive Membrane Theory (in)

WP ..... Graphical Peak Capacity Within the Author's Compressive Membrane Theory (psi) or Incremented Deflection Associated With the Graphical Peak Capacity (in)

WDI ..... Deflection Indexed Capacity Within the Author's Compressive Membrane Theory (psi)

WTI ..... Peak Thrust Indexed Capacity Within the Author's Compressive Membrane Theory (psi) or the Incremented Deflection Associated With the Peak Thrust (in)

WES ..... United States Army Waterways Experiment Station

Y ..... Yield

YL ..... Yield Line

z ..... Distance from the Section of Maximum Moment to the Section of Zero Moment (in)

z_y ..... Yield Deflection (in)

z_u ..... Ultimate Deflection (in)

β ..... Percentage of Slab Length Between Hinge Point at the Support and the Next Hinge Along the Length

$\beta 1$ ..... Ratio of the Depth of the Equivalent Stress Block to the Neutral-Axis Depth

δ ..... Midspan Deflection (in)

Δ ..... Midspan Deflection (in)

Δ/h ..... Midspan Deflection to Thickness ratio

ε ..... Strain (in/in)

ε_o ..... Peak Strain (in/in)

ε_u, ε_{cu} ..... Ultimate Concrete Strain (in/in)

Iε ..... Inelastic Strain (in/in)

ϕ ..... Curvature (in^{-1}) or Angle in Figure 4.6

ϕ_{spl} ..... Extension or Shortening of Lateral Spring (in)

ϕ_{spr} ..... Rotation of the Spring (rad)

ν ..... Poisson's Ratio

ℓ ..... Span Length (in)

ρ ..... Tensile Reinforcement Ratio

ρ' ..... Compressive Reinforcement Ratio

ρ_S ..... Shear Reinforcement Ratio

θ ..... Support Hinge Rotation (degrees)

θ_u ..... Inelastic Rotation in Length d/2

θ_{tu} ..... Total Inelastic Rotation in Length z

Θ ..... Rotational Restraint (lb/degree)

σ ..... Stress (psi)

σ_{spl} ..... Load in Lateral Spring (lb/in)

σ_{spr} ..... Load in Rotational Spring (lb/rad)

CHAPTER 1

INTRODUCTION

1.1. Introduction

It was generally recognized in Europe during World War II that bomb shelters of various types, which had moderate spans and relatively rigid supports, seemed to accommodate higher than expected loading (Hall, 1997). Failures of such structures, as observed in laboratory tests, were somewhat explosive (i.e., sudden and brittle). Arching and/or compressive membrane forces, followed by subsequent snap through, were suspected to be contributory factors in the enhancement. With the ensuing postwar economic boom in America and reconstruction of Europe, slab research naturally focused on testing, as well as evaluation, of Johansen's (1943) revolutionary yield line theory which does not consider lateral edge restraint (A-B'-C, Figure 1.1). Johansen's theory greatly improved the engineer's ability to estimate the capacity of a slab, thereby leading to construction of less expensive structures.

In 1955, Ockleston unleashed a flurry of research activity on laterally restrained reinforced concrete two-way slabs after reporting on a lightly-reinforced concrete interior two-way slab which supported over two times the accepted upper bound yield line load capacity. It is now understood that the surrounding slabs laterally restrained the interior slab allowing the development of internal compressive thrusts which enhanced the flexural strength at critical sections of the slab. It is the compressive thrust (T, Figure 1.2) generation in these laterally restrained slabs that highlights the primary difference between yield line theory and compressive membrane theory. The formation of support and midspan hinges (Figure 1.3) during increased loading lengthens the bottom fiber which subsequently is resisted by the surrounding slabs, beams, or walls (Figure 1.4). The resulting thrust enhances the moment capacity at the hinge lines through axial force-moment interaction.

Once the complete failure mechanism forms in the slab (Point B, Figure 1.1), the load decreases with increasing deflections (i.e., snaps through to tensile resistance) until catenary action of the reinforcement catches the load at Point C, Figure 1.1. Obviously, tensile membrane load

capacity (i.e., catenary action, Point C to D, Figure 1.1) can occur only if the rebar is adequately anchored into the supports or surrounding slabs. Reinforcement fracture defines the ultimate capacity at Point D, Figure 1.1. The increased load capacity during compressive membrane action (Point B, Figure 1.1) can be substantial in slabs containing low amounts of reinforcement and high concrete compressive strengths. However, forty years later engineers still cannot estimate reliably, without prior testing, the peak capacity of these laterally restrained reinforced concrete slabs which are strengthened by in-plane compressive forces. This issue provided motivation for this thesis.

Current compressive membrane theories, i.e., the modified rigid-plastic theory and the flow theory, use an estimate of the peak capacity deflection to point to, or index, the ultimate compressive membrane load capacity. However, at large reinforcement ratios ($\rho > 1$ percent) and small span-to-thickness ratios ($L/h < 8$), this technique has been shown to be extremely inaccurate such that the predicted capacity barely approaches the yield line load capacity (Woodson, 1993 and 1994).

Research reported herein shows that the compressive thrust developed within the slab, arising from partial lateral edge restraint, is a better index, than even experimentally measured deflections, for predicting the peak compressive membrane load capacity. The capacity associated with the generated peak compressive thrust within the compressive membrane theory is, on average, a slightly smaller prediction of the experimentally measured peak compressive membrane capacity. The superb correlation between predicted peak compressive membrane capacities and the experimental data should lead to inclusion of compressive membrane capacity enhancements, when appropriate, within the current building and military design codes.

This dissertation focused on the static flexural behavior of laterally restrained reinforced concrete one-way slabs for the following reasons:

- one-way slabs provide clearly defined membrane action (i.e., they do not include the additional complication of twisting moments as in two-way slabs);

- most dynamic analysis uses a statically developed resistance function with or without a dynamic increase factor (i.e., strain rate effects) to predict dynamic performance since flexural failure is similar in both dynamically and statically loaded slabs;
- current threat assessments (i.e., mail and car bombs) and any civilian required enhanced capacities generally point to loading rates that are dominated by flexural response, thereby precluding punching which is normally uneconomical to prevent in many situations;
- there is a large experimental data base available through the United States Army Waterways Experiment Station Laboratory (WES) of 73 recently tested, gradually loaded, one-way slabs dominated by flexural behavior to combine with the 42 previously tested one-way slabs of the 1960's (i.e., 115 slabs with L/h's ranging from 3 to 28);
- current military protective construction uses the one-way slab as the primary structural element; and
- the proposed prediction technique can be extended to the analysis of laterally restrained two-way slabs by considering the capacity of slab strips in orthogonal directions (i.e., the strip method used by Park, September 1964).

The use of "rigid-plastic" in Park's compressive membrane theory refers to the approximate slab behavior at peak compressive membrane capacity. The slab generally remains rigid, or elastic, during the flexural response except for the inelastic rotation at the support and midspan plastic hinge locations. The widely used version of the compressive membrane theory or "modified" rigid-plastic theory (Park and Gamble, 1980) includes numerous improvements made by Park and other researchers (Chapter 2) to the original theory presented by Park in 1964.

The primary difference between Park and Gamble's modified rigid-plastic theory and Morley's flow theory centers on the strain level at which they are applicable. The modified rigid-plastic theory is applied at the peak compressive membrane capacity when hinges have formed at both the supports and midspan for a one-way slab (i.e., peak compressive strain, Figures 1.3 and 1.4). The flow theory slowly increments the compressive strain from initial elastic conditions until reaching the peak load capacity. Each method provides quite similar results near peak load

capacity, while the flow theory generally provides a more rapidly descending curve from Point B to C, Figure 1.1, than the modified rigid-plastic theory. However, neither the flow nor the rigid-plastic theory when plotted with the experimental curves descends as rapidly as the post-peak experimental curves. With neither theory truly representing the behavior of the crushed and spalling concrete during post-peak behavior (Point B to C, Figure 1.1), the author believes that neither theory should be employed beyond making an estimate for the peak compressive membrane load capacity. Once the peak and ensuing trough points are known (Points B and C, Figure 1.1), a simple parabolic curve should be used to represent the descending post-peak portion of the load-deflection curve until intersection with the tensile membrane curve.

The following definitions are presented here to assist in managing the lengthy terminology associated with membrane behavior. The slab's load capacity at Points B, C, or D, Figure 1.1, represents the uniformly distributed load resisted by the slab at that time. Peak capacity and peak deflection identifies the peak compressive membrane behavior at Point B, Figure 1.1. Trough capacity and trough deflection denotes the membrane behavior at Point C, Figure 1.1. Ultimate capacity and ultimate deflection depicts the peak tensile membrane behavior at Point D, Figure 1.1. Peak thrust (T) represents the thrust occurring nearly simultaneously with the peak compressive membrane load capacity used to index the peak capacity, while the peak deflection at Point B, Figure 1.1, is used in current methods to index the peak capacity.

1.2. Background

The current American Concrete Institute (ACI) code (1995) does not address membrane behavior in slabs, but only in thin shell members. To the best of the author's knowledge, none of the currently used versions of the military's many protective construction and accidental explosion design manuals discuss additional resistance arising from compressive membrane behavior even though the defense community, through Picatinny Arsenal, supported a large amount of research on membrane behavior during the 1960's (i.e., over 100 slabs, Woodson, 1993). In these manuals, the only mention of increased moment capacity is through axial force-moment interaction

associated with beam-columns; obviously, any available compressive membrane enhancements normally are considered as simply uncertain, yet beneficial, increases in the load capacity.

The basic load capacity modeling approach for commercially designed slabs is yield line theory (Curve A-B'-C, Figure 1.1) even though many engineers know that the actual capacity can be several times larger due to the lateral restraint provided by the surrounding slabs. This situation is partially understandable since most designers never really know the actual loading a slab will need to resist, nor can they always prevent the occasional over-loading. However, there may be a need to safely overload certain slabs within a building for a short time or possibly even extended periods of time. Additionally, the loading requirements frequently change with changes in use over time. For example, an entire floor may first support a corporate headquarters, while later supporting a law firm with a large library. Or floors in a manufacturing plant may be converted to heavy merchandise storage areas. The existing slab system may already possess sufficient strength and serviceability for heavier loads than designed for. Or with limited support system strengthening (i.e., added lateral restraint), existing slabs may easily support the new loads without excessive deflections or cracking. The ability to accurately assess the structural strength with compressive membrane theory could extend the life of existing buildings by allowing the owner to economically accommodate client needs.

Within the defense community, yield line theory is also the primary method of estimating the peak load capacity of protective structures. Of course the reserve load capacity, as reflected in the tensile membrane capacity, is included and equally important (Curve A-B'-C-D, Figure 1.1). Unfortunately, current design and analysis procedures (i.e., yield line theory based) result in excessive costs by requiring thicker slabs, and greatly underestimate peak load capacity for targeting missions. These analysis limitations still exist in the military design manuals even though during the 1960's and early 1970's numerous tests were conducted on laterally restrained two-way slab systems which showed that yield line theory greatly under-estimates the experimentally measured load capacity. Perhaps the test results did improve protective structure design and targeting techniques in some past classified documents, but the currently referenced military design

manuals lack any discussion of compressive thrust enhancements. At a minimum, compressive membrane enhancements should be considered for targeting of enemy protective structures.

At the height of the Cold War (late 1970's and early 1980's), the Federal Emergency Management Agency (FEMA) developed a plan to construct thousands of key worker blast shelters throughout the United States (Guice et. al., 1986). These shelters would protect key personnel and industries during and after a nuclear attack. The need for a large number of these shelters coupled with shrinking defense budgets prevented construction of the past, overly designed and uneconomical, protective structures. FEMA funded a research program to develop techniques for efficiently designed shelters which would resist severe loading, while experiencing only moderate damage. These lofty goals led WES engineers to consider the additional resistance available in a laterally restrained reinforced concrete slab through compressive membrane action. Efficient internal space utilization within these protective shelters led to long rectangular structures with a square cross-section (i.e., one-way slab construction). Measured strengths for buried structures at WES exceeded capacities predicted by yield line theory, renewing the focus on understanding the behavior of laterally restrained one-way slabs throughout the entire loading range.

With the demise of the Berlin Wall, the need for key worker blast shelters disappeared and much of the defense research effort focused on soldier needs in Desert Storm and other peace keeping operations such as in Somalia, Bosnia, etc. However, bombing of the World Trade Center in New York City, the Murray Building in Oklahoma City, and the Khobar Towers in Saudi Arabia, to name but a few, highlighted the escalating need to protect key operations (i.e., personnel and equipment) within existing structures from terrorist activity. The desire to economically contain the blast and protect other occupants and/or the building's life support equipment requires efficiently modified/designed slab systems, and naturally points to use of compressive membrane theory if at all possible. Fully understanding and predicting compressive membrane capacity is critical within the defense community for properly designed protective structures and effective targeting of enemy protective structures.

1.3. Objectives

Initial review of past test results highlighted that using even the experimentally measured peak midspan deflections in the compressive membrane theory did not always provide an accurate prediction of peak capacity. Thus the major objectives of this thesis were as follows:

1. to develop an accurate estimate for the peak compressive membrane capacity in a partial laterally restrained, gradually loaded (i.e., static) reinforced concrete one-way slabs;
2. to develop a simple load-deflection curve, based on the statically loaded experimental results, to be used within both static and dynamic analysis;
3. to provide engineers with a quick method for making an estimate of compressive membrane capacity for either targeting missions (i.e., in the field) or rapid evaluation of the peak load capacity available in existing commercial structures; and
4. to evaluate the capability of finite element techniques in analyzing the behavior of laterally restrained reinforced concrete slabs experiencing large deflections.

1.4. Scope of Dissertation

The author conducted a thorough review of the numerous compressive membrane studies made over the past 40 years to fully comprehend what was, and was not, considered in development of the currently used compressive membrane theories. A summary of these contributions is presented in Chapter 2. Of course, no review on membrane behavior would be complete without a section summarizing tensile membrane behavior which provides reserve strength once the compressive membrane capacity is exceeded.

The results of the finite element analysis for previously tested laterally restrained reinforced concrete one-way slabs are presented in Chapter 3. This investigation using finite element analysis furnishes supplemental information to use along with the actual experimental results listed in Appendix A. The observed trends in stresses, strains, and forces at the support locations reinforced the use of the peak thrust as the primary index for predicting the peak capacity, and also led to the use of larger compressive strains than the recommended ACI

maximum (i.e., 0.003 in/in) within the deflection estimates. The limitations which prevented development of the entire load-deflection curve for one-way slabs experiencing large deflections and material instability are summarized. The input parameters required in the ABAQUS finite element analysis program are presented in Appendix B, while an evaluation of ABAQUS' capability, including required subroutines, to analyze laterally restrained reinforced concrete one-way slabs is furnished in Appendix C.

The theoretical derivations, analysis and methods for predicting the peak load capacity and producing a complete load-deflection curve for laterally restrained reinforced concrete one-way slabs are presented in Chapter 4. Even though the author's derivation generally follows Park and Gamble's modified rigid-plastic theory, his modifications to their compressive membrane derivation does lead to prediction of a larger peak capacity. This modification produced a marked difference for thin reinforced slabs ($L/t > 18$) which greatly improved the overall correlation with the experimental results. The peak compressive membrane deflection estimate is curvature based, even though the curvature is primarily concentrated within the hinges at the supports and midspan. The author's simple peak capacity estimate uses the ratio, T/P_o, based on the analytical results of 115 one-way slabs, of the peak thrust (T) to the peak axial capacity (P_o) to determine the thrust used within the axial force-moment interaction diagram. The thrust enhanced support and midspan moments are then used to determine the peak capacity without considering any P-Δ effects.

Conclusions and recommendations are presented in Chapter 5.

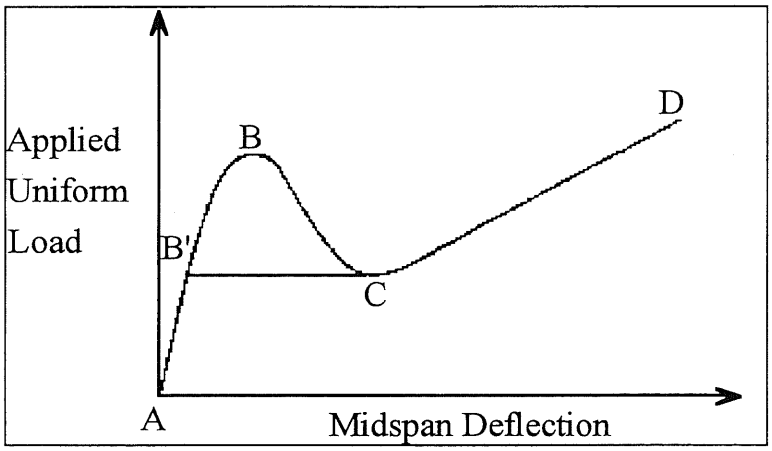

Figure 1.1. Restrained Slab Load-Deflection Curve (Park and Gamble, 1980)

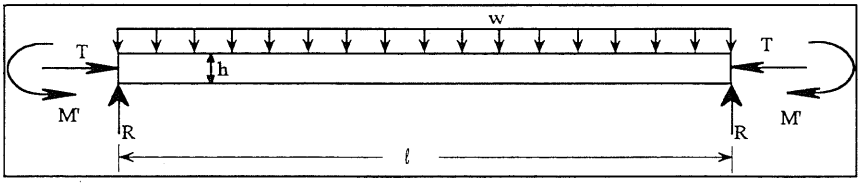

Figure 1.2. Structural Free-Body Diagram

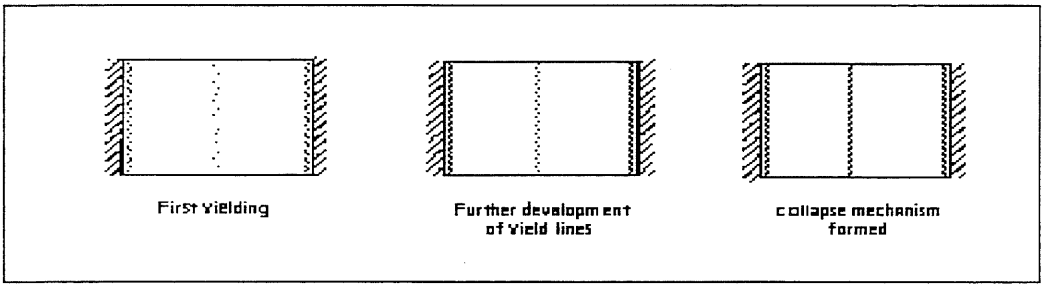

Figure 1.3. Formation of Yield Lines in One-Way Slabs

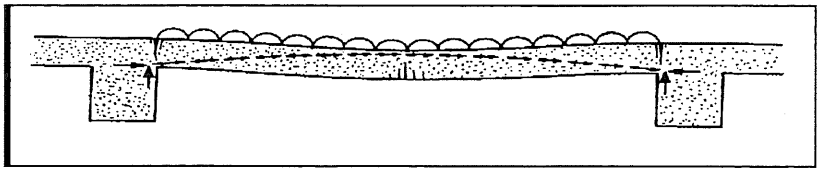

Figure 1.4. Thrust Generation (Ockleston, 1958)

CHAPTER 2

HISTORICAL OVERVIEW OF MEMBRANE DEVELOPMENT

2.1. Introduction

Hundreds of journal papers, theses, and books discuss the behavior of reinforced concrete slabs. Some cover experimental results, others present theoretical work, and many do both. Each provides valuable insight into reinforced concrete slab behavior. This chapter summarizes the most important contributions illustrating what has, and has not, been considered in past research on compressive and tensile membrane behavior in slabs. These references discuss membrane behavior and analytical models used to predict compressive and tensile membrane action.

Within both of the widely used compression membrane theories, namely the modified rigid-plastic theory and the flow theory, the yield line approach is used to define the failure mode and establish hinge locations for each unit width slab strip. Initial slab behavior is first elastic, then elastic-plastic, with hinges located along yield lines (Figure 1.3). The all important in-plane compressive thrusts increase because of the edge restraints provided by the surrounding slabs and beams which prevent slab lengthening during increased deflections (Figure 1.4). The larger loading capacities are attributed to the enhanced resisting moments present along the yield lines resulting from these compressive thrusts (i.e., axial force-moment interaction). Therefore, any discussion of membrane behavior must begin with a cursory review of elastic theories, plastic theories (i.e., yield line), and the moment-thrust interaction diagram since they are fundamental to the theory, and continue to be the starting points for compressive and tensile membrane theory development

A general overview of the entire load-deflection curve for membrane behavior precedes the detailed discussion of significant contributions made to the compressive and tensile membrane theories. Key points for each researcher are summarized within Table 2.1 (Summary of Two-Way Slab Experimentation and Analysis), Table 2.2 (Summary of One-Way Slab Experimentation and Analysis), and Table 2.3 (Summary of Tensile Membrane Experimentation and Analysis). The

discussion on compressive membrane action is divided between two-way and one-way slabs since early research (i.e., 1960's and 1970's) was primarily on two-way slabs and defined basic membrane behavior, while research in the 1980's, especially within the defense community, focused on one-way slab resistance for protective construction.

The tensile membrane capacity, sometimes referred to as the reserve capacity, is a function of reinforcement catenary action if the rebar is properly anchored at the supports. Normally, classical tensile membrane theory is employed to estimate the reserve capacity through use of the rupture stress for an upper bound estimate, and the yield stress as a lower bound estimate.

The numerous experiments on laterally restrained reinforced concrete slabs highlight the available load capacity enhancements above the capacity predicted by Johansen's yield line theory. Ockleston (1955) tested an existing slab and beam floor system, while Gamble et al. (1969) and Criswell (1972) tested one-quarter scale models. Gamble's experiment was a nine panel (three by three) reinforced concrete slab and beam floor system, while Criswell's experiment was a nine panel (three by three) reinforced concrete flat slab supported by a continuous perimeter wall and four interior columns. Numerous laterally restrained single panel tests also have been reported by Powell (1956), Wood (1961), Christiansen (1963), Park (1964-1965), Sawczuk (1965), Brotchie et al. (1965), Keenan (1969), Roberts (1969), Girolami et al. (1970), Hung and Nawy (1971), Black (1975), Desayi and Kulkarni (1977), Kiger et al. (1984), Baylot et al. (1985), Woodson (1985, 1993, 1994), Guice (1986), and others.

As experimental data became available, a number of theories and techniques for predicting the peak load capacity (Point B, Figure 1) emerged. Wood (1961) developed an analytical solution for laterally restrained circular slabs using a rigid-plastic material model and large-deflection plate theory. He felt that his technique could be applied indirectly (does not consider torsional moment effects) to laterally restrained rectangular slabs since a generally circular yield line developed along the outer edge of the rectangular slabs. Park (1964) expanded the rigid-plastic theoretical approach, sometimes referred to as the deformation theory, of Powell (1956) and Wood (1961) to rectangular slabs by considering unit width slab strips in each

orthogonal direction. Park used Johansen's yield line failure mechanism to establish the hinge points in each slab strip; thereby, defining the geometry for the slab strip at peak load capacity. Sawczuk (1965) used energy methods to develop a capacity estimate for isotropically reinforced slabs. Morley (1967) adapted basic yield line theory to account for membrane forces by considering displacement rates and equilibrium along yield lines. He used flow theory, which increments the strain rather than establishing a total strain condition at peak load capacity as in Park's deformation theory, to equate work done by the loads to the dissipated energy. Each of these methods requires a pre-determined peak load capacity midspan deflection to select a capacity.

Keenan (1969) developed a curvature based deflection equation to estimate the midspan deflection when experimental data are lacking. Researchers at WES have used Keenan's equation while assuming no lateral support movement. The estimated deflection is usually smaller than the experimentally measured deflection such that a larger (i.e., upper bound) load capacity is selected from the compressive membrane theoretical curve.

Gamble et al. (1970) provided an alternative peak load capacity prediction method that did not require a pre-determined deflection, but instead required a pre-determined thrust value. The known thrust (i.e., prestress) was used in the axial force-moment interaction relationships to determine increased moments which were then substituted into the yield line theory equations to calculate the capacity.

The use of "rigid-plastic" in Park's rigid-plastic method refers to the approximate slab behavior at peak compressive membrane capacity. The slab generally remains rigid during the flexural response except for the inelastic rotation of the plastic hinges located at the supports and midspan for one-way slabs. The current version of the compressive membrane theory or "modified" rigid-plastic theory (Park and Gamble, 1980) includes numerous improvements made by Park and other researchers (Chapter 2) to the original theory presented by Park in 1964.

The two widely used forms of the compressive membrane theory are Park's modified rigid-plastic theory and Morley's flow theory in which both were initially developed to predict only the peak load capacity. Comparison of the two theories by Braestrup (1980) in Figure 2.23 shows that

up to a midspan deflection-to-thickness ratio (w_o/h) of 0.4, both theories generally predict the same load capacity for the three different reinforcement schemes. A comparison at $w_o/h = 0.3$ is provided on the figure. It was not until researchers began using the theoretically generated compressive membrane curves to model post-peak behavior that the differences between the two compressive membrane theories became appreciated (i.e., at $w_o/h > 0.6$). Maybe neither compressive membrane theory should be used to predict post-peak behavior since the developmental assumptions were based on pre-peak conditions. For the span-to-thickness (L/h) ratios used within this thesis ($2.7 < L/h < 28.3$), either compressive membrane theory could be used to provide load capacity predictions since the midspan deflections-to-thickness ratios associated with the peak load capacity ranged from 0.03 - 0.4.

The author's review of the experimental results and the peak load capacity prediction techniques, the following salient points for compressive membrane resistance were chosen for further investigation:

- when the thrust was measured, it was noted to peak only slightly after the load capacity,
- a lateral stiffness equal to the slab's stiffness produced over 90 percent of the enhancement afforded from infinitely stiff supports,
- the testing of slabs with the same span-to-thickness ratio (L/h) and various reinforcement ratios and concrete compressive strengths produced a nearly constant peak load capacity midspan deflection-to-thickness ratio (Δ/h).

For tensile membrane resistance, the prominent details were:

- the trough capacity (Point C, Fig. 1) was generally defined by Johansen's fixed-supported yield line capacity,
- failure at the ultimate point is determined through an incipient collapse deflection,
- with support rotations during compressive membrane resistance limited to less than 2 degrees for thick slabs ($L/h < 18$), it was noted that there was an increase in the tensile membrane load capacity and the collapse deflection.

With this introduction to set the stage, the detailed presentation that follows begins with a brief review of concrete elastic theory, plasticity theories, axial-moment interaction and general membrane behavior. In this way the basic "building blocks" of the compressive membrane theory, and the progression of development, are demonstrated herein. This historical overview is key to fully appreciating the contributions of this current study.

2.1.1. Elastic Theory

The first investigators used elastic theory to analyze slab response in an effort to replace the need to load test every slab, but the slab shapes and boundary conditions common in construction made it nearly impossible to determine deflection functions, especially at higher loads, which would satisfy the boundary conditions (Park and Gamble, 1980). Difficulty with obtaining closed form solutions led to extensive research with approximate methods such as finite differences, and later, finite elements. The elastic approach, which is still present in the 1995 version of the ACI Building Code Requirements for Reinforced Concrete, defines acceptable moment distributions using conservative assumptions and approximations within the elastic theory.

However, continued testing highlighted the greatly under-estimated capacities of these elastic theory designs. This extremely large margin of safety meant over design and lost profits for the owners and financiers. What the engineers needed was a rational method of estimating the capacity of a reinforced concrete slab and a better estimate of the factor of safety.

2.1.2. Plasticity Theories

Fortunately, the emergence of plasticity theories, eventually coupled with load/reduction factors, provided a basis for practical safety levels and greater accuracy in predicting the available ultimate strength. Even though an exact solution is not always possible when using plastic theory, upper or lower bound limits are available depending on the chosen solution method.

Yield Line analysis which was credited to A. Ingerslev (1923), but greatly extended by K.W. Johansen (1943), provides an upper bound, or correct, solution for slabs with no lateral edge

restraint. Review of the commercial and military design manuals demonstrates its wide use in estimating the peak capacity of a slab. Through the principle of virtual work and/or the equations of equilibrium, an estimated peak load is calculated which will be either correct or too high based on whether or not the correct collapse mechanism is chosen (Park and Gamble, 1980). Any collapse mechanism chosen must be compatible with the boundary conditions (Figure 2.1). Yield line theory assumes that the reinforcement crossing plastic hinge lines is yielding (i.e., the so-called ultimate moment of resistance), while the points between the yield lines do not exceed the ultimate moment of resistance and behave elastically, if the correct failure mechanism is selected. The correct failure mechanisms for most common slab shapes and associated boundary conditions are well known and have been verified experimentally (Wood, 1961; Park and Gamble, 1980). Yield line theory employs a pure flexural failure mode which neglects in-plane forces and assumes sufficient shear strength, or shear reinforcement, to ensure flexural behavior.

Loading of the slab creates a concentration of strain in the concrete and reinforcing steel along lines of maximum resistance. Cracks develop and spread to form a distinct pattern which divides the slab into segments where eventually the moment capacity at these critical sections is exceeded (Figure 2.2). Each slab segment is assumed to be a plane segment that rotates at the critical sections (i.e., hinge lines) to form the actual collapse mechanism. Ultimate flexural resistance is limited by the forces, usually only moments, which cross each yield line before material failure of the critical section. At failure, the elastic deformations are usually assumed to be negligible in comparison to the inelastic deformations because of the concentration of the curvature at the yield lines.

An alternative to yield line's upper bound solution was a lower bound plastic solution developed at Brown University which predicted a correct capacity, or possibly an even lower capacity, for the slab by using equilibrium equations and selected distributions of moments to determine the peak load of the slab (Park and Gamble, 1980). The lower bound limit analysis assumes that equilibrium is satisfied at every point, no point exceeds initial yielding, and all

boundary conditions are met. This method, which really did not gain widespread use, under-predicted the capacity, but not quite as low as the elastic method.

In yield line theory, the forces that cross the critical sections or plastic hinge lines limit the peak capacity of the reinforced concrete slab. Up to this point only moment distributions or moments at the plastic hinges were mentioned, but any membrane forces generated through lateral restraint at the boundaries are extremely important. In fact, many early investigators prevented the development of compressive thrusts in order to observe and verify pure yield line behavior (Braestrup, 1980). In most reinforced concrete structures, the boundary conditions do restrict lateral movement and induce membrane forces. Tests on slabs with rigid supports have shown that yield line theory under-predicts the peak load capacity of these laterally restrained reinforced concrete slabs (Wood, 1961; Park, 1964; Brotchie et. al., 1965, etc.), especially for lightly reinforced thin slabs.

2.1.3. Axial Force-Moment Interaction

The axial force-moment interaction diagram (Figure 2.3) developed by Hognestad (1952) clearly depicts the effect of axial forces on the ultimate moment capacity of a reinforced concrete section. The curve represents all combinations of thrust and moment which constitute material failure (i.e., concrete crushing and/or steel yielding), while normally ignoring any concrete tensile strength and steel strain hardening (i.e., rebar defined as perfectly elastic-plastic). The peak moment capacity coincides with the balance point, represented by a horizontal dashed line in Figure 2.3, where there is simultaneous yielding of the tensile reinforcement and crushing of the extreme concrete fiber. Obviously, thrust-moment combinations below the balance point provide the more desired ductile behavior, while the points above the balance point represent an increasing tendency toward brittle behavior. Brittle failure is usually marked by a sudden drop in capacity and only partial formation of the collapse mechanism (Keenan, 1969, R621), while ductile behavior normally produces relatively constant capacity with continued deflection.

Pfrang et. al. (1964) further refined the basic understanding of load/moment/curvature (ϕ) interaction by studying the effects of the reinforcement ratio, yield strength, and reinforcement concrete cover on load-moment, load-curvature, and moment-curvature relationships. These authors used symmetrical reinforcement and the same cross-section dimensions for all analyses. Increased reinforcement ratios increased the cross-sectional stiffness through increased moment capacity and resistance to rotation, but it did not increase the balanced point axial load which appears independent, nor the ductility, except for a small decrease in rotation (i.e., represented by curvature times the thickness, ϕt) at low axial loads (Figure 2.4). The effect of increasing the yield strength (f_y) is similar to increasing the reinforcement ratio (Figure 2.5). Increased concrete cover, defined by the depth to the compression steel (d') to the thickness (t), decreases the moment capacity, as well as the stiffness and the ductility at extremely low load levels, but has no effect on axial load capacity (Figure 2.6). In summary, the interaction diagram is an efficient way of illustrating the strength and ductility of a reinforced concrete cross section when subjected to axial forces.

2.1.4. General Membrane Behavior

The membrane forces generated through lateral support stiffness modify the slab load-deflection relationship (Figure 1.1). Instead of a bi-linear resistance curve (A-B'-C), the membrane forces increase early (B'-B-C) and late (C-D) member resistance (A-B-C-D). Walls which are monolithic with the slab, adjacent slabs, and even friction between simply-supported deep members can provide the lateral restraint necessary to induce significant in-plane compressive and tensile membrane forces. These in-plane membrane forces interact with the moments already crossing the plastic hinge lines of the yield line collapse mechanism to ultimately increase capacity.

As the load increases from Point A to Point B (i.e., the Compression Zone), the yield line pattern develops until the collapse mechanism is formed at Point B, i.e., the peak capacity (Figure 1.1). Concurrently, the generated compressive thrusts increase the stiffness and the moment capacity at the plastic hinge locations which, in turn, increases the load capacity of the slab. Test

results show that the compressive forces generated by rigid supports or arching of slab segments from boundary to boundary usually do not exceed the balanced thrust condition (i.e., the balanced point, Figure 2.3) which ultimately ensures an increased ultimate moment capacity, yielding of the steel, and a ductile response (Park and Gamble, 1980). If pre-compression exists within the slab, it is possible to develop slab conditions located above the balanced point, a decrease in the moment capacity, and ultimately a brittle failure (Figure 2.3).

Once the collapse mechanism forms, increased deflections lead to decreased compressive thrusts and less stiffness because of slab instability (i.e., material or geometric) which usually leads to a rapid transition, or snap through, from the compression zone to the tension zone (Figure 1.1). Thick slabs normally experience material instability with concrete crushing, while thin slabs undergo geometric instability. If sufficient reinforcement is properly embedded in the supports, the slab will catch the load as the membrane forces begin changing from compression to tension at the center of the slab. Test results in Park and Gamble (1980) support a midspan deflection at Point C (Figure 1.1) approximately equal to the slab thickness.

From Point C to D, the load is initially supported by both tensile membrane action and bending until the stretching of the of the slab develops full depth concrete cracking, especially over the central region. The orthogonal reinforcement forms a steel net that supports additional load through pure tensile membrane or catenary action as the deflection increases. Normally tensile membrane action is important in order to prevent catastrophic failure if the peak capacity is exceeded. However, in heavily reinforced concrete slabs, such as those used within the defense community, the tensile membrane capacity (Point D) is designed to exceed the peak capacity (Point B) and assist in the absorption of the energy from nuclear and conventional weapon blasts. Eventually, increasing deflection leads to fracture of the reinforcement.

2.2. Compressive Membrane Experimentation and Analysis

In 1939, Gvozdev of the Soviet Union, who presented yield line theory in Russia at about the same time as Johansen did in Copenhagen, wrote a discussion -- that was never translated -- on

the new Russian code allowing a 20 percent reinforcement reduction in interior panels (discussed in Braestrup, 1980). Gvozdev cited tests on restrained slabs that showed compressive membrane forces naturally exist since the neutral axes at the positive and negative yield lines were at different heights. With the immediate calamity of World War II and the ensuing Cold War silence behind the Iron Curtain, Gvozdev's early work on yield line theory and compressive membrane strength enhancements, evident in the Russian structural code, were unavailable to the free world for many years. Additionally, most tests after World War II primarily focused on the validity of Johansen's yield line theory.

The British were extremely curious after World War II about their reinforced concrete protective shelters that had resisted larger than expected loads during the war (Hall, 1997). It was suspected that membrane forces performed a significant role in enhancing slab performance. Later in 1955, A.J. Ockleston statically load tested a hospital's lightly-reinforced concrete interior panel. To his surprise, the slab supported more than twice the load predicted by yield line theory (Ockleston, 1955). Upon further study, Ockleston reported that the interior slab sustained the additional load by "arching" through the lateral restraint provided by the surrounding unloaded reinforced concrete panels (Ockleston, 1958). The slab's increased structural capacity was attributed to in-plane compressive forces and not the often quoted enhancers, such as concrete tensile strength, catenary action, or reinforcement strain hardening.

Ockleston's results led to a flurry of research activity on statically-loaded slabs to establish both a data base and a theoretical approach to predict this new structural enhancement. Much of the research focused on two-way slabs (Park and Gamble, 1980). The testing showed that yield line theory significantly under-predicted the capacity in lightly-reinforced laterally restrained concrete slabs. The defense community quickly embraced this unexpected structural capacity and initiated it's own testing of two-way slabs supervised by Picatinny Arsenal (discussed in Woodson, 1993). More recently, WES initiated a series of tests sponsored by FEMA on laterally restrained reinforced concrete one-way slabs (discussed in Guice and Slawson, 1986).

2.2.1. Two-Way Slabs

Currently, many engineers use the analytical procedures presented in Park and Gamble (1980) to predict the capacity of reinforced concrete slabs strengthened through compressive and/or tensile membrane action. These procedures represent the accumulated experimental and analytical contributions of numerous investigators. A recent proposal to include compressive membrane enhancements within the reinforced concrete design codes simply added prestress forces to Park and Gamble's current equations and the use of the modified compression field theory to relate the sectional forces at a point to the stresses and strains (Meamarian et. al., 1994). The following historical overview lists the many contributions in defining the behavior of laterally restrained reinforced concrete two-way slabs (summarized in Table 2.1).

Ockleston's report and analysis (1955, 1958) established the occurrence of moment-thrust interaction (Figure 2.7) and established many of the early assumptions used by others to analyze their work. These assumptions are as follows: membrane forces normal to the yield line are invariant along the yield line; equilibrium of horizontal forces requires that membrane forces are equal at the support and midspan; elastic deformations are negligible in comparison to the plastic deformations at the hinge lines; and prediction of the load capacity requires a pre-existing knowledge deflection at peak load capacity. In laboratory tests on isotropic slabs with laterally restrained edges, Ockleston noted that capacity enhancement was dependent on the percentage of reinforcement, being greatest for slabs containing small steel percentages, and that post-peak capacity was the result of tensile membrane action.

Powell (1956) conducted the first laboratory tests on uniformly loaded laterally restrained reinforced concrete small-scale single panels with large span-to-depth ratios (discussed in Guice, 1986, SL-86-32). His analysis included a rigid-plastic solution (i.e., approximated the peak capacity slab behavior as rigid except at the plastic hinges) based on kinematic relations and equilibrium equations, and established a range of empirical deflections associated with the peak capacity at 33 to 50 percent of the slab depth. Powell's dissertation established the starting point

for a number of researchers including Park who later developed the widely used compressive membrane theory referred to by many as the modified rigid-plastic theory.

Wood (1961) developed an analytical procedure using rigid-plastic material (i.e., perfectly rigid-plastic reinforcement behavior) and large deflection plate theory for an isotropic thin circular slab subject to uniform loading. The use of equipotential yield criteria within his theory predicted the maximum capacity at zero deflection, while plastic membrane actually starts in a thin circular slab at a deflection near 20 percent of the depth. Accurate peak capacity prediction required an empirically derived deflection (i.e., 0.35 to 0.5h) (Figure 2.8). Wood also tested five rectangular two-way slabs with isotropic reinforcement patterns and variable boundary conditions including simple, rigid, and supported on encased steel beams. All slabs showed enhancements, with the greatest for the rigidly restrained slab. Even though torsional moments in rectangular slabs prevented the direct application of his technique, Wood felt an estimate was possible since laterally restrained rectangular slabs generally develop a circular crack pattern along the outer edges. Wood noted that capacity enhancement in thin slabs was not really "arching" between supports, but more a change of the character of the yield phenomenon due to in-plane compression. Wood warned that the capacity should not be increased through consideration of compressive membrane theory if the supporting beams were part of the collapse mechanism, if the slab is a one-way slab defined by his limit of $L_1/L_2 > 2.0$), if the slab is restrained by walls, or if the slab's long span leads to geometric instability. Moreover, he noted that long term creep effects must be considered, and that his solution should have included the elastic in-plane deformations due to in-plane compressive forces.

Park (1964-1965) expanded the rigid-plastic theory of Powell (1956) and Wood (1961) to predict the capacity of rectangular slabs with various boundary conditions using a rigid-plastic strip approximation and an empirical peak capacity deflection estimate. Park's deflection estimate of 0.5h for a fully restrained slab and 0.4h for a slab with one edge simply supported and three edges fully restrained were based on his and Powell's test results. Park determined the additional compression at the yield lines by considering the geometry of the strips at peak capacity (Figures

2.9 (i.e., small deflections) and 2.10), and using virtual work and the empirical peak capacity deflection estimates to solve for the peak capacity. He used yield line patterns to define strip lengths, assumed torsional moments were zero along yield lines which is similar to yield line theory, neglected axial shortening of the slab strips, and assumed symmetrical reinforcement about the yield lines. His theoretical curves which represent the slab's rigid-plastic behavior only apply at the point of peak capacity for a fully fixed-supported slab. The behavior before the peak, which is associated with fully plastic hinges, is first elastic then elastic-plastic, while after the peak, the crushing of the concrete reduces the concrete area which is not represented by the equations (Figure 2.11). Cracks were not visible until after 32 percent of the peak load capacity for the slabs with one edge simply supported and three edges restrained, and after 42 percent of the peak load capacity for a slab with all four edges restrained. Park extended his method to two-way slabs by summing the contribution of strips in both directions (Figure 2.12).

Park later included the effects of axial shortening and support movement by assuming that the elastic creep and shrinkage axial strains and the outward lateral support displacement were the same in all strips in the same direction. Large elastic axial strains can reduce or eliminate compressive membrane action in thin slabs, while having little effect in thick slabs. Service loads less than one-third of the peak capacity (Slabs E5 and E-7, E-8, Figure 2.13) produced small creep strains because of the negligible compressive membrane forces present at those low load levels. The thrust in laterally restrained slabs rapidly increases after the loading exceeds the yield line capacity.

Park studied the lateral restraint provided by surrounding panels (Figure 2.14) and determined the following: (i) the use of square slabs to surround and laterally restrain an interior slab reduced lateral bowing to negligible amounts; (ii) increasing the cross-sectional area of the reinforcement around the interior panel does not result in a proportionate increase in the peak capacity (i.e., increasing the steel area by three times only increased the capacity by 60 percent); (iii) there will always be local edge deformations; and (iv) tie reinforcement should be placed

continuously around the supporting beams if failure of the exterior panels is to be avoided (Figure 2.14).

Brochie et. al. (1965 and 1971) tested 45 isotropically reinforced concrete slabs using the three boundary conditions of lateral restraint only, fully clamped, and no lateral or rotational restraint while varying the span-to-thickness and the reinforcement ratios. The results were as follows: (i) unreinforced laterally restrained slabs were stronger than normally reinforced unrestrained slabs; (ii) full restraint provided the greatest enhancement in slabs with the largest span-to-thickness ratio; (iii) peak capacity increases more with lateral restraint than with reinforcement; (iv) increasing the slab thickness decreases the enhancement from increasing the reinforcement; (v) external restraint provides greater stiffness after cracking but before crushing; (vi) a larger reinforcement ratio increases the deflection at peak capacity; (vii) post-peak capacity reduction is less in thicker slabs and slabs with high reinforcement ratios; (viii) the transition between compressive membrane action and tensile membrane action is smooth unless there is a shear failure; (ix) the large compressive stress apparently increased the deforming or crushing strain of the concrete which resulted in larger rotation at the yield lines; (x) thicker slabs can accept larger edge movements with little loss in peak load capacity; (xi) the restraining force which is proportional to slab thickness remains essentially constant as the reinforcement ratio increases; (xii) the thrust distribution across the slab width is larger along the edges near the supports while it is larger in the center near midspan; and (xiii) the thrust peaked at a slightly larger deflection and slightly smaller capacity in comparison with the peak capacity. As shown in Figure 2.15 and 2.16, Brotchie et. al concluded that placing the lateral restraint, which is the most important parameter, at the level of the bottom reinforcement provides nearly the same capacity as a fully clamped slab. Unfortunately, their analytical method also required a pre-existing knowledge of the relationship between deflection and peak capacity.

Sawczuk and Winnicki (1965) analyzed laterally restrained simply-supported slabs using energy methods to represent the plastic deformations by defining the total energy of the plastic action in terms of the energy dissipated along the yield lines (i.e., through the bending and

membrane stresses). Their load-deflection curve was similar to Park's and also used an empirical peak capacity deflection to determine the peak capacity.

Taylor and Hayes (1965) used a concentrated load to test simply-supported reinforced concrete slabs with and without lateral edge restraint to investigate the effect of compressive membrane behavior on punching strength. Generally, lateral edge restraint increased punching shear strength by 24-60 percent when the slab was near flexural failure and 0-16 percent when the slab was not near flexural failure. Large reinforcement ratios increased the flexural strength to the point that the edge restraint had little effect on peak capacity.

Morley (1967) adapted conventional yield line theory to account for membrane forces by considering the displacement rates and the in-plane equilibrium along yield lines during gradual, static loading. He used flow theory which considers strain increments rather than the strain condition at the peak capacity (i.e., modified rigid-plastic theory) to equate the work done by the loads to the energy dissipated plastically. Morley felt that using strain increments accounted for the elastic unloading paths as the strains decreased during post-peak behavior because of the thrusts decreasing faster than predicted in Park's rigid-plastic theory. The overall results were similar to Park, but Morley's equations were limited to isotropic slabs and did not account for elastic shortening nor lateral support movement because of the mathematical difficulty involved in the solution of the differential equations by iterative methods. Morley's method provided good results for square slabs, while Park's method provided better results for rectangular slabs with an aspect ratio of 1.75. Morley mathematically proved that in-plane compressive forces and displacement rates do not affect yield line positions and that assuming compressive membrane forces are zero with yield line theory is not necessarily an upper-bound solution since moments generated with a strain gradient will be greater. Comparison of Morley's predicted post-peak behavior with experimental results showed a sharper decrease in the experimental thrust and capacity.

Jacobson (1967) defined the peak capacity through evaluation of the load-deflection behavior prior to peak capacity with first elastic and then elastic-plastic material theories which led

eventually to formation of plastic hinges at the supports. The thrust and the load capacity increase gradually until initiation of either geometric or material instability at the peak capacity. Jacobson's modifications to Park's rigid-plastic theory resulted in a prediction that did not require a predetermined deflection-capacity relationship, but it over-predicted the capacity, especially at low reinforcement ratios, at a deflection which was only half of the experimental deflection (Figure 2.17). His solution technique led to the following insights: (i) if lateral restraint leads to compression failure, then the restraining effect is reduced because of geometrical changes and a complete plastic hinge will develop; (ii) significant vertical stress at the supports produces a three-dimensional state of compressive stress which results in increased capacity and greater ductility; (iii) if the bottom reinforcement above the support does not yield while a plastic hinge develops at the support, the equivalent location of the restraint is near the bottom of the slab preserving the restraint through increasing deflections; (iv) if an elastic condition remains at the boundary for thin slabs, the equivalent restraint location is located near mid-depth resulting in a unrestrained effect; (v) if the bottom reinforcement yields, the center of restraint moves toward the slab mid-depth which is equivalent to the introduction of a displacement release at the restraint; and (vi) the greatest effect on restraint is caused by horizontal displacement due to the changes in geometry.

Gamble et. al. (1961 and 1969) tested a one-quarter scale model of a nine square panel (3 panel x 3 panel) slab/beam system with uniform and patterns loads. The behavior at the design load and even twice the design load (i.e., overload) was satisfactory with neither excessive deflections nor high reinforcement stresses causing unacceptable cracking. Since the interior panel was not overly stressed when the corner and edge panels eventually experienced large deflections during snap through to tensile membrane capacity, Gamble et. al. loaded the corner panels to half of their design capacity and then the interior panel to failure. The beams failed in combined shear and torsion when the load exceeded twice the yield line prediction for the slab. The torsional moment developed at the beam-column connections was virtually the same as the flexural capacity of the slab. This test demonstrated that local sections of the structure may be over stressed without

seriously affecting the overall structural behavior, and that the edge beams only needed a minimum amount of torsional stiffness and rigidity.

Keenan's (1969) experimental and analytical studies on uniformly loaded laterally restrained square slabs provided the following insights: (i) compressive steel allows an increase in the enhancement factor as the ratio of compressive reinforcement to tensile reinforcement (ρ'/ρ) increases; (ii) compressive thrust is maximum at the peak capacity deflection; (iii) cracking occurred at approximately 67-96 percent of the yield line capacity since the compressive thrusts increased the slab stiffness; (iv) post-peak capacity decreased to near yield line capacity before increasing through tensile membrane action; (v) enhancements during static testing are available during dynamic loading; (vi) strain rate effects which further increased the capacity during dynamic loading are represented by dynamic increase factors, DIF, ranging from 1.3 to 1.6; (vii) edge movements decreased the enhancement as L/h increased; (viii) consistent with the test data, varying the ultimate compressive strain produced minimal differences in the interaction curves just below the balance condition and at the point with zero thrust; and (ix) a review of Wood and Brochie et. al.'s test results, indicates that geometric instability occurs at a deflection of approximately 0.42h for slabs with $L/h > 18$.

Keenan derived an expression for the peak capacity deflection using Park's rigid-plastic theory and curvature with hinge lengths of d at the supports and 2d at midspan even though the rigid strip is assumed to only rotate/bend at the hinge points and axially deform. He focused on the condition that crushing of concrete along the yield line produces material instability or failure in thick slabs similar to those in protective construction, thereby developing the first non-empirical relationship for estimating peak capacity deflection. WES analysts have used Keenan's equation and an infinite stiffness at the supports to determine upper bound solutions for peak capacity with Park and Gamble's modified rigid-plastic theory equations. Since the deflection from Keenan's equation is usually less than the experimental deflections, the deflection indexed capacity is selected from higher on the curve. Keenan predicted the peak capacity by solving his deflection equations for a deflection estimate, used this deflection to determine the neutral axis depth and

geometrical configuration leading to a peak thrust estimate, in turn used the thrust to solve for an increased moment capacity in the axial force-moment interaction diagram, and finally solved for the peak capacity while including the P-Δ effects with Δ equal to the peak capacity deflection estimate.

Girolami et. al. (1970) focused on developing a simple and reasonably accurate method of analysis of compressive membrane action with various boundary conditions. The method was similar to Keenan's with the exception that it started with an independently determined load-deflection curve and used an iterative method to solve for the peak capacity. The iterative method consisted of initially calculating the load-capacity using thrust increased moments from the axial force-moment interaction diagram, determining the associated deflection for this capacity from the previously developed load-deflection curve, recalculating the capacity for the new geometrical configuration resulting from the associated midspan deflection, and then repeating the last two steps until convergence. The deflections were off by a factor of two even though peak capacities were somewhat reasonable. The measured in-plane forces were consistent with changes in mid-depth length and strain measurements. Beam flexibility determined the final collapse mechanism with flexible beams allowing initial formation of a typical cross pattern yield mechanism in the slab which later included the beam, while non-deflecting beams limited the yield mechanism to the slab.

Gamble et. al. (1970) tested slabs with common reinforcement ratios of 0.01 and 0.005 and three levels of external compressive forces applied through mid-depth prestress cables. Gamble et. al. accurately predicted the peak capacity using conventional thrust-moment interaction diagrams (Figure 2.18). A 138 psi in-plane force produced increased moment capacities of 16 and 32 percent in slabs with 0.01 and 0.005 reinforcement ratios, respectively, while 275 psi resulted in 37 and 57 percent increases, respectively. In each case crushing of the concrete produced material instability leading to a drop in capacity and termination of the experiment. For the lower reinforcement ratio of 0.005, strain hardening increased the moment by 11 to 13 percent with respect to the theoretical values. Gamble et. al. felt that strain hardening of the reinforcement in sections subject to moment gradients may produce larger sustained deformations/rotations (i.e., 10-

20 degree hinge rotation with little to no shear reinforcement) and even larger moment enhancements than predicted through the axial force-moment interaction curve.

Hopkins and Park (1971) tested a slab/beam system with shear reinforcement in the beams to resist the tension and torsion generated by the compressive forces of the center and center-edge panels. The design peak capacity of 800 psf was twice the yield line capacity. The loading reached 850 psf when the center panel snapped through to tensile membrane action (Figure 2.19f). After reducing the center panel load to 600 psf, they loaded the other panels until failure resulting in 966 psf (Figure 2.19e) on the center-edge panel and 1170 psf (Figure 2.19d) on the corner panel. The panels supported 2.18, 1.55 and 1.46 times their yield line capacity versus the expected 2.00, 1.35, and 1.00 for the center, center-edge and corner panels, respectively. There was little evidence of tension in the beams apart from the steeply inclined shear cracks. The snap through of the central panel greatly eased the tension burden of the interior beams. Hopkins and Park believed that had the outer panels not cracked the interior panel would have carried even larger loads. The effect of the full service loading of 375 psf for 66 hours was minimal with rapid recovery to the original load path once additional load was applied. Park (1971) reflected on this test by stating that ductile beams stiff enough to first force development of yield line behavior in the slabs will increase capacity 66-88 percent over yield line theory.

Hung and Nawy (1971) used the test results of over 119 two-way slabs with varying boundary conditions to extend Sawczuk's work to consider isotropically reinforced concrete slabs with at least two fully restrained opposite edge conditions and the other two opposite edge conditions either simply supported, hinged, free, or fully restrained (Hung and Nawy and Nawy and Blair (1971)). They used their own experimentally derived peak capacity deflection estimate which varied from 0.4 to 1.0h depending on the slab parameters and the boundary conditions. Estimates for peak capacity were acceptable except for the extreme capacity under-prediction for the slabs with two hinged edges. The inelastic stage of the load-deflection curve began at about 12.5 percent of depth.

Tong and Batchelor (1971) studied punching failure in two-way slabs loaded through a concentrated force. Conventional edge beams induced significant compressive membrane action which resulted in higher failure loads than predicted by yield line theory regardless of mode of failure (i.e., flexure or shear). Low reinforcement ratios prevented punching failure and nearly guaranteed a flexural failure mode. Tong and Batchelor developed a relationship between flexural and shearing strength considering compressive membrane enhancement to predict the punching load.

Criswell (1972) tested two one-quarter scale models of a nine panel slab (3 panel x 3 panel) supported on four interior columns and a continuous perimeter wall. The monolithic connection between the slab and wall supported a 30 percent capacity increase due to compressive membrane action which was contrary to Wood's earlier assessment. Criswell felt that bottom reinforcement should run throughout the entire slab to develop the local membrane action along supporting walls and around columns. Splicing at columns should alternate sides so that bars from each span are continuous through the column capital. Round column capitals avoided the shearing force concentrations present at rectangular column capital corners. The column areas need to be sufficiently tied together with shear reinforcement to minimize shear crack size.

Ramesh and Datta (1973 and 1975) extended Park's method to include the lateral bowing effect of edge beams which remain elastic as the slab yields. Park's theory only considered an identical lateral translation for all slab strips while Ramesh and Datta included the larger support movement at the slab's center line because of the edge beams greater lateral deflection at it's center. Ramesh and Datta tested 19 isotropically reinforced concrete two-way square slabs with either the slab cast at the center of the edge beam (BN1, CN1, DN1) or cast at the top of the edge beam (B1, C1, D1) to verify their analytical work. All slabs developed increased capacity, but casting the edge beams at the top of slab increased capacity by 20 percent because of T-beam action which generates greater torsional resistance and compressive stresses in the perimeter of the slab (i.e., greater resistance to lateral movement) (Figure 2.20). Ramesh and Datta's dimensionless parameter representing the restraint provided by the edge beams is based on the lateral deflection of

the edge beam from the generated in-plane thrust in the slab strip. The partial lateral restraint of the edge beams translated into increased peak capacity deflections and a gradual post-peak decrease in compressive membrane action in contrast to the completely restrained slab which has less deflection and a steeper decline.

Batchelor and Tissington (1976) loaded bridge spans with a concentrated load to study the effects of support conditions on shear strength. In their A-Series, all four beam edges were simply supported, while only the abutment ends were simply supported in their C-Series. The beam action in the C-series induced in-plane compressive stresses and increased strengths 1.46 times those of the A-series (Figures 2.21 and 2.22). Working load deflections were less than $^1/_{600}$ of the span.

Desayi and Kulkarni (1977) defined the load-deflection behavior for fully restrained slabs with elastic shortening in two stages: up to Johansen's capacity with a semi-empirical approach and then with rigid-plastic membrane action up to the peak capacity. They tracked the behavior by slowly incrementing the plastic deflection. In comparison with the analysis of Hung and Nawy (1971) and Park (1964), Desayi and Kulkarni's method was not much better than Hung and Nawy's for isotropic square slabs, while Park's method was better for orthotropically reinforced rectangular slabs. Park and Gamble's (1980) equations for compressive membrane behavior employs the technique of incrementing the plastic deflection.

Braestrup (1980) and Braestrup and Morley (1980) used elastic and elastic-plastic material models to define the pre-peak behavior of the load-deflection curve and the flow theory which increments the strain for the post-peak behavior. In Figure 2.23, Braestrup presents the differences between flow theory and the modified rigid-plastic theory (also known as the deformation theory). The differences in the two theories are not really significant for the peak capacity predicted near a dimensionless deflection value of $0.3w_o/h$ where w_o is the central deflection and h is the slab thickness. This deflection value is within the usual range of observed experimental peak capacity deflections for two-way slabs with Park's (1964) suggested deflection for indexing the peak capacity as the upper limit at $0.5w_o/h$. However, there is a noticeable difference in predicted capacity when using the theories to predict post-peak behavior, i.e., at a

dimensionless deflection value beyond $0.6w_o/h$. The deformation theory curve eventually falls below the yield line capacity which is contrary to Braestrup's contention. Most test results analyzed by the author also supports the tensile membrane action initiating at about the yield line capacity. However, there are a few experimental one-way slab results listed in Appendix A where the post-peak capacity drops below the yield line capacity before initiation of tensile membrane resistance. Additionally, the experimental results usually show an even steeper post-peak decline than either method shown in Figure 2.23 due to possible strain-softening of the concrete in the compression zone. Braestrup noticed that slabs with the same L/h ratio had approximately the same peak capacity deflection even though increasing reinforcement ratios should have decreased the deflections due to increased stiffness.

Fang et. al. (1994) tested with a concentrated load 18 partial lateral edge restrained reinforced concrete slabs reinforced isotropically. Ductility decreased with increasing reinforcement ratio and slab thickness. The steel grade did not significantly affect the load capacity which was dominated by concrete strength and slab thickness. A lower span-to-thickness and reinforcement ratio had a greater duration of and enhancement from compressive membrane action.

Ghoneim and MacGregor (1994) tested 19 reinforced concrete slabs loaded to failure under combined compressive in-plane and lateral loads to investigate the effect of loading type, plate slenderness, in-plane load level, aspect ratio, reinforcement ratios, and loading sequence. The slabs were simply-supported on all four edges. The experimental results were as follows: (i) uniaxial in-plane compression reduced the capacity of slender plates due to the secondary moments (P-Δ effects) increasing more rapidly than the internal resisting moments pointing to the importance of rotational restraint; (ii) secondary moments accelerated yielding at hinges; (iii) increased reinforcement ratios perpendicular to the in-plane load increased the capacity more efficiently than increasing reinforcement parallel to the in-plane load, especially in the short span; (iv) the in-plane forces significantly redistributed (i.e., lateral redistribution) near the maximum applied lateral load with larger in-plane forces in the center of the span; (v) in thick slabs, only slight surface crushing

occurred at the peak capacity with a corresponding compressive strain of 0.00498 in/in parallel to the in-plane load; (vi) biaxial in-plane compression generated a stiffer response in the pre-cracking stage and increased the capacity by 25 percent; (vii) the interaction of in-plane forces and geometric non-linearity in rectangular slabs initiates earlier than in square slabs because of larger deflections; (viii) the moment capacity for the slabs with the in-plane load level in the ductile region of axial force-moment interaction diagram is 25 percent higher than the slab with the in-plane load level in the brittle region; and (ix) applying in-plane forces after the full lateral loads results in a loss of capacity and sudden failure.

2.2.2. One-Way Slabs

In order to accurately and simply investigate compressive membrane or tensile membrane behavior, some testing must naturally focus on laterally restrained one-way slabs (i.e., width larger than thickness) with an aspect ratio $\ell_1/\ell_2 > 2$. One-way slabs differ from beams in that normally lateral instability is insignificant in slabs, shear stresses and deformation are relatively small, and transverse reinforcement in the form of temperature steel is usually provided. In Table 2.2 there is presented a summary of the following detailed contributions in defining compressive membrane action in one-way slabs.

In the 1980's (i.e., height of the Cold War), WES statically tested 61 one-way slabs under various programs sponsored by the Defense Nuclear Agency (DNA), the Office, Chief of Engineers (OCE), the Federal Emergency Management Agency (FEMA), and the Air Force Engineering and Services Center (AFESC). Most of the experiments focused on the flat-roofed, shallow-buried FEMA key worker structures designed to resist low yield nuclear weapons (Guice et. al., 1986). Generally, initial failure, denoted by concrete crushing, was in a flexural mode with continued loading leading to rupture of the reinforcement during the tensile membrane stage. The tensile membrane or reserve capacity is extremely important in economically designed blast resistant structures. Even though many of the WES tests focused on tensile membrane behavior, the researchers did record and sometimes analyzed the compressive membrane action. In support

of the tensile membrane loading, many of the slabs contained shear reinforcement which is critical for the development of large deflections, but only moderately critical in the development of compressive membrane capacity beyond prevention of compressive reinforcement buckling. With the WES focus being on protective structures, their program limited the span-to-thickness ratios to less than 15. However, the conventionally reinforced concrete slab strips tested by Christiansen (1963) and Roberts (1969) do provide experimental one-way slab data for L/h's ranging from 17 to 29. A detailed summary of the experimental results used within this dissertation for analytical comparisons are presented in Appendix A.

Christiansen (1963) tested four conventionally reinforced concrete one-way slab strips to eliminate torsional considerations, and to validate his equations predicting the load arching to the supports. He estimated the peak capacity by considering separately the bending capacity through yield line theory and the compressive membrane capacity generated by the thrust. Christiansen related the depth of the additional compressive stresses induced through resistance to lengthening of the slab sections along the tension side resulting from rotations at plastic hinges (i.e., rigid-plastic strip) to the relative plastic deflection from hinge rotation. The additional compression at midspan and the supports produced greater internal moment resistance. The thrust was a maximum when the vertical distance between the additional compression at midspan and the supports is zero (i.e., distance a_1 equals zero, Figure 2.24).

Gurfinkel and Siess (1968) performed an analysis on laterally restrained reinforced concrete beams/slab strips which highlighted the following points: eccentric longitudinal reaction forces increased capacity similar to rotational edge restraint when placed below the mid-depth; restrained beams have larger ultimate deflections with increased reinforcement ratios; and their approximate method had acceptable precision for low reinforcement ratios.

Roberts (1969) tested laterally restrained (i.e., 83 percent of infinitely stiff) reinforced concrete slab strips only reinforced along the entire bottom. He extended Wood's rigid-plastic theory to include plastic stretch and rotation and did not require an empirical deflection estimate as did Park's derivation. Roberts had to adjust the concrete cube strength to obtain acceptable results

due to the concrete strength enhancements from biaxial and triaxial stresses. An analysis of support stiffness showed that a stiffness equal to the slab strip stiffness reduced the increased load by only 10 percent from a support stiffness nearly 11 times greater. Roberts was hoping that the peak capacity deflections were a fixed proportion of the thickness, but the deflection appeared to be a function of L/h. The ratio of the midspan deflection-to-thickness (Δ/h) for the two inch thick slabs was approximately 0.269, while it was 0.158 for the three inch thick slabs. Increasing the concrete strength and slab thickness increased the capacity more than increasing the reinforcement ratio. Experimentally, the maximum thrust and maximum load capacity occurred nearly at the same deflection with the thrust peaking at a slightly larger deflection (Figures 2.25 and 2.26). The experimental thrust and capacity decreased faster than Roberts' theory predicted.

Keenan (1969) tested heavily reinforced laced concrete one-way slabs with L/h = 12 in which the loading type, static or dynamic, did not change the collapse mechanism, failure mode, support rotation capacity, nor the extent of cracked or crushed concrete. His theory provided acceptable correlation with the experimental results and he recommended providing equal amounts of compressive and tensile reinforcement to increase the moment resistance.

Woodson and Garner (1985) tested laterally restrained reinforced concrete one-way slabs similar to other Woodson tests (1985) except that reinforcement was not placed equally in the compressive and tensile faces. Their experimental results were: (i) placing most of the reinforcement in the tension zones produced a high yield line capacity but little compressive membrane enhancement; (ii) equal compressive and tensile reinforcement lowered the yield line capacity, but increased the capacity by 40 percent through compressive membrane action; (iii) reinforcement placement in heavily reinforced slabs (i.e., $\rho > 1.5$ percent) had little effect on peak capacity; and (iv) using a peak deflection of 0.4h in Park and Gamble's modified rigid-plastic equations achieved greater accuracy than 0.5h.

Baylot et. al. (1985) tested three laterally restrained reinforced concrete one-way slabs in which the static results indicated that the peak resistance occurred at 0.5h for his thin slabs with an L/h = 10 and at 0.25h for his thick slabs with an L/h = 5. The transition to tensile membrane

action occurred between 0.5h to h. Baylot et. al. dynamically tested similar slabs with conventional blasts resulting in the thin slab with light reinforcement being breached, while a similar slab with increased reinforcement and a thicker slab exposed to an even closer blast were not breached.

Guice (1986) tested a series of laterally restrained reinforced concrete slabs similar to Woodson's slabs in 1985 except that the supports were not rigidly restrained from rotating (i.e., no monolithic slab-wall connection). The small support rotational freedom increased the peak capacity deflection, but did not always reduce the peak capacity. Large rotational freedoms between 2.0 to 2.5 degrees, depending on the slab thickness, eliminated any compressive membrane action in some slabs. The large early rotations allowed the slabs to snap through to the tensile membrane stage before development of significant thrusts and compressive membrane resistance. Rotational restraint and not just lateral restraint at mid-depth is required to achieve significant compressive membrane capacity, while rotational freedoms less than 1.5 degrees increased tensile membrane capacity and incipient collapse deflection. Guice predicted within 10 percent the peak capacity using Park and Gamble's compressive membrane theory with a realistic lateral support stiffness value. An infinite support stiffness value greatly over predicted the capacity. Guice used energy methods with a reduction in axial stiffness of 50 percent for L/h = 14.8 and 25 percent for L/h = 10.4 to develop the load-deflection curve from the initial loading through the transition zone to intersection with the tensile membrane curve. Guice's predicted peak capacities using energy methods were lower than Park and Gamble's or Hung and Nawy's analytical results since Guice used a linear displacement field to represent the rigid slab sections between hinges.

Woodson (1993) tested 16 laterally restrained reinforced concrete slabs to investigate the effectiveness of shear stirrups versus lacing. Lacing was only slightly more effective than stirrups in enhancing the ultimate capacity of the slabs, but provided little difference in peak capacity. The lacing results in better confinement, but is very labor intensive and costly. The span-to-thickness ratio, principal reinforcement quantity and spacing, and support conditions are more significant than shear reinforcement in affecting the failure mode and total response of the slab. The average

Δ/h ratio was 0.29 and did not appear to be affected by the various construction parameters (i.e., constant for $L/h = 8$). Park and Gamble's compressive membrane theory acceptably predicted the peak capacity for the slabs with $\rho = \rho' = 0.0025$ and 0.0056 when the experimentally obtained deflections were used (i.e., $\Delta/h = 0.29$ versus 0.5), but Woodson required a Δ/h value of approximately 0.1 to predict the capacity of the slabs having a reinforcement of 0.0097. Woodson concluded that slabs reinforced with more than 0.5 percent of reinforcement need shear reinforcement to prevent shear failure.

Woodson (1994) tested deep slabs with an $L/h < 5$ to evaluate the contribution of shear reinforcement on compressive and tensile membrane capacity. With similar results for stirrups or lacing, his experimentation showed that a relatively large amount of shear reinforcement is critical to achieve peak flexural resistance in a deep slab. Park and Gamble's compressive membrane theory provided a good estimate of the peak capacity provided that appropriate values of Δ/h are used in the computations: 0.07 for an L/h of 4.4 and 0.03 to 0.05 for an L/h of 2.7. These Δ/h values are much smaller than the experimental Δ/h results.

Meamarian et. al. (1994) developed a computer-based design program in which they modified the compressive membrane equations in Park and Gamble to include the effects of prestressing forces and long-term deflections. Once the peak capacity is determined, equilibrium equations determine the sectional forces at any point and an iterative method uses the recently developed modified compression field theory to relate these sectional forces to stresses, strains and curvature. Meamarian et. al. recommended higher load factors when using this design method, especially for sustained loads, because of the sensitivity of the membrane action to axial deformations and the relatively large discrepancies observed in test results. Their theoretical deflections at peak capacity are nearly half of the experimental values for high reinforcement and thickness ratios.

2.3. Tensile Membrane Experimentation and Analysis

After a laterally restrained reinforced concrete slab reaches the peak load capacity, the load resistance decreases as a result of material or geometric instability. If the lateral restraint, reinforcement ratio, and steel embedment are sufficient, the membrane forces will gradually change from compression to tension as the reinforcement yielding spreads and provides reserve capacity through catenary action. Pure tensile membrane behavior is marked by full-depth cracking, large deflections, and a load capacity carried entirely by the steel. If the reinforcement ratio is large enough, the tensile membrane ultimate load capacity could exceed the peak compressive membrane capacity. During the transition between compressive and tensile membrane action, the load is carried by combined bending and tensile membrane action, especially in thicker slabs ($L/h < 18$). Normally steel strain hardening and any bending capacity are ignored once the load is carried by tensile membrane action. Of course for many engineers reaching tensile membrane action means a serviceability failure, but for those concerned with protective structures, tensile membrane capacity is an inherent part of the resistance and energy absorption measures available.

The following researchers have compiled experimental and analytical knowledge which is summarized in Table 2.3 concerning tensile membrane behavior even though the results were occasionally a secondary focus after compressive membrane experimentation.

As secondary efforts to their compressive membrane study, Powell (1956) suggested that incipient collapse would occur at one-eighth of span length, while Wood (1961) used plate theory to show that tensile membrane action could not increase the capacity until deflections greater than the slab depth had occurred. However, Park (1964) provided the first real effort toward defining tensile membrane behavior in reinforced concrete slabs. He used classical membrane theory to develop a linear relationship between load and deflection, while assuming that the concrete does not contribute because of full depth cracking, there is no reinforcement strain hardening, and the reinforcement throughout the slab reaches yielding (Figure 2.27). Park suggested using a safe estimate of the incipient collapse deflection as one-tenth of the short span length. He developed a widely used chart comparing aspect ratios and tensile membrane capacity from square to one-way

slabs (Figure 2.28). Park suggested that slabs using draped reinforcement should have considerable tensile strength because of the large load carrying capacity of the reinforcement at relatively small deflections (investigated by Woodson and Garner, 1985).

Sawczuk and Winnicki (1965) extended their compressive membrane work to include tensile membrane capacity. From their experiments, they observed that during post-yield response (i.e., large deflections) the bending response yield line patterns did not change and generally forced localization of post-yield membrane action at the hinges. This localization basically shifted up the pure membrane response (Figure 2.29 and 2.27). In Figure 2.30 they depict the effect of using the reinforcement ultimate strength (i.e., the top dashed line) rather than yield strength (i.e., the bottom dashed line).

Taylor (1965) observed that tensile membrane action in simply-supported reinforced concrete slabs did not alter the bending action collapse mechanism since additional deflections were caused by rotations of the segments at the yield lines. The large deflections at midspan caused the central portions of the supported edges to move inward, but the adjacent outer edges restrained the movement allowing the development of catenary action.

Taylor et. al. (1966) tested simply-supported reinforced concrete two-way slabs with L/h's of 41, 36, and 24 with reinforcement spacing according to elastic bending moment distributions (i.e., yield line or strip method). The arrangement of the reinforcement increased tensile membrane load capacity 26 to 80 percent. The variably reinforced slabs were slightly stiffer than uniformly reinforced slabs, but the stiffness of the slabs with top cut-off bars deteriorated rapidly with the subsequent square yield line pattern following the ends of the cut-off bars. Tensile membrane strength ultimately depended on the yield line failure mode which produced the lowest load capacity for the slabs (e.g., cut-off bars).

Keenan (1969) used tensile membrane behavior as reserve energy absorption capacity in protection against total collapse. He suggested empirical modifications to Park's formulation with $k = 20$ rather than 13.5 (i.e., square slabs, Figure 2.28) to account for strain hardening and

combined action of flexure and tension. Keenan also used one-tenth the short span length for marking incipient collapse.

Nawy and Blair (1971) pointed out the need to limit the spacing of the principal reinforcement to control cracking. If the reinforcement grid spacing is too large, the stress concentration magnitudes and energy absorbed is too small to force the cracks along the reinforcing bars or wires. This results in early cracking in the plain concrete with a few, wide cracks ultimately limiting the crack band and hinge size. The smaller the spacing of the equally important transverse reinforcement, the smaller should be the diameter of the longitudinal bars.

Regan (1975) focused on the slab tensile strength required in structures due to local failures such as the loss of a column. A slab must provide tensile strength, extendibility and horizontal restraint for other slabs. Reinforcement was required throughout in orthogonal directions, but Regan felt that it really should not matter whether the steel was in the top or the bottom at any one point in the slab. All tests had an initial compressive membrane phase which terminated with the load capacity falling to a minimum before rising again in a catenary action. Two tests failed immediately after the peak capacity because of limited ties which fractured after large rotations at a single crack, i.e., strain concentration. Many of the slabs failed when the bottom bars tore out of the concrete at the cut-off point for the ties (Figure 2.31). When the end cantilevers yielded in flexure before any tearing out of the bottom reinforcement, the cantilever bent down and a catenary extended from support to support. Plain round ties allowed some bond slip and decreased the resistance at the ends so that a catenary could form. The better bond provided by deformed bars produced brittle failures particularly when concentrated rotations occurred at the ends of the member (deformed bars, Figure 2.32, and plain round bars, Figure 2.33).

Black (1975) tested fully restrained reinforced concrete slabs and compared them with previously tested (WES) simply-supported slabs to provide an upper and lower bound solution of actual structures supported on flexible beams. Black felt a value of one-tenth of the short span was too conservative for incipient collapse deflection after recording an incipient collapse of one-fifth the span length for a flexible slab system (Figure 2.34) and one-sixth for a stiffer slab system.

During his analysis, Black used Park's tensile membrane equation with suggestions from Keenan. For the statically loaded square slabs, Black had good results using k = 20 as Keenan suggested versus Park's k = 13.5 (Figure 2.28), an incipient collapse deflection of 0.15L, and the yield stress (f_y) as the reinforcement stress. For the dynamically loaded slabs, he used k = 20, a collapse deflection of 0.1L, and $f_s = f_u$ (i.e., steel stress = ultimate steel stress) or k = 13.5, the deflection as 0.25L, and $f_s = f_y$. Concrete confinement is extremely important during tensile membrane action to ensure that the concrete distributes the loading. Failure was initiated by rupture of the individual bars around the periphery of the slab.

Hawkins and Mitchell (1979) provided recommendations to defend against progressive collapse caused by punching shear failures. Punching failures occur with little warning either from increasing crack widths or deflections since the inclined shear cracks develop in the plane of the slab and are indistinguishable from flexural cracks except at discontinuous edges. Additionally, the shear strength decreases as the stiffness of the connection decreases. Their defensive measures called for continuous bottom reinforcement through the connections (Figure 2.35), especially if $M/V_c > 1$ (length) (moment divided by the plain concrete shear strength), and/or additional reinforcement to support tensile membrane action which is controlled usually by the small amount of midspan reinforcement. Reinforcement through the connections provides proper embedment for the tensile membrane stage and a post-punching shear transfer mechanism that is recommended to be 0.5 times the yield strength of the continuous bottom reinforcement. Splice and anchorage lengths within supports must ensure the development of the bars tensile strength, while the surrounding structure must provide horizontal restraint. Damage is further reduced and the strength increased by the provision of integral beam stirrup reinforcement.

Woodson (1985) tested laterally restrained reinforced concrete one-way slabs subject to large deflections to evaluate the use of different types of stirrups. Generally, failure was a three hinge mechanism with little spreading of the cracks. The lowest reserve capacity occurred in the slabs having no stirrups, while the slabs with 90-135 degree bend stirrups only achieved 88 to 93 percent of the tensile capacity of the slabs with two 135 degree bend stirrups. Double leg stirrups

only slightly improved the performance over the two 135 degree bend stirrups. The 90-135 degree bend stirrups performed similarly to the two 135 degree bend stirrups up to a deflection of 0.125L. Slabs with a large number of closely spaced ($< d/2$) stirrups exhibited increased load resistance at large deflections. Larger stirrup spacing did not greatly improve performance over slabs with no stirrups. Slabs with principal reinforcement spaced less than the effective depth (d) had little improvement with closely spaced stirrups. Therefore, any construction detail that improved confinement or increases the size of the confined core greatly increased ductile reserve or tensile capacity, but did little to affect peak capacity. Woodson used Park's equations for tensile membrane behavior initiating at a deflection near the slab's depth.

Woodson and Garner (1985) tested 15 laterally restrained reinforced concrete slabs to determine the reinforcing pattern that would provide the greatest tensile membrane capacity for a given slab depth and total area of steel. Slab reinforcement configurations that produce the greatest yield line capacity exhibited the best tensile membrane behavior. The case of bending all the principal reinforcement into the tension zones provided the best tensile membrane behavior as Park predicted, but significant spalling occurred due to the lack of concrete confinement. To control spalling 50 percent of the reinforcement was bent into the tension zones and the other 50 percent split between the top and bottom faces which resulted in a 50 percent reduction in the tensile membrane capacity. The combination of closely spaced stirrups with temperature steel placed exterior to the principal steel improved the load response of similarly reinforced slabs. The symmetrically reinforced slab performed nearly as well during compressive/tensile membrane action with a lot less spalling and damage to entire slab.

Guice (1986) tested both thick (i.e., L/h = 10.4) and thin (i.e., L/h = 14.8) laterally restrained reinforced concrete slabs with some support structure rotation. Most of the support rotations occurred prior to peak capacity. Initial support rotations greater than 2.0 to 2.5 degrees for thick slabs and 1.5 to 2.0 for thinner slabs produced early snap through to the tensile membrane stage without development of any compressive membrane resistance (i.e., less stiffness). Guice used both the yield stress and the rupture stress in Park's tensile membrane theory to bound the

tensile membrane response of the slabs prior to rupture of the reinforcement. The thinner slabs carried a larger percentage of load by tensile membrane action with a broader crack pattern, narrower cracks, and evenly distributed yielding throughout the slab. Higher tensile capacities in the thicker slabs were achieved as the rotational freedoms increased. Small or no perceptible rotational freedom results in more of the reinforcement strain energy being required during the flexural stage leading to earlier rupture in the tensile membrane stage and reduction of the slope of the tensile membrane resistance curve. For the thinner slabs, small support rotational freedom results in more of the load being carried by combined flexure and tension. Most of the slabs initiated tensile membrane response at a deflection between d and h with an average incipient collapse deflection of one-eighth of the span for the thick group and slightly greater for the thin slabs which equates to over 20 degree hinge rotations. Small rotational support freedoms do not significantly affect the compressive membrane capacity, but do increase the tensile membrane capacity and incipient collapse deflection. Sufficient reinforcement ductility must be provided to develop tensile membrane resistance through the use of Grade 60 or lower reinforcement.

Woodson (1993) tested laterally restrained slabs to evaluate the effect of stirrups versus lacing on tensile membrane behavior. In all slabs significant spreading of cracking did not occur along the length of the slab resulting in limited tensile membrane behavior. Lacing appeared to provide the best enhancement in slabs with $\rho = 0.0025$, while stirrups provided the best enhancement for the slabs with $\rho = 0.0097$. Both shear reinforcement techniques performed equally well in the slabs with $\rho = 0.0056$. The reinforcement ratio was the significant parameter determining the peak reserve capacity with tensile membrane capacity best predicted by using only one-half of the principal steel for the large ρ values and all the reinforcement with the small ρ values. Crack widths were slightly less in the laced slabs since lacing was mobilized earlier in the slab's response (i.e., based on the strain readings). However, the overall performance of laced and stirrup slabs were very similar.

Polak and Vecchio (1994) tested large scale reinforced concrete shell elements under the conditions of biaxial bending and in-plane normal forces to evaluate current models representing

post-cracking tensile stresses in concrete. When imposed in-plane loads were in line with the reinforcement, there was little interaction between the orthogonal directions except for a decrease in cracking moments. Tensile loads skewed to the reinforcement generated a nonlinear response with a redistribution of forces, a reorientation of cracks, and a greatly decreased capacity.

Woodson (1994) tested laterally restrained reinforced concrete deep slabs with an $L/h < 5$ to investigate the effect of lacing and stirrup shear reinforcement on behavior. A substantial amount of reserve capacity is available in deep slabs with large quantities of principal reinforcement. The slabs with relatively low levels of principal reinforcement (i.e., $\rho = 0.0034$) were considerable less ductile. Woodson determined that with adequate shear reinforcement spaced less than 0.5d and principal steel ratios of 0.01, the recommended response limit is approximately 12 degrees of rotation. For any smaller amount of principal reinforcement, hinge rotation should be limited to approximately 8 degrees.

2.4. Summary

Even though most discussion in the literature is on lateral restraint, laterally restrained reinforced concrete slabs require some support rotational rigidity to activate substantial compressive membrane behavior. Prior to peak compressive capacity, the slab behavior is defined by a combination of elastic, and then, elastic-plastic material behavior influenced by compressive axial thrusts. Failure deformations are concentrated along yield lines even though yield line theory, which determines the failure pattern, under-predicts the capacity for laterally restrained slabs. The peak capacity is a function of axial force-moment interaction along the yield lines, which increases the yield line moments. Presently, peak capacity for lightly-reinforced thin slabs can be reasonably predicted, even though the capacity is 10 percent lower than experimental results, using an empirical peak capacity deflection as an index point in the modified rigid-plastic theory (i.e., Park's final version in Chapter 12 of Park and Gamble, 1980). However, a deflection indexed peak capacity for thick slabs (i.e., $L/h < 8$) and heavily reinforced slabs (i.e., $\rho > 1$ percent) is some times inaccurate to the point that the estimated capacity barely exceeds the yield line capacity.

After the peak capacity, the capacity decreases with increasing deflections because of material instability for thick slabs, L/h < 18, and geometric instability for thin slabs. During the tensile membrane stage, the principal reinforcement provides reserve capacity through catenary action if the rebar is properly anchored. Classical tensile membrane theory provides an upper bound estimate of tensile membrane capacity by using the rupture stress and a lower bound estimate by using the yield stress. Heavily reinforced slabs (i.e., $\rho > 1$ percent) may only mobilize approximately one-half of the reinforcement during tensile membrane action.

Whether the slab is one-way or two-way, increasing f'_c, ρ or the slab thickness provides capacity enhancement while maintaining a given support stiffness. Closely spaced principal reinforcement and stirrups increase the capacity and ductility during compressive and tensile action through improved confinement of the concrete core. Infinitely stiff support structures are not necessarily the best condition since support rotations less than 1.5 degrees produce increased tensile membrane behavior with little, if any, decrease in peak capacity. Lateral stiffness equal to the slab stiffness will generate up to 90 percent of the capacity of infinitely stiff supports. The peak thrust occurs nearly simultaneously (i.e., at a slightly larger deflection) with the peak capacity; thereby, possibly providing a better index for peak capacity within the modified rigid-plastic theory than an empirical deflection index.

Once the peak capacity and peak capacity deflection are known, a simple parabolic curve may be the best estimate, based on current knowledge, for the load-deflection curve up to the peak capacity and then back down until intersection with the tensile membrane curve, since the post-peak portions of the modified rigid-plastic and flow theory curves are not usually as steep as the experimental results. Peak capacity deflections appear to be a function of L/h and are larger than expected because of the high concrete compressive strains in excess of 0.005 in/in, in the support hinge regions, resulting from biaxial and triaxial conditions.

The two widely used forms of the compressive membrane theory are Park's modified rigid-plastic theory and Morley's flow theory in which both were initially developed to predict only the peak load capacity. Comparison of the two theories by Braestrup (1980) in Figure 2.23 shows that

up to a midspan deflection-to-thickness ratio (w_o/h) of 0.4, both theories generally predict the same load capacity for the three different reinforcement schemes. A comparison at $w_o/h = 0.3$ is provided on the figure. It is not until researchers began using the theoretical compressive membrane curves to model post-peak behavior that the differences between the two compressive membrane theories became significant (i.e., at $w_o/h > 0.6$). Maybe neither compressive membrane theory should be used to predict post-peak behavior since the developmental assumptions were based on pre-peak conditions. For the span-to-thickness (L/h) ratios used within this thesis ($2.7 < L/h < 28.3$), either compressive membrane theory could be used to provide load capacity predictions since the midspan deflections-to-thickness ratios associated with the peak load capacity ranged from 0.03 - 0.4.

Upon review of the experimental results and the peak load capacity prediction techniques, the following salient points for compressive membrane resistance were chosen for further investigation:

- when the thrust was measured, it peaked only slightly after the load capacity,
- a lateral stiffness equal to the slab's stiffness produced over 90 percent of the enhancement afforded from infinitely stiff supports, and
- the testing of slabs with the same span-to-thickness ratio (L/h) and various reinforcement ratios and concrete compressive strengths produced nearly constant peak load capacity midspan deflection-to-thickness ratios (Δ/h).

For tensile membrane resistance, the prominent details were:

- the trough capacity (Point C, Fig. 1) was generally defined by Johansen's fixed-supported yield line capacity,
- failure at the ultimate point is determined through an incipient collapse deflection, and
- support rotations during compressive membrane resistance limited to less than 2 degrees for thick slabs ($L/h < 18$), increased tensile membrane load capacity and the collapse deflection.

Table 2.1. Summary of Two-Way Slab Experimentation and Analysis

Two-Way Slabs - Compressive Membrane Action	
Gvozdev, 1939	Recommended a 20 percent reinforcement reduction for interior panels in Russian code.
Ockleston, 1955, 1958	Confirmed that lateral stiffness generated compressive thrust enhanced capacity either through arching action or moment-thrust interaction.
Powell, 1956	Conducted first laboratory tests which lead to a general rigid-plastic solution using empirical deflections (i.e., deformation theory).
Wood, 1961	Developed first analytical solution for circular slabs using a rigid-plastic material model, large-deflection plate theory, and an empirically derived deflection; described basic mechanics as a change of yield criterion due to compression.
Park, 1964-1965	Expanded Powell and Wood's work for rectangular slabs using a rigid-plastic strip method; strip hinge points followed traditional yield lines; applied to two-way slabs by summing the contribution of strips in orthogonal directions; rigid-plastic curves apply only at peak capacity; later included partial lateral restraint to include axial shortening and support movement; sustained loads of less than one-third of the service load had little effect on capacity; recommended using 0.5h as a peak compressive membrane deflection estimate.
Brochie, Holley, and Okubo, 1965	Determined that unreinforced laterally restrained slabs are stronger than normally reinforced unrestrained slabs; greatest enhancement in lightly reinforced thin slabs; load capacity increases with increased reinforcement ratio but more with increased slab thickness; post-peak capacity reduction less in thicker slabs; the compressive stress apparently increased the concrete crushing strain; thicker slabs withstood larger edge displacement with little loss in capacity; thrust is a function of slab thickness; thrust peaked at a slightly larger deflection and at a slightly reduced capacity; lateral restraint the most important parameter.
Sawczuk and Winnicki, 1965	Predicted capacity with energy method which related the total energy of plastic action to the energy dissipated along yield lines; results similar to Park.
Taylor and Hayes, 1965	Determined that the lateral edge restraint increased punching strength; greatest for slabs near ultimate flexural capacity.
Morley, 1967	Adapted basic yield line theory to account for elastic unloading by incrementing the strain rather than consider the strain at peak capacity as in Park's theory; equated work to energy dissipation; descending curve steeper than Park's, but not steep enough; limited to isotropically reinforced slabs.
Jacobson, 1967	Defined peak capacity through evaluation of pre-peak behavior through elastic/elastic-plastic behavior until formation of plastic hinges; not extremely accurate but no predetermined deflection value required; just another modified the rigid-plastic theory.
Gamble, Sozen, and Siess, 1961, 1969	Tested nine panel slab/beam system with the following results: rigidly designed beams not necessary; interior panel exceeded twice the yield line capacity with tensile action in edge/corner panels; overall structural behavior not affected by over-stressed slab sections.

Table 2.1. Summary of Two-Way Slab Experimentation and Analysis (cont.)

Two-Way Slabs - Compressive Membrane Action	
Keenan, 1969	Showed that compressive reinforcement can increase the enhancement; maximum compressive thrust and load capacity occur nearly simultaneously; post-peak capacity decreases to yield line capacity; derived a peak compressive membrane deflection estimate using rigid-plastic theory and curvature with crushing denoting peak capacity; estimated capacity using the axial-moment interaction curve; used quadratic equations to approximate the ascending and descending portions of compressive membrane action in the load-deflection curve.
Girolami, Sozen, and Gamble, 1970	Used an experimentally derived load-deflection curve and an iterative solution to determine the peak capacity from the axial force-moment interaction curve.
Gamble, Flug, and Sozen, 1970	Predicted accurately the capacity of slabs using conventional reinforced concrete thrust-moment interaction diagrams based on predetermined thrust values; felt strain hardening within section containing moment gradients may produce larger deformations through larger hinge rotations and enhanced moment capacity.
Hopkins and Park, 1971	Determined that cracking of outer panels precipitated interior panel snap-through at 2.18 times yield line capacity; 66-88 percent increase over yield line capacity if beam stiffness forces yield-line development in slabs first.
Hung and Nawy, 1971	Extended Sawczuk's work to include fully restrained isotropically reinforced concrete slabs; used their own experimental deflection values of 0.4t to t.
Tong and Batchelor, 1971	Enhanced punching capacity with edge beams; low reinforcement ratios precluded any punching failure; developed estimate for punching capacity.
Criswell, 1972	Generated a 30 percent capacity enhancement with monolithic construction between walls and slab.
Ramesh and Datta, 1973 and 1975	Extended Park's work to include the lateral bowing of elastic edge beams; slabs cast at the top of edge beams enhanced capacity by 20 percent over slabs cast at the center of the edge beams.
Batchelor and Tissington, 1976	Determined that beam action in slabs only supported at the two longitudinal edges increased capacity 1.46 times over slabs with all beam edges simply supported.
Desayi and Kulkarni, 1977	Used the modified rigid-plastic approach from the yield line capacity through peak capacity; same general approach as presented in Park and Gamble (1980).
Braestrup and Morley, 1980	Compared flow theory and modified rigid-plastic theories; flow theory provides steeper descending curve, but not as steep as experimental load-deflection curves; modified rigid-plastic theory will drop below the yield line capacity while flow theory is generally level at yield line capacity; noted that L/h appeared to control peak compressive membrane deflection.
Fang, Lee and Chen, 1994	Decreased the ductility with increased thickness and reinforcement ratio; lower span-to-thickness and reinforcement ratios had greater duration and enhancement through compressive membrane action.
Ghoneim and MacGregor, 1994	Measured a strain of 0.00498 with minimal surface crushing; secondary moments increase faster than resisting moments in thin plates (reduce capacity); in-plane forces redistribute near maximum capacity to be greater in the center of the cross-section at midspan; biaxial in-plane compression produced stiffer response during the pre-cracked stage and increased capacity by 25 percent; compressive in-plane loads within the ductile region of the axial force-moment interaction diagram produced a 25 percent capacity increase.

Table 2.2. Summary of One-Way Slab Experimentation and Analysis

One-Way Slabs - Compressive Membrane Action	
Christiansen, 1963	Considered separately yield and arching capacity; related generated thrust to lengthening of section; maximum thrust when vertical distance between the additional compression (thrust generated) at midspan and supports is zero.
Gurfinkel and Siess, 1968	Correlated enhancement to eccentric longitudinal reaction forces with a maximum when the thrust is at the bottom of the slab; restrained beams have larger peak capacity deflections with increasing reinforcement ratios.
Roberts, 1969	Extended Wood's rigid-plastic theory to include plastic stretch and rotation; did not require an empirical deflection estimate; support stiffness equal to slab stiffness only reduced capacity by 10 percent from infinitely stiff supports; appears deflection is a function of L/h; increasing the concrete strength and thickness increased capacity more than increasing reinforcement ratios; thrust peaked at a slightly larger deflection than the capacity.
Keenan, 1969	Determined that loading type, static or dynamic, did not change collapse mechanism, failure mode, support rotations, nor the extent of crushed and cracked concrete.
Woodson and Garner, 1985	Placed most of reinforcement in the tension zones and produced a high yield line capacity but little compressive membrane enhancement; equal placement of reinforcement in tension and compression zones produces lower yield line capacity and a 40 percent compressive membrane enhancement; recommended using 0.4h as a peak compressive membrane deflection estimate.
Baylot et. al., 1985	Used 0.25t as a deflection estimate in Park and Gamble's (1980) equations for slabs with an L/h = 5, while 0.5h still worked for slabs with L/h = 10.
Guice, 1986	Tested slabs while allowing some support rotational freedom; small support rotation increased the tensile membrane deflections, but did not always reduce the compressive membrane capacity; support rotational freedom greater than 2.0/2.5 degrees for slabs with L/h = 14.8/10.4, respectively, allowed snap through to tensile membrane action before significant thrust developed (i.e., no compressive membrane enhancement); rotational restraint is important.
Woodson, 1993	Showed that lacing only slightly more effective than stirrups in confining the concrete; span-to-thickness ratio, reinforcement quantity and spacing, and support conditions are more significant during compressive membrane action than shear reinforcement; used the experimental deflection which was nearly the same for all slabs to predict the capacity with Park's equations for slabs with reinforcement ratios, $\rho = 0.0025$ and 0.0056, but needed only a third of the deflection for $\rho = 0.0097$; slabs with reinforcement ratios > 0.5 percent need shear reinforcement to prevent shear failure.
Woodson, 1994	Evaluated shear reinforcement in deep slabs (i.e., L/h = 2.7 and 4.4); a large amount of shear reinforcement is critical to produce flexural response; used a $\Delta/h = 0.07$ for L/h = 4.4 and 0.04 for L/h = 2.7 in Park's equations rather than 0.4 to 1.0 reported in previous reports.
Meamarian et al., 1994	Added the effects of prestress forces and long-term deflections to Park's modified rigid-plastic theory; used the modified compression field theory to determine stresses and strains from sectional forces.

Table 2.3. Summary of Tensile Membrane Experimentation and Analysis

Tensile Membrane Action	
Powell, 1956	Estimated incipient collapse deflection at $^1/_8$ of span length.
Wood, 1961	Calculated that the tensile membrane action initiates with deflections usually greater than the depth.
Park, 1964	Developed a linear relationship from classical membrane theory; concrete does not contribute, no strain hardening, all reinforcement reaches yielding; estimated incipient collapse at a deflection of $^1/_{10}$ of span length.
Sawczuk and Winnicki, 1965	Showed that yield line patterns did not change during large deflection response; generally forced localization of post-yield membrane action at the previously determined hinge points; the combination of bending and tensile membrane action shifts the pure membrane response curve upward.
Taylor, 1965	Increased deflections during tensile membrane action resulted from rotations at hinge points; outer edge restraint from inward movement supports the catenary action.
Taylor et. al., 1966	Determined that tensile membrane strength depends on the yield line failure mode.
Keenan, 1969	Suggested a value of k = 20 versus 13.5 for square slabs.
Nawy and Blair, 1971	Limited the spacing of principal reinforcement to control cracking; too large of spacing does not force the cracks along the reinforcement resulting in a few wide cracks in plain concrete.
Regan, 1975	Felt reinforcement should extend throughout in orthogonal directions and does not matter whether in top or bottom; sufficient ties are necessary to prevent large rotations at a single crack; better performance when the edges yielded flexurally before any tearing out of bars.
Black, 1975	Recorded incipient collapse deflections of $^1/_5$ of span length for a flexible slab system and $^1/_6$ of span length for a stiffer slab system; used a k = 20, a collapse deflection of 0.15L, and the yield stress for statically loaded slabs; used a k = 20, a collapse deflection of 0.1L, and the rupture stress or k = 13.5, a deflection of 0.25L, and the yield stress for dynamically loaded slabs; need to contain the concrete to ensure it distributes the loading.
Hawkins and Mitchell, 1979	Used continuous bottom reinforcement through connections to guard against punching failure; damage is reduced and strength enhanced by the provision of integral beam stirrup reinforcement.
Woodson, 1985	Determined that stirrups with 135-90 degree bends achieved 88 - 93 percent of the reserve capacity of stirrups with two 135 degree bends; stirrups spaced less than $^d/_2$ produced increased resistance at large deflections; slabs with principal reinforcement spaced less than d had little improvement with closely spaced stirrups; core confinement increases reserve capacity.
Woodson and Garner, 1985	Verified that slab reinforcement patterns that produce the greatest yield line capacity exhibited the best tensile membrane behavior; all reinforcement in the tension zones provided excellent tensile capacity but also tremendous spalling; the symmetrically reinforced slab performed nearly as well with little spalling.

Table 2.3. Summary of Tensile Membrane Experimentation and Analysis (cont.)

Tensile Membrane Action	
Guice, 1986	Prevented premature rupture of reinforcement and enhanced tensile membrane capacity with limited support rotation; using both the yield stress and the rupture stress bounded the experimental tensile stress capacity; thinner slabs carry more of the capacity through tensile membrane action; tensile membrane action initiated between a deflection of the d and h; estimated incipient collapse deflection as $^1/_8$ of the span length; small support rotations (i.e., < 2 degrees) do not significantly affect the compressive membrane capacity, but do enhance the tensile membrane capacity and the incipient collapse deflection.
Woodson, 1993	Showed that the reinforcement ratio was the most significant parameter determining reserve capacity while using only half of the reinforcement for large ρ values and all the reinforcement for low ρ values; stirrups and lacing performed similarly.
Polak and Vecchio, 1994	Showed that tensile in-plane forces skewed to the reinforcement directions reduced capacity; little interaction between orthogonal directions when in-plane forces are in line with reinforcement except to lower the cracking moment.
Woodson, 1994	Determined that in deep slabs, the response should be limited 12 degrees if the steel ratios are > 1 percent and the shear reinforcement spacing < 0.5d, otherwise limit rotation to 8 degrees.

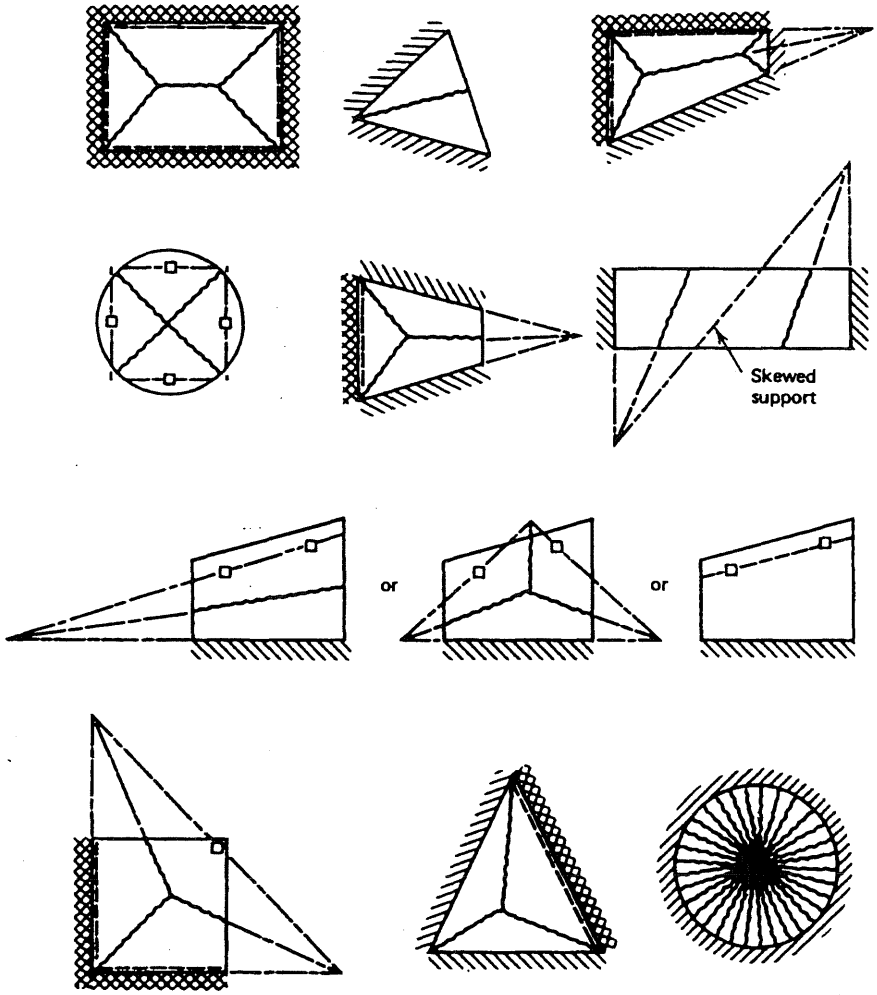

Figure 2.1. Examples of Yield Line Patterns for Uniformly Loaded Slabs (Park and Gamble, 1980)

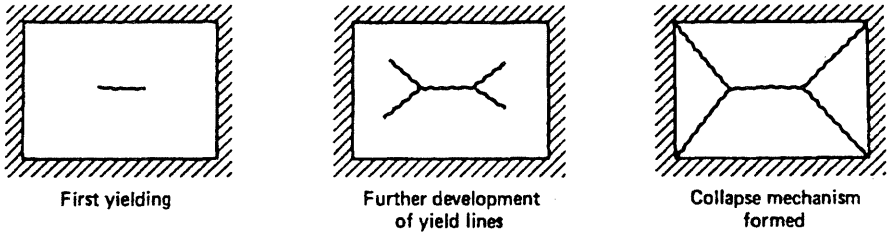

Figure 2.2. Yield Lines Developing in a Uniformly Loaded Simply Supported Slab (Park and Gamble, 1980)

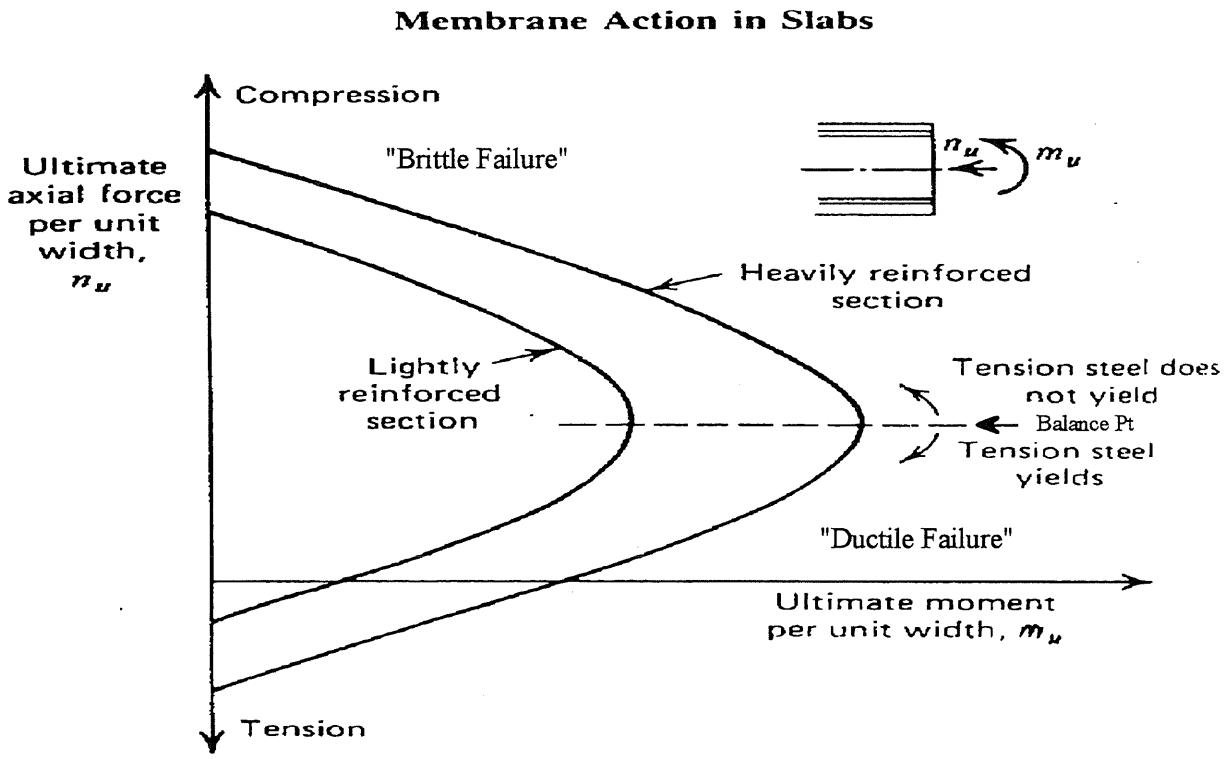

Figure 2.3. Ultimate Moment-Axial Force Interaction of Symmetrically Reinforced Concrete Section (Park and Gamble, 1980)

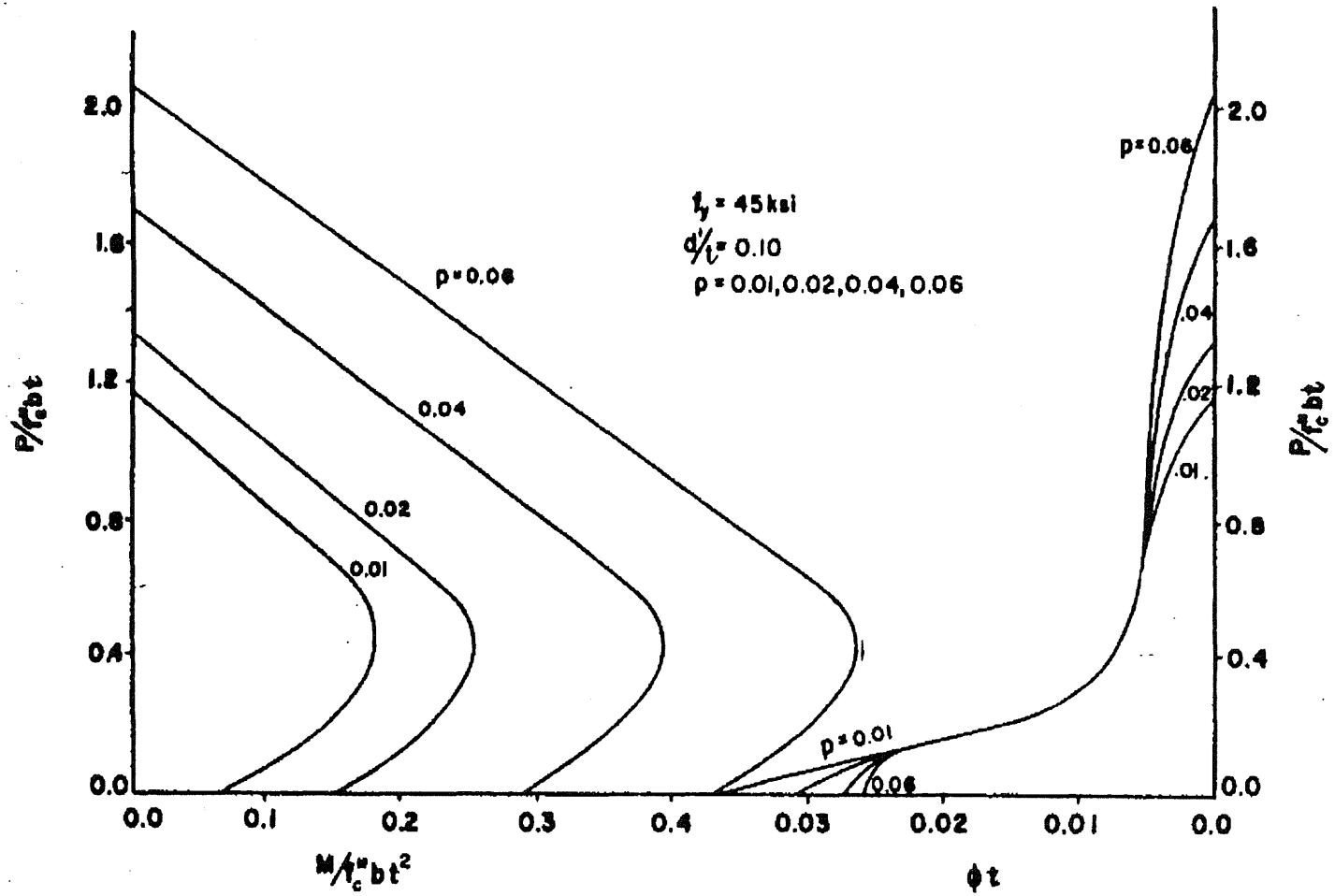

Figure 2.4. Interaction Diagrams for Different Values of Reinforcement Ratio
(Pfrang et. al., 1964)

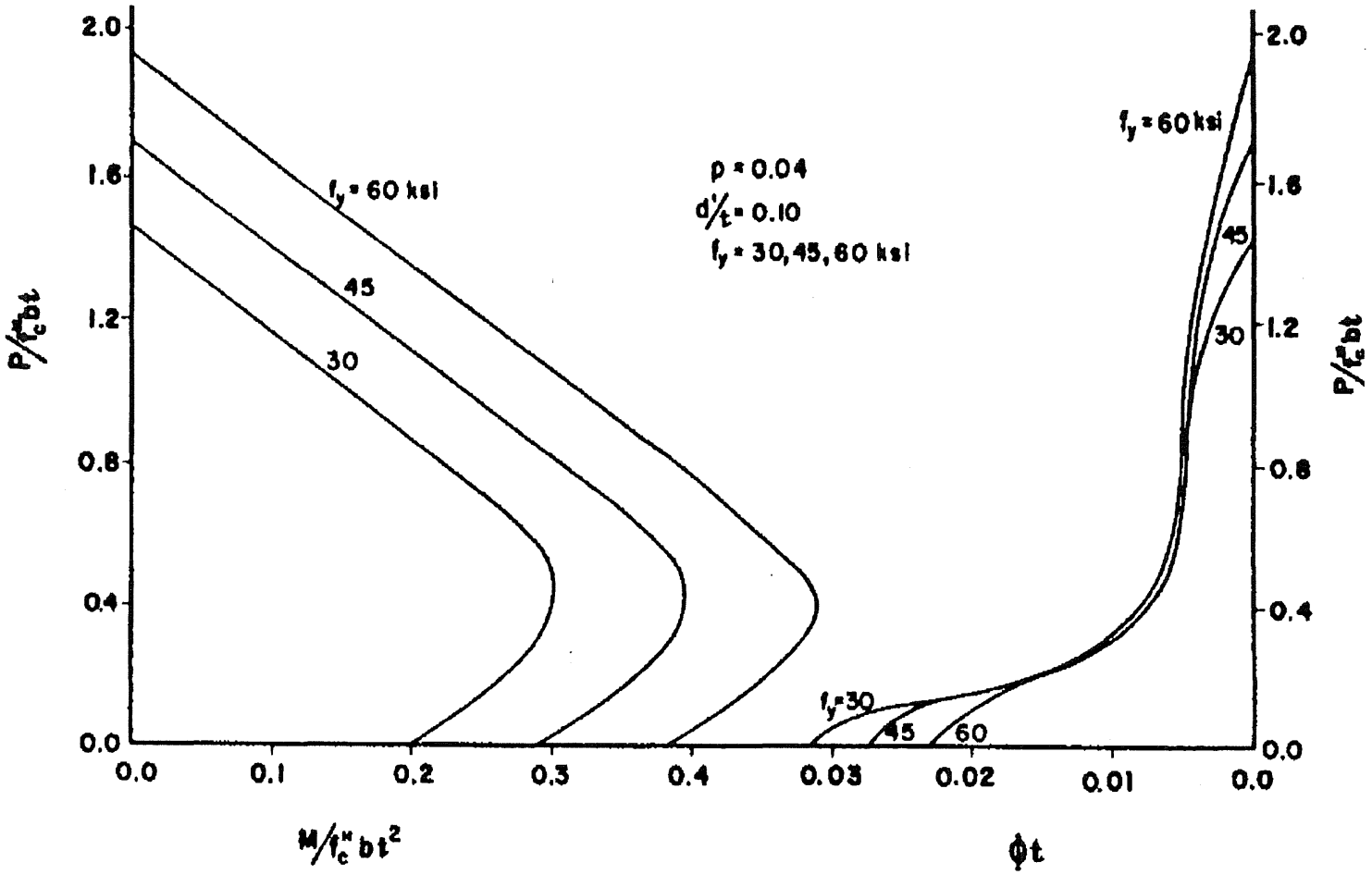

Figure 2.5. Interaction Diagrams for Different Values of Reinforcement Yield Stress (Pfrang et. al., 1964)

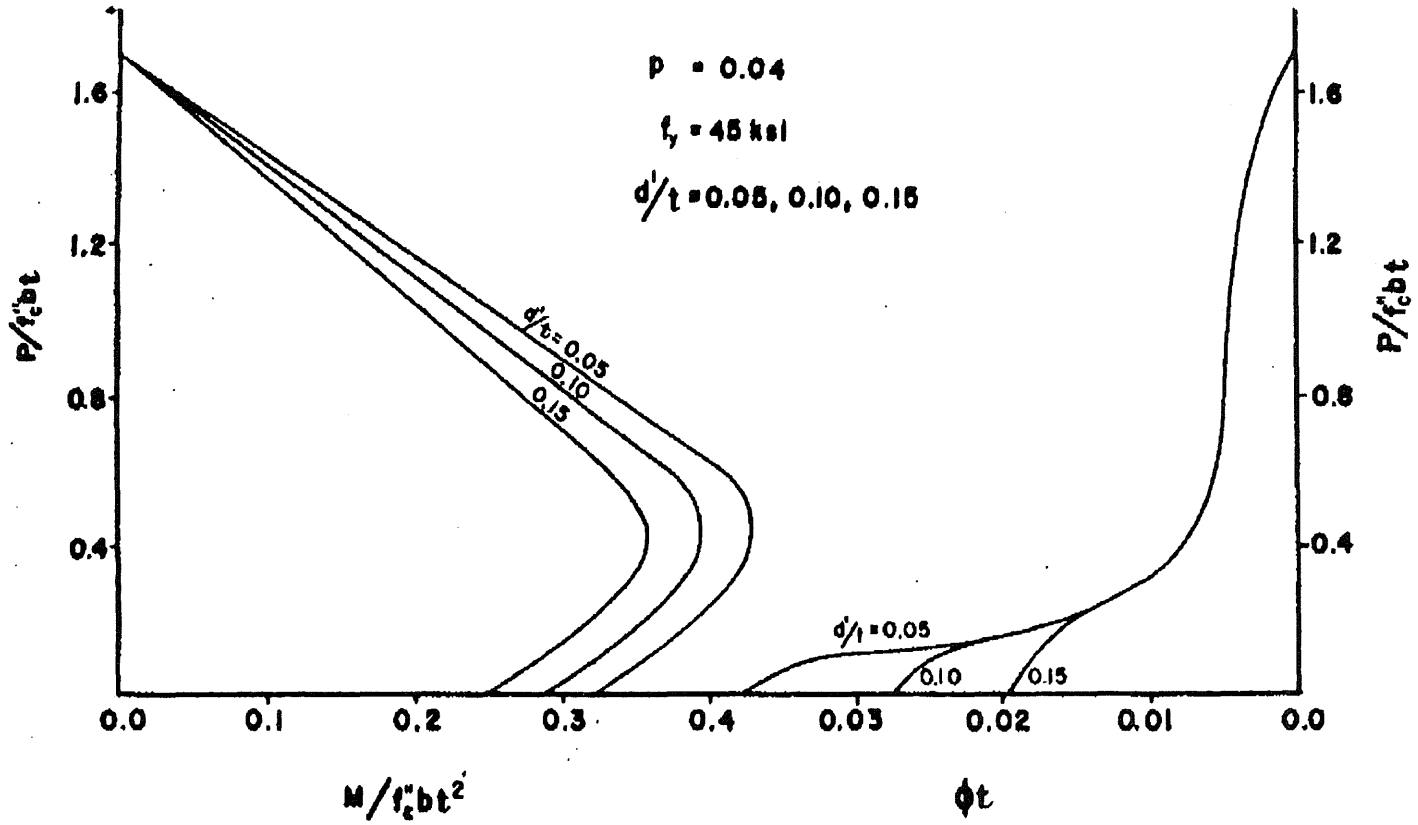

Figure 2.6. Interaction Diagrams for Different Values of d'/t (Pfrang et. al., 1964)

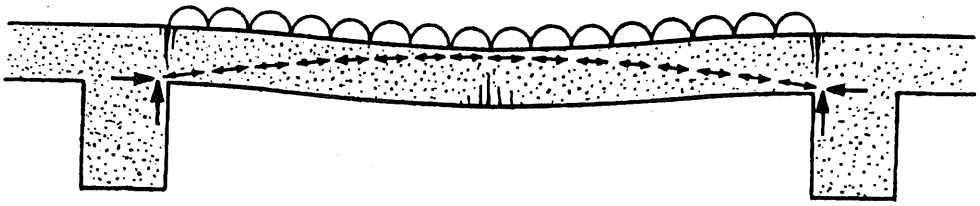

Figure 2.7. Compressive Forces Forming Arching Action (Ockleston, 1958)

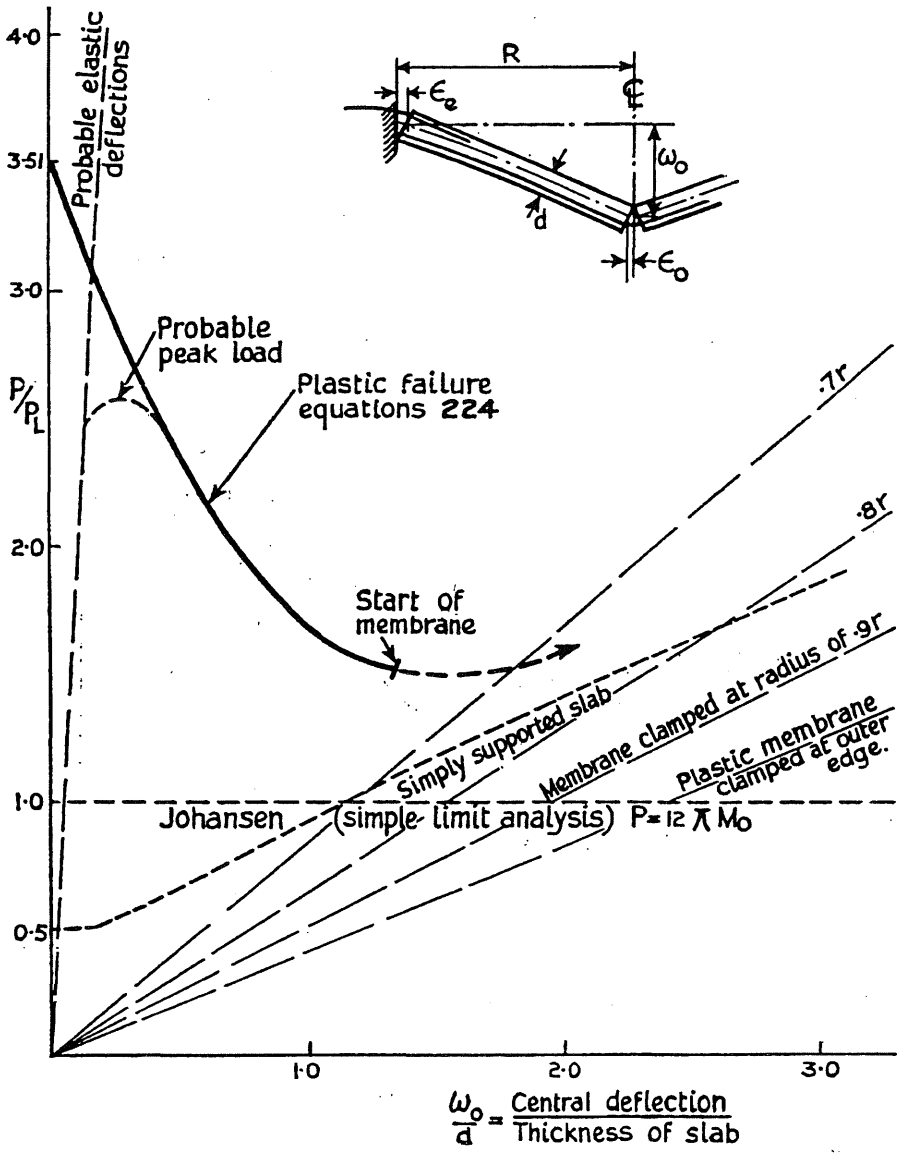

Figure 2.8. Plastic Collapse and Instability of a Clamped Circular Slab (Wood, 1961)

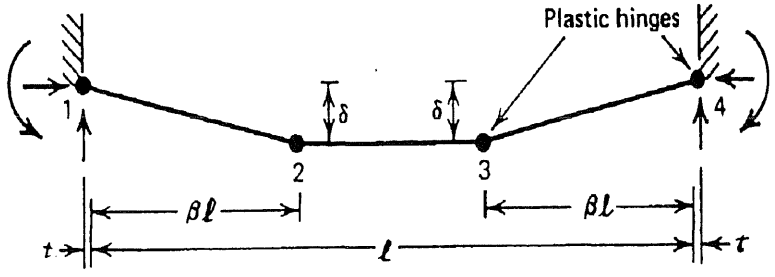

Figure 2.9. Plastic Hinges of Restrained Strip (Park and Gamble, 1980)

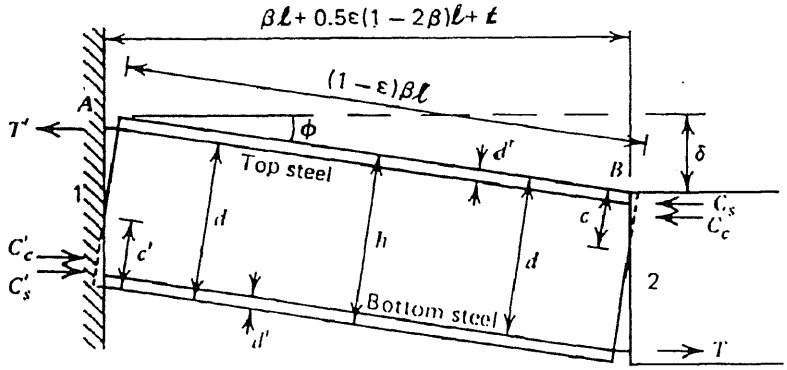

Figure 2.10. Portion of Strip Between Yield Sections 1 and 2 of Figure 2.10 (Park and Gamble, 1980)

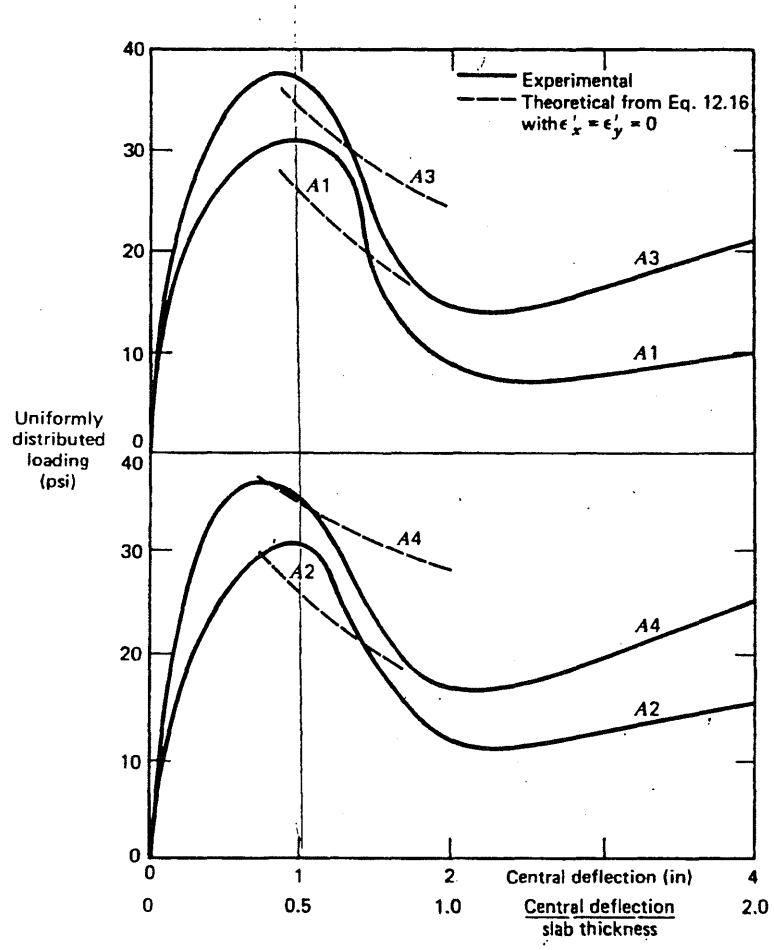

Figure 2.11. Load-Central Deflection Curves for Slabs With All Edges Restrained (Park and Gamble, 1980)

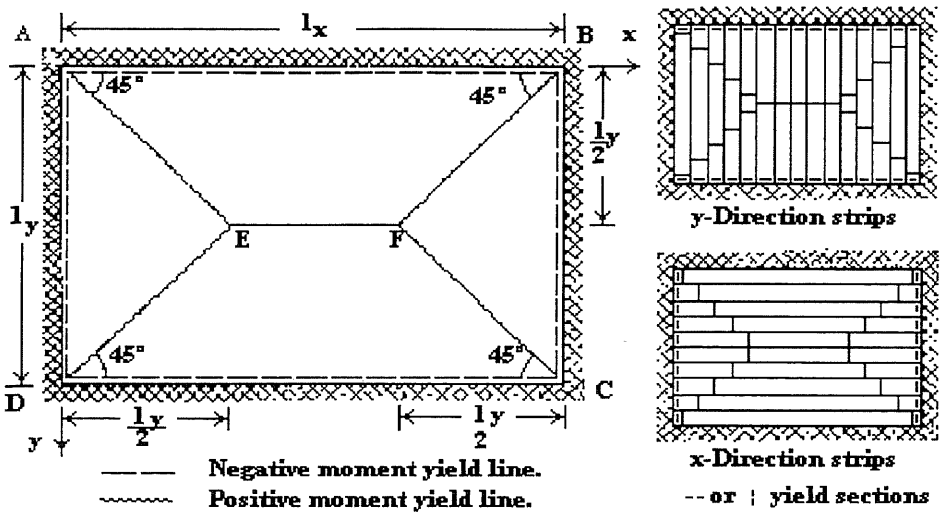

Figure 2.12. Assumed Yield Line Pattern for Uniformly Loaded Slab With Restrained Edges (Park and Gamble, 1980)

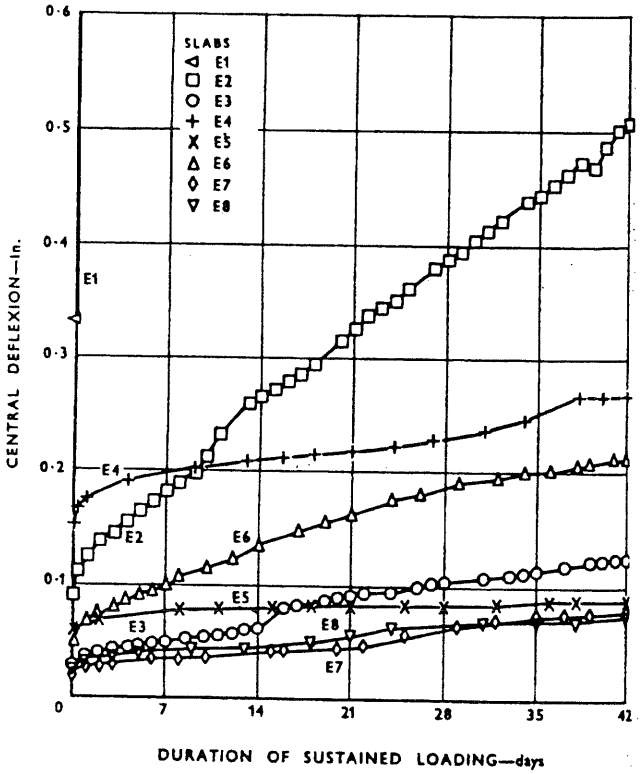

Figure 2.13. Central Deflection of Slabs During Periods of Sustained Loading (Park, September 1964)

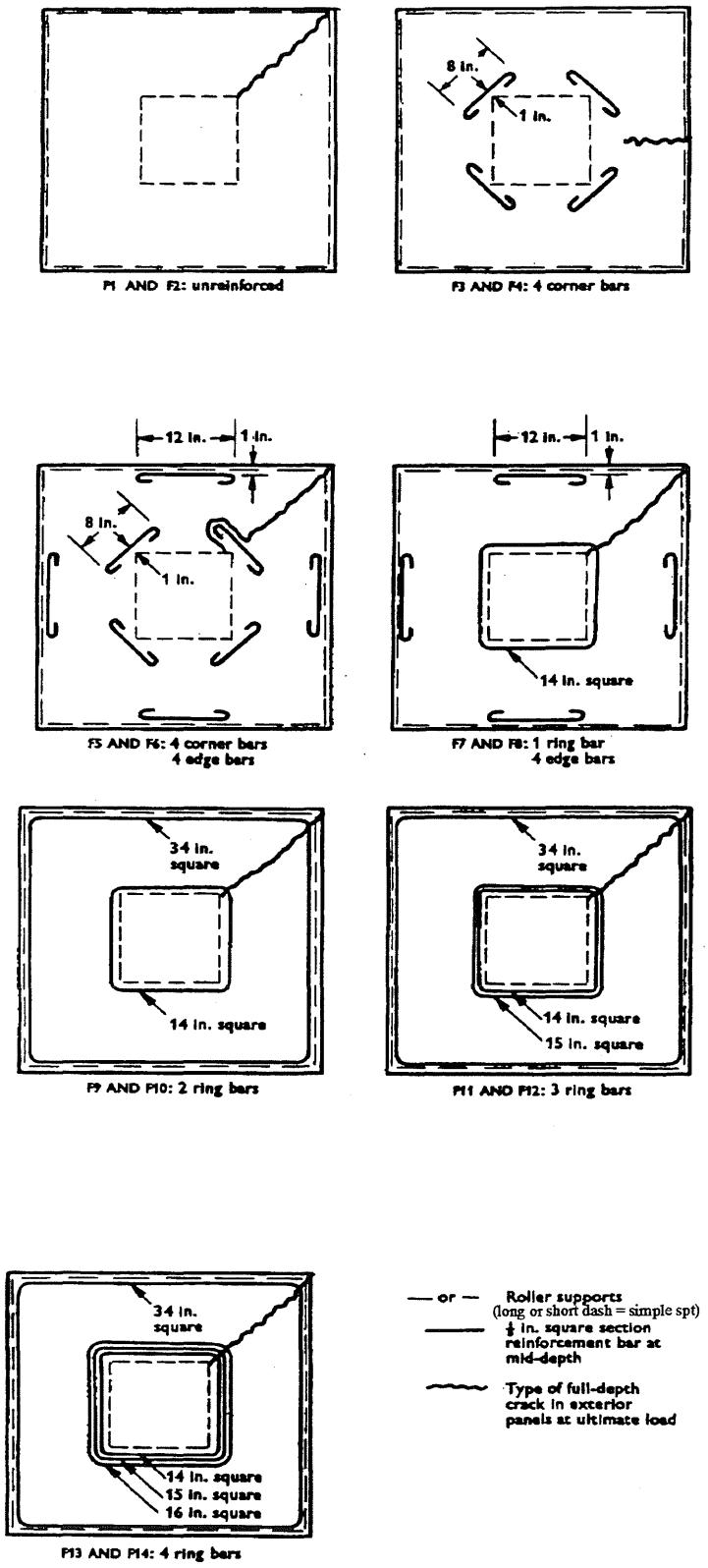

Figure 2.14. Positions of Reinforcement, Support Rollers and Full-Depth Cracks in Exterior Panels at Failure (Park, 1965)

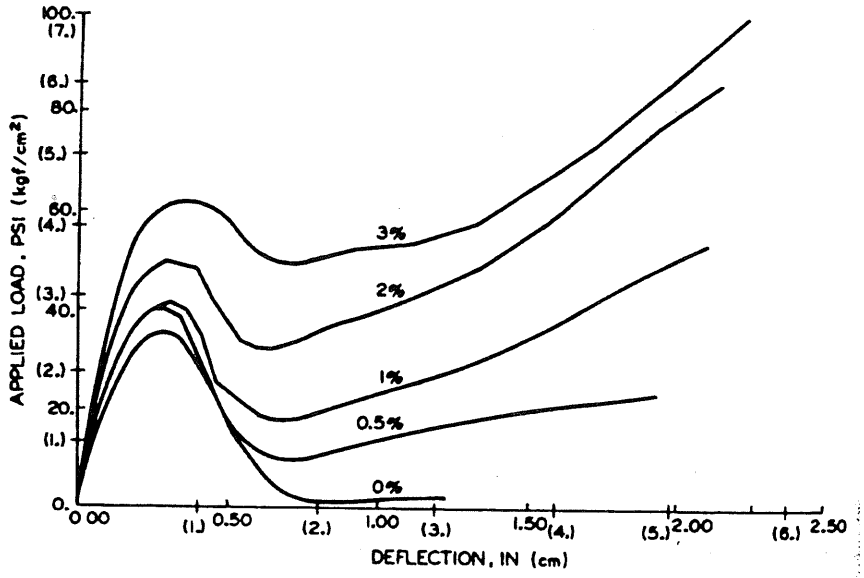

Figure 2.15. Load-Deflection Relation for Restrained Slabs (Restraint at Level of Bottom Steel) With Various Reinforcement Ratios and With Span-Depth Ratio of 20 (Brochie and Holley, 1971)

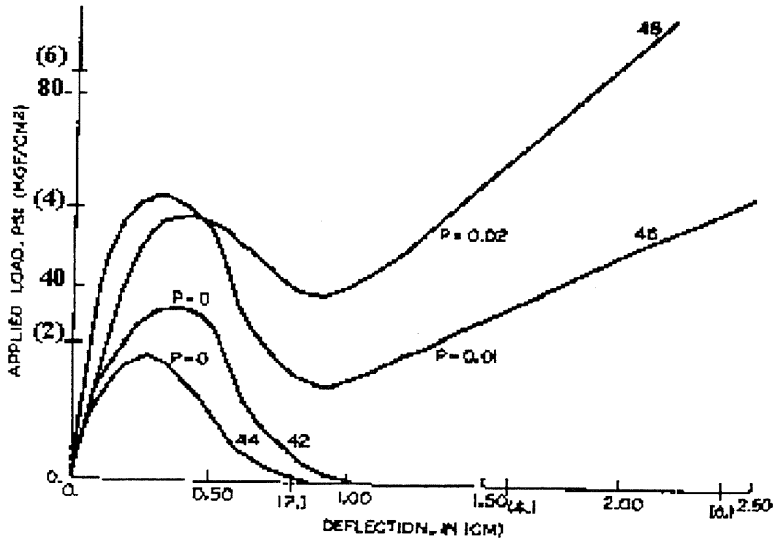

Figure 2.16. Load-Deflection Relation for Restrained Slabs (Fully Clamped) With Various Reinforcement Ratios and Span-Depth Ratio of 20 (Brochie and Holley, 1971)

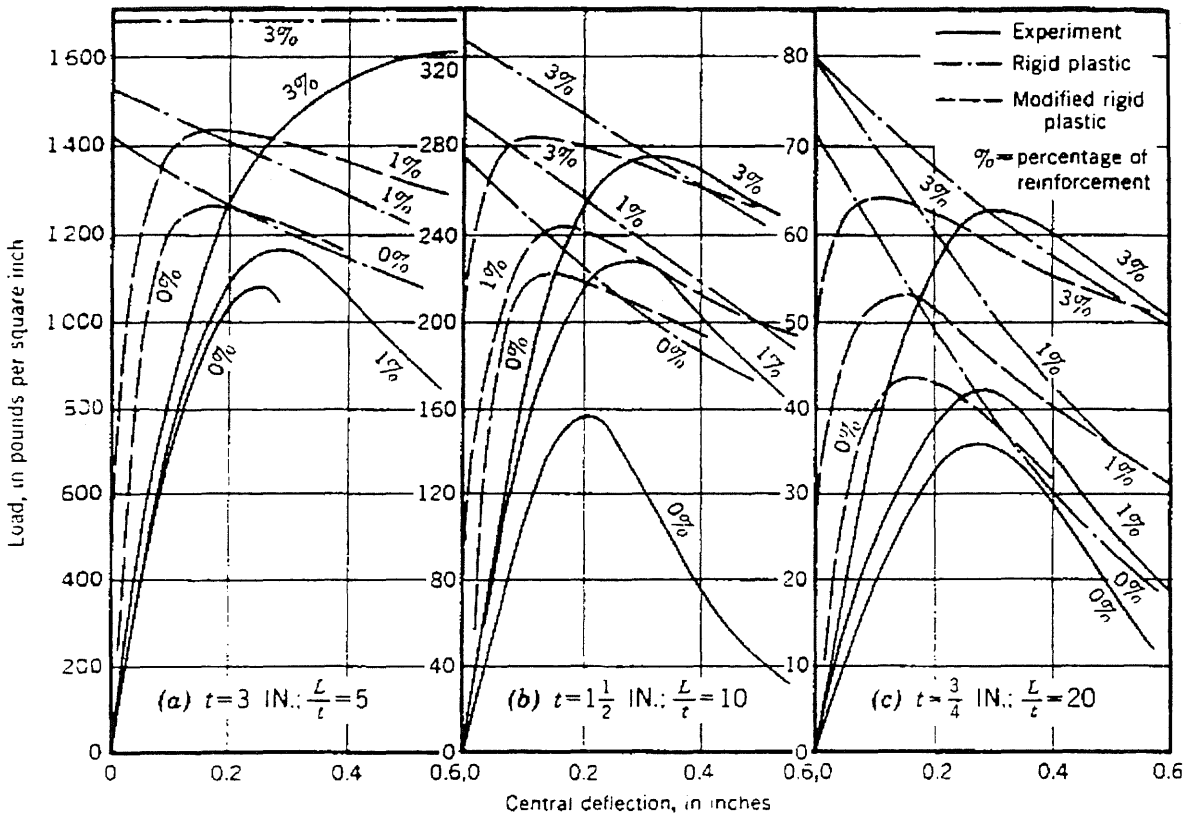

Figure 2.17. Rigid-Plastic Solutions: Comparison with MIT Tests (Jacobson, 1967)

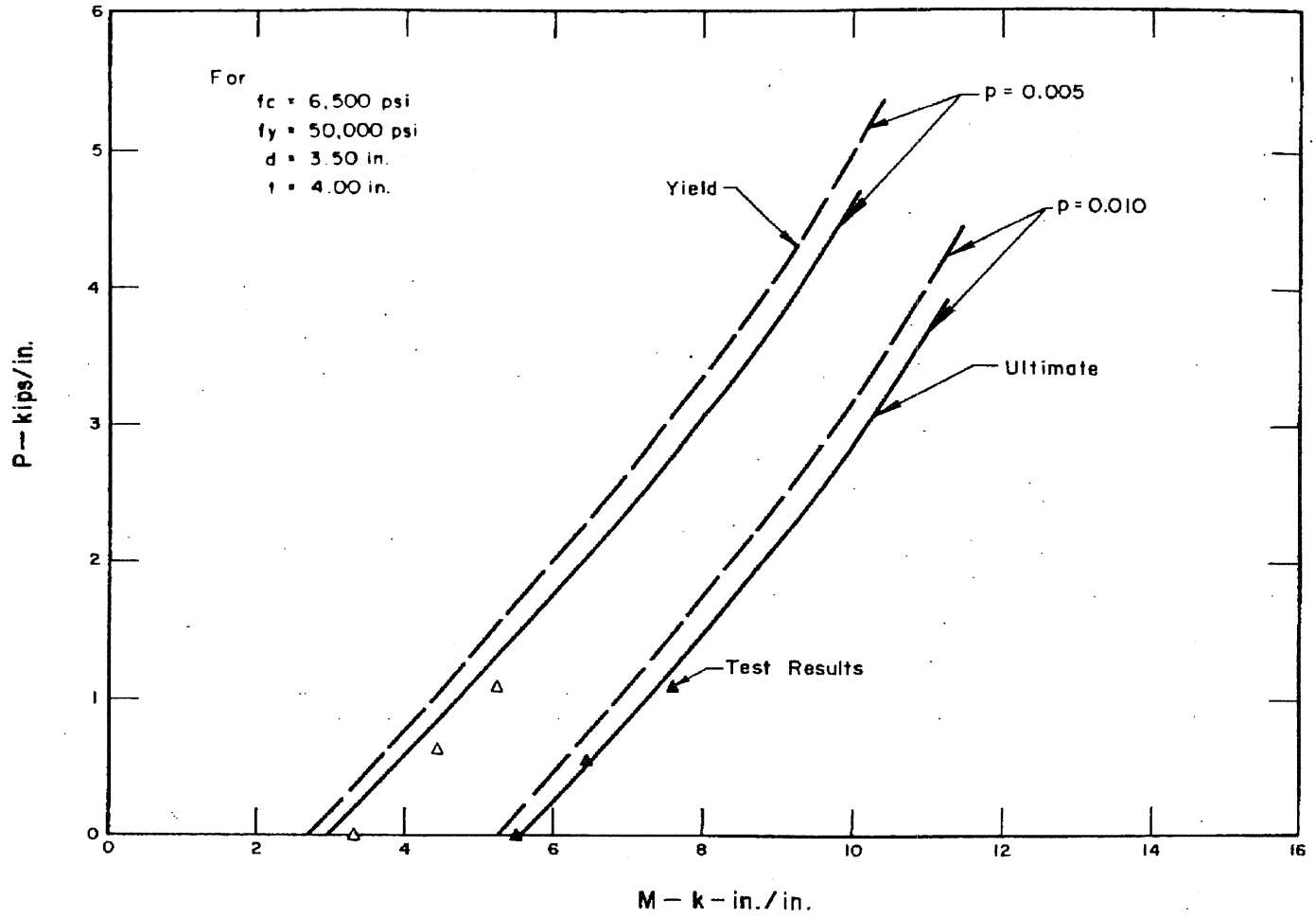

Figure 2.18. Partial Moment-Thrust Interaction Diagram (Gamble et. al., 1970)

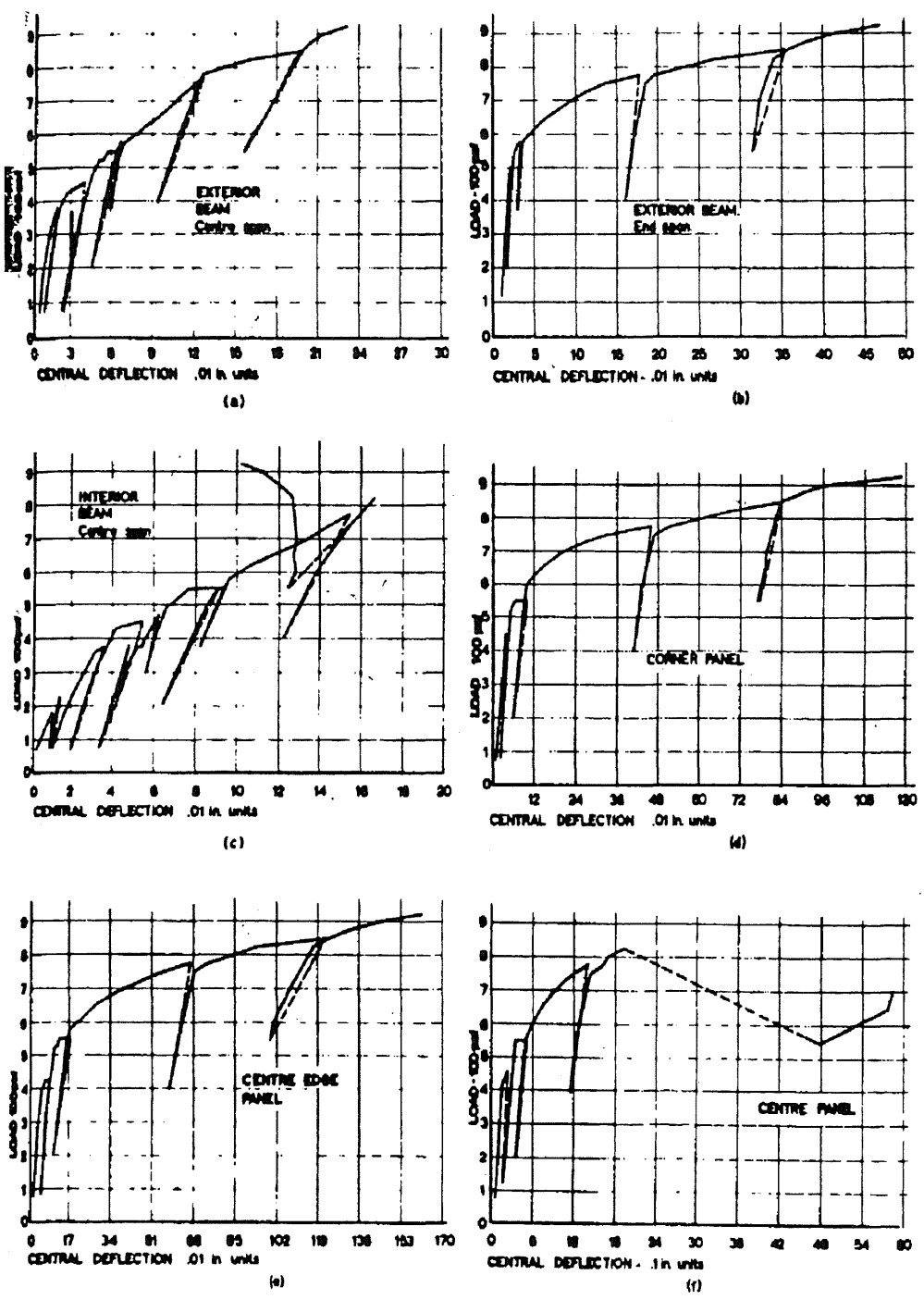

Figure 2.19. Load-Deflection Relationships (Hopkins and Park, 1971)

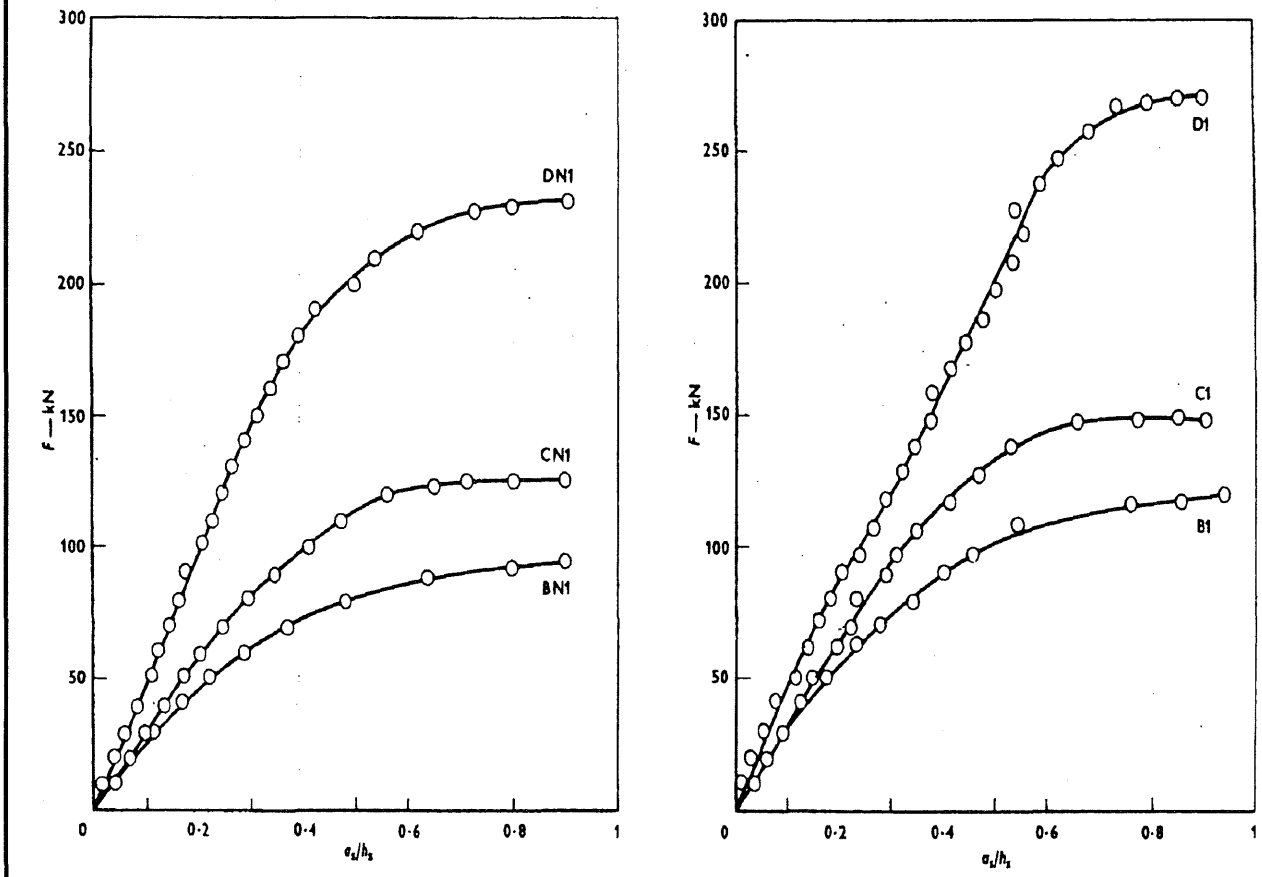

(a) Models BN1, CN1 and DN1

(b) Models B1, C1 and D1

Figure 2.20. Load-Deflection Curves From Experiments on Slab-Beam Panels (Datta and Ramesh, 1975)

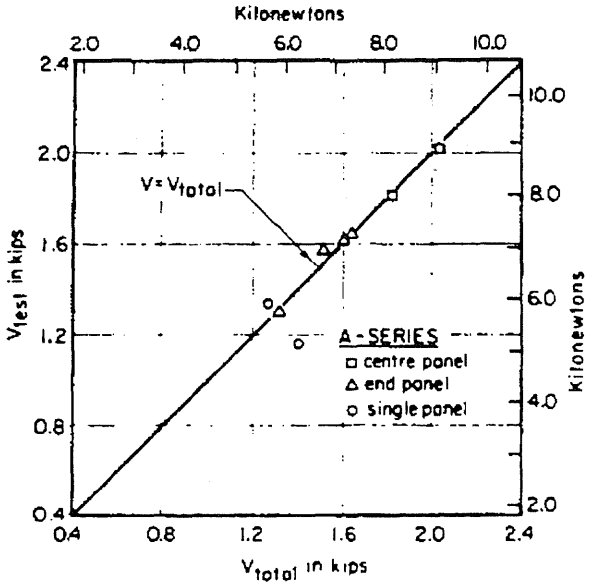

Figure 2.21. V_{test} Versus V_{total} for A-Series - Proposed Method (Batchelor and Tissington, 1976)

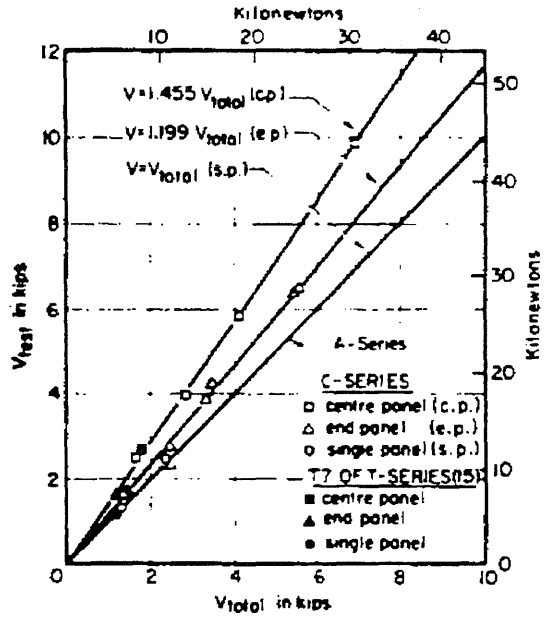

Figure 2.22. V_{test} Versus V_{total} for C-Series - Proposed Method (Batchelor and Tissington, 1976)

a.

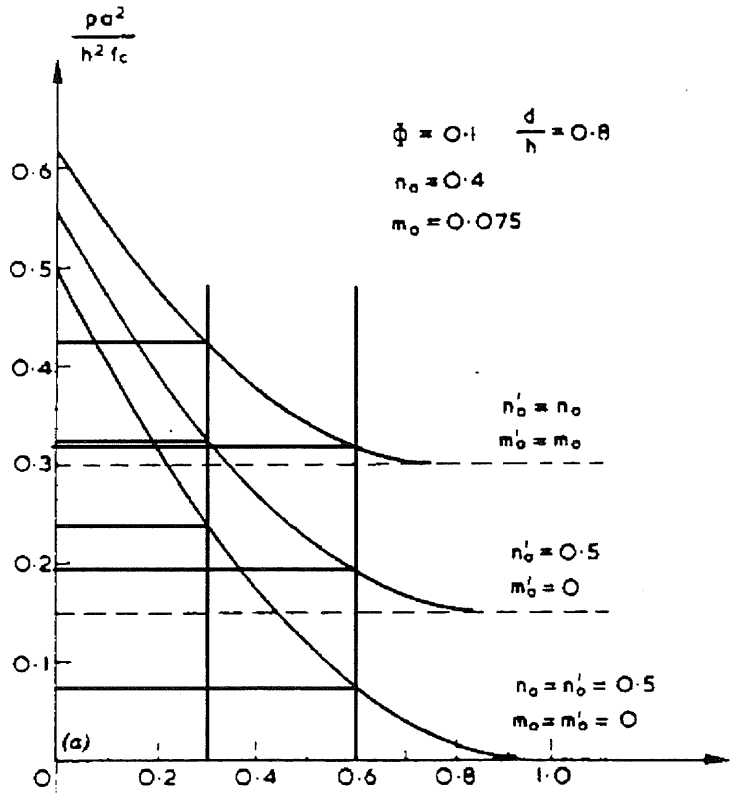

b.

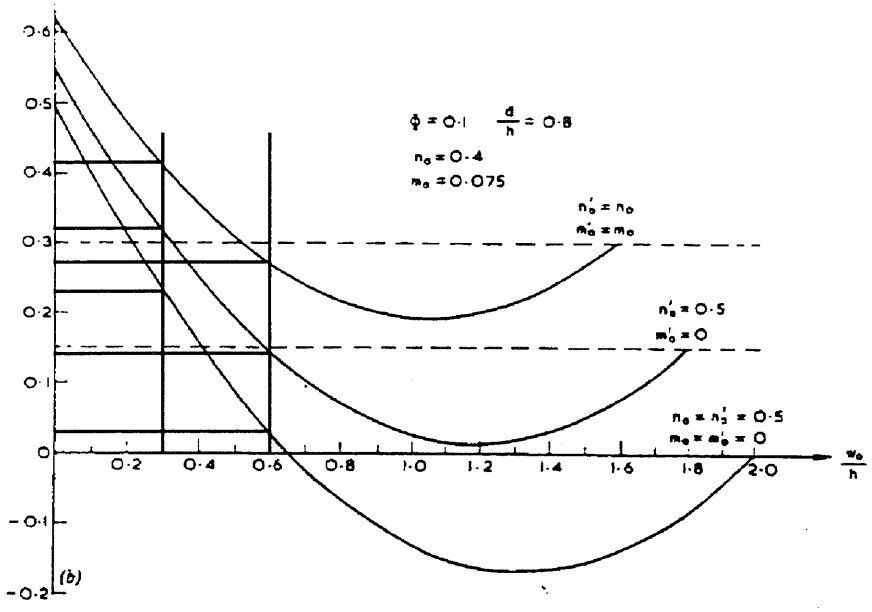

Figure 2.23. Rigid-Plastic Load-Deflection Curves for Slab Strips: a) Flow Theory; and b) Deformation Theory (Braestrup, 1980)

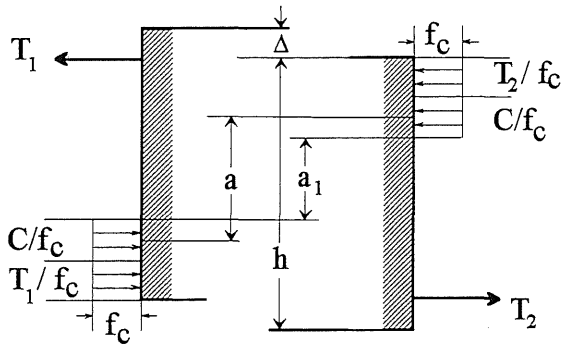

Figure 2.24. Horizontal Forces at Support (1) and at Midspan (2) (Christiansen, 1963)

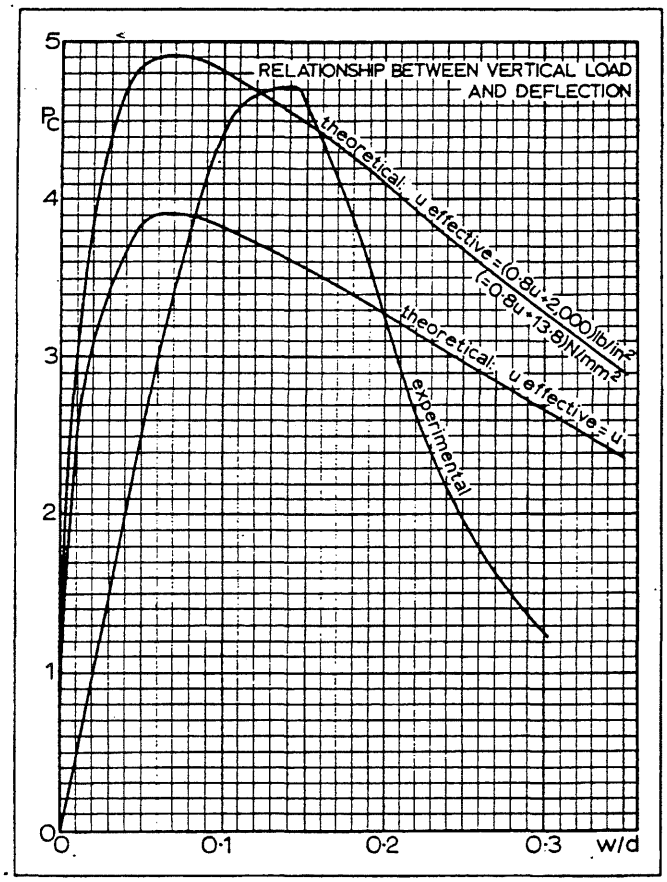

Figure 2.25. Theoretical and Experimental Relationship Between P_C and w:d - Beam RB18 (Roberts, 1969)

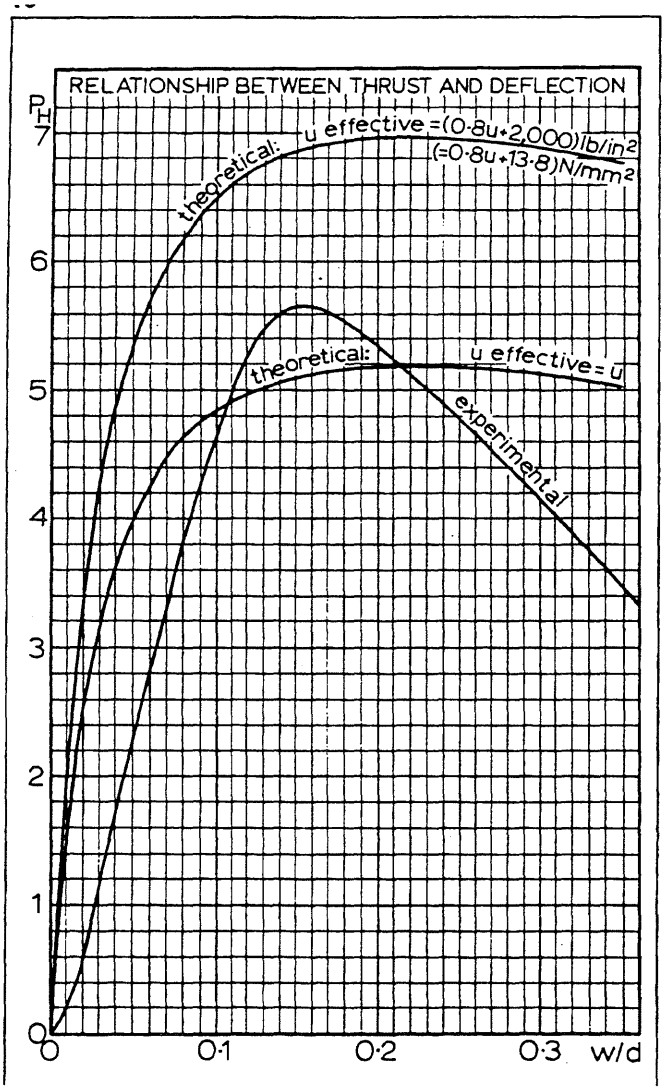

Figure 2.26. Theoretical and Experimental Relationship Between P_H and w:d - Beam RB18 (Roberts, 1969)

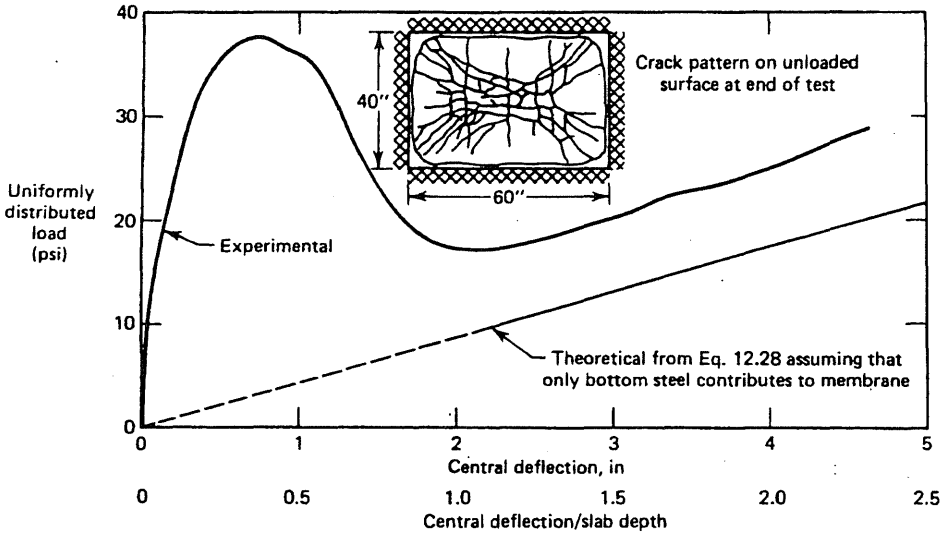

Figure 2.27. Load-Deflection Curves and Cracking for Slab A4 (Park, March 1964)

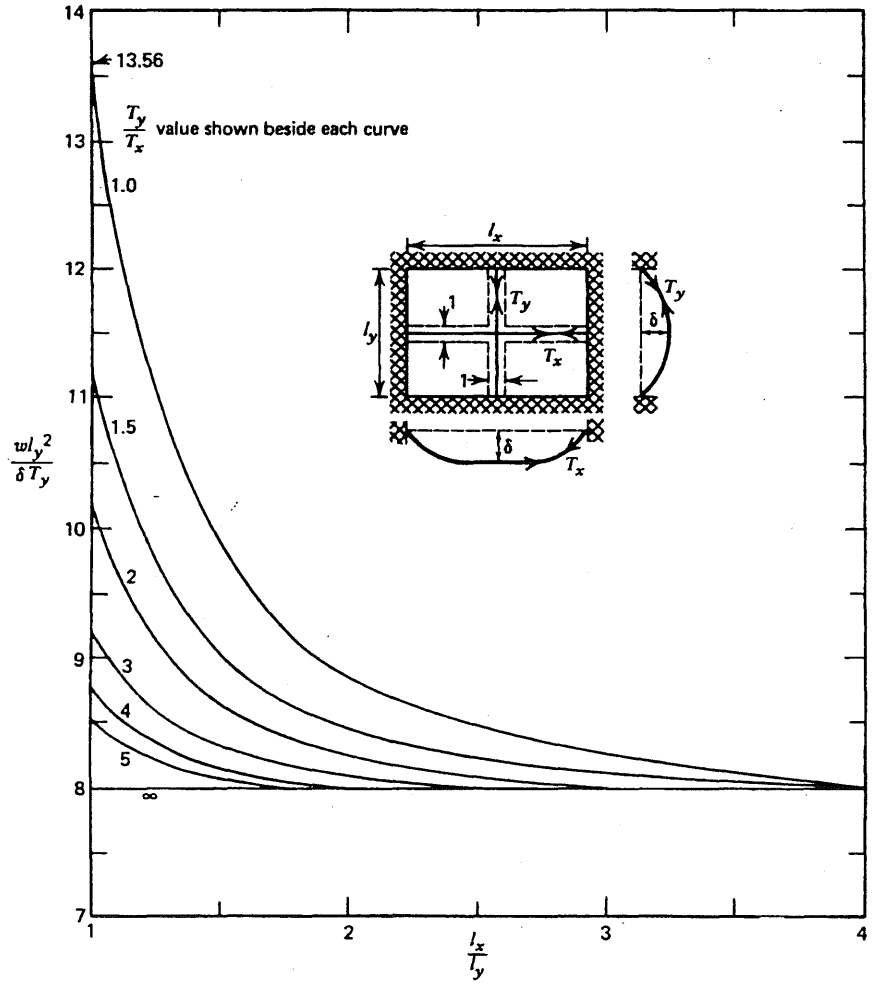

Figure 2.28. Load-Central Deflection Relationships for Uniformly Loaded Rectangular Plastic Tensile Membranes (Park, March 1964)

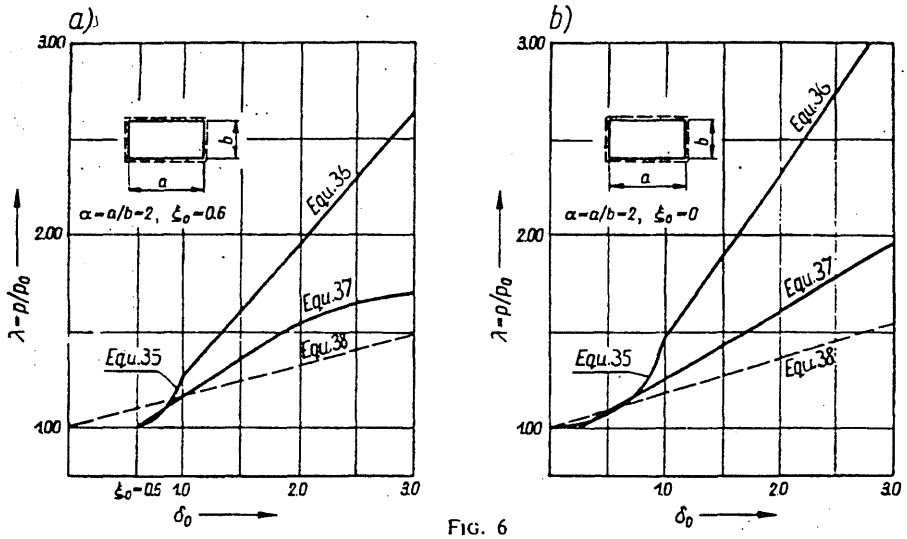

FIG. 6

Figure 2.29. Tensile Membrane Load-Deflection for Varying Neutral Axis Depth (Sawczuk and Winnicki, 1965)

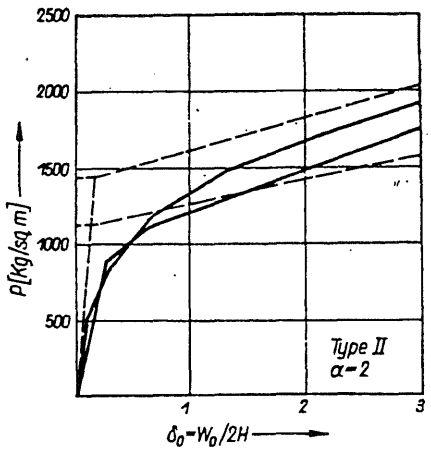

Figure 2.30. Tensile Membrane Load-Deflection (Sawczuk and Winnicki, 1965)

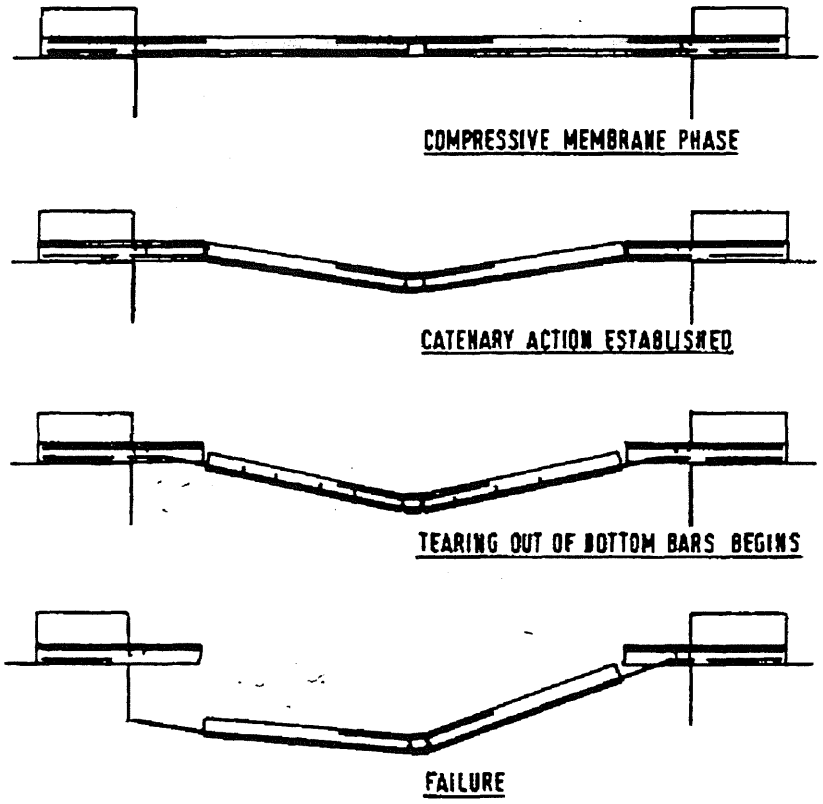

Figure 2.31. Stages of Behavior in PCL Catenary Tests (Regan, 1975)

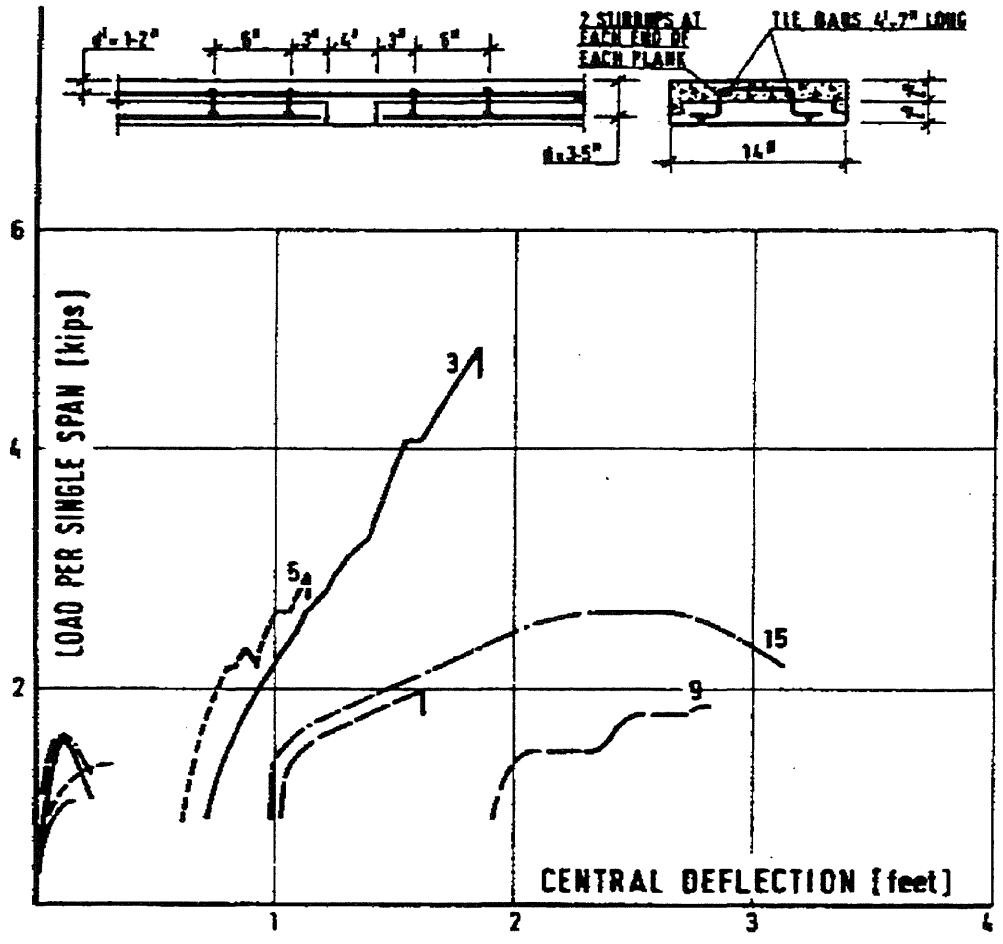

SPEC.	MAIN STEEL	TIE STEEL
3	2 No. 0.31" def.	2 No. 0.31" def.
5	2 No. 0.31" def.	2 No. 0.31" def.
9	2 No. 0.31" def.	2 No. 0.24" plain
15	2 No. 0.16" plain *	2 No. 0.31" def.

* prestressed

Figure 2.32. Load-Deflection Curves From PCL Catenary Tests, Type I Specimens (Regan, 1975)

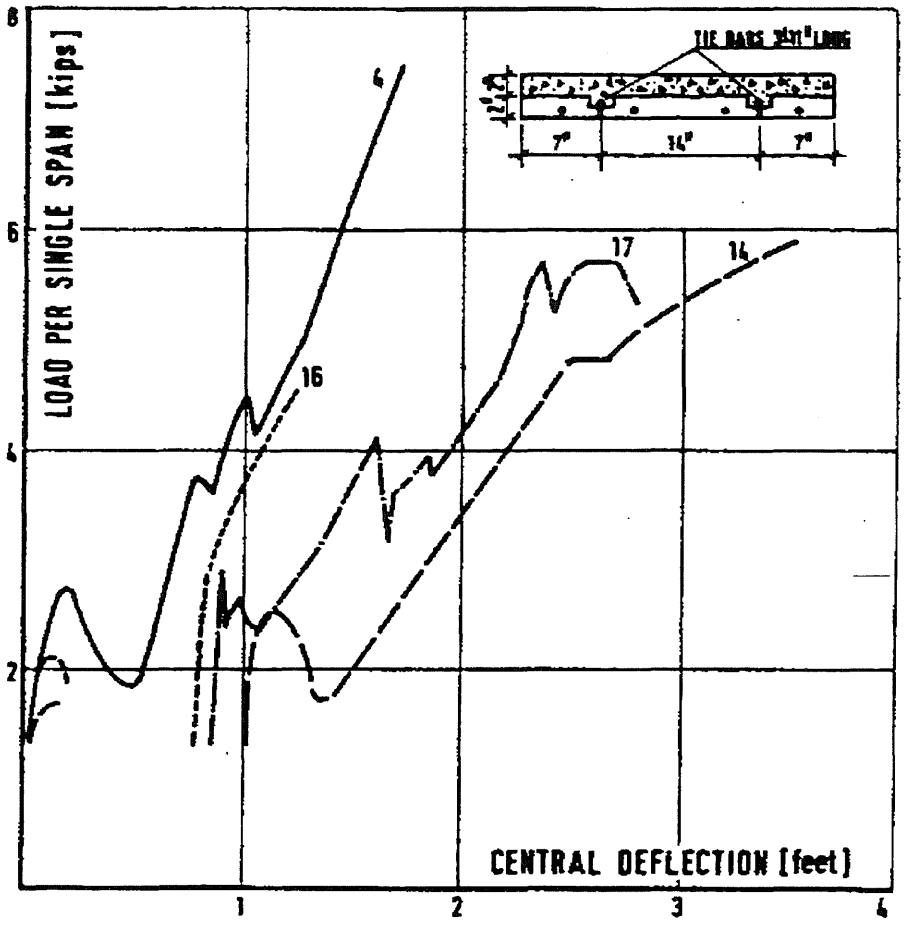

SPEC.	MAIN STEEL	TIE STEEL
4	4 No. 0.31" def.	2 No. 0.47" def.
14	4 No. 0.31" def	2 No. 0.31" plain
16	4 No. 0.31" def	2 No. 0.31" def
17	4 No. 0.16" plain *	2 No. 0.31" plain

* prestressed

Figure 2.33. Load-Deflection Curves From PCL Catenary Tests, Type II Specimens (Regan, 1975)

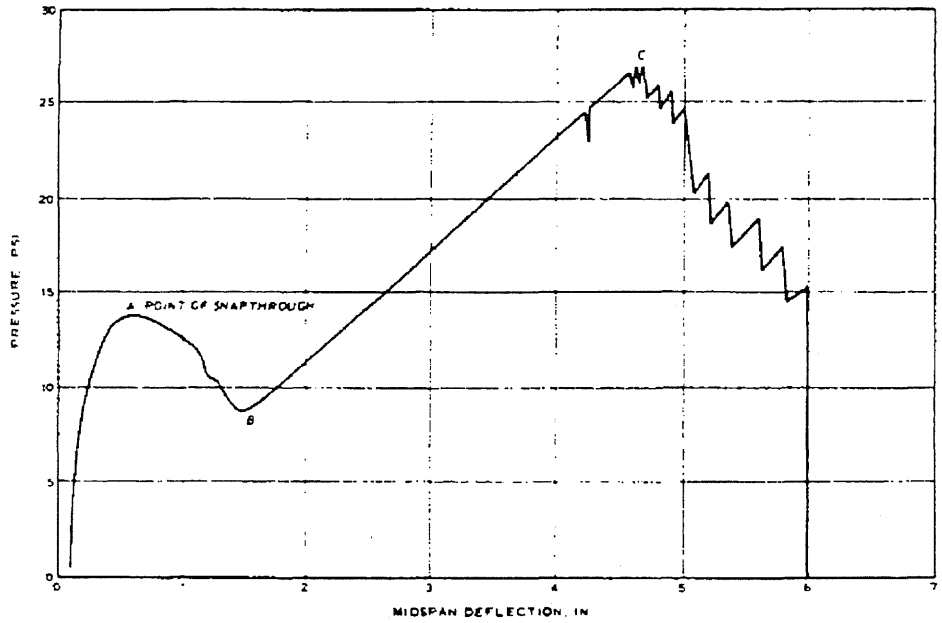

Figure 2.34. Pressure-Midspan Deflection Curve, Static Slab S3 (Black, 1975)

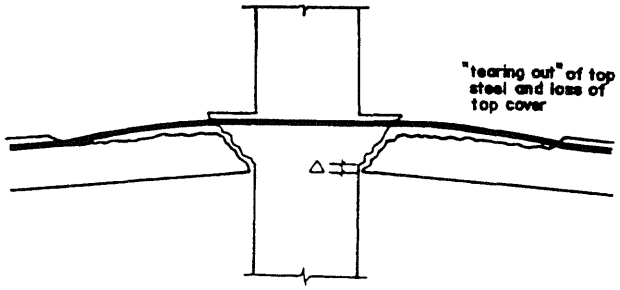

(a) WITHOUT CONTINUOUS BOTTOM BARS

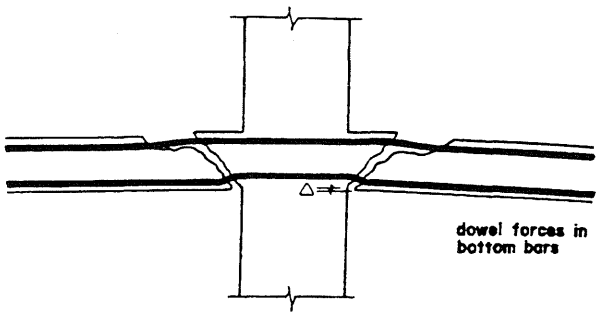

(b) WITH CONTINUOUS BOTTOM BARS

Figure 2.35. Geometry of Deformation After a Punching Shear Failure in a Slab (Hawkins and Mitchell, 1979)

CHAPTER 3

FINITE ELEMENT ANALYSIS

3.1. Introduction

The experimental results for the 115 laterally restrained reinforced concrete one-way slabs presented in Appendix A (Table 3.1) provides invaluable information on slab behavior. However, there is little consistency between the researchers on the type and quality of data collected since each researcher had different experimental objectives. The varied experimental data usually consisted of some of the following: the peak compressive membrane load capacity, the associated midspan deflection, the plastic hinge rotation, the support rotation, the thrust, the slab damage resulting from concrete cracking and crushing, the tensile membrane capacity, and the occasional stress and strain reading when concrete cracking or crushing did not prematurely damage the gages before reaching the peak load capacity.

Of course, instrumentation failure affected data collection and accuracy. For example, if key instrumentation failed (i.e., the midspan deflection gage), one researcher would stop the test, fix the gage, and reload the structure, while another would provide measurements based on the final unloaded permanent conditions. These final measurements are not entirely accurate representations, but they do provide some insight into the slab's behavior (i.e., the associated peak capacity deformations depending on when the gage failed and the test was terminated). Additionally, the support structure and/or the rubber membrane providing a water tight seal for the preferred hydrostatic loading method (Figure A.18) usually blocked any visual observation of the concrete cracking and crushing. Most observation of cracks and plastic hinge zones occurred after completion of the test and unloading of the structure.

As a result of the foregoing observations and the simple fact that none of the previous researchers discussed finite element analysis results, the author investigated the use of modern analysis techniques in an attempt to match the experimental data and to evaluate the behavior of laterally restrained reinforced concrete one-way slabs during gradual loading, especially near the

supports. A static finite element (FE) analysis was conducted only on a representative number of the slabs listed in Appendix A (bold and italicized in Table 3.2) because of the early termination of the analysis before a defined peak load capacity for thick slabs, $L/h < 18$. The excessive cracking/crushing of the concrete during compressive membrane resistance normally damaged the finite elements at or near the supports to the point that the elements could no longer mathematically converge to an equilibrium solution during successive load increments.

Additionally, the modeling of the experimental constraints as fixed-supported boundary conditions produced acceptable peak capacity results in thin slabs, but for thick slabs where the analysis terminated before denoting a peak capacity, the final load capacity was much larger than the experimentally measured peak load capacity. This result led to an unsuccessful attempt to decrease the support rigidity through the use of lateral and rotational springs. The additional instability of the springs coupled with the instability of the cracking concrete resulted in even earlier termination of the analysis.

Even though the FE analysis capability was less than desired (i.e., hoped for observation of the complete load-deflection behavior through FE analysis), the available FE analysis of the pre-peak behavior of thick slabs and the small amount of post-peak behavior for thin slabs provided invaluable insight to the slab's behavior at peak capacity. The useful observations were:

- The less sensitive the individual element, the better the performance when the elements became severely damaged near the peak load capacity. For the analyzed one-way slabs, beam elements provided further analysis along the load-deflection curve than continuum elements. Continuum elements also require a very fine mesh in order to provide concrete stress and strain values near the surface of the compressive face.
- When a defined peak load capacity occurred in finite element analysis, the thrust peaked nearly simultaneously.
- The peak load capacity and midspan deflection for thin slabs using beam elements were very close to the experimentally measured data, but the analysis did not proceed far into post-peak behavior.

- The concrete compressive strain at peak load capacity exceeded the ACI maximum recommended value of 0.003 in/in (i.e., 0.005 to 0.007 in/in).
- The experimental reaction structures did not provide fixed-supported edge conditions.

The limited success using finite element analysis to predict the peak load capacity, not to mention the need for the entire load-deflection curve, refocused the study on the use of analytical methods to match empirical data. Analytical methods are needed to predict all of the behavior for thick slabs (L/h < 18), and at least the post-peak behavior for thin slabs (L/h > 18).

Before discussing in detail the results of the finite element analysis, it should be pointed out that there is a short discussion of the detailed development of the required input parameters in Appendix B and an evaluation of the ABAQUS finite element package in Appendix C. As with any experiment, the material properties (concrete and steel), the construction details (L, ρ, ρ ', h, f'_c, f_y, d, d', one-way slab, etc.), the testing apparatus (finite elements analysis), the loading technique (statically applied uniform loading), the boundary conditions (simply-supported, lateral and rotational springs, and fully-fixed), the instrumentation (node/elements of interest), and the testing procedures (data collection and experiment termination) must be reviewed and verified.

3.1.1. Input Parameters

Before any accurate analysis is possible, sound input data are required (Appendix B). Since most analysis techniques ignore strain hardening and this research is focused on compressive membrane behavior which usually occurs prior to significant strain hardening, the Modulus of Elasticity and yield strength are the only input parameters required for the reinforcement to represent a perfectly plastic stress-strain curve. This also means that the concrete will control the analysis since the rebar will never actually rupture in ABAQUS, but just continue to yield.

Concrete, on the other hand, has numerous input requirements with each being a function of the concrete compressive strength. With the early anticipation of extending this research to include high strength concrete, concrete input parameters were determined for concrete compressive strengths ranging from 3000 to 20,000 psi. This large range of concrete compressive

strengths greatly affects not only the shape of the uniaxial compressive stress-strain curve, but also the tensile capacity and the biaxial stress-strain relationship.

The uniaxial compressive concrete stress-strain curve has a longer linear ascending curve and a steeper descending curve as the concrete compressive strength increases. The descending curve normally is complete and becomes relatively horizontal by a strain of 0.0038 to 0.004 in/in with an associated stress of approximately 100 to 300 psi which is a function of the testing apparatus. However, high strength concrete can fail in a brittle mode after passing the peak and descending only partially down the descending portion of the curve. Examples of generated curves and ABAQUS input parameters are presented in Appendix B (Figures B.12 and B.13 and Table B.2).

Young's Modulus (E_c) increases at a decreasing rate as the concrete compressive strength increases. The ACI 363-92 Committee Report provides a representative curve up to 12,000 psi, while Kakizaki (1992) provides a curve from 12,000 to 20,000 psi. Unfortunately these two curves do not meet at 12,000 psi. So a gradual transition was developed between the two curves from 10,000 to 14,000 psi (Table B.1 and Figure B.2). For Poisson's ratio (ν), there are numerous conflicting reports as to the affect of concrete compressive strength. After reviewing the data, a gradually decreasing Poisson's Ratio from 0.22 to 0.15 was used within the analysis for concrete compressive strengths ranging from 3000 to 20,000 psi (Table B.1).

Experimentally, once a crack in the concrete develops, the concrete between cracks will still carry tensile stresses using the rebar as a conduit. Deep cracks beyond the level of the reinforcement force the reinforcement to carry all of the tensile stresses. Until the development of the deep cracks, "Tension Stiffening" in the ABAQUS code allows the concrete between cracks, or planes of damaged elasticity, to transfer tensile stresses. Based on comparisons with actual experiments, a value of 10^{-3} (Appendix B) will represent the total post cracking strain softening across the crack with the concrete providing a gradually decreasing load transfer through the rebar.

"Shear Retention" in the ABAQUS code is the shear load transfer across cracks. Using the discussions on the crack width that supports aggregate interlock for shear transfer, a total strain

value of 0.0083 across a crack after the formation of the crack marks the point of zero shear transfer at that point (Appendix B).

The four "Failure Ratios" in the ABAQUS code assist in defining the biaxial failure surface for concrete. The first failure ratio is the ultimate biaxial compressive stress to the uniaxial compressive stress. The reported ratios were from 1.16 to 1.27 depending on if the conditions were equal biaxial compressive stresses or high strength concrete, since the biaxial strength decreases as the compressive strength increases. Because the one-way slab experiments rarely develop equal biaxial conditions at even the supports, a gradually decreasing ratio will be used: 1.27 at 3000 psi to 1.16 at 20,000 psi (Table B.1).

The second failure ratio is the uniaxial tensile stress at failure to the uniaxial compressive stress at failure. The first question to address is whether the tensile capacity is represented by splitting or rupture strength since the tension zones are controlled more by a splitting stress, while the compression zones are controlled more by rupture stress. Additionally, there is variability in the equations predicting tensile strength (i.e., rupture vs. splitting). An actual tensile test could provide an average result for use in ABAQUS. Fortunately, there has been some recent effort to perform actual tensile tests on cylinders. An average of equations established while tensile testing concrete cylinders is used to determine the ratio of the uniaxial tensile stress at failure to the uniaxial compressive stress at failure (Table B.1).

The third failure ratio is the magnitude of the principal component of plastic strain in biaxial compression to the plastic strain at ultimate stress in uniaxial compression. Using the available charts (Figures B.24 - B.25), the ratio could vary anywhere from 1.25 to as high as 1.6, so a consistent, cautious value of 1.33 was used.

The fourth failure ratio is the tensile principal stress at cracking when the other non-zero principal stress component is at ultimate compressive stress versus the cracking stress under uniaxial tension. Since failure during uniaxial compressive testing is most likely the result of tensile cracking due to the tensile strain from Poisson's effect in the unloaded direction, it would take very little tensile stress in the perpendicular direction to cause cracking when the other

principal stress component is approaching peak compressive capacity. Upon comparison of Figures B.24 and B.25, the resulting ratio is between 0.2 and 0.3, so an average value is taken at 0.25.

3.1.2. Model Verification

In order to analyze an actual structure with a finite element package, the analyst must select the proper elements, boundary conditions, loading techniques, material properties, and matrix manipulation techniques to model and analyze the structure. For this dissertation, ABAQUS (Hibbitt, 1996) was chosen for its availability at the National Center for Super-Computing Applications (NCSA) and robustness. Since dynamic analysis techniques generally use statically generated resistance functions and a wealth of experimental results exist for statically loaded laterally restrained reinforced concrete one-way slabs (Appendix A), only static analyses were performed. The following discussion is a summary of the detailed evaluation of ABAQUS in Appendix C (Finite Element Model Verification).

Since the experimental one-way slab behavior is dominated by flexural action, beam (i.e., linear and quadratic) or solid continuum (i.e., 20 node brick) elements were chosen to model the laterally restrained reinforced concrete slabs. Of course the actual behavior of each element is somewhat different. The continuum element better represents the true flexural behavior of a structure, but extreme damage levels prevented convergence due to either divergence of equilibrium, or the time step was not small enough (i.e., $< 10^{-10}$). With the deflections being off an order or more of magnitude, mesh refinement is usually the key. However, refining the mesh or increasing the number of elements along the length or width within the support or midspan areas, which contained the greatest damaged areas, resulted in even earlier termination of the analysis. Smaller continuum elements were completely damaged faster and unable to converge compared to a larger continuum element which still had some undamaged portions at the same point in the analysis. Extreme damage may be preventing the transfer of load from a node to the rest of the structure. When material instability controls the post-peak behavior, the analysis is terminated

before any peak point is clearly established. With geometric instability, some post-peak analysis usually is possible.

The beam elements provided a little less detail and flexibility in use than the continuum elements, but the inherent assumptions of plane sections remain plane, only one element across the width, etc., produced a more stable element capable of proceeding further along the load-deflection curve. If the slab was thin (L/h > 18), the beam element, based on the number of elements used, would carry the analysis into at least the transition zone (Figure 3.1). Too many beam elements, which resulted in a small beam element length, had the same effect as mesh refinement with continuum elements, produced convergence problems and early termination.

Analysis of a 10 in x 10 in x 1 in single element block in pure compression and then in pure tension with or without reinforcement produced acceptable results (Appendix C). Cracking and crushing is represented by a plane of damage to the Modulus of Elasticity (E or E_o) when the stress-strain reaches one of the boundaries established by the biaxial stress-strain curve. In pure compression, the stress-strain at the integration points followed the stress-strain curve provided as part of the input parameters. Cracking was observed as the lateral tensile strains reached the tensile failure strain. The inclusion of rebar provided additional strength and earlier variation in stress-strain values at the integration points after the peak compressive capacity, which represented the variation in material performances. Without the inclusion of "NLGEOM", which prepares ABAQUS to track the highly nonlinear behavior of geometric instability, in the ABAQUS commands, ABAQUS would unload the block or reverse the loading once the element experienced any inelastic strains. Even with NLGEOM, the "STATIC RIKS" method in ABAQUS, which is controlled incremental loading while expecting a decrease in the loading with increased deflections, would change the load path direction and unload the element with the observance of large stress-strain variation at the integration points. Eventually, the quantity and multiple orientation of cracks in the continuum elements produced so much damage that either an extremely small time step (i.e., > 1.0E-15) was required for limited continued analysis, or at that step, the number of attempts at equilibrium was exceeded.

In pure tension, the element would unload while continuing to strain once the ratio between the tensile stress to compressive stress was reached. Rebar inclusion arrested or caught the capacity decrease after the concrete cracked, and then increased the capacity until the rebar yielded. Ultimate capacity was determined by the reinforcement yield strength.

The steel reinforcement was modeled through smearing of the rebar as a layer within the concrete elements. The smearing of the rebar proved just as reliable as discretely modeling the rebar as truss bars connected to the nodes, and produced a simpler model. The boundary conditions were idealized as either fixed-supported or partially fixed-supported with lateral and rotational springs. The STATIC RIKS loading method with a distributed load allowed for a gradual uniform loading of the slab very similar to the hydrostatic loading performed at WES, which comprises a major portion of the experimental data.

3.2. Finite Element Investigation

Some of the slabs presented in Appendix A (i.e., the 115 one-way laterally restrained reinforced concrete slabs) consisted of identical construction details except for the variation in shear reinforcement (i.e., none, lacing, and stirrups), which had little to no effect on the peak load capacity, since many of the WES experiments focused on tensile membrane behavior. Therefore, the finite element analysis is compared with the averaged results from these groupings of slabs (Table 3.2). Based on the solution convergence issues presented in the previous section, only a few of the different L/h's and reinforcement ratio combinations were analyzed at this time with finite elements (bold and italicized in Table 3.2). Each slab group was analyzed with fixed-supports using both beam and continuum elements in order to develop additional behavioral information (i.e., stresses, strains, cracking. yielding, etc.) and to compare the findings with experimental and compressive membrane theory analytical models. Thick slabs were analyzed also with partially fixed-supports (i.e., springs) in an effort to more closely match the experimental results. Additionally, each slab group was analyzed with simple-supports to provide a check with the most

reliable analytical equations to validate FE performance against the changing concrete strengths and reinforcement ratios.

Before discussing the results in detail, the terminology within the Tables should be explained. Looking at Table 3.3, the table was separated into two parts - Part One, the average of simply-supported results for a number of different elements along the half-length, and Part Two, the fixed-supported results. From left to right each column represented the following items:

- the number of elements along the half-length (# elem)
- the time step increment at which it was chosen to record data (Inc)
- the peak compressive longitudinal stress (σ_{11}) and location - support (s) or midspan (m)
- the peak compressive longitudinal strain (ε_{11}) and location
- the associated peak inelastic longitudinal strain ($I\varepsilon_{11}$)
- the peak rebar longitudinal tensile stress (σ_{11}) - at the support and then at midspan once the rebar at the support has yielded unless noted otherwise with either an s or m
- the applied uniform load (Load)
- the midspan peak deflection (Δ_{mid})
- the generated total thrust at the support (Thrust)
- the remarks to point out initiation of cracking, yielding, peak capacity and peak thrust

The recorded points of interest were crack initiation at the supports or midspan, rebar yielding at the supports or midspan, peak compressive concrete strength at the support or midspan, peak capacity, peak thrust, and termination of the analysis. These points usually define the key behavioral changes of a reinforced concrete section during compressive membrane resistance. The number of elements within the half-length varied to investigate the affect of the element aspect ratio on the analysis. As can be seen in Table 3.3, increasing the number of elements decreased the deflection and capacity at the peak point, i.e., more flexibility.

For the thick slabs ($L/h < 18$), lateral and rotational support springs were used in an attempt to decrease the support rigidity since fully fixed-supported conditions greatly over-

estimated the peak compressive membrane capacity. The additional notation in these tables (e.g., Table 3.5) is as follows:

- the load in the rotational spring (σ_{spr})
- the rotation of the rotational spring (ϕ_{spr})
- the load in the longitudinal spring (σ_{spl})
- the extension (or shortening) of the longitudinal spring (ϕ_{spl})
- the resisting moment generated for a rotationally fixed-supported condition to compare with the rotational spring-supported condition
- the resistance (lb/rad or lb/in) of the rotational (R1E8) or longitudinal (L1E7) spring
- the possibility that the longitudinal/rotational direction was fully fixed-supported (L_{full}/R_{full}) with the type of element (i.e., B22 - quadratic beam element; C3D20 - 20 node continuum element; C3D20R - 20 node continuum element with reduced integration) representing the structure if more than one element is presented in the table.

Tables 3.3 through 3.10 contain the results for select thick slabs (L/h < 18) using beam and continuum elements (with or without springs), while Tables 3.11 through 3.15 present the results for select thin slabs (L/h > 18). The experimental peak compressive membrane capacity and deflection are placed in the title of the table to assist in comparisons.

3.2.1. Capacity

Beam elements with fully fixed-supported conditions greatly over-estimated, by 16 to 68 percent, the capacity for the thick slabs (Table 3.3, L/h = 4.4; Table 3.4, L/h = 8; Table 3.7, L/h = 10.4; and Table 3.9, L/h = 14.8), as compared to the experimental data listed in the title of the tables, no matter how many elements were used within the half-length which also was summarized in first half of Table 3.16. More than 15 elements produced too much instability and terminated the analysis well before the peak capacity. Replacing the lateral and rotational support conditions with springs (Table 3.5, L/h = 8; Table 3.8, L/h = 10.4; and Table 3.10, L/h = 14.8) increased the

flexibility which was probably closer to reality and lowered the peak capacity (summarized in Table 3.17). Unfortunately, the increased flexibility produced even earlier instability and termination of the analysis without a defined peak point. Adjustments of the spring strength created a capacity at termination nearly matching the experimental capacity (Table 3.17). However, final compressive stress/strain values were smaller by at least 50 percent than the peak compressive stress/strain for fully fixed-supported conditions (i.e., comparing values in Table 3.16 with Table 3.17). The increase in capacity in the fully fixed-supported analysis from the spring-supported termination stress/strain values was approximately 10 to 20 percent. Decreasing the spring resistance to produce a plausible termination stress/strain that could be extrapolated to the experimental capacity provides little valuable information. Therefore, the additional mathematical instability generated by the springs did not allow the analysis to progress far enough to reap substantial benefits. However, the analysis using springs for support conditions did prove that the laboratory support conditions were not truly fixed-supported.

The use of continuum elements with or without springs never produced a prominent peak compressive membrane capacity (Tables 3.6, L/h = 8; 3.8, L/h = 10.4; and 3.10, L/h = 14.8). The results for continuum elements without springs were similar to those using beam elements except that the stress/strain values were even smaller (i.e., compare Table 3.16 and 3.17 for L/h = 8, 10.4 and 14.8) since the integration points are located farther away from the element edges at the element's quarter or third points for fully or reduced integration schemes, respectively. Overall, the results using continuum elements did not assist in the investigation.

Beam elements without springs produced good results for thin slabs, L/h > 18 (i.e., second half of Table 3.16). The results for Roberts Slabs RB18 and RB11 using continuum elements are also presented in the second half of Table 3-16 to allow comparison with the results from using beam elements. Load capacity was generally comparable, while the discrepancies were noted for stress, strain, deflection and thrust. Generally, 7 to 10 beam elements along the half-length produced comparable peak compressive membrane capacities with the analysis terminated somewhere in the transition zone between the peak capacity and the tensile membrane resistance.

The success in matching the experimental peak compressive membrane capacity in thin slabs was similar to the results in a recent ASCE article by Famiyesin and Hossain (1998) where 3D degenerated shell elements were used to analyze thin two-way slabs. Fortunately, the beam elements also provided somewhat comparable deflection results when using only 3 beam elements in the half-length, while the deflections needed to be increased by 3.32 using the shell elements for two-way slabs. The deflections are discussed further in next section.

Normally the peak capacity occurred after cracking at both the supports and midspan, after yielding of the tension steel at the supports, after reaching the peak compressive capacity of the concrete at the supports (i.e., usually meant that the concrete at the support was into the descending portion of the uniaxial stress-strain curve), and either before, for thick slabs, or right after, for thin slabs, the yielding of the tension steel at midspan and reaching peak compressive capacity of the concrete at midspan. The compressive strain at the supports was approximately 0.005 in/in (Table 3.16) at the peak compressive membrane capacity.

Once the geometric or material instability produced a drop in capacity, the capacity would level off and increase, if the analysis went this far, as the thrust eventually turned into a tensile force. Continued concrete crushing at the supports as the reinforcement pulls down trying to form a steel net or catenary from support to support terminated the analysis before achieving reinforcement rupture strains.

3.2.2. Deflections

The only acceptable deflections occurred during the analysis of thin slabs (L/h >18) using a small number (< 3) of quadratic beam elements along the half length (Tables 3.11 - 3.14). Even the deflection results associated with the best peak capacity estimates were acceptable (i.e., summarized from Tables 3.11 - 3.15 in second half of Table 3.16). Deflection estimates using beam or continuum elements for thick slabs (L/h < 18) were off by at least an order of magnitude. The experimental results were at least 10 to 20 times the finite element deflection results (Tables 3.16, the first half, and 3.17).

All attempts to use continuum elements to analyze one-way slabs produced deflection estimates smaller than the experimental values. Only the estimates for thin slabs were even close (Table 3.16), and they were less than half of the experimental deflections associated with peak capacity, compared to very close deflection estimates using beam elements.

Recently, researchers have used deflection enhancement factors (Famiyesin and Hossain, 1998) with the finite element deflection results when their peak capacity results were acceptable. However, using deflection factors to improve the finite element deflection results would not be practical in this dissertation. The thin slabs already can be reasonably represented for both capacity and deflection using quadratic beam elements and there were no consistent capacity estimates for the thick slabs no matter what finite element/support condition combination was used. There is the possibility of using a reduction factor for the capacity and an enlargement factor for the deflections when using fixed-supported end conditions and beam elements for thick slab analysis, but using more than one improvement factor within a set of finite element results does not appear wise. Additionally, the current use of compressive membrane enhancements is within the defense community where thick slabs are the norm. Therefore, a more reliable technique than current finite element techniques is needed for use with thick slabs.

3.2.3. Compressive Strain

The compressive strain levels at peak capacity were much higher than currently allowed in analysis by the ACI Building Code (1995). This correlates well with the researchers listed in Chapter 2 who mentioned compressive strains at hinge locations near 0.005 in/in when gages did not break before reaching the peak capacity. The ABAQUS analysis using quadratic beam elements provided peak capacity compressive strains ranging from 0.005 to 0.007 in/in for the peak capacity through the capacity associated with the peak thrust (Tables 3.3, 3.4, 3.7, 3.9, 3.11-3.14). This result supports the use of larger compressive strains (i.e., greater than 0.005 in/in) in curvature based deflection estimates since a compressive strain of 0.003 in/in yields deflection estimates smaller than the experimental deflections.

The compressive strains recorded through the analysis of thick slabs are associated with compressive membrane capacities higher than the experimental capacities (Table 3.16). However, this researcher believes that the compressive strains for the thick slabs near the supports at peak capacity with slightly less than fully fixed-supported conditions (i.e., less capacity and greater deflections) would be near at least 0.005 in/in when the concrete is crushing and experiencing pop-outs based on the following: (i) the consistency of the compressive strains near the supports during the peak compressive membrane capacity for thick and thin slabs with fully fixed-supported end conditions (Table 3.16), (ii) the occasional strain reading near 0.005 in/in (Chapter 2) at the peak capacity for slabs not fully fixed-supported and considered thick slabs, and (iii) the study by Mattock (1965) on the rotation capacity of hinging regions.

3.2.4. Thrust

For thin slabs with L/h > 18, the analysis with finite beam elements continued well into the post-peak response and offered a complete view of thrust development (Tables 3.11 - 3.14). The thrust generally peaked slightly after the peak compressive capacity at a slightly larger deflection and smaller capacity. Increasing the number of elements decreased the capacity change between peak capacity and peak thrust to the point that occasionally the peak thrust and capacity occurred simultaneously. Too many beam elements, such as 15 beam elements in the half-span, produced convergence problems whether the span-to-thickness ratio was 8 or 28.3.

The thrust appeared to be more a function of the length-to-thickness ratio (Figure 3.2) rather than the reinforcement ratio, as shown by comparing the peak thrust in Table 3.18 comprised of peak thrust entries using 7 beam elements from the following Tables: 3.7 ($\rho = 0.52$, L/h = 10.4), 3.9 ($\rho = 0.58$, L/h = 14.8), 3.11 ($\rho = 0.578$, L/h = 18.8), 3.12 ($\rho = 0.924$, L/h = 18.8), 3.13 ($\rho = 0.556$, L/h = 28.3), and 3.14 ($\rho = 0.926$, L/h = 28.3). Even though the finite element analysis for thick slabs did not always denote a distinct peak capacity, in the few times that it did (Tables 3.3, 3.4, 3.7 and 3.9), the peak thrust occurred after the peak capacity at a slightly less capacity - which is a capacity closer to the experimental results when using fully fixed-

supported end conditions. Therefore, the author believes that using the point of peak thrust in the compressive membrane theory will provide a better index for denoting the peak capacity than the currently used deflection indexed point.

3.2.5. Concrete Damage

The location and band width of cracking on the top and bottom of the elements matched the experimental results, if available, fairly well. Termination of finite element analysis, especially for thick slabs, usually coincided with large crushing or concrete pop-outs at the peak capacity within the experimental data base. The massive cracking, or softening of the modulus of elasticity, of the finite elements near the supports and at midspan near the peak capacity eventually prevented equilibrium convergence within the acceptable number of attempts or led to solution divergence. Even though improvements usually result from increasing the number of elements through mesh refinement, the mesh refinement for reinforced concrete structures experiencing massive damage decreased the possible analysis since the smaller element became completely cracked, or unstable, earlier in the analysis; thereby, stopping the analysis sooner. Attempts to decrease the minimum time step (< 1E-10) led to load reversal before reaching the previously determined capacity at a larger time step.

3.2.6. Hinge Development Length

The two primary methods for predicting the deflection at the peak capacity are either empirical results or curvature based equations. This deflection presently is used as an index point within the modified rigid-plastic or the flow theory to determine the peak compressive membrane capacity and to represent the deflection at point B in Figure 1.1. For curvature based deflection equations, the hinge length is just as crucial as the associated compressive strain when estimating the deflection at the peak capacity. Keenan (1969) used a hinge length of d at the supports and 2d at midspan when developing his curvature based deflection equations. These values appear reasonable compared to the available data on cracking and crushing band widths in Appendix A.

In ABAQUS, the stress in the reinforcement is provided at two integration points located at 0.1666L from each end of the rebar length in each concrete finite element. By tracking the stress in the reinforcement at the integration points for both the support and midspan regions, the author had hoped to develop a little insight into the hinge length available at the supports and at midspan (Table 3.19). Unfortunately, the location of the integration points (i.e., 0.1666L from each end) does not always provide enough distance along the length to accurately determine how much of the reinforcement is yielding. For thick slabs, a low number of beam elements (< 5) makes the model too stiff (Table 3.3), while too many elements (> 15) makes the model unstable. It did appear that as L/h became smaller, so did the hinge length. The ABAQUS program does not provide the location of a crack in an individual element, not does it provide the width of the crack to allow any estimate of the strain at the crack and, therefore, whether the reinforcement near the crack may be yielding. So at the present time, the time honored hinge distances of d at the support and 2d at midspan, based on experimental observation, will be used for thin slabs, while a smaller hinge length of 0.6d at the supports will used for the thicker slabs (i.e., based on Table 3.19).

3.3. Material Model Issues

The material model, or algorithm, does not allow for much analysis past the peak capacity if large amounts of concrete cracking or crushing are associated with it. Total destruction of an element through crushing prevents mathematical convergence; thereby terminating the analysis, especially for slabs controlled by material instability. The smaller the L/h (< 18), the more flexibility required at the supports through the use of springs to achieve acceptable capacity results. Unfortunately, the more flexibility provided at the supports through springs, the greater the instability and the earlier the termination of the analysis.

The concrete material and element models eventually need to allow for an element to just transfer the load (i.e., like rubble) once the damage is such that the element is nearly destroyed. If the analysis waits until complete destruction of the element, the analysis will terminate prematurely. Of course, peak compressive membrane capacity is normally associated with

concrete crushing or complete destruction of elements depending on how small they are (i.e., element length less than d near the support leads to complete destruction).

The deflection estimates for thick slabs (L/h < 18) will never be acceptable as long as the damage to elements prevents convergence. Deflection estimates will only improve if the mesh is refined (i.e., smaller and more elements), but smaller element dimensions just leads to quicker convergence problems and termination well before the peak capacity. Other, presently unknown, improvements to the finite element method are needed.

3.4. Summary

The studies undertaken as a part of this dissertation, and summarized briefly herein suggest that based on observations, finite element analysis cannot at this time replace analytical expressions in predicting the load capacity of laterally restrained reinforced concrete one-way slabs, especially thick slabs (L/h < 18). However, the behavioral trends observed during finite element analysis further validate the use of the thrust as an index for the peak capacity within the compressive membrane theory and the use of compressive strains between 0.005 to 0.007 in/in in deflection estimates predicting the deflection associated with the peak capacity.

The uniformity of the peak thrust occurring nearly simultaneously or slightly after the peak capacity for thick or thin slabs supports the use of the peak thrust as an index for selecting the peak compressive membrane capacity in the compressive membrane theory rather than the currently used peak capacity deflection estimate. The consistent compressive strain (Table 3.16) associated with peak capacity for thick and thin slabs while using beam elements is about 0.005 to 0.007 in/in. These values correspond to the available compressive strains at peak capacity casually mentioned in Chapter 2. This range of compressive strains will be used in curvature based deflection equations to estimate the peak deflection for use in the load-deflection curve.

Analysis with quadratic beam elements produces acceptable capacities and deflections for thin slabs (L/h > 18). However, for thick slabs (L/h < 18), the analysis with the quadratic beam elements and fixed-supported end conditions over-estimates the capacity by 1.2 to 1.7 times and

greatly under-estimates the deflection by 10 to 15 times. Replacement of the rotational and lateral end conditions with springs does lower the capacity and increase the deflection, but it also increases the instability which led to earlier termination of the analysis. The springs were adjusted to produce a termination capacity near the experimental capacity, but the compressive strains were only half of the peak capacity compressive strains associated with fixed-supported conditions (i.e., 0.005 in/in). These lower compressive strains suggest that the termination capacities are not peak capacities (i.e., based on the consistency in Table 3.16). Weaker springs led to termination values that could be extrapolated to experimental peak capacities based on strains versus capacities with fully fixed-supported end conditions, but there is doubt as to the accuracy.

The midspan deflections using beam elements for thick slabs may be smaller than experimental deflections by an order of magnitude, but the over-all shape and generally the capacities are acceptable (Figures 3.3 - 3.6). The finite element analysis usually stopped before denoting a peak capacity because of the mathematical instability resulting from the massive concrete cracking in individual elements. The load-deflection relationship for thin slabs (Figures 3.1, 3.7 - 3.9) not only displayed acceptable deflections, but also a gradual decline after the peak capacity before mathematical instability ended the analysis.

The use of continuum elements decreases the analysis value further since the analysis terminates even earlier because of the increased instability of the 3D continuum elements. The only way to use finite element results for thick slabs is to use some type of reduction factor with the capacity when analyzing the slabs with fully fixed-supported end conditions and quadratic beam elements. This does not seem appropriate considering that the deflections are also off by an order of magnitude. Therefore, currently used analytical expressions derived from physical observations, either the modified rigid-plastic or flow theory, provide the best option of estimating the capacity, short of experimentation, for laterally restrained thick one-way slabs. Use of the observed behavioral trends at peak capacity from FE analysis with the compressive membrane theory should improve the prediction capability for the capacity and deflection as compared to the current form presented in Park and Gamble (1980).

Table 3.1. Parameter Values for Experimental Slabs Used Within the Analysis

L/h	# Slab	L (in)	h (in)	b (in)	f'_c (psi)	f_y (ksi)	E_c (psi) x 10^6	A_s (in^2)	d (in)	A'_s (in^2)	d' (in)	S (lb/in) x 10^3	ρ_{mid} (%)	ρ'_{mid} (%)	ρ_{spt} (%)	ρ'_{spt} (%)	w_{exp} (psi)	Δ_{exp} (in)
2.7	7	24	8.9	24	5900	60	4.10	1.86	8.0	1.86	0.9	58	0.969	0.969	0.969	0.969	1486	0.41
2.7	3	24	8.9	24	5900	60	4.10	0.66	8.0	0.66	0.9	58	0.344	0.344	0.344	0.344	1620	0.39
4.4	3	24	5.5	24	5900	60	4.10	1.10	4.8	1.10	0.8	58	0.955	0.955	0.955	0.955	557	0.41
5.0	1	24	4.8	24	6030	70	4.10	0.4718	4.3	.4718	0.5	58	0.457	0.457	0.457	0.457	290	0.53
8.0	6	24	3.0	24	4000	55.75	3.53	0.15	2.4	0.15	0.6	58	0.26	0.26	0.26	0.26	68.8	0.835
8.0	4	24	3.0	24	4000	61.75	3.53	0.32	2.4	0.32	0.6	58	0.55	0.55	0.55	0.55	86.0	0.885
8.0	4	24	3.0	24	4000	64.69	3.53	0.5587	2.4	0.5587	0.6	58	0.97	0.97	0.97	0.97	133	0.893
8.3	1	24	2.9	24	3560	60.3	3.37	0.5875	2.4	0.5875	0.5	58	1.02	1.02	1.02	1.02	126	0.8
8.3	1	24	2.9	24	6740	90.2	4.30	0.2774	2.3115	0.2774	0.589	580	0.5	0.5	0.5	0.5	174	0.21
10.0	1	24	2.4	24	6080	70	4.10	0.2172	1.95	0.2172	0.45	58	0.464	0.464	0.464	0.464	61	0.50
10.0	1	24	2.4	24	6080	70	4.10	0.4718	1.88	0.4718	0.52	58	1.045	1.045	1.045	1.045	101	0.86
10.4	8	24	2.3125	24	4975	59.8	3.83	0.3441	1.9375	0.3947	0.375	58	0.74	0.85	0.85	0.74	68.7	0.813
10.4	2	24	2.3125	24	4800	62.4	3.83	0.3488	1.9375	0.3999	0.375	58	0.75	0.86	0.86	0.75	73.5	0.825
10.4	1	24	2.3125	24	4470	66.0	3.68	0.3441	1.9375	0.3441	0.625	58	0.74	0.74	0.74	0.74	66.0	1.0
10.4	1	24	2.3125	24	4470	66.0	3.68	0.3434	1.8125	0.3434	0.5	58	0.79	0.79	0.79	0.79	64.0	0.8
10.4	1	24	2.3125	24	4470	63.0	3.68	0.4959	1.8125	0.174	0.5	58	1.14	0.40	0.40	1.14	68.0	1.2
10.4	2	24	2.3125	24	4490	63.0	3.68	0.4959	1.8125	0.5176	0.5	58	1.14	0.40	1.19	1.14	72.5	1.1
10.4	1	24	2.3125	24	4490	66.0	3.68	0.6873	1.8125	0.0	0.5	58	1.58	0.0	1.58	0.0	68.0	0.25
10.4	7	24	2.3125	24	4170	66.0	3.53	0.4916	1.8125	0.1958	0.5	58	1.13	0.45	1.13	0.45	69.0	0.857
10.4	1	24	2.3125	24	3560	66.0	3.37	0.3437	1.8125	0.1958	0.5	58	0.79	0.45	0.79	0.45	52.0	1.0
10.4	2	24	2.3125	24	4341	50	3.60	0.2418	1.9375	0.2418	0.375	100	0.52	0.52	0.52	0.52	52.0	0.798
10.4	4	24	2.3125	24	4267	58.47	3.60	0.344	1.9375	0.344	0.375	100	0.74	0.74	0.74	0.74	72.0	1.335
10.4	2	24	2.3125	24	4365	58.47	3.60	0.493	1.9375	0.493	0.375	100	1.06	1.06	1.06	1.06	95.0	1.179
12.0	1	72	6.0	24	5010	49.9	3.83	2.4687	4.875	2.4687	1.125	7600	2.11	2.11	2.11	2.11	110	1.00
14.8	2	24	1.625	24	4996	67.33	3.83	0.175	1.25	0.175	0.375	100	0.58	0.58	0.58	0.58	27.5	0.805
14.8	4	24	1.625	24	4984	58.47	3.83	0.342	1.25	0.342	0.375	100	1.14	1.14	1.14	1.14	41.0	0.601
14.8	2	24	1.625	24	4996	58.47	3.83	0.441	1.25	0.441	0.375	100	1.47	1.47	1.47	1.47	46.0	0.65

Table 3.1. Parameter Values for Experimental Slabs Used Within the Analysis (cont.)

L/h	# Slab	L (in)	h (in)	b (in)	f'_c (psi)	f_y (ksi)	E_c (psi) x 10^6	A_s (in^2)	d (in)	A'_s (in^2)	d' (in)	S (lb/in) x 10^3	ρ_{mid} (%)	ρ'_{mid} (%)	ρ_{spt} (%)	ρ'_{spt} (%)	w_{exp} (psi)	Δ_{exp} (in)
17.1	1	60	3.5	6	3276	40.0	3.19	0.0982	3.125	0.0982	0.375	176	0.52	0.0	0.52	0.0	16.5	0.65
17.1	1	60	3.5	6	4528	40.0	3.68	0.0982	3.125	0.0982	0.375	176	0.52	0.0	0.52	0.0	18.3	0.65
18.8	2	56.5	3.0	9	6032	35.0	4.10	0.0553	2.66	0.0	0.0	3290	0.231	0.0	0.0	0.231	23.3	0.446
18.8	2	56.5	3.0	9	2976	35.0	3.36	0.0553	2.66	0.0	0.0	3290	0.231	0.0	0.0	0.231	15.7	0.441
18.8	2	56.5	3.0	9	3130	35.0	3.36	0.1384	2.66	0.0	0.0	3290	0.578	0.0	0.0	0.578	15.6	0.462
18.8	2	56.5	3.0	9	5552	35.0	3.97	0.1384	2.66	0.0	0.0	3290	0.578	0.0	0.0	0.578	24.5	0.474
18.8	2	56.5	3.0	9	3328	35.0	3.37	0.1384	2.66	0.0	0.0	3290	0.578	0.0	0.0	0.578	19.3	0.551
18.8	2	56.5	3.0	9	2104	35.0	3.19	0.2212	2.66	0.0	0.0	3290	0.924	0.0	0.0	0.924	16.2	0.447
18.8	2	56.5	3.0	9	3496	35.0	3.37	0.2212	2.66	0.0	0.0	3290	0.924	0.0	0.0	0.924	18.5	0.45
18.8	2	56.5	3.0	9	6528	35.0	4.22	0.2212	2.66	0.0	0.0	3290	0.924	0.0	0.0	0.924	26.9	0.512
20.0	1	60	3.0	6	3744	40.0	3.53	0.0982	2.625	0.0982	0.375	176	0.623	0.0	0.623	0.0	13.3	0.65
24.0	1	72	3.0	6	3976	40.0	3.53	0.0982	2.625	0.0982	0.375	176	0.623	0.0	0.623	0.0	8.8	0.65
28.3	2	56.5	2.0	9	3048	35.0	3.19	0.0554	1.66	0.0	0.0	3290	0.371	0.0	0.0	0.371	6.0	0.50
28.3	2	56.5	2.0	9	6008	35.0	4.10	0.0554	1.66	0.0	0.0	3290	0.371	0.0	0.0	0.371	8.0	0.55
28.3	3	56.5	2.0	9	2864	35.0	3.19	0.0831	1.66	0.0	0.0	3290	0.556	0.0	0.0	0.556	5.1	0.506
28.3	1	56.5	2.0	9	5840	35.0	4.10	0.0831	1.66	0.0	0.0	3290	0.556	0.0	0.0	0.556	7.9	0.576
28.3	2	56.5	2.0	9	3800	35.0	3.53	0.1107	1.66	0.0	0.0	3290	0.741	0.0	0.0	0.741	7.0	0.545
28.3	3	56.5	2.0	9	3496	35.0	3.37	0.1107	1.66	0.0	0.0	3290	0.741	0.0	0.0	0.741	5.7	0.506
28.3	3	56.5	2.0	9	5760	35.0	4.10	0.1107	1.66	0.0	0.0	3290	0.741	0.0	0.0	0.741	7.9	0.536
28.3	2	56.5	2.0	9	2796	35.0	3.19	0.1383	1.66	0.0	0.0	3290	0.926	0.0	0.0	0.926	5.9	0.507
28.3	2	56.5	2.0	9	6176	35.0	4.12	0.1383	1.66	0.0	0.0	3290	0.926	0.0	0.0	0.926	7.3	0.562

Table 3.2. Groupings of One-Way Laterally Restrained Reinforced Concrete Slabs

L/h	Researcher, Year	Reinforcement Ratios (%)
2.7	Woodson, 1994	0.344, 0.96
4.4	***Woodson, 1994***	***0.96***
5.0	Baylot, 1985	0.457
8.0	***Woodson, 1993***	***0.25***, 0.55, 0.97
8.3	Kiger, 1984	0.5
10.0	Baylot, 1985	0.464, 1.045
10.4	Woodson, 1985	0.74
10.4	Woodson/Garner, 1985	top and bottom steel varied
10.4	***Guice, 1986***	***0.52***, 0.74, 1.06
12.0	Keenan, 1969	2.11
14.8	***Guice, 1986***	***0.58***, 1.14, 1.47
17.1	Christiansen, 1964	0.623
18.8	***Roberts, 1969***	0.231, ***0.578***, ***0.924***
20.0	Christiansen, 1964	0.623
24.0	Christiansen, 1964	0.52
28.3	***Roberts, 1969***	0.371, ***0.556***, 0.741, ***0.926***

Table 3.3. ABAQUS Results for Woodson Slab (L/h = 4.4)
Using Beam Elements (B22) With a Peak Capacity of 557 psi and a Deflection of 0.41 inches

# elem	Inc	σ_{11} (psi)	ε_{11} (in/in)	$I\varepsilon_{11}$ (in/in)	σ_{11} rebar (psi)	Load (psi)	Δ_{mid} (in)	Thrust (lb)	Remarks
Part	**One**								
5-15	466	-584(m)	-1.426E-04(m)	--	3070	-48.5	-0.003	--	Crk (m)
	4617	-3695(m)	-9.011E-04(m)	--	60000	-174.4	-0.036	--	Yield/Pk
Part	**Two**								
5	794	-579(s)	-1.414E-04(s)	--	2922	-82.7	-0.002	+5.7	Crk (s)
	1432	-1140(s)	-2.781E-04(s)	--	7166	-142.2	-0.003	-1919	Crk (m)
	6473	-4843(s)	-1.419E-03(s)	-2.377E-04	60000	-479.3	-0.016	-75402	Yield (s)
	11531	-6000(s)	-3.005E-03(s)	-1.542E-03	39893	-717.3	-0.028	-167660	
	13691	-5478(m)	-3.986E-03(s)	-2.901E-03	47366	-782.3	-0.033	-195470	Pk
	13724	-5481(m)	-4.018E-03(s)	-2.985E-03	47493	-781.7	-0.034	-195540	Pk Thrust
	14804	-5570(m)	-4.986E-03(s)	-4.492E-03	51610	-777.9	-0.036	-195490	Error
7	764	-580(s)	-1.415E-04(s)	--	2924	-79.6	-0.002	+5.1	Crk (s)
	1431	-1218(s)	-2.970E-04(s)	--	7988	-142.0	-0.003	-1804	Crk (m)
	6192	-4815(s)	-1.395E-03(s)	-2.215E-04	60000	-455.7	-0.015	-71082	Yield (s)
	10660	-6000(s)	-3.005E-03(s)	-1.542E-03	35703	-663.0	-0.026	-155900	
	11178	-5980(s)	-3.205E-03(s)	-1.747E-03	37057	-684.0	-0.027	-164360	Time Inc
10	742	-580(s)	-1.414E-04(s)	--	2922	-77.3	-0.002	+4.9	Crk (s)
	1431	-1273(s)	-3.104E-04(s)	--	8555	-141.8	-0.003	-1790	Crk (m)
	5873	-4781(s)	-1.364E-03(s)	-1.978E-04	60000	-432.0	-0.014	-65127	Yield (s)
	9700	-6000(s)	-2.975E-03(s)	-1.512E-03	32256	-608.0	-0.023	-140030	
	12750	-5239(m)	-5.356E-03(s)	-4.907E-03	41280	-699.0	-0.030	-183390	Pk/Thrust
	13000	-5208(m)	-5.535E-03(s)	-5.125E-03	41496	-694.0	-0.031	-183200	Unload
15	726	-580(s)	-1.414E-04(s)	--	2922	-75.6	-0.002	+4.8	Crk (s)
	1431	-1315(s)	-3.208E-04(s)	--	8998	-141.7	-0.003	-1781	Crk (m)
	5592	-4740(s)	-1.324E-03(s)	-1.688E-04	60000	-412.0	-0.013	-59953	Yield (s)
	8600	-6000(s)	-2.896E-03(s)	-1.434E-03	27782	-552.0	-0.020	-119180	
	11500	-5093(s)	-5.703E-03(s)	-5.286E-03	36349	-648.0	-0.027	-165620	Time Inc

Table 3.4. ABAQUS Results for Woodson Slab (L/h = 8)
Using Beam Elements (B22) With a Peak Capacity of 68.8 psi and a Deflection of 0.835 inches

# elem	Inc	σ_{11} (psi)	ε_{11} (in/in)	$I\varepsilon_{11}$ (in/in)	σ_{11} rebar (psi)	Load (psi)	Δ_{mid} (in)	Thrust (lb)	Remarks
Part	**One**								
5-15	235	-453(m)	-1.283E-04(m)	--	2235	-9.79	-0.005	--	Crk (m)
	535	-1206(m)	-3.417E-04(m)	--	11887	-16.4	-0.012	--	Attempts
Part	**Two**								
5	41	-462(s)	-1.309E-04(s)	--	2285	-17.1	-0.002	+0.27	Crk (s)
	75	-925(s)	-2.621E-04(s)	--	6114	-28.4	-0.004	-963	Crk (m)
	311	-2985(s)	-1.149E-03(s)	-3.041E-04	55750	-67.9	-0.017	-28921	Yield (s)
	626	-4000(s)	-2.653E-03(s)	-1.520E-03	44486	-103	-0.036	-60025	
	924	-3911(m)	-4.682E-03(s)	-3.980E-03	55750	-116	-0.053	-75437	Pk/Yield (m)
	1081	-4000(m)	-6.051E-03(s)	-5.537E-03	55750	-113	-0.062	-80080	
	1255	-3921(m)	-7.616E-03(s)	-7.263E-03	55750	-110	-0.072	-83956	Pk Thrust
	1869	-3043(m)	-1.153E-02(s)	-1.143E-02	55750	-92.3	-0.091	-72228	Time Inc
7	39	-457(s)	-1.294E-04(s)	--	2256	-16.2	-0.002	+2.3	Crk (s)
	75	-1003(s)	-2.840E-04(s)	--	7021	-28.4	-0.004	-924	Crk (m)
	232	-2758(s)	-9.754E-04(s)	-1.939E-04	55750	-53.6	-0.012	-19554	Yield (s)
	548	-4000(s)	-2.651E-03(s)	-1.518E-03	39510	-93.1	-0.030	-54010	
	789	-3755(m)	-4.786E-03(s)	-4.106E-03	46458	-109	-0.045	-71648	Pk
	832	-3871(m)	-7.021E-03(s)	-6.610E-03	55750	-101	-0.053	-70856	Yield (m)
	874	-3990(m)	-8.541E-03(s)	-8.265E-03	55750	-100	-0.061	-75888	Pk Thrust
	895	-4000(m)	-9.681E-03(s)	-9.483E-03	55750	-96.2	-0.065	-74741	Unloading
10	38	-459(s)	-1.298E-04(s)	--	2264	-15.8	-0.002	+2.3	Crk (s)
	77	-1133(s)	-3.210E-04(s)	--	9410	-28.3	-0.004	-1262	Crk (m)
	177	-2617(s)	-8.590E-04(s)	-1.176E-04	55750	-43.7	-0.009	-13270	Yield (s)
	470	-4000(s)	-2.651E-03(s)	-1.518E-03	37482	-83.5	-0.025	-46426	
	764	-3674(m)	-5.331E-03(s)	-4.732E-03	43729	-103	-0.041	-68670	Pk/Thrust
	1556	-3804(m)	-1.133E-02(s)	-1.121E-02	55750	-85.2	-0.055	-66472	Yield (m)
15	37	-456(s)	-1.292E-04(s)	--	2251	-15.4	-0.002	+2.8	Crk (s)
	78	-1313(s)	-3.720E-04(s)	--	13245	-27.9	-0.004	-1530	Crk (m)
	135	-2511(s)	-7.710E-04(s)	-5.984E-05	55750	-36.0	-0.007	-8665	Yield (s)
	421	-4000(s)	-2.652E-03(s)	-1.519E-03	30156	-74.2	-0.021	-39022	
	557	-3542(s)	-3.429E-03(s)	-2.425E-03	36071	-81.5	-0.025	-45924	Unloading

Table 3.5. ABAQUS Results for Woodson Slab (L/h = 8) Using 10 Beam Elements (B22) and Springs With a Peak Capacity of 68.8 psi and a Deflection of 0.835 inches

Restraint	Inc	σ_{11} (psi)	ε_{11} (in/in)	$l\varepsilon_{11}$ (in/in)	σ_{11} rebar (psi)	σ_{spr} (lb /rad)	ϕ_{spr} (rad)	σ_{spl} (lb/in)	ϕ_{spl} (in)	Load (psi)	Δ_{mid} (in)	Thrust * or Moment (lb) or (in-lb)	Remarks
L_{full}	46	-453(s)	-1.284E-04(s)	--	2238	18309	2.288E-04	--	--	-19.2	-0.004	+12.9	Crk (s)
R8E7	53	-529(s)	-1.497E-04(s)	--	2658	21049	2.631E-04	--	--	-22.1	-0.004	+2.3	Crk (m)
	310	-2757(s)	-9.738E-04(s)	-1.929E-04	55750	49411	6.176E-04	--	--	-53.0	-0.016	-19917	Yield (s)
	1368	-3440(s)	-1.547E-03(s)	-5.727E-04	38532	64597	8.074E-04	--	--	-69.6	-0.023	-33376	Time Inc
L5.1E7	38	-458(s)	-1.298E-04(s)	--	2264	--	--	-1.6	-3.173E-08	-15.8	-0.002	-18233	Crk (s)
R_{full}	76	-1114(s)	-3.155E-04(s)	--	9341	--	--	871	1.708E-05	-27.9	-0.004	-30810	Crk (m)
	167	-2530(s)	-7.874E-04(s)	-7.060E-05	55750	--	--	9425	1.848E-04	-39.6	-0.009	-37216	Yield (s)
	340	-3420(s)	-1.526E-03(s)	-5.579E-04	18067	--	--	25312	4.963E-04	-60.1	-0.017	-54734	Time Inc
L1E8	188	-452(s)	-1.281E-04(s)	--	2230	18018	1.801E-06	-2.8	-2.785E-08	-15.7	-0.002	--	Crk (s)
R1E10	376	-1090(s)	-3.087E-04(s)	--	8763	30892	3.089E-06	918	9.181E-06	-27.9	-0.004	--	Crk (m)
	850	-2561(s)	-8.129E-04(s)	-8.735E-05	55750	38985	3.898E-06	10916	1.091E-04	-41.2	-0.009	--	Yield (s)
	3000	-3990(s)	-2.507E-03(s)	-1.376E-03	38345	73753	7.375E-06	41273	4.127E-04	-78.3	-0.025	--	Inc Comp
L1E8	191	-452(s)	-1.281E-04(s)	--	2231	18038	1.803E-05	-3.15	-3.156E-08	-15.9	-0.002	--	Crk (s)
R1E9	356	-982(s)	-2.782E-04(s)	--	6908	30320	3.032E-05	584	5.843E-06	-27.5	-0.004	--	Crk (m)
	837	-2564(s)	-8.150E-04(s)	-8.869E-05	55750	39152	3.915E-05	11034	1.103E-04	-41.6	-0.009	--	Yield (s)
	1645	-3495(s)	-1.604E-03(s)	-6.137E-04	19059	59266	5.926E-05	28998	2.899E-04	-64.3	-0.018	--	Time Inc
L1E8	45	-461(s)	-1.306E-04(s)	--	2281	18539	1.853E-04	-7.6	-7.600E-08	-18.7	-0.003	--	Crk (s)
R1E8	55	-572(s)	-1.623E-04(s)	--	2903	22584	2.258E-04	5.3	5.257E-08	-22.8	-0.004	--	Crk (m)
	598	-2834(s)	-1.033E-03(s)	-2.309E-04	55750	47329	4.732E-04	18539	1.853E-04	-51.3	-0.016	--	Yield (s)
	6166	-3487(s)	-1.595E-03(s)	-6.077E-04	39093	61758	6.175E-04	30737	3.073E-04	-66.8	-0.023	--	Time Inc

* If the restraint (lateral or rotational) was fully rigid, the generated thrust or moment is listed.

Table 3.6. ABAQUS Results for Woodson Slab (L/h = 8) Using 14 (7/2/1) Continuum Elements (C3D20/R) and Springs With a Peak Capacity of 68.8 psi and a Deflection of 0.835 inches

Restraint	Inc	σ_{11} (psi)	ε_{11} (in/in)	$I\varepsilon_{11}$ (in/in)	σ_{11} rebar (psi)	σ_{spr} (lb/ rad)	ϕ_{spr} (rad)	σ_{spl} (lb/in)	ϕ_{spl} (in)	Load (psi)	Δ_{mid} (in)	Thrust * or Moment (lb) or (in-lb)	Remarks
L_{full}	173	-406(s)	-1.021E-04(s)	--	2206	--	--	--	--	-17.3	-0.002	-136	Crk (s)
R_{full}	436	-1108(s)	-2.770E-04(s)	--	12207	--	--	--	--	-33.8	-0.005	-3150	Crk (m)
	1500	-2599(s)	-6.723E-04(s)	-5.321E-05	55750	--	--	--	--	-73.8	-0.018	-30477	Yield (s)
	3000	-4449(s)	-1.222E-03(s)	-2.815E-04	26291	--	--	--	--	-121	-0.036	-65052	Time Inc
L_{full}	242	-403(s)	-1.025E-04(s)	--	3089	--	--	--	--	-24.2	-0.003	-188	Crk (s)
R_{full}	948	-861(s)	-2.392E-04(s)	--	50170	--	--	--	--	-49.8	-0.011	-15856	Crk (m)
Reduced	1277	-1288(s)	-3.075E-04(s)	--	55750	--	--	--	--	-55.5	-0.016	-29476	Yield(s)
	1850	-1821(s)	-4.332E-04(s)	--	55750	--	--	--	--	-77.8	-0.023	-43618	Yield (m)
	2200	-2256(s)	-5.219E-04(s)	--	55750	--	--	--	--	-91.9	-0.030	-59840	Time Inc
L1E7	260	-402(s)	-1.016E-04(s)	--	3524	--	--	195.3	1.953E-05	-25.7	-0.004	7425	Crk (s)
R_{full}	690	-768(s)	-2.139E-04(s)	--	41554	--	--	12420	1.242E-03	-43.0	-0.011	12389	Crk (m)
Reduced	1220	-1334(s)	-3.194E-04(s)	--	55750	--	--	28617	2.861E-03	-58.8	-0.020	16931	Yield (s&m)
	1940	-2074(s)	-4.918E-04(s)	--	55750	--	--	48579	4.857E-04	-83.0	-0.032	23904	Attempts
L1E6	260	-378(m)	-1.054E-04(m)	--	12734(m)	--	--	857	8.573E-04	-22.0	-0.008	6345	Crk (m)
R_{full}	460	-445(s)	-1.080E-04(s)	--	55750(m)	--	--	4881	4.881E-03	-24.1	-0.015	6935	Yield (m)
Reduced	700	-698(s)	-1.687E-04(s)	--	3963(s)	--	--	8770	8.770E-03	-32.6	-0.025	9374	Crk (s)
	880	-817(s)	-1.939E-04(s)	--	27318(s)	--	--	13143	1.314E-02	-37.4	-0.032	10786	Attempts
L2E6	350	-418(s)	-1.022E-04(s)	--	34079(m)	--	--	4275	2.137E-03	-20.3	-0.009	5837	Crk (s&m)
R_{full}	600	-717(s)	-1.753E-04(s)	--	55750(m)	--	--	8198	4.099E-03	-34.6	-0.016	9952	Yield (m)
Reduced	1150	-1316(s)	-3.170E-04(s)	--	55750(s)	--	--	24531	1.226E-02	-52.9	-0.032	15242	Yield (s)
	1550	-1793(s)	-4.324E-04(s)	--	55750	--	--	34354	1.717E-02	-68.0	-0.044	19597	Attempts

* If the restraint (lateral or rotational) was fully rigid, the generated thrust or moment is listed.

Table 3.7. ABAQUS Results for Guice Slab (L/h = 10.4)
Using Beam Elements (B22) With a Peak Capacity of 52.0 psi and a Deflection of 0.798 inches

# elem	Inc	σ_{11} (psi)	ε_{11} (in/in)	$I\varepsilon_{11}$ (in/in)	σ_{11} rebar (psi)	Load (psi)	Δ_{mid} (in)	Thrust (lb)	Remarks
Part	**One**								
5-15	160	-492(m)	-1.337E-04(m)	--	2622	-6.67	-0.007	--	Crk (m)
	541	-1835(m)	-4.986E-04(m)	--	26485	-12.1	-0.023	--	Unloading
Part	**Two**								
5	110	-494(s)	-1.343E-04(s)	--	1495	-11.5	-0.003	+4.5	Crk(s)
	203	-982(s)	-2.667E-04(s)	--	6715	-19.4	-0.005	-723	Crk(m)
	792	-3174(s)	-1.079E-03(s)	-2.170E-04	50000	-47.2	-0.020	-19479	Yield (s)
	1850	-4500(s)	-2.815E-03(s)	-1.592E-03	37562	-77.7	-0.048	-52818	
	2445	-4191(m)	-4.206E-03(s)	-3.349E-03	47879	-86.3	-0.064	-62717	Pk
	2573	-4229(m)	-4.649E-03(s)	-3.989E-03	50000	-86.1	-0.067	-63297	Yield (m)
	3531	-4487(m)	-7.907E-03(s)	-7.601E-03	50000	-79.6	-0.094	-69012	Pk Thrust
	3681	-4462(m)	-8.405E-03(s)	-8.137E-03	50000	-78.3	-0.097	-68254	Time inc
7	263	-492(s)	-1.335E-04(s)	--	2620	-10.9	-0.003	+4.9	Crk (s)
	507	-1055(s)	-2.866E-04(s)	--	7576	-19.3	-0.005	-685	Crk (m)
	1600	-3010(s)	-9.599E-04(s)	-1.419E-04	50000	-40.1	-0.016	-14073	Yield (s)
	4096	-4500(s)	-2.815E-03(s)	-1.592E-03	32842	-70.8	-0.042	-47591	
	6079	-4128(m)	-5.211E-03(s)	-4.635E-03	45450	-81.5	-0.062	-61486	Pk/Pk Thrust
	6215	-4081(m)	-5.886E-03(s)	-5.386E-03	48025	-77.4	-0.064	-57985	Time inc
10	110	-532(s)	-1.444E-04(s)	--	2857	-11.4	-0.003	-0.19	Crk (s)
	210	-1167(s)	-3.170E-04(s)	--	9213	-19.7	-0.006	-845	Crk (m)
	540	-2911(s)	-8.874E-04(s)	-9.646E-05	50000	-35.4	-0.013	-10664	Yield (s)
	1420	-4500(s)	-2.810E-03(s)	-1.587E-03	28018	-63.9	-0.035	-41316	
	2260	-3969(m)	-5.603E-03(s)	-5.071E-03	39926	-77.2	-0.056	-59130	Time Inc
15	250	-492(s)	-1.335E-04(s)	--	2619	-10.4	-0.002	+4.6	Crk (s)
	513	-1195(s)	-3.246E-04(s)	--	9814	-19.3	-0.005	-782	Crk (m)
	1321	-2894(s)	-8.752E-04(s)	-8.877E-05	50000	-34.4	-0.012	-10213	Yield (s)
	3092	-4500(s)	-2.814E-03(s)	-1.592E-03	22711	-57.9	-0.030	-35122	
	3950	-3483(s)	-4.018E-03(s)	-3.071E-03	30450	-65.7	-0.039	-44630	Time Inc

Table 3.8. ABAQUS Results for Guice Slab (L/h = 10.4) Using 10 Beam Elements (B22) / 14 (7/2/1) Continuum Elements (C3D20/R) and Springs With a Peak Capacity of 52.0 psi and a Deflection of 0.798 inches

Restraint	Inc	σ_{11} (psi)	ε_{11} (in/in)	σ_{11} rebar (psi)	σ_{spr} (lb/ rad)	ϕ_{spr} (rad)	σ_{spl} (lb/in)	ϕ_{spl} (in)	Load (psi)	Δ_{mid} (in)	Thrust * or Moment (lb) or(in-lb)	Remarks
L1E7	120	-533(s)	-1.448E-04(s)	2866	13275	1.327E-04	-1.68	-1.687E-07	-12.5	-0.004	--	Crk (s)
R1E8	170	-812(s)	-2.205E-04(s)	5069	18267	1.826E-04	58.6	5.855E-06	-17.3	-0.005	--	Crk (m)
B22	460	-2729(s)	-7.545E-04(s)	50000	30445	3.044E-04	4430	4.430E-04	-31.0	-0.015	--	Yield (s)
	1490	-4500(s)	-2.791E-03(s)	44155	51309	5.130E-04	28090	2.809E-03	-55.4	-0.048	--	
	1740	-4154(s)	-3.475E-03(s)	50000	55332	5.533E-04	32766	3.276E-03	-60.4	-0.057	--	Yield (m)
	2470	-4398(m)	-6.139E-03(s)	50000	64591	6.459E-04	45312	4.531E-03	-70.4	-0.083	--	Pk/hhrust
	2530	-4417(m)	-6.698E-03(s)	50000	62936	6.293E-04	44760	4.476E-03	-69.1	-0.084	--	Time Inc
L4.6E6	120	-532(s)	-1.444E-04(s)	2857	13244	1.365E-04	-1.04	-2.253E-07	-12.5	-0.004	--	Crk (s)
R9.7E7	170	-809(s)	-2.198E-04(s)	5058	18230	1.879E-04	33.2	7.216E-06	-17.3	-0.005	--	Crk (m)
B22	440	-2617(s)	-7.112E-04(s)	50000	28666	2.955E-04	2509	5.454E-04	-29.3	-0.014	--	Yield(s)
	1610	-4500(s)	-2.799E-03(s)	49561	44107	4.547E-04	20199	4.391E-03	-49.3	-0.053	--	
	1640	-4498(s)	-2.849E-03(s)	50000	44458	4.583E-04	20568	4.471E-03	-49.7	-0.054	--	Yield (m)
	1940	-4497(s)	-2.849E-03(s)	50000	44447	4.582E-04	20567	4.471E-03	-49.7	-0.054	--	Unloading
L_{full}	120	-451(s)	-1.092E-04(s)	2660	--	--	--	--	-11.9	-0.003	-68.6	Crk (s)
R_{full}	290	-1168(s)	-2.817E-04(s)	11709	--	--	--	--	-23.3	-0.007	-2074	Crk (m)
C3D20	900	-2596(s)	-6.270E-04(s)	50000	--	--	--	--	-48.5	-0.021	-20194	Yield (s)
	1000	-2790(s)	-6.825E-04(s)	13885	--	--	--	--	-51.9	-0.023	-23569	File to large
L_{full}	170	-448(s)	-1.093E-04(s)	3980	--	--	--	--	-16.9	-0.004	-146.8	Crk (s)
R_{full}	590	-876(s)	-2.261E-04(s)	46643	--	--	--	--	-33.8	-0.013	-10975	Crk (m)
Reduced	670	-1025(s)	-2.395E-04(s)	50000	--	--	--	--	-36.5	-0.015	-14069	Yield (s)
C3D20R	1270	-1877(s)	-4.352E-04(s)	50000	--	--	--	--	-56.6	-0.029	-34432	Yield (m)
	1980	-2763(s)	-6.599E-04(s)	50000	--	--	--	--	-77.3	-0.047	-58582	File to large
L1E6	180	-482(m)	-1.289E-04(m)	5362(m)	--	--	57.9	5.792E-05	-17.8	-0.011	5134	Crk (s)
R_{full}	340	-578(s)	-1.495E-04(m)	50000(m)	--	--	3860	3.859E-03	-23.1	-0.022	6645	Yld/Crk (m)
Reduced	1000	-1612(s)	-3.796E-04(s)	50000(s)	--	--	22160	2.216E-02	-44.8	-0.068	12920	Yield (s)
C3D20R	1210	-1952(s)	-4.603E-04(s)	50000	--	--	27837	2.783E-02	-51.5	-0.082	14824	Attempts

* If the restraint (lateral or rotational) was fully rigid, the generated thrust or moment is listed.

Table 3.9. ABAQUS Results for Guice Slab (L/h = 14.8)
Using Beam Elements (B22) With a Peak Capacity of 27.5 psi and a Deflection of 0.805 inches

# elem	Inc	σ_{11} (psi)	ε_{11} (in/in)	$I\varepsilon_{11}$ (in/in)	σ_{11} rebar (psi)	Load (psi)	Δ_{mid} (in)	Thrust (lb)	Remarks
Part	**One**								
5-15	33	-532(m)	-1.387E-04(m)	--	2174	-3.44	-0.010	--	Crk (m)
	92	-1433(m)	-3.741E-04(m)	--	11899	-5.87	-0.027	--	Time Inc
Part	**Two**								
5	56	-526(s)	-1.374E-04(s)	--	2151	-5.8	-0.004	+7.11	Crk (s)
	104	-1055(s)	-2.754E-04(s)	--	5776	-9.8	-0.007	-554	Crk (m)
	645	-4495(s)	-1.787E-03(s)	-6.135E-04	67330	-31.6	-0.045	-24945	Yield (s)
	947	-5000(s)	-2.835E-03(s)	-1.530E-03	23290	-38.8	-0.067	-36937	
	1347	-4652(m)	-4.687E-03(s)	-4.258E-03	50855	-42.2	-0.096	-45792	Pk
	1459	-4804(m)	-5.398E-03(s)	-5.174E-03	51998	-41.1	-0.104	-47043	Pk Thrust
	1914	-4885(m)	-9.532E-03(s)	-9.516E-03	67330	-31.1	-0.136	-39074	Yield (m)
	2306	-5000(m)	-1.278E-02(s)	-1.277E-02	67730	-28.5	-0.166	-36130	
7	54	-528(s)	-1.378E-04(s)	--	1179	-5.6	-0.003	+6.7	Crk (s)
	104	-1140(s)	-2.976E-04(s)	--	2083	-9.8	-0.007	-528	Crk (m)
	502	-4184(s)	-1.496E-03(s)	-4.043E-04	67330	-26.9	-0.035	-18816	Yield (s)
	835	-5000(s)	-2.830E-03(s)	-1.525E-03	32976	-35.8	-0.058	-33428	
	1184	-4542(m)	-4.830E-03(s)	-4.452E-03	42495	-39.3	-0.083	-42601	Pk
	1219	-4576(m)	-5.101E-03(s)	-4.803E-03	43803	-39.1	-0.085	-42784	Pk Thrust
	1226	-4576(m)	-5.101E-03(s)	-4.803E-03	43804	-39.1	-0.085	-42784	Time Inc
10	52	-523(s)	-1.365E-04(s)	--	1137	-5.4	-0.003	+6.9	Crk (s)
	105	-1231(s)	-3.214E-04(s)	--	7851	-9.7	-0.007	-601	Crk (m)
	507	-4172(s)	-1.485E-03(s)	-3.965E-04	67330	-26.3	-0.034	-18428	Yield (s)
	18400	-5000(s)	-2.821E-03(s)	-1.516E-03	29578	-33.6	-0.053	-31143	
	30000	-4209(m)	-3.997E-03(s)	-3.209E-03	35471	-36.4	-0.066	-37431	File to Large
15	51	-524(s)	-1.368E-04(s)	--	2142	-5.3	-0.003	+6.7	Crk (s)
	106	-1346(s)	-3.515E-04(s)	--	9668	-9.7	-0.007	-668	Crk (m)
	5195	-4107(s)	-1.434E-03(s)	-3.618E-04	67330	-24.9	-0.032	-16793	Yield (s)
	6245	-4226(s)	-1.533E-03(s)	-4.299E-04	17201	-25.5	-0.033	-17887	File to Large

Table 3.10. ABAQUS Results for Guice Slab (L/h = 14.8) Using 10 Beam Elements (B22)/14 (7/2/1)
Continuum Elements (C3D20/R) and Springs With a Peak Capacity of 27.5 psi and a Deflection of 0.805 inches

Restraint	Inc	σ_{11} (psi)	ε_{11} (in/in)	$I\varepsilon_{11}$ (in/in)	σ_{11} rebar (psi)	σ_{spr} (lb/rad)	ϕ_{spr} (rad)	σ_{spl} (lb/in)	ϕ_{spl} (in)	Load (psi)	Δ_{mid} (in)	Thrust * or Moment (lb) or (in-lb)	Remarks
L1E8	54	-527(s)	-1.378E-04(s)	--	2155	6295	6.294E-05	-7.73	-7.729E-08	-5.6	-0.004	--	Crk (s)
R1E8	96	-1070(s)	-2.794E-04(s)	--	6077	10238	1.023E-04	303	3.029E-06	-9.3	-0.007	--	Crk (m)
B22	1740	-4138(s)	-1.458E-03(s)	-3.782E-04	67330	26711	2.671E-04	17611	1.761E-04	-25.8	-0.037	--	Yield (s)
	6954	-5000(s)	-2.837E-03(s)	-1.532E-03	33420	33917	3.391E-04	30202	3.020E-04	-33.3	-0.058	--	
	10000	-4225(m)	-3.959E-03(s)	-3.143E-03	38061	35913	3.591E-04	36063	3.606E-04	-35.9	-0.070	--	Inc Compl
L6E7	60	-521(s)	-1.361E-04(s)	--	2132	6287	3.143E-04	-16.8	-2.809E-07	-6.3	-0.006	--	Crk (s)
R2E7	80	-724(s)	-1.890E-04(s)	--	3208	8288	4.144E-04	12.2	2.031E-07	-8.3	-0.008	--	Crk (m)
B22	60000	-4122(s)	-1.445E-03(s)	-3.694E-04	64251	26763	1.338E-03	18583	3.097E-04	-26.3	-0.046	--	Inc Compl
L1E7	70	-545(s)	-1.423E-04(s)	--	2199	6506	6.506E-04	-16.2	1.627E-06	-7.3	-0.008	--	Crk (s&m)
R1E7	60000	-3577(s)	-9.858E-04(s)	-5.187E-05	53927	18292	1.829E-03	7880	7.879E-03	-18.5	-0.039	--	Inc Compl
L_{full}	70	-557(s)	-1.297E-04(s)	--	2772	--	--	--	--	-6.9	-0.004	-72.7	Crk (s)
R_{full}	150	-1258(s)	-2.924E-04(s)	--	10081	--	--	--	--	-11.8	-0.009	-1509	Crk (m)
C3D20	700	-3946(s)	-9.207E-04(s)	--	67330	--	--	--	--	-32.8	-0.044	-24723	Yield (s)
	1020	-5323(s)	-1.330E-03(s)	-1.745E-04	23193	--	--	--	--	-43.0	-0.064	-38694	File to large
L_{full}	90	-484(s)	-1.137E-04(s)	--	3857	--	--	--	--	-8.7	-0.006	-165.7	Crk (s)
R_{full}	320	-982(s)	-2.415E-04(s)	--	47336	--	--	--	--	-16.6	-0.019	-9012	Crk (m)
Reduced	550	-1804(s)	-4.156E-04(s)	--	67330	--	--	--	--	-23.8	-0.036	-20858	Yield (s)
C3D20R	920	-2772(s)	-6.354E-04(s)	--	67330	--	--	--	--	-35.1	-0.059	-37126	Yield (m)
	1360	-3863(s)	-9.046E-04(s)	-3.809E-05	67330	--	--	--	--	-46.4	-0.089	-56301	Attempts
L6E6	90	-470(s)	-1.106E-04(s)	--	3093	--	--	12.9	2.160E-06	-8.9	-0.008	2588	Crk (s)
R_{full}	230	-828(m)	-2.139E-04(m)	--	39004	--	--	6888	1.148E-03	-14.2	-0.019	4105	Crk (m)
Reduced	490	-1775(s)	-4.128E-04(s)	--	67330	--	--	19474	3.245E-03	-24.2	-0.043	6980	Yield (s)
C3D20R	570	-1995(s)	-4.633E-04(s)	--	63271	--	--	22905	3.817E-03	-27.1	-0.050	7811	Attempts

* If the restraint (lateral or rotational) was fully rigid, the generated thrust or moment is listed.

Table 3.11. ABAQUS Results for Roberts Slab RB18 (L/h = 18.8)
Using Beam Elements (B22) With a Peak Capacity of 15.6 psi and a Deflection of 0.462 inches

# elem	Inc	σ_{11} (psi)	ε_{11} (in/in)	$I\varepsilon_{11}$ (in/in)	σ_{11} rebar (psi)	Load (psi)	Δ_{mid} (in)	Thrust (lb)	Remarks
Part	**One**								
2-15	29	-410(m)	-1.271E-04(m)	--	2639	-1.61	-0.027	--	Crk
	187	-1686(m)	-6.289E-04(m)	-1.069E-04	35000	-4.16	-0.186	--	Yield/Pk
Part	**Two**								
2	58	-357(s)	-1.104E-04(s)	--	1697	-3.22	-0.011	+7.45	Crk (s)
	92	-571(s)	-1.762E-04(s)	--	2596	-4.78	-0.018	-237	Crk (m)
	935	-2801(m)	-1.702E-03(m)	-8.379E-04	35000	-17.4	-0.216	-19612	Yield
	1252	-3000(m)	-2.348E-03(m)	-1.422E-03	35000	-18.7	-0.294	-23188	
	1299	-3000(s)	-2.445E-03(m)	-1.521E-03	35000	-18.8	-0.306	-23549	
	1487	-2947(s)	-2.851E-03(m)	-1.959E-03	35000	-18.9	-0.352	-24826	Pk
	1880	-2640(m)	-3.769E-03(m)	-3.007E-03	35000	-18.1	-0.452	-26102	Pk Thrust
3	51	-358(s)	-1.108E-04(s)	--	1525	-2.83	-0.009	+5.91	Crk (s)
	94	-678(s)	-2.101E-04(s)	--	2604	-4.64	-0.018	-374	Crk (m)
	1043	-2984(s)	-2.163E-03(s)	-1.239E-03	35000	-16.6	-0.229	-21186	Yield
	1122	-3000(s)	-2.346E-03(s)	-1.417E-03	35000	-16.9	-0.247	-22107	
	1263	-3000(m)	-2.712E-03(s)	-1.801E-03	35000	-17.2	-0.281	-23312	
	1463	-2915(m)	-3.227E-03(s)	-2.387E-03	35000	-17.4	-0.329	-24498	Pk
	1806	-2473(m)	-4.130E-03(m)	-3.401E-03	35000	-16.6	-0.413	-25390	Pk Thrust
5	47	-363(s)	-1.124E-04(s)	--	1418	-2.61	-0.009	+4.42	Crk (s)
	97	-822(s)	-2.454E-04(s)	--	2581	-4.53	-0.019	-512	Crk (m)
	908	-3000(s)	-2.351E-03(s)	-1.422E-03	26030	-14.5	-0.188	-19586	
	1178	-2922(m)	-3.199E-03(s)	-2.355E-03	35000	-15.8	-0.245	-22441	Yield
	1319	-3000(m)	-3.673E-03(s)	-2.889E-03	35000	-16.1	-0.276	-23797	
	1411	-2971(m)	-3.999E-03(s)	-3.254E-03	35000	-16.2	-0.297	-24450	Pk
	1585	-2701(m)	-4.769E-03(s)	-4.110E-03	35000	-15.9	-0.338	-24782	Pk Thrust
7	45	-361(s)	-1.119E-04(s)	--	1361	-2.49	-0.009	+4.45	Crk (s)
	103	-987(s)	-3.057E-04(s)	--	2566	-4.46	-0.020	-773	Crk (m)
	778	-3000(s)	-2.350E-03(s)	-1.421E-03	19411	-13.1	-0.156	-17544	
	1239	-2922(m)	-4.313E-03(s)	-3.605E-03	35000	-15.4	-0.250	-22462	Yield
	1370	-3000(m)	-4.947E-03(s)	-4.308E-03	35000	-15.5	-0.279	-23490	
	1396	-2996(m)	-5.082E-03(s)	-4.456E-03	35000	-15.5	-0.285	-23638	Pk
	1401	-2995(m)	-5.116E-03(s)	-4.494E-03	35000	-15.5	-0.286	-23640	Pk Thrust
10	44	-364(s)	-1.127E-04(s)	--	1333	-2.44	-0.008	+4.23	Crk (s)
	157	-1593(s)	-5.467E-04(s)	-5.354E-05	2355	-3.96	-0.029	-3542	Crk (m)
	663	-3000(s)	-2.326E-03(s)	-1.397E-03	15253	-11.7	-0.129	-15896	
	1275	-2898(m)	-6.197E-03(s)	-5.672E-03	35000	-14.5	-0.251	-21777	Yield
	1295	-2921(m)	-6.343E-03(s)	-5.830E-03	35000	-14.5	-0.255	-21912	Pk/Thrust
	1460	-3000(m)	-8.205E-03(s)	-7.827E-03	35000	-14.0	-0.290	-21612	
15	102	-1190(s)	-3.683E-04(s)	--	2096	-3.64	-0.017	-829	Attempts

Table 3.12. ABAQUS Results for Roberts Slab RB22 (L/h = 18.8) Using Beam Elements (B22) With a Peak Capacity of 18.5 psi and a Deflection of 0.45 inches

# elem	Inc	σ_{11} (psi)	ε_{11} (in/in)	$I\varepsilon_{11}$ (in/in)	σ_{11} rebar (psi)	Load (psi)	Δ_{mid} (in)	Thrust (lb)	Remarks
Part	**One**								
2-15	34	-472(m)	-1.402E-04(m)	--	2802	-1.89	-0.029	--	Crk
	235	-2070(m)	-7.549E-04(m)	-1.408E-04	35000	-6.01	-0.219	--	Yield/Pk
Part	**Two**								
2	65	-380(s)	-1.127E-04(s)	--	1723	-3.61	-0.012	+7.87	Crk (s)
	107	-629(s)	-1.866E-04(s)	--	2716	-5.49	-0.019	-323	Crk (m)
	1193	-3386(m)	-2.070E-03(m)	-1.066E-03	35000	-22.1	-0.255	-24272	Yield
	1451	-3500(m)	-2.570E-03(m)	-1.531E-03	35000	-22.9	-0.313	-27135	
	1632	-3500(s)	-2.930E-03(m)	-1.908E-03	35000	-23.2	-0.355	-28497	
	1688	-3496(s)	-3.044E-03(m)	-2.031E-03	35000	-23.3	-0.369	-28847	Pk
	2674	-2911(s)	-5.515E-03(m)	-4.883E-03	35000	-19.8	-0.601	-30805	Pk Thrust
3	57	-379(s)	-1.125E-04(s)	--	1540	-3.17	-0.010	+6.5	Crk (s)
	109	-747(s)	-2.216E-04(s)	--	2696	-5.30	-0.020	-485	Crk (m)
	1371	-3497(s)	-2.479E-03(m)	-1.442E-03	35000	-20.8	-0.277	-26303	Yield
	1415	-3500(s)	-2.569E-03(s)	-1.531E-03	35000	-20.9	-0.287	-26765	
	1520	-3500(m)	-2.783E-03(s)	-1.750E-03	35000	-21.2	-0.310	-27832	
	1717	-3407(m)	-3.185E-03(s)	-2.197E-03	35000	-21.4	-0.354	-29459	Pk
	2368	-2931(m)	-5.325E-03(m)	-4.667E-03	35000	-18.8	-0.503	-30894	Pk Thrust
5	52	-381(s)	-1.130E-04(s)	--	1418	-2.89	-0.009	+5.4	Crk (s)
	116	-939(s)	-2.787E-04(s)	--	2673	-5.15	-0.021	-796	Crk (m)
	1125	-3500(s)	-2.570E-03(s)	-1.531E-03	24978	-17.7	-0.215	-23554	
	1529	-3473(m)	-3.730E-03(s)	-2.834E-03	35000	-19.6	-0.293	-27041	Yield
	1626	-3500(m)	-4.027E-03(s)	-3.178E-03	35000	-19.7	-0.313	-27899	
	1778	-3462(m)	-4.495E-03(s)	-3.719E-03	35000	-19.8	-0.346	-29031	Pk
	2015	-3425(m)	-5.087E-03(s)	-4.396E-03	35000	-19.3	-0.389	-29929	Pk Thrust
7	50	-381(s)	-1.130E-04(s)	--	1367	-2.78	-0.009	+5.2	Crk (s)
	133	-1247(s)	-3.699E-04(s)	--	2616	-4.92	-0.024	-1585	Crk (m)
	988	-3500(s)	-2.568E-03(s)	-1.530E-03	20506	-16.3	-0.183	-22149	
	1594	-3466(m)	-5.054E-03(s)	-4.359E-03	35000	-18.9	-0.297	-26721	Yield
	1686	-3500(m)	-5.467E-03(s)	-4.828E-03	35000	-18.9	-0.315	-27372	
	1707	-3497(m)	-5.565E-03(s)	-4.939E-03	35000	-19.0	-0.319	-27507	Pk
	1848	-3475(m)	-6.267E-03(s)	-5.729E-03	35000	-18.7	-0.349	-28097	Pk Thrust
10	48	-376(s)	-1.115E-04(s)	--	1315	-2.66	-0.009	+5.3	Crk (s)
	187	-1823(s)	-5.728E-04(s)	-3.199E-05	2422	-4.55	-0.032	-4326	Crk (m)
	840	-3500(s)	-2.568E-03(s)	-1.530E-03	16143	-14.5	-0.151	-19896	
	1626	-3422(m)	-7.369E-03(s)	-6.954E-03	35000	-17.6	-0.294	-25410	Yield
	1631	-3428(m)	-7.404E-03(s)	-6.993E-03	35000	-17.7	-0.296	-25436	Pk
	1679	-3479(m)	-7.740E-03(s)	-7.361E-03	35000	-17.6	-0.305	-25694	Pk Thrust
	2083	-3500(m)	-1.389E-02(s)	-1.385E-02	35000	-14.0	-0.384	-19167	
12	48	-381(s)	-1.129E-04(s)	--	1315	-2.67	-0.009	+5.0	Crk (s)
	197	-1923(s)	-6.466E-04(s)	-7.611E-05	2399	-4.57	-0.033	-4756	Crk (m)
	767	-3500(s)	-2.567E-03(s)	-1.529E-03	14177	-13.6	-0.136	-18631	
	1373	-3288(m)	-5.839E-03(s)	-5.248E-03	26957	-17.5	-0.246	-25651	Pk/Thrust
	1426	-3303(m)	-6.552E-03(s)	-6.048E-03	28213	-17.3	-0.252	-24979	Time Inc

Table 3.13. ABAQUS Results for Roberts Slab RB11 (L/h = 28.3)
Using Beam Elements (B22) With a Peak Capacity of 5.1 psi and a Deflection of 0.506 inches

# elem	Inc	σ_{11} (psi)	ε_{11} (in/in)	$I\varepsilon_{11}$ (in/in)	σ_{11} rebar (psi)	Load (psi)	Δ_{mid} (in)	Thrust (lb)	Remarks
Part	**One**								
2-15	13	-422(m)	-1.324E-04(m)	--	2383	-0.72	-0.043	--	Crk
	80	-1660(m)	-6.121E-04(m)	-9.188E-05	35000	-1.57	-0.269	--	Yield/Pk
Part	**Two**								
2	26	-372(s)	-1.167E-04(s)	--	1529	-1.44	-0.017	+10.4	Crk (s)
	41	-590(s)	-1.849E-04(s)	--	2319	-2.11	-0.028	-157	Crk (m)
	407	-2779(m)	-1.685E-03(m)	-8.126E-04	35000	-6.31	-0.327	-11817	Yield
	529	-2987(m)	-2.194E-03(m)	-1.258E-03	35000	-6.49	-0.429	-13767	Pk
	569	-3000(m)	-2.360E-03(m)	-1.420E-03	35000	-6.47	-0.464	-14302	
	952	-2596(s)	-4.000E-03(m)	-3.246E-03	35000	-4.96	-0.791	-16051	Pk Thrust
3	23	-375(s)	-1.176E-04(s)	--	1377	-1.27	-0.015	+8.1	Crk (s)
	41	-686(s)	-2.153E-04(s)	--	2264	-2.01	-0.028	-231	Crk (m)
	434	-2946(s)	-2.028E-03(m)	-1.105E-03	35000	-5.87	-0.330	-12536	Yield
	506	-3000(s)	-2.341E-03(s)	-1.401E-03	35000	-5.99	-0.388	-13798	
	519	-2998(s)	-2.396E-03(s)	-1.456E-03	35000	-6.00	-0.399	-13991	Pk
	554	-3000(m)	-2.548E-03(s)	-1.613E-03	35000	-5.98	-0.427	-14544	
	838	-2487(m)	-3.992E-03(m)	-3.236E-03	35000	-4.95	-0.663	-16099	Pk Thrust
5	21	-377(s)	-1.183E-04(s)	--	1269	-1.16	-0.014	+7.2	Crk (s)
	42	-827(s)	-2.593E-04(s)	--	2231	-1.97	-0.028	-303	Crk (m)
	395	-3000(s)	-2.356E-03(s)	-1.416E-03	28738	-5.30	-0.283	-11955	
	497	-2880(m)	-2.991E-03(s)	-2.107E-03	35000	-5.60	-0.357	-13709	Yield
	581	-3000(m)	-3.499E-03(s)	-2.683E-03	35000	-5.60	-0.420	-14700	Pk
	680	-2800(m)	-4.490E-03(s)	-3.793E-03	35000	-5.11	-0.539	-15799	Pk Thrust
7	20	-373(s)	-1.171E-04(s)	--	1212	-1.11	-0.013	+7.07	Crk (s)
	44	-977(s)	-3.065E-04(s)	--	2197	-1.93	-0.294	-441	Crk (m)
	325	-3000(s)	-2.338E-03(s)	-1.398E-03	21099	-4.83	-0.225	-10369	
	527	-2900(m)	-4.000E-03(s)	-3.245E-03	35000	-5.45	-0.369	-13845	Pk/Yield
	595	-3000(m)	-4.619E-03(s)	-3.935E-03	35000	-5.38	-0.418	-14481	
	652	-2910(m)	-5.490E-03(s)	-4.895E-03	35000	-5.08	-0.486	-15029	Pk Thrust
10	19	-365(s)	-1.144E-04(s)	--	1154	-1.05	-0.013	+7.00	Crk (s)
	67	-1610(s)	-5.618E-04(s)	-5.935E-05	1895	-1.67	-0.043	-2181	Crk (m)
	272	-3000(s)	-2.341E-03(s)	-1.401E-03	13260	-4.42	-0.183	-9225	
	491	-2806(m)	-4.741E-03(s)	-4.071E-03	31956	-5.25	-0.335	-13246	Pk
	534	-2869(m)	-5.524E-03(s)	-4.932E-03	35000	-5.21	-0.365	-13380	Yield
	605	-3000(m)	-6.644E-03(s)	-6.148E-03	35000	-5.04	-0.416	-13912	
	612	-2996(m)	-6.751E-03(s)	-6.264E-03	35000	-5.01	-0.422	-13973	Pk Thrust

Table 3.14. ABAQUS Results for Roberts Slab RB15 (L/h = 28.3)
Using Beam Elements (B22) With a Peak Capacity of 5.9 psi and a Deflection of 0.507 inches

# elem	Inc	σ_{11} (psi)	ε_{11} (in/in)	$I\varepsilon_{11}$ (in/in)	σ_{11} rebar (psi)	Load (psi)	Δ_{mid} (in)	Thrust (lb)	Remarks
Part	**One**								
2-15	14	-448(m)	-1.406E-04(m)	--	2434	-0.77	-0.044	--	Crk
	108	-1886(m)	-7.876E-04(m)	-1.964E-04	35000	-2.33	-0.356	--	Yield/Pk
Part	**Two**								
2	26	-355(s)	-1.113E-04(s)	--	1445	-1.44	-0.017	+11.2	Crk (s)
	42	-576(s)	-1.806E-04(s)	--	2231	-2.16	-0.028	-163	Crk (m)
	507	-2964(m)	-2.075E-03(m)	-1.146E-03	35000	-7.15	-0.393	-13304	Yield
	546	-2996(m)	-2.257E-03(m)	-1.318E-03	35000	-7.17	-0.425	-13919	Pk
	568	-3000(m)	-2.360E-03(m)	-1.420E-03	35000	-7.16	-0.443	-14237	
	701	-3000(s)	-3.021E-03(m)	-2.141E-03	35000	-6.89	-0.554	-15574	
	841	-2958(s)	-3.766E-03(m)	-2.983E-03	35000	-6.26	-0.671	-16164	Pk Thrust
3	23	-357(s)	-1.121E-04(s)	--	1301	-1.27	-0.015	+8.7	Crk (s)
	43	-688(s)	-2.156E-04(s)	--	2217	-2.09	-0.028	-265	Crk (m)
	561	-3000(s)	-2.360E-03(m)	-1.419E-03	34484	-6.55	-0.411	-14140	
	570	-2998(s)	-2.392E-03(s)	-1.452E-03	35000	-6.56	-0.418	-14236	Yield
	572	-2998(s)	-2.399E-03(s)	-1.460E-03	35000	-6.57	-0.419	-14265	Pk
	597	-3000(m)	-2.492E-03(s)	-1.554E-03	35000	-6.55	-0.439	-14616	
	808	-2745(m)	-3.768E-03(m)	-2.985E-03	35000	-5.86	-0.610	-16077	Pk Thrust
5	21	-359(s)	-1.127E-04(s)	--	1199	-1.16	-0.014	+7.4	Crk (s)
	45	-851(s)	-2.667E-04(s)	--	2174	-2.02	-0.028	-408	Crk (m)
	422	-3000(s)	-2.359E-03(s)	-1.418E-03	22817	-5.64	-0.291	-12257	
	637	-2998(m)	-3.552E-03(s)	-2.742E-03	35000	-6.13	-0.442	-14744	Pk/Yield
	646	-3000(m)	-3.599E-03(s)	-2.796E-03	35000	-6.12	-0.448	-14849	
	787	-2916(m)	-4.355E-03(s)	-3.642E-03	35000	-5.65	-0.559	-15594	Pk Thrust
7	20	-356(s)	-1.116E-04(s)	--	1145	-1.11	-0.013	+7.2	Crk (s)
	50	-1089(s)	-3.415E-04(s)	--	2125	-1.96	-0.032	-738	Crk (m)
	350	-3000(s)	-2.360E-03(s)	-1.420E-03	15951	-5.12	-0.233	-10799	
	674	-2999(m)	-4.693E-03(s)	-4.018E-03	34981	-5.93	-0.454	-14975	Pk
	678	-3000(m)	-4.732E-03(s)	-4.061E-03	35000	-5.92	-0.457	-14992	Yield
	713	-2994(m)	-5.094E-03(s)	-4.461E-03	35000	-5.82	-0.484	-15070	Pk Thrust
10	20	-367(s)	-1.151E-04(s)	--	1147	-1.11	-0.013	+6.8	Crk (s)
	72	-1626(s)	-5.822E-04(s)	-7.257E-05	1852	-1.73	-0.045	-2360	Crk (m)
	289	-3000(s)	-2.362E-03(s)	-1.422E-03	12032	-4.61	-0.187	-9584	
	654	-2989(m)	-5.709E-03(s)	-5.135E-03	31891	-5.76	-0.430	-15051	Pk/Thrust
	676	-3000(m)	-6.241E-03(s)	-5.712E-03	33566	-5.70	-0.444	-14756	
	697	-2954(m)	-7.005E-03(s)	-6.536E-03	35000	-5.50	-0.453	-13777	Yield
12	19	-352(s)	-1.102E-04(s)	--	1090	-1.06	-0.012	+6.8	Crk (s)
	75	-1712(s)	-6.556E-04(s)	-1.189E-04	1802	-1.72	-0.046	-2577	Crk (m)
	260	-3000(s)	-2.360E-03(s)	-1.421E-03	10282	-4.34	-0.166	-8896	
	642	-2978(m)	-6.406E-03(s)	-5.891E-03	30558	-5.67	-0.417	-14966	Pk/Thrust
	665	-2978(m)	-6.691E-03(s)	-6.198E-03	31142	-5.62	-0.421	-14736	Time Inc

Table 3.15. ABAQUS Results for Roberts Slabs RB18 (L/h = 18.8) and RB11 (L/h = 28.3) Using 7/10 Continuum Elements (C3D20) With a Peak Capacity of 15.6 psi and Deflection of 0.462 inches for RB18 and a Peak Capacity of 5.1 psi and a Deflection of 0.506 inches for RB11

Restraint	Inc	σ_{11} (psi)	ε_{11} (in/in)	$I\varepsilon_{11}$ (in/in)	σ_{11} rebar (psi)	Load (psi)	Δ_{mid} (in)	Thrust or * Moment (lb) or (in-lb)	Remarks
L_{full}	28	-327(s)	-9.121E-05(s)	--	1521	-2.79	-0.009	-3.94	Crk (s)
R_{full}	111	-899(s)	-2.478E-04(s)	--	3455	-5.87	-0.037	-3705	Crk (m)
RB18(7)	496	-2450(m)	-1.079E-03(m)	-3.598E-04	21291	-14.7	-0.159	-19050	Time Inc
L_{full}	27	-324(s)	-9.053E-05(s)	--	1476	-2.70	-0.009	-1.81	Crk (s)
R_{full}	134	-893(s)	-2.585E-04(m)	--	3462	-5.94	-0.044	-5549	Crk (m)
RB18(10)	518	-2495(s)	-1.095E-03(s)	-3.702E-04	21159	-14.3	-0.164	-19696	Unloading
L_{full}	13	-350(s)	-9.724E-05(s)	--	1395	-1.29	-0.015	+1.35	Crk (s)
R_{full}	43	-841(s)	-2.323E-04(s)	--	2806	-2.46	-0.048	-1789	Crk (m)
RB11(7)	240	-2300(m)	-9.544E-04(m)	-2.752E-04	18107	-5.50	-0.216	-10714	Unloading
L_{full}	12	-355(s)	-9.332E-05(s)	--	1302	-1.19	-0.014	+6.00	Crk (s)
R_{full}	56	-847(s)	-2.447E-04(m)	--	2782	-2.48	-0.062	-3337	Crk (m)
RB11(10)	221	-2453(s)	-1.043E-03(s)	-3.325E-04	19775	-5.5	-0.237	-11422	Time Inc
* If the restraint (lateral or rotational) was fully rigid, the generated thrust or moment is listed.									

Table 3.16. Summary of ABAQUS Results at Peak Capacity
Using Beam Elements (B22) Except as Noted

L/h	# Elem	σ_{11} (psi)	ε_{11} (in/in)	σ_{11} rebar (psi)	Load EXP (psi)	Load FE (psi)	Δ_{mid} EXP (in)	Δ_{mid} FE (in)	Thrust (lb)
4.4	10	-5239(m)	-5.356E-03(s)	41280	-557	-699	-0.41	-0.030	-183390
8	10	-3674(m)	-5.331E-03(s)	43729	-68.8	-103	-0.84	-0.041	-68670
10.4	7	-4128(m)	-5.211E-03(s)	45450	-52.0	-81.5	-0.79	-0.062	-61486
14.8	7	-4576(m)	-5.101E-03(s)	43803	-27.5	-39.1	-0.81	-0.085	-42784
18.8[1]	7	-2996(m)	-5.082E-03(s)	35000	-15.6	-15.5	-0.46	-0.285	-23638
18.8[2]	7	-3497(m)	-5.565E-03(s)	35000	-18.5	-19.0	-0.45	-0.319	-27507
28.3[3]	5	-2800(m)	-4.490E-03(s)	35000	-5.1	-5.11	-0.51	-0.539	-15799
28.3[4]	7	-2999(m)	-4.693E-03(s)	34981	-5.9	-5.93	-0.51	-0.454	-14975
18.8[5]	10	-2495(s)	-1.095E-03(s)	21159	-15.6	-14.3	-0.46	-0.164	-19696
28.3[6]	10	-2453(s)	-1.043E-03(s)	19775	-5.1	-5.50	-0.51	-0.237	-11422

1 Roberts Slab RB18 ($\rho = 0.578$).
2 Roberts Slab RB22 ($\rho = 0.924$).
3 Roberts Slab RB11 ($\rho = 0.556$).
4 Roberts Slab RB15 ($\rho = 0.926$).
5 Roberts Slab RB18 using Continuum elements.
6 Roberts Slab RB11 using Continuum elements.

Table 3.17. Summary of ABAQUS Results at Peak Capacity Using Beam Elements (B22) With Springs and Continuum Elements (C3D20/R) With/Without Springs

Restraint	L/h - [1] Elem Type	σ_{11} (psi)	ε_{11} (in/in)	σ_{11} rebar (psi)	σ_{spr} (lb/ rad)	ϕ_{spr} (rad)	σ_{spl} (lb/in)	ϕ_{spl} (in)	Load[2] (psi)	Δ_{mid}[2] (in)	Thrust (-) or Moment (lb) or (in-lb)
L/R1E8	8-B	-3487(s)	-1.595E-03(s)	39093	61758	6.175E-04	30737	3.073E-04	-66.8	-0.023	--
L_{full}/R_{full}	8-C	-4449(s)	-1.222E-03(s)	26291	--	--	--	--	-121	-0.036	-65052
$L2E6/R_{full}$	8-CR	-1793(s)	-4.324E-04(s)	55750	--	--	34354	1.717E-02	-68.0	-0.044	19597
L1E7/R1E8	10.4-B	-4398(m)	-6.139E-03(s)	50000	64591	6.459E-04	45312	4.531E-03	-70.4	-0.083	--
L4.6E6/R9.7E7	10.4-B	-4497(s)	-2.849E-03(s)	50000	44447	4.582E-04	20567	4.471E-03	-49.7	-0.054	--
L_{full}/R_{full}	10.4-CR	-2763(s)	-6.599E-04(s)	50000	--	--	--	--	-77.3	-0.047	-58582
$L1E6/R_{full}$	10.4-CR	-1952(s)	-4.603E-04(s)	50000	--	--	27837	2.783E-02	-51.5	-0.082	14824
L6E7/R2E7	14.8-B	-4122(s)	-1.445E-03(s)	64251	26763	1.338E-03	18583	3.097E-04	-26.3	-0.046	--
L_{full}/R_{full}	14.8-CR	-3863(s)	-3.809E-05(s)	67330	--	--	--	--	-46.4	-0.089	-56301
$L6E6/R_{full}$	14.8-CR	-1995(s)	-4.633E-04(s)	63271	--	--	22905	3.817E-03	-27.1	-0.050	7811

[1] B- beam element, C - continuum element, CR- continuum element with reduced integration.

[2] Experimental load capacity and deflection: L/h = 8, Load = 68.8 psi, Δ_{mid} = 0.835 inches
L/h = 10.4, Load = 52.0 psi, Δ_{mid} = 0.798 inches
L/h = 14.8, Load = 27.5 psi, Δ_{mid} = 0.805 inches

Table 3.18. Peak Thrust Comparison

Peak Thrust Using 7 Beam Elements	Inc	σ_{11} (psi)	ε_{11} (in/in)	$I\varepsilon_{11}$ (in/in)	σ_{11} rebar (psi)	Load (psi)	Δ_{mid} (in)	**Thrust (lb)**	Remarks
ρ = 0.52, L/h = 10.4	6079	-4128(m)	-5.211E-03(s)	-4.635E-03	45450	-81.5	-0.062	**-61486**	Pk/Pk Thrust
ρ = 0.58, L/h = 14.8	1219	-4576(m)	-5.101E-03(s)	-4.803E-03	43803	-39.1	-0.085	**-42784**	Pk Thrust
ρ = 0.578, L/h = 18.8	1401	-2995(m)	-5.116E-03(s)	-4.494E-03	35000	-15.50	-0.286	**-23640**	Pk Thrust
ρ = 0.924, L/h = 18.8	1848	-3475(m)	-6.267E-03(s)	-5.729E-03	35000	-18.7	-0.349	**-28097**	Pk Thrust
ρ = 0.556, L/h = 28.3	652	-2910(m)	-5.490E-03(s)	-4.895E-03	35000	-5.08	-0.486	**-15029**	Pk Thrust
ρ = 0.926, L/h = 28.3	713	-2994(m)	-5.094E-03(s)	-4.461E-03	35000	-5.82	-0.484	**-15070**	Pk Thrust

Table 3.19. Approximate Length of Reinforcement Yielding at the Supports and Midspan

L/h	d (in)	h (in)	L_p (in)	Location
4.4	4.8	5.5	0.6	spt
4.4	4.8	5.5	did not yield	midspan
8	2.4	3.0	0.5	spt
8	2.4	3.0	4.0	midspan
10.4	1.9375	2.3125	0.45	spt
10.4	1.9375	2.3125	4.0	midspan
14.8	1.25	1.625	1.6	spt
14.8	1.25	1.625	did not yield	midspan
18.8[1]	3.0	2.66	no rebar	spt
18.8	3.0	2.66	7.0	midspan
28.3	2.0	1.66	no rebar	spt
28.3	2.0	1.66	7.0	midspan

[1] With the section doubly-reinforced, the amount of yielding at midspan did not change and the yielding at the supports was out to 0.5 inches.

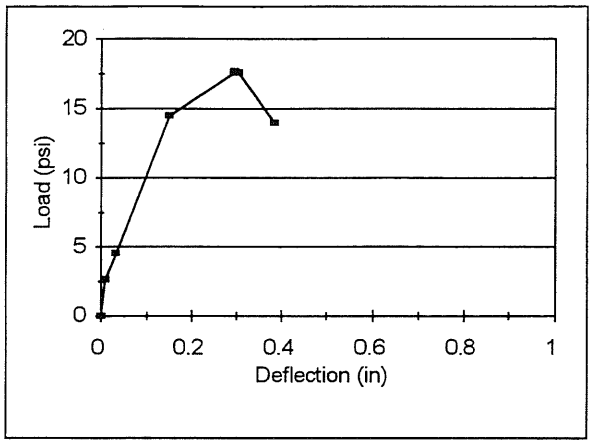

Figure 3.1. Load-Deflection Results From Finite Element Analysis for Roberts Slab RB22 (L/h = 18.8)

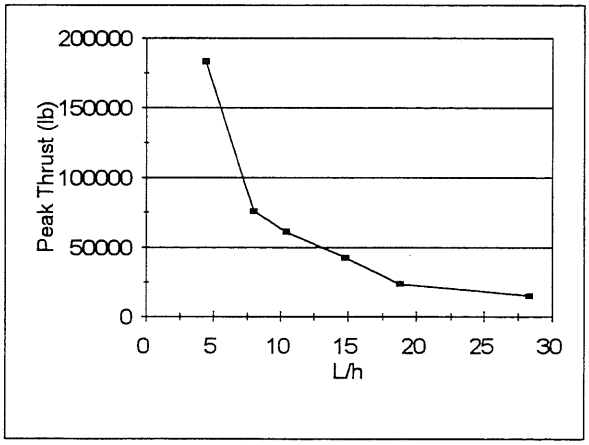

Figure 3.2. Peak Thrust (Finite Element Analysis) Versus L/h

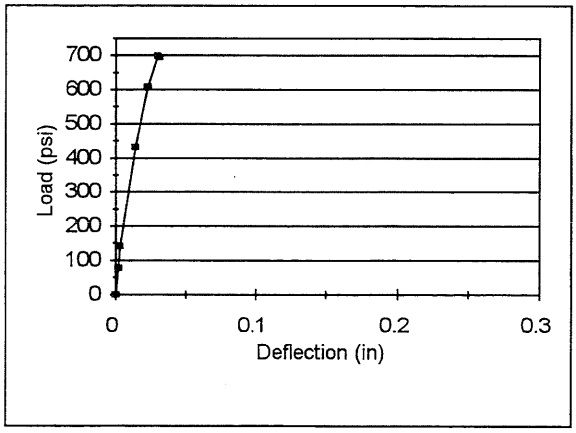

Figure 3.3. Load-Deflection Results From Finite Element Analysis for Woodson Slab (L/h = 4.4)

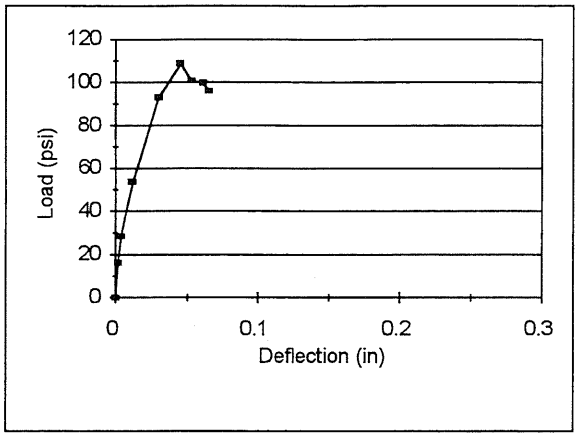

Figure 3.4. Load-Deflection Results From Finite Element Analysis for Woodson Slab (L/h = 8)

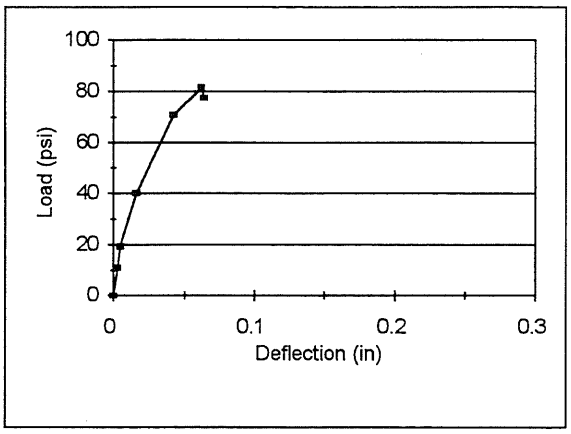

Figure 3.5. Load-Deflection Results From Finite Element Analysis for Guice Slab (L/h = 10.4)

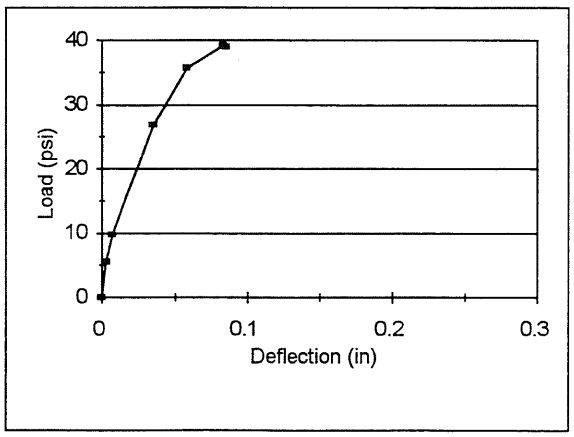

Figure 3.6. Load-Deflection Results From Finite Element Analysis for Guice Slab (L/h = 14.8)

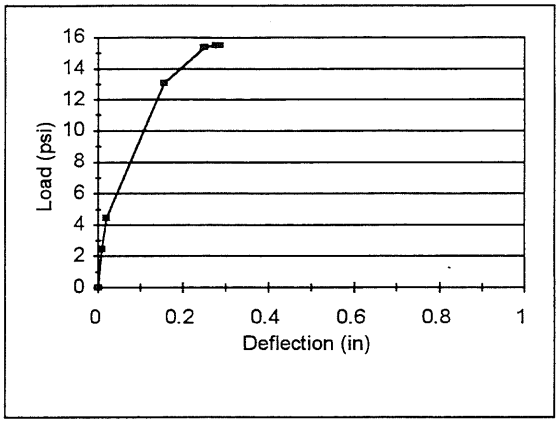

Figure 3.7. Load-Deflection Results From Finite Element Analysis for Roberts Slab RB18 (L/h = 18.8)

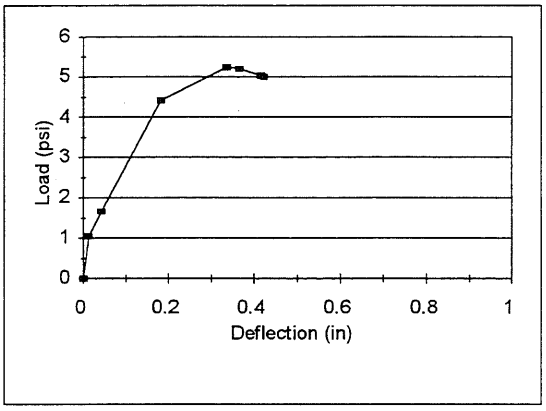

Figure 3.8. Load-Deflection Results From Finite Element Analysis for Roberts Slab RB11 (L/h = 28.3)

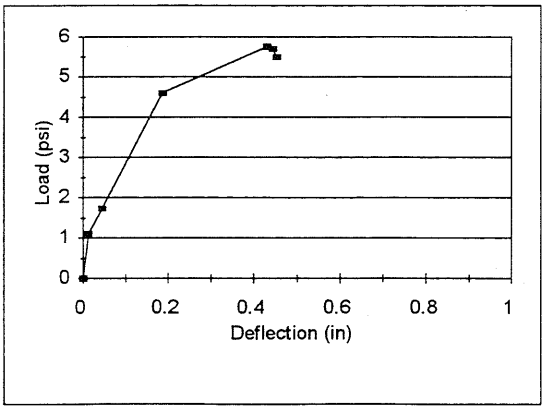

Figure 3.9. Load-Deflection Results From Finite Element Analysis for Roberts Slab RB15 (L/h = 28.3)

CHAPTER 4

AN ENHANCED MEMBRANE THEORY

4.1. Introduction

In Chapter 2, the author presented a comprehensive summary of previous experiments and analytical work, which served to show what had, and had not, been investigated, to compare the different compressive membrane theories, and to highlight research results which led to this current study on membrane behavior, i.e., that the peak thrust occurred right after the peak load capacity and that the concrete compressive strain at peak capacity exceeded 0.003 in/in. In Chapter 3, the author summarized an exhaustive finite element method investigation which was only partially successful in arriving at a better definition of laterally restrained slab behavior. However, the analysis did show that the peak thrust occurs nearly simultaneously with the peak load capacity, that the concrete compressive strain in the hinge regions at peak capacity greatly exceeded the ACI (1995) maximum value of 0.003 in/in (i.e., 0.005 - 0.01 in/in), and that the slab behavior at peak capacity is controlled by the type of instability which occurs, i.e., material instability for thick slabs ($L/h < 18$) and geometric instability for thin slabs ($L/h > 18$). The finite element analysis did fail to generate, for thick slabs, a defined peak capacity and a midspan deflection within an order of magnitude, while also failing to delineate a complete load-deflection curve for thick or thin slabs. Here in Chapter 4, these findings are brought together by the author in an effort to develop a membrane behavioral model that more fully depicts the entire load-deflection curve for a laterally restrained reinforced concrete one-way slab, with the focus on peak capacity prediction.

Few researchers have tried to predict the entire load-deflection curve. Most focus on estimating either the peak compressive membrane capacity or the ultimate tensile membrane capacity. The complete load-deflection curve is usually needed to perform any type of dynamic analysis. In order to predict the entire load-deflection curve, the capacity and deflection at Points B, C, and D in Figure 4.1 are required. A compressive membrane theory is developed herein in which the calculated value for the peak thrust is used to point to (i.e., to index) the peak capacity.

This peak capacity is paired with a curvature based midspan deflection to establish Point B. Since it is generally recognized by many researchers that Point C and D lie along the tensile membrane curve, a capacity (i.e., Point C) or a deflection (i.e., Point D) estimate is used to calculate the corresponding deflection or capacity with Park's (1964) tensile membrane theory. Point C is defined through an appropriate yield line capacity, while Point D is located with an incipient collapse deflection. Upon determining Points B, C, and D, the load-deflection curve consists of three sections: 1) a roughly parabolic curve representing the ascending curve from Point A to B (Figure 4.1); 2) a roughly parabolic curve representing the descending curve from Point B until intersection with the tensile membrane curve at Point C (Figure 4.1); and 3) a linear tensile membrane curve for one-way slabs between Points C and D (Figure 4.1).

Numerous researchers listed in Chapter 2 used Park's derivations (1964-1965) as either their starting point or for comparison purposes. Even recent WES experiments of laterally restrained reinforced concrete one-way slabs were analyzed through use of Park and Gamble's (1980) compressive and tensile membrane theories which incorporate many of the important contributions listed in Chapter 2. In this dissertation Park and Gamble's compressive membrane theory also is used for comparison purposes, and their basic definition of the problem is used as the starting point for the development of a modified compressive membrane theory. When using the currently popular method of indexing the peak capacity with a midspan deflection estimate, or within this dissertation using the experimentally measured midspan deflections listed in Appendix A, the peak load capacity prediction using a modified compressive membrane theory was closer to the experimental peak capacity than Park and Gamble's compressive membrane theory, especially for the thin slabs.

The research reported herein has shown that the peak thrust indexes in the compressive membrane theories an even closer approximation of the experimental peak capacity than using the current deflection index method. In this dissertation, the word "index" is used to reference or point to another value, which in this case is calculated simultaneously. For example, for every increment of the deflection within the compressive membrane theory, an associated thrust and capacity, as

well as other important variables, are calculated. At an increment of deflection which matches the experimentally measured midspan deflection, or when the thrust has peaked, the associated capacity is "indexed" by these values. The use of the peak thrust to index the peak capacity reflects the results of the finite element analysis of Chapter 3, where it is noted that the peak thrust occurred either simultaneously with, or slightly after, the peak capacity. Since the thrust is already an integral calculation within the compressive membrane theory, indexing the peak capacity with the peak thrust eliminates the necessity of first, estimating a midspan deflection, and then using that deflection to index the peak capacity. Even though the peak deflection is eventually estimated for use in defining the load-deflection curve, the peak midspan deflection is difficult to estimate (i.e., large standard deviation) when the experimental deflection data are lacking. The peak capacity prediction is more accurate when using the peak thrust as the index, and is, on average, slightly smaller than the experimentally measured peak capacity.

For the engineer in the field, the most important assessment of a slab's predicted performance is usually the peak compressive membrane capacity. The peak thrust indexed capacity provides a superb peak capacity prediction if the engineer has a computer available. However, it is not always possible to have a computer in the field, nor can the analyst always wait until returning to the office. In some instances, such as in military targeting missions, a calculator may be the only tool available to the engineer. The basic equations inherent within axial force-moment interaction and an experimentally developed ratio were successfully used, as developed herein, to provide the field engineer with a simple method for estimating the peak compressive membrane capacity. Most civil engineers are familiar with the basic axial force-moment interaction equations since they used them in their first concrete design course. The experimentally based ratio, T/P_o, relates the compressive thrust (T) used in the axial force-moment interaction equations to the cross section's ultimate axial force capacity (P_o). The thrust enhanced moments at midspan and the supports determined through the axial force-moment interaction equation can be substituted into the fundamental yield line equation to estimate the peak load capacity. The

accuracy of this simple method for predicting peak capacities is remarkable, with the average predicted peak load capacity being slightly larger than the experimentally measured peak capacity.

The derivations and summarized results that support the findings are presented in the expanded discussion within the following sections: Section 4.2, the peak compressive membrane load capacity predictions (Point B, Figure 4.1); Section 4.3, the peak compressive membrane capacity deflection estimates (Point B, Figure 4.1); Section 4.4, the tensile membrane capacity at Points C and D (Figure 4.1); Section 4.5, the development of the complete load-deflection curve; and Section 4.6, the simple estimate for the peak compressive membrane load capacity. The detailed tables summarized in Sections 4.2 - 4.6 are available in Appendix D.

4.2. Compressive Membrane Behavior

A slowly applied uniform load produces elastic, then elastic-plastic, deflections in a one-way slab until plastic hinges form first at the supports, and then at midspan, producing a three-hinge yield line pattern (Figure 1.3). The deflections change the slab geometry causing the slab edges to rotate and move outward against the stiff boundary (Figure 1.4). This outward movement generates in-plane compressive forces which enhance the flexural capacity at the critical sections (i.e., the hinge locations, Figure 1.2). The enhanced flexural capacity is both a function of axial force-moment interaction and a larger sectional compression zone which leads to an increased internal couple; thus, the phenomenon known as compressive membrane behavior.

Park and Gamble's compressive membrane theory, which is sometimes referred to as the modified rigid-plastic or deformation theory, actually defines only the plastic theory portion of the load-deflection behavior at the peak compressive membrane capacity (Point B, Figure 4.1). Some engineers actually use the entire generated theoretical curve to represent the complete load-deflection history. However, the computed peak capacity of Park and Gamble's theoretical compressive membrane curve (CMC) usually occurs at a smaller deflection than the peak capacity of the experimental curve (Exp, Figure 4.2), because the theory does not take into account the additional plastic rotation possible during biaxial/triaxial stress conditions at the supports (among

various possible causes). Additionally, the experimental post-peak behavior is usually steeper than predicted by the rigid-plastic theoretical post-peak curve (Figure 4.2). Occasionally, the theoretical curve will even drop below zero capacity, as mentioned in Chapter 2 by Braestrup (1980), before eventually showing an increase in resistance (Figure 4.3). Review of the assumptions and initial conditions of the compressive membrane theory reaffirms the limitation of the theory to estimating only the peak capacity. The compressive membrane theory assumes full rotational and vertical edge restraint, and only partial lateral edge restraint. The ultimate goal of the theory is to establish a relationship between the incremental deflections and the uniformly distributed load, while considering the axial deformations, the lateral support movements, and the equilibrium and deformations associated with full plastic hinge rotation of the rigid-plastic slab strips at peak capacity.

Presently, both the support lateral stiffness and the peak capacity midspan deflection used within the current compressive membrane theories are very difficult to determine accurately. The techniques presented later for predicting the midspan deflection result in a large variability (i.e., large standard deviation) when compared to the experimental data. Park and others use an empirically based midspan deflection as an index for determining the peak compressive membrane capacity, while some simply use the peak computed capacity generated by the theoretical equations (i.e., the peak point on the compressive membrane curve (CMC) in Figure 4.2). When using a deflection estimate, or within this dissertation, the experimentally measured midspan deflections listed in Appendix A, to index the peak capacity, the modified compressive membrane theory derived herein provided a closer prediction of the peak capacity to the experimental peak capacity than Park and Gamble's compressive membrane theory, especially for thin slabs.

Additionally, the peak compressive thrust is adopted, rather than the peak capacity midspan deflection, to index a peak capacity which is even closer to the experimental results within both the new theory and Park and Gamble's compressive membrane theory. Since the thrust is already an integral calculation within the compressive membrane theory, indexing the peak capacity with the peak thrust eliminates the necessity of estimating a deflection to use as an index,

especially when experimental midspan deflection data are lacking. Now only the lateral support stiffness needs to be estimated. Fortunately in the area of support stiffness, a stiffness (lb/in) with a scalar magnitude on the order of 0.05 to $0.1E_c$, where E_c is the Young's Modulus of the concrete, generates membrane action close to experimentally provided rigid supports, while a support stiffness with a scalar magnitude greater than E_c provides limited additional enhancement.

4.2.1. Peak Compressive Membrane Capacity Derivation

The compressive membrane theory is developed in general terms (i.e., for four-hinge points) for a slab strip so that it can be applied in the future to possibly analyze two-way slabs comprised of orthogonal strips, which usually fail in a four-hinge mechanism. The slab strip (Figure 4.4) of length ℓ is rotationally and vertically fixed at the edge supports, but only partially restrained against lateral edge movement (t). The deflections in Figure 4.4 are exaggerated for computed purposes, i.e., they are small. The reasonableness of the boundary conditions shown in Figure 4.4 are supported by the experimental results of Guice (1986) who allowed small support rotations to coincide with a partial lateral edge restraint. His experiment demonstrated that compressive membrane behavior is not quite as sensitive to support rotations that are less than 2.0 degrees as it is to lateral movement, especially for thin slabs. Outward lateral support movement limits the development of compressive thrusts, and therefore, enhanced moment capacity. The peak compressive membrane load capacity in Guice's work was negligibly affected by support rotations limited to less than 2.0 degrees for slabs with L/h's of 10.4 and 14.8, while support rotations greater than 2.0 degrees allowed premature snap-through to tensile membrane resistance before generation of substantial compressive thrusts.

It is further assumed that the tension reinforcement has yielded, that the plastic hinges are symmetrically located, that the tension reinforcement area at both supports is identical, that the tension steel areas at the supports and midspan may be different, that the concrete tensile strength is ignored, and that the concrete has reached its ultimate compressive strength, which is defined by the ACI concrete compressive stress block (Figure 4.5). The sections between hinges are assumed

to remain straight, but can shorten due to elastic, creep and shrinkage strains (ε) which are summed and assumed constant, since the compressive membrane thrust is assumed constant along the length.

The axial shortening will decrease the middle section 2-3 (Figure 4.4) by $\varepsilon(1-2\beta)\ell$ and the end sections 1-2 and 3-4 by $\varepsilon\beta\ell$ (β defines end section length). Due to the symmetry, the edges of section 2-3 will move toward the center of the section by $0.5\varepsilon(1-2\beta)\ell$. Since the outward movement of each support is t (Figure 4.4), the horizontal distance of section 1-2 in Figure 4.4, and a close-up view in Figure 4.6, is $(1-\varepsilon)\beta\ell + 0.5\varepsilon(1-2\beta)\ell + t$. Park and Gamble (1980) used a horizontal distance of $\beta\ell + 0.5\varepsilon(1-2\beta)\ell + t$ in their derivation. Since the peak capacity deformation state is under consideration, the end portions must also shorten in the horizontal direction. For a one-way slab strip (i.e., $\beta = 0.5$), Park's equation for the length would remove axial shortening from this horizontal distance, while the new length would not.

The change in dimensions of section 1-2 due to midspan deflections, ε, and t is shown in detail in Figure 4.6. The distance from A (i.e., top of slab at the support, Figure 4.6) to B (i.e., center of midspan hinge, Figure 4.6) through geometry of the deformations is

$$\{(1-\varepsilon)\beta\ell + 0.5\varepsilon(1-2\beta)\ell + t\} \sec\phi = (h-c')\tan\phi + (1-\varepsilon)\beta\ell - c\tan\phi \qquad \text{EQN 4.1}$$

in which

ℓ is the slab length,

h is the slab thickness,

c and c' are the neutral axis depths at hinge sections 1 and 2, respectively,

ε is the axial strain,

β defines the end section length, and

ϕ is the angle formed by the slab center line with the horizontal when deforming.

The neutral axis depths, c and c', can be different since the compressive and tensile steel areas can differ. Rearranging EQN 4.1 leads to

$$h - c' - c = \frac{(1-\cos\phi)(1-\varepsilon)\beta\ell + 0.5\varepsilon\,(1-2\beta)\ell + t}{\sin\phi} \quad \text{or}$$

$$h - c' - c = \frac{2\beta\ell(1-\varepsilon)\sin^2(\frac{\phi}{2}) + 0.5\varepsilon\,(1-2\beta)\ell + t}{\sin\phi} \quad \text{EQN 4.2}$$

Since ϕ and ε are small,

$$\sin\phi = 2\sin\frac{\phi}{2} = \frac{\delta}{\beta\ell(1-\varepsilon)}$$

$$\sin^2(\frac{\phi}{2}) = \frac{\delta^2}{4(\beta\ell)^2(1-\varepsilon)^2}$$

in which δ is the midspan deflection, EQN 4.2 becomes

$$c' + c = h - \frac{\delta}{2} - \frac{\beta\ell^2}{2\delta}(1-\varepsilon)(\varepsilon + \frac{2t}{\ell} - 2\beta\varepsilon) \quad \text{EQN 4.3}$$

Equilibrium of sectional forces leads to

$$C_c' + C_s' - T' = C_c + C_s - T \quad \text{EQN 4.4}$$

in which

C'_c and C_c are the concrete compressive forces at the support and midspan, respectively,

C'_s and C_s are the steel compressive forces at the support and midspan, respectively, and

T' and T are the tensile forces at the support and midspan, respectively.

The concrete compressive forces are further defined by the ACI concrete compressive stress block (Figure 4.5) for a unit width as

$$C_c' = 0.85f_c'\beta_1 c' \quad \text{EQN 4.5}$$

and

$$C_c = 0.85f_c'\beta_1 c \quad \text{EQN 4.6}$$

in which

f'_c is the concrete cylinder strength, and

β_1 is the ratio of the depth of the equivalent stress block to the neutral-axis depth.

Substituting EQNs 4.5 and 4.6 into EQN 4.4 and rearranging provides

$$c' - c = \frac{T' - T - C'_s + C_s}{0.85f'_c\beta_1} \qquad \text{EQN 4.7}$$

Solving EQNs 4.3 and 4.7 simultaneously provides

$$c' = \frac{h}{2} - \frac{\delta}{4} - \frac{\beta\ell^2}{4\delta}(1-\varepsilon)(\varepsilon + \frac{2t}{\ell} - 2\beta\varepsilon) + \frac{T' - T - C'_s + C_s}{1.7f'_c\beta_1} \qquad \text{EQN 4.8}$$

$$c = \frac{h}{2} - \frac{\delta}{4} - \frac{\beta\ell^2}{4\delta}(1-\varepsilon)(\varepsilon + \frac{2t}{\ell} - 2\beta\varepsilon) - \frac{T' - T - C'_s + C_s}{1.7f'_c\beta_1} \qquad \text{EQN 4.9}$$

These equations only apply when the deflections are significant since the third term tends to negative infinity when the deflections are very small. The internal forces at a positive moment section (Figure 4.5) are statically equal to the compressive membrane force n_u at mid-depth and the resisting moment m_u when summed about mid-depth. For a unit width strip,

$$n_u = C_c + C_s - T = 0.85f'_c\beta_1 c + C_s - T \qquad \text{EQN 4.10}$$

and

$$m_u = 0.85f'_c\beta_1 c(0.5h - 0.5\beta_1 c) + C_s(0.5h - d') + T(d - 0.5h) \qquad \text{EQN 4.11}$$

where EQN 4.9 is substituted for c. For a negative moment section, m'_u is similar to EQN 4.11 except for primed terms and $n'_u = n_u$.

The sum of the moments of the internal forces about the mid-depth of one end (section 1-2 or 3-4) is $m'_u + m_u - n_u\delta$. Upon substitution:

$$m_u' + m_u - n_u\delta = 0.85f_c'\beta_1 h[\frac{h}{2}(1-\frac{\beta_1}{2}) + \frac{\delta}{4}(\beta_1-3) + \frac{\beta\ell^2}{4\delta}(\beta_1-1)(1-\varepsilon)(\varepsilon+\frac{2t}{\ell}-2\beta\varepsilon)$$

$$+ \frac{\delta^2}{8h}(2-\frac{\beta_1}{2}) + \frac{\beta\ell^2}{4h}(1-\frac{\beta_1}{2})(1-\varepsilon)(\varepsilon+\frac{2t}{\ell}-2\beta\varepsilon) - \frac{\beta_1\beta^2\ell^4}{16h\delta^2}\{(1-\varepsilon)(\varepsilon+\frac{2t}{\ell}-2\beta\varepsilon)\}^2]$$

$$-\frac{1}{3.4f_c'}(T' - T - C_s' + C_s)^2 + (C_s' + C_s)(\frac{h}{2}-d'-\frac{\delta}{2}) + (T' + T)(d-\frac{h}{2}+\frac{\delta}{2}) \qquad \text{EQN 4.12}$$

For a one-way strip of unit width, the failure mode is a three-hinge mechanism (i.e., $\beta = 0.5$) with a negative-moment plastic hinge at each support and a positive-moment hinge at midspan. If the strip (section 1-2) is given a virtual rotation θ, the external virtual work (i.e., the uniform distributed load going through the virtual displacement $\theta\ell/4$) is equal to the internal virtual work (i.e., internal moments going through the virtual rotation θ) producing an equation relating the strip midspan deflection to the external loading. The right side of EQN 4.13 is given by EQN 4.12.

$$\frac{w\ell}{2}\frac{\theta\ell}{4} = (m_u' + m_u - n_u\delta)\theta$$

$$\frac{w\ell^2}{8} = m_u' + m_u - n_u\delta \qquad \text{EQN 4.13}$$

To evaluate axial shortening and support movement in EQN 4.12, ε and t are related to the axial thrust n_u (i.e., $\varepsilon = (n_u)/(hE_c)$ and $t = n_u/S$) which has been substituted from EQN 4.10 where E_c is the Young's Modulus for the concrete and S is the support stiffness. The expression $[(1-\varepsilon)(\varepsilon + 2t/\ell - 2\beta\varepsilon)]$ is located not only in EQN 4.12, but also in the equation for n_u, EQN 4.10. Once the expression is expanded above and n_u is substituted, it must be rearranged to determine $(1-\varepsilon)(\varepsilon + 2t/\ell - 2\beta\varepsilon)$ (EQN 4.14).

The all-important geometrical changes of axial shortening and lateral support movement are represented in EQN 4.14, and when they become large enough, the slab will snap-through to tensile membrane resistance. When $(1-\varepsilon)(\varepsilon + 2t/\ell - 2\beta\varepsilon)$ is a maximum, the thrust is a maximum

$$(1-\varepsilon)(\varepsilon + \frac{2t}{\ell} - 2\beta\varepsilon) = \varepsilon + \frac{2t}{\ell} - 2\beta\varepsilon - \varepsilon^2 - \frac{2t\varepsilon}{\ell} + 2\beta\varepsilon^2$$

$$= \frac{n_u}{hE_c} + \frac{2n_u}{\ell S} - \frac{2\beta n_u}{hE_c} - (\frac{n_u}{hE_c})^2 - \frac{2n_u^2}{\ell ShE_c} + 2\beta(\frac{n_u}{hE_c})^2$$

$$= \frac{J(\frac{Qh}{2} - \frac{Q\delta}{4} - QF + C_s - T) + K(\frac{Q^2h^2}{4} - \frac{Q^2h\delta}{4} - Q^2hF + QhC_s - QhT + \frac{Q^2\delta^2}{16} + \frac{Q^2\delta F}{2} - \frac{Q\delta C_s}{2} + \frac{Q\delta T}{2} + Q^2F^2 - 2QFC_s + 2QFT + C_s^2 - 2C_sT + T^2)}{1 + J(\frac{Q\beta\ell^2}{4\delta}) + K(\frac{Q^2h\beta\ell^2}{4\delta} - \frac{Q^2\beta\ell^2}{8} - \frac{Q^2\beta^2\ell^4}{16\delta^2} - \frac{Q^2\beta\ell^2F}{2\delta} + \frac{Q\beta\ell^2C_s}{2\delta} - \frac{Q\beta\ell^2T}{2\delta}}$$

where:

$$J = \frac{1}{hE_c} + \frac{2}{\ell S} - \frac{2\beta}{hE_c}$$

$$K = -\frac{1}{h^2E_c^2} - \frac{2}{\ell ShE_c} + \frac{2\beta}{h^2E_c^2}$$

$$Q = 0.85f_c'\beta_1$$

$$F = \frac{T' - T - C_s' + C_s}{1.7f_c'\beta_1}$$

EQN 4.14

and indexes the peak capacity. The peak thrust produces the necessary axial shortening and lateral support movement in combination with plastic hinge rotation to generate snap-through in thin slabs and concrete crushing and pop-outs in thick slabs. The concrete crushing or pop-outs in thick slabs ultimately leads to snap-through to tensile membrane resistance. Similarly in Park and Gamble's compressive membrane theory, when $(\varepsilon + 2t/l)$ is a maximum, the thrust is a maximum and indexes the peak capacity.

The deflection (δ) is increased incrementally in EQN 4.13 until the point of peak thrust, which is determined through evaluation of EQN 4.10 at each increment, indexes the peak capacity. The incremented deflection associated with the peak thrust indexed capacity is usually smaller than the experimental deflection for the same capacity since the derivation does not include the biaxial compressive stress condition at the support hinges. The biaxial compressive stress condition allows larger rotational capacity and, therefore, much larger midspan deflections (Figure 4.2).

In its current form Equation 4.14 does not always provide a defined computed peak point. The curve is somewhat similar to that developed by Wood (1961) (shown as Figure 2.8) in which the curve continually descends from left to right. A theoretical curve without a defined peak point is not important if a thrust or a deflection is used to index a peak capacity. However, it was desired to investigate the accuracy of the sometimes used computed peak capacity, and also an average between the computed peak capacity and the thrust indexed peak capacity. Determination of a computed peak capacity is possible in Park and Gamble's (1980) derivation. Removal of the term, $(G^2\beta^2t^4)/(16\delta^2)$, from the denominator in EQN 4.14 results in a defined computed peak capacity similar to Park and Gamble's derivation (Figure 4.7, a and b). The top figure is before removal of the term and the bottom figure is after removal of the term. As can be seen, the removed term only affects the early portion of the curve which is actually dominated by elastic behavior, and not truly represented by the modified compressive membrane theory nor Park and Gamble's compressive membrane theory curve.

4.2.2. Peak Compressive Membrane Capacity Results

The construction details for some of the 115 one-way slabs listed in Appendix A were identical except for the availability and type of shear reinforcement. Since the shear reinforcement usually had little effect on the peak capacity (Chapter 2) besides keeping the compressive reinforcement from buckling prematurely, the 115 one-way slabs were evaluated with both Park and Gamble's and the modified compressive membrane theories through the 48 subgroups listed in Table 4.1. As shown in Figures 4.8 - 4.9, there is a small, but appreciable, difference between the two theories for thick slabs. However, for thin slabs, there is a substantial difference noted.

The two theories were evaluated by predicting the peak capacity through the current methods of using either the computed peak capacity (PP or WP) or the deflection indexed capacity (PDI or WDI), and the proposed approach of using either the peak thrust indexed capacity (PTI or WTI) or the average between the computed peak capacity and the peak thrust indexed capacity (P_{avg} or W_{avg}). The first abbreviation represents the predicted capacity with Park and Gamble's compressive membrane theory, while the second abbreviation delineates the capacity with the modified compressive membrane theory. Additionally, the code recommended capacity, i.e., the yield-line capacity with fixed-supports (YL), was provided for comparison with the other compressive membrane theory predictions.

The load capacity and deflection estimates were calculated with a spreadsheet for both Park and Gamble's compressive membrane theory and the modified compressive membrane theory. Selected columns and rows from the Wood3 spreadsheet are provided in Figure 4.10. Additional examples of spreadsheet output are presented in Appendix D for three of the analyzed slabs (Wood4, W45, and G4). As the deflection, δ, is incremented, a number of values are simultaneously calculated, i.e., the capacity w, the thrust N_u, the curvature based deflection (delta), etc. In Figure 4.10 it is shown how the experimental deflection, 0.41 inches, indexes a capacity (WDI) of 595.2 psi, which is prior to the computed peak capacity (WP) of 614.3 psi. The peak thrust (i.e., 171723 lb), which is less than the balanced thrust (i.e., 258150 lb), indexes or points to a capacity (WTI) of 541.4 psi. These capacities for Wood3 are listed in Table D.2 along with the

average (W_{avg}) between the computed peak capacity (WP) and the peak thrust indexed capacity (WTI). The experimental capacity was 557 psi.

To improve comparison efforts, each of the predicted capacities was divided by the experimentally measured capacity listed in Appendix A. These normalized capacities were further evaluated by taking the average and standard deviation for all the slabs (first two rows of Table 4.2), the thick slabs (L/h < 18), the thin slabs (18 <L/h < 22), and the very thin slabs (L/h > 22) (the rest of Table 4.2). The detailed listing of the capacities used for the averages and standard deviations presented in Table 4.2 is in Appendix D. The predicted capacities using Park and Gamble's compressive membrane theory are presented in Table D.1, while the new compressive membrane theory results are presented in Table D.2.

Upon evaluation of all the slabs, the computed peak capacity (PP, column 3, Table 4.2) followed by the average peak capacity (P_{avg}, column 6, Table 4.2) provides the best peak capacity estimate using Park and Gamble's compressive membrane theory, while the peak thrust indexed capacity (WTI, column 9, Table 4.2) and average peak capacity (W_{avg}, column 10, Table 4.2) provides the best estimates using the new compressive membrane theory (Table 4.2). When operating under the currently popular method of indexing the peak capacity with a peak capacity midspan deflection estimate, or within this dissertation, using the experimentally measured peak capacity midspan deflections listed in Appendix A, the modified compressive membrane theory (WDI, column 8, Table 4.2) provided a peak capacity prediction that was closer to the experimentally measured peak capacity than Park and Gamble's compressive membrane theory (PDI, column 4, Table 4.2), especially for the thin slabs. As shown in Table 4.2, the peak thrust indexed peak capacity estimate (PTI, column 5, and WTI, column 9, Table 4.2) provides as close an estimate of the experimental peak capacity as the deflection indexed peak capacity (PDI, column 4, and WDI, column 8, Table 4.2), especially with the new compressive membrane theory, without the need to estimate a deflection first. As will be seen in the next section, the available methods to estimate the peak capacity deflection produce a lot of scatter (i.e., large standard deviation). The peak thrust indexed capacity (WTI, column 9, Table 4.2) provides the best estimate with the

smallest standard deviation for both the thick and thin slabs, while slightly over-estimating the peak capacity for the very thin slabs. However, very thin slabs will not normally be used to provide additional protection in blast environments.

Most of the past researchers either did not test their support structure for an effective lateral stiffness or they did not mention the effective lateral stiffness in their reports. Additionally, none of the researchers discussed the support stiffness used within their compressive membrane calculations. The lateral support stiffness and the peak capacity deflection estimate, if used as an index, should have been key parameters in their methods of estimating the peak capacity. In the absence of definitive statements, it is assumed that past researchers used their experimental peak capacity midspan deflections to index the peak capacity in the compressive membrane theory, while using a low lateral stiffness value. For the one-way slabs listed in Appendix A, only Roberts (1969) tested and listed the lateral support stiffness of his reaction structure. In order to estimate the lateral support stiffness for the other experimental results in Appendix A, the author used Park and Gamble's derivation (1980) for the relationship between the uniform load-central deflection and a range of lateral support stiffness varying from very flexible to infinitely rigid (Figure 4.11). In Figure 4.11, Woodson's slab (1993) had a peak capacity of 68.8 psi which is an enhancement of approximately 3 times the expected Johansen yield line capacity of 22.7 psi. The lateral support stiffness (lb/in) required to generate this level of enhancement is approximately a scalar magnitude of $0.015E_c$. The WES testing generally used the same support and reaction structure, which had an average lateral support stiffness less than a scalar magnitude of $0.05E_c$. The lateral support stiffness used within this study are listed along with all the other individual slab parameters in Table 3.1.

Even though the purpose of the reaction structure was to impose relatively fixed-supported edge conditions, the magnitudes of the lateral support stiffness listed in Table 3.1 are smaller, except for Robert's slabs, than the scalar magnitude of the Young's Modulus of the slab. The results of the author's study on the affect of lateral support stiffness versus peak capacity, for a select number of the slabs listed in Appendix A, is presented in Table 4.3. The peak capacity was

estimated for each slab using the compressive membrane theory and a lateral support stiffness of scalar magnitude E_c, $0.1E_c$, and $0.01E_c$. The estimated peak capacity using a lateral support stiffness between a scalar magnitude of 0.1 and $0.01E_c$ for the thick slabs generally bracketed the experimental peak capacity. Of course a lateral stiffness value nearly equal to a scalar magnitude of E_c was required to estimate the capacity for the thin slabs, since the experimental reaction structure was known to have a lateral stiffness close to a scalar magnitude of E_c. A lateral support stiffness as low as a scalar magnitude of $0.01E_c$ generally predicted a peak capacity 1.5 to 2.0 times the yield line capacity for all of the evaluated slabs.

In Chapter 3, the finite element results for thick slabs using fixed-supported edge conditions greatly over-estimated the peak capacity (Tables 3.3, 3.4, 3.7, 3.9). A lateral stiffness value of scalar magnitude E_c has been noted by past researchers (Chapter 2) to represent fully fixed-supported lateral edge conditions. Therefore, a lateral support stiffness of scalar magnitude E_c in the newly derived compressive membrane theory should generate the same results as the fully fixed-supported finite element results. Upon comparison of the compressive membrane peak load capacities (columns 6-9, Table 4.4) with the average finite element (FE, column 10-13, Table 4.4) peak capacities, the compressive membrane results were very close to the FE peak capacities. The average FE peak capacity is used to calculate the normalized value listed in the parentheses of Table 4.4 (i.e., compressive membrane capacity divided by the FE capacity), and it is then averaged at the bottom of the table. Once again, the peak thrust indexed capacity (i.e., column 3, Table 4.4) provides the best overall peak load capacity estimate for the estimated lateral support stiffness of scalar magnitude of E_c (i.e., 1.043).

The results in Tables 4.3 - 4.4 validate the use of the compressive membrane theory to estimate the peak compressive membrane capacity in thick slabs, while using the peak thrust to index the load capacity. The compressive membrane theory is able to match, not only the acceptable results when using finite element analysis methods for thick slabs, i.e., fixed-supported edge conditions, but also the peak capacity when the lateral supports are not fixed. Deflections are not required to estimate the peak load capacity since the peak load capacity can be successfully

indexed with the peak thrust. However, a plausible peak capacity deflection estimate is still required if there is a need for the load-deflection curve.

4.3. Peak Compressive Membrane Capacity Deflection

Many engineers estimate the peak capacity with Park and Gamble's (1980) compressive membrane theory using a peak capacity deflection estimate as an index point. This practice may have more to do with tradition, since the initial theoretical curves (Wood, 1961; Park, 1964) generally did not have a defined peak capacity, as they do now in Park and Gamble's (1980) compressive membrane theory or the new compressive membrane theory, than with the deflection actually being the best index value. However, some engineers have noted that the computed peak capacity will usually be larger than experimental peak capacities when the lateral support stiffness is equal to or greater than the correct stiffness. Therefore, Park and others usually chose a safe deflection estimate, approximately 0.5h, to index the peak capacity, which was based on their limited empirical results.

Upon close evaluation of the empirical deflection results for the one-way slabs listed in Appendix A, there is a large range of experimental peak capacity deflections. The deflections range from a low of 0.03h to a high of 0.4h. The deflection estimate of 0.5h used by Park and others would greatly under-estimate the peak capacity for a large number of these slabs. Prediction of such a low peak capacity would be disastrous in military targeting missions. Additionally, the experimentally measured peak capacity deflections for the deep slabs (i.e., $L/h < 5$) indexed a peak capacity with the compressive membrane theory that was prior to the computed peak capacity (Tables D.1 - D.2). Some researchers accept a capacity predicted prior to the compressive membrane theory computed peak capacity, but this author cannot. The early portion of the compressive membrane theoretical curve, i.e., prior to and in some cases including the computed peak capacity, does not accurately represent the elastic and then elastic-plastic behavior of the slab during initial loading. Based on the underlying assumptions, the theoretical compressive membrane curve can represent the inelastic behavior at peak capacity, which should be at or after the

computed peak capacity (Figure 4.2). The wide range and relative inaccuracy of deflection estimate procedures coupled with the limited discussion on the estimates for the lateral support stiffness used in the compressive membrane theories inspired this compressive membrane study, which has led to his use of the peak thrust to index the peak capacity rather than a deflection estimate.

The use of the peak thrust to index the peak capacity would appear to eliminate the need for any peak capacity deflection estimate. However, in dynamic analysis, especially in the blast arena, there is still the need for a complete load-deflection curve as input. The load-deflection history provides invaluable insight into the energy absorption capability of the slab. Fortunately, the peak capacity midspan deflection (Δ) is a function of L/h and the concrete compressive strength as shown in the raw data of Figures 4.12 and 4.13. As observed in Figure 4.13, the axial concrete compressive strain, used within the curvature based deflection relationship developed herein to match the experimental peak capacity midspan deflections, is generally related to the concrete compressive strength. As will be discussed later in more detail, the curvature based deflection relationship (Figure 4.13) provided the most accurate peak capacity midspan deflection estimate, while estimating the midspan deflection with the span-to-thickness ratio (Figure 4.12) was the least complicated.

A number of techniques for estimating the deflection were evaluated, to include: empirically based linear relationships, deflections corresponding to the compressive membrane theory computed peak load capacity and the peak thrust indexed load capacity, general concrete deflection equations available in most textbooks, and curvature based deflection relationships. The format for comparing the different deflection techniques is similar to the peak load capacity estimates in Section 4.2.2 in that for each slab the deflection estimate is normalized by dividing the deflection estimate by the experimentally measured midspan deflection. The accuracy of each prediction technique is evaluated by the overall average and standard deviation when considering all the slabs or just the thick slabs, the thin slabs, or the very thin slabs. The detailed deflection

estimates for each slab group provided by the different prediction techniques are available in Appendix D.

4.3.1. Deflection Estimate Using General Deflection Equations

The midspan deflection estimates listed in most standard analysis textbooks were evaluated. The equations ranged from modeling one-half of the slab as a cantilever (i.e., first hinge forms at midspan) to modeling the slab as simply-supported (i.e., hinges form first at the supports). The moment of inertia was adjusted to represent the amount of cracking (i.e., fully cracked conditions) since most of the general equations assume fully elastic behavior. The best overall estimate, using general equations, for the peak capacity midspan deflection was through modeling the slab as simply-supported (SS) with a fully cracked moment of inertia. The detailed deflection estimates (SS) are presented in both Tables D.7 and D.8 for comparison with the other deflection estimates. As shown in the second column of Table 4.5, the use of simply-supported edge conditions with a fully cracked moment of inertia estimated the peak capacity midspan deflection fairly well for the thin slabs ($18 < L/h < 22$), but under-estimated the deflection for thick slabs ($L/h < 18$) and over-estimated the deflection for very thin slabs ($L/h > 22$).

4.3.2. Deflection Estimate Using Empirically Based Curves

Since the peak load capacity appears to be more a function of the slab thickness and the concrete strength rather than the reinforcement ratio, a number of researchers divided the midspan deflection by the thickness to develop a dimensionless parameter to use in their equations to predict the peak load capacity. This same parameter, Δ/h, can be used when estimating the peak capacity midspan deflection. Roberts (1969) and Woodson (1993) each tested a large number of slabs with the same L/h ratio while varying the concrete compressive strength and reinforcement ratio. They noted that Δ/h was almost a constant for the slabs with the same L/h, no matter what combination of concrete compressive strength and reinforcement ratio they used.

The Δ/h for each L/h grouping in Appendix A was averaged and plotted in Figure 4.12. There was an obvious correlation between L/h and Δ/h depending on whether the slabs were thick (L/h < 18) or thin (L/h > 18). The only real outlier was the Δ/h value for Christiansen's (1963) two slabs which had an L/h of 17.1. The best correlation between the experimental and estimated peak capacity midspan deflections was when the data for L/h of 17.1 (i.e., in the transition zone between material and geometric instability) were left out. It should be noted that Christiansen only listed one representative deflection for his four tested slabs with three different L/h ratios. How to handle slabs within the transition zone (15 < L/h < 18) is explained below. A linear curve provided the best fit to the data points (Figures 4.14 and 4.15). The linear equation for the thick slabs (L/h < 15) is

$$\frac{\Delta}{h} = 0.034423\left(\frac{L}{h}\right) - 0.03757 \qquad \text{EQN 4.15,}$$

while for the thin slabs (L/h > 18) the linear equation is

$$\frac{\Delta}{h} = 0.008764\left(\frac{L}{h}\right) + 0.007527 \qquad \text{EQN 4.16}$$

The deflection estimates from these empirically based curves (EC) for each slab are presented in the last two columns of Table D.7, while the corresponding normalized deflection averages and standard deviations for the thick, the thin and the very thin slabs are presented in the last column of Table 4.5 (EC/Δ). The predicted deflection value for Wood3 (L/h = 4.4, h = 5.5) was 0.626 inches, while the experimentally measured deflection was 0.41 inches (0.63/0.41 = 1.54).

The fact that the peak capacity deflection for Christiansen's slabs, C1 and C2 (Table 4.1), was between the range of values provided by substituting an L/h of 17.1 into EQNs 4.15 and 4.16 does makes sense. The deflection behavior of the thick slabs is controlled by material instability, while the thin slab behavior is dominated by geometric instability. The switch from material to geometric instability does not occur magically at a given L/h ratio. Without additional testing of slabs with L/h ratios ranging from 15 to 18, it is difficult at this time to define the exact range of

L/h ratios where the transition occurs. Therefore, it is recommended for slabs with an L/h between 15 and 18 that the results from the two equations are weighted based on L/h.

For example, for an L/h of 17.1, the Δ/h values from EQNs 4.15 and 4.16 when substituting 17.1 for L/h are 0.551 and 0.1574, respectively. With 17.1 being about 2/3 of the difference between 15 and 18, an estimate for Δ/h can be determined by simply multiplying 0.333 times 0.551 and adding it to 0.666 times 0.1574 which equals 0.288. With a thickness of 3.5 inches for slabs C1 and C2, the estimated peak capacity midspan deflection is 1.0 inches compared to the experimental deflection of 0.65 inches. Even though there are no experimental results for a slab with an L/h of 16, this simple procedure would result in Δ/h values of 0.3418 and 0.0492 from EQNs 4.15 and 4.16, respectively. With an L/h of 16 being about 1/3 of the difference between 15 and 18, an estimate for Δ/h would be determined by multiplying 0.666 times 0.3418 and adding it to 0.333 times 0.0492 for a Δ/h of 0.3909. The peak capacity midspan deflection estimate would be the slab thickness (inches) times 0.3909.

The empirically based curves provide a good over-all estimate of the midspan peak capacity deflection (EC/Δ, last column, Table 4.5). Even the standard deviation is small except for the thick slab estimates. The thick slab standard deviation is greatly improved from 0.65 to 0.25 when the extreme outliers for the single slab tests K1, K2, and W6 are dismissed (Table 4.1). K1 and K2 were single event slabs tested to establish parameters for follow-on dynamically loaded slabs. Slab W6 was a thick slab with only very heavy tensile reinforcement while most of the other tested slabs were doubly reinforced with equal tensile and compressive reinforcement ratios. Since there can be large variations in the concrete properties and testing procedures, slabs K1, K2, and W6 would not be possible outliers if more than a single slab test represented the data point.

4.3.3. Deflection Estimate Using the Compressive Membrane Theory

The goal of the compressive membrane theory is to relate the midspan deflection to the uniform load supported by the slab. This premise is the basis for current users to index the peak capacity using an estimated peak capacity deflection. In Section 4.2.2, it was shown that the

ability to estimate accurately the peak capacity using even the experimental peak capacity deflection was not more accurate than using the peak thrust as the index point. Additionally, the experimental deflection indexed a capacity before the computed peak capacity, between the computed and thrust indexed peak capacity, and even after the thrust indexed peak capacity (Tables D.1 and D.2). Therefore, it is possible that the deflection associated with either the computed peak point or the peak thrust capacity could produce an accurate estimate of the peak capacity deflection. The average normalized deflection and standard deviation for the deflections associated with the computed peak capacity (PP or WP, columns 3 and 4) and the peak thrust indexed peak capacity (PTI or WTI, columns 5 and 6) are provided in Table 4.5, while the detailed listing of deflection estimates are in Tables D.7 (i.e., using Park and Gamble's compressive membrane theory, PP, PTI) and D.8 (i.e., using the new compressive membrane theory, WP, WTI).

The smaller deflection at the computed peak capacity clearly points to the fact that the computed peak capacity does not truly represent the stress conditions (i.e., biaxial and triaxial) near the supports. The biaxial and sometimes triaxial stress conditions at the supports accommodate large hinge rotations leading to even larger deflections at peak capacity. The deflection associated with the peak thrust in Park and Gamble's compressive membrane theory is larger than the experimental deflections for thick and thin slabs, while the deflection associated with the peak thrust in the new compressive membrane theory over-estimates the peak capacity deflection for thick slabs and under-estimates the peak capacity deflection for thin slabs. As an interesting exercise, the associated deflections for peak thrust from both Park and Gamble's and the new compressive membrane theories were averaged and compared with the experimental peak capacity deflections (Table 4.6). The estimated deflections for the thin slabs correlated very well with the experimental peak capacity deflections.

4.3.4. Deflection Estimate Using Mattock's Equations

Mattock (1965) performed a number of experiments to develop a relationship for the rotational capacity of hinging regions in reinforced concrete beams. His goal was to determine the magnitude of the strains in the hinging sections during the redistribution of moments. The ACI code suggests limiting the ultimate concrete compressive strain to 0.003 in/in. However, this value was determined when measuring the strain within the constant moment region of beams loaded with two point loads. If the moment-curvature relationship from a beam loaded at only two points is used to calculate the rotation of the hinges at the supports, the calculated rotation is less than the observed rotation. A number of researchers have noted this discrepancy and simply recommended increasing the calculated rotation in the support region by a factor.

Mattock's investigation had the following conclusions:

1. The maximum concrete compressive strain at the section of maximum moment over a support or under a single concentrated point load can greatly exceed 0.003 in/in;
2. Using the principles of equilibrium and compatibility of strain provides a close estimate of the moments and a safe limiting estimate of the curvature and rotation at the section of maximum concrete compressive strain, if the strain hardening of the reinforcement and the variation of maximum concrete strain with shear span are taken into account; and
3. The plasticity zone spreads outward along the beam from the section of maximum moment as z/d increased and the net tension reinforcement decreased.

Control beams were tested with the concrete compressive strain measured between two equal concentrated point loads. Once again, the maximum concrete compressive strain was approximately 0.003 in/in in the constant moment regions, while the strain in regions of moment gradients (i.e., at the supports or under a single point load) was larger than 0.003 in/in by an order of magnitude or more.

Mattock developed a relationship for the maximum concrete compressive strain (EQN 4.17) and a relationship between the total inelastic rotation θ_{tu} in length z and the inelastic rotation θ_u in length d/2 (EQN 4.18).

$$\varepsilon_u = 0.003 + 0.5z \qquad \text{EQN 4.17}$$

$$\frac{\theta_{tu}}{\theta_u} = 1 + (1.14\sqrt{\frac{z}{d}} - 1)[1-(\frac{q-q'}{q_b})\sqrt{\frac{d}{16.2}}] \qquad \text{EQN 4.18}$$

in which

z is the distance from the section of maximum moment to the section of zero moment,

d is the distance from the extreme concrete compressive fiber to the tensile reinforcement,

q is the reinforcement index ($\rho f_y/f'_c$) with the prime superscript for compression reinforcement and the b subscript for the balanced ultimate strength condition determined using an maximum concrete compressive strain of 0.003 in/in.

Mattock's conclusion that the strain near the supports (i.e., in the plastic regions) is larger than 0.003 in/in is supported by the results using finite element methods in Chapter 3. The average normalized deflection and standard deviation for the deflection estimates using Mattock's equations (listed as M/Δ) and a strain of 0.005 in/in are presented in Table 4.5 (column 9), while the individual deflection estimates are listed in Table D.7 (listed as M). The deflection estimate was either lower than the experimental peak capacity deflection or produced invalid data (i.e., an error message) at such a low level of strain.

The ultimate concrete compressive strain was adjusted in Mattock's equations until the experimental peak capacity deflection was matched (listed as ε(M), Table D.7). The large ultimate compressive strain values for the thick slabs supported Mattock's test results of strains greater than 0.003 in/in near the support. For the thin slabs (L/h > 18), no adjusted strain value was determined that would provide a match with the experimental peak capacity deflections, except for the slabs with tension reinforcement in the negative and positive moment regions (i.e., Christiansen's slabs C1-C4). However, for slabs C1 through C4, the adjusted strains were less than half the finite element method suggested value of 0.005 in/in. The reinforcement ratio (ρ), the

reinforcement index (q), the length-to-thickness ratio (L/h), and the concrete compressive uniaxial strength (f'_c) were plotted against the adjusted strains for the thick slabs used in Mattock's EQN 4.18. The best fit of a curve to the data occurred when using a linear curve to represent the relationship between the slab's uniaxial concrete compressive strength and the adjusted strains (Figure 4.16).

Mattock's equations and the uniaxial concrete compressive strength - adjusted axial strain relationship presented in Figure 4.16 should only be used to predict the peak capacity deflection for thick slabs with tension reinforcement at both the positive and negative moment regions. Additional experimental data for doubly reinforced thin slabs are necessary before attempting to correlate Mattock's equations for use with thin slabs. Since this technique could not estimate the peak capacity deflections for the thin slabs, the comparison with other methods was stopped after estimating the concrete compressive strains from the relationship established in Figure 4.16 for the thick slabs (column 3, Table 4.7).

4.3.5. Deflection Estimate Using Curvature Based Equations

Another area that received some emphasis in the past is curvature based deflection equations. Keenan (1969) initiated his work with Park's (1964) assumption that the slab strip behaves in a rigid-plastic manner. If the plastic behavior only occurs at the hinge lines, the geometry of the slab for a small deflection at peak capacity is shown in Figure 4.6. Keenan assumed that concrete crushing defined the peak capacity (i.e., the ultimate concrete compressive strain in the outer fiber). If the slab strip is assumed to remain rigid between the hinge points, then the lengthening of the outer edge when the member is loaded must be concentrated at the hinge points on each end of the slab strip. Through tan ϕ (Figure 4.6), Keenan related the slab geometry to the curvature of the slab section

$$\tan\phi = \frac{x\varepsilon_u}{2c_e} = \frac{u}{x + \frac{sL}{2}} \qquad \text{EQN 4.19}$$

in which

ε_u is the ultimate axial strain as the concrete begins to crush,

c_e is the neutral axis depth at the support,

x is less than or equal to L/2,

u is the midspan deflection,

sL/2 represents the outward movement of the supports.

In Park and Gamble's notation (Figure 4.6), EQN 4.19 would be

$$\tan\phi = \frac{\beta\ell\varepsilon_u}{2c'} = \frac{\delta}{\beta\ell + t} \qquad \text{EQN 4.20}$$

in which

$\beta\ell$ defines the section length,

c' is the neutral axis depth at the support,

δ is the peak midspan deflection, and

t is the support lateral movement.

Keenan did not include axial shortening and he assumed half of the lengthening due to curvature occurred at each hinge (Keenan, 1998). Expansion of EQN 4.19 by Keenan results in an estimate for the midspan deflection (z_u) which has been used recently by some of the researchers at WES (Guice, 1986).

$$\frac{z_u}{h} = \left(1+q_e\frac{d_e}{hk_1}-q_d\frac{d_d}{hk_1}\right) - \sqrt{\left(1+q_e\frac{d_e}{hk_1}-q_d\frac{d_d}{hk_1}\right)^2 - \frac{1}{2}\left(\frac{L}{h}\right)^2[s(1+\varepsilon_u)+\varepsilon_u]} \qquad \text{EQN 4.21}$$

in which

d is the distance from the compressive face to the tensile reinforcement,

k_1 is a parameter defining the concrete stress block (based on shape of stress-strain curve),

ρ is the reinforcement ratio,

f_y is the yield stress of the reinforcement,

f''_c is the uniaxial concrete compressive strength, and

$q_e = (\rho_e - \rho_e')f_y/f''_c$, $q_d = (\rho_d - \rho_d')f_y/f''_c$ (reinforcement index)

where subscript e and d represent the sections at the support and midspan, respectively. When $q_e = q_d$, EQN 4.21 reduces to

$$\frac{z_u}{h} = 1 - \sqrt{1 - \frac{1}{2}\left(\frac{L}{h}\right)^2 [s(1+\varepsilon_u) + \varepsilon_u]} \qquad \text{EQN 4.22}$$

Keenan's equations were modified to include axial shortening. The value s was replaced by $(\varepsilon+2t/\ell)$ for use with Park and Gamble's equations and by $(1-\varepsilon)(\varepsilon+2t/\ell-2\beta\varepsilon)$ for use with the newly derived compressive membrane theory equations. The two terms each represent both the elastic axial shortening within the section and the support movement. The first term is defined in Park and Gamble (1980), while the second term is defined by EQN 4.14. The deflection (K(P), column 7, Table 4.5) represented by EQN 4.21 was used with Park and Gamble's compressive membrane theory and a concrete compressive strain of 0.005 in/in, while EQN 4.22 was used with the new compressive membrane theory and a concrete compressive strain of 0.005 in/in (K(W), column 8, Table 4.5). The peak thrust also indexes the peak deflection value for EQN 4.21 and 4.22 when using $(\varepsilon+2t/\ell)$ in Park and Gamble and $(1-\varepsilon)(\varepsilon+2t/\ell-2\beta\varepsilon)$ in the new compressive membrane theory to represent the axial shortening and the support outward movement. The predicted deflections for the thick slabs were close to the experimentally measured deflections with the best results from EQN 4.22 (K(W), column 8, Table 4.5), while EQN 4.21 produced invalid data (i.e., an error message) when predicting a deflection estimate for the thin slabs.

The individual deflection estimates, when using a concrete compressive strain of 0.005 in/in and then the adjusted strain values which produced deflections that matched the experimentally measured midspan deflections, are listed in Table D.7 (listed as K(P)) for EQN 4.21, and Table D.8 (listed as K(W)) for EQN 4.22. When adjusting the strain, EQN 4.21 still produced invalid data (i.e., an error message) for thin slab deflection estimates. Even though EQN 4.22 assumes that the slab is reinforced with equal amounts of tensile and compressive

reinforcement at the supports and midspan, it was used to determine an adjusted ultimate strain which produced a matching peak capacity deflection (Table D.8) for the thin slabs with only bottom reinforcement (columns 8 and 9, Table 4.7). The adjusted concrete compressive strains for the thin slabs were much smaller than the expected strain of 0.005 in/in which was computed during finite element analysis in Chapter 3.

A curvature based deflection equation was developed for use with the new compressive membrane equations, while using Park and Gamble's geometry and the modified length for the distance between Points A and B (Figure 4.6). The relation between the slab geometry and the curvature is

$$\tan\phi = \frac{\beta\ell(1-\varepsilon)\varepsilon}{2c'} = \frac{\delta}{\beta\ell(1-\varepsilon) + 0.5\varepsilon(1-2\beta)\ell + t} \qquad \text{EQN 4.23}$$

Upon substituting EQN 4.8 for c', the maximum midspan deflection, δ, can be determined by solving for the root of the resulting quadratic equation (EQN 4.24).

$$\delta = 2\left(\frac{h}{2} + \frac{T' - T - C_s' + C_s}{1.7 f_c' \beta_1}\right) - \left\{2\left(\frac{h}{2} + \frac{T' - T - C_s' + C_s}{1.7 f_c' \beta_1}\right)^2 - 2\left[\frac{\beta\ell^2 (1-\varepsilon)\left(\varepsilon + \frac{2t}{\ell} - 2\beta\varepsilon\right)}{2}\right.\right.$$

$$\left.\left. + (\beta\ell)^2 (1-\varepsilon)^2 \varepsilon + 0.5\beta\ell\varepsilon^2 (1-\varepsilon)(1-2\beta)\ell + + \beta\ell(1-\varepsilon)\varepsilon t\right]\right\}^{0.5} \qquad \text{EQN 4.24}$$

The value $(1-\varepsilon)(\varepsilon+2t/\ell-2\beta\varepsilon)$ is given by EQN 4.14 and $t = n_u/S$, which leaves ε as the only unknown. The best results were obtained by adjusting ε versus using $\varepsilon = n_u/hE_c$. The averaged normalized deflection results and standard deviation (listed as W(W)) for an ε of 0.005 in/in used within EQN 4.24 and the new compressive membrane theory are presented in Table 4.5 (column 11). For the very thin slabs, the ultimate concrete compressive strain of 0.005 in/in produced invalid data (i.e., an error message for a negative value under the square root), while excellent deflection estimates were observed for the thick slabs. The individual deflection estimates for a

concrete compressive strain of 0.005 in/in (W(W)) and the adjusted strain values which generated deflections that matched the experimental deflections are listed in Table D.8 (listed as ε(W(W))). Strains on the order of 0.001 in/in were necessary to achieve matching deflections for the thin slabs (W(W), column 6, Table 4.7).

A deflection relationship similar to EQN 4.24 was developed for use with Park and Gamble's equations with the relation between the slab geometry and curvature being

$$\tan\phi = \frac{\beta\ell\varepsilon}{2c'} = \frac{\delta}{\beta\ell + 0.5\varepsilon(1-2\beta)\ell + t} \qquad \text{EQN 4.25}$$

The value for c' and (ε+2t/ℓ) are presented in Park and Gamble (1980). The results (W(P)) using an ultimate concrete compressive strain of 0.005 in/in are listed in Table 4.5 (column 10). The overall results for the predicted deflections with Park and Gamble's compressive membrane theory (W(P), column 10, Table 4.5) were not quite as good as the results (W(W), column 11, Table 4.5) using EQN 4.24 in the new compressive membrane theory. Once again, an ultimate concrete compressive strain of 0.005 in/in produced invalid data (i.e., an error message) when considering Robert's thin slabs, and a small strain value (ε(W(P)), Table D.7, column 4, Table 4.7) was necessary to match the experimental deflections for those thin slabs.

Keenan's EQN 4.21 could not match the experimental peak capacity midspan deflections for thin slabs even when the ultimate concrete compressive strain was varied. Since Keenan's EQN 4.22 provided better overall results for the thick slabs than his EQN 4.21 (Table 4.5), EQN 4.21 was dropped from further evaluation. The reinforcement ratio (ρ), the reinforcement index (q), the span length-to-thickness ratio (L/h), and the concrete compressive uniaxial strength (f'_c) were plotted against the adjusted strains for the thick slabs used in Keenan's EQN 4.22 and the modified curvature based deflection equation (EQN 4.24) used within both Park and Gamble's and the new compressive membrane theories (Appendix D). Neither a linear nor exponential curve really fit the data in any of the graphs as long as the strain values for the thin slabs were included. Since the

adjusted thin slab strain values are rather constant and below a value of 0.002 in/in (Table 4.7), those data points were removed and averaged (Table 4.7) so that the focus could be on thick slabs. The best fit of a curve to the thick slab data occurred when plotting the slab's uniaxial concrete compressive strength against the adjusted strains (Figure 4.17). The linear equation for the thick slabs (L/h < 17) represented in Figure 4.17 is

$$\varepsilon = -2.420668E-06(f_c') + 0.018938 \quad (in/in) \qquad \text{EQN 4.26}$$

Similar equations are available for the adjusted strain data sets from Keenan's and Mattock's deflection equations in Appendix D. The comparison of the estimated (ε_{est}) strain values using EQN 4.26 to the adjusted (i.e., ε_{adj}) strain values for the thick slabs is presented in the first row of Table 4.7. The best correlated strain values between the estimated and adjusted strain values came from using the modified curvature based deflection equation with either Park and Gamble's or the new compressive membrane theory. The individual strain estimate for each slab used in the comparison of the estimated strain values to the adjusted strain values are listed in Table D.12.

For the thin slab strain values removed from consideration above, the strain values were averaged for use in the curvature based deflection equations. The averages and standard deviations for the thin (17 <L/h <22) and the very thin (22 < L/h < 29) slabs are listed at the bottom of Table 4.7. The strain values are much smaller than what the finite element results (i.e., 0.005 in/in) would have predicted. However, the curvature based deflection equation does assume crushing of the concrete at peak capacity, which does not always occur in thin slabs, and the average cross sectional concrete compressive strain which produces snap-through is usually small in thin slabs.

4.3.6. Deflection Estimate Results

From the previous discussions in Section 4.3, the viable methods for predicting the peak capacity midspan deflections are either using the slab's L/h ratio in the empirically based deflection curves or using a concrete compressive strain estimate in a curvature based deflection equation. In

order to estimate the concrete compressive strain, linear curves were used for the thick slabs (i.e., Figure 4.17), while the average of the adjusted strain values (Table 4.7) were used for the thin ($17 < L/h < 22$) and very thin ($22 < L/h < 29$) slabs. The comparison of the four viable deflection estimates (Table D.13) is presented in Table 4.8.

The empirically based deflection curves (Figures 4.14 and 4.15) are probably the simplest to use, except when evaluating a slab with an L/h within the range of $15 < L/h < 18$. However, simple interpolation between the results provided by substituting the given L/h into both equations, 4.15 and 4.16, results in estimates close to the experimentally measured deflection (EC, column 5, Table 4.8). The curves in Figures 4.14 - 4.15 point out a direct correlation between the span-to-thickness ratio and the peak capacity midspan deflection-to-thickness ratio. The curves also highlight the behavioral change at peak capacity for thick slabs controlled by material instability and thin slabs controlled by geometric instability.

The curvature based deflection estimates shed light on the fact that the concrete compressive strength plays a major role in determining the concrete compressive strain used to estimate the peak capacity deflection. The shaded strain value (i.e., 0.004656 in/in, column D, Figure 4.10) is the estimated strain value based on f'_c (Wood3, column 9, Table D.12). The curvature based deflection estimate is a maximum when the peak thrust is a maximum (i.e., $\Delta =$ 0.437 inches, shaded in column O, Figure 4.10), and is a better estimate of the experimentally measured deflection (i.e., 0.41 inches) than the empirically based deflection estimate of 0.63 inches (Section 4.3.2). Even though Keenan's simplified deflection estimate assumes equal tensile and compressive reinforcement ratios, the estimated deflections were fairly close to the experimental deflections (column 4, Table 4.8). However, the modified curvature based deflection equation used with either Park and Gamble's (column 2, Table 4.8) or the new (column 3, Table 4.8) compressive membrane theory provides the best correlation and the smallest standard deviation from the experimental deflections without assuming equal tensile and compressive reinforcement. As can be seen in the bottom half of Table 4.8, disregarding a few of the experimental deflection outliers improves the accuracy and nearly cuts in half the standard deviation. However, inclusion of all

data points has little affect on the overall positive results from use of the curvature based deflection equations.

The peak thrust should be used to index the peak load capacity with the newly derived version of the compressive membrane theory and the corresponding peak capacity midspan deflection with the modified curvature based deflection equation. Together these two values represent Point B in Figure 4.1.

4.4. Tensile Membrane Behavior

Once the slab fails or snaps-through due to material or geometric instability (Point B, Figure 4.1), tensile membrane action will initiate gradually as the capacity decreases. The ability to generate tensile membrane behavior assumes adequate anchorage of the reinforcement. If the boundary elements, i.e., slabs, walls, or beams, are stiff enough, the central membrane forces transition from compression to tension as the boundary elements resist the slab's inward edge movement. The stretching of the slab produces full-depth cracks forcing the reinforcement to act as a tensile membrane (Point C, Figure 4.1) with the concrete ultimately capable of only transferring the uniform load vertically to the reinforcement. Additional deflection generates gradual spreading of the tension or catenary zone until the reinforcement fractures (Point D, Figure 4.1). Tensile membrane action is normally used as a reserve capacity to catch the loaded slab if the compressive membrane capacity is exceeded, but within the defense community, the tensile membrane resistance and ultimate load capacity are used to resist the blast loading. At times, the tensile membrane load capacity may even be designed to exceed the compressive membrane capacity.

4.4.1. Tensile Membrane Capacity Derivation

Park's (1964) widely accepted load-deflection relationship for uniformly loaded rectangular plastic tensile membranes (Figure 4.18) provides the standard plastic tensile membrane

theory equation. The limiting condition, T_y/T_x equal to infinity, represents the equation for one-way slabs:

$$\frac{w}{\delta} = \frac{8T_y}{\ell_y^2} \qquad \text{EQN 4.27}$$

in which

T_y is the tension force carried by the steel reinforcement (i.e., steel stress multiplied by the cross-sectional area) in the one-way span direction,

ℓ_y is the one-way span length,

w is the uniform distributed load, and

δ is the midspan deflection.

Park used the yield stress for the reinforcement stress, while researchers at WES have used the rupture stress and yield stress to provide upper and lower bound estimates, respectively (Guice, 1986). For thick slabs, some WES experimental results, based on the number of ruptured bars, have suggested to only using half of the reinforcement cross-sectional area in the calculation of T_y (Woodson, 1993).

If the reinforcement is properly anchored, rupture of the reinforcement produces failure during the tensile membrane resistance phase. Even though the experimental data does show some scatter, the incipient tensile membrane collapse appears to be a function of L/h. Table 4.9 lists the average span length fraction which represents the experimental incipient collapse deflection. Upon considering the experimental results listed in Table 4.9 and close scrutiny of the experimental data for the slabs listed in Appendix A (column 3 and 4, Table 4.11), the following values for incipient collapse or tensile failure for one-way slabs were chosen: one-tenth of the span length for $L/h < 6$, one-seventh the span length for $6 < L/h < 18$, and one-sixth the span length for $L/h > 18$.

4.4.2. Tensile Membrane Capacity Results

Since not all of the thin one-way slabs (L/h > 18) listed in Appendix A were anchored at the supports to allow for development of tensile membrane resistance, the tensile membrane results in Chapter 2 for thin two-way slabs established the incipient collapse values for thin one-way slabs until additional experimental data is available.

The experimental results for the thick one-way slabs listed in Appendix A at first display a large amount of scatter as to when the tensile membrane resistance begins (Point C, trough load capacity, Figure 4.1) and ends (Point D, ultimate load capacity, Figure 4.1). Park and Gamble (1980) and others state that the capacity drops after the peak capacity until about the Johansen yield line capacity for fixed edge conditions before the tensile membrane resistance catches the load and increases the capacity. However, the inclusion of deep slabs (L/h < 6) and the availability of small support rotation affects the capacity and deflection at which tensile membrane resistance initiates.

In some cases, the capacity at which tensile membrane resistance began (Point C, Figure 4.1) could be lower than the simply-supported capacity for the one-way slab. At other times the initiation capacity was larger than the fixed-supported yield line capacity. Of course, sometimes the capacity at initiation of tensile membrane resistance was somewhere between the capacity for simply-supported and fixed-supported. The author used the easily established yield line capacities (YL) for simply-supported edge conditions, fixed-supported edge conditions, and the average between the two (listed as s, f, and m, respectively, Table 4.10) to compare with the experimental capacities at Point C, Figure 4.1. In some cases more than one comparison was made in order to establish trends in the behavior based on L/h.

For L/h's less than 6, the trough capacity was close to the yield line capacity for fixed-supported edge conditions, while the capacity for slabs with an L/h greater than 6 was closer to the yield line capacity for simply-supported edge conditions (column 4, Table 4.10). When the thick slab did not have equal amounts of compressive and tensile reinforcement, the capacity at initiation of tensile membrane resistance was sometimes closer to the average capacity between simply-

supported and fixed-supported conditions. When the support conditions were limited to less than two degrees of rotation as they were in Guice's (1986) research (i.e., slabs G1-G6), the capacity at initiation of tensile membrane resistance is very close to the yield-line capacity for fixed-supported edge conditions (Table 4.10). The general rules established to determine the capacity for initiation of tensile membrane resistance (Point C, Figure 4.1) were as follows:

- if $L/h < 6$, the capacity can be estimated as the yield line capacity for fixed-supported edge conditions;
- if $6 < L/h < 18$, the capacity can be estimated as the yield line capacity for simply-supported edge conditions; and
- if the support conditions are such that the rotation is less than 2 degrees (Guice, 1986) and $6 < L/h < 18$, then the capacity can be estimated as the yield line capacity for fixed-supported edge conditions.

The second part to locating Point C, Figure 4.1, is to determine the associated midspan deflection. In order to use Park's tensile membrane curve to represent the tensile resistance, this deflection must lie on the curve. As noted before, there is a question as to whether all or only the tensile reinforcement at midspan in doubly reinforced members is considered. The capacity determined in the preceding paragraph was used to calculate the associated deflection (ΔYL, column 7, Table 4.10) with EQN 4.27 while considering all the reinforcement at midspan, the tensile reinforcement at midspan, or the average reinforcement between the other two (d, s, and a, respectively, column 7, Table 4.10). The following pattern emerged when calculating the associated deflection in column 7, Table 4.10:

- if $L/h < 6$, all the reinforcement at midspan should be used to calculate the deflection;
- if $6 < L/h < 18$, only the tensile reinforcement at midspan should be used to calculate the deflection; and
- if the support conditions are such that the rotation are less than 2 degrees and $6 < L/h < 18$, all of the reinforcement should be used to calculate the deflection.

The listed averages and standard deviations for the normalized YL capacities and deflections at the bottom of Table 4.10 are the results when using the recommended values in the two preceding paragraphs.

The controlling factor for how much reinforcement is contributing to tensile membrane resistance appears to be a function of how much straining has occurred in the reinforcement prior to initiation of tensile membrane resistance. When there is support rotation limited to less than 2 degrees, there is less early plastic rotation along the support hinge line resulting in less damage (i.e., strain) to the reinforcement. Once the tensile membrane resistance begins, more of the reinforcement supports the load rather than rupturing prematurely as in members where a lot of straining occurred during the compressive membrane plastic hinge rotation. Thin slabs exhibit some of the same behavior since their behavior is controlled by geometric instability, i.e., usually no concrete crushing and small hinge rotation before snapping through to tensile membrane resistance. For most thick slabs, there is no support rotation and a large amount of the hinge rotation during the compressive membrane phase generates a large amount of straining in the tensile reinforcement. Once the tensile membrane phase begins, half of the reinforcement for thick slabs has little straining capability left before rupturing. For the deep slabs ($L/h < 6$), when the concrete crushing/pop-outs occurs, the small amounts of rotation which has occurred has not greatly limited the tensile membrane resistance of most of the reinforcement. Additionally, in order for the associated tensile membrane deflections for deep slabs to be closer to the experimental deflections at the calculated capacities, the entire tensile membrane curve should be shifted upward an amount equal to at least the capacity for a simply-supported edge condition, if not as high as the fixed-supported yield line capacity.

At the point of incipient collapse (Point D, Figure 4.1), the yield stress and rupture stress were both evaluated within EQN 4.27. Generally, the same trends were observed for Point D as there were for Point C, Figure 4.1 (Table 4.11). The following deflection values for tensile failure for one-way slabs were used to determine the incipient collapse capacity: one-tenth of the span

length for L/h < 6, one-seventh the span length for 6 < L/h < 18, and one-sixth the span length for L/h >18 (Table 4.11).

Even when using all the reinforcement at midspan and the rupture stress (symbol d, first four rows in column 9, Table 4.11), the predicted capacity for the deep slabs (L/h < 6) was smaller than the experimental collapse capacity (column 5, Table 4.11). The tensile membrane curve needs to be shifted upward by an amount equal to at least the capacity for the simply-supported edge condition in order to improve the predicted collapse capacity for the deep slabs. For the rest of the thick slabs (6 < L/h <18), the reinforcement yield stress, rather than the rupture stress, generated more acceptable predicted capacities based on the normalized capacity averages and standard deviations listed at the bottom of Table 4.11. If the support is rigidly restrained against rotation, only the tensile reinforcement (symbol s, Table 4.11) at midspan should be used to predict the capacity at a deflection of one-seventh of the span length, while all of the available reinforcement at midspan should be used when the supports can possibly rotate an amount less than 2 degrees. When adhering to the suggested amounts of reinforcement for thick slabs based on whether the supports can rotate or not, the average and standard deviation for the predicted collapse capacities are acceptable (Table 4.11).

4.5. Load-Deflection Curve

The load-deflection curve provides insight into the complete response of a structural element. Even though most structures are never loaded to failure, protective structures, on the other hand, are designed to resist extremely heavy loading with moderate (i.e., some concrete crushing) to severe damage (i.e., tensile membrane resistance without collapse). In order to achieve economical designs which can resist these types of loading, compressive and tensile membrane resistance must be employed. Even for conventional slabs strengthened naturally by the surrounding slabs or through a beam/wall system, knowledge of the complete load response allows for the proper assessment of the available strength afforded by the peak compressive membrane capacity and the reserve tensile membrane capacity. In dynamic analysis, engineers use numerical

integration schemes and the load-deflection curve to determine the slab's energy absorption capability and overall ductility during loading. Therefore, an accurately constructed load-deflection response for a given slab design is an extremely valuable asset.

Synthesis of the numerous dynamic and static load tests for laterally restrained reinforced concrete slabs reinforces the idea that the general shape of the load-deflection curve for a laterally restrained reinforced concrete one-way slab has a parabolic rise in capacity to the peak compressive membrane capacity, a roughly parabolic decline in load capacity until the tensile membrane action catches the load, and an approximately linear increase in capacity until rupture of the reinforcement during tensile membrane resistance (Figure 4.1). The transition between compressive and tensile membrane resistance is usually smooth unless there is a shear failure.

The efforts by some researchers listed in Chapter 2 to mirror the early elastic and then the elastic-plastic behavior before peak capacity resulted in a fairly parabolic curve up to the peak capacity. Park's (1964) modified rigid-plastic theory and Morley's (1967) flow theory have been used by a few researchers to represent the descending portion of the compressive membrane zone with a smooth transition at intersection with the tensile membrane curve. However, the compressive membrane theories only truly represent the slab's material conditions at the peak capacity (i.e., the steel yielding and the concrete at the maximum compressive strength or disintegrating). Additionally, when both the flow and the modified rigid-plastic theories are plotted with the experimental load-deflection curve, the flow and the modified rigid-plastic theories are usually not as steep during the post-peak phase as the experimentally observed decline in capacity. Therefore, each theory could result in an unrealistic representation of the energy absorption capability, or area under the curve.

The following system of curves is proposed: the use of a roughly parabolic ascending curve up to the peak capacity, a descending parabolic curve from the peak capacity until intersection with the tensile membrane curve, and a linear extension along the tensile membrane curve to represent the tensile membrane resistance. This method of developing the load-deflection

curve will provide a simple, and possibly a more accurate, representation of the experimental results.

4.5.1. Load-Deflection Curve Development

A good parabolic representation of the ascending and descending portions of the compressive membrane curve was provided by Keenan (1969). His roughly parabolic curves will use the peak thrust indexed compressive membrane capacity (Section 4.2) for q_u and the curvature based deflection estimate (Section 4.3) for z_u (representing the peak compressive membrane deflection) to define the ascending (EQN 4.28) and the descending (EQN 4.29) portions of the compressive membrane behavior while incrementing the deflection, z.

$$q = q_u\left[1-\left(1-\frac{z}{z_u}\right)^n\right]^{\frac{1}{n}} \qquad \text{EQN 4.28}$$

for the ascending curves (i.e., A to B, Figure 4.1) and

$$q = \frac{1}{2}q_u\left\{1+\left(\frac{q_y}{q_u}\right)+\left[1-\left(\frac{q_y}{q_u}\right)\right]\cos\left[\frac{\pi\,(z-z_u)}{(z_s-z_u)}\right]\right\} \qquad \text{EQN 4.29}$$

for the descending curves (i.e., B to C, Figure 4.1). The appropriate yield line capacity, q_y (Section 4.4), for Point C of Figure 4.1 is based on L/h (Section 4.4), while z_s is the corresponding tensile membrane deflection at the chosen yield line capacity (Section 4.4). The values for q_y and z_s define the end point for EQN 4.29. Keenan's suggested value of n = 1.3 for one-way slabs was used. EQN 4.29 is only valid for cosine angles from 0.0 to π, or the first half of the curve shown in Figure 4.19. The resulting curve will gradually decrease from the capacity q_u (i.e., cos = 1, smooth transition at the peak capacity) to q_y (i.e., cos = -1, smooth transition at the tensile membrane curve) at a deflection of z_s. From the point q_y and z_s (Point C, Figure 4.1) until incipient collapse which is defined in Section 4.4, the linear tensile membrane curve, based on

considering only the tensile reinforcement or all of the reinforcement at midspan (Section 4.4), represents the slab's final resistance capacity.

4.5.2. Load-Deflection Curve Results

The estimated load-deflection curve (Figures 4.20 - 4.21) is comprised of the following:

- the ascending portion of the compressive membrane resistance curve (C1, from EQN 4.28, ascending curve of Figures 4.20 - 4.21), using the peak thrust indexed capacity and the strain controlled curvature based deflection to define the peak point (Point B, Figure 4.1);
- the descending portion of the compressive membrane resistance curve until intersection with the tensile membrane resistance curve (C2, from EQN 4.29, descending curve of Figures 4.20 - 4.21), which uses the L/h ratio and whether support rotation occurs to determine first the appropriate yield line capacity, and then the associated deflection from EQN 4.27 to define Point C, Figure 4.1 (i.e., intersection of curve T1 which considers only tensile reinforcement at midspan or T2 which considers all of the reinforcement at midspan); and
- the linear tensile membrane resistance curve (Ten), which uses an L/h based incipient collapse deflection and lies along the previously selected tensile membrane curve (T1 or T2) to construct the linear curve from Point C to Point D (Figure 4.1).

In Figures 4.20 - 4.21, the experimental curve (Exp), the newly derived compressive membrane curve (CMC), and the linear tensile membrane curves (T1, tensile reinforcement at midspan; T2, all of the reinforcement at midspan) are presented for comparison with the author's estimated load-deflection curve. A larger sample of estimated load-deflection curves for a variety of span length-to-thickness ratios is presented in Appendix D.

Since the estimation techniques for the deflections have large standard deviations, there is the possibility that the estimated peak capacity deflection, z_u (Point B, Figure 4.1), could be as large or slightly larger than the deflection, z_s (Point C, Figure 4.1). This happened for Slab G4 (Figure 4.21) in which the deflection z_s was only 0.04 inches larger than the deflection z_u. This small difference in deflection between the Points B and C resulted in an incomplete curve between

Points B and C. The solution to the problem was to slightly reduce z_u by ten percent increments of the standard deviation [i.e., 0.448, column 3, W(W), thick slabs, Table 4.8] until a reasonable curve could be generated. A small reduction in z_u only slightly affects the area under the estimated curve which is generally smaller than the area under the experimental curve. Since there is no really effective way of knowing whether the actual deflection would be slightly smaller or larger than the estimated deflection, the deflection z_u was chosen to be decreased rather than increasing the deflection for z_s, which could increase the area under the curve.

The experimental curves plotted in Figures 4.20 - 4.21 are as accurate as possible. The data points were generated from graphs in the literature through hand-drawn lines determining the experimental capacities at constant increments of deflection. All peak and trough points were captured by using a small deflection increment. In general, the estimated load-deflection curves match the response of the experimental curves. For the thin slabs, the experiments were stopped shortly after the peak capacity since the edges were restrained only for outward lateral movement. The continuation of the predicted curves beyond the peak capacity is based on the experimental results presented in Chapter 2 for two-way thin slabs rigidly restrained at the edges. For the thick slabs, the averaged capacity (W_{avg}, Table D.2) between the peak thrust indexed capacity and the computed peak capacity was used for q_u in Figures 4.22 - 4.23. In most cases, there was an improvement in the correlation between the experimental peak load capacity and the estimated peak load capacity. It should be noted that a simple straight line between the origin, the peak point, the trough point, and the ultimate point also provides a simple estimate of the load-deflection curve.

4.6. Simple Estimate for the Peak Capacity

Most civil engineers are taught how to construct an axial force-moment interaction diagram for a reinforced concrete section during their first or second concrete design course. If the peak thrust developed during compressive membrane action can be estimated, then the peak thrust enhanced moments available at the supports and midspan can be determined. Since the P-Δ effects

are generally small in structural elements experiencing double curvature (i.e., both ends fixed-supported), the capacity can be predicted by substituting the enhanced moments into

$$\frac{w\ell^2}{8} = m_u' + m_u \qquad \text{EQN 4.30}$$

where the moments are calculated for a unit slab width.

Unfortunately, most of the research listed in Chapter 2 and detailed in Appendix A for one-way slabs does not include any measurements for the thrust generated during compressive membrane action. Therefore, the thrust (column 3, Table 4.12) used in the axial force-moment interaction equations to predict the peak capacity was determined by trial and error. The thrusts in the third column do not include P-Δ effects (i.e., EQN 4.30). The thrust in the fifth column includes P-Δ effects with the deflection represented by the experimental peak capacity deflection (i.e., subtracting T x Δ from the right side of EQN 4.30). In most cases the experimental peak capacity could not be matched by even the balanced thrust conditions when considering P-Δ effects. Therefore, only the thrust without P-Δ effects was considered when calculating the peak capacity.

The thrust was divided by the slab's ultimate axial capacity (P_o, Table D.15) in an effort to determine a trend. The averages and standard deviation for the T/P_o ratio while considering all the slabs, thick or thin slabs, and thick, thin or very thin slabs are listed in the second column of Table 4.13. It was obvious that a single ratio should not represent all the slabs. The simple peak capacity estimate (SP (tt)) using the T/P_o ratio for thick ($L/h < 18$) or thin ($L/h > 18$) slabs is presented in the seventh column of Table 4.12. Additionally, the simple peak capacity estimate (SP (ttvt)) using the T/P_o ratio for thick ($L/h < 18$), thin ($18 < L/h < 22$), or very thin ($L/h > 22$) slabs is presented in the ninth column of Table 4.12 for comparison. The normalized capacity averages and standard deviations for the various slab groupings are presented in the third and fourth columns of Table 4.13. The best average and lowest standard deviation is obtained when using a separate T/P_o ratio for the thick ($T/P_o = 0.167$), thin ($T/P_o = 0.319$) and very thin ($T/P_o =$

0.197) slab groupings (i.e., column 4, Table 4.13). A simple estimate for the thrust is $P_o/6$ for thick slabs, $P_o/3$ for thin slabs, and $P_o/5$ for the very thin slabs.

In order for the engineer to quickly estimate the peak compressive membrane capacity for a thick slab, he/she will use the cross-sectional ultimate axial capacity (P_o) to determine the thrust (T) from the ratio $T/P_o = 0.167$. Since most of the data supports a peak thrust less than the balanced point thrust, the balanced thrust will be used only if the calculated thrust is greater than the balanced point thrust. The peak thrust is used within the axial force-moment interaction equations to obtain the enhanced (i.e., hinge) moments to substitute into EQN 4.30. The calculation for the enhanced moment should be repeated for the supports and midspan (i.e., different reinforcement ratios possible at each). This simple calculation for the peak capacity of laterally restrained reinforced concrete one-way slabs is something that most engineers can do in even remote locations.

For example, P_o for the slab Wood3 is 33079 lb/in (width of 24 inches, Table D.15) which results in a thrust of $T = (33079)(0.167) = 5524$ lb/in. The thrust is less than P_{bal} (i.e., 10753 lb/in, Table D.15) so it is used in the axial force-moment interaction equations. There is equal tensile and compressive reinforcement at both the supports and midspan. Upon substitution of T = 5524 lb/in into the axial force-moment interaction equations, the enhanced moment is 21378 in-lb/in at the supports and midspan. With a span length (ℓ) of 24 inches, the estimated capacity is 593 psi which is slightly larger than the experimental capacity of 557 psi (i.e., 593/557 = 1.06, row 3, column 8, Table 4.12).

4.7. Summary

As presented in Chapter 2, the peak compressive membrane capacity for laterally restrained reinforced concrete one-way slabs generally has been estimated through a deflection indexed capacity in either the flow or rigid-plastic compressive membrane theories. Efforts to improve the original theories has resulted in the compressive and tensile membrane theories presented in Park and Gamble (1980). In order to estimate the peak capacity of a laterally

restrained slab, two key unknowns must be estimated: the lateral stiffness and the peak capacity midspan deflection. A deflection of approximately 0.45 - 0.5h has been suggested for indexing the peak capacity within the various compressive membrane theories. Past research has shown that a lateral restraint greater than a scalar magnitude of E_c is unwarranted since a larger lateral restraint provides very limited increase in peak capacity. Recent tests on laterally restrained reinforced concrete one-way slabs at WES have highlighted the large variation in deflection estimates (i.e., 0.05 to 0.45h) required to accurately predict the peak capacity for the large range of span-to-thickness ratios (i.e., $2.7 < L/h < 28.3$).

The method presented herein of using the peak thrust to index the capacity within Park and Gamble's compressive membrane theory and the newly derived compressive membrane theory provides a predicted peak capacity which is closer to the experimental peak capacity than that obtained by using the actual experimental peak capacity midspan deflection to index the peak capacity. The thrust calculation is an integral part of the current compressive membrane theories and the peak thrust indexed capacity eliminates the difficult task of first, estimating the peak capacity midspan deflection, and then, indexing the peak capacity. Additionally, methods to estimate the peak capacity deflection can produce large discrepancies (Tables D.7 and D.8). The close comparisons of the generated peak thrusts (Table D.15) within the different analysis methods, the nearly simultaneous occurrence of the peak capacity and the peak thrust in finite element analysis, and the accuracy of the presented prediction technique provides efficacy in using the generated peak thrust in the compressive membrane theories to index the peak capacity.

The study on the sensitivity of the lateral stiffness (Table 4.3) shows that using a lateral stiffness with a scalar magnitude of approximately 0.05 - 0.01E_c usually generates acceptable enhanced results for the tested slabs which had fairly rigid supports (Appendix A). In this dissertation, the lateral stiffness was varied in order to determine the appropriate stiffness corresponding to the support structure used for the large number of slabs tested at WES (Table 3.1).

Since the load-deflection history is important in the evaluation of the dynamic response of one-way slabs subjected to blast events, several methods were developed for predicting the peak capacity midspan deflection. All of the methods produced large discrepancies as noted by the large standard deviations listed in Table 4.8. The easiest method to use is the empirically based deflection curves (Figures 4.14 and 4.15 or EQNs 4.15 and 4.16). The best deflection estimate (Tables 4.8) was determined through the modified curvature based deflection equation used in the newly derived compressive membrane theory, in which the peak concrete compressive strain for thick slabs was estimated through a relationship established with the slab's concrete uniaxial compressive strength (Figure 4.17 and EQN 4.26), while a simple averaged strain value was used for thin slabs.

The curvature based peak capacity midspan deflection and peak thrust indexed capacity locate Point B, Figure 4.1. Points C and D, which lie along the tensile membrane curve, are determined after choosing the slope of the tensile membrane curve, i.e., whether only the tensile reinforcement or all of the reinforcement at midspan is considered.

The following procedure is offered to generate the complete load-deflection curve (example: for a slab of given $L/h = 4.4$):

1. Determine the estimated strain from the concrete compressive strength, i.e., 0.004656, column D, Figure 4.10 [EQN 4.26 for thick slabs ($L/h < 18$), $\varepsilon = 0.00142$ for thin slabs ($18 < L/h < 22$), or $\varepsilon = 0.00095$ for very thin slabs ($22 < L/h < 28.3$)].
2. Locate point of peak thrust (i.e., 171723 lb, column L, Figure 4.10).
3. Use the peak thrust to index (i.e., point to) the peak capacity (i.e., 541.45 psi, column J, Figure 4.10) and the peak deflection (i.e., 0.437, column O, Figure 4.10). The peak capacity and the peak deflection establish Point B, Figure 4.1.
4. a) If the slab has an $L/h < 6$ or $L/h > 18$, then the trough capacity at Point C (Figure 4.1) is the fixed-supported yield line capacity (i.e., Johansen yield line capacity), while the trough deflection at Point C is calculated with EQN 4.27, using the fixed-supported yield line capacity

and all of the reinforcement at midspan. The trough capacity and deflection establish Point C, Figure 4.1.

4. b) If the slab has an $6 < L/h < 18$ with the support rotation limited to less than 2 degrees, then the trough capacity at Point C (Figure 4.1) is the fixed-supported yield line capacity, while the trough deflection at Point C is calculated with EQN 4.27, using the fixed-supported yield line capacity and all of the reinforcement at midspan. The trough capacity and deflection establish Point C, Figure 4.1.

4. c) If $6 < L/h < 18$ and there is no support rotation, then the trough capacity at Point C (Figure 4.1) is the simply-supported capacity, while the trough deflection at Point C is calculated with EQN 4.27, using the simply-supported capacity and only the tensile reinforcement at midspan. The trough capacity and deflection establish Point C, Figure 4.1.

5. The ultimate deflection at Point D (Figure 4.1) is either one-tenth of the span length for an $L/h < 6$, one-seventh of the span length for $6 < L/h < 18$, or one-sixth the span length for an $L/h > 18$, while the associated capacity is determined by substituting the deflection at Point D into EQN 4.27 and using the appropriate reinforcement area determined in steps 4a/b or 4c to determine the deflection of Point C.

6. The load-deflection curve is plotted using the peak capacity and deflection values at Point B in EQN 4.28 (the ascending curve, A-B), the peak and trough capacity and deflection values at Point B and C in EQN 4.29 (the descending curve, B-C), and the appropriate linear tensile membrane relationship (i.e., only the tensile reinforcement or all of the reinforcement, EQN 4.27) between Points C and D.

Example load-deflection curves are presented in Figures 4.20 - 4.21 with the curve C1 representing the generally parabolic ascending compressive membrane resistance curve, curve C2 representing the generally parabolic descending compressive membrane resistance curve, and curve Ten representing the linear tensile membrane resistance. The experimental curve (Exp), the theoretical compressive membrane curve (CMC), and the tensile membrane curves when considering only the tensile membrane reinforcement at midspan (T1) or all of the reinforcement at midspan (T2) are

included for comparison. The generated load-deflection curves match the experimental data extremely well.

A simple, but accurate, estimate of the peak capacity is possible through use of the axial force-moment interaction equations. The appropriate thrust-to-axial capacity (T/P_o) for thick (0.167), thin (0.319) and very thin (0.197) slabs (Table 4.13) is multiplied by the ultimate axial capacity for the given slab parameters at midspan to calculate the thrust used within the axial force-moment interaction equations. Once the enhanced moments at midspan and the supports are determined separately from the axial force-moment interaction equations and substituted into EQN 4.30, the peak capacity is easily calculated. The thrust enhanced moments at midspan and the supports may be different if the reinforcement ratios vary between the supports and midspan.

Engineers now have a method for accurately predicting the peak compressive membrane capacity and the entire load-deflection curve, while only needing to estimate the lateral support stiffness. The lateral support stiffness can be estimated between a scalar magnitude of 0.05 and $0.01E_c$. Additionally, a simple procedure that most engineers can use and easily understand is available for estimating the peak capacity in the field. This simple estimate will be very useful in targeting methods and the early stages of design.

Table 4.1. Grouping of Experimental Slabs Used Within the Analysis

L/h	# Slabs	L (in)	h (in)	Symbol	w_{exp} (psi)	Δ_{exp} (in)	L/h	# Slabs	L (in)	h (in)	Symbol	w_{exp} (psi)	Δ_{exp} (in)
2.7	7	24	8.9	Wood1	1486	0.41	17.1	1	60	3.5	C1	16.5	0.65
2.7	3	24	8.9	Wood2	1620	0.39	17.1	1	60	3.5	C2	18.3	0.65
4.4	3	24	5.5	Wood3	557	0.41	18.8	2	56.5	3.0	RB26	23.3	0.446
5.0	1	24	4.8	B1	290	0.53	18.8	2	56.5	3.0	RB27	15.7	0.441
8.0	6	24	3.0	Wood4	68.8	0.835	18.8	2	56.5	3.0	RB18	15.6	0.462
8.0	4	24	3.0	Wood5	86.0	0.885	18.8	2	56.5	3.0	RB20	24.5	0.474
8.0	4	24	3.0	Wood6	133	0.893	18.8	2	56.5	3.0	RB19	19.3	0.551
8.3	1	24	2.9	W14	126	0.8	18.8	2	56.5	3.0	RB21	16.2	0.447
8.3	1	24	2.9	K2	174	0.21	18.8	2	56.5	3.0	RB22	18.5	0.45
10.0	1	24	2.4	B2	61	0.50	18.8	2	56.5	3.0	RB23	26.9	0.512
10.0	1	24	2.4	B3	101	0.86	20.0	1	60	3.0	C3	13.3	0.65
10.4	8	24	2.3125	W18	68.7	0.813	24.0	1	72	3.0	C4	8.8	0.65
10.4	2	24	2.3125	W910	73.5	0.825	28.3	2	56.5	2.0	RB25	6.0	0.50
10.4	1	24	2.3125	W1	66.0	1.0	28.3	2	56.5	2.0	RB24	8.0	0.55
10.4	1	24	2.3125	W2	64.0	0.8	28.3	3	56.5	2.0	RB11	5.1	0.506
10.4	1	24	2.3125	W3	68.0	1.2	28.3	1	56.5	2.0	RB10	7.9	0.576
10.4	2	24	2.3125	W45	72.5	1.1	28.3	2	56.5	2.0	RB12	7.0	0.545
10.4	1	24	2.3125	W6	68.0	0.25	28.3	3	56.5	2.0	RB13	5.7	0.506
10.4	7	24	2.3125	W713	69.0	0.857	28.3	3	56.5	2.0	RB14	7.9	0.536
10.4	1	24	2.3125	W15	52.0	1.0	28.3	2	56.5	2.0	RB15	5.9	0.507
10.4	2	24	2.3125	G1	52.0	0.798	28.3	2	56.5	2.0	RB17	7.3	0.562
10.4	4	24	2.3125	G2	72.0	1.335							
10.4	2	24	2.3125	G3	95.0	1.179							
12.0	1	72	6.0	K1	110	1.00							
14.8	2	24	1.625	G4	27.5	0.805							
14.8	2	24	1.625	G5	41.0	0.601							
14.8	2	24	1.625	G6	46.0	0.65							

Table 4.2. Comparison of Normalized Capacity Averages/Standard Deviations for Park and Gamble's and the Modified Compressive Membrane Theories

	YL/w [a]	PP/w [b]	PDI/w [c]	PTI/w [d]	P_{avg}/w [e]	WP/w [b]	WDI/w [c]	WTI/w [d]	W_{avg}/w [e]
Average - All:	0.490	1.012	0.907	0.846	0.929	1.121	0.933	0.991	1.056
Standard Deviation:	0.244	0.142	0.152	0.137	0.137	0.159	0.153	0.159	0.156
Average - Thick (L/h < 18):	0.644	1.078	0.954	0.918	0.999	1.098	0.960	0.941	1.019
Standard Deviation:	0.169	0.116	0.159	0.116	0.11286	0.114	0.163	0.114	0.109
Average - Thin (18 < L/h < 22):	0.235	0.844	0.804	0.711	0.778	1.000	0.846	0.931	0.965
Standard Deviation:	0.133	0.091	0.094	0.079	0.084	0.100	0.106	0.087	0.092
Average - Very Thin (L/h > 22)	0.276	0.971	0.864	0.760	0.866	1.298	0.934	1.193	1.245
Standard Deviation:	0.118	0.101	0.108	0.087	0.093	0.167	0.125	0.164	0.163

w - experimental capacity.

[a] YL - yield line with fixed-supported edge conditions.

[b] Compressive membrane theory computed peak capacity: PP - Park and Gamble; WP - Newly Derived.

[c] Compressive membrane theory experimental deflection indexed capacity: PDI - Park and Gamble; WDI - Newly Derived.

[d] Compressive membrane theory peak thrust indexed capacity: PTI - Park and Gamble; WTI - Newly Derived.

[e] Average between the computed peak capacity and the peak thrust indexed capacity: P_{avg} - Park and Gamble; W_{avg} - Newly Derived.

Table 4.3. Peak Compressive Membrane Capacity Estimates (Point B, Figure 4.1) With the Modified Compressive Membrane Theory for Varying Lateral Support Stiffness

Slab Group	S[1] (lb/in)	w_{exp} (psi)	Simply Spt (SS)(psi)	YL (psi)	YL/w	Computed Peak (WP)(psi)	WP/w	Defl Indexed (WDI)(psi)	WDI /w	Thrust Indexed (WTI)(psi)	WTI /w	W_{avg} (WP+WTI)/2 (psi)	W_{avg}/w
Wood1	E_c	1486	486	972	0.654	2159	1.453	2101	1.413	2122	1.427	2140	1.440
Wood1	$0.1E_c$					2047	1.377	2044	1.375	1952	1.313	1999	1.346
Wood1	$0.01E_c$					1751	1.178	1607*	1.081	1557	1.047	1654	1.113
B1	E_c	290	80.4	160.8	0.554	507	1.748	454	1.565	494	1.701	500	1.724
B1	$0.1E_c$					463	1.596	444	1.531	428	1.476	445	1.536
B1	$0.01E_c$					354	1.221	347*	1.196	290.7	1.002	322.3	1.111
Wood4	E_c	68.8	14.4	28.9	0.420	115	1.672	72.9	1.059	110	1.599	112.5	1.635
Wood4	$0.1E_c$					102	1.482	72.9	1.059	89.6	1.302	95.8	1.392
Wood4	$0.01E_c$					70.6	1.026	65.6	0.953	51.5	0.748	61.1	0.888
B2	E_c	61	18.4	36.9	0.604	115	1.885	89.4	1.466	110.6	1.813	112.8	1.849
B2	$0.1E_c$					100	1.639	87.4	1.433	88.9	1.457	94.5	1.548
B2	$0.01E_c$					67.6	1.108	67.6	1.108	52.1	0.854	59.8	0.981
G2	E_c	72.0	21.2	42.4	0.588	97.3	1.351	46.3	0.643	94.2	1.308	95.8	1.329
G2	$0.1E_c$					87.9	1.221	46.7	0.649	79.4	1.103	83.7	1.162
G2	$0.01E_c$					66.4	0.922	48.3	0.671	54.4	0.756	60.4	0.839
G4	E_c	27.5	9.2	18.3	0.665	45.9	1.669	21.6	0.785	43.9	1.596	44.9	1.633
G4	$0.1E_c$					39.4	1.433	21.8	0.793	33.9	1.233	36.6	1.333
G4	$0.01E_c$					26.1	0.949	21.1	0.767	19.5	0.709	22.8	0.829
RB18	E_c	15.6	3.5	3.5	0.224	16.8	1.076	13.9	0.891	15.8	1.013	16.3	1.045
RB18	$0.1E_c$					14.3	0.918	13.4	0.859	12.1	0.776	13.2	0.847
RB18	$0.01E_c$					9.1	0.585	8.9*	0.568	6.5	0.417	7.8	0.501
RB13	E_c	5.7	1.7	1.7	0.298	7.8	1.366	5.5	0.965	7.2	1.263	7.5	1.316
RB13	$0.1E_c$					6.3	1.101	5.3	0.929	5.1	0.895	5.7	1.000
RB13	$0.01E_c$					3.5	0.614	3.5	0.614	2.3	0.403	2.9	0.509

* Capacity is located before the computed peak capacity.

[1] E_c portrays a magnitude only and not the units.

Table 4.4. Peak Compressive Membrane Capacity Estimates (Point B, Figure 4.1) With the Modified Compressive Membrane Theory for Lateral Support Stiffness of Scalar Magnitude E_c Versus Finite Element Results for Fully Fixed-Supported Edge Conditions

Slab Group	S [1] (lb/in)	w_{exp} (psi)	Simply Spt (SS)(psi)	YL (psi)	Computed Peak (WP)(psi)	Defl Indexed (WDI)(psi)	Thrust Indexed (WTI)(psi)	W_{avg} (WP+WTI)/2 (psi)	Peak FE [2] 5 Elements (psi)	Peak FE 7 Elements (psi)	Peak FE 10 Elements (psi)	Average FE (psi)
Wood3	E_c	557	174	347	774 (1.072)*	734 (1.017)	760 (1.053)	767 (1.062)	782	684	699	722
Wood4	E_c	68.8	14.4	28.9	115 (1.055)	73 (0.669)	110 (1.009)	113 (1.032)	116	109	103	109
G1	E_c	52.0	14.0	26.2	84 (1.024)	51 ((0.623)	81 (0.983)	82.1 (1.001)	86.3	81.5	77.2	82
G4	E_c	27.5	9.2	18.3	46 (1.177)	22 (0.554)	44 (1.126)	44.9 (1.151)	42.2	39.3	36.4	39
AVG:					1.082	0.716	1.043	1.061				

[1] E_c portrays a magnitude only and not the units.
[2] FE - Finite Element.
* Values in parentheses are normalized by dividing the capacity by the average FE capacity in the last column of the table.

Table 4.5. Comparison of Average Normalized Capacity/Standard Deviations for the Deflection Estimates in Tables D.7 - D.8 Determined Through Park and Gamble's and the Modified Compressive Membrane Theories

	SS/Δ [a]	PP/Δ [b]	WP/Δ [b]	PTI/Δ [c]	WTI/Δ [c]	K(P)/Δ [d]	K(W)/Δ [d]	M/Δ [e]	W(P)/Δ [f]	W(W)/Δ [f]	EC/Δ [g]
Average - All:	0.799	0.634	0.475	1.587	1.208	0.550	1.293	0.175	0.621	0.708	1.108
Standard Deviation:	0.676	0.424	0.475	1.068	1.196	0.725	1.492	0.277	0.729	0.943	0.514
Average - Thick (L/h < 18):	0.375	0.693	0.651	1.723	1.636	0.911	0.956	0.237	1.028	0.995	1.163
Standard Deviation:	0.289	0.533	0.534	1.344	1.359	0.736	0.656	0.284	0.678	0.636	0.649
Average - Thick (no outliers):						0.746	0.800		0.867	0.845	0.944
Standard Deviation:						0.434	0.332		0.342	0.327	0.254
Average - All Thin (L/h > 18):	1.447	0.545	0.026	1.380	0.555	-	1.807	0.081	-	0.270	1.024
Standard Deviation:	0.576	0.082	0.129	0.231	0.301	-	2.128	0.236	-	1.146	0.103
Average - Thin (18 < L/h < 22):	0.958	0.581	0.229	1.457	0.623	-	3.815	0.077	-	0.570	1.070
Standard Deviation:	0.335	0.085	0.116	0.270	0.259	-	1.378	0.217	-	1.612	0.108
Average - Very Thin (L/h > 22):	1.887	0.512	0.185	1.311	0.495	-	-	0.084	-	-	0.982
Standard Deviation:	0.346	0.062	0.136	0.161	0.323	-	-	0.253	-	-	0.078

[a] Deflection estimate for simply-supported slab with a fully cracked moment of inertia.
[b] Deflection associated with the compressive membrane computed peak capacity: PP - Park and Gamble; WP - Modified.
[c] Deflection associated with the compressive membrane peak thrust indexed capacity: PTI - Park and Gamble; WTI - Modified.
[d] Deflection estimate using Keenan's curvature based equation within a compressive membrane theory: K(P) - Park and Gamble; K(W) - Modified.
[e] Mattock's deflection estimate.
[f] Deflection estimate using the modified curvature based equation with a compressive membrane theory: W(P) - Park and Gamble; W(W) -Modified.
[g] Empirical curve deflection estimate.

Table 4.6. Normalized Deflection Estimate Using the Average of the Peak Thrust Indexed Capacities From Park and Gamble's and the Modified Compressive Membrane Theories

Slab Group	PTI/Δ [a]	WTI/Δ [b]	TI_{avg}/Δ
Average - All:	1.587	1.208	1.398
Standard Deviation:	1.068	1.196	1.116
Average - Thick:	1.723	1.636	1.679
Standard Deviation:	1.344	1.359	1.349
Average - All Thin:	1.380	0.555	0.968
Standard Deviation:	0.231	0.301	0.239
Average - Thin:	1.457	0.622	1.041
Standard Deviation:	0.270	0.259	0.216
Average - Very Thin:	1.311	0.495	0.903
Standard Deviation:	0.161	0.323	0.241

[a] Normalized deflection associated with Park and Gamble's compressive membrane peak thrust indexed capacity.
[b] Normalized deflection associated with the modified compressive membrane peak thrust indexed capacity.

Table 4.7. Comparison of Computed Strains

Slab Group	$\varepsilon(M)$ [a] (in/in)	$\varepsilon(M)_{est}/\varepsilon(M)_{adj}$ [b]	$\varepsilon(W(P))$ (in/in)	$\varepsilon(W(P))_{est}/\varepsilon(W(P))_{adj}$ [c]	$\varepsilon(W(W))$ (in/in)	$\varepsilon(W(W))_{est}/\varepsilon(W(W))_{adj}$ [d]	$\varepsilon(K(W))$ (in/in)	$\varepsilon(K(W))_{est}/\varepsilon(K(W))_{adj}$ [e]
Average (Thick):		1.218		1.118		1.116		1.133
Standard Deviation:		0.548		0.489		0.489		0.537
Average (Thin):	-		0.00117		0.00142		0.00161	
Standard Deviation:	-		0.00024		0.00024		0.00013	
Average (Very Thin):	-		0.00070		0.00095		0.00111	
Standard Deviation:	-		0.00021		0.00018		0.00013	

[a] No thin slab calculations possible because of invalid data generation (i.e., error message).
[b] Estimated strain to the adjusted strain - Mattock's equations.
[c] Estimated strain to the adjusted strain - Modified curvature based equation used with Park and Gamble's compressive membrane theory.
[d] Estimated strain to the adjusted strain - Modified curvature based equation used with his compressive membrane theory.
[e] Estimated strain to the adjusted strain - Keenan's curvature based equation used with the author's compressive membrane theory.

Table 4.8. The Average Normalized Deflections and Standard Deviation for the Deflection Estimates Generated With Strain Estimates and the Empirically Based Deflection Curve

Slab Group	W(P) [a] (in)	W(W) [b] (in)	K(W) [c] (in)	EC [d] (in)
Average - All:	1.085	1.089	1.097	1.108
Standard Deviation:	0.356	0.364	0.415	0.514
Average - Thick:	1.121	1.128	1.172	1.163
Standard Deviation:	0.443	0.448	0.539	0.649
Average - Thin:	1.061	1.059	1.003	1.070
Standard Deviation:	0.229	0.243	0.072	0.108
Average - Very Thin:	1.015	1.019	0.997	0.982
Standard Deviation:	0.113	0.135	0.055	0.078
Average - All (No W6, K1, G5, G6):	1.003	1.004	0.985	1.016
Standard Deviation:	0.191	0.201	0.159	0.274
Average - Thick (No W6):	1.069	1.066	1.103	1.099
Standard Deviation:	0.327	0.324	0.419	0.564
Average - Thick (No W6, K1, G5, G6):	0.971	0.970	0.971	1.013
Standard Deviation:	0.190	0.196	0.211	0.349

[a] Deflection estimate using the modified curvature based equation with Park and Gamble's compressive membrane theory.
[b] Deflection estimate using the modified curvature based equation with the modified compressive membrane theory.
[c] Deflection estimate using Keenan's simplified curvature based equation with the modified compressive membrane theory.
[d] Deflection estimate using the empirically based deflection curve.

Table 4.9. Incipient Collapse Values

Researcher[1]	L/h	Incipient Collapse[2]
Powell, 1958	16	$1/8$
Park, 1964	20 - 40	$1/10$*
Keenan, 1969	12	$1/12$
Black, 1975	33	$1/6$
Guice, 1986	10.4 - 14.8	$1/8$
Woodson, 1993	8	$1/5$ - $1/7$
Woodson, 1994	3 - 5	$1/9$ - $1/13$

* Noted as much less than experimental.
[1] Span length fraction either stated in the reference or determined through evaluation of experimental data.
[2] The midspan deflection at incipient collapse is estimated by this fraction of the span length.

Table 4.10. Capacity and Deflection for Point C, Figure 4.1

Slab [a] Group	L/h	w_{exp} (psi)	YL [b] (psi)	YL/w	Δ_{exp} (in)	ΔYL_c (in)	$\Delta YL/\Delta$
Wood1	2.7	958	971-f	1.013	1.85	7.0-d	3.78
Wood2	2.7	146[d]	358-f	2.452	4.0[1]	4.0-d	1.0
Wood3	4.4	260	340-f	1.30	1.0	3.5-d	3.5
B1	5.0	243[e]	160-f	0.658	0.77[2]	6.0-d	7.79
Wood4	8.0	7.0	14.4-s	2.06	2.75	3.0-s	1.09
Wood5	8.0	23.6	27.8-s	1.17	2.9	2.45-s	0.827
Wood6	8.0	17.5	45.8-s	2.62	3.0	2.25-s	0.75
W14	8.3	25.0	44.1-s	1.76	3.5	2.15-s	0.614
K2	8.3	5.0	32.1-s	6.4	1.16	1.13-d (2.25-s)	0.97 (1.94)
B2	10.0	25.0	24.9-m (18.4-s)	0.996 (0.736)	1.85	2.1-s	1.135
B3	10.0	42.6	34.4-s	0.807	1.90	1.75-s	0.921
W18	10.4	46.2	47.5-f (22.9-s)	1.028 (0.495)	2.50	1.85-d	0.74
W910	10.4	38.2	36.5-m (23.3-s)	0.956 (0.61)	2.75	2.9-s	1.05
W1	10.4	36.9	44.3-m (25.9-s)	1.2 (0.701)	2.25	2.25-a (3.5-s)	1.0 (1.55)
W2	10.4	37.5	33.7-m (23.1-s)	0.898 (0.616)	2.65	2.55-s	0.96
W3	10.4	37.5	36.7-m (29.7-s)	0.978 (0.792)	3.00	2.05-s	0.68
W45	10.4	49.6	45.2-m (29.9-s)	0.911 (0.602)	3.00	2.5-s	0.833
W6	10.4	42.0	41.1-s	0.978	0.5	1.6-s	3.2

[a] The slabs with L/h > 15 were not mounted nor tested for tensile membrane capacity.
[b] The descriptive symbols are -s for simply-supported capacity, -f for fixed-supported capacity, or -m for the mean capacity when considering only tensile reinforcement.
[c] The descriptive symbols are -s for only tensile reinforcement at midspan, -d for all the reinforcement at midspan, or -a for the average deflection between the other two.
[d] Catastrophic failure.
[e] Test stopped early because the mounting bolts broke.

Table 4.10. Capacity and Deflection for Point C, Figure 4.1 (cont.)

Slab [a] Group	L/h	w_{exp} (psi)	YL [b] (psi)	YL/w	Δ_{exp} (in)	ΔYL_c (in)	$\Delta YL/\Delta$
W713	10.4	50.6	45.7-m (30.5-s)	0.904 (0.603)	3.00	2.45-s	0.816
W15	10.4	24.3	21.7-s	0.893	3.5	1.65-s	0.471
G1	10.4	21.9	20.1-m (26.2-f)	0.917 (1.19)	3.00	2.90-s (1.4-d)	0.966 (0.477)
G2	10.4	63.2	42.4-f	0.67	2.25	2.45-m (1.8-d)	1.08 (0.80)
G3	10.4	88.5	59.2-f	0.66	1.75	2.35-d	1.34
K1	12.0	88.2	67.6-f	0.766	5.5	4.25-d	0.77
G4	14.8	23.5	18.3-f	0.778	1.5	1.37-d	0.91
G5	14.8	37.6	26.7-f	0.71	1.1	1.16-d	1.05
G6	14.8	44.6	33.5-f	0.751	1.1	1.13-d	1.02
AVG	(All):			1.2145			1.4731
STD	DEV:			1.1583			1.5096
AVG	(Deep):			1.3560			4.0175
STD	DEV:			0.6729			2.4321
AVG	(Thick):			1.1677			1.3122
STD	DEV:			1.2005			1.4614

Table 4.11. Capacity and Deflection for Point D, Figure 4.1

Slab [a] Group	Δ_{exp} (in)	Incipient Collapse Ratio (ICR)	Conser. (CICR)	w_{exp} (psi)	Load [b] CICR Yield (psi)	LCICR(Y) $/w_{exp}$	f_y (psi)	Load [b] CICR Rupture (psi)	LCICR(R) $/w_{exp}$	f_u (psi)
Wood1	3.00	1/8	1/8	1242	309-d	0.248	60.0	387-d	0.311	75000
Wood2	-	-	1/10	-	109-d	-	60.0	137-d	-	75000
Wood3	2.0	1/12	1/13	400	141-d	0.352	60.0	176-d	0.44	75000
B1	-	-	1/10	-	90-d	-	70.0	110-d	-	78200
Wood4	4.5	1/5.33	1/7	25	18.2-s	0.728	55.75	27-m	1.08	60050
Wood5	4.5	1/5.33	1/7	42.1	40.0-s	0.950	61.752	46.7-s	1.109	72052
Wood6	4.5	1/5.33	1/7	70.9	73.2-s	1.032	64.688	81.8-s	1.11	72360
W14	5.0	1/4.8	1/7	94	71.5-s	0.761	90.2	90-s	0.957	76650
K2	1.52	1/15.7	1/16	73.3	50.7-s	0.692	70.0	52-d	0.709	109900
B2	2.2	1/10.9	1/11	32.6	30.5-s	0.945	70.0	32.4-s	0.993	78200
B3	2.4	1/10	1/10	52.0	45-s	0.86	59.8	51-s	0.980	78200
W18	4.0	1/6	1/7	58.6	41.7-s	0.711	62.4	70.5-m	1.20	65450
W910	3.5	1/7	1/7	71.2	44.1-s	0.619	66.0	82-m	1.15	74440
W1	4.0	1/6	1/7	47.5	46-s	0.960	66.0	51-s	1.07	73200
W2	4.0	1/6	1/7	52.5	45-s	0.857	63.0	50-s	0.952	73200
W3	4.5	1/5.33	1/7	57.5	63.3-s	1.10	63.0	81.4-s	1.415	81000
W45	4.5	1/5.33	1/7	57.5	63.3-s	1.10	66.0	81.4-s	1.41	81000
W6	3.0	1/8	1/8	100	78.8-s/d	0.788	66.0	87.3-s/d	0.873	73200
W713	5.5	1/4.36	1/7	62.4	65.7-s	1.05	60.3	72-s	1.15	73200
W15	5.0	1/4.8	1/7	35.5	45.9 -s	1.29	66.0	50.9-s	1.43	73200

[a] The slabs with L/h > 15 were not mounted nor tested for tensile membrane capacity.

[b] The descriptive symbols are -s for using tensile reinforcement at midspan, -d for using all the reinforcement at midspan, or -m for the mean capacity.

Table 4.11. Capacity and Deflection for Point D, Figure 4.1 (cont.)

Slab [a] Group	Δ_{exp} (in)	Incipient Collapse Ratio (ICR)	Conser. (CICR)	w_{exp} (psi)	Load [b] CICR Yield (psi)	LCICR(Y) /w_{exp}	f_y (psi)	Load [b] CICR Rupture (psi)	LCICR(R) /Exp	f_u (psi)
G1	3.5	1/6.85	1/7	35.1	48.9-d	1.393	50	30-s	0.854	61420
G2	4.5	1/5.33	1/6	97.5	93.1-d	0.958	58.47	91.5-m	0.938	76680
G3	3.5	1/6.86	1/7	103.1	116.8-d	1.13	58.47	114-m	1.11	76680
K1	5.5	1/13	1/13	88.2	87-d	0.980	49.9	96.9-m	1.09	74000
G4	3.5	1/6.86	1/7	27.0	47.7-d	1.76	67.33	27.5-s	1.01	77730
G5	3.5	1/6.86	1/7	92.7	80-d	0.86	58.47	106-d	1.14	76680
G6	3.5	1/6.86	1/7	116.3	104-d	0.894	58.47	102-m	0.877	76680
	AVG	(All):				0.9278			1.0145	
	STD	DEV:				0.2234			0.2544	
	AVG	(Deep):				0.3000			0.3755	
	STD	DEV:				0.0520			0.0645	
	AVG	(Thick):				0.9823			1.0701	
	STD	DEV:				0.1295			0.1772	

Table 4.12. Simple Estimate for Peak Capacity and Deflection

Slab Group	w_{exp} (psi)	Thrust T (lb)	T/P_o [3]	Thrust (P-Δ) (lb)	T/P_o (P-Δ)	SP(tt) [4] (psi)	SP(tt) /w	SP(ttvt) [5] (psi)	SP(ttvt) /w	Δ_{exp} (in)	EC [6] (in)	EC/Δ
Wood1	1486	160000	0.124	170000	0.132	1763	1.186	1763	1.186	0.41	0.493	1.201
Wood2	1620	403000	0.350	430244*	0.374	1112	0.686	1112	0.686	0.39	0.493	1.264
Wood3	557	120500	0.152	130500	0.164	593	1.064	593	1.064	0.41	0.626	1.527
B1	290	75300	0.115	85300	0.129	373	1.280	373	1.280	0.53	0.646	1.218
Wood4	68.8	41700	0.159	74900	0.286	71.8	1.043	71.8	1.043	0.835	0.713	0.854
Wood5	86.0	44700	0.157	76700	0.269	90.9	1.057	90.9	1.057	0.885	0.713	0.805
Wood6	133	61000	0.192	86753*	0.273	120.8	0.908	120.8	0.908	0.893	0.713	0.798
W14	126	51100	0.182	85168*	0.303	119.5	0.948	119.5	0.948	0.8	0.719	0.898
K2	174	97855[2]	0.218	97855*	0.218	132.9	0.764	132.9	0.764	0.21	0.719	3.426
B2	61	38300	0.117	52000	0.158	79.4	1.301	79.4	1.301	0.50	0.735	1.470
B3	101	61700	0.169	83926*	0.231	100.1	0.991	100.1	0.991	0.86	0.735	0.854
W18	68.7	38400	0.138	58400[1]	0.209	80.0	1.164	80.0	1.164	0.813	0.7409	0.911
W910	73.5	40700	0.149	58000[1]	0.212	80.1	1.089	80.1	1.089	0.825	0.7409	0.898
W1	66.0	26300	0.103	26300[1]	0.103	68.7	1.041	68.7	1.041	1.0	0.7409	0.741
W2	64.0	41600	0.162	70394*	0.275	65.7	1.026	65.7	1.026	0.8	0.7409	0.926
W3	68.0	35700	0.141	42000[1]	0.166	73.8	1.085	73.8	1.085	1.2	0.7409	0.617
W45	72.5	43000	0.169	56183*	0.220	72.0	0.993	72.0	0.993	1.1	0.7409	0.673
W6	68.0	32567	0.127	32567*	0.127	68.3	1.004	68.3	1.004	0.25	0.7409	2.963
W713	69.0	41200	0.170	44700[1]	0.185	68.5	0.993	68.5	0.993	0.857	0.7409	0.864
W15	52.0	30800	0.151	49709*	0.244	55.4	1.065	55.4	1.065	1.0	0.7409	0.741
G1	52.0	33700	0.147	69700	0.304	58.0	1.115	58.0	1.115	0.798	0.7409	0.928
G2	72.0	41900	0.173	61900[1]	0.256	70.2	0.975	70.2	0.975	1.335	0.7409	0.555
G3	95.0	50900	0.193	70900[1]	0.269	86.9	0.915	86.9	0.915	1.179	0.7409	0.628
K1	110	201300	0.234	253149*	0.294	91.0	0.827	91.0	0.827	1.00	2.250	2.250
G4	27.5	24500	0.129	17100[1]	0.0904	30.3	1.102	30.3	1.102	0.805	0.766	0.952

* Balance condition not matching the experimental capacity.

[1] The large deflection decreased the capacity at any other value for P.

[2] P_{bal} required to match experimental peak capacity.

Table 4.12. Simple Estimate for Peak Capacity and Deflection (cont.)

Slab Group	w_{exp} (psi)	Thrust T (lb)	T/P_o [3]	Thrust (P-Δ) (lb)	T/P_o (P-Δ)	SP(tt) [4] (psi)	SP(tt) /w	SP(ttvt) [5] (psi)	SP(ttvt) /w	Δ_{exp} (in)	EC [6] (in)	EC/Δ
G5	41.0	38500	0.188	55695*	0.271	37.4	0.912	37.4	0.912	0.601	0.766	1.270
G6	46.0	39800	0.183	54300*	0.250	42.9	0.933	42.9	0.933	0.65	0.766	1.178
C1	16.5	12900	0.207	26474*	0.424	14.6	0.884	14.6	0.884	0.65	0.755	1.162
C2	18.3	13700	0.161	36788*	0.434	18.8	1.027	18.8	1.027	0.65	0.755	1.162
RB26	23.3	35500	0.253	63573*	0.453	23.0	0.987	26.5	1.137	0.446	0.517	1.160
RB27	15.7	34772[2]	0.495	34772*	0.495	12.0	0.764	13.8	0.879	0.441	0.517	1.170
RB18	15.6	21600	0.282	28900[1]	0.377	13.4	0.936	16.4	1.051	0.462	0.517	1.120
RB20	24.5	35772	0.270	57386*	0.434	23.4	0.955	26.6	1.086	0.474	0.517	1.090
RB19	19.3	36206[2]	0.446	36206*	0.446	15.4	0.798	17.3	0.896	0.551	0.517	0.939
RB21	16.2	18209[2]	0.325	18209*	0.325	11.9	0.734	13.7	0.845	0.447	0.517	1.150
RB22	18.5	23500	0.267	35379*	0.402	17.9	0.967	19.8	1.070	0.45	0.517	1.150
RB23	26.9	34400	0.218	60803*	0.386	28.9	1.074	32.7	1.216	0.512	0.517	1.010
C3	13.3	12000	0.196	25258*	0.413	15.1	1.350	16.9	1.271	0.65	0.548	0.844
C4	8.8	10800	0.167	27067*	0.418	11.0	1.250	9.7	1.102	0.65	0.762	1.172
RB25	6.0	13300	0.274	21522	0.443	5.6	0.933	4.7	0.783	0.50	0.510	1.020
RB24	8.0	16300	0.174	38844*	0.414	10.4	1.300	8.8	1.100	0.55	0.510	0.928
RB11	5.1	10300	0.220	19138*	0.409	5.6	1.098	4.6	0.902	0.506	0.510	1.008
RB10	7.9	15800	0.171	37180*	0.403	10.5	1.329	8.9	1.126	0.576	0.510	0.886
RB12	7.0	14300	0.231	25376*	0.409	7.5	1.071	6.1	0.872	0.545	0.510	0.936
RB13	5.7	11500	0.200	23035*	0.401	6.9	1.211	5.6	0.983	0.506	0.510	1.008
RB14	7.9	15500	0.168	35872*	0.389	10.8	1.367	9.1	1.228	0.536	0.510	0.951
RB15	5.9	11900	0.249	16681*	0.350	5.8	0.983	5.5	0.932	0.507	0.510	1.006
RB17	7.3	11400	0.115	36614*	0.369	11.9	1.630	9.9	1.356	0.562	0.510	0.907

[3] Thrust from axial force-moment interaction divided by the slab's pure axial capacity located in Table D.15.
[4] Simple peak capacity estimate using the T/P_o ratio for the thick (0.167) and all of the thin (0.248) slabs.
[5] Simple peak capacity estimate using the T/P_o ratio for the thick (0.167), the thin (0.319) and the very thin (0.197) slabs.
[6] Deflection estimate using the empirically based L/h - Δ/h curve.

Table 4.13. Comparison of Averages/Standard Deviations for the Simple Estimate Results

	T/P_o [a]	SP (tt)/w [b]	SP (ttvt)/w [c]	EC/Δ [d]
Average - All:	0.199			1.108
Standard Deviation:	0.078			0.514
Average - Thick (L/h < 18):	0.167	0.979	0.979	1.163
Standard Deviation:	0.046	0.227	0.227	0.649
Average - All Thin (L/h > 18):	0.248	1.080	1.044	
Standard Deviation:	0.091	0.222	0.156	
Average (thick and all thin T/P_o values):		1.019		
Standard Deviation:		0.230		
Average (thick, thin, very thin T/P_o values):			1.005	
Standard Deviation:			0.204	
Average - Thin (18 < L/h < 22):	0.319	0.902	1.023	1.070
Standard Deviation:	0.092	0.113	0.125	0.108
Average - Very Thin (L/h > 22):	0.197	1.198	1.073	0.982
Standard Deviation:	0.043	0.184	0.171	0.078

[a] Thrust from axial force-moment interaction divided by the slab's ultimate axial capacity located in Table D.15.

[b] Normalized simple peak capacity estimate using the T/P_o ratio for the thick (0.167) and all of the thin (0.248) slabs.

[c] Normalized simple peak capacity estimate using the T/P_o ratio for the thick (0.167), the thin (0.319) and the very thin (0.197) slabs.

[d] Deflection estimate using the empirically based L/h - Δ/h curve.

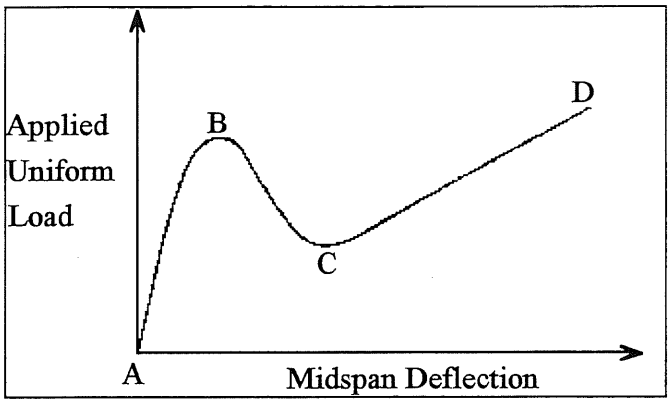

Figure 4.1 Restrained Slab Load-Deflection Curve

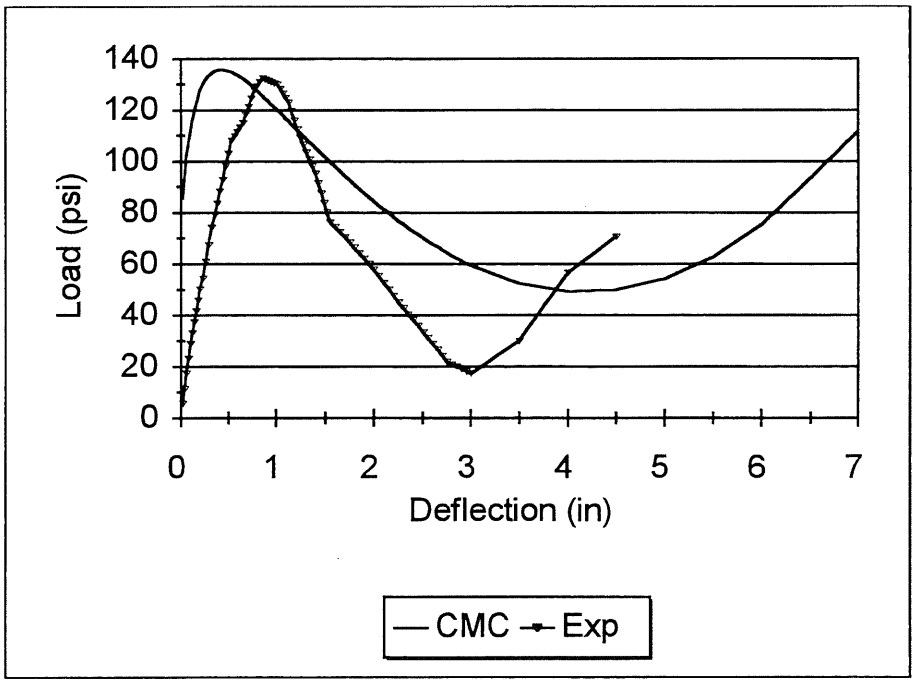

Figure 4.2. Compressive Membrane Theoretical Curve vs. Experimental Load-Deflection Curve For Woodson Slab (Wood6, L/h = 8, $\rho = 0.97\%$) (1993)

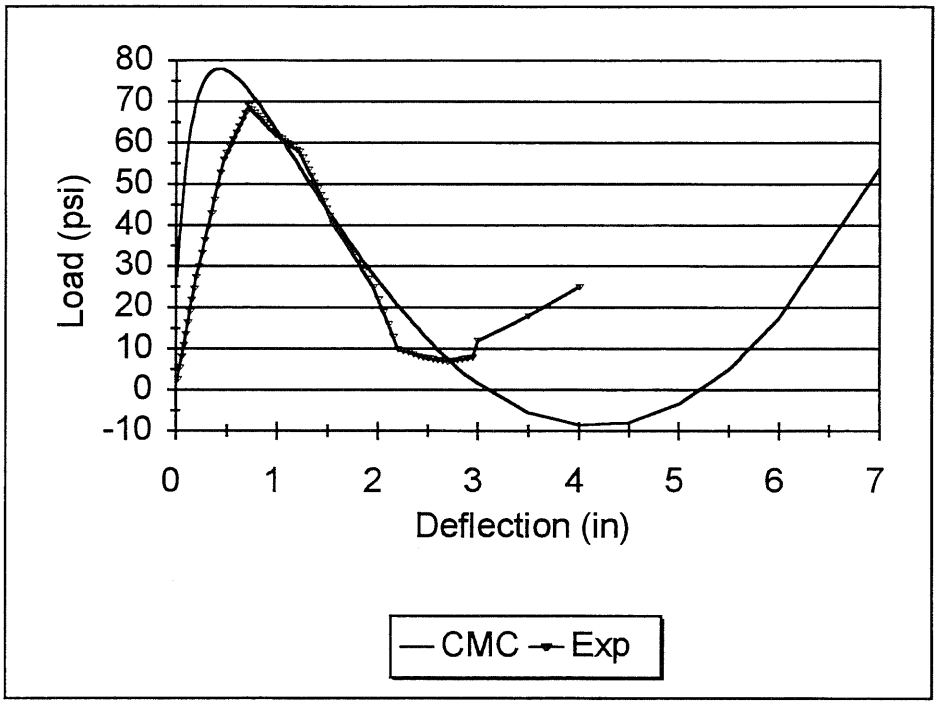

Figure 4.3. Compressive Membrane Theoretical Curve vs. Experimental Load-Deflection Curve For Woodson Slab (Wood4, L/h = 8, ρ = 0.26%) (1993)

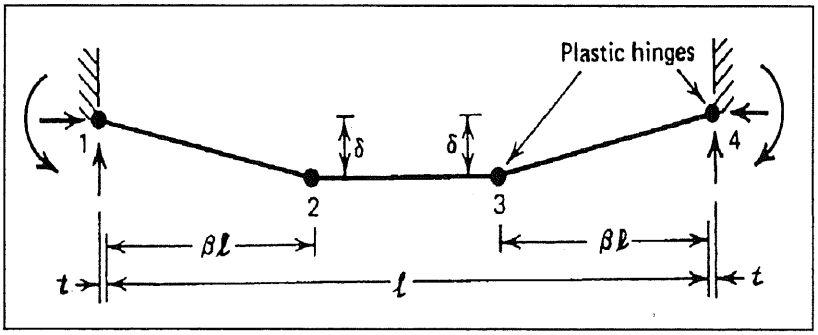

Figure 4.4. Plastic Hinges of Restrained Strip (Park and Gamble, 1980)

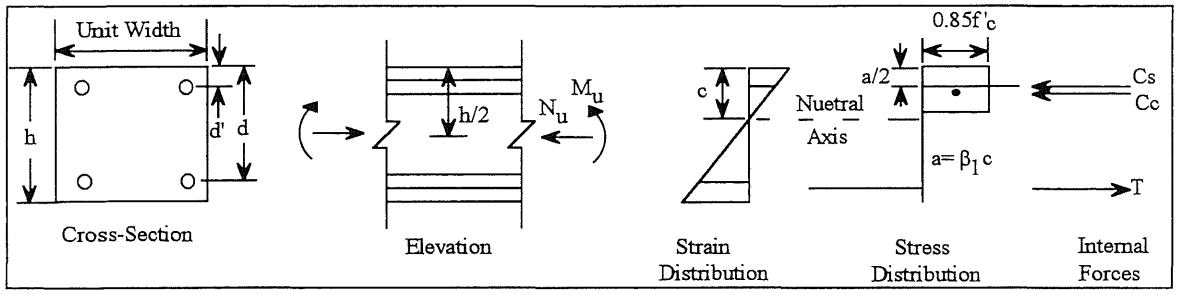

Figure 4.5. Positive Moment Section

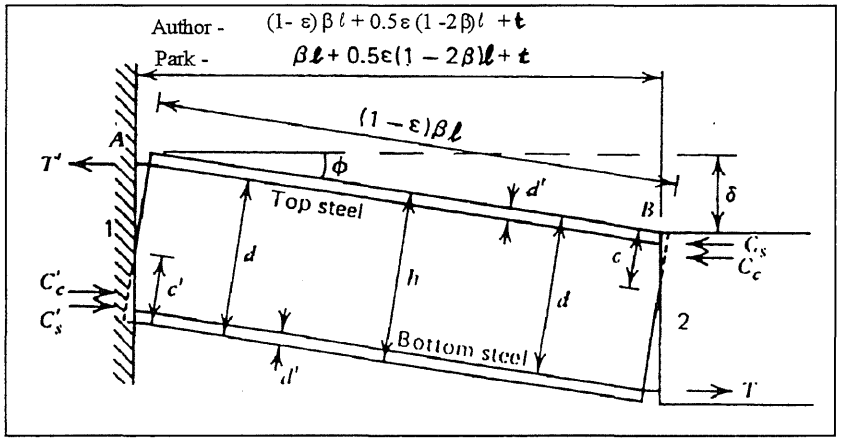

Figure 4.6. Portion of Strip Between Yield Sections 1 and 2 of Figure 12.10 (Park and Gamble, 1980)

a.

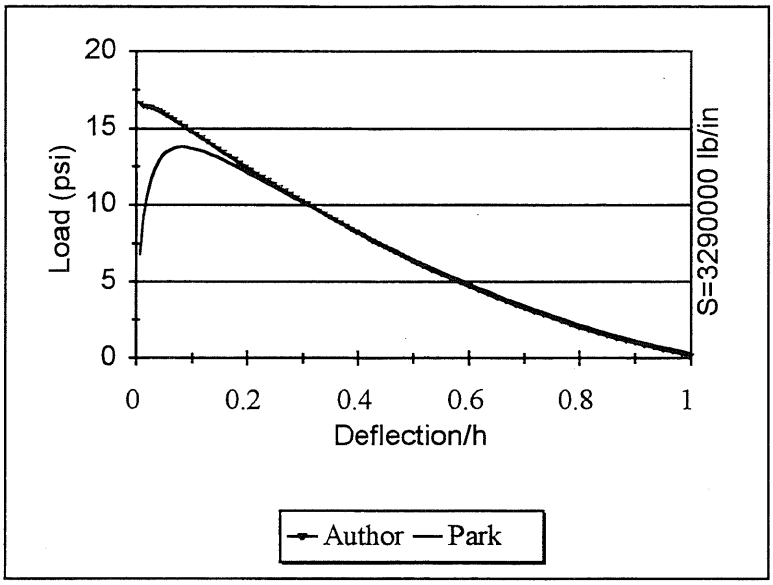

b.

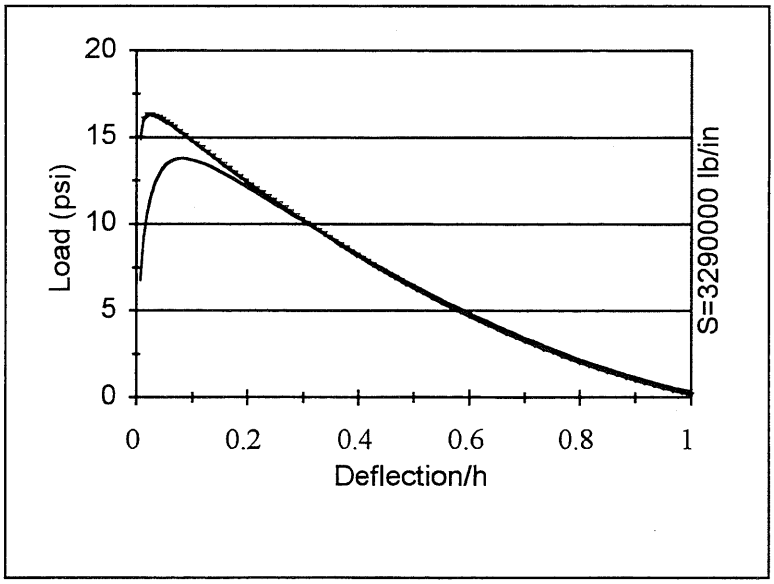

Figure 4.7. Compressive Membrane Theoretical Curves for Park and Gamble's and the Modified Equations for Roberts' Slab RB18 (L/h = 18.8) (1969):
a) Before Removal and b) After Removal

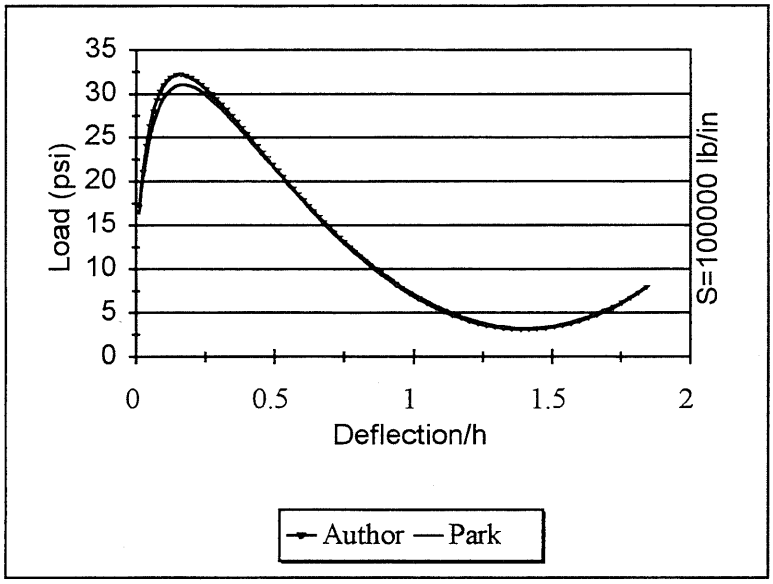

Figure 4.8. Comparison of Park and Gamble's vs. the Modified Compressive Membrane Theory for a Thick Slab (G4, L/h = 14.8)

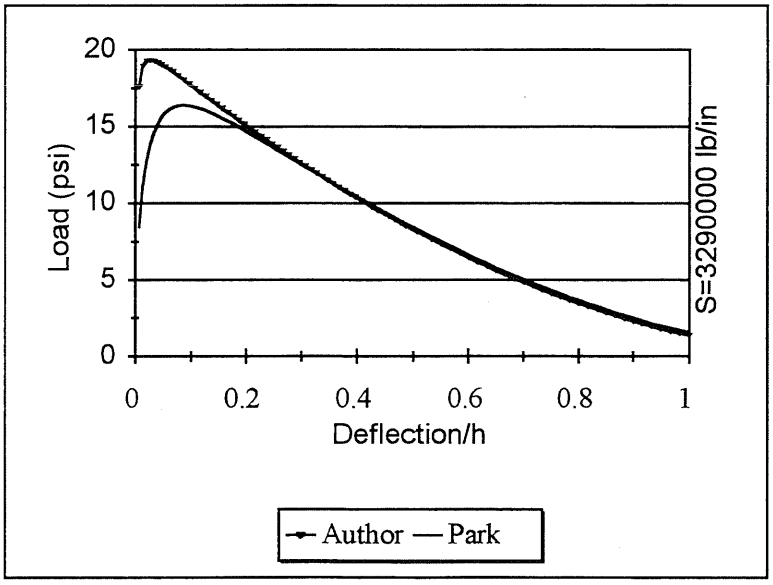

Figure 4.9. Comparison of Park and Gamble's vs. the Modified Compressive Membrane Theory for a Thin Slab (RB22, L/h = 18.8)

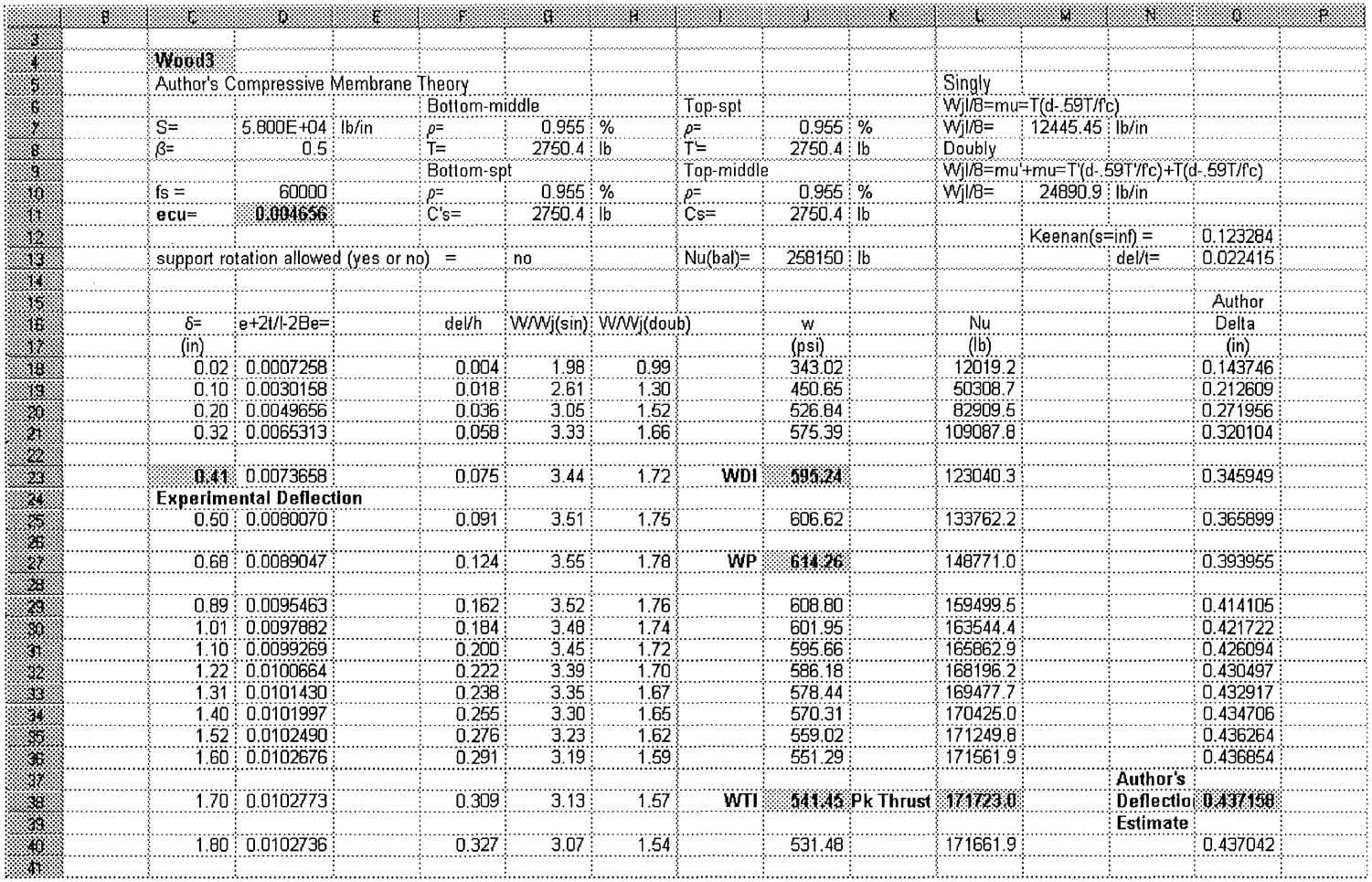

	C	D	E	F	G	H	I	J	K	L	M	N	O
4	**Wood3**												
5	Author's Compressive Membrane Theory									Singly			
6				Bottom-middle			Top-spt			Wjl/B=mu=T(d-.59T/f'c)			
7	S=	5.800E+04	lb/in	ρ=	0.955	%	ρ=	0.955	%	Wjl/B=	12445.45	lb/in	
8	β=	0.5		T=	2750.4	lb	T=	2750.4	lb	Doubly			
9				Bottom-spt			Top-middle			Wjl/B=mu'+mu=T'(d-.59T'/f'c)+T(d-.59T/f'c)			
10	fs =	60000		ρ=	0.955	%	ρ=	0.955	%	Wjl/B=	24890.9	lb/in	
11	**ecu=**	**0.004656**		C's=	2750.4	lb	Cs=	2750.4	lb				
12											Keenan(s=inf) =		0.123284
13	support rotation allowed (yes or no) =				no		Nu(bal)=	258150	lb			del/t=	0.022415
14													
15													Author
16	δ=	e+2t/l-2Be=		del/h	W/Wj(sin)	W/Wj(doub)		w		Nu			Delta
17	(in)							(psi)		(lb)			(in)
18	0.02	0.0007258		0.004	1.98	0.99		343.02		12019.2			0.143746
19	0.10	0.0030158		0.018	2.61	1.30		450.65		50308.7			0.212609
20	0.20	0.0049656		0.036	3.05	1.52		526.84		82909.5			0.271956
21	0.32	0.0065313		0.058	3.33	1.66		575.39		109087.8			0.320104
22													
23	**0.41**	0.0073658		0.075	3.44	1.72	**WDI**	**595.24**		123040.3			0.345949
24	**Experimental Deflection**												
25	0.50	0.0080070		0.091	3.51	1.75		606.62		133762.2			0.365899
26													
27	0.68	0.0089047		0.124	3.55	1.78	**WP**	**614.26**		148771.0			0.393955
28													
29	0.89	0.0095463		0.162	3.52	1.76		608.80		159499.5			0.414105
30	1.01	0.0097882		0.184	3.48	1.74		601.95		163544.4			0.421722
31	1.10	0.0099269		0.200	3.45	1.72		595.66		165862.9			0.426094
32	1.22	0.0100664		0.222	3.39	1.70		586.18		168196.2			0.430497
33	1.31	0.0101430		0.238	3.35	1.67		578.44		169477.7			0.432917
34	1.40	0.0101997		0.255	3.30	1.65		570.31		170425.0			0.434706
35	1.52	0.0102490		0.276	3.23	1.62		559.02		171249.8			0.436264
36	1.60	0.0102676		0.291	3.19	1.59		551.29		171561.9			0.436854
37												**Author's**	
38	1.70	0.0102773		0.309	3.13	1.57	**WTI**	**541.45**	**Pk Thrust**	**171723.0**		**Deflectio**	**0.437158**
39												**Estimate**	
40	1.80	0.0102736		0.327	3.07	1.54		531.48		171661.9			0.437042
41													

Figure 4.10. Portion of Slab Wood3 Spreadsheet

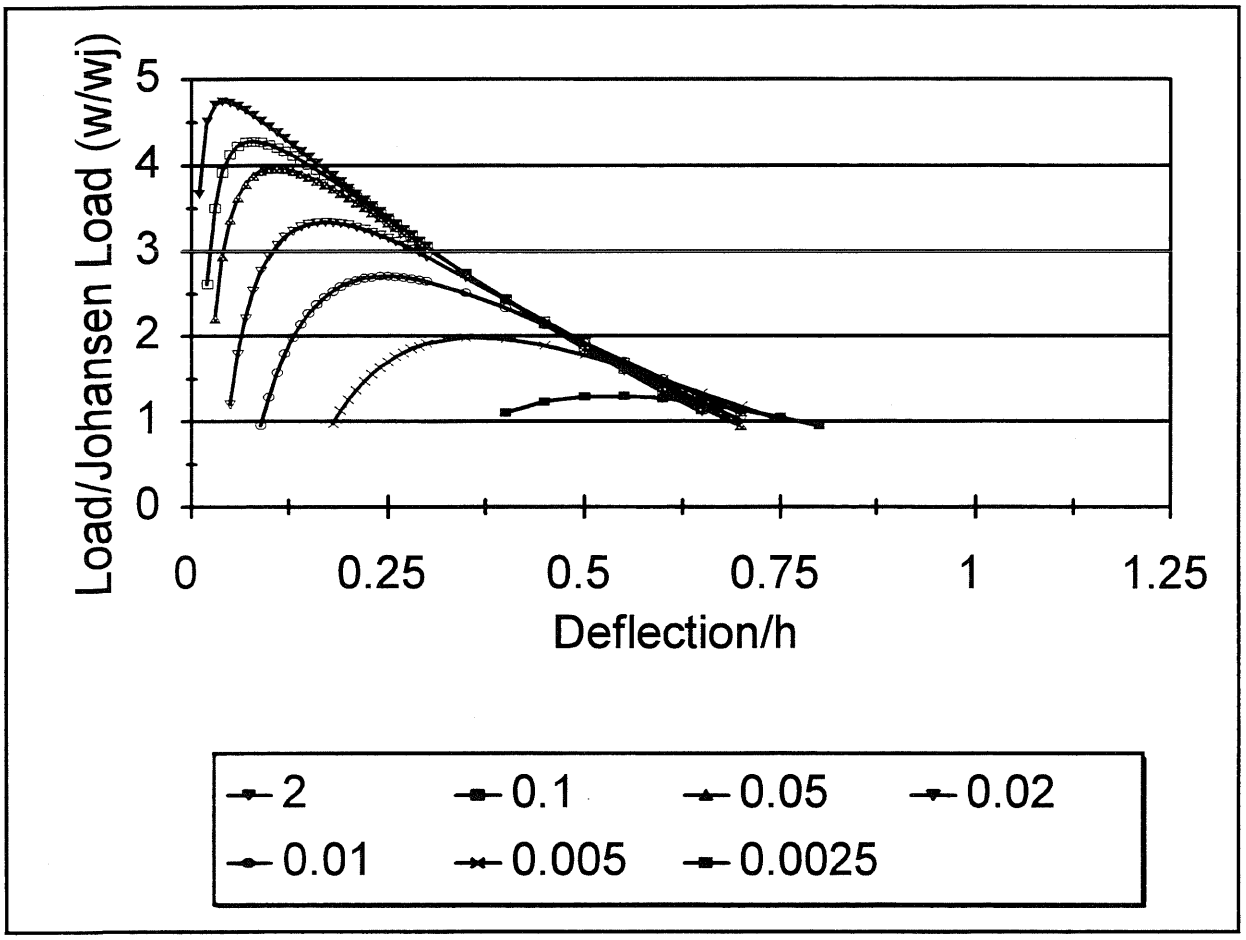

Figure 4.11 Compressive Membrane Theoretical Curves for Park and Gamble's Equations With Varying Support Stiffness (Scalar Magnitude from 2 to $0.0025E_c$) for Woodson's Slab (Wood4, L/h = 8, $\rho = 0.26\%$, w = 68.8 psi, $w_j = 22.7$ psi) (1993)

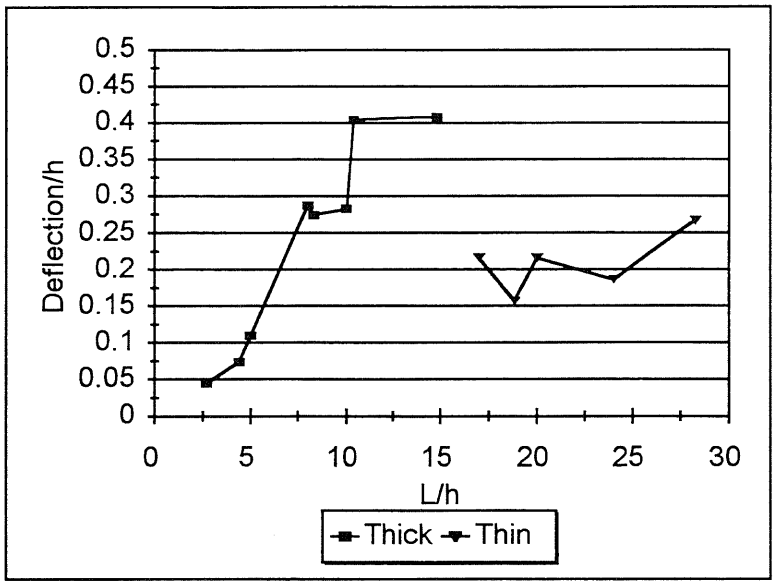

Figure 4.12. Empirical Data for Span Length-to-Thickness (L/h) vs. Peak Midspan Deflection-to-Thickness (Δ/h) for Thick and Thin Slabs

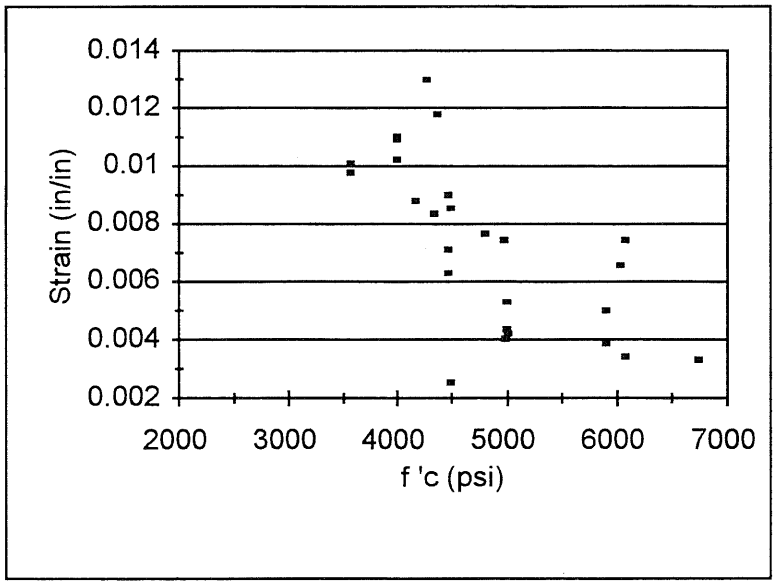

Figure 4.13. Concrete Compressive Strength vs. Adjusted Concrete Compressive Strain Used in the Modified Curvature Based Deflection Estimate for Thick Slabs

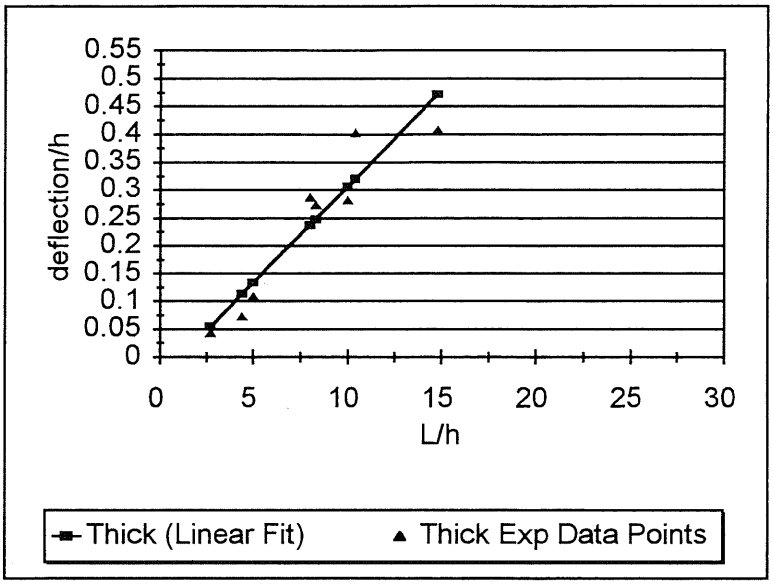

Figure 4.14. Empirical Data for Span Length-to-Thickness (L/h) vs. Midspan Deflection-to-Thickness (Δ/h) for Thick Slabs

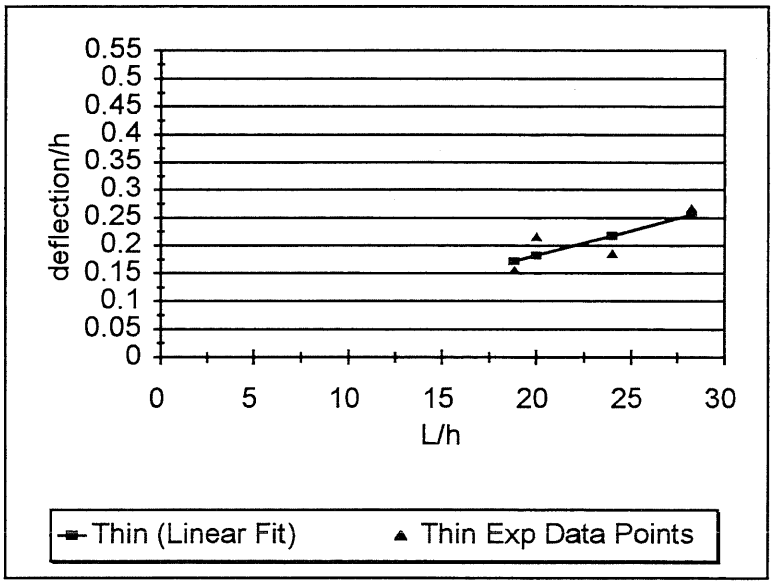

Figure 4.15. Empirical Data for Span Length-to-Thickness (L/h) vs. Midspan Deflection-to-Thickness (Δ/h) for Thin Slabs

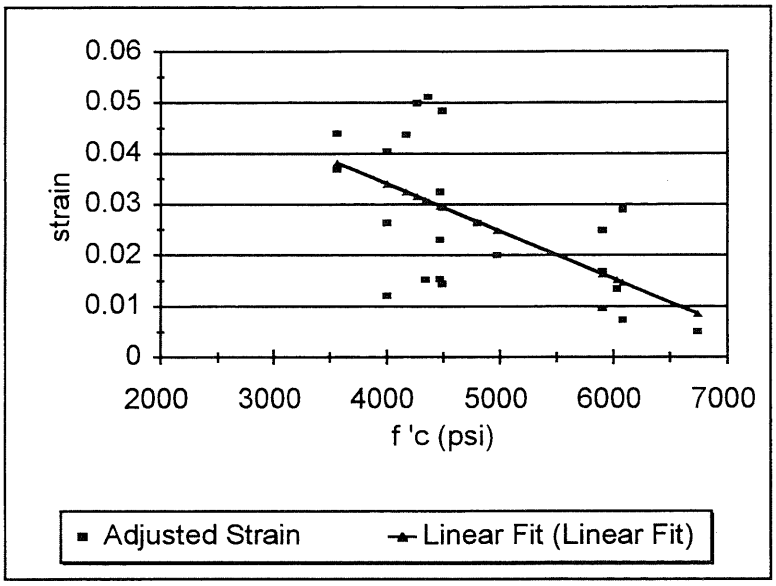

Figure 4.16. Concrete Compressive Strength vs. Adjusted Concrete Compressive Strain Used in Mattock's Deflection Estimate for Thick Slabs

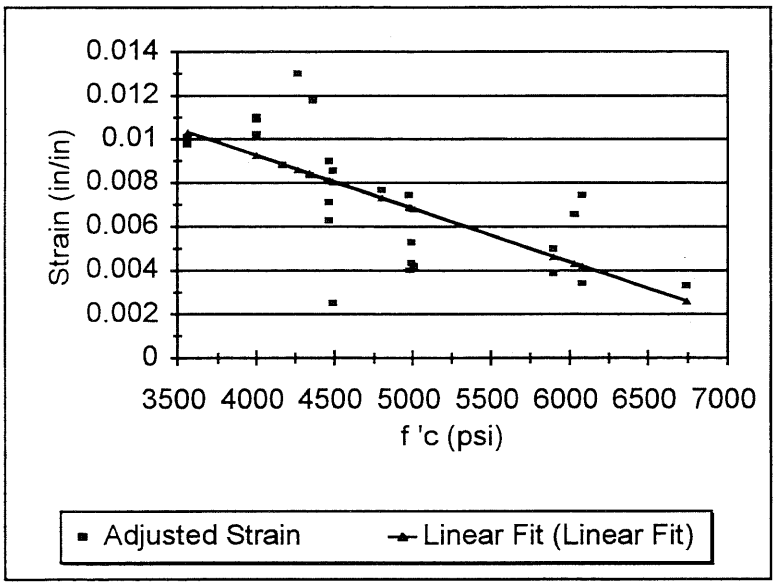

Figure 4.17. Concrete Compressive Strength vs. Adjusted Concrete Compressive Strain Used in the Modified Curvature Based Deflection Estimate for Thick Slabs

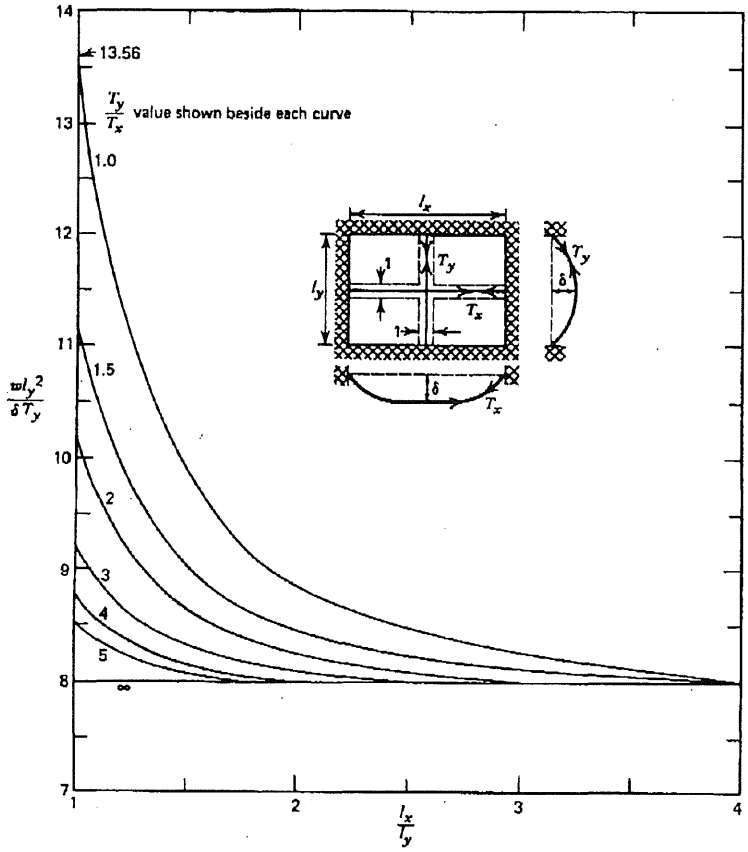

Figure 4.18. Load-Central Deflection Relationships for Uniformly Loaded Rectangular Plastic Tensile Membranes (Park, March 1964)

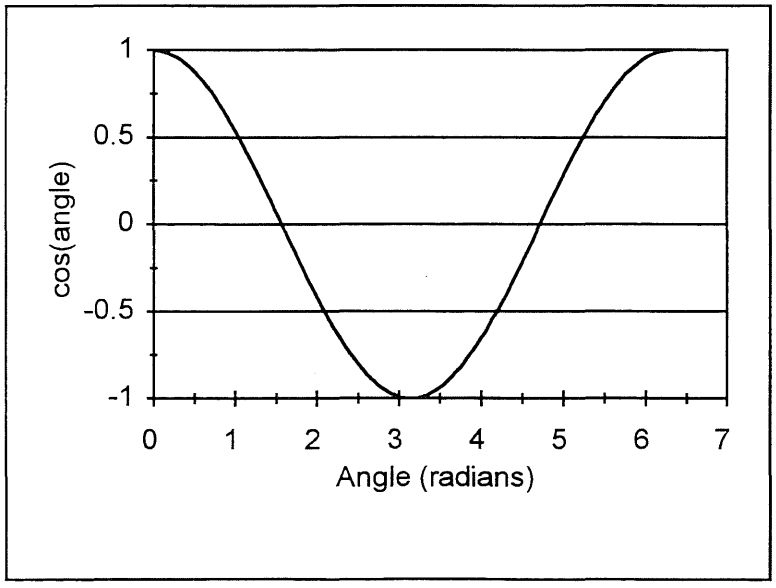

Figure 4.19. Angle (Radians) vs. COS (Angle)

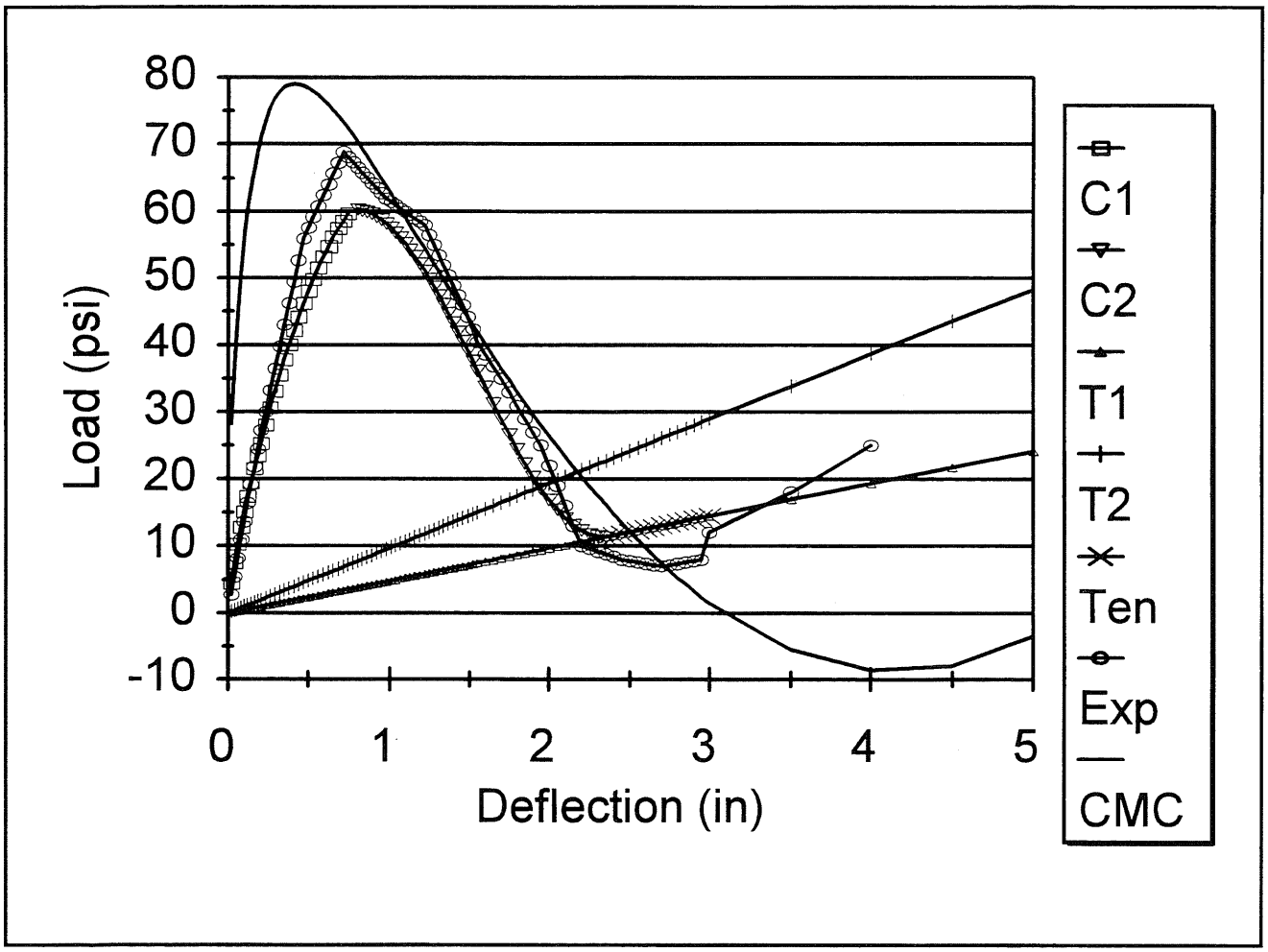

Figure 4.20. Compressive Membrane Theoretical Curve, Experimental Load-Deflection Curve, and the Peak Thrust Estimated Load-Deflection Curve for Woodson's Slab (Wood4, L/h = 8, $\rho = 0.26\%$) (1993)

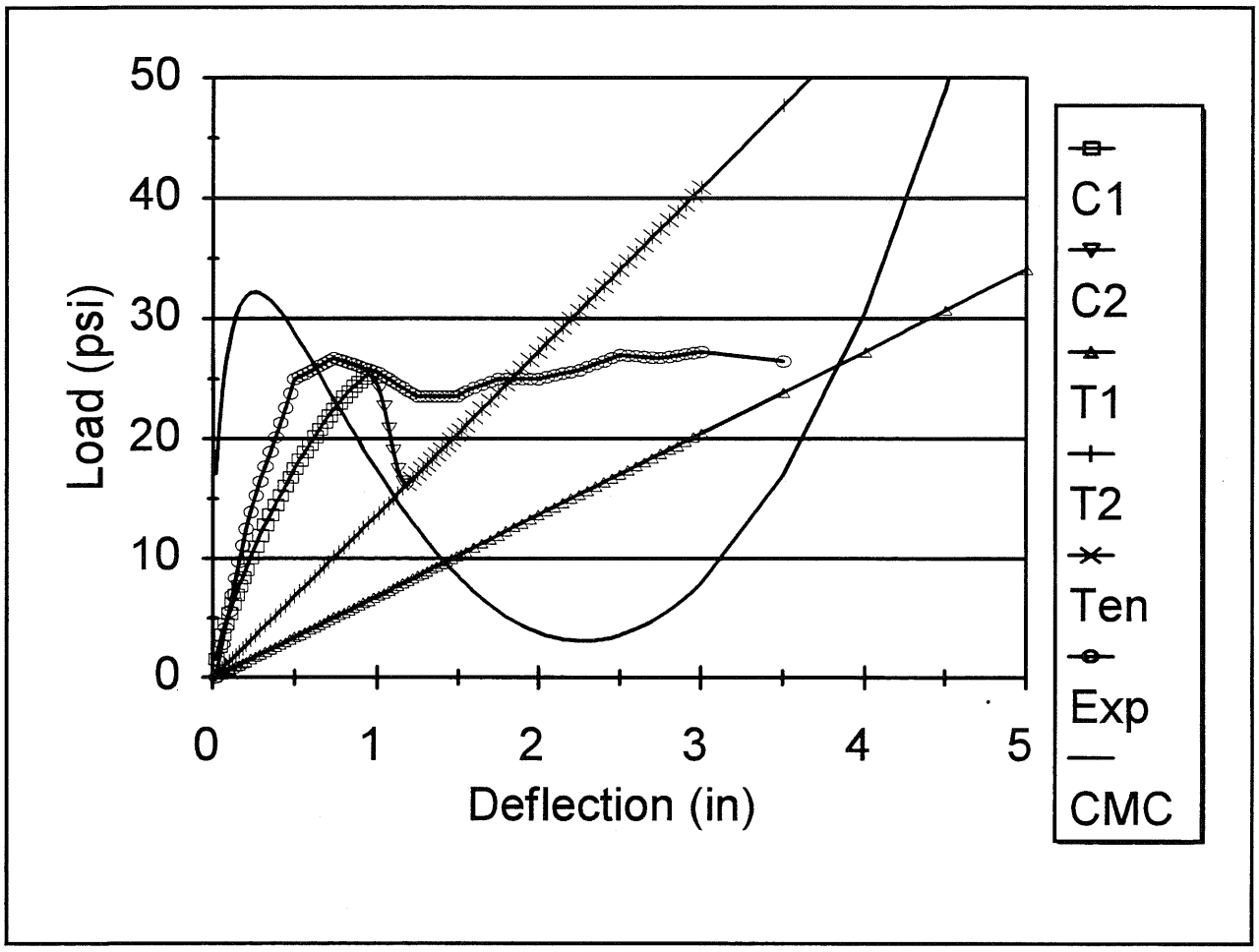

Fiigure 4.21. Compressive Membrane Theoretical Curve, Experimental Load-Deflection Curve, and the Peak Thrust Estimated Load-Deflection Curve for Guice's Slab (G4, L/h = 14.8, $\rho = 0.58\%$) (1986)

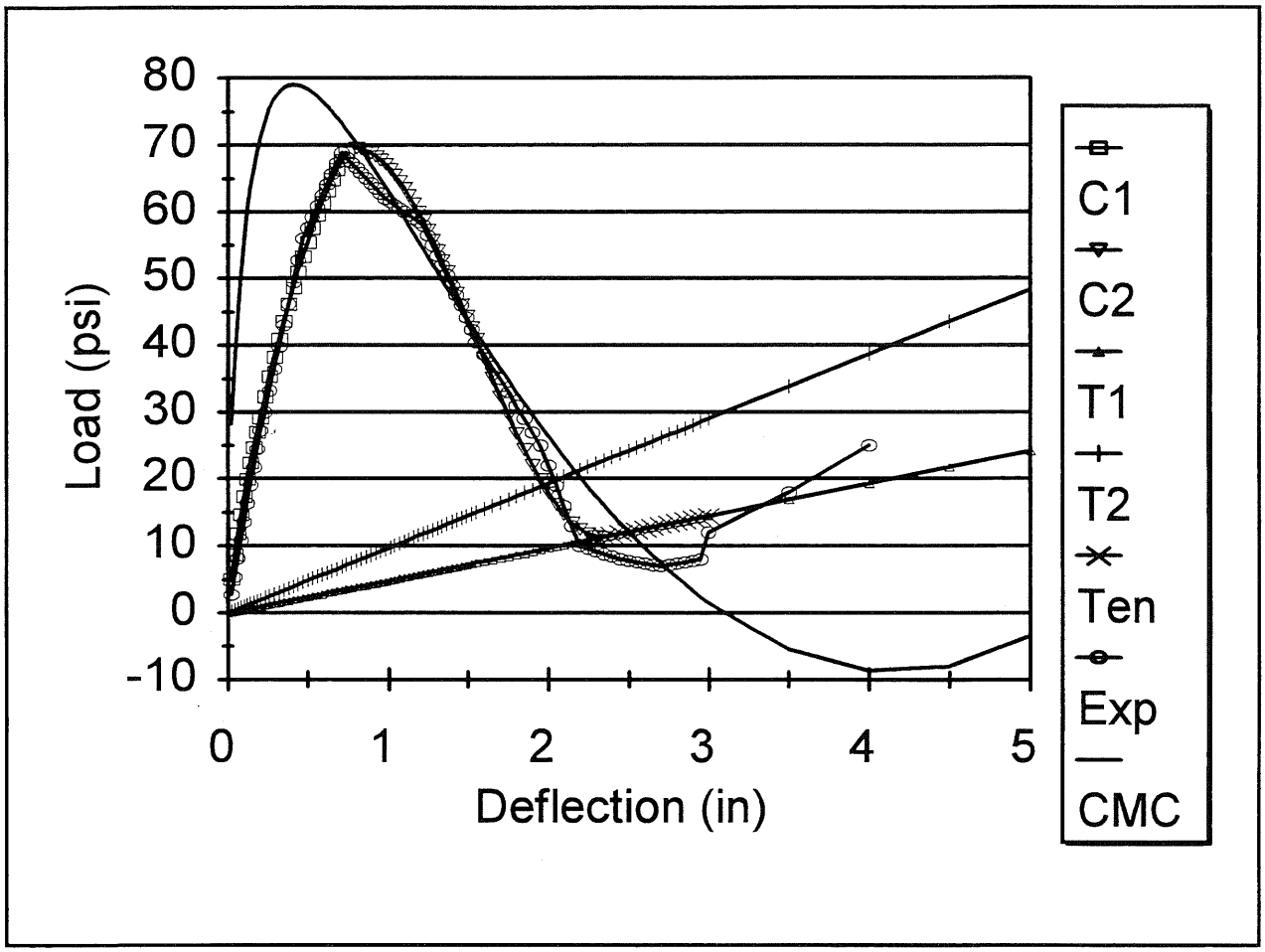

Figure 4.22. Compressive Membrane Theoretical Curve, Experimental Load-Deflection Curve, and the Averaged Peak Thrust and Computed Peak Capacity Estimated Load-Deflection Curve for Woodson's Slab (Wood4, L/h = 8, $\rho = 0.26\%$) (1993)

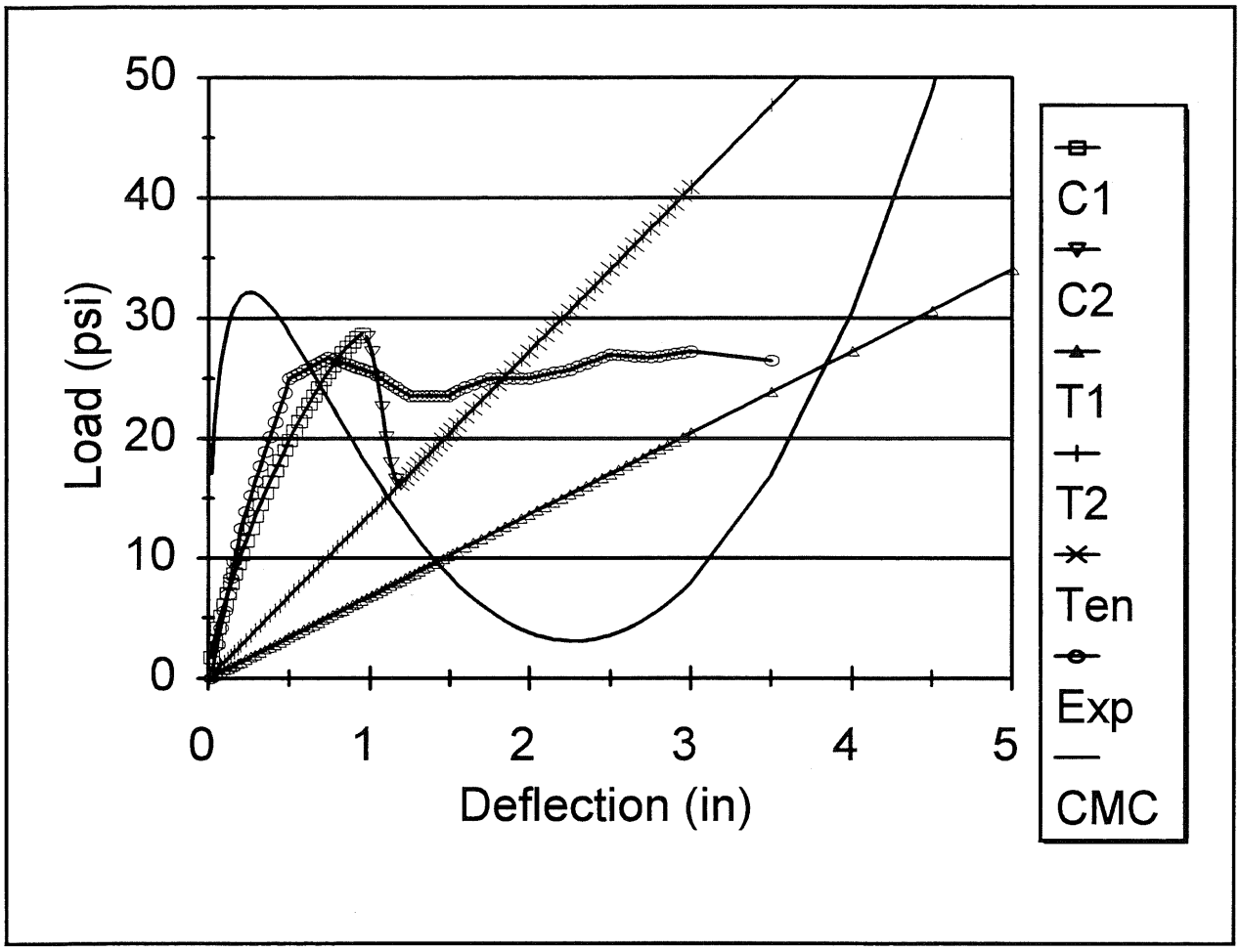

Figure 4.23. Compressive Membrane Theoretical Curve, Experimental Load-Deflection Curve, and the Averaged Peak Thrust and Computed Peak Capacity Estimated Load-Deflection Curve for Guice's Slab (G4, L/h = 14.8, $\rho = 0.58\%$) (1986)

CHAPTER 5

CONCLUSIONS AND RECOMMENDATIONS

5.1. Conclusions

The research presented herein achieved its stated objectives which were: (i) to develop an accurate estimate for the peak compressive membrane capacity in a partial laterally restrained, gradually loaded (i.e., static) reinforced concrete one-way slabs; (ii) to develop a simple load-deflection curve, based on the statically loaded experimental results, to be used within both static and dynamic analysis; (iii) to provide engineers with a quick method for making an estimate of compressive membrane capacity for either targeting missions (i.e., in the field) or rapid evaluation of the peak load capacity available in existing commercial structures; and (iv) to evaluate the capability of finite element techniques in analyzing the behavior of laterally restrained reinforced concrete slabs experiencing large deflections.

The peak compressive thrust developed within a one-way slab, arising from partial lateral restraint at the supports, is a better index, than even experimentally measured midspan deflections, for pointing to an accurate estimate of the peak load capacity within the compressive membrane theory. The capacity associated with the peak compressive thrust is, on average, only slightly smaller than the experimentally measured peak capacity. Since calculation of the thrust is an essential part of the compressive membrane theory, using the peak thrust to select the peak load capacity eliminates the currently difficult task of estimating a peak deflection to use in selecting the peak capacity, especially if no experimental data exists.

Since the load-deflection curve, and not just the peak capacity, is important in the evaluation of the dynamic response of one-way slabs subjected to blast events, a series of equations was developed to predict the peak capacity midspan deflection. Even though the deflection equations reasonably predicted the peak deflections, there was some variability in the results when compared to the experimentally measured peak deflections (i.e., large standard deviations). The equations derived from the empirically based deflection curves, which were a function of L/h, were

the easiest to use in estimating the peak deflection, while the improved curvature based deflection equation provided the best deflection estimate. The peak concrete compressive strain employed in the curvature based deflection equation was estimated from a linear equation relating the slab's concrete uniaxial compressive strength to the concrete compressive strain.

After the peak capacity, the capacity decreases with increasing deflections because of material instability for thick slabs, $L/h < 18$, and geometric instability for thin slabs. During the tensile membrane stage, the principal reinforcement provides reserve capacity through catenary action if the rebar is properly anchored. Classical tensile membrane theory (EQN 4.27) provides an upper bound estimate of tensile membrane resistance by using the rupture stress and a lower bound estimate by using the yield stress. Heavily reinforced slabs (i.e., $\rho > 1$ percent) may only mobilize approximately one-half of the reinforcement during tensile membrane action.

The pairing of the curvature based peak deflection and the compressive membrane theory capacity associated with the peak thrust locates the peak point on the load-deflection curve. The ensuing trough and ultimate points are determined after choosing the proper slope of the tensile membrane curve, i.e., whether only the tension reinforcement, or all of the reinforcement at midspan, is considered, and if the steel stress is either the yield or rupture stress.

Evaluation of the experimental data for the 115 slabs listed in Appendix A produces the following trends for locating the trough and ultimate points for the load-deflection curve:

(1) If the slab has an $L/h < 6$ or $L/h > 18$, then the capacity at the trough point is the fixed-supported yield line capacity, while the deflection at the trough point is calculated with the tensile membrane equation (EQN 4.27), using the fixed-supported yield line capacity and all of the reinforcement at midspan.

(2) If the slab has an $6 < L/h < 18$ with the support rotation limited to less than 2 degrees, then the capacity at the trough point is the fixed-supported yield line capacity, while the deflection at the trough point is calculated with EQN 4.27, using the fixed-supported yield line capacity and all of the reinforcement at midspan.

(3) If $6 < L/h < 18$ and there is no support rotation, then the capacity at the trough point is the simply-supported load capacity, while the associated deflection is calculated with EQN 4.27, using the simply-supported load capacity and only the tension reinforcement at midspan.

(4) The incipient collapse deflection at the ultimate point is either one-tenth of the span length for an $L/h < 6$, one-seventh of the span length for $6 < L/h < 18$, or one-sixth the span length for an $L/h > 18$, while the associated ultimate capacity is determined by substituting the incipient collapse deflection into EQN 4.27 and using the appropriate reinforcement area determined in (1 and 2) or (3) to calculate the deflection of the trough point.

(5) The steel yield stress, rather than the rupture stress, provided the best slope for the tensile membrane resistance curve.

An extremely accurate load-deflection curve subsequently is plotted using the peak, trough and ultimate point capacities and deflections in equations representing the generally parabolic ascending curve, the generally parabolic descending curve, and the ascending linear curve.

Irrespective of whether or not the slab is one-way or two-way, increasing the concrete compressive strength (f'_c), the reinforcement ratio (ρ), or the slab thickness (h) provides enhanced compressive and shear capacity for a given support stiffness, but changes in the thickness and concrete compressive strength generate the largest variation in capacity. Increased reinforcement improves the overall ductility observed through larger hinge rotations and peak deflections at midspan.

Analytically, infinitely stiff lateral supports are ideal. However, they are not only impossible to produce in practice, but a lateral support stiffness (i.e., vertical and rotational stiffness assumed to be infinite) equal in scalar magnitude to the slab's Modulus of Elasticity, will usually produce 90 percent of the total enhancement available through infinitely stiff lateral supports. The presented study on the sensitivity of the lateral stiffness shows that using a lateral stiffness with a scalar magnitude of approximately $0.05 - 0.1E_c$ generated a capacity that accurately predicted the experimentally measured capacity for the available one-way slabs listed in

Appendix A, which had fairly rigid supports. Additionally, a support rotation less than 1.5 degrees enhanced tensile membrane behavior with usually little, if any, decrease in compressive membrane action. Support rotation greater than 2.0 degrees effectively removed any compressive membrane enhancement because of premature snap-through to tensile membrane action. Therefore, rotational rigidity is required to achieve at least the fixed-supported yield line capacity, while lateral restraint is required to produce compressive membrane enhancements.

Finite element analysis cannot at this time replace the use of analytical expressions to predict the complete resistance function of laterally restrained reinforced concrete one-way slabs, especially for thick slabs (L/h < 18). Unfortunately, the element and material models (i.e., algorithm solutions) are not yet mathematically capable of continuing the analysis beyond the level of damage associated with the peak capacity for laterally restrained reinforced concrete slabs dominated by material instability, i.e., crushing and pop-outs which result in rapid snap-through to tensile membrane action (L/h < 18). For slabs controlled by geometric instability (i.e., similar to progressive buckling in slender columns, L/h > 18), the finite element analysis was able to extend past the peak capacity, and clearly demonstrate that the peak thrust did occur simultaneously with the peak capacity, or at a slightly larger deflection and slightly smaller capacity. The behavioral trends observed during finite element analyses validate the use of the peak thrust as an index for the peak capacity within the compressive membrane theory, and the use of compressive strains between 0.005 to 0.007 in/in in curvature based equations predicting the deflection associated with the peak capacity.

Analysis with quadratic beam elements produced capacities and deflections for thin slabs (L/h > 18) that were close to the experimental results. However, for thick slabs (L/h < 18), the analysis with the quadratic beam elements and fixed-supported end conditions over-estimated the capacity by 1.2 to 1.7 times, and greatly under-estimated the deflection by 10 to 15 times. Replacement of the rotational and lateral support edge conditions with springs does lower the capacity and increase the deflection, but it also increases the instability which led to even earlier termination of the analysis. The stiffness of the springs was adjusted to produce a computationally

determined termination capacity near the experimental capacity, but the concrete compressive strains were less than half of the peak capacity compressive strains associated with fixed-supported conditions (i.e., 0.005 in/in). These lower concrete compressive strains suggest that the termination capacities were not peak capacities. Weaker springs led to termination values that could be extrapolated to experimental peak capacities based on strains versus capacities with fully fixed-supported end conditions, but there is a level of doubt as to the accuracy. The finite element analysis usually stopped before indicating a peak capacity because of the mathematical instability resulting from the massive concrete cracking in individual elements. The compressive membrane theory was able to match closely, not only the finite element results for fixed-supported edge conditions, but also, the partially-restrained lateral edge conditions of the actual test configurations.

A simple, but accurate estimate of the peak capacity is possible through use of the axial force-moment interaction equations. The appropriate thrust-to-ultimate axial capacity (T/P_o) for thick (0.167), thin (0.319) and very thin (0.197) slabs is multiplied by the ultimate axial capacity for the given slab parameters at midspan to calculate the thrust used within the axial force-moment interaction equations. Once the enhanced moments at midspan and the supports are determined separately from the axial force-moment interaction equations and substituted into the general yield line equation which ignores P-Δ effects (EQN 4.30), the peak capacity is easily calculated. The thrust enhanced moments at midspan and the supports may be different if the reinforcement ratios vary between the supports and midspan.

The analytical techniques presented in this thesis provide the engineer with not only an accurate prediction of the peak compressive membrane load capacity for partial laterally restrained, reinforced concrete one-way slabs, but also, a reasonable representation of the entire load-deflection curve (i.e., generated curve usually underneath the experimental curve). The only parameter that is still somewhat uncertain is the lateral support stiffness, and the research herein has shown that it can be estimated between a scalar magnitude of 0.01 and $0.05E_c$ for the experimental reaction structures. Additionally, a simple procedure that most engineers can use and

easily understand is available for estimating the peak load capacity in the field, especially for targeting missions.

The innovative method developed herein for predicting the peak capacity provided outstanding results when compared to the available experimental data for partial laterally restrained one-way slabs. The predicted peak capacity is the capacity associated with the peak thrust in the modified compressive membrane theory. The correlation between the predicted peak compressive membrane capacities and the experimental data should lead to inclusion of compressive membrane capacity enhancements, when appropriate, within the current building and military design codes, instead of relying strictly on yield line theory capacity estimates.

5.2. Recommendations

Even with the recently acquired large experimental data base developed at WES for laterally restrained reinforced concrete one-way slabs, a number of areas still need to be investigated. A series of tests should be conducted for thick and thin one-way slabs in which the lateral stiffness of the support structure is known and the generated thrust is measured (i.e., advanced load cells, etc.). Not only would this type of experiment allow physical observance of the peak thrust and peak capacity occurring nearly simultaneously, but would also validate the relative accuracy of the compressive membrane theory in predicting the peak thrust, which in turn, indexes the peak capacity, and whether the thrust is truly a function of the slab thickness and concrete compressive strength as currently believed.

The measurement of the support structure lateral stiffness would permit an evaluation of how important is the accuracy of the lateral stiffness used within the compressive membrane theory. Presently, only a range of lateral stiffness used within the theory to bracket the experimental peak capacities is provided. Support structures of varying lateral stiffness should be tested to further evaluate the accuracy of the compressive membrane theory for a range of lateral stiffness. However, without the testing of the lateral stiffness of a surrounding slab system or a perimeter wall monolithically placed with the one-way slab, and the testing of slabs supported by

such systems, the analyst will not have complete confidence in the lateral stiffness chosen for use in the compressive membrane theory.

The prediction of the load-deflection curve could be improved with the testing of doubly reinforced thin slabs which have adequate resistance to inward movement, and the testing of slabs with an L/h between 15 and 18. The experimental data for thin one-way slabs only includes measurement of compressive membrane capacity and not tensile membrane capacity since the edges were not bolted to the support structure; thereby, preventing the development of tensile membrane resistance. Additionally, the behavior of slabs within the transition zone (i.e., $15 < L/h < 18$) between thick slabs controlled by material instability and thin slabs controlled by geometric instability is not well defined.

If thin one-way slabs are to be analyzed, quadratic beam elements can be used successfully to estimate the peak capacity and deflection by averaging the results for a range of beam elements along the length (i.e., 3 to 10 elements). However, there is a need for a finite element that can continue to transfer load vertically to the lower elements (i.e., to maintain the mesh and to act like rubble), while not requiring calculation of stresses and strains. The element would need to turn off after a certain amount of damage from cracking and not require equilibrium within. If damaged elements could be turned off even partially, then the analyst could use even finer meshes to investigate the slab behavior at peak and post peak resistance. At the present time, in the absence of improvements in the algorithms, analytical methods should be used to predict the peak capacity and the associated load-deflection curve for laterally restrained reinforced concrete one-way slabs, especially for thick slabs.

When designing one-way slabs for enhanced capacity through lateral restraint, some details are equally important during the compressive and tensile membrane resistance phases for different reasons. There should be equal amounts of reinforcement in the top and bottom of the slab to improve spall control during the tensile membrane stage, while providing additional compressive membrane resistance through the capacity of the compression reinforcement. Shear stirrups, which prevent the compressive reinforcement from buckling during the compressive

membrane phase and allows the concrete core to transfer the load directly to the reinforcement during the tensile membrane resistance, are just as effective as lacing, if the spacing is less than d/2. Shear reinforcement is critical in deep slabs if flexural resistance is desired. The principal reinforcement should be spaced less than d (i.e., core confinement), and the bottom reinforcement should run throughout the slab, especially through the walls and columns. Any splicing of reinforcement should not be placed all on one side of a column or a wall. The smaller the spacing of the principal reinforcement, the smaller the crack widths which lead to a larger crack band and hinge widths, i.e., greater ductility. It is extremely important that there is adequate anchoring of the reinforcement if tensile membrane resistance is to be expected. To assist in core confinement, the temperature steel should be placed outside of the principal reinforcement mat, while the principal reinforcement must be oriented with the expected tensile and compressive forces to ensure there is no degradation in capacity. Service loads must be limited to less than one-third of the expected peak capacity, if the designer is going to limit the reduction of the peak capacity from long-term creep affects.

BIBLIOGRAPHY

Air Force Manual for Design and Analysis of Hardened Structures, California Research and Technology, Inc., 1986, and Applied Research Associates, Inc., 1989.

American Concrete Institute, "Building Code Requirements for Reinforced Concrete (318-95)," American Concrete Institute, Detroit, Michigan, 1995.

American Concrete Institute Committee Report 363R, "High Strength Concrete," American Concrete Institute, Detroit, Michigan, 1992.

Batchelor, B., and Tissington, I.R., "Shear Strength of Two-Way Bridge Slabs," Journal of the Structural Division, Proceedings, ASCE, Vol. 102, No. ST12, December 1976, pp. 2315-2331.

Baylot, J.T., Kiger, S.A., Marchand, K.A., and Painter, J.T., "Response of Buried Structures to Earth-Penetrating Conventional Weapons," ESL-TR-85-09 (WES), November 1985, Engineering and Services Laboratory, Tyndall Air Force Base, FL.

Black, M.S., "Ultimate Strength Study of Two-Way Concrete Slabs," Journal of the Structural Division, ASCE, Vol. 101, No. ST1, January 1975, pp. 311-324.

Braestrup, M.W., "Dome Effect in RC Slabs: Rigid-Plastic Analysis," Journal of the Structural Division, ASCE, Vol. 106, No. ST6, June 1980, pp. 1237-1253.

Braestrup , M.W. and Morley, C.T., "Dome Effect in RC Slabs: Elastic-Plastic Analysis," Journal of the Structural Division, ASCE, Vol. 106, No. ST6, June 1980, pp. 1255-1262.

Brochie, J.F. and Holley, M.J., "Membrane Action in Slabs," Cracking, Deflection, and Ultimate Load of Concrete Slab Systems, ACI Special Publication SP-30, American Concrete Institute, Detroit, Michigan, 1971, pp. 345-375.

Brochie, J.F., Holley, M.J., and Okubo, S., "Effect of Membrane Action on Slab Behavior," Research Report R65-25, Department of Civil Engineering, Massachusetts Institute of Technology, Cambridge, Massachusetts, August 1965.

Chinn, J. and Zimmerman, R.M., "Behavior of Plain Concrete Under Various High Triaxial Compression Loading Conditions," Technical Report WLTR-64-163, August 1965, Air Force Weapons Laboratory, Kirkland AFB, N.M.

Crisfeld, M.A., "Snap-Through and Snap-Back Response in Concrete Structures and the Dangers of Under-Integration," International Journal for Numerical Methods in Engineering, Vol. 22, 1986, pp. 751-767.

Christiansen, K.P., "The Effect of Membrane Stresses on the Ultimate Strength of the Interior Panel in a Reinforced Concrete Slab," The Structural Engineer, Vol. 41, pp. 261-265, August 1963.

Criswell, M.E., "Design and Testing of a Blast-Resistant Reinforced Concrete Slab System," Technical Report N72-10, U.S. Army Engineer Waterways Experiment Station, Vicksburg, MS, 1972.

Datta, T.K. and Ramesh, C.K., "Some Experimental Studies on a Reinforced Concrete Slab-Beam System," Magazine of Concrete Research, London, England, Vol. 27, No. 91, June 1975, pp. 111-120.

Department of the Army, "Response Limits and Shear Design for Conventional Weapons Resistant Slabs," Engineer Technical Letter 1110-9-7, Washington, D.C., 1990.

Department of the Army, the Navy, and the Air Force, "Structures to Resist the Effects of Accidental Explosions," Army TM 5-1300, Navy NAVFAC P-397, Air Force AFR 88-22, Washington, D.C., November 1990.

Desayi, P., and Krishnan, S., "Equation for the Stress-Strain Curve of Concrete," Journal of the American Concrete Institute, Vol. 61, March 1964, pp. 345-350.

Desayi, P. and Kulkarni, A.B., "Load-Deflection Behavior of Restrained Reinforced Concrete Slabs," Journal of the Structural Division, ASCE, Vol. 103, No. ST2, Feb. 1977, pp. 405-419.

Famiyesin, O.O.R., and Hossain, K.M.A., "Optimized Design Charts For Fully Restrained Slabs By FE Predictions, Journal of Structural Engineering, ASCE, Vol. 124, No. 5, May 1998, pp. 560-569.

Fang, I.K., Lee, J.H., and Chen, C.R., "Behavior of Partially Restrained Slabs Under Concentrated Load," ACI Structural Journal, Vol. 91, No. 2, March-April 1994, pp. 133-139.

Fenwick, R.C. and Paulay, T., "Mechanisms of Shear Resistance of Concrete Beams," Journal of the Structural Division, ASCE, Vol. 94, No. ST10, October 1968, pp. 2325-2350.

Gamble, W.L., Sozen, M.A., and Siess, C.P., "An Experimental Study of a Reinforced Concrete Two-Way Floor Slab," Civil Engineering Studies, Structural Research Series No. 211, University of Illinois, Urbana, Illinois, October 1961.

Gamble, W.L., Sozen, M.A., and Siess, C.P., "Tests of Two-Way Reinforced Concrete Floor Slab," Journal of the Structural Division, Proceedings of the American Society of Civil Engineers, Vol. 95, No. ST6, June 1969.

Gamble, W.L., Flug, H., and Sozen, M.A., Strength of Slabs Subjected to Multiaxial Bending and Compression," Civil Engineering Studies, Structural Research Series No. 369, University of Illinois, Urbana, Illinois, October 1970.

Gerstle, K.H., Aschl, H., Belloti, R., Bertocchi, P., Kotsovos, M.D., Ko, H., Linse, D., Newman, J.B., Rossi, P., Schickert, G., Taylor, M.A., Traina, L.A., Winkler, H., and Zimmerman, R.M., "Behavior of Concrete Under Multiaxial Stress States," Journal of Engineering Mechanics Division, ASCE, December 1980, pp. 1383-1403.

Ghoneim, M.G., and MacGregor, J.G., "Tests of Reinforced Concrete Plates Under Combined Inplane and Lateral Loads," ACI Structural Journal, Vol. 91, No. 1, January-February 1994, pp. 19-30.

Ghoneim, M.G., and MacGregor, J.G., "Behavior of Reinforced Concrete Plates Under Combined Inplane and Lateral Loads," ACI Structural Journal, Vol. 91, No. 2, March-April 1994, pp. 188-197.

Ghoneim, M.G., and MacGregor, J.G., "Prediction of the Ultimate Strength of Reinforced Concrete Plates Under Combined Inplane and Lateral Loads," ACI Structural Journal, Vol. 91, No. 6, November-December 1994, pp. 688-696.

Girolami, A.G., Sozen, M.A., and Gamble, W.L., "Flexural Strength of Reinforced Concrete Slabs with Externally Applied Inplane Forces," Civil Engineering Studies, Structural Research Series No. 369, University of Illinois, Urbana, Illinois, October 1970.

Guice, L.K. and Slawson, T.R., "Static and Dynamic Slab Tests Conducted at WES: FY 78-84," Technical Report SL-86-1, February 1986, U.S. Army Engineer Waterways Experiment Station, Vicksburg, MS.

Guice, L.K., "Effects of Edge Restraint on Slab Behavior," Technical Report SL-86-2, February 1986, U.S. Army Engineer Waterways Experiment Station, Vicksburg, MS.

Guice, L.K., "Effects of Edge Restraint on Slab Behavior," Technical Report SL-86-32, September 1986, U.S. Army Engineer Waterways Experiment Station, Vicksburg, MS.

Gurfinkel, G. and Siess, C.P., "Longitudinally Restrained Reinforced Concrete Beams," Journal of the Structural Division, Proceedings of the American Society of Civil Engineers, Vol. 94, ST 3, March 1968, pp. 709-735.

Hall, W.J., Discussion with Ronald Welch Concerning the Conference with the British Army (Early 1950's) Reference the Performance of Bomb Shelters During W.W.II, January 1997.

Hall, W.J., Discussion with Ron Welch Concerning the Load Testing of Slabs (Manufacturing and Distribution Plants) to Determine Actual Ultimate Safe Capacity, January 1998.

Hawkins, N.M., and Mitchell, D., "Progressive Collapse of Flat Plate Structures," ACI Journal, Title No. 76-34, July 1979, pp. 775-807.

Headquarters, Department of the Army, "Fundamentals of Protective Design for Conventional Weapons," Technical Manual 5-855-1, November 1986, Washington, D.C.

Hegemier, G.A., Cheverton, K.J., Hagerman, L.J., and Lade, P.V., "On the Development of Constitutive Relations for Plain and Reinforced Concrete," DNA-TR-81-65, Defense Nuclear Agency, Washington, D.C., July 1985.

Hibbitt, Karlson and Sorensen, Inc., ABAQUS/Standard Manuals, Version 5.6, 1996.

Hognestad, E., "A Study of Combined Bending and Axial Load in Reinforced Concrete Members," University of Illinois Engineering Experiment Station Bulletin No. 399, November 1951, 128 pp.

Hognestad, E., "Inelastic Behavior in Tests of Eccentrically Loaded Short Reinforced Concrete Columns," American Concrete Institute, Journal, Proceedings, Vol. 49, No. 2, October 1952, pp. 117-139.

Hognestad, E., Hanson, N.W., and McHenry, D., "Concrete Stress Distribution in Ultimate Strength Design," Journal of the American Concrete Institute, Vol. 27, No. 4, December 1955, pp. 455-479.

Hopkins, D.C., and Park, R., "Test on a Reinforced Concrete Slab and Beam Floor Designed with Allowance for Membrane Action," Cracking, Deflection, and Ultimate Load of Concrete Slab Systems, ACI Special Publication SP-30, American Concrete Institute, Detroit, Michigan, 1971, pp. 223-250.

Houde, J. and Mirza, M.S., "A Finite Element Analysis of Shear Strength of Reinforced Concrete Beams," Shear in Reinforced Concrete, Vol. 1, Special Publication SP-42, American Concrete Institute, 1974.

Huff, W.L., "Test Devices, Blast Load Generator Facility," Miscellaneous Paper N-69-1, April 1969, US Army Engineer Waterways Experiment Station, Vicksburg, Mississippi.

Hung, T.Y. and Nawy, E.G., "Limit Strength and Serviceability Factors in Uniformly Loaded, Isotropically Reinforced Two-Way Slabs," Cracking, Deflection, and Ultimate Load of Concrete Slab Systems, ACI Special Publication SP-30, American Concrete Institute, Detroit, Michigan, 1971, pp. 301-323.

Ingerslev, A., "The Strength of Rectangular Slabs," Institution of Structural Engineers, Journal, Vol. 1, 1923.

Jacobson, A., "Membrane-Flexural Failure Modes of Restrained Slabs," Journal of the Structural Division, ASCE, Vol. 93, No. ST5, Oct. 1967, pp. 85-111.

Johansen, K.W., "Brudineie Teorier," Gjellerups Forlag, Copenhagen, 1943. ("Yield-Line Theory," translated by the Cement and Concrete Association, London, 1962).

Kakizaki, M., Edahiro, H., Tochigi, T., and Niki, T., "Effect of Mixing Method on Mechanical Properties and Pore Structure of Ultra High Strength Concrete," ACI SP-132, CONMET/ACI, 1992.

Keenan, W.A., "Strength and Behavior of Laced Reinforced Concrete Slabs Under Static and Dynamic Loading," Technical Report R-620, April 1969, Naval Civil Engineering Laboratory, Port Hueneme, CA.

Keenan, W.A., "Strength and Behavior of Restrained Reinforced Concrete Slabs Under Static and Dynamic Loading," Technical Report R-621, April 1969, Naval Civil Engineering Laboratory, Port Hueneme, CA.

Keenan, W.A., Phone conversation with Ron Welch concerning equations in R-621, November 1998.

Kiger, S.A., Eagles, P.S., and Baylot, J.T., "Response of Earth-Covered Slabs in Clay and Sand Backfills," Technical Report SL-84-18, October 1984, U.S. Army Engineer Waterways Experiment Station, Vicksburg, MS.

Kupfer, H., Hilsdorf, H.K., and Rusch, H., "Behavior of Concrete Under Biaxial Stresses," ACI Journal, Vol. 66, 1969, pp. 656-666.

Mattock, A., "Rotational Capacity Of Hinging Regions In Reinforced Concrete Beams," ACI SP-12, 1965.

Meamarian, N., Krauthammer, T., and O'Fallon, J., "Analysis and Design of Laterally Restrained Structural Concrete One-Way Members," ACI Structural Journal, Vol. 91, No. 6, Nov-Dec 1994, pp. 719-725.

Morley, C.T., "Yield Line Theory for Reinforced Concrete Slabs at Moderately Large Deflections," Magazine of Concrete Research, Vol 19, No. 61, pp. 211-222, December 1967.

Nawy, E.G. and Blair, K., "Further Studies on Flexural Crack-Control in Structural Slab Systems," Cracking, Deflection, and Ultimate Load of Concrete Slab Systems, ACI Special Publication SP-30, American Concrete Institute, Detroit, Michigan, 1971, pp. 1-41.

Neville, A.M., Properties of Concrete, Fourth and Final Edition, John Wiley and Sons, Inc., NY, 1996.

Norman, C.D., "Evaluation of Nonlinear Constitutive Properties of Concrete," Technical Report SL-90-1, Final Report, February 1990, U.S. Army Engineer Waterways Experiment Station, Vicksburg, MS.

Ockleston, A.J., "Load Test on a Three-Story Reinforced Building in Johannesburg," Structural Engineer, Vol. 33, No. 10, pp. 304-322, October 1955.

Ockleston, A.J., "Arching Action in Reinforced Concrete Slabs," Structural Engineer, Vol. 36, No. 6, pp. 197-201, June 1958.

Oluokun, F.A., "Prediction of Concrete Tensile Strength From Compressive Strength: Evaluations of Existing Relations for Normal Weight Concrete," ACI Material Journal, Vol. 88, No. 3, 1991, pp. 302-309.

Park, R., "Tensile Membrane Behavior of Uniformly Loaded Rectangular Reinforced Concrete Slabs With Fully Restrained Edges," Magazine of Concrete Research, London, England, Vol. 16, No. 46, March 1964, pp. 39-44.

Park, R., The Lateral Stiffness and Strength Required to Ensure Membrane Action at the Ultimate Load of a Reinforced Concrete Slab and Beam Floor," Magazine of Concrete Research, London, England, Vol. 17, No. 50, March 1965, pp. 29-38.

Park, R., "The Ultimate Strength and Long-Term Behaviour of Uniformly Loaded Two-Way Concrete Slabs With Partial Lateral Restraint at All Edges," Magazine of Concrete Research, London, England, Vol. 16, No. 48, September 1964, pp. 139-152.

Park, R., "Ultimate Strength of Rectangular Concrete Slabs Under Short-Term Uniform Loading With Edges Restrained Against Lateral Movement," Proceedings of the Institute of Civil Engineers, London, England, Vol. 28, June 1964, pp. 125-150.

Park, R., "Further Test on a Reinforced Concrete Floor Designed by Limit Procedures," Cracking, Deflection, and Ultimate Load of Concrete Slab Systems, ACI Special Publication SP-30, American Concrete Institute, Detroit, Michigan, 1971, pp. 251-269.

Park, R. and Gamble, W.L., Reinforced Concrete Slabs, John Wiley and Sons, New York, pp. 562-609, 1980.

Park, R. and Paulay, T., Reinforced Concrete Structures, John Wiley and Sons, N.Y., 1975.

Paulay, T. and Loeber, P.S., "Shear Transfer by Aggregate Interlock," Shear in Reinforced Concrete, Vol. 1, Special Publication SP-42, American Concrete Institute, 1974.

Pfrang, E.O., Siess, C.P., and Sozen, M.A., "Load-Moment Curvature Characteristics of Reinforced Concrete Sections," American Concrete Institute, Journal, Proceedings, Vol. 61, No. 7, July 1964, pp. 763-778.

Polak, M.A., and Vecchio, F.J., "Reinforced Concrete Shell Elements Subjected to Bending and Membrane Loads," ACI Structural Journal, Vol. 91, No. 3, May-June 1994, pp. 261-268.

Powell, D.S., "The Ultimate Strength of Concrete Panels Subjected to Uniformly-Distributed Loads," Thesis presented to Cambridge in partial fulfillment of the requirements for the degree of Doctor of Philosophy.

Ramesh, C.K. and Datta, T.K., "Ultimate Strength of Reinforced Concrete Slab-Beam Systems: A New Approach," Indian Concrete Journal, Bombay, India, Vol. 47, 1973, pp. 301-308.

Raphael, J.M., "Tensile Strength of Concrete," ACI Materials Journal, Vol. 81, No. 2, 1984, pp. 158-65.

Regan, P.E., "Catenary Action in Damaged Concrete Structures," Industrialization in Concrete Building Construction, ACI Special Publication SP-48, American Concrete Institute, Detroit, Michigan, 1975, pp. 191-224.

Roberts, E.H., "Load-Carrying Capacity of Slab Strips Restrained Against Longitudinal Expansion," Concrete, Vol. 3, No. 9, pp. 369-378, September 1969.

Saadeghvaziri, M.A., "Inelastic Response of Reinforced Concrete Bridges Under Horizontal and Vertical Earthquake Motions," University of Illinois, SRS #540, June 1988.

Sawczuk, A., "Membrane Action in Flexure of Rectangular Plates With Restrained Edges," in Flexural Mechanics of Reinforced Concrete; Proceedings of the International Symposium, Miami, Florida, November 10-12, 1964, New York, American Society of Civil Engineers, 1965, pp. 347-358.

Sawczuk, A., and Winnicki, L., "Plastic Behavior of Simply-Supported Reinforced Concrete Plates at Moderately Large Deflections," International Journal of Solids and Structures, Vol. 1, 1965, pp. 97-111.

Smith, G.M. and Young, L.E., "Ultimate Theory in Flexure by Exponential Function," Journal of the American Concrete Institute, Vol. 52, No. 3, November 1955, pp. 349-359.

Talbot, A. N., "Tests of Concrete and Reinforced Concrete Columns," University of Illinois Engineering Experiment Station Bulletin No. 20, December 1907, 59 pp.

Taylor, R., "A Note on a Possible Basis for a New Method of Ultimate Load Design of Reinforced Concrete Slabs," Magazine of Concrete Research, London, England, Vol. 17, No. 53, December 1965, p. 183-186.

Taylor, R., and Hayes, B., "Some Tests on the Effect of Edge Restraint on Punching Shear in Reinforced Concrete Slabs," Magazine of Concrete Research, London, England, Vol. 17, No. 50, March 1965, p. 39-44.

Taylor, R., Maher, D.R.H., and Hayes, B., "Effect of the Arrangement of Reinforcement on the Behavior of Concrete Slabs," Magazine of Concrete Research, London, England, Vol. 18, No. 55, June 1966, p. 85-94.

Timoshenko, S., Strength of Materials, Second Edition, Parts I and II, D. Van Nostrand Co., Inc., 1940 and 1941.

Tong, P.Y., and Batchelor, B., "Compressive Membrane Enhancement in Two-Way Bridge Slabs," Cracking, Deflection, and Ultimate Load of Concrete Slab Systems, ACI Special Publication SP-30, American Concrete Institute, Detroit, Michigan, 1971, pp. 271-286.

University of Illinois, "FINITE Manual," Via the Network, May 1997.

U.S. Department of the Army, 1990, "Structures To Resist the Effects of Accidental Explosions," Technical Manual 5-1300, Navy NAVFAC P-397, AFR 88-22, Washington, D.C.: Departments of the Army, Air Force, and Navy.

Vecchio, F.J. and Collins, M.P., "The Modified Compression Field Theory for Reinforced Concrete Elements Subjected to Shear," ACI Journal, Proceedings, Vol. 83, No. 2, March-April 1986, pp. 219-231.

White, R.N., and Holley, M.J., "Experimental Studies of Membrane Shear Transfer," Journal of the Structural Division, American Society of Civil Engineers, No. ST3, August 1972, pp. 1835-1852.

Wood, R.H., Plastic and Elastic Design of Slabs and Plates, Thames and Hudson, pp. 225-261, London, England, 1961, pp. 225-261.

Woodson, S.C., "Effects of Shear Stirrup Details on Ultimate Capacity and Tensile Membrane Behavior of Reinforced Concrete Slabs," Technical Report SL-85-4, August 1985, U.S. Army Engineer Waterways Experiment Station, Vicksburg, MS.

Woodson, S.C. and Garner, S.B., "Effects of Reinforcement Configuration on Reserve Capacity of Slabs," Technical Report SL-85-5, August 1985, U.S. Army Engineer Waterways Experiment Station, Vicksburg, MS.

Woodson, S.C., "Effects of Shear Reinforcement on the Large-Deflection Behavior of Reinforced Concrete Slabs," Doctoral Thesis, University of Illinois, IL, 1993.

Woodson, S.C., "Shear Reinforcement in Deep Slabs," Technical Report SL-94-24, November 1994, U.S. Army Engineer Waterways Experiment Station, Vicksburg, MS.

APPENDIX A

EXPERIMENTAL RESULTS OF LATERALLY RESTRAINED ONE-WAY SLABS

A.1. Introduction

The following experimental data from 115 gradually loaded, laterally restrained one-way reinforced concrete slabs/slab strips will provide the data base for use with theoretical and finite element analytical comparisons contained in this dissertation. Each section will briefly outline the experimental objectives, procedures, testing apparatus, parameters, and outcome for each investigation. The ensuing paragraphs set the historical stage preceding the accompanying experiments on laterally restrained one-way reinforced concrete slabs.

In 1955, A.J. Ockleston statically load tested a hospital's lightly-reinforced concrete interior panel. To his surprise, the slab supported more than twice the load predicted by "yield-line" theory, the state-of-the-art ultimate load analysis procedure (Ockleston, 1955). Upon further study, Ockleston reported that the interior slab sustained the additional load by "arching" or "dome action" through the lateral restraint provided by the surrounding unloaded reinforced concrete panels (Ockleston, 1958). The slab's enhanced structural capacity was the result of in-plane compressive forces and not the often quoted enhancers: concrete tensile strength, catenary action, and reinforcement strain hardening.

Ockleston's experimental and investigative results led to a flurry of research activity on statically loaded two-way slabs to establish both a data base and a theoretical approach to predict this new structural enhancement. Much of the research focused on 56 nearly square slabs (Park and Gamble, 1980). The defense community quickly embraced this unexpected structural capacity and initiated dynamic testing of over 110 two-way reinforced concrete slabs under the supervision of Picatinny Arsenal (discussed in Woodson, 1993). The additional capacity would possibly eliminate strengthening of existing protective structures and produce significant economic savings in new protective structures by allowing thinner slabs (i.e., Cuban Missile Crisis, Cold War, etc.).

Unfortunately, much of the research was on nearly square slabs which often obscures the pure mechanics of compressive membrane behavior. Even a simply supported square slab develops a compressive ring around the outer edge which provides arching of the slab's central load to the supports (Park and Gamble, 1980). To accurately investigate compressive membrane or tensile membrane behavior, it became apparent that testing should focus on one-way slabs. Two of the early researchers did test reinforced concrete slab strips in an effort to develop supporting data for their compressive membrane theories (Christiansen, 1963; Roberts, 1969). However, these slab strips did not exactly mirror the two-way slabs tested by others, which had equal amounts of tension and compression steel along entire length of member. Christiansen only placed tension reinforcement where it was required at the top of slab strip near the supports and at the bottom of slab strip near midspan, while Roberts only placed bottom reinforcement along the entire slab strip length.

In the late 1970's and early 1980's (height of the Cold War), Waterways Experiment Station (WES) statically (61 slabs) and dynamically (76 slabs) tested one-way slabs under various programs sponsored by the Defense Nuclear Agency (DNA), the Office, Chief of Engineers (OCE), the Federal Emergency Management Agency (FEMA), and the Air Force Engineering and Services Center (AFESC). Most of the experiments focused on the flat-roofed, shallow-buried FEMA key worker structures designed to resist low yield nuclear weapons (Guice et. al., 1986). Tests were made on either reinforced concrete slab strip elements or on one-way roof slabs of reinforced concrete box structures which were the basic structural element in the FEMA key worker design. Generally, failure was in a flexural mode for the highly impulsive loads with the exception of direct shear failures in thick slabs ($L/h < 5$) and in slabs experiencing extremely high over pressures. Additionally, the shear reinforcement ratio and spacing are critical for the development of large deflections, but only moderately critical in the development of compressive membrane capacity beyond the need to keep compressive reinforcement from buckling.

The primary parameters investigated at WES were: L/h, reinforcement ratio (ρ & ρ'), stirrup spacing (s_s), principal steel spacing (s), concrete compressive strength (f'_c) and

connections. The concrete compressive strength ranged from 3600 to 5000 psi with a few tests in the 6100 to 6900 psi range. Reinforcement ratios were approximately 0.5, 0.75. 1.0, and 1.6 percent with the reinforcement yield strengths ranging from 60,000 to 66,000 psi with a few tests in the 70,000 to 90,000 psi range. The WES slabs had equal amounts of tensile and compressive reinforcement except for the 15 slabs tested by Woodson (1985) in which he provided a lower percentage of compressive reinforcement compared to the tensile reinforcement.

Even though several of the WES experiments were not planned to provide input for a general data base (i.e., failed to record all key characteristics pertinent to slab behavior), most slabs were fully restrained reinforced concrete one-way slabs while the rest were at least, partially restrained one-way slabs. Since the WES program focused on protective structures, the span-to-thickness ratios were limited to less than 15. However, the conventionally reinforced concrete slab strips tested by Christiansen and Roberts do provide experimental data for L/h's ranging from 17 to 29. One key drawback to most of the experiments was the oversight of the investigators in determining the support stiffness, and understandably, the motions at the supports.

A.2. K. P. Christiansen, 1963 [Table A.1 and Figures A.1-A.2]

Christiansen conducted four experiments on laterally restrained reinforced concrete one-way slab strips to verify his analytical study of Ockleston's previous reports (1955, 1958). Focus was on the apparent arching of the load to the supports as a result of compressive thrusts developed in the laterally restrained slab strips. Christiansen desired to estimate the ultimate strength of interior panels, while considering separately the action of bending and compressive membrane stresses. With the action of bending for non-laterally restrained members well documented through yield line theory (Wood, 1961), Christiansen's primary effort was on the enhancement due to development of compressive membrane stresses.

The compressive thrusts develop within a member as a function of the support resistance to slab elongation when loaded perpendicular to the longitudinal axis. If the deflection at midspan (Δ) is relatively small compared to the depth of the member, an arch will form when the additional

thrust (i.e., the compressive force divided by the concrete compressive strength, C/f_c) at the midspan is acting above the additional thrust (C/f_c) at the supports (Figure A.1). The maximum thrust or arching capacity occurs when the vertical distance, a_1, between the additional compression at midspan and the additional compression at the supports is zero.

Christiansen tested four conventionally reinforced concrete one-way slab strips while laterally restrained by a welded steel frame (Figure A.2). Reinforcement consisted of only tensile rebar in the top of the slab strip at the supports and in the bottom of the slab strip at midspan. A concentrated force at midspan with a constant rate of application loaded the member through the peak capacity. Similar loading of four simply supported reinforced concrete slabs identical to the laterally restrained slabs provided calibration of the testing procedures and analytical techniques.

All slab strips were six inches wide. The reinforcement consisted of two one-quarter inch diameter mild steel rods which were assumed to have a yield strength of 36 ksi and one-quarter inch of concrete cover. The test on the fourth laterally restrained reinforced concrete slab strip differed from the others in that additional horizontal forces were applied to the ends of the steel frame preventing any support spreading. The experimental results for the four laterally restrained slabs are presented in Table A.1.

Christiansen's equations provided a low estimate with actual arching loads being at least 8 percent higher than calculated. The deflection for the calculated peak arching capacity was two-thirds less than the experimental peak arching capacity deflection (only mentioned a constant experimental deflection of 0.65 inches). He felt the additional compressive membrane stresses permitted increased rotation at the hinges which led to larger deflections at peak capacity. When Christiansen applied his equations to two way slabs, he experienced even greater inaccuracy.

A.3. W. A. Keenan, 1969 [Tables A.2-A.3 and Figures A.3-A.6]

The Naval Civil Engineering Laboratory (NCEL) conducted experiments on laced reinforced concrete slabs under the sponsorship of the Department of the Army, Picatinny Arsenal. They evaluated the following characteristics of laced shear reinforcement in laterally restrained

reinforced concrete members subject to short duration dynamic loads from high-explosive detonations: (i) the dynamic strength throughout the entire range of ductile response; (ii) rotation capacity of the member at clamped supports; and (iii) dynamic versus static response under uniform load.

Laced shear reinforcement distributes the loading, resists diagonal tension stresses, confines the concrete core, minimizes spalling, improves rotational capacity, and enhances strain energy to absorb the blast load (Keenan, R620, 1969). The lacing process begins with the placement of transverse reinforcement exterior to the principal reinforcement (Figure A.3). The diagonal lacing bars are continuous and span in the direction of the principal reinforcement, while being bent around the exterior edge of the transverse reinforcement.

Keenan tested four laced one-way reinforced concrete slabs (i.e., 1-statically, 3-dynamically) with edges restrained against rotation and longitudinal movement. All slabs were loaded with uniform pressure in the NCEL slab loader (Figure A.4) which produces uniform static or dynamic pressures up to 300 psi. The loader can accommodate slabs with clear spans of 6 feet and widths up to 5 feet. The NCEL loader is a reinforced concrete box with a steel lined cavity (Figure A.5). Bolts anchor the slab to the loader's edges. Each slab is loaded on the bottom face either statically by hydrostatic pressure or dynamically by expanding gases created by detonating primacord with decay controlled by vents.

The four one-way slabs were eight feet two and one-half inches long with a clear span of six feet, a width of 24 inches, and a thickness of six inches (i.e., L/h = 12). Eight No. 5 bars at a spacing of three inches provided the principal tensile and compressive reinforcement ratio of 2.11 percent. All reinforcement was continuous and extended into the support where it was welded to a 3" x 2.5" x 23" steel block. The transverse reinforcement, which was U-shaped with a four inch overlap, was No. 2 bars also spaced at three inches.

Both slab ends were clamped between the top face of the loader and a 15/50 steel channel which had six studs anchored into the loader perimeter to prevent rotation (Figure A.3). There were three horizontal bolts threaded into the steel plate welded to the principal reinforcement to

provide lateral connection of the slab to the loader. Once the slab was seated in the loader, the three bolts on each end were unthreaded to provide firm lateral restraint. To prevent inward movement of the edges, a plate-washer assembly kept the head of the bolts against the edge of the loader. The vertical and horizontal studs were strain gaged to measure thrust and vertical reaction, but frictional restraint coupled with the interaction of thrust, shear, and moment prevented any accurate measurements.

Each slab was cast from a different batch of Victor Type II Portland cement. The mix proportions were: 1.00:2.95:2.24 with a water to cement ratio (w/c) of 0.69 by weight. The reinforcement bars were from the same lot with a flat yield range out to 1.6 and 2.2 percent for No. 4 and 5 bars, respectively. Six control cylinders (6"x12") were cast for each slab and cured under wet burlap. A summary of the slab details for the statically loaded slab is in Table A.2. The loaded face of the slab was cast against a steel mold to ensure a smooth surface.

The hydrostatically loaded slab required three cycles of loading due to early seal rupture (Figure A.6, Table A.3). Cracking and crushing of the concrete was concentrated generally near the supports and at midspan. During tensile membrane loading, some hairline cracks appeared between the supports and midspan, but these closed on slab removal from the loader.

A.4. E. H. Roberts, 1969 [Table A.4 and Figures A.7-A.10]

Roberts tested 36 laterally restrained, conventionally reinforced concrete one-way slab strips to investigate compressive membrane action in its simplest form. This research effort was a starting point to logically analyze the results of previous experiments on laterally restrained, reinforced concrete two-way slabs. Roberts used the rigid plastic theory developed by R. H. Wood (1961) in his analysis without relying on a constant value for ultimate deflection as many earlier researchers had done with two-way slabs (Park and Gamble, 1980). Additionally, he included in his equations a value for the support stiffness and the axial compressibility of the slab.

A large concrete support system, 7' x 20"(depth) x 22.5" (width), provided lateral resistance through the concrete tensile capacity of the surrounding support system which was

reinforced by one inch diameter steel rebar to prevent catastrophic failure (Figure A.7). The compressive strength of the concrete in the supports was at least 10,000 psi. The measured stiffness of the support system was 3.29E6 psi. The relative stiffness of the supports to the two inches deep slab strips was between eight to 12; and for the three inches deep slab strips it was five to nine. The opening in the support system was three-eighths inch longer than the slab strips which were to be supported on their edges by steel plates one-half inch square and nine inches long (Figure A.7). Slab loading occurred through a four point system after the end gaps were filled with two-day cured grout to prevent any grout crushing before slab failure. Roberts tested at least pairs for all parameter sets except one, RB10 (Figure A.8 and Table A.4).

Each slab was 57.5 inches long with a clear span of 56.5 inches, nine inches wide, and either two inches (i.e., 20 each, L/h = 28.25, d = 1.66 inches) or three inches deep (i.e., 16 each, L/h = 18.83, d = 2.66 inches). The slab reinforcement consisted of annealed mild steel which was three-sixteenths inch diameter with a defined yield point of 35 psi. Reinforcement was placed only along the entire bottom length.

Resulting compressive membrane enhancements ranged from 3 to 17 with the largest increase in capacity within slab strips possessing the highest compressive strength and lowest reinforcement ratio (i.e., RB24 and RB26, Table A.4). Concrete crushing occurred in the top of the slab strip at midspan and in the bottom at the edges producing a three-hinge mechanism. To improve the correlation with his analytical equations, Roberts adjusted the cube strengths by using 0.6 x cube strength + 2000 psi for the two inch slabs and 0.8 x cube strength + 2000 psi for the three inch slabs (Figures A.9 and A.10). However, no acceptable correlation existed between experimental and calculated deflections during any adjustment to compressive strength. Roberts further investigated the generated thrust by loading wedge-shaped specimens which represented the edge of the previously tested slabs. The measured thrust was three times the load applied to the beam or six times the vertical reactions.

A.5. S. A. Kiger et. al., 1984 [Tables A.5-A.6 and Figures A.11-A.15]

Kiger, Eagles, and Baylot tested five one-way slabs to evaluate the effect of soil cover on the static and dynamic capacity of earth-covered reinforced concrete slabs. The only parameters varied between tests were the backfill type and loading mechanism. They statically tested three slabs with two being buried, one in sand and one in clay, and dynamically tested with blast loading two buried slabs, one in sand and one in clay. The unburied statically tested slab was the control for the buried slabs.

Kiger used the Small Blast Load Generator (SBLG) (Huff, 1969) which can produce up to 2000 psi pressures to test all three statically loaded slabs (Figure A.11). After placing the reaction structure which was a steel box with a concrete inner lining (Figure A.12 and A.13) into the SBLG, six studs on each end of the reaction structure and a steel plate rigidly clamped each slab into place. With the slab rigidly connected, they buried the reaction structure until the sand was flush with the surface of the control slab. A flexible rubber membrane separated the slab and sand from the pressurized water uniformly loading the slab. The reaction structure design resisted any in-plane thrusts generated through the loading of the sand surrounding the reaction structure.

All five slabs were cast from the same concrete batch (Table A.5) with a 24 inch clear span, a 24 inch width, a 2.9 inch thickness (L/h = 8.3), and a 0.5 inch cover of concrete over the reinforcement. The principal reinforcement which was allowed to rust to obtain surface roughness was small diameter wire with an average yield strength of 90,200 psi (Table A.6). The steel spacing of two inches on center provided a reinforcement ratio of $\rho = 0.005$ for both the tension and compressive reinforcement (Figure A.14). The temperature and shear steel had average yield strengths of 97,500 and 84,300 psi, respectively.

Three successively incremental loadings of the control, surface mounted slab provided an opportunity to investigate the damage at each stage of capacity. The first loading was up to 163 psi and a deflection of 0.11 inches with the formation of tension cracks at the support and initiation of crushing at the midspan. The second loading went through the peak capacity at 174 psi to a load of 110 psi with a total deflection of 0.21 inches. The third loading of 85 psi took the slab to

failure which resulted in a three-hinge mechanism with a final deflection of 4.5 inches. The bottom reinforcement was broken along the entire width at midspan of the slab (Figure A.15).

After considering the results of all five slabs, Kiger's testing program clearly demonstrated that "soil arching" distributed much of the load from the center of the slab to the supports if cohesiveless soils like sand are used as cover. However, the actual mechanics of "soil arching" are still somewhat a mystery.

A.6. S. C. Woodson, 1985 [Tables A.7-A.11 and Figures A.16-A.19]

Woodson tested 10 laterally restrained, reinforced concrete one-way slabs to investigate the effect of stirrups and stirrup details on the flexural response. He believed that TM 5-1300's requirements for shear lacing in protective structures was possibly unnecessary. Shear lacing not only is expensive to construct based on the amount of man-hours, but may not greatly enhance performance. Using three stirrup types (Figure A.16) and varying stirrup spacing, the tests were carefully monitored to allow comparison with previously tested laced reinforced concrete slabs with the same dimensions.

Woodson mirrored Kiger et. al.'s (1984) loading procedures and used their reaction structure, which was modified with a removable side door, with a different Small Blast Load Generator (Figures A.17 and A.18). Once the slabs were mounted in the reaction structure, all slabs had a clear span of 24 inches, a width of 24 inches, and a thickness of 2.3125 inches (L/h = 10.4). Instrumentation recorded displacement at one-eighth of the span and midspan, principal and stirrup steel strains, and water pressure. Once the instrumentation and removable door were in place, Woodson buried the reaction structure in sand up to the top surface of the slab.

All 10 slabs were cast from the same concrete batch with an anticipated 28-day design strength of 4,000 psi. Twelve test cylinders were cast which provided for testing of two at 28 days and one on the day of each slab test (Table A.7). Woodson used heat treated deformed wire for the principal reinforcement, the temperature reinforcement, and the stirrups (Table A.8). The reinforcement ratio for Slabs 9 and 10 was slightly higher because of the closer spacing of

principal reinforcement. The shear reinforcement, if present, consisted of double-leg and single-leg stirrups with different combinations of 90 and 135 degree bends (Table A.9).

The load-deflection summary for the 10 slabs is in Table A.10. Woodson observed total support rotations between 13 degrees and a maximum of 21 degrees since he stopped the test at 21 degrees of hinge rotation (Table A.11). Closely spaced stirrups and principal reinforcing steel and exterior placement of temperature steel increased ductility within tensile membrane action through an improved confinement of a larger concrete core. Even the slab with no shear reinforcement reached 16 degrees of support rotation without collapse (Figure A.19). These results exceeded maximum plastic hinge rotations allowed by TM 5-1300 for slabs with shear stirrups. Overall reserve capacity was generally the same whether the shear reinforcement was in the form of closely spaced stirrups or lacing. Acceptable compressive membrane results were obtained by using the experimentally obtained deflections (Table A.11).

A.7. S. C. Woodson et. al., 1985 [Tables A.12-A.15 and Figures A.20-A25]

Woodson and Garner tested 15 laterally restrained, reinforced concrete one-way slabs to investigate the effects of principal reinforcement configurations on slab response during primarily tensile membrane action. Many of the slabs maintained the same overall reinforcement ratios as the previous Woodson report, but the steel distribution and details varied through the use of dowels at the supports, bent-up bars, bars not extending into the supports, etc. The focus was on the cost and performance benefits of the varying principal steel details.

Woodson et. al. used the same Small Blast Load Generator, reaction structure, and general slab details (24" clear span and 24" wide) from the previous Woodson experiment in order to provide direct data comparison. The primary parameter varied was the steel ratios at midspan and the supports (Figures A.20 and A.21 and Table A.12). Slabs 1-8 were cast from one batch of concrete, while Slabs 9-15 were cast from a second batch (Table A.13). Reinforcement yield strengths are listed in Table A.14. Instrumentation recorded displacement at the quarter-span and

midspan, principal and stirrup steel strains, and water pressure. The shear reinforcement, if present, consisted of single-leg stirrups (Figure A.22).

The best compressive membrane enhancement occurred through equal amounts of compressive and tensile reinforcement at midspan and supports (Slabs 1 and 2; Figure A.23; Table A.15). The best overall performance of reinforcement details during both compressive and tensile membrane behavior consisted of a combination of bent-up and straight rebars which resulted in 75 percent of the total longitudinal reinforcement being placed in the tension zones at midspan and the supports (Slabs 7, 8, 9, and 12; Figure A.24). Many slabs contained no shear reinforcement and still reached support rotations greater than 20 degrees (Table A.15). The best tensile membrane enhancement occurred in Slab 6 with all reinforcement in tension regions through use of only bent-up bars for longitudinal reinforcement and no shear reinforcement. However, spalling was unacceptable in Slab 6 (Figure A.25). These tests demonstrated that principal steel details affect the large-deflection behavior of the one-way slab.

A.8. J. T. Baylot et. al., 1985 [Tables A.16-A.17]

Baylot et. al. dynamically tested 11 reinforced concrete one-way slabs to establish a data base of pressure distributions on buried structures from conventional weapons since previous data only noted peak pressure. A secondary objective was to develop an analytical procedure for computing the conventional weapons blast response for buried structures. The study focused on intermediate weapon stand-off since moderate to severe damage normally occurs. Closer blasts produce a breach or sure kill which would require a costly design to prevent.

Since experimental data seems to confirm that the static and dynamic failure modes are essentially the same, WES analysts relate the dynamic strength of the slab to the ultimate static capacity. To ensure accurate static resistance and response information for their analytical model, Baylot et. al. statically tested three reinforced concrete one-way slabs. The test facility, reaction structure and loading procedures were the same as Woodson (1985). Instrumentation recorded displacements, steel strains, and water pressure.

The structural parameters for the three statically loaded one-way slabs were as follows: ρ = 0.0047, 0.0104, and 0.0046, for the tension and compressive reinforcement; the shear reinforcement ratio (ρ_s) was 0.0023, 0.0098, and 0.0041 with single-leg stirrups; and L/h = 10, 10, and 5; respectively. WES heat treated the wire to conform to Grade 60 Number 2 and Number 3 bars (Table A.16). All three 24" x 24" gradually loaded slabs were cast from the same concrete batch with the testing of control cylinders just prior to loading of each slab (Table A.17). Predicted values for the peak capacity were over 10 percent less than experimental results (Table A.17).

Slab 1 failed in a three-hinge mechanism with several broken tension reinforcing bars at midspan. The peak capacity was 60.5 psi at a deflection of 0.5 inches. After dropping to a load of 30 psi at a deflection of 1.5 inches, the ultimate capacity was 54 psi at a deflection of 2.2 inches.

Slab 2 failed in a three-hinge mechanism with broken tension reinforcement at both the supports and midspan. The peak capacity on the first test of the slab was 101.1 psi with a deflection of 0.69 inches. On retest, the peak capacity was 100 psi at a deflection of 0.86 inches. After dropping to a capacity of 42 psi at a deflection of 1.8 inches, the ultimate capacity was 55 psi at a deflection of three inches.

Slab 3 required three loadings to reach a point where the mounting bolts broke. The load was 290 psi at a deflection of 0.53 inches. The cracks were not as wide as Slabs 1 and 2 nor was any reinforcement broken since the test was stopped before reaching peak capacity.

A.9. L. K. Guice, 1986 [Tables A.18-A.23 and Figures A.26-A.34]

Guice statically tested 16 reinforced concrete one-way slabs to investigate the effects of edge restraint on slab behavior. Previous investigators provided relatively fixed rotational and lateral edge conditions when testing their slabs. However, the roof of the box type FEMA key worker blast shelter is not quite as rigidly restrained, especially the rotational restraint, as the support clamping provided in previous tests. Current theories also assume variable lateral restraint

with full rotational restraint. These static tests increase the data base and improve the understanding of fundamental slab behavior.

Guice used previous WES test procedures with the exception that the reaction structure design permitted partial support rotation (Figure A.26 and A.27). Partial rotations of between 0.4 to 2.8 degrees would resemble the rotations possible in a box-type structure. Symmetrically placed shafts and springs, which adjusted the rack stiffness, transferred loads from the slab to the entirely steel reaction structure (Figures A.27 and A.28). Instrumentation recorded support displacement (Figure A.29), support thrusts or tensions, support moments (Figure A.30), water pressure, steel reinforcement strains, concrete strains, and slab midspan deflections.

Rack assemblies (Figure A.27) were preloaded to 20,000 pounds to ensure full lateral restraint before tightening the support rack bolts. Slack rubber membranes prevented any tension developing in the rubber membrane during large slab deflections. The slow, uniform rate of deflection was further controlled through monitoring the slab's load-midspan deflection plot. Loading ceased after significant tensile membrane action. Unfortunately, effective gap adjustments were not possible and prevented any controlled rotational restraint during testing. Support rotation could only be evaluated after testing. Post test activities included the recording of crack and spall behavior, steel rupture, and the amount of support rotation.

Slab construction was similar to previous WES investigations with a different concrete batch for each thickness of slabs (Table A.18). All slabs had equal percentages of compressive and tensile principal reinforcement with three-eighths inch concrete cover and identical temperature steel spaced at three inches in the transverse direction (Table A.19). Most principal reinforcement was No. 2 deformed bars with a few slabs reinforced by heat-treated deformed wire to maintain appropriate reinforcement ratios and bar spacing. To complete the structural cage and confine the concrete, Guice used Woodson's (1985) recommendation for shear reinforcement and provided single-leg stirrups of 0.11 inch diameter wire with 135/90 degree bends on opposite ends at the transverse reinforcement locations (Figure A.31). Three different reinforcement ratios were used for each slab thickness (Table A.20).

Since many of the slabs were identical to previous investigations, direct comparison was possible. Large values of support rotational freedom (Table A.21) prevented the development of compressive membrane capacity in Slabs 10 and 10A by allowing easier snap through to the tensile membrane stage before sufficient in-plane thrusts were developed (Table A.22 and A.23). For thinner slabs, even smaller support rotation would result in snap through. However, some small rotational freedom at the supports enhanced the tensile membrane capacity and increased the collapse deflection because of the decreased support stiffness. With little to no breakage of reinforcement during the compressive membrane stage, greater tensile membrane capacity existed. Tests did indicate that the percentage of load carried by tensile membrane action is related to the span-to-thickness ratio.

Performance of most slabs was comparable to the previously tested slabs even with the small amounts of support rotation (i.e., Slab 3, Figures A.32 to A.34). The small enhancement in Slabs 8 and 12 was the result of the loss of lateral restraint after attaining large thrusts (Table A.22). Review of the results for Slabs 1 and 2 (Table A.23) directly shows the effect of precompression since Slab 1 was prestressed. Guice used Keenan's deflection equation with the compressive membrane theory to estimate capacities for compressive membrane behavior (Table A.23). The assumed support stiffness resulted in estimated capacities greater than experimental values for the thick slabs and less than experimental values for the thin slabs.

A.10. S. C. Woodson, 1993 [Tables A.24-A.29 and Figures A.35-A.41]

Woodson statically tested 16 laterally restrained, one-way reinforced concrete slabs to evaluate the effects of shear reinforcement on large-deflection behavior. The objective was to compare the ductility enhancement of reinforced concrete one-way slabs when using either stirrups or lacing bars for shear reinforcement. The ultimate goal was development of new guidelines for shear reinforcement in blast-resistant structures which would result in safety and cost effectiveness improvements.

Testing procedures mirrored previous Woodson investigations. A four-foot diameter blast load generator (similar to Figure A.17) hydrostatically loaded the slabs rigidly clamped into the reaction structure (Figure A.13) over several minutes. Woodson varied three principal reinforcement ratios with an effective depth of 2.4 inches and three shear reinforcement ratios within the sixteen 24" x 24" x 3" slabs (Table A.24). He maintained the ratio of principal steel spacing to slab effective depth at approximately 0.6 while varying the shear reinforcement spacing between d, 0.75d, and 0.5d (Figures A.35). The temperature steel was identical for all slabs except that the location varied slightly between the laced shear reinforced slabs, which was placed outside the principal steel, and the stirrup shear reinforced slabs, which was placed inside the principal steel (Figures A.36 and A.37).

The 16 slabs were cast from one batch of concrete proportioned to provide approximately 4000 psi compressive strength at test time (Table A.25). The reinforcement was heat-treated deformed wire with an approximate defined yield-point of 60,000 psi (Table A.26). Each slab was instrumented for strain (Figures A.37 and A.38), displacement, and water pressure measurements.

Woodson measured final hinge rotations (Table A.27) and deflections at the one-quarter span and midspan points (Table A.28) throughout entire load history. In slabs with no shear reinforcement, the failure mode changed from flexure to flexure-shear to shear as the reinforcement ratio increased (Figures A.39 to A.41). A small amount of shear reinforcement quickly changed the failure mode from shear to flexural in heavily reinforced members. There was greater ductility during tensile membrane action if the temperature steel was placed exterior to the principal steel. Woodson also compared his results to compressive membrane theory by using the experimental peak deflection values with varying support stiffness. The greater the reinforcement ratio, the smaller the deflection required in the theory to obtain acceptable results (Table A.29).

A.11. S.C. Woodson, 1994 [Tables A.30-A.32 and Figures A.42-A.45]

Woodson statically tested 13 laterally restrained, reinforced concrete one-way deep slabs to investigate the behavior of deep slabs reinforced with details typical of protective structures.

Specifically, the study compared shear reinforcement performance for stirrups versus lacing. Results of previous Woodson experiments guided parameter decisions: quantity and spacing of primary and shear reinforcement, support conditions, testing procedures, and span-to-thickness ratios. Efficiently designed deep slabs with reserve capacity was the ultimate goal.

Testing procedures once again mirrored previous WES investigations except that a different blast load generator (Figure A.42) was required to provide the large hydrostatic load on the deep slabs. Each slab was 24" x24" with either a thickness of 5.5 (d = 4.8) or 8.9 inches (d = 8.0) (Table A. 30). For the slabs with an L/h = 4.4, the principal reinforcement was No. 3 Grade 60 rebar and the shear reinforcement was D2 deformed wire. For the slabs with an L/h of 2.7, the principal reinforcement was No. 5 Grade 60 rebar and the shear reinforcement was D3 deformed wire. Each slab had equal percentages of tensile and compressive reinforcement. The deformed wire was annealed to yield at approximately 60 ksi.

The ratio between the principal steel spacing and the effective depth was maintained at approximately 0.5. The three shear reinforcement spacing were 0.17d, 0.31d, and 2d since 0.5d is a typical value for blast structures tested at WES. Temperature steel was identical for all slabs with the exception of exterior placement in slabs with laced shear reinforcement. The average concrete compressive strength was approximately 5900 psi. Instrumentation recorded shear reinforcement strain, displacement at quarter-span and midspan, and pressure measurements.

The typical experimental load-deflection curve for the deep slabs was different from the general curve for laterally restrained slabs (Figure A.43). The deep slabs provided stiffer resistance up to the peak capacity with a more gradual decline before tensile membrane action occurred (Table A.31). Both the decline in resistance and tensile membrane action are characterized by straight lines. The sketches of damage and deflections across the slab which were similar at quarter-span and midspan indicate general dominance by shear action (Figures A.44 and A.45).

The two parameters, midspan deflection-to-thickness ratio and support hinge rotation, do not correlate well with past laterally restrained slab performances. The rotations were greater than

expected being 9-16 degrees, but less than previous results which were 12-20 degrees for thinner slabs even when using sufficient shear reinforcement (Table A.32). The greater observed stiffness resulted in Δ/h values of 0.07 and 0.04 for L/h's of 4.4 to 2.7, respectively. Using these values in Park and Gamble's modified rigid-plastic theory (W_c, Table A.32) resulted in over estimation of the capacity.

Therefore, to obtain the potential ultimate deep slab resistance, relatively large amounts of lacing or stirrup shear reinforcement is critical (i.e., > 0.6 percent). Adequate ductile reserve capacity is possible with reinforcement ratios of greater than one percent for both tensile and compressive reinforcement.

Table A.1. Slab Strip Test Results (Christiansen, 1963)

Test No.	1	2	3	4
Span (in)	60	60	60	72
Depth (in)	3.5	3.5	3	3
Cube Strength (psi)	4090	5660	4680	4970
f 'c (psi) (0.8 x cube strength)	3272	4528	3744	3976
E_c (psi)	3.6×10^6	5.4×10^6	3.8×10^6	4.2×10^6
Free Shrinkage Strain	30×10^{-5}	10×10^{-5}	32×10^{-5}	10×10^{-5}
k (calculated)	1.19	0	1.07	1.20
Rate of Deflection (in./min.)	0.006	0.004	0.010	0.016
Maximum Load (lb)	3970	4275	3180	2530
Load due to bending (lb)	2700	1150	2240	1715
Load due to arching (lb)	1270	3125	940	815
Calculated load due to arching (lb)	1122	3120	824	781
Experimental arch load/calculated arch load	1.13	1.00	1.14	1.05

Table A.2. Slab Details (Condensed from Table 1, Keenan 1969, R-620)

Slab	b (in)	h (in)	L (in)	d (in)	d' (in)	f'_c (psi)	f_y (ksi)	f_u (ksi)	Size (No.)	Spacing (in)	ρ (%)	ρ' (%)
1	24	6	72	4.875	1.125	5010	49.9	74.0	5	3	2.11	2.11
Dimensions are for both the supports and midspan.												

Table A.3. Statically Loaded Slab Results (Condensed from Table 2, Keenan 1969, R-620)

Source	At Flexural Ultimate ($N = N_u$)			At Flexural Yield ($N = 0$)[1]	
	Resistance q_u (psi)	Deflection z_u (in)	Concrete Strain ε_u	Resistance q_y (psi)	Deflection z_y (in)
Measured	110.0	1.00	0.0026	88.0	< 5.80
Computed[2]	98.6	0.90	0.0038	76.0	4.81
Measured/ Computed	1.11	1.11	--	1.15	< 1.20

[1] Post ultimate behavior at $N = 0$, just prior to initiation of tensile membrane action.
[2] All computed values based on ε_u (support) = ε_u (midspan) = 0.0038 in/in, $S = 0$, and no strain hardening of reinforcement.

Table A.4. Roberts Experimental Results (Adapted from Table 1, Roberts, 1969)

Slab[1] Strip	Depth (in)	ρ (%)	Cube Strength, 4 in (psi)	f 'c[2] (psi)	P_C	P_H	w:d
RB10	2	0.556	7300	5840	6.14	*	0.288
RB11	2	0.556	3580	2864	3.95	*	0.254
RB11	2	0.556	3580	2864	3.92	*	0.262
RB11	2	0.556	3580	2864	4.05	*	0.245
RB12	2	0.741	4750	3800	4.05	*	0.270
RB12	2	0.741	4750	3800	4.10	*	0.275
RB13	2	0.741	4370	3496	3.51	*	0.279
RB13	2	0.741	4370	3496	3.10	*	0.243
RB13	2	0.741	4370	3496	3.33	*	0.238
RB14	2	0.741	7200	5760	4.31	*	0.305
RB14	2	0.741	7200	5760	4.59	*	0.287
RB14	2	0.741	7200	5760	4.85	*	0.306
RB15	2	0.926	3495	2796	2.91	*	0.266
RB15	2	0.926	3495	2796	2.87	*	0.241
RB17	2	0.926	7720	6176	3.45	3.62	0.262
RB17	2	0.926	7720	6176	3.27	3.71	0.300
RB18	3	0.578	3910	3130	4.72	5.61	0.143
RB18	3	0.578	3910	3130	4.46	4.87	0.165
RB19	3	0.578	4160	3328	5.54	6.58	0.189
RB19	3	0.578	4160	3328	5.63	6.54	0.178
RB20	3	0.578	6940	5552	7.43	8.95	0.166
RB20	3	0.578	6940	5552	6.78	7.93	0.150
RB21	3	0.924	2630	2104	3.19	*	0.141
RB21	3	0.924	2630	2104	3.01	2.64	0.157
RB22	3	0.924	4370	3496	3.33	3.07	0.147
RB22	3	0.924	4370	3496	3.63	3.62	0.153
RB23	3	0.924	8160	6528	5.04	4.99	0.169
RB23	3	0.924	8160	6528	4.79	4.96	0.172
RB24	2	0.371	7510	6008	9.60	11.93	0.270
RB24	2	0.371	7510	6008	8.50	10.43	0.280
RB25	2	0.371	3810	3048	6.80	9.62	0.240
RB25	2	0.371	3810	3048	7.21	9.85	0.260
RB26	3	0.231	7540	6032	16.30	20.62	0.160
RB26	3	0.231	7540	6032	17.24	22.24	0.137
RB27	3	0.231	3720	2976	10.91	15.41	0.133
RB27	3	0.231	3720	2976	11.72	16.22	0.161

Experimental values of P_C, P_H and w:d at maximum experimental load.

[1] Length was 56.5 inches and the width was 9 inches for all slab strips.

[2] f 'c = 0.8 x cube strength.

* No readings taken.

P_C: ratio of P_M to P_L.

P_L: theoretical limit analysis load (bending only).

P_M: load applied to beam (M for existence of membrane action).

P_H: ratio of P to T.

T: load required to cause yielding of reinforcement in tension (i.e., steel area multiply yield stress).

P: thrust exerted on surround by slab.

w:d: ratio of central deflection of element to depth.

Table A.5. Concrete Compressive Strength/Modulus of Elasticity (Day of Test) (Kiger, 1984)

Test #	Sample #	Compressive Strength f'_c (psi)	Modulus of Elasticity E (10^6 psi)
1	1	6590	4.29
1	2	6890	4.50
2	1	6590	4.39
2	2	6950	4.50
3	1	7130	4.73
3	2	6710	4.28
4/5	1	7020	4.62
4/5	2	6840	4.50

Table A.6. Static Tensile Test, Steel Wire Reinforcement (Condensed from Table 2.2, Kiger, 1984)

Sample #[1]	Ultimate Stress (psi)	Yield Stress (psi)	Diameter (in)	Area (in^2)	Elongation 8-in gage Length (%)
1	97,561	89,431	0.177	0.0246	5.0
2	99,187	90,447	0.177	0.0246	4.2
3	99,187	89,837	0.177	0.0246	4.6
4	101,220	91,870	0.177	0.0246	5.4
5	98,374	89,431	0.177	0.0246	4.5
6	118,400	100,000	0.126	0.0125	3.6
7	119,200	97,600	0.126	0.0125	3.5
8	117,600	94,400	0.126	0.0125	5.0
9	118,400	97,600	0.126	0.0125	3.9
10	120,000	98,000	0.126	0.0125	3.4
11	105,600	87,000	0.080	0.0050	3.1
12	103,000	82,600	0.080	0.0050	3.4
13	102,400	84,000	0.080	0.0050	3.4
14	100,600	83,000	0.080	0.0050	2.2
15	103,400	85,000	0.080	0.0050	2.4

[1] Samples 1-5 are for main steel, 6-10 are for temperature steel, 11-15 are for shear steel.

Table A.7. Results of Concrete Cylinder Tests (Woodson, 1985)

Concrete Batch	Age Days	Compressive Strength (psi)	Corresponding Slab Test
1	28	4120	--
1	28	3960	--
1	103	4860	4
1	118	5060	3
1	124	4920	2
1	140	4850[1]	6
1	144	5110[1]	8
1	154	5020[1]	7
1	158	5060[1]	5
1	163	4700[1]	9
1	166	4930	10
1	168	4830	1

[1] Strain-gaged cylinder.

Table A.8. Tensile Test for Steel Reinforcement (Deformed Wire) (Woodson, 1985)

Wire Diameter (in)	Yield Stress (psi)	Ultimate Stress (psi)
0.11	68,500	69,400
Temperature Steel, All Slabs	57,760	61,580
Stirrup Steel, Slabs 1-8	65,040	67,650
	57,310	61,130
0.247	64,300	66,700
Principal Steel, Slabs 1-8	58,000	65,500
	59,290	65,570
	57,620	65,990
	59,490	60,960
	61,200	68,480
	58,460	64,930
0.179	66,400	71,200
Principal Steel, Slabs 9-10	65,600	72,000
	66,200	77,400
	58,000	72,400
	55,600	79,200
0.080	63,360	81,470
Stirrup Steel, Slabs 9-10	64,360	82,040
	63,650	80,620
	62,660	80,600

Table A.9. Static Test Results (Compiled From Text and Table 3.4, Woodson, 1985)

Slab	ρ mid %	ρ' mid %	ρ spt %	ρ' spt %	f_y ksi	f'_c ksi	h in	d in	d' in	ρ_s %	Stirrup Type	P_A psi	Δ_A in
1	0.72	0.83	0.83	0.72	59.8	4.83	2.313	1.9375	0.629	-	none	59.7	0.75
2	0.72	0.83	0.83	0.72	59.8	4.92	2.313	1.9375	0.629	0.36	135-S-135	66.1	0.75
3	0.72	0.83	0.83	0.72	59.8	5.06	2.313	1.9375	0.629	0.18	135-S-135	71.6	0.75
4	0.72	0.83	0.83	0.72	59.8	4.86	2.313	1.9375	0.629	0.09	135-S-135	76.0	0.75
5[1]	0.72	0.83	0.83	0.72	59.8	5.06	2.313	1.9375	0.629	0.18	135-S-135	75.2	0.65
6	0.72	0.83	0.83	0.72	59.8	4.85	2.313	1.9375	0.629	0.18	135-S-90	66.6	1.10
7[1]	0.72	0.83	0.83	0.72	59.8	5.02	2.313	1.9375	0.629	0.18	135-S-90	65.5	0.85
8	0.72	0.83	0.83	0.72	59.8	5.11	2.313	1.9375	0.629	0.18	D-135	69.5	0.80
9	0.76	0.87	0.87	0.76	62.4	4.70	2.313	1.9375	0.629	0.19	135-S-135	71.0	0.75
10	0.76	0.87	0.87	0.76	62.4	4.93	2.313	1.9375	0.629	0.38	135-S-135	77.4	0.90

[1] Temperature steel outside principal steel.

Table A.10. Load-Deflection Summary (Woodson, 1985)

Slab	P_A (psi)	Δ_A (in)	P_B (psi)	Δ_B (in)	P_C (psi)	Δ_C (in)	P_D (psi)	Δ_D (in)
1	59.7	0.75	42	1.8	35	3.1	43	3.7
2	66.1	0.75	39	2.1	41	3.1	66	4.1
3	71.6	0.75	32	1.7	45	3.0	*	*
4	76.0	0.75	52	1.7	45	2.8	*	*
5	75.2	0.65	47	1.6	47	2.4	67	3.2
6	66.6	1.10	55	1.8	49	3.1	*	*
7	65.5	0.85	42	1.8	42	2.7	55	3.4
8	69.5	0.80	51	2.0	48	2.8	54	3.1
9	71.0	0.75	41	1.6	37	2.9	56	3.4
10	77.4	0.90	42	1.7	42	2.8	85	3.4

* No increase in load-carrying capacity experienced.

Table A.11. Membrane Theory Comparison and Hinge Rotation
(Adapted Tables 4-6, 4-7, and 4-10, Woodson, 1985)

	Experimental		Predicted Resistance from Compressive Membrane Theory for Δ/h =					Support Hinge Rotations	
Slab	Resistance (psi)	Δ/h	0.17	0.3	0.4	0.5	Exp	Rotation (degrees)	Δ_{max} / L (%)
1	59.7	0.32	80.7	67.1	57.5	48.9	66.6	16.3	14.6
2	66.1	0.32	80.7	67.1	57.5	48.9	66.6	20.6	18.8
3	71.6	0.32	80.7	67.1	57.5	48.9	66.6	14.0	12.5
4	76.0	0.32	80.7	67.1	57.5	48.9	66.6	13.1	11.7
5	75.2	0.28	80.7	67.1	57.5	48.9	70.5	15.4	13.8
6	66.6	0.48	80.7	67.1	57.5	48.9	52.5	14.0	12.5
7	65.5	0.37	80.7	67.1	57.5	48.9	61.9	14.5	12.9
8	69.5	0.35	80.7	67.1	57.5	48.9	63.7	14.0	12.5
9	71.0	0.32	82.8	69.3	59.7	51.2	69.1	16.3	14.6
10	77.4	0.39	82.8	69.3	59.7	51.2	62.6	18.4	16.7

Table A.12. Static Test Results (Adapted From Tables 2.1 and 4.1, Woodson et. al., 1985)

Slab	ρ Mid %	ρ' Mid %	ρ Spt %	ρ' Spt %	f_y ksi	f'_c ksi	h in	d in	d' in	ρ_s %	Stirrup Type	P_B psi	Δ_B in
1	0.74	0.74	0.74	0.74	66.0	4.47	2.313	1.9375	0.625	-	none	66	1.00
2	0.79	0.79	0.79	0.79	66.0	4.47	2.313	1.8125	0.500	-	none	64	0.80
3	1.14	0.40	0.40	1.14	63.5	4.47	2.313	1.8125	0.500	-	none	68	1.20
4[1]	1.14	0.40	1.19	1.14	63.5	4.49	2.313	1.8125	0.500	-	none	68	1.10
5[2]	1.14	0.40	1.19	1.14	63.5	4.49	2.313	1.8125	0.500	-	none	77	1.00
6[3,4]	1.58	0.0	1.58	0.0	66.0	4.49	2.313	1.8125	0.500	-	none	68	0.25
7[3,5]	1.13	0.45	1.13	0.45	66.0	4.27	2.313	1.8125	0.500	-	none	67	1.00
8[5]	1.13	0.45	1.13	0.45	66.0	4.27	2.313	1.8125	0.500	0.06	135-S-90	68	0.80
9[5]	1.13	0.45	1.13	0.45	66.0	4.03	2.313	1.8125	0.500	0.22	135-S-90	67	0.80
10[5]	1.13	0.45	1.13	0.45	66.0	4.03	2.313	1.8125	0.500	0.22	135-S-90	73	0.90
11[5]	1.13	0.45	1.13	0.45	66.0	4.16	2.313	1.8125	0.500	0.22	135-S-90	73	0.95
12[6]	1.13	0.45	1.13	0.45	66.0	4.16	2.313	1.8125	0.500	0.22	135-S-90	71	0.80
13[7]	1.13	0.45	1.13	0.45	66.0	4.16	2.313	1.8125	0.500	-	none	64	0.75
14	1.02	1.02	1.02	1.02	60.3	3.56	2.9	2.4	0.500	1.53	135-S-90	126	0.80
15[8]	0.79	0.45	0.79	0.45	66.0	3.56	2.313	1.8125	0.500	-	none	52	1.00

[1] No. 2 dowels extended 0.97t at supports.
[2] No. 2 dowels extended 2.22t at supports.
[3] Reloaded.
[4] No. 2 pairs bent.
[5] Alternate No. 2 pairs bent.
[6] Alternate No. 2 pairs bent, temperature steel outside.
[7] Alternate No. 2 pairs cut.
[8] Alternate No. 2's bent.

Table A.13. Concrete Compressive Test Cylinder Results (Woodson et. al., 1985)

Batch	Slab	28-Day Strength (psi)	60-Day Strength (psi)	Approximate Test-Day Strength (psi)
1	1-8	4440	4050	
		4780	4490	
	1			4470
	2			4470
	3			4470
	4			4490
	5			4490
	6			4490
	7			4270
	8			4270
2	9-15	3500	4400	
		3360	3660	
	9			4030
	10			4030
	11			4160
	12			4160
	13			4160
	14			3560
	15			3560

Table A.14. Reinforcement Tensile Test Results (Woodson et. al., 1985)

Specimen	Yield Stress (ksi)	Ultimate Stress (ksi)
D1 Wire	72.56	74.34
	67.69	71.24
	51.32	56.64
	52.21	56.64
D2.5 Wire	62.00	72.73
	62.20	75.91
	64.78	76.71
0.25 Inch Diameter Wire	73.90	78.90
	73.70	78.70
	51.10	61.90
No. 2 Rebar	59.94	--
	58.43	75.0
	62.53	78.3
0.3 Inch Diameter Rebar	63.4	81.47
	64.35	82.03
	63.65	80.62
	62.66	80.02

Table A.15. Summary of Test Results (Adapted From Tables 4.1 and 5.1, Woodson et.al., 1985)

	Compressive Membrane Region				Tensile Membrane Region			Posttest Analysis	
Slab	P_B exp (psi)	Δ_B (in)	Δ_B/h	P_B[1] theor (psi)	P_D exp (psi)	Δ_D (in)	Yield Line Resistance (psi)	P_B[2] theor (psi)	Mechanism[3]
1	66	1.00	0.43	46.3	48	4.1	46.7	56.5	3-H
2	64	0.80	0.35	45.7	55	4.3	46.3	62.9	3-H
3	68	1.20	0.52	43.6	58	4.6	43.9	45.8	3-H
4	68	1.10	0.48	43.6	60	4.5	43.9	50.0	Mod 3-H
5	77	1.00	0.43	59.3	55	5.1	60.9	68.0	Mod 3-H
6	68	0.25	0.11	86.5	122	4.9	51.6	71.6	4-H
7	67	1.00	0.43	57.7	63	5.7	61.2	66.6	Mod 3-H
8	68	0.80	0.35	57.7	70	5.2	61.2	71.3	Mod 3-H
9	67	0.80	0.35	57.7	71	5.3	61.2	67.4	Mod 3-H
10	73	0.90	0.39	57.7	62	5.2	61.2	67.4	Mod 3-H
11	73	0.95	0.41	57.7	54	4.2	61.2	67.1	3-H
12	71	0.80	0.35	57.7	76	5.5	61.2	70.5	Mod 3-H
13	64	0.75	0.32	57.7	47	5.4	61.2	--	Mod 3-H
14	126	0.80	0.28	100.7	96	5.0	88.5	123.7	3-H
15	52	1.00	0.43	45.1	36	5.4	44.2	49.9	3-H

[1] Using Park and Gamble's (1980) equations with $\beta = 0.5$ and $\Delta/h = 0.5$.
[2] Using Park and Gamble's (1980) equations with $\beta = 0.5$ (0.21 for Slab 6) and experimental Δ/h.
[3] A modified 3-hinge mechanism has a larger midspan crushing zone and cracking zone at the supports.

Table A.16. Reinforcing Steel Tensile Tests (Adapted from Table 3, Baylot et.al., 1985)

Slab	Steel Use	Dia (in)	Area (in^2)	Yield (psi)	Ultimate (psi)	Rupture (psi)
1	Principal	0.152	0.0181	82,000	86,000	56,100
	Temperature	0.106	0.0088	45,500	47,700	47,700
	Shear	0.106	0.0088	45,500	47,700	47,700
2	Principal	0.207	0.0337	70,000	78,200	72,100
	Temperature	0.106	0.0088	45,500	47,700	47,700
	Shear	0.152	0.0181	82,000	86,000	56,100
3	Principal	0.207	0.0337	70,000	78,200	72,100
	Temperature	0.120	0.0113	59,500	64,600	50,900
	Shear	0.120	0.0113	59,500	64,600	50,900

Table A.17. Static Test Results (Expanded Table 11 From Text, Baylot et. al., 1985)

Slab	Area (in^2)	ρ (%)	L/h	f'c (psi)	E (10^6 psi)	ν	h (in)	d (in)	δ (in)	Act w (psi)	Pred w (psi)
1	0.2172	0.464	10	6080	4.75	0.25	2.4	1.95	0.50	60.5	55
2	0.4718	1.045	10	6080	4.75	0.25	2.4	1.88	0.86	101.1	83
3	0.4718	0.457	5	6030	5.00	0.22	4.8	4.30	0.53	290*	252

* Test stopped before ultimate load was reached.

Table A.18. Concrete Properties (Guice, 1986, SL-86-32)

Cylinder	Compressive Strength (psi)	Age When Tested (days)	Average Strength (psi)
Batch 1			
1	3420	29	
2	3420	29	3420
3	3950	75	
4	4220	75	4090
5	4340	77	
6	4140	77	4240
7	4610	82	
8	3920	82	4270
9*	4230	88	
10*	4720	88	
11*	4160	88	4370
12	4220	103	
13	4550	103	
14	4610	103	
15	4720	103	
16	4140	103	
17	4310	103	
18	4500	103	4440
Batch 2			
19	4770	29	
20	4750	29	4760
21	3700	12	3700
22	3840	14	3840
23	5290	89	
24	5390	89	5340
25	4380	106	
26	4130	106	
27	5210	106	4570
28	4380	109	
29	5500	109	
30	4770	109	4880
31*	5180	110	
32*	5230	110	
33*	5030	110	5150
34	5510	111	
35	5230	111	
36	4660	111	5130
37	5110	112	
38	5270	112	5190
* Indicates cylinders instrumented with strain gages.			

Table A.19. Experimental Steel Properties (Guice, 1986, SL-86-32)

Bar Type[1]	Yield Stress (psi)	Yield Strain (in/in)	Ultimate Stress (psi)	Rupture Strain[2] (in/in)
No. 2	59,590	0.0020	79,180	0.165
	56,730	0.0015	75,510	0.188
	58,780	0.0017	75,510	0.135
	58,780	0.0015	76,530	0.170
Average	58,470	0.0017	76,680	0.174
D3	53,330	0.0015	65,000	0.091
	39,330	0.0015	50,670	0.198
	50,000	0.0016	59,330	0.039
	57,330	0.0014	70,670	0.075
Average	50,000	0.0015	61,420	0.101
D2.5	64,000	0.0019	76,000	0.053
	76,000	0.0020	82,400	0.109
	62,000	0.0019	74,800	0.073
Average	67,330	0.0019	77,730	0.078
D1	95,000	0.0028	97,000	0.058
	87,000	0.0028	86,000	0.029
	86,000	0.0038	86,000	0.017
	89,000	0.0028	89,000	0.020
	96,000	0.0030	97,000	0.015
Average	90,600	0.0030	91,000	0.028

[1] Corresponding areas and diameters of bars are: D3 - area = 0.030 sq. in., diameter = 0.195 in.; D2.5 - area = 0.025 sq. in., diameter = 0.178 in.; D1 - area = 0.010 sq. in., diameter = 0.110 in.; No. 2 - area = 0.049 sq. in., diameter = 0.250 in.

[2] Failure occurred outside the gage length in the third sample of No. 2.

Table A.20. Slab Design/Construction Details (Adapted From Tables 2.1, 2.2, and 4.1, Guice, 1986, SL-86-32)

Slab[1]	L/h	ρ [2] (%)	$A_s=A'_s$	f_y (psi)	Type[3]/ Spacing (in)	h (in)	depth (in)	f'_c (psi)
1	10.4	0.52	0.2418	50,000	D3/3	2.3125	1.9375	4414
2	10.4	0.52	0.2418	50,000	D3/3	2.3125	1.9375	4269
3	10.4	0.74	0.3441	58,470	#2/3.75	2.3125	1.9375	4443
4	10.4	0.74	0.3441	58,470	#2/3.75	2.3125	1.9375	4258
4A	10.4	0.74	0.3441	58,470	#2/3.75	2.3125	1.9375	4165
4B	10.4	0.74	0.3441	58,470	#2/3.75	2.3125	1.9375	4201
5	10.4	1.06	0.4929	58,470	#2/2.5	2.3125	1.9375	4450
6	10.4	1.06	0.4929	58,470	#2/2.5	2.3125	1.9375	4279
7	14.8	0.58	0.1740	67,330	D2.5/3.75	1.625	1.25	5023
8	14.8	0.58	0.1740	67,330	D2.5/3.75	1.625	1.25	4968
9	14.8	1.14	0.3420	58,470	#2/3.75	1.625	1.25	5015
9A	14.8	1.14	0.3420	58,470	#2/3.75	1.625	1.25	5005
10	14.8	1.14	0.3420	58,470	#2/3.75	1.625	1.25	4965
10A	14.8	1.14	0.3420	58,470	#2/3.75	1.625	1.25	4963
11	14.8	1.47	0.4410	58,470	#2/3.75	1.625	1.25	5018
12	14.8	1.47	0.4410	58,470	#2/3.75	1.625	1.25	4973

[1] All slabs had lengths = 24 inches, widths = 24 inches, depths to compressive steel = 0.375 inches, and ultimate strain assumed = 0.003.
[2] Steel percentages were the same in top and bottom.
[3] Corresponding areas and diameters of bars are: D3 - area = 0.030 sq. in., diameter = 0.195 in.; D2.5 - area = 0.025 sq. in., diameter = 0.178 in.; D1 - area = 0.010 sq. in., diameter = 0.110 in.; No. 2 - area = 0.049 sq. in., diameter = 0.250 in.

Table A.21. Support Rotations (Guice, 1986, SL-86-32)

	Lateral Deflection (inches)			Rack Rotation (degrees)		
Slab	at D3	at D4	Average	at D3	at D4	Average
1	0.14	0.20	0.170	1.50	2.14	1.82
2	0.10	0.19	0.145	1.08	2.04	1.56
3	0.01	0.22	0.115	0.14	2.36	1.24
4	0.10	0.18	0.140	1.08	1.93	1.50
4A	0.19	0.28	0.235	2.04	3.00	2.52
4B	0.12	0.29	0.205	1.29	3.12	2.20
5	0.05	0.05	0.050	0.55	0.55	0.55
6	0.14	0.24	0.190	1.50	2.57	2.04
7	0.10	0.01	0.055	1.08	0.14	0.61
8	0.21	0.20	0.205	2.25	2.14	2.20
9	0.04	0.20	0.120	0.45	2.14	1.29
9A	0.01	0.06	0.035	0.14	0.66	0.40
10	0.30	0.22	0.260	3.22	2.36	2.79
10A	0.20	0.18	0.19	2.14	1.93	2.04
11	0.12	0.02	0.07	1.29	0.24	0.76
12[1]	0.21	0.16	0.19	2.25	1.72	2.04

[1] Denotes slab with substantial rotation occurring after the peak capacity was reached.

Table A.22. Load-Washer Data (Guice, 1986, SL-86-32)

	Left Support				Right Support				Average	
Slab	F1 (kips)	F2 (kips)	T (kips)	M (in-k)	F1 (kips)	F2 (kips)	T (kips)	M (in-k)	T (kips)	M (in-k)
1	30.9	7.2	38.1	120.0	20.6	21.8	42.4	63.3	40.3	91.7
2	16.7	4.1	20.8	58.6	11.7	3.1	14.8	31.1	17.8	44.9
3	15.8	0.8	16.6	40.9	7.3	1.6	8.9	-5.8	12.8	17.6
4	24.5	1.9	26.4	89.2	21.6	*	*	73.2	26.4	81.2
4A	19.8	0.8	20.6	64.7	15.7	*	*	42.2	20.6	53.5
4B	23.6	0.4	24.0	80.4	19.4	*	*	57.3	24.0	68.9
5	16.1	2.4	18.5	26.0	22.6	6.2	28.8	61.7	23.7	30.9
6	29.9	4.0	33.9	106.3	24.9	1.7	26.6	78.8	30.3	92.6
7	*	4.5	*	*	*	4.4	*	*	*	*
8	*	1.7	*	*	4.8	9.0	13.8	11.8	13.8	11.8
9	14.8	3.8	18.6	55.9	15.0	6.3	21.3	56.5	39.9	56.5
9A	6.7	3.0	9.7	10.7	9.9	5.8	15.7	19.5	12.7	19.5
10	4.4	1.5	5.9	6.2	5.1	1.1	6.2	8.2	6.1	8.2
10A	7.0	1.8	8.8	20.5	4.9	1.2	6.1	14.8	7.5	14.8
11	14.0	4.2	18.2	47.7	*	4.1	*	47.7	18.2	47.7
12	0.0	*	*	-14.0	0.9	*	*	-11.5	*	-11.5

* Denotes unavailable or erroneous data.
Some of the averages are actually based on single records when second records are unavailable.

Table A.23. Results of Compressive Membrane Analyses (Guice, 1986, SL-86-32)

	Analytical						Experimental	
Slab	Condition A[1]		Condition B[1]		Condition C[1]			
	W_{ua} [2] (psi)	δ/h [3]	W_{ub} [2] (psi)	δ/h	W_{uc} [2] (psi)	δ/h	W_u (psi)	δ/h
1	74.4	0.11	66.6	0.16	63.5	0.17	78	0.32
2	72.9	0.11	65.4	0.16	62.5	0.17	52	0.37
3	89.3	0.11	81.3	0.16	78.2	0.17	72	0.52
4	89.3	0.11	79.9	0.16	77.0	0.17	71	0.65
4A	86.2	0.11	79.1	0.16	76.3	0.17	69	0.58
4B	86.6	0.11	79.4	0.16	76.6	0.17	77	0.56
5	105.1	0.11	97.1	0.16	94.0	0.17	98	0.37
6	103.5	0.11	96.0	0.16	93.1	0.17	91	0.65
7	32.6	0.25	28.2	0.32	26.2	0.35	32	0.37
8	32.4	0.25	28.0	0.32	25.7	0.36	23	0.62
9	40.9	0.25	37.4	0.32	34.1	0.33	40	0.43
9A	40.9	0.25	37.4	0.32	34.1	0.33	41	0.31
10	40.7	0.25	37.2	0.32	34.1	0.33	--	--
10A	40.7	0.25	37.2	0.32	33.9	0.33	--	--
11	46.6	0.25	43.3	0.32	39.7	0.32	46	0.40
12	46.4	0.25	43.1	0.32	39.7	0.32	22	0.31

[1] Condition A - Support Stiffness = 1.0E20 lb/in, Condition B - Support Stiffness = 5.4E6 lb/in, Condition C - Support Stiffness = 3.0 E6 lb/in.
[2] W_{ua}, W_{ub}, W_{uc} = Peak Capacity for Condition A, B, C, respectively.
[3] δ/h = peak capacity deflection/hhickness.

Table A.24. Slab Characteristics (Woodson, 1993)

Slab	$\rho_{tension}$	ρ_{shear}	Lacing	Stirrups	Principal Steel Type / Spacing (type[1] / inches)	Shear Steel Spacing (inches)
1	0.0025	none	-	-	D1 / 1.60	-
2	0.0056	none	-	-	D2 / 1.50	-
3	0.0097	none	-	-	D3 / 1.33	-
4	0.0025	0.0026	x		D1 / 1.60	2.40
5	0.0097	0.0031	x		D3 / 1.33	2.40
6	0.0025	0.0034	x		D1 / 1.60	1.85
7	0.0056	0.0036	x		D2 / 1.50	1.85
8	0.0025	0.0052	x		D1 / 1.60	1.20
9	0.0097	0.0063	x		D3 / 1.33	1.20
10	0.0025	0.0026		x	D1 / 1.60	2.40
11	0.0025	0.0034		x	D1 / 1.60	1.85
12	0.0056	0.0036		x	D2 / 1.50	1.85
13[2]	0.0056	0.0036		x	D2 / 1.50	1.85
14	0.0025	0.0052		x	D1 / 1.60	1.20
15	0.0097	0.0031		x	D3 / 1.33	2.40
16	0.0097	0.0063		x	D3 / 1.33	1.20

[1] D1, D2, and D3 deformed wires have nominal cross-sectional areas of approximately 0.01, 0.02, 0.03 inches^2, respectively.
[2] Temperature steel placed exterior to principal steel.

Table A.25. Concrete Cylinder Test Results (Woodson, 1993)

Cylinder	Age (days)	Compressive Strength (psi)
1	7	2780
2	7	2600
3	28	3400
4	28	3660
5	243	4400
6	243	4050
7	243	4260
8	243	4100
9	243	4120
10	243	3980

Table A.26. Steel Reinforcement Tensile Tests (Heat Treated Deformed Wire)
(Expanded Table 4.4, Woodson, 1993)

Wire Type [1]	Yield Stress (psi)	Ultimate Stress (psi)
D1	52,860	58,040
	52,680	58,040
	60,710	62,500
	58,040	62,050
	54,460	59,820
average	55,750	60,090
D2	62,500	72,320
	61,610	73,210
	67,860	77,230
	61,430	72,320
	55,360	65,180
average	61752	72,052
D3	62,280	71,170
	64,290	72,770
	66,070	72,770
	64,730	71,880
	66,070	73,210
average	64,688	72,360

[1] D1, D2, and D3 deformed wires have nominal cross-sectional areas of approximately 0.01, 0.02, 0.03 inches^2, respectively.

Table A.27. Hinge Rotation and Ratio of Midspan Deflection to Clear Span (Posttest Measurements) (Woodson, 1993)

Slab	Midspan Deflection [1] (Δ) (inches)	Δ/L (percent)	θ (degrees)
1	4.4	18.3	20.1
4	5.5	22.9	24.6
10	5.0	20.8	22.6
6	5.5	22.9	24.6
11	5.9	24.6	26.2
8	5.5	22.9	24.6
14	5.7	23.8	25.4
2[2]	1.5	7.1	8.1
7	4.5	18.8	20.6
12	5.7	23.8	25.4
13	7.0	29.2	30.3
3[3]	2.2	9.2	10.4
5	7.0	29.2	30.3
15	5.3	22.1	23.8
9	5.3	22.1	23.8
16	5.1	21.3	23.0

[1] Presented deflection values were manually measured following removal of the neoprene membrane.
[2] Experiment terminated early due to water leak.
[3] Slab failed in shear.

Table A.28. Midspan Load-Deflection Summary (Combined Tables 5.2 and 5.6, Woodson, 1993)

Slab	YL (psi)	P_A (psi)	P_A /YL	Δ_A (in)	Δ_A /h	P_B (psi)	Δ_B (in)	P_C (psi)	Δ_C (in)	P_D (psi)	Δ_D[4] (in)	Shear[6] (ρ_s)	$\rho_{tension}$
1	22	57[1]	2.6	0.52	0.19	8	2.41	8	2.41	23	3.61	none	0.0025
4	22	71	3.2	0.80	0.27	10	2.31	10	2.96	31	4.36	L 0.0026	0.0025
10	22	63	2.9	0.65	0.22	3	2.33	8	3.59	25	4.77	S 0.0026	0.0025
6	22	88	4.0	0.79	0.26	10	2.58	10	2.58	31	4.80	L 0.0034	0.0025
11	22	63	2.9	0.91	0.30	2	2.65	2	2.65	22	5.00	S 0.0034	0.0025
8	22	64	2.9	1.00	0.33	8	2.50	8	3.10	26	4.50	L 0.0052	0.0025
14	22	64	2.9	0.87	0.29	4[2]	2.60	-	-	23[3]	-	S 0.0052	0.0025
2	53	87	1.6	0.80	0.27	44	1.10	44	1.10	53	1.65	none	0.0056
7	53	83	1.6	0.88	0.29	38	2.32	11	3.61	43	4.00	L 0.0036	0.0056
12	53	85	1.6	1.10	0.37	19[2]	3.10	-	-	43[3]	-	S 0.0036	0.0056
13	53	89	1.7	0.74	0.25	25	2.00	25	3.19	41	4.63	S 0.0036	0.0056
3[5]	92	106	1.2	0.45	0.15	59	0.51	59	0.51	88	2.18	none	0.0097
5	92	135	1.5	0.89	0.30	70	1.69	27	3.88	41	4.96	L 0.0031	0.0097
15	92	130	1.4	0.81	0.27	58	2.30	14	3.11	75	4.00	S 0.0031	0.0097
9	92	137	1.5	0.91	0.31	17	2.85	17	2.85	73	4.22	L 0.0063	0.0097
16	92	132[2,3]	1.4	-	-	-	-	-	-	79[3]	-	S 0.0063	0.0097

[1] Actual experimental value was greater than shown due to data record clip during experiment.
[2] Large crack formed directly at deflection gage connection on slab, causing loss of connection.
[3] Taken from data recorded at the one-quarter-span location.
[4] Deflection values presented were electronically recorded during the experiment.
[5] Shear failure occurred prior to attainment of potential flexural capacity.
[6] L is for lacing; S is for stirrups.

Table A.29. Compressive Membrane Analysis (Woodson, 1993)

Experimental Ultimate Resistance and Deflection			Predicted (Computed) Ultimate Resistance (P_A) Using Compressive Membrane Theory For Δ/h =		
Slab	P_A (psi)	Experimental Δ_A/h	Experimental Δ_A/h (psi)	$\Delta_A/h = 0.1$ (psi)	$\Delta_A/h = 0.5$ (psi)
1	57[1]	0.19	77	89	40
4	71	0.27	67	89	40
10	63	0.22	73	89	40
6	88	0.26	69	89	40
11	63	0.30	63	89	40
8	64	0.33	59	89	40
14	64	0.29	64	89	40
2	87	0.27	86	105	63
7	83	0.29	63	105	63
12	85	0.37	75	105	63
13	89	0.25	88	105	63
3[2]	106	0.15	123	128	95
5	135	0.30	109	128	95
15	130	0.27	112	128	95
9	137	0.31	108	128	95
16	132[3]	0.31[4]	108	128	95

[1] Actual experimental value was greater than shown due to the data record clip during experiment.
[2] Shear failure occurred prior to attainment of potential ultimate flexural capacity.
[3] Based on the one-quarter span load deflection curve.
[4] Based on midspan deflection measured for similar slab (slab #9).

Table A.30. Slab Characteristics (Combined Tables 1 and 2, Woodson 1994)

Slab	$\rho_{tension}$ (%)	ρ_{shear} (%)	Shear Type[1]	Principal Steel Spacing (in)	Shear Steel Spacing (in)	L/h
1	0.96	none	-	0.5d, #3 @2.4	-	4.4
2	0.96	0.60	S	0.5d, #3 @2.4	0.31d, D2 @ 1.5	4.4
3	0.96	0.60	L	0.5d, #3 @2.4	0.31d, D2 @ 1.5	4.4
4	0.34	none	-	0.5d, #3 @4.0	-	2.7
5	0.96	none	-	0.5d, #5 @4.0	-	2.7
6	0.96	none	-	0.5d, #5 @4.0	-	2.7
7	0.34	0.60	S	0.5d, #3 @4.0	0.17d, D3 @1.33	2.7
8	0.96	0.60	S	0.5d, #5 @4.0	0.17d, D3 @1.33	2.7
9	0.96	0.60	S	0.5d, #5 @4.0	0.17d, D3 @1.33	2.7
10	0.96	0.13	S	0.5d, #5 @4.0	2d, D3 @ 6.0	2.7
11	0.34	0.60	L	0.5d, #3 @4.0	0.17d, D3 @1.33	2.7
12	0.96	0.13	L	0.5d, #5 @4.0	2d, D3 @ 6.0	2.7
13	0.96	0.60	L	0.5d, #5 @4.0	0.17d, D3 @1.33	2.7

[1] L is for lacing and S is for stirrups.

Table A.31. Midspan Load-Deflection Summary (Combined Tables 3 and 5, Woodson, 1994)

Slab	P_A (psi)	Δ_A (in)	Δ_A/h	P_B (psi)	Δ_B (in)	Δ_B/h	P_C (psi)	Δ_C (in)	Δ_C/h
1	399	0.20	0.036	264	1.01	0.18	349	1.98	0.36
2	571	0.40	0.073	396	0.96	0.17	369	1.80	0.33
3	543	0.41	0.075	319	1.32	0.24	-	-	-
4	572	0.33	0.037	-	-	-	-	-	-
5	1169	0.24	0.027	869	1.30	0.15	1211	1.92	0.35
6	1222	0.33	0.037	824	1.43	0.16	1150	2.66	0.30
7	1860	0.40	0.045	-	-	-	-	-	-
8	1550	0.40	0.045	975	1.74	0.20	1225	2.58	0.29
9	1365	0.29	0.033	1285	0.44	0.05	1260	0.87	0.16
10	1337	0.29	0.033	-	-	-	-	-	-
11	1380	0.37	0.042	-	-	-	-	-	-
12	1210	0.27	0.030	926	1.21	0.14	1163	2.93	0.33
13	1545	0.65	0.073	1315	1.79	0.20	1445	3.48	0.39

Table A.32. Compressive Membrane and Hinge Rotation (Combined Tables 6 and 7, Woodson, 1994)

Slab	W_y (psi)	W_c (psi)	W_{exp} (psi)	ρ_{shear} (%)	Δ_A/h exp	θ_A (degrees)	θ_B (degrees)	θ_C (degrees)
1	348	606	399	none	0.036	1.0	4.8	9.4
2	348	595	571	0.60	0.073	1.9	4.6	8.5
3	348	594	543	0.60	0.075	2.0	6.3	-
4	352	1331	572	none	0.037	1.6	-	-
5	966	1718	1169	none	0.027	1.1	6.2	9.1
6	966	1713	1222	none	0.037	1.6	6.8	12.5
7	352	1322	1860	0.60	0.045	1.9	-	-
8	966	1705	1550	0.60	0.045	1.9	8.3	12.1
9	966	1716	1365	0.60	0.033	1.4	2.1	4.1
10	966	1716	1337	0.13	0.033	1.4	-	-
11	352	1326	1380	0.60	0.042	1.8	-	-
12	966	1717	1210	0.13	0.030	1.3	5.8	13.7
13	966	1668	1545	0.60	0.073	3.1	8.5	16.2

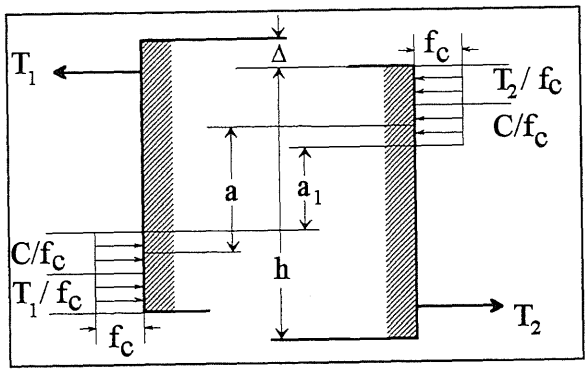

Figure A.1. Horizontal Forces at Support (1) and at Midspan (2) (Christiansen, 1963)

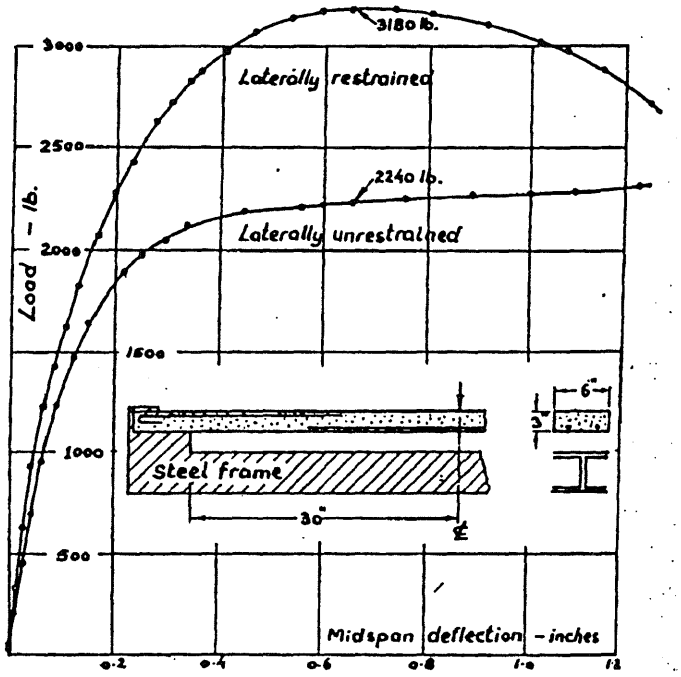

Figure A.2. Load Deflection Curves for Beam 2 (Christiansen, 1963)

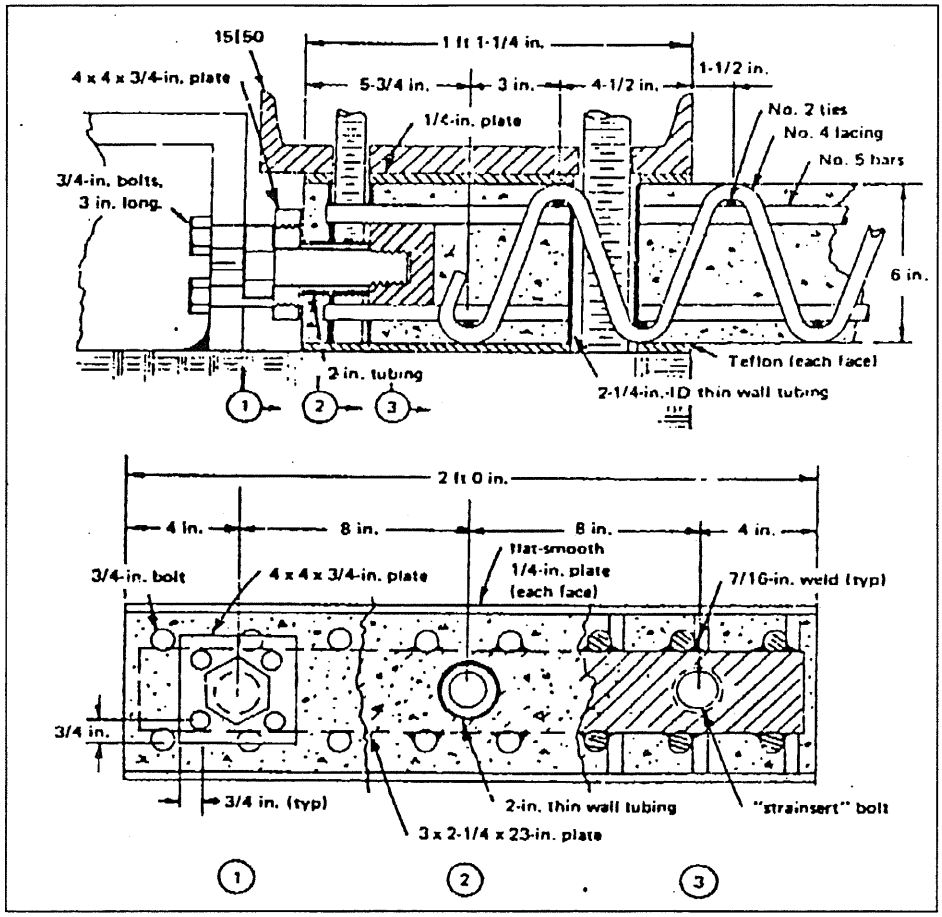

Figure A.3. Slab Details at Supports (Keenan, 1969, R620)

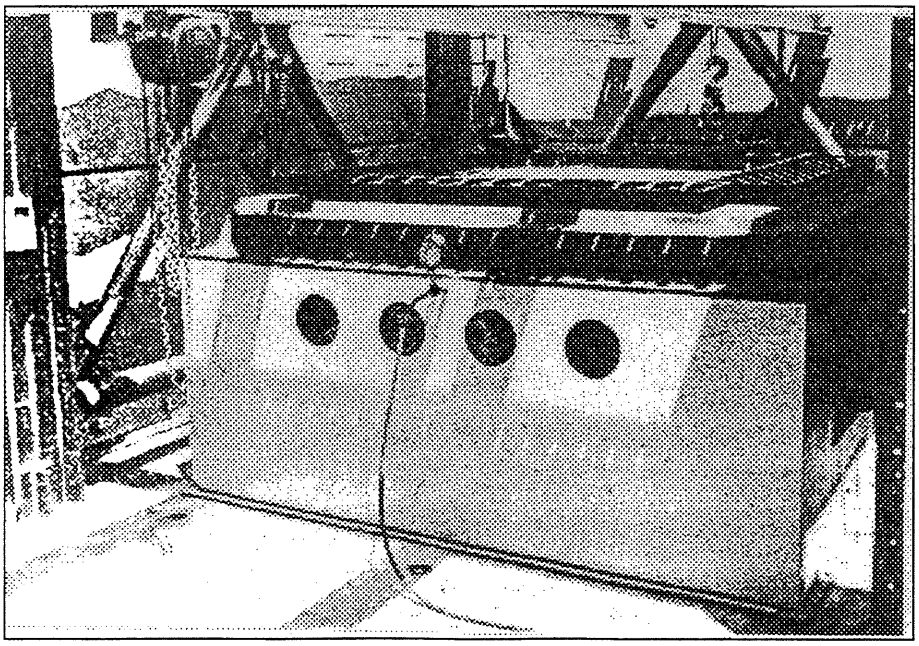

Figure A.4. NCEL Slab Loader (Keenan, 1969, R621)

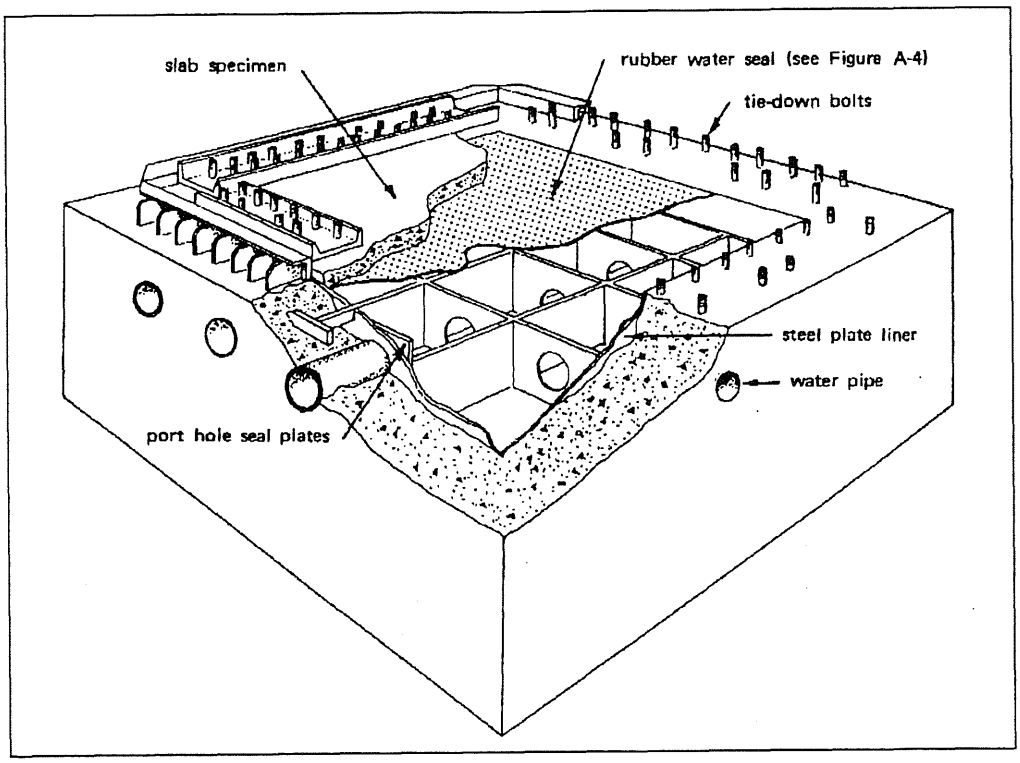

Figure A.5. NCEL Slab Loader Details (Keenan, 1969, R621)

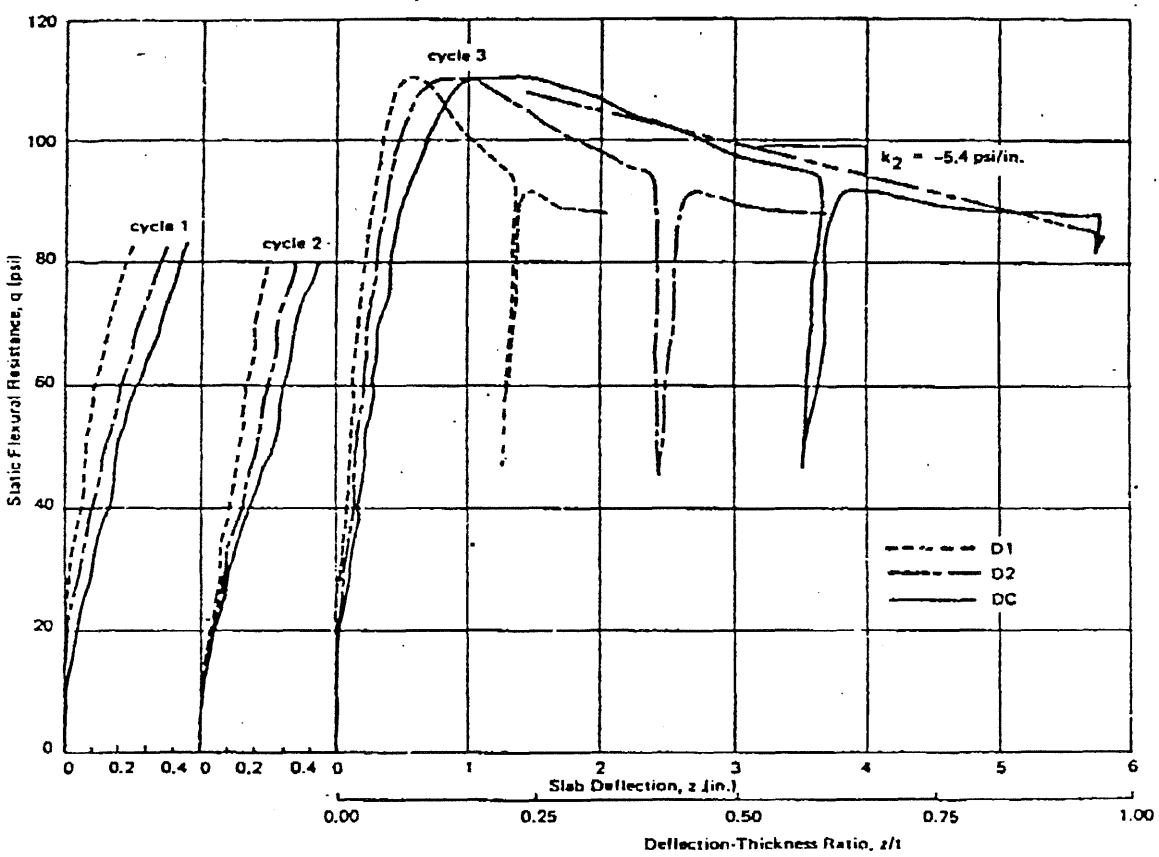

Figure A.6. Static Load-Deflection Relationship for Slab 1 (Keenan, 1969, R620)

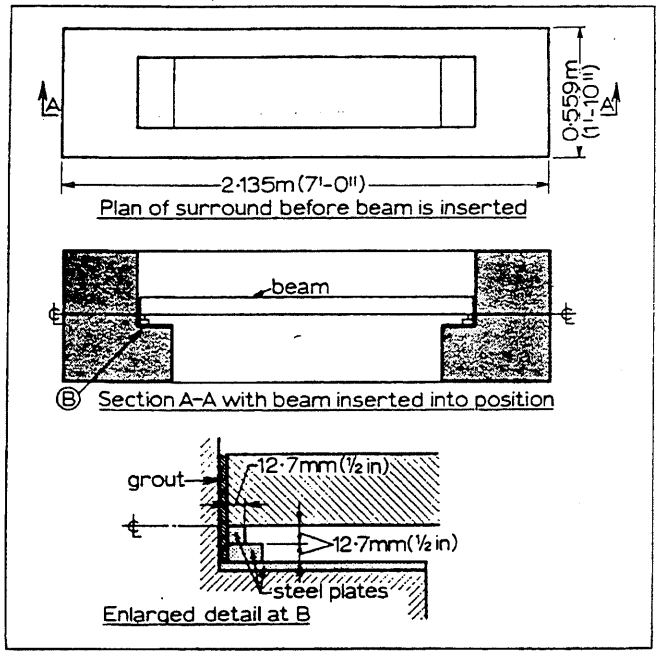

Figure A.7. Test Beam and Surround Details (Roberts, 1969)

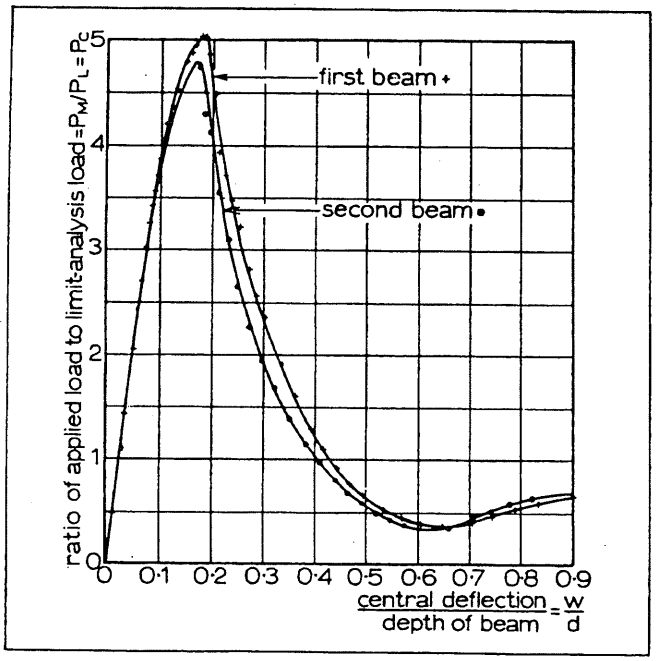

Figure A.8. Experimental Load-Deflection Curves for Beams RB23 (Roberts, 1969)

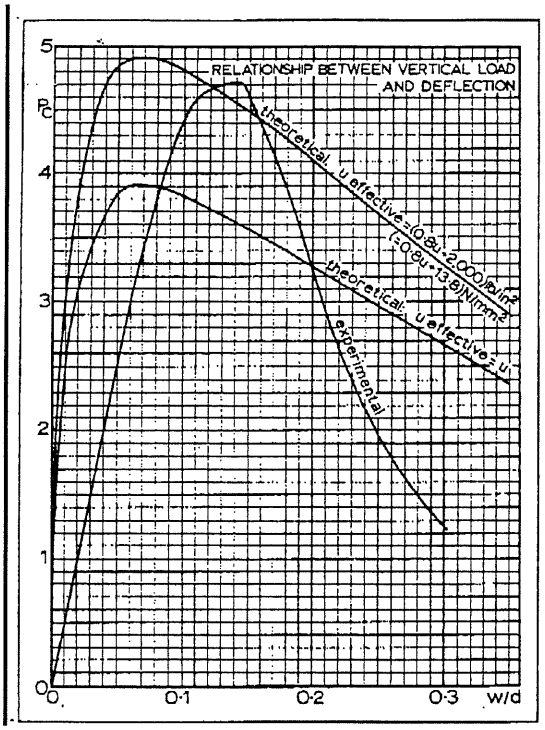

Figure A.9. Theoretical and Experimental Relationship Between P_C and w:d - Beam RB18 (Roberts, 1969)

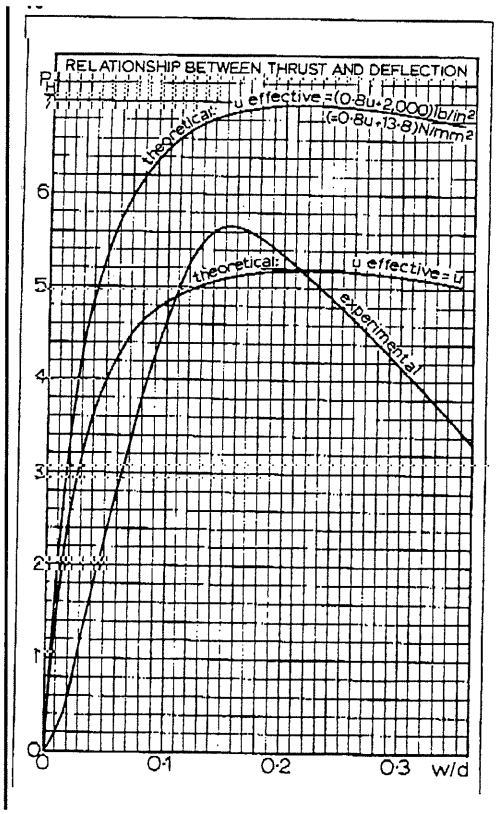

Figure A.10. Theoretical and Experimental Relationship Between P_H and w:d - Beam RB18 (Roberts, 1969)

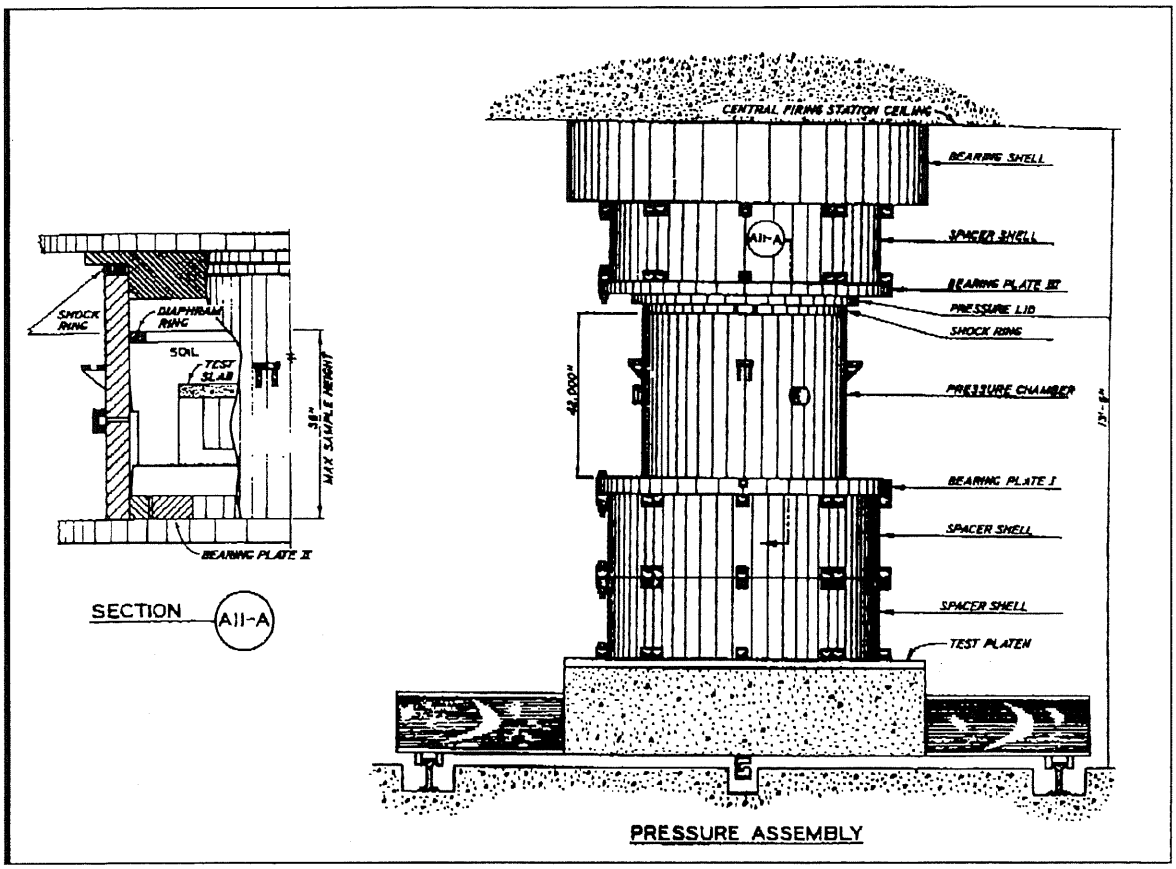

Figure A.11. Small Blast Load Generator (Kiger et. al., 1984)

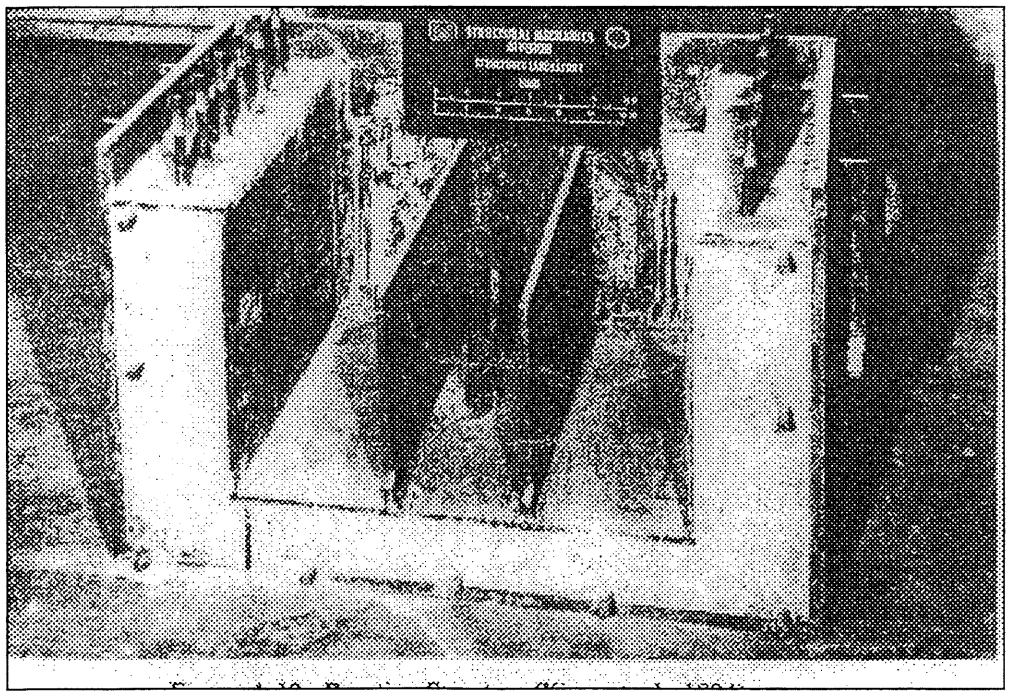

Figure A.12. Reaction Structure (Kiger et. al., 1984)

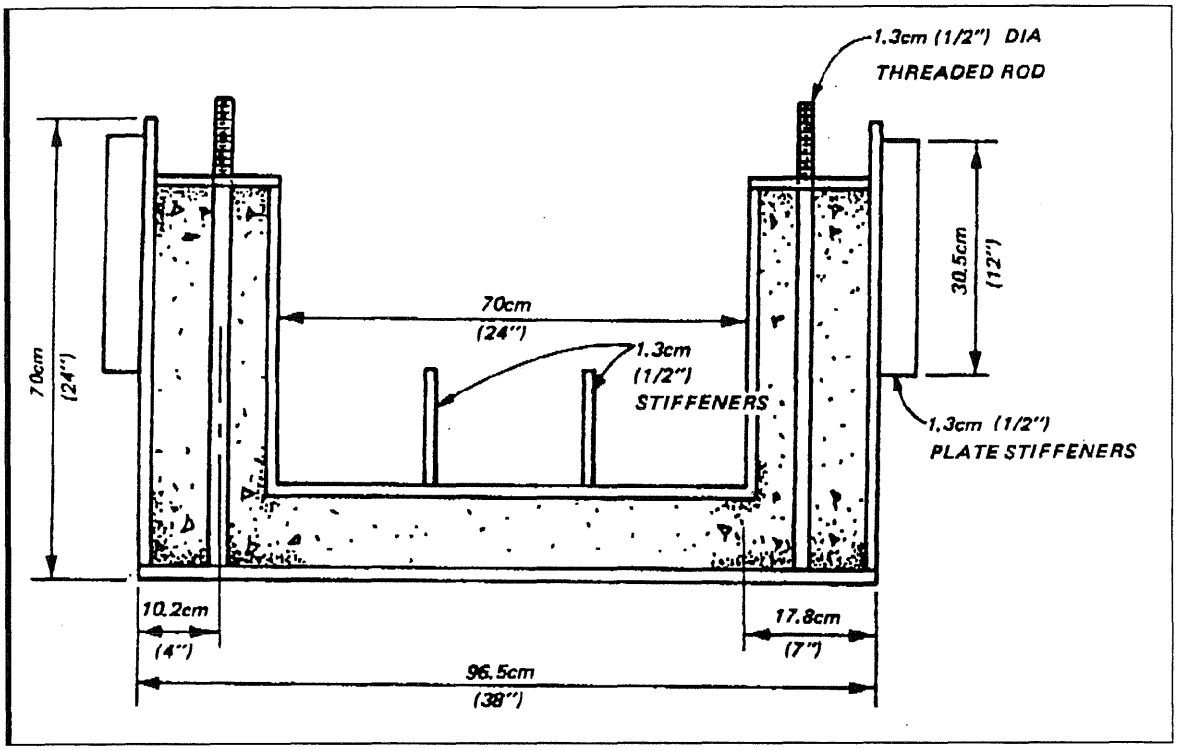

Figure A.13. Reaction Structure (Woodson, 1985)

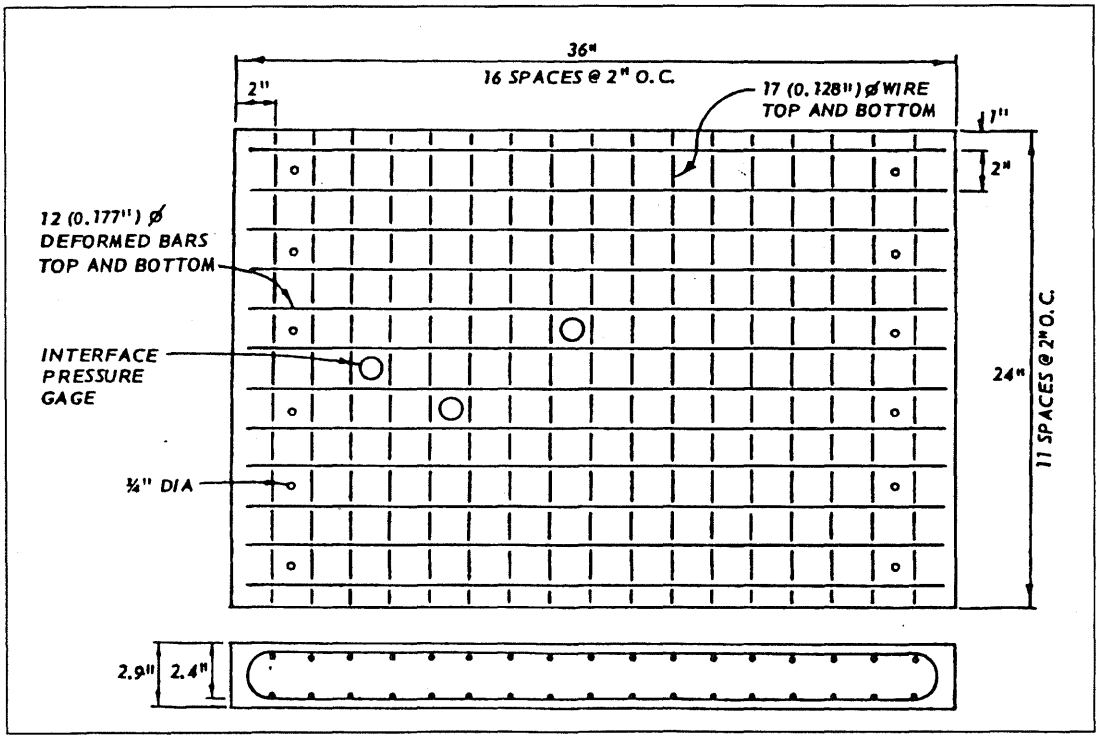

Figure A.14. Reinforcement Pattern (Kiger et. al., 1984)

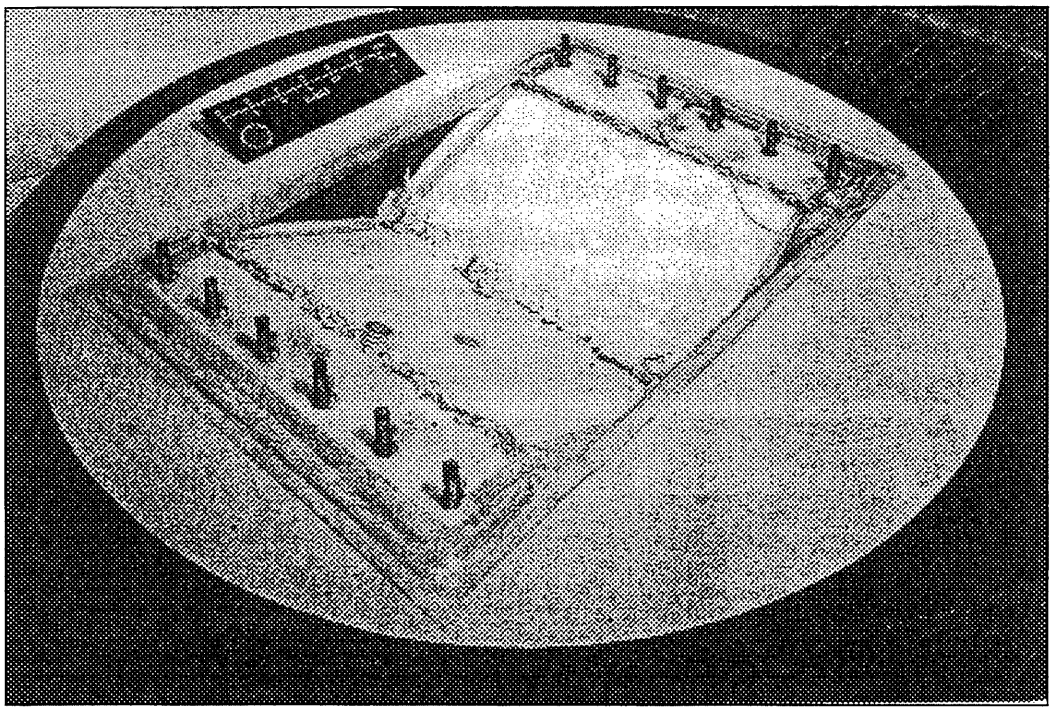

Figure A.15. Failure of the Surface-Flush Static Slab Test (Kiger et. al., 1984)

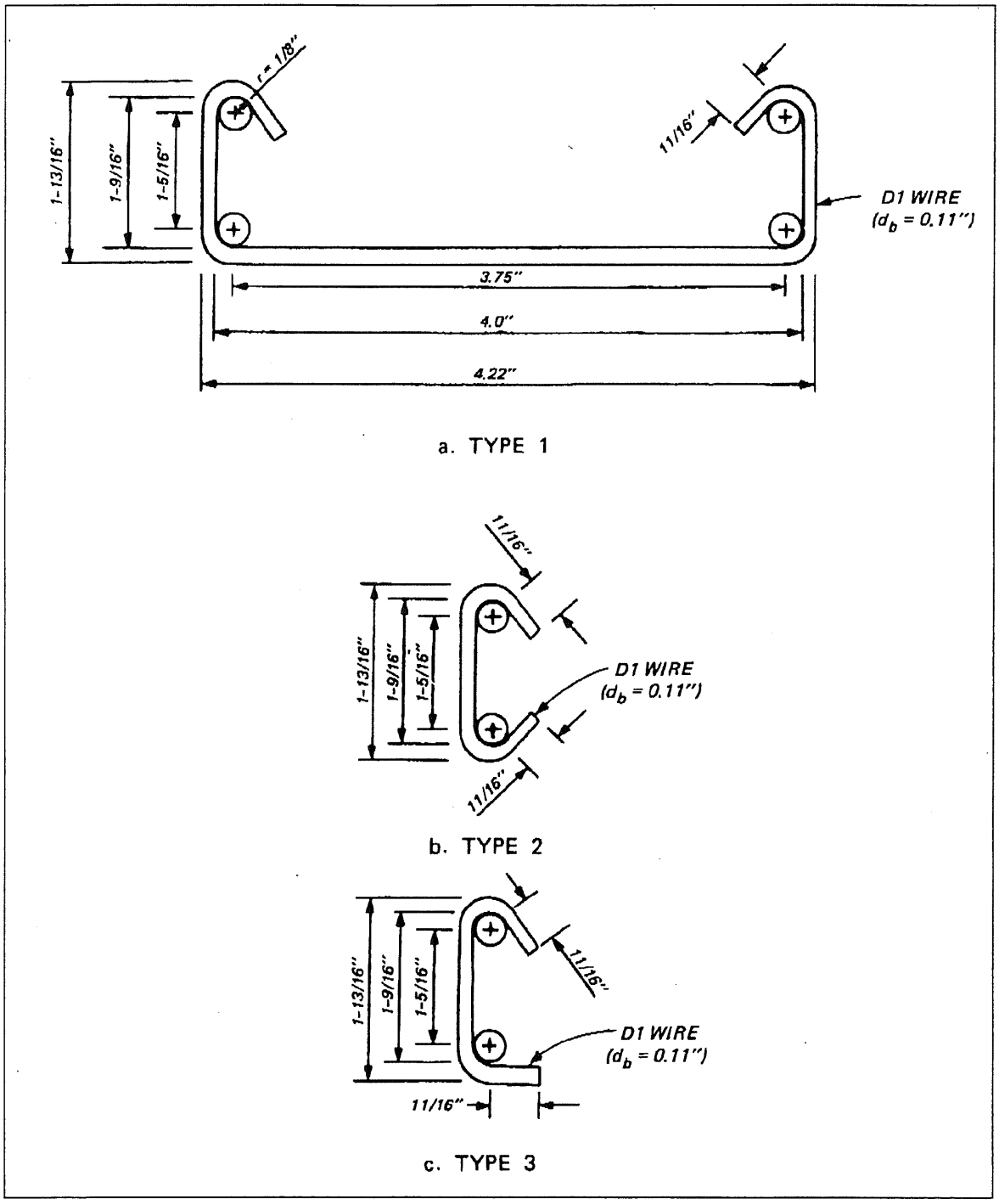

Figure A.16. Stirrup Details (Woodson, 1985)

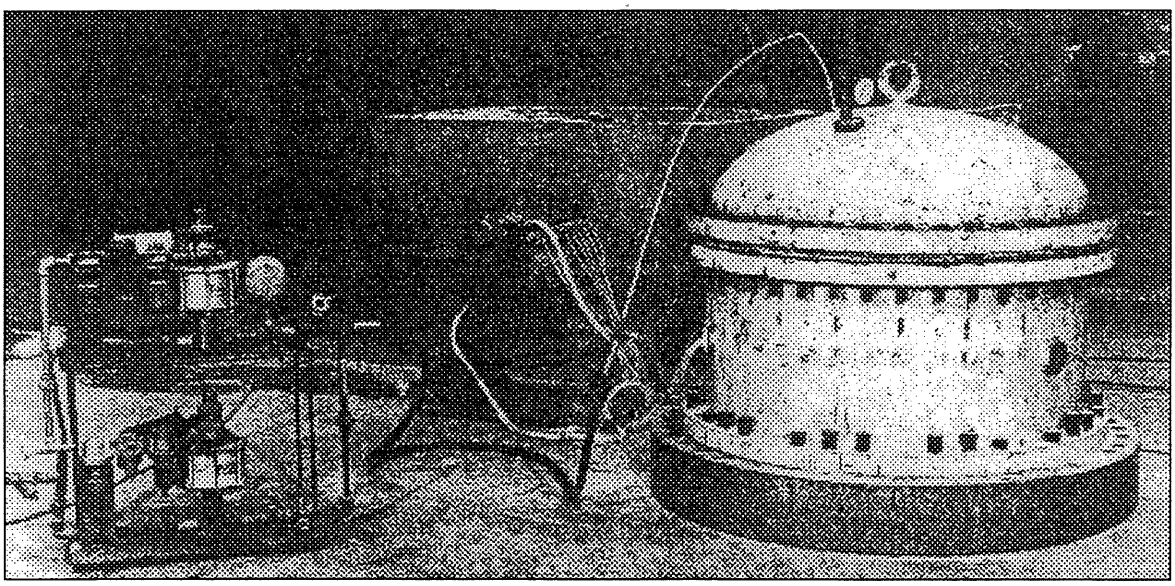

Figure A.17. Blast Load Generator (Woodson, 1985)

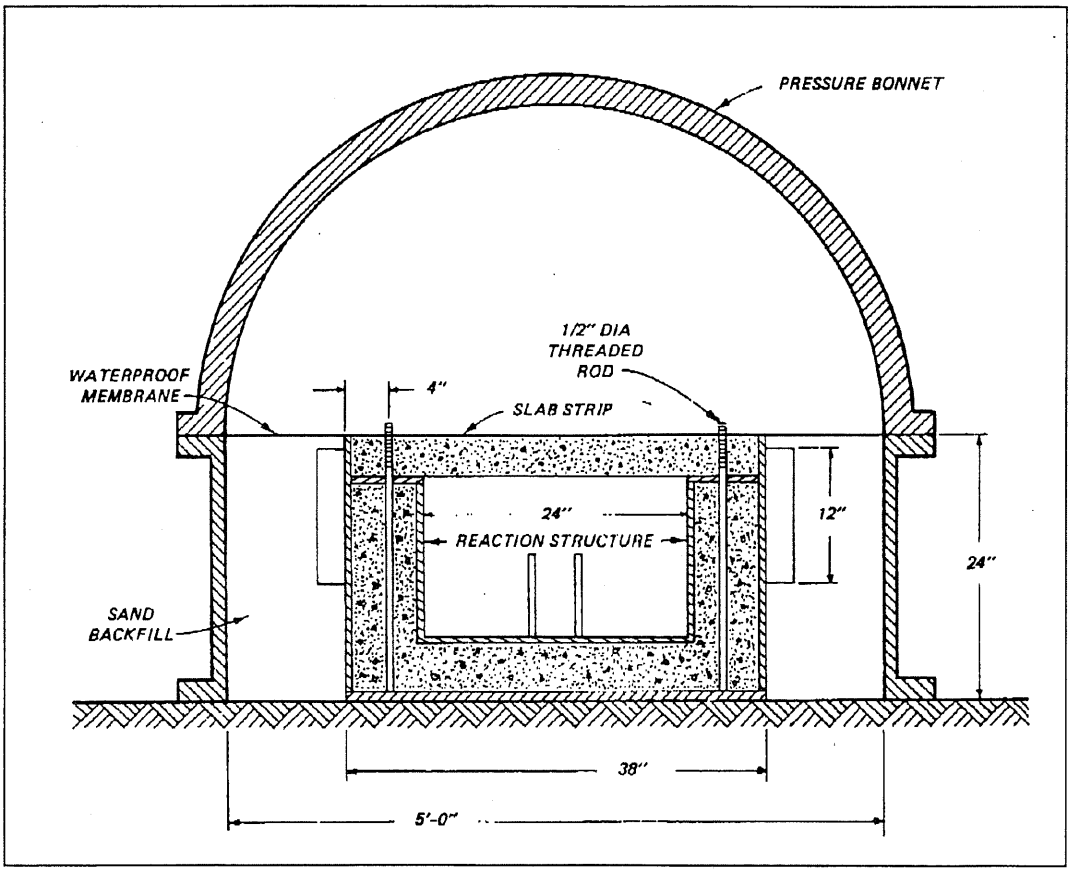

Figure A.18. Small Blast Load Generator Facility and Rigid Reaction Structure (Guice et. al., 1986)

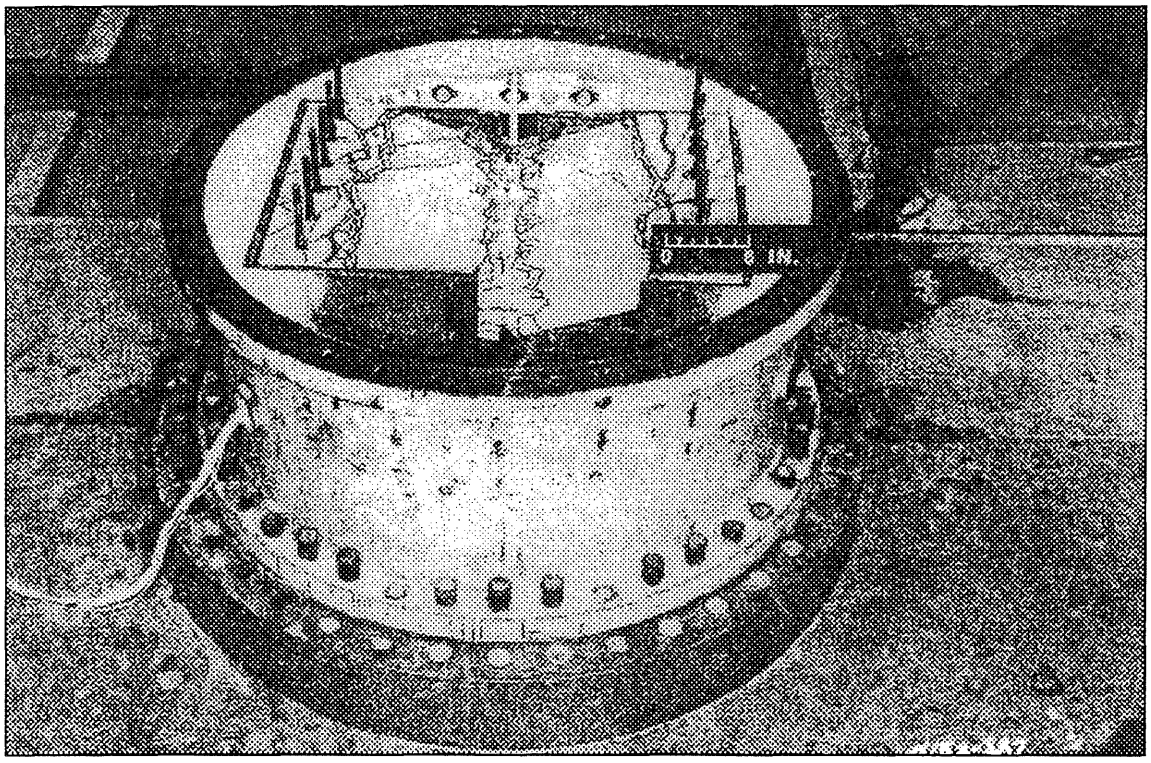

Figure A.19. Slab 1 Posttest (Woodson, 1985)

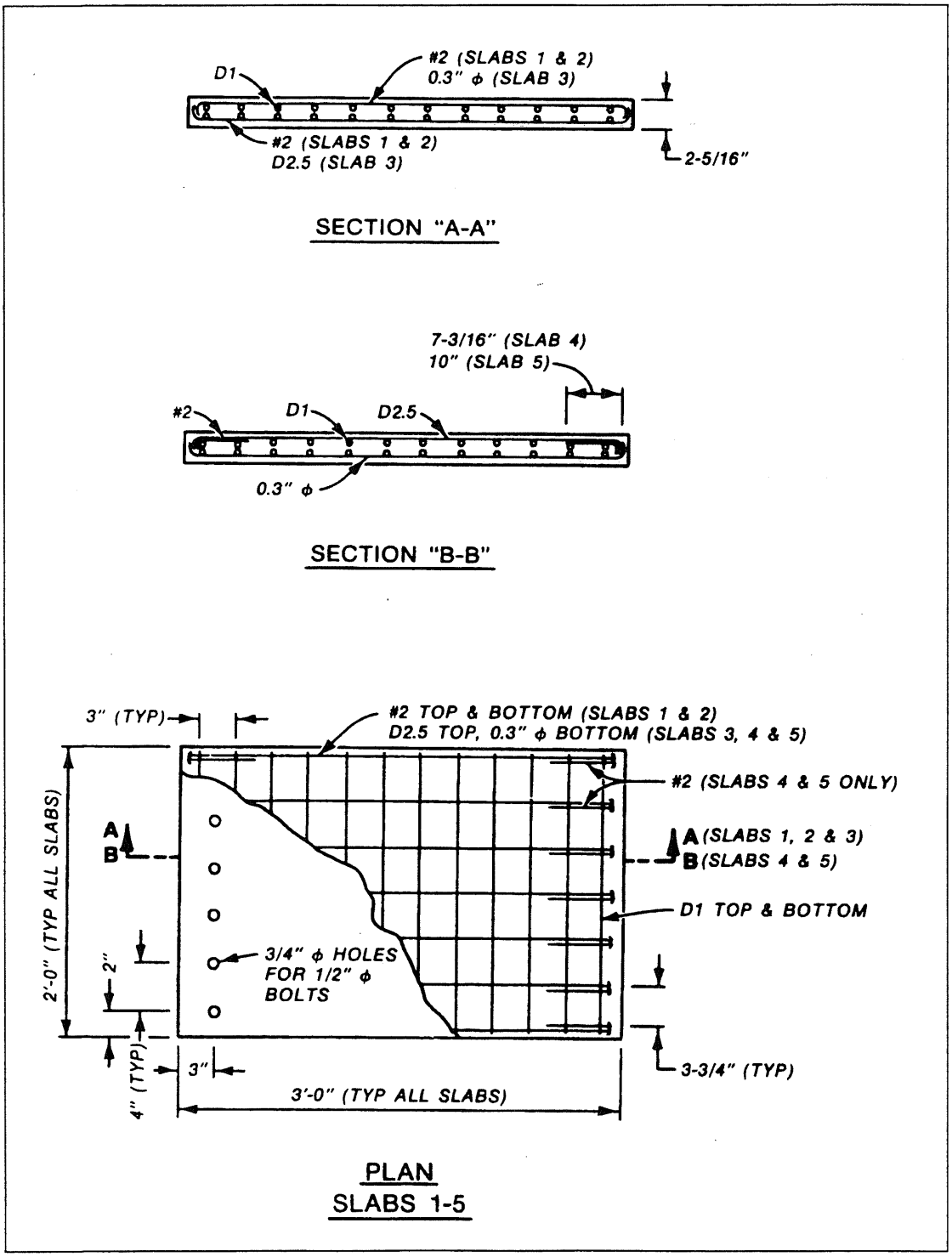

Figure A.20. Slabs 1-5 Plan Details (Woodson et. al., 1985)

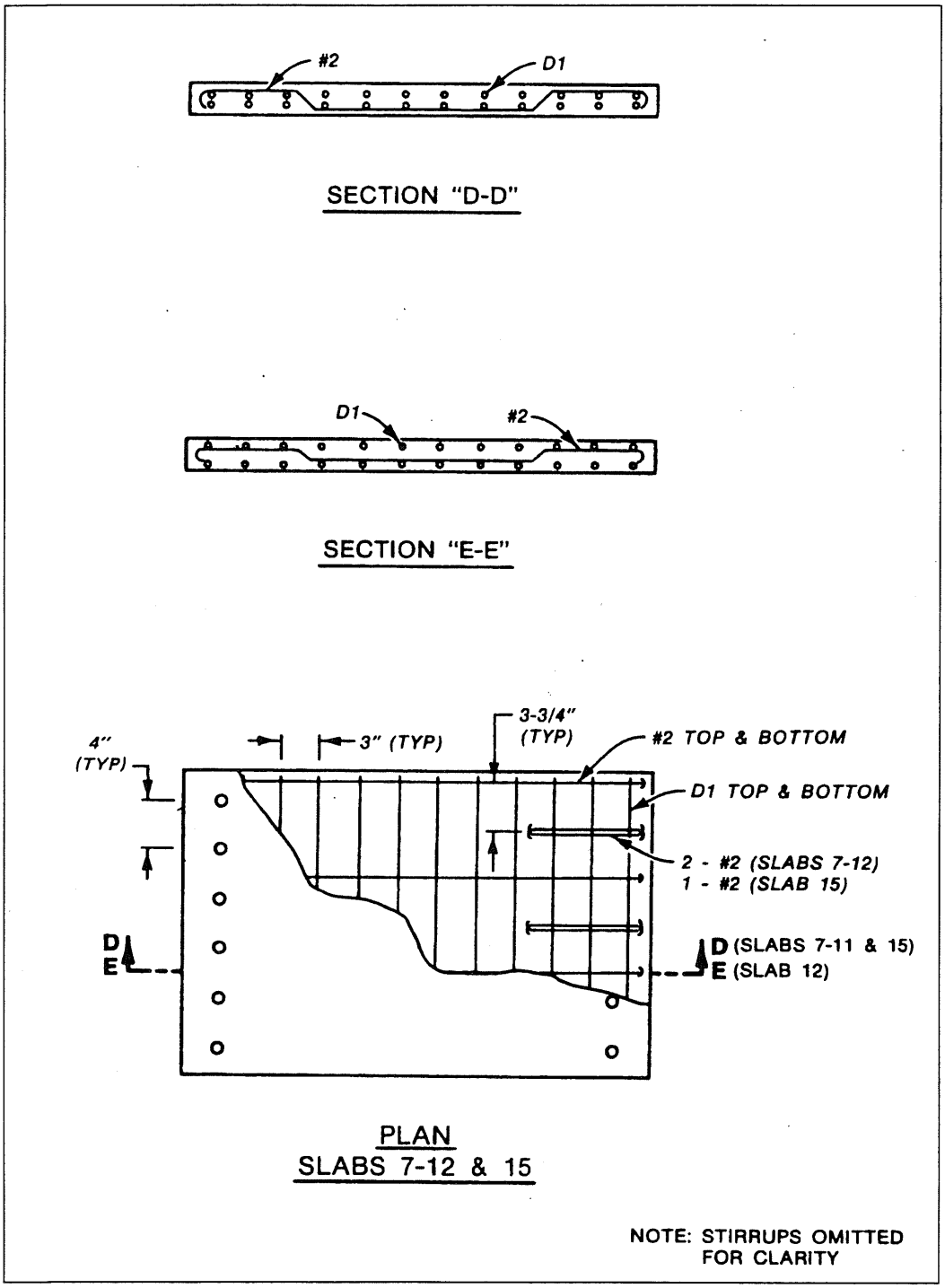

Figure A.21. Slabs 7-12 & 15 Plan Details (Woodson et. al., 1985)

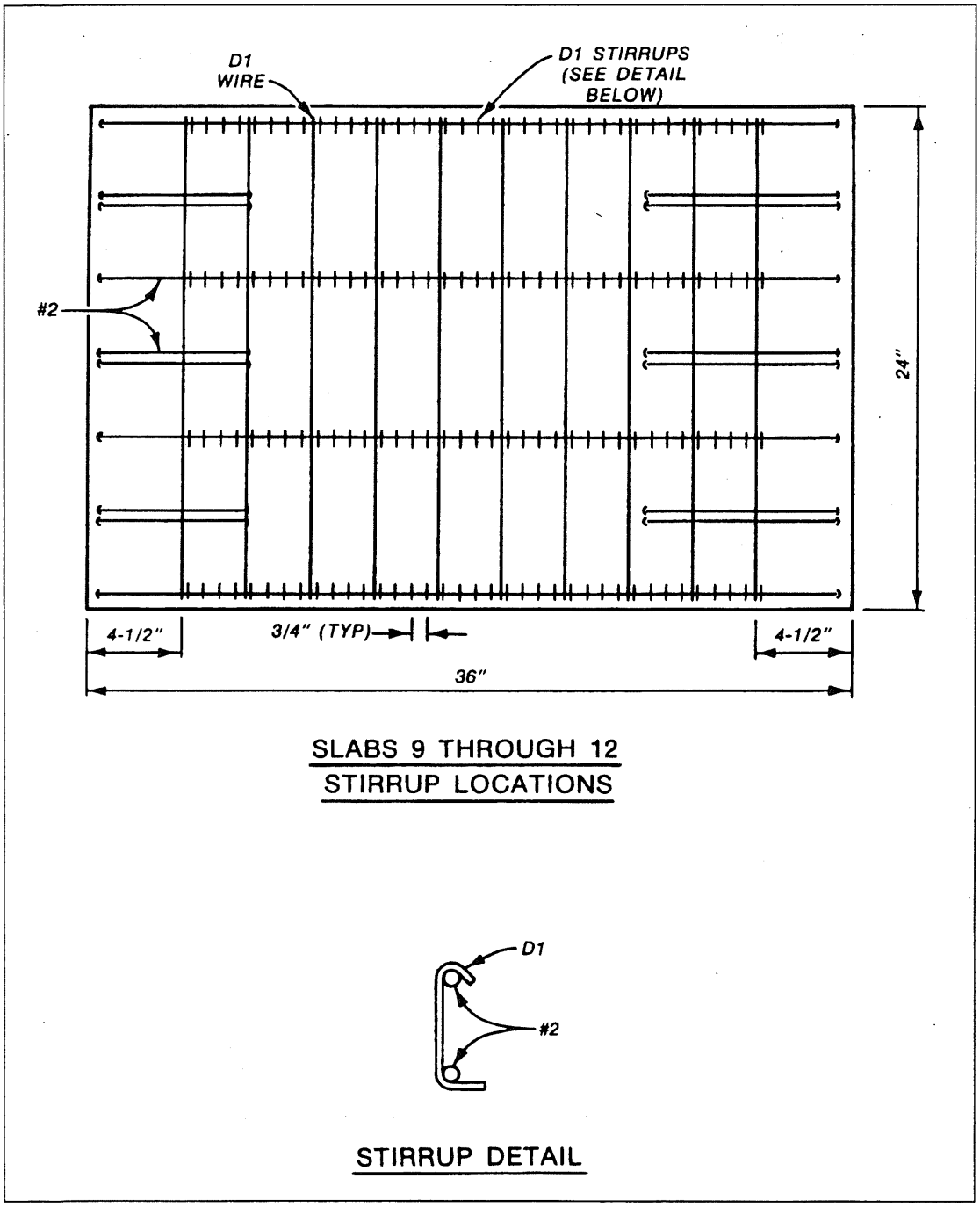

Figure A.22. Stirrup Details, Slabs 9-12 (Woodson et. al., 1985)

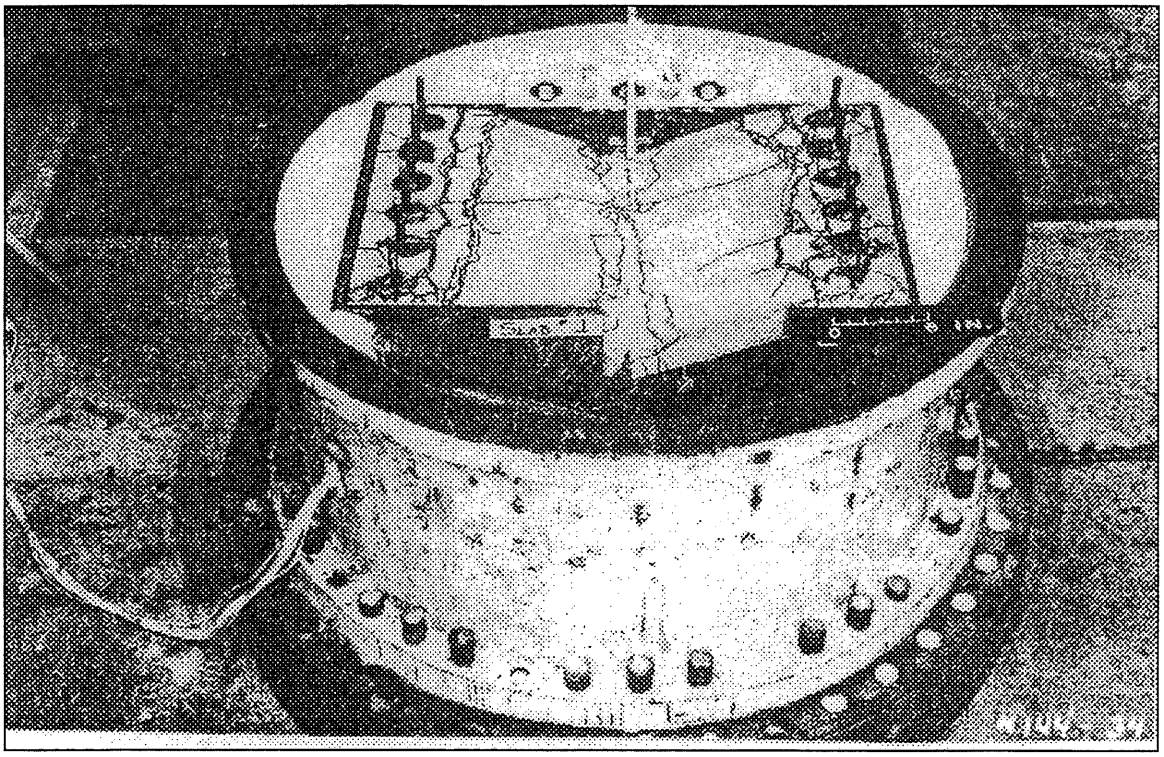

Figure A.23. Slab 1, Posttest (Woodson et. al., 1985)

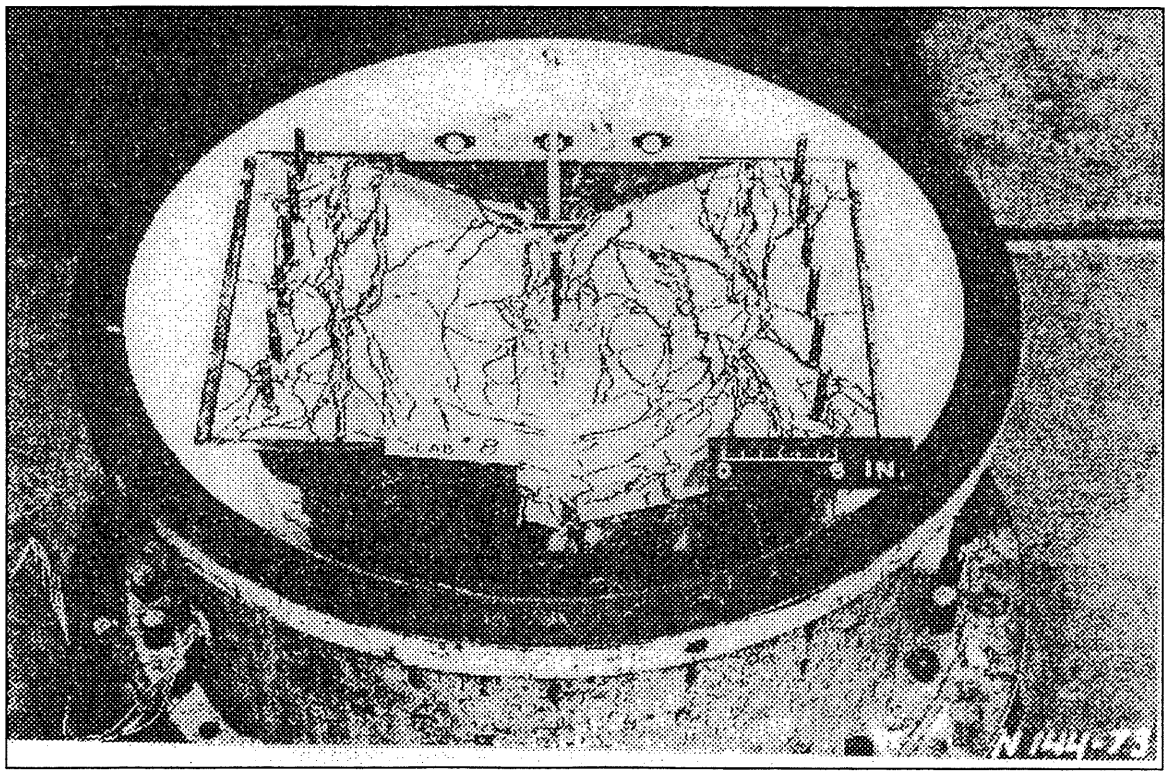

Figure A.24. Slab 8, Posttest (Woodson et. al., 1985)

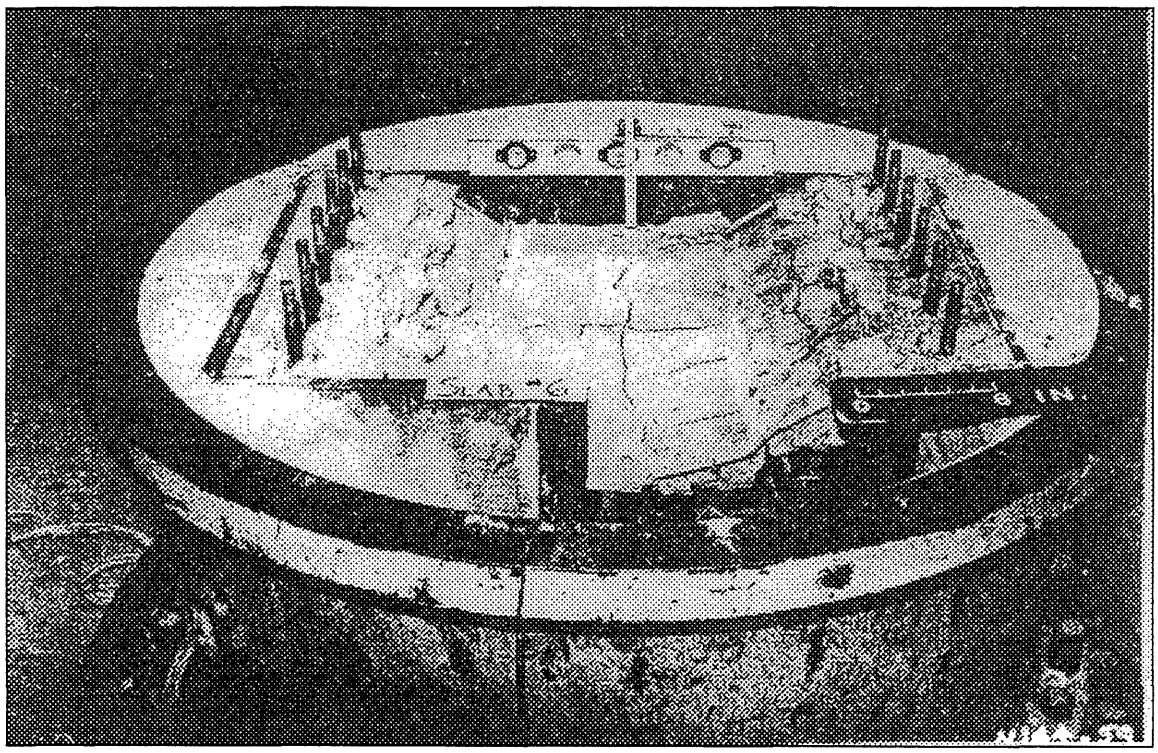

Figure A.25. Slab 6, Posttest (Woodson et. al., 1985)

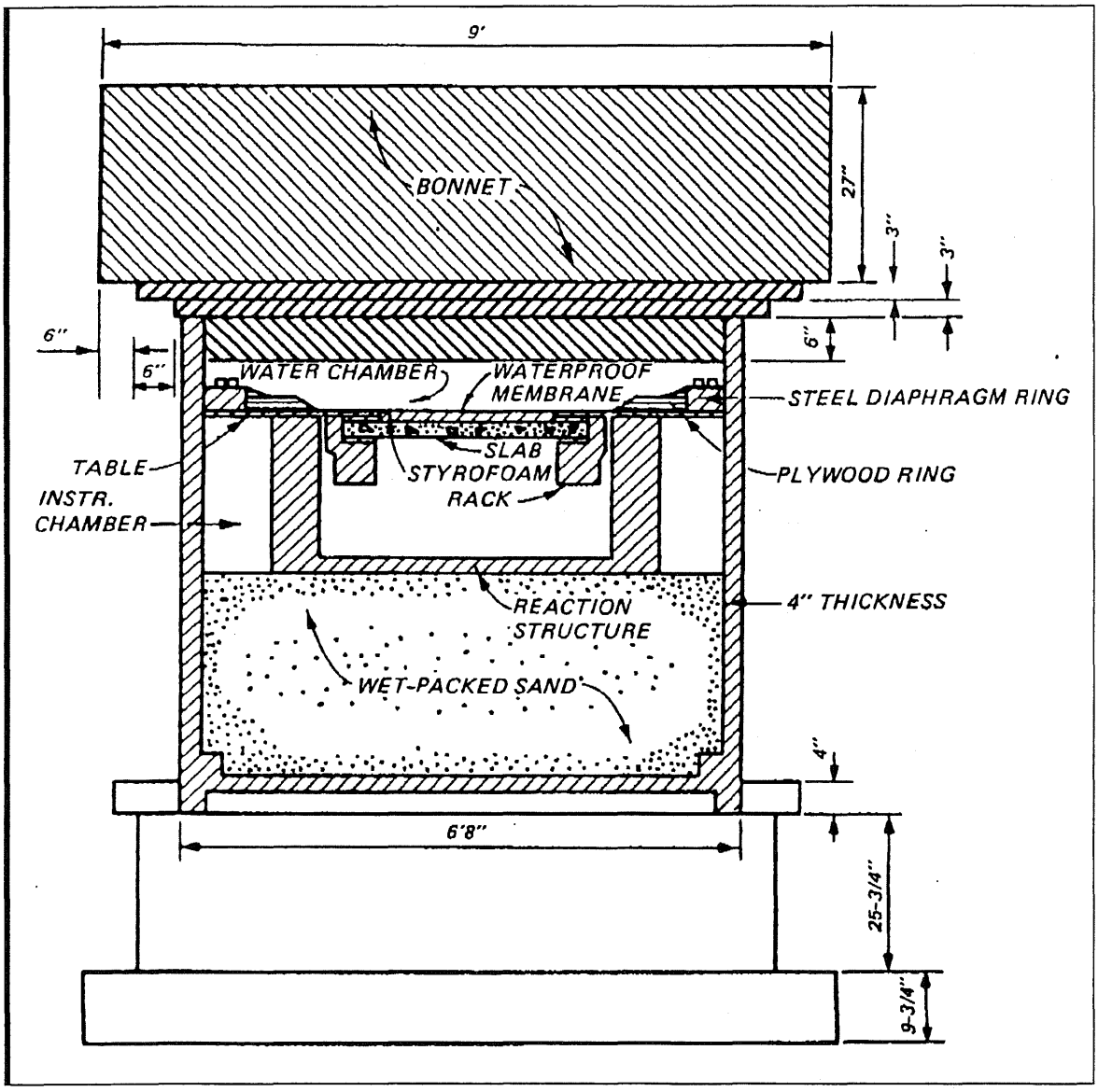

Figure A.26. Cross-Section of Reaction Structure in Test Configuration (Guice, 1986, SL-86-2)

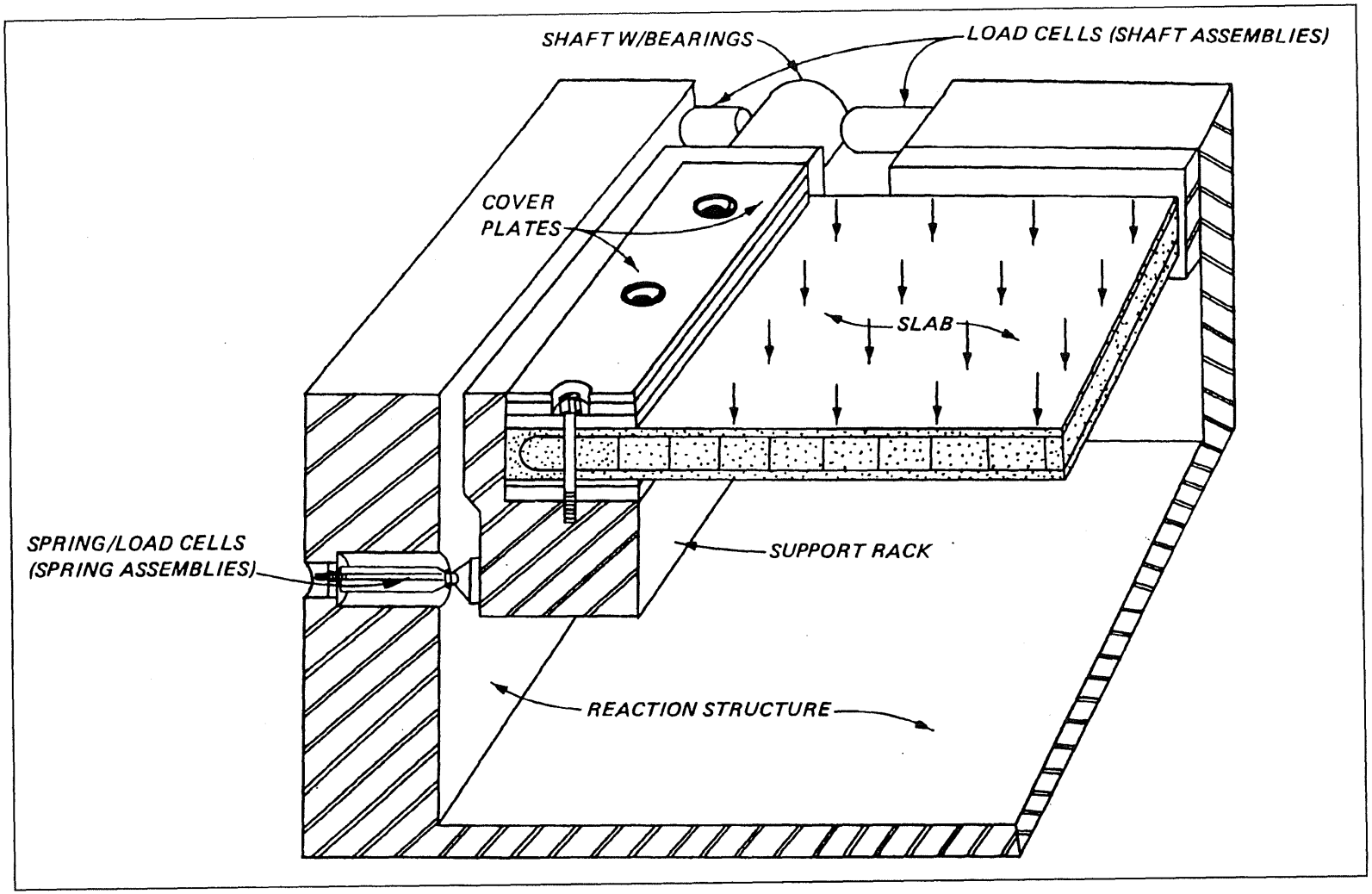

Figure A.27. Quarter-Section View of Reaction Structure with Slab in Place
(Guice, 1986, SL-86-2)

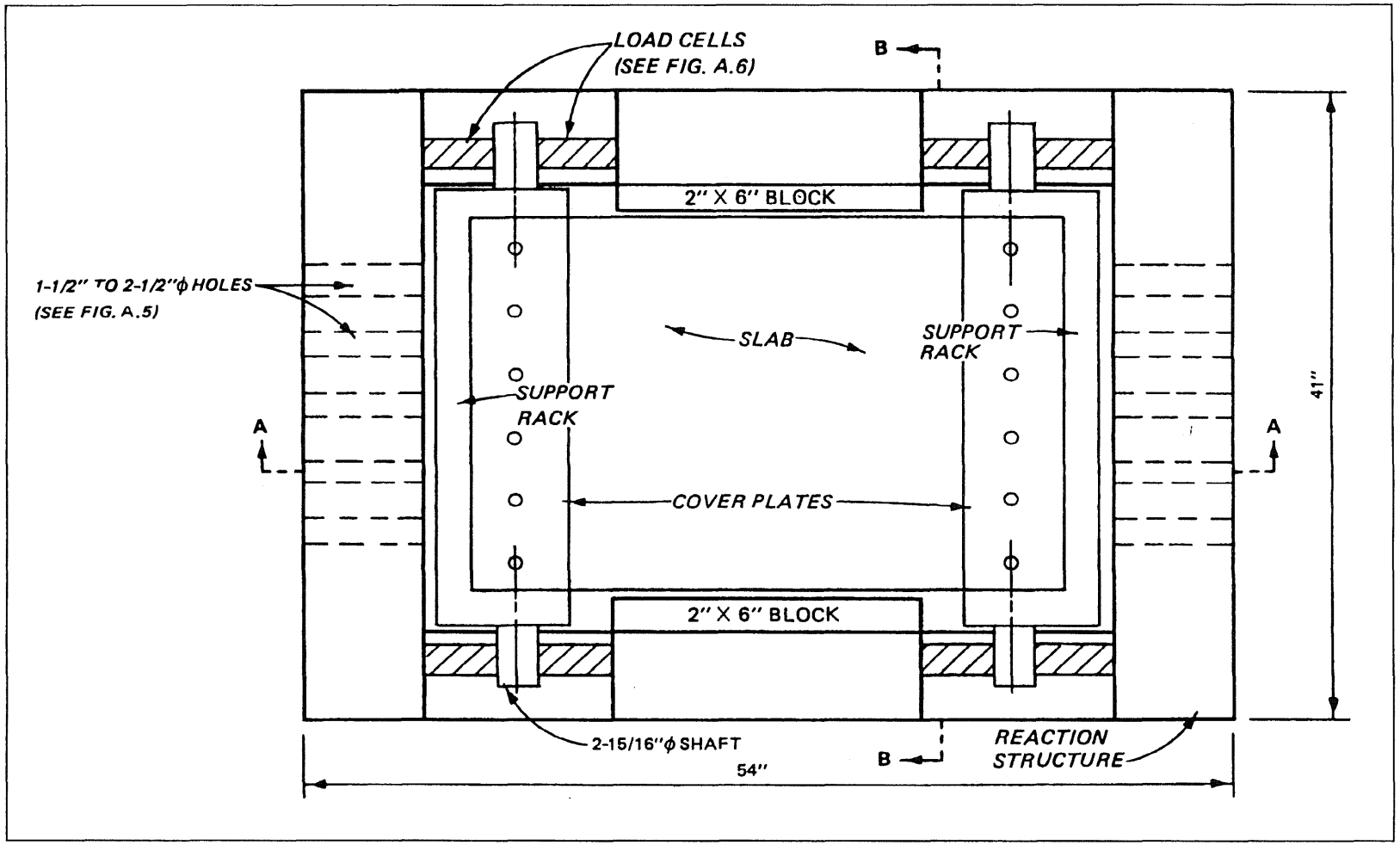

Figure A.28. Plan View of Reaction Structure and Assemblies (Guice, 1986, SL-86-2)

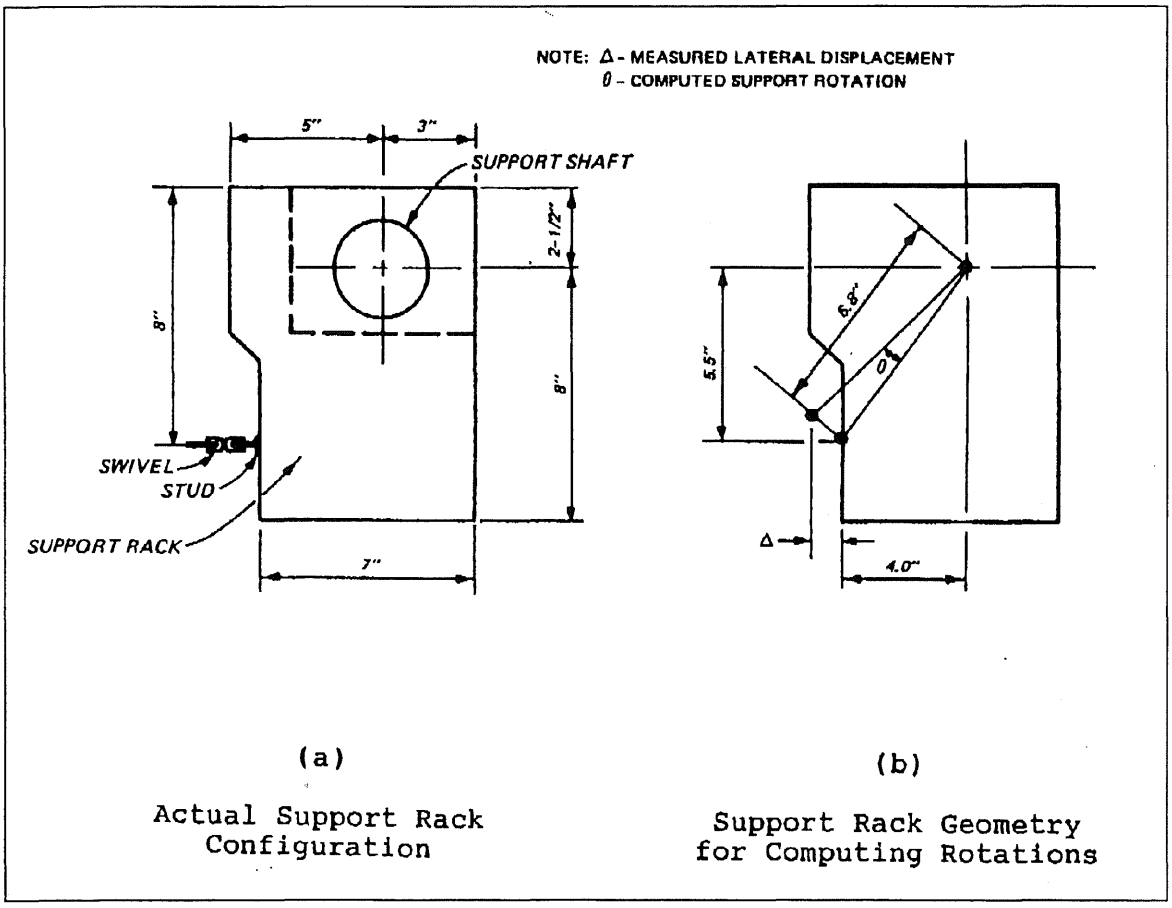

Figure A.29. Actual Support Rack Configuration and Geometry (Guice, 1986, SL-86-32)

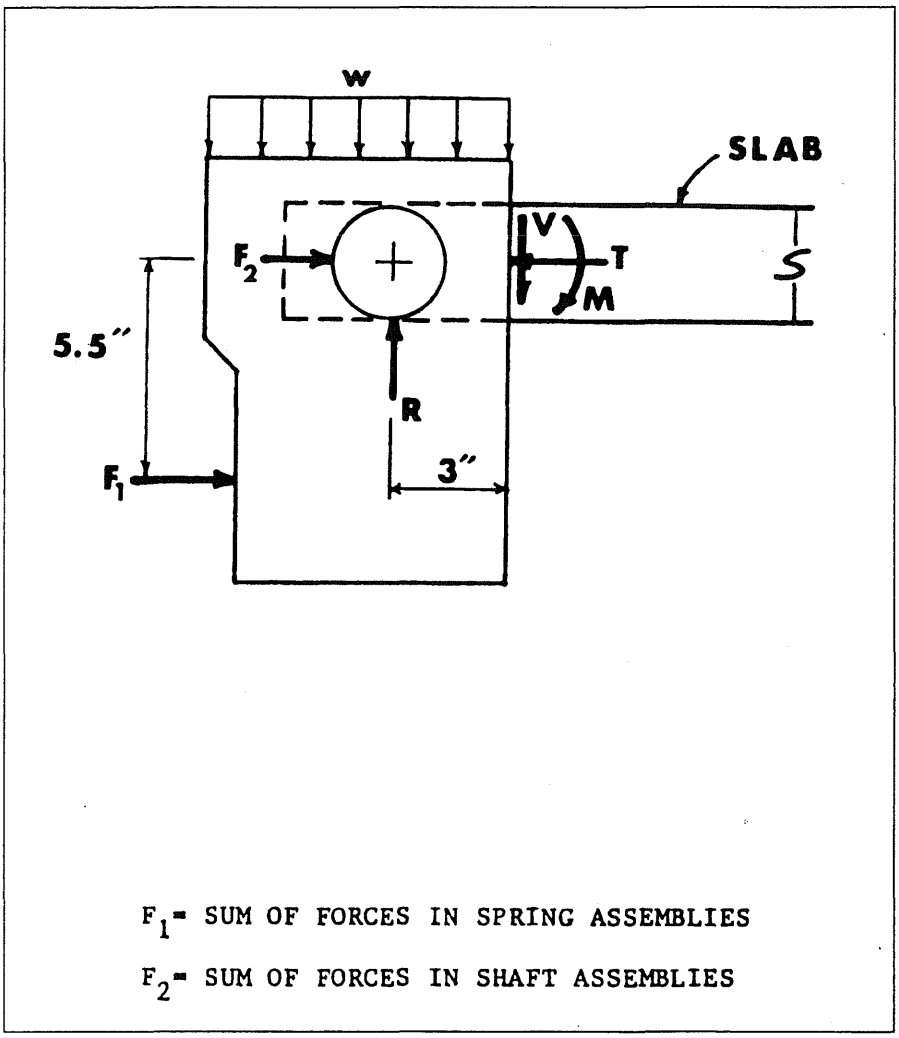

Figure A.30. Free-Body Diagram Used in Computing Support Thrusts and Moments (Guice, 1986, SL-86-32)

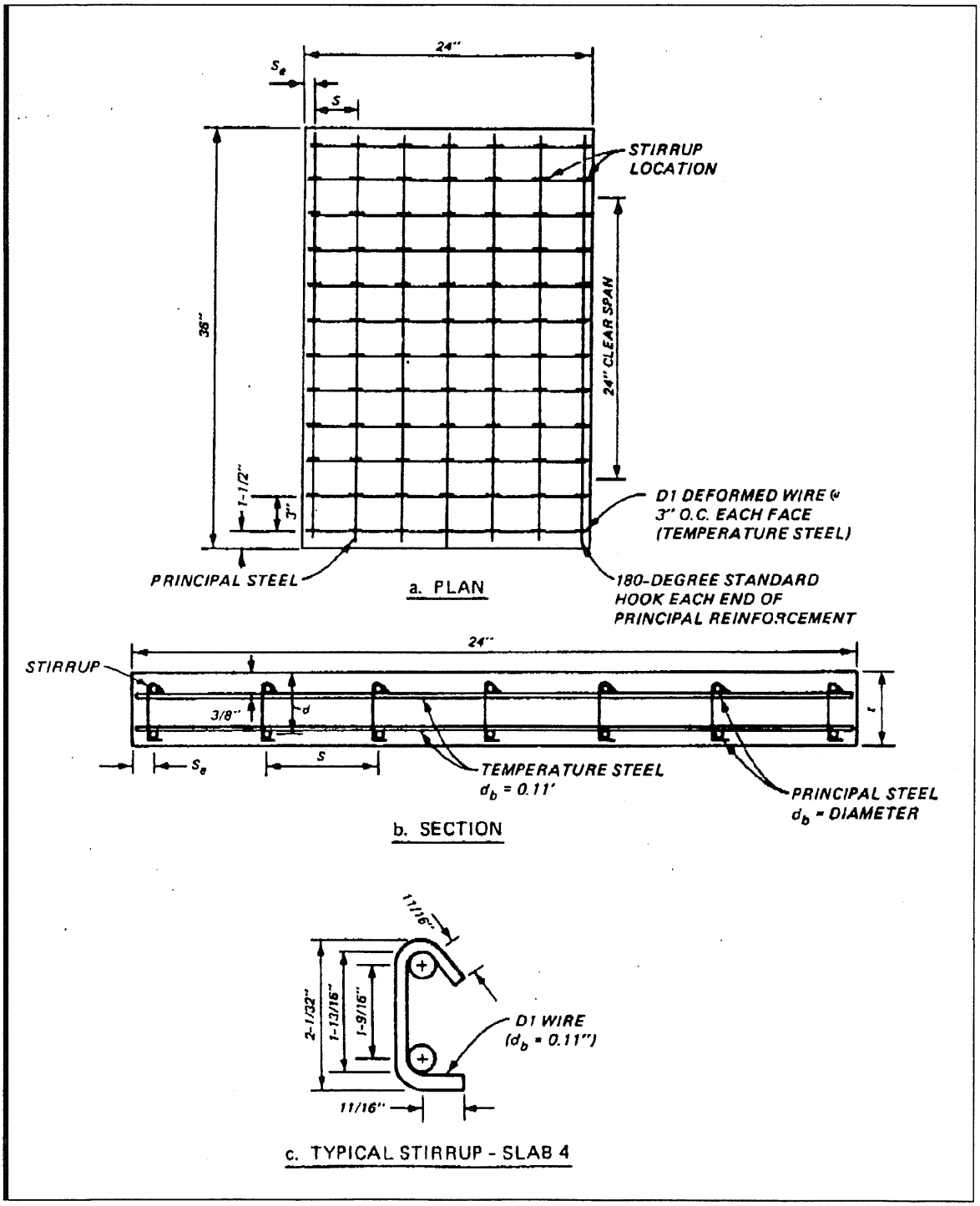

Figure A.31. Slab Construction Details (Guice, 1986, SL-86-32)

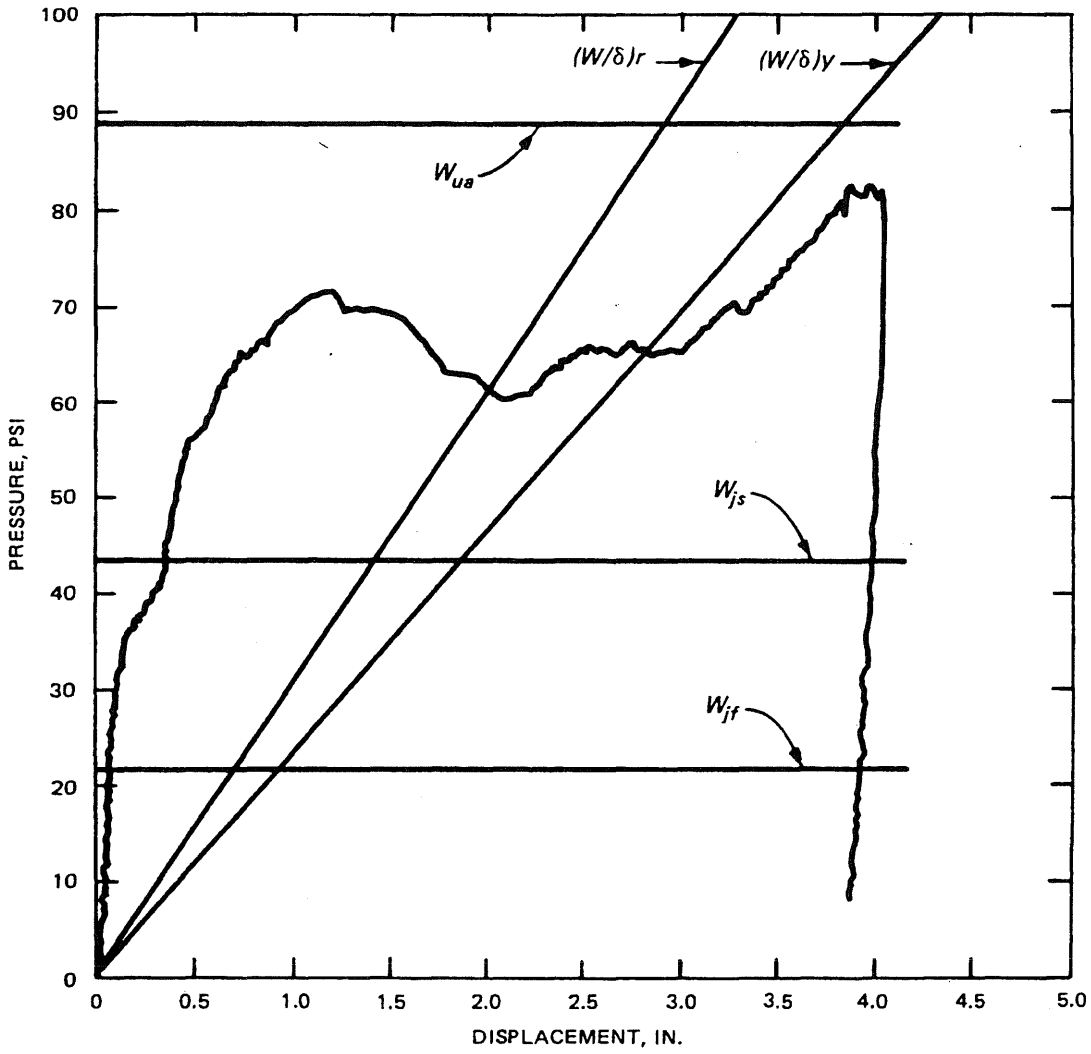

Figure A.32. Experimental and Analytical Comparisons for Slab 3 (Guice, 1986, SL-86-2)

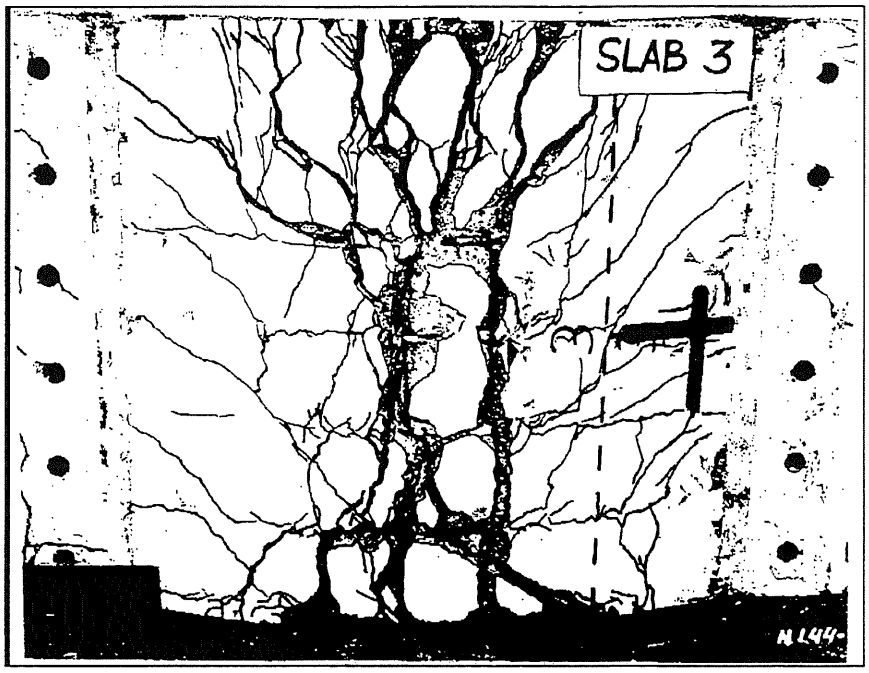

Figure A.33. Bottom View of Slab 3 (Guice, 1986, SL-86-2)

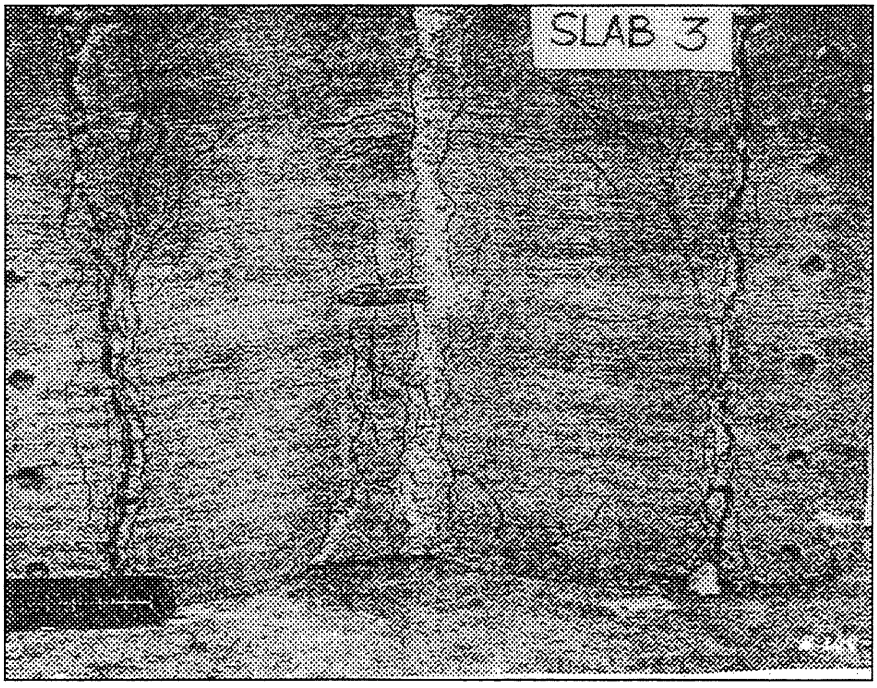

Figure A.34. Top View of Slab 3 (Guice, 1986, SL-86-2)

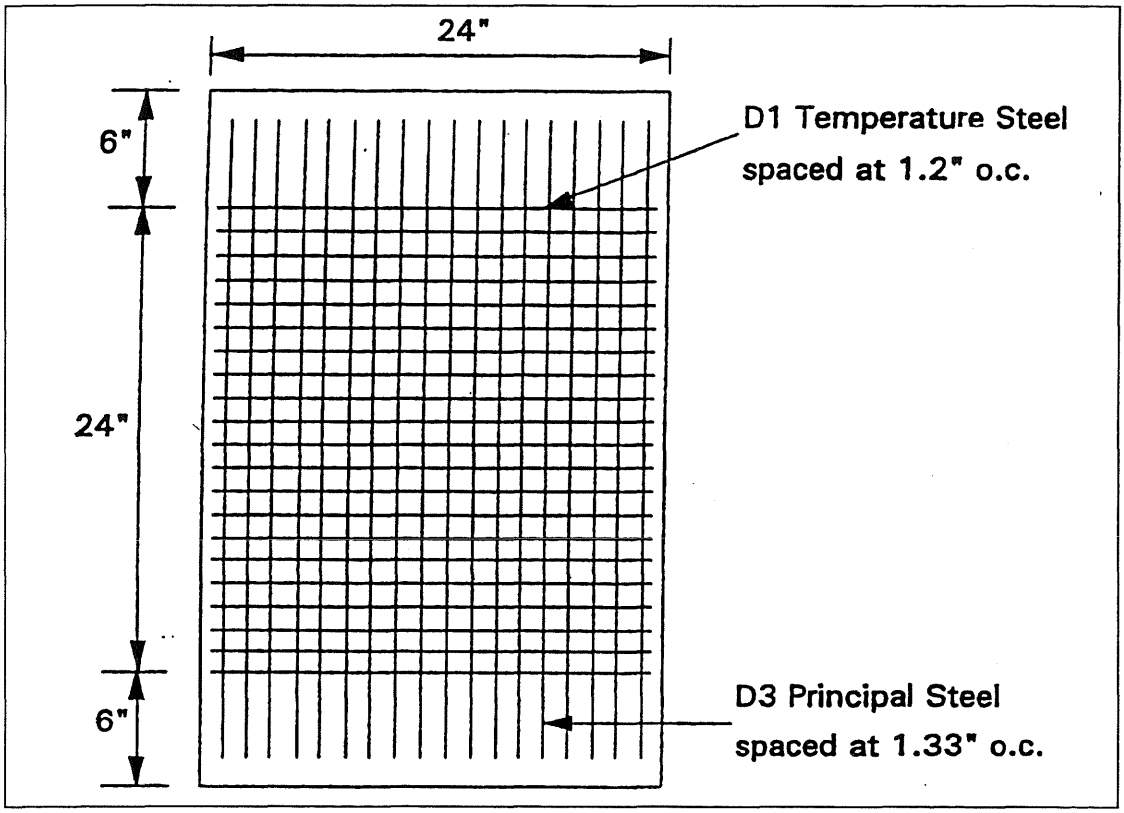

Figure A.35. Plan View of Slabs 3, 5, 9, 15, and 16 (Woodson, 1993)

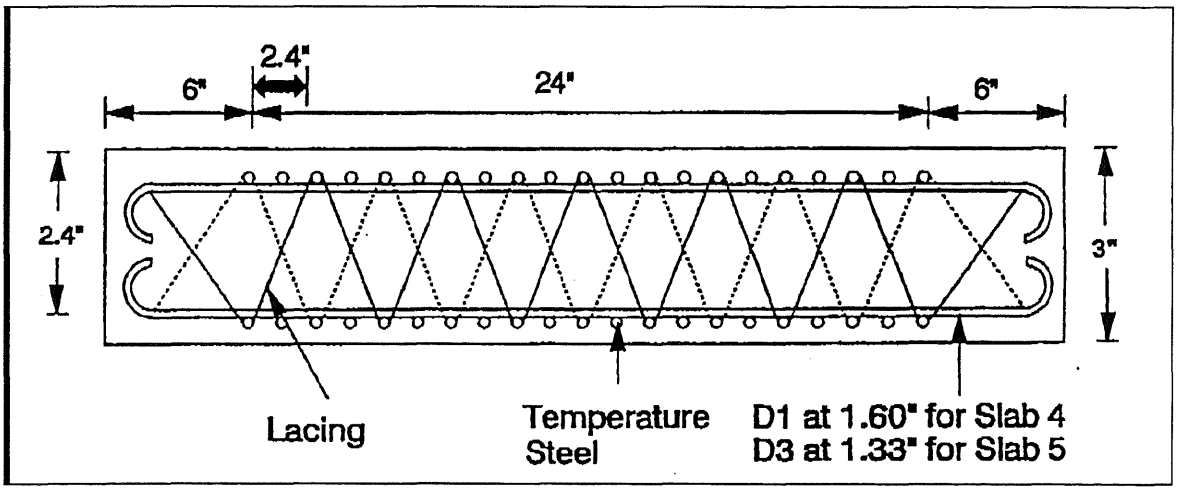

Figure A.36. Sectional View Through Length of Slabs 4 and 5 (Woodson, 1993)

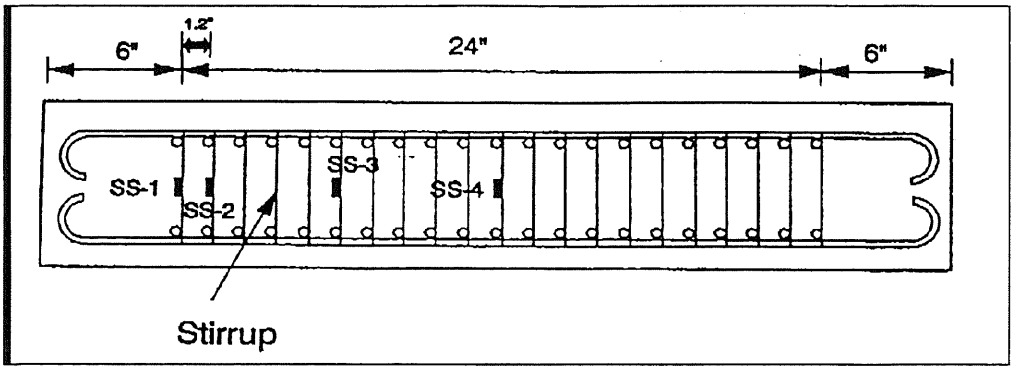

Figure A.37. Strain Gage Locations on Stirrups in Slabs 14 and 15 (Woodson, 1993)

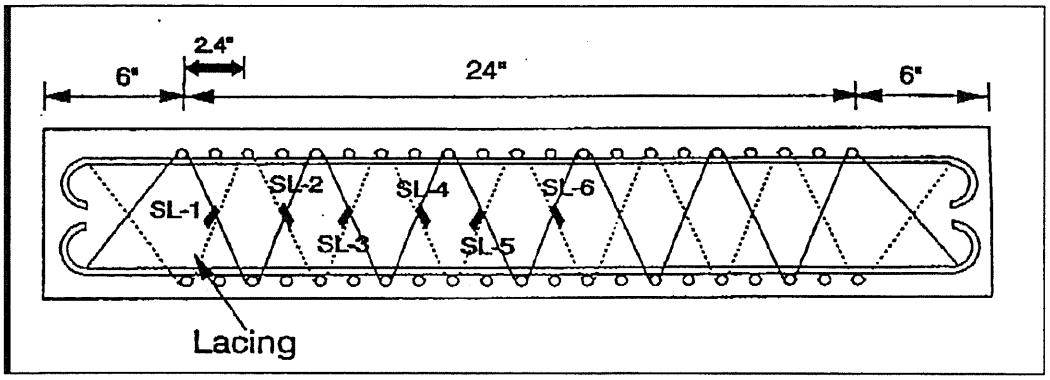

Figure A.38. Strain Gage Locations on Lacing in Slabs 4 and 5 (Woodson, 1993)

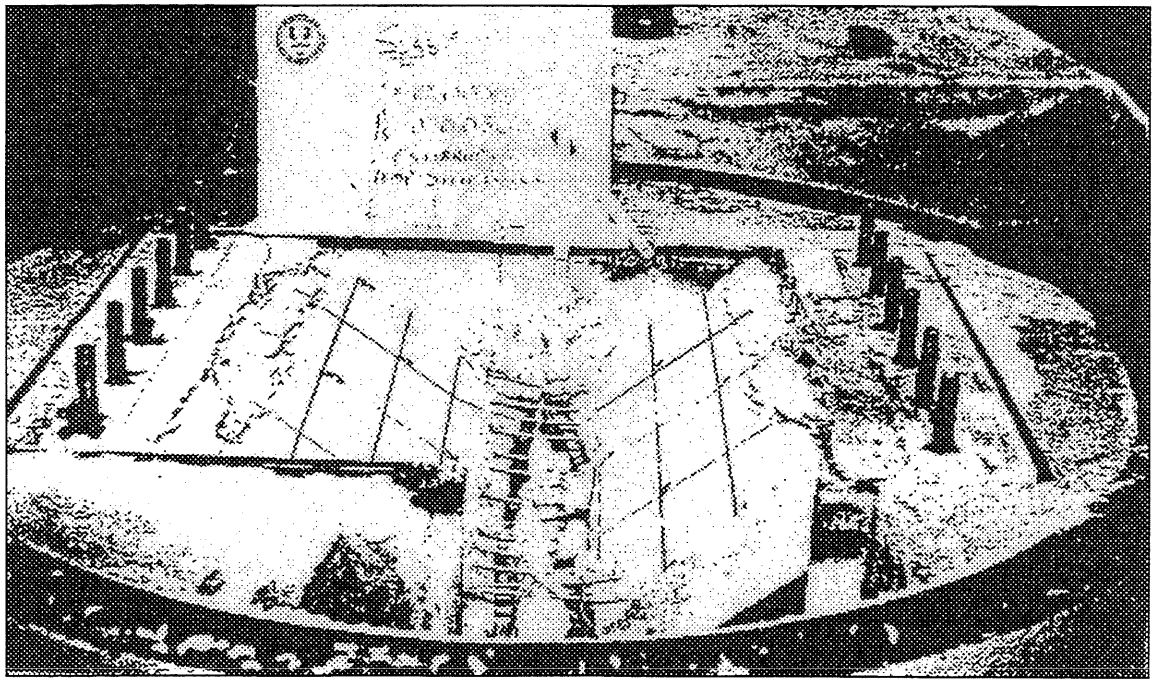

Figure A.39. Posttest View of Slab 13 (Woodson, 1993)

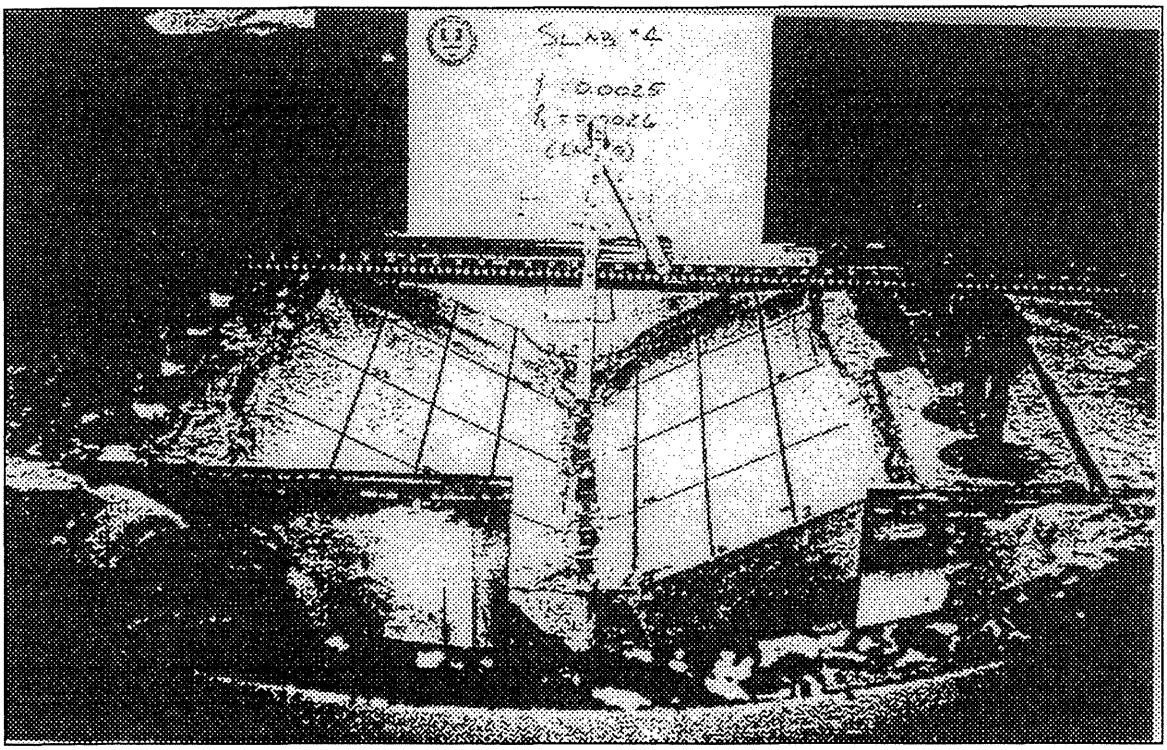

Figure A.40. Posttest View of Slab 4 (Woodson, 1993)

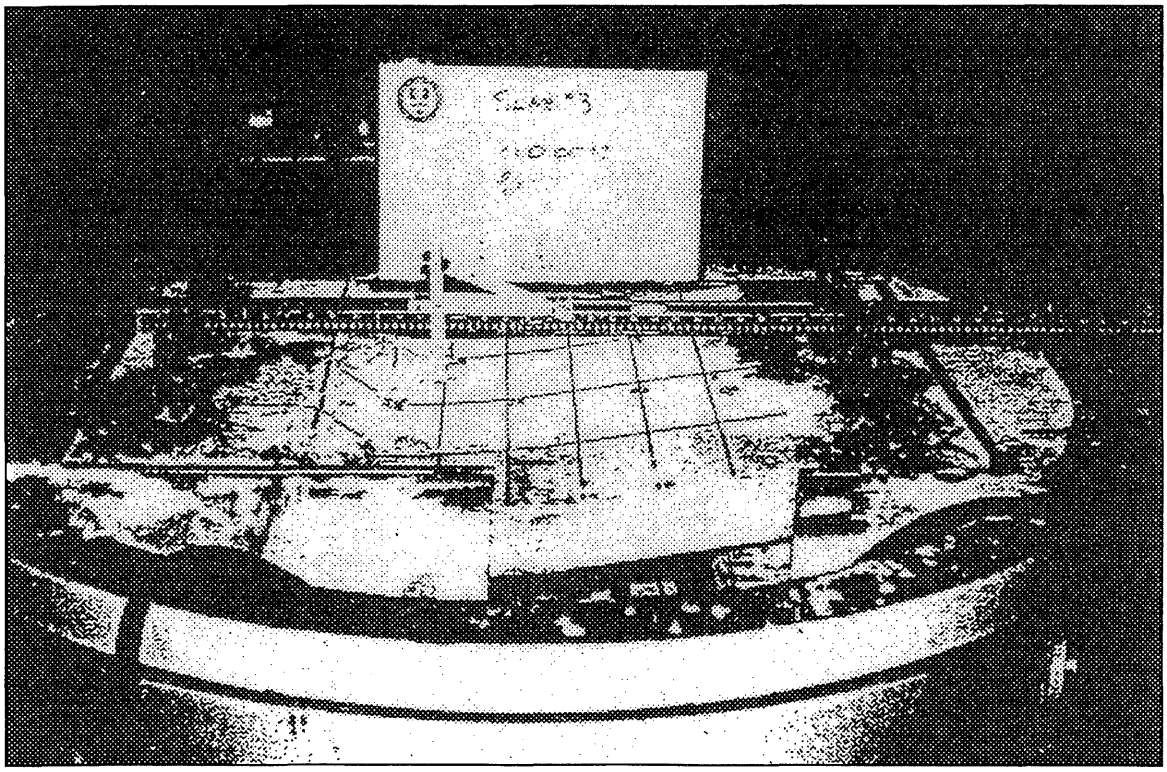

Figure A.41. Posttest View of Slab 3 (Woodson, 1993)

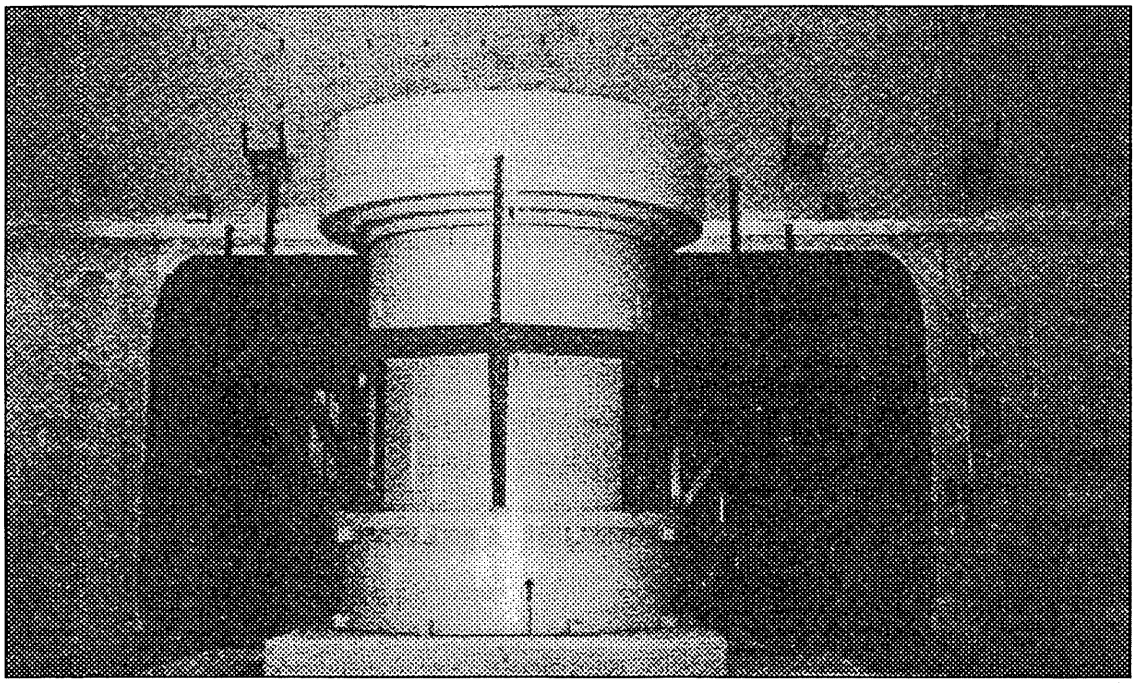

Figure A.42. Test Chamber Ready to Roll Inside Large Reaction Structure (Woodson, 1994)

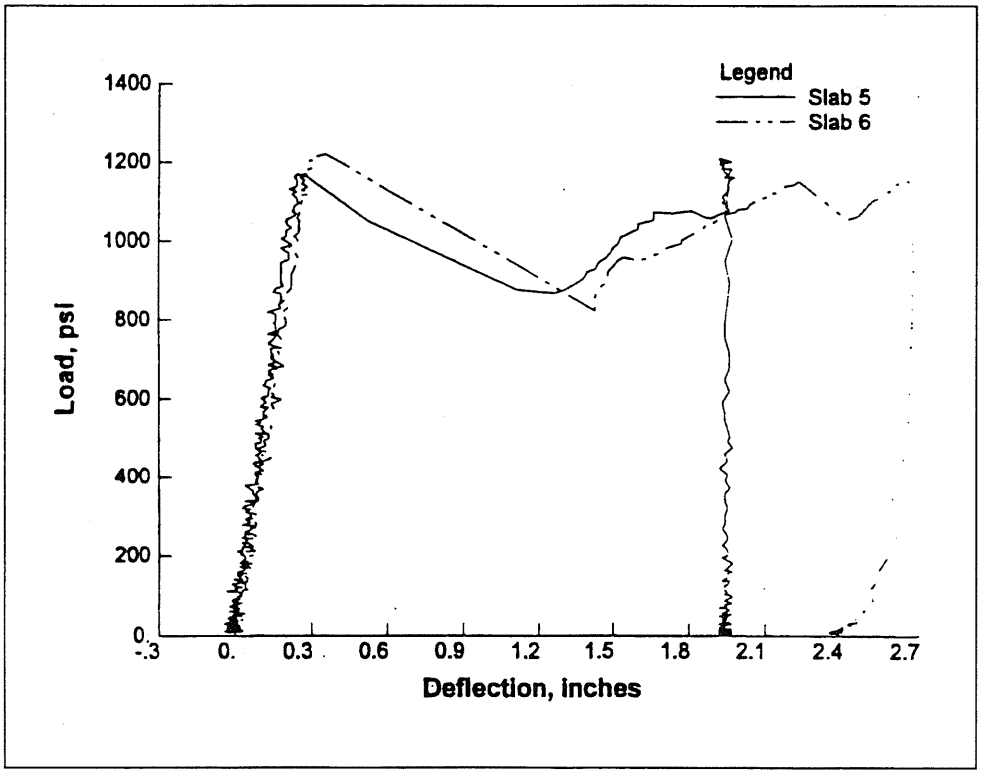

Figure A.43. Composite Midspan Load-Deflection Data for Slabs 5 and 6 (Woodson, 1994)

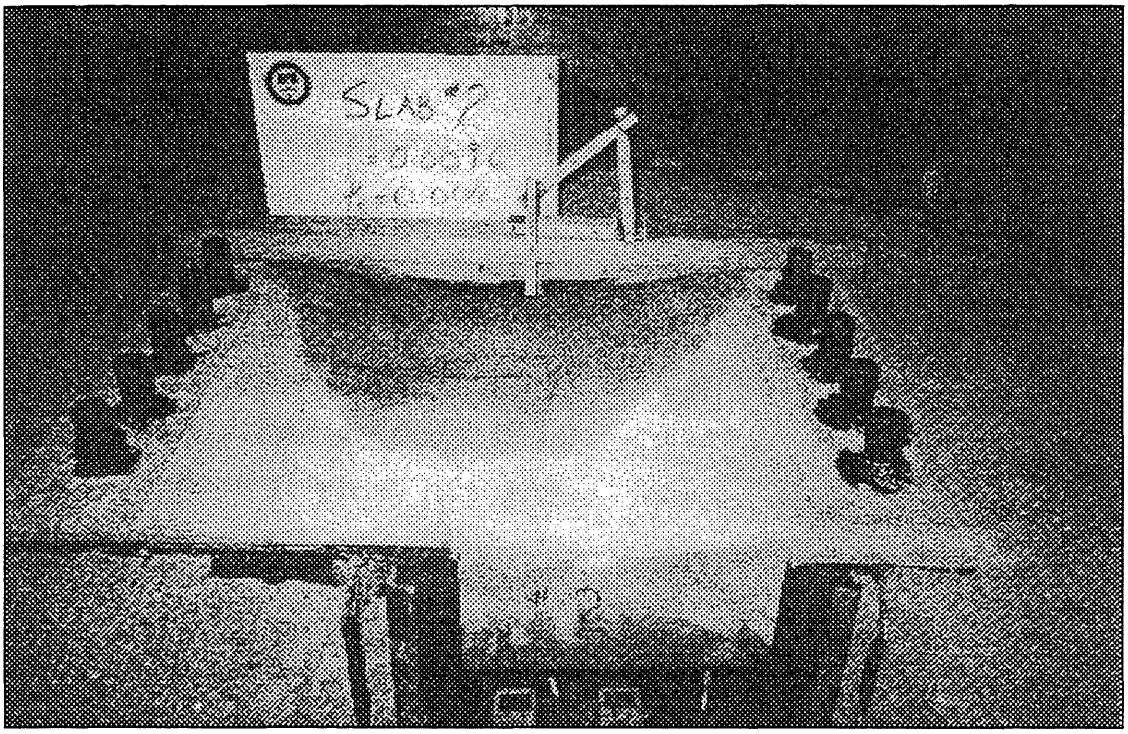

Figure A.44. Posttest View of Slab 2 (Woodson, 1994)

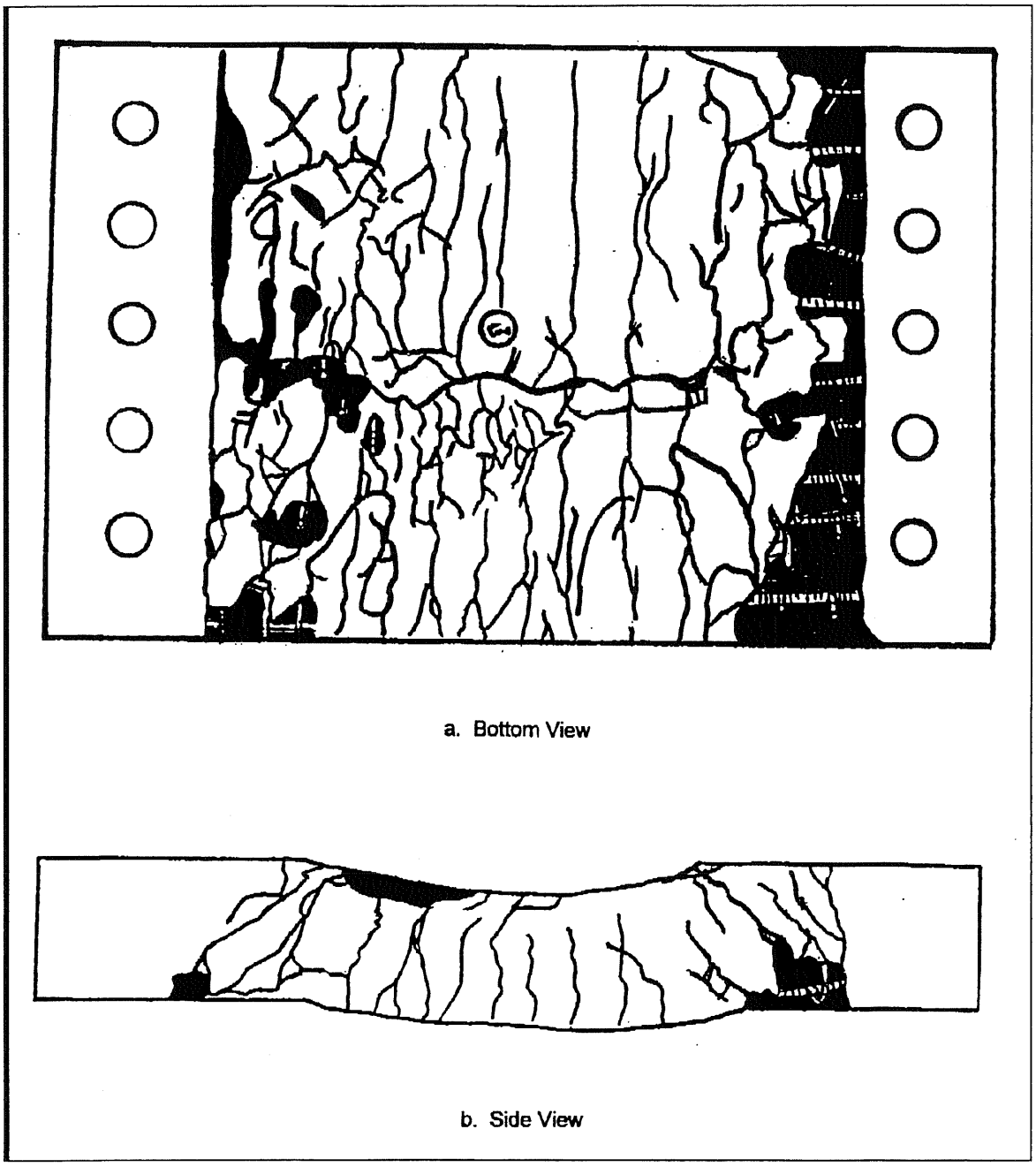

Figure A.45. Sketch of Damage for Slab 2 (Woodson, 1994)

APPENDIX B

ABAQUS INPUT PARAMETERS

B.1. Introduction

To be successful and ultimately obtain accurate data with ABAQUS or any other finite element analysis program, the numerous subroutines within ABAQUS and the required input must be well understood. These subroutines not only create the geometry of the model and print out the results, but also define the material and loading properties. Properly using material models and unique loading schemes are critical in any analysis in order to capture the structural response, but quite possibly even more important in laterally restrained members where both compressive and tensile membrane resistance occurs, "snap through " phenomenon exists, and high strength concrete are being considered in design.

The characteristics and engineering properties of high strength concrete is noticeably different than the lower strength concrete prevalent in most construction. One of the traits not normally expected is even greater brittleness associated with the increased strength. This is not saying that high strength concrete is not used in current construction, but that there are not as many instances such as in high rise buildings, super highway overpasses, and large bridges where the decrease in required material over shadows the higher cost per cubic yard nor the uncertainties associated with the material properties of higher strength concrete. Fortunately recent research efforts have provided better insight into high strength concrete behavior to facilitate its wider use in military construction and skyscrapers.

In order to define the concrete model in ABAQUS, the following parameters must be determined: Young's Modulus, Poisson's Ratio, the Uniaxial Stress vs. Strain Curve, the Failure Ratios (i.e., parameters establishing the biaxial failure curve), the Shear Retention Ratio (i.e., Shear Modulus reductions due to decreased shear transfer as cracks widen), and Tension Stiffening (i.e., the loss of tensile load transfer by the concrete between cracks once the cracks form). Numerous references (i.e., Park and Paulay (1975), Hognestad (1951), ACI Committee Reports

(1992), etc.) were consulted to determine realistic ranges for these necessary concrete parameters required in ABAQUS. The Failure and Shear Retention Ratios are set to default values within ABAQUS unless otherwise adjusted during material model generation. This is acceptable for normal loading scenarios, but when loading any structure past peak capacity, large cracks are expected to exist and a resulting reduction in shear capacity should follow. Additionally, some of the Failure Ratios vary according to the uniaxial compressive strength.

It is important to remember that the published results of any stress-strain curve or any other experimentally derived concrete properties are a function of the testing procedure and concrete composition. The testing procedure is influenced by the testing machine type (i.e., loading limits and especially its stiffness for post peak unloading), loading rate, platen design (i.e., the friction level), specimen shape (i.e., cylinder or cube), and whether failure was explosive or progressive. The concrete composition is a function of the water/cement ratio, aggregate size and properties, sand quantity and properties, cement quality, curing procedures, etc.

The concrete model in ABAQUS (1996) consists of a compressive yield/flow surface to model the concrete response in predominantly compressive states of stress and planes of damaged elasticity or a decrease in Young's Modulus to represent cracking from tensile states of stress. Since the underlying loading condition is monotonic, not cyclic, at the macro level with fairly low confining pressures (i.e., < 4 to $5\ f'_c$), the concrete model maintains elastic responses for unload and reload even though the loading may go beyond the ultimate stress point (Hibbitt et. al., 1996). Most concrete is reinforced with rebar which can be added to the structure through three usual methods: a truss bar element attached at nodes, the placement of single bars within an element, or the placement of a layer within an element. ABAQUS provides a fairly robust concrete model (Appendix C, Finite Element Model Verification) to define the biaxial and uniaxial material behavior subject to generally monotonic loading through a variety of input parameters.

B.2. Concrete Elastic Properties

B.2.1. Young's Modulus

Young's Modulus is defined in Park and Paulay (1975) (< 6000 psi) as:

$$E = 33 w_c^{1.5} \sqrt{f_c'} \quad \text{(psi)} \qquad \text{EQN B.1}$$

where w_c is the density of the concrete and f'_c is the compressive cylinder strength. For normal weight concrete (w_c = 145 lb/ft^3), Young's Modulus may be considered to be (ACI 318-1995):

$$E = 57000 \sqrt{f_c'} \quad \text{(psi)} \qquad \text{EQN B.2}$$

Hognestad (1951) provided the following equation during his study on short columns:

$$E = 1800000 + 460 f_c' \ \text{(psi)} \qquad \text{EQN B.3}$$

However, when comparing the ACI 318 equation (i.e., Hognestad's equation provides even larger values) with experimental results for high strength concrete (Figure B.1), the equation overestimates the modulus of elasticity for concrete with compressive strengths greater than 6000 psi. Many investigations presented in the ACI 363-92 Committee Report on High Strength Concrete note a Modulus of Elasticity's from 4.2 to 6.5 x 10^6 psi for concrete having compressive strengths ranging from 10,000 to 11,000 psi. Their correlation between the modulus of elasticity and compressive strength for compressive strengths from 3000 psi < f'_c < 12,000 psi was:

$$E_c = 40{,}000 \sqrt{f_c'} + 1.0 \times 10^6 \ \text{(psi)} \qquad \text{EQN B.4}$$

which will be used in this research effort.

Neville (1996) noted that Young's Modulus continuously increases at a decreasing rate as the compressive strength increases and predicted that the ACI 363 equation will over estimate the Elastic Modulus past 12,000 psi. The first equations for Young's Modulus were based on test data for compressive strengths up to 6000 psi and the ACI Committee 363 (1992) equation is based on experimental data up to 12,000 psi. Fortunately, Neville reported on Kakizaki et. al. (1992) who provided a Modulus of Elasticity equation:

$$E = 43950 \sqrt{f_c'} \ \text{(psi)} \qquad \text{EQN B.5}$$

based on testing of concrete with compressive strengths between 12,000 and 20,000 psi. The ACI 363 and Kakizaki equations provide differing results at 12,000 psi, so a gradual transition of

Young's Modulus values was developed between compressive strengths of 10,000 to 14,000 psi. From 14,000 to 20,000 psi, Kakizaki's equation will be used to estimate Young's Modulus (Figure B.2 and Table B.1).

B.2.2. Poisson's Ratio

Park and Paulay (1975) define Poisson's ratio as the ratio between the transverse strain and the strain in the direction of the applied uniaxial loading. Normally Poisson's ratio for concrete is defined within the range of 0.15 to 0.2 with the applied loading being a compressive uniaxial loading. Neville (1996) notes that Poisson's ratio appears to be the same whether the direction of loading is either compressive or tensile. Park and Paulay and Neville state that the ratio is normally lower for high strength concrete. However, ACI Committee Report 363R (1992) conflicts with this statement. Researchers referenced by the ACI 363 committee report larger Poisson's ratios for high strength concrete: 0.23 to 0.32 have been found regardless of compressive strength (i.e., 2500 to 11,500 psi), 0.20 to 0.28 for high strength concrete from 8000 to 11,600 psi, and 0.20 for lightweight-aggregate concrete regardless of concrete strength up to 10,570 psi. The difference in these reported values can possibly be summed by Talbot (1907) who determined Poisson's ratios of 0.1 to 0.16 for low loads and 0.25 to 0.3 near failure, i.e., undefined at failure, during tests of concrete and reinforced concrete columns. The high strength concrete appears to have less micro-cracking (ACI 363) so there is less lateral strain at low loads, but the increased brittleness develops large lateral strains at failure because of the lack of progressive crack growth. Based on these conflicting results and the fact that Poisson's ratio is required in ABAQUS to define the elastic properties of the concrete, a gradually decreasing Poisson's ratio from 0.22 to 0.15 will be used within the analysis for concrete compressive strengths ranging from 3000 to 20,000 psi (Table B.1).

B.3. Uniaxial Concrete Compressive Stress-Strain Curve

Algebraically defining the Uniaxial Compressive Stress-Strain Curve has long been a subject of great debate. The curve has been defined with straight lines representing triangular and rectangular shapes and second order equations such as parabolas. The clamor for simplicity lead to great popularity within the United States for using the Whitney Rectangular Stress Block for flexural analysis. Even ACI Committee 363 (1992) has obtained good results while using the Whitney stress block with high strength concrete. However, the ACI Committee also states that an accurate representation of the concrete stress pattern is important in combined bending and axially loaded structures, especially for members failing in flexural compression since there is a 15 percent difference in the axial force-moment interaction curve in the compression failure zone (Figure B.3). A study by the committee showed that actual curves were the best prediction for test data, while the rectangular and triangular approximations provided acceptable lower bounds for lightly-reinforced concrete members failing in tension. Since combined bending and axial loading mirrors the loading conditions within this dissertation, there is a need to accurately represent the compressive stress pattern. Fortunately, ABAQUS allows the user to define the uniaxial compressive stress-strain curve by defining points along the curve, while ABAQUS uses straight lines between the points. The primary purpose of inputting the stress-strain curve is to define the concrete inelastic behavior.

Hognestad et. al. (1955) equations for the stress-strain curve were used initially to develop curves based upon f'_c. Upon comparison with experimentally developed compressive stress-strain curves in Park and Paulay (1975) and Neville's (1996) books and the report by ACI Committee 363 (1992), the stress associated with peak strain was greatly over estimated, especially for high strength concrete, but also moderately so for even $f'_c > 4000$ psi (Figure B.4 compared to Figures B.5 to B.7). In order to input into ABAQUS a set of generally algebraically and geometrically correct compressive stress-strain curves, curves were developed that approximated the published experimental curves. It is important to remember that the published results of any stress-strain

curve are a function of the testing procedure and concrete composition. Therefore, the developed curves are an idealization for the predetermined concrete compressive strengths in this study.

The initial linear portion of the curve for low strength concrete (< 6000 psi) was defined by using a Young's Modulus from either the ACI Committee 363 (1992) or the Kakizaki (1992) equations based on the compressive strength and 45 percent of the strain associated with peak stress. The value of 45 percent was determined through observing published experimental results (Figures B.5 to B.7) and referred to by Park and Paulay (1975). For high strength concrete Norman (1990) pointed out that the linear portion continues until 0.75 to 0.8 f'_c. Upon comparison with Figures B.6 and B.7, the curves were approximately linear until at least .75 f'_c for compressive strengths up to 12,000 psi. Therefore, for high strength concrete (> 6000 psi) a gradually increasing percentage of the strain associated with peak compressive strength (0.65 to 0.8) defines the elastic limit (σ, Table B.1).

The strain associated with the peak compressive stress of 3000 psi was approximately 0.0019, while for 12,000 psi it was 0.0032 (Figure B.6). Using gradually increasing values for Young's Modulus and mirroring the available curves (Figures B.5 to B.7), approximate values for strain associated with peak stress were estimated as 0.0033 and 0.0035 for peak compressive stresses of 15,000 and 20,000 psi, respectively (Table B.1). Neville (1996) states that the strain associated with peak compressive stress of 15,000 psi will be typically between 0.003 and 0.004. In comparison with low strength concrete which has a descending portion that is usually not as steep as the ascending portion (i.e., more parabolic) of the curve, high strength concrete is nearly linear up to peak and decreases linearly at a even steeper slope than the ascending slope.

The approximately parabolic peak portion of the uniaxial compressive stress-strain curve was initially represented solely by the Desayi-Krishnan (1964) equation:

$$\sigma = \frac{2f'_c\varepsilon}{\varepsilon_o[1+(\frac{\varepsilon}{\varepsilon_o})^2]} \qquad \text{EQN B.6.}$$

When Equation B.6 is compared with the equations by Hognestad (1955) and Smith-Young (1955):

$$\sigma = 0.85 f_c' [2(\frac{\varepsilon}{\varepsilon_o}) - (\frac{\varepsilon}{\varepsilon_o})^2] \quad \text{(Hognestad)}$$

$$\text{where } \varepsilon_o = \frac{1.7 f_c'}{E_c} \qquad \text{EQN B.7}$$

$$\sigma = 0.85 s e^{(1-s)} \quad \text{(Smith - Young)}$$

$$\text{where } s = \frac{\varepsilon}{\varepsilon_o},\ \varepsilon_o \text{ is peak strain} \qquad \text{EQN B.8}$$

with the linear portion as part of Hognestad's uniaxial compressive stress-strain curve (Figures B.8 to B.10), the equation by Desayi-Krishnan provides the best continuance of the initially linear portion of the stress-strain curve.

A conservative value for the ultimate strain in concrete without lateral reinforcement is 0.003 (Figure B.11), but as the figure points out, it is not as conservative for high strength concrete. Hognestad (1951) recommended a peak strain of 0.0038 for combined bending and axially loaded members. In a separate study, Hognestad et. al. (1955) stated that the ultimate strain was from 0.0034 to 0.0038 and was largely independent of f'_c. Park and Paulay (1975) noted that in Europe the CEB-FIP uses a curve similar to Hognestad with the peak stress at 0.002 strain and then a straight horizontal branch to a maximum strain of 0.0035. Newmark even recommended a strain value of 0.004 for biaxial loaded structures with heavy shear confinement (noted in Park and Paulay, 1975). Based upon the curves for high strength concrete and the loading conditions within this study (i.e., combined bending and axially loaded slab strips performing under some biaxial compression), a peak compressive strain of 0.0038 was determined for all compressive strengths since the research effort is considering members with adequate shear reinforcement or lateral support. An important note in ABAQUS is that there is continued straining past the defined peak strain while maintaining the defined associated stress, which is similar to being confined until the analysis is terminated either through displacement controls or element instability from extensive cracking. Therefore, the stress-strain curves will be extended until the final stress is less than 100 psi which is a reasonably low value that thoroughly cracked concrete could transmit. This will ensure that crushing and cracking of concrete technically

removes the element from providing effective resistance as the structure transitions from compressive membrane resistance to tensile membrane action. Examples of the approximated curves are shown in Figures B.12 and B.13.

The stress-strain values representing the curves in Figures B.12 and B.13 are listed in Table B.2. The top value is the concrete compressive strength (f'_c, ksi), while the value just below it is the stress value (psi) defining the initial straight portion of the stress-strain curve. ABAQUS uses the previously defined Young's Modulus to determine the corresponding strain. The remaining values in the table are the required input (stress, accumulative strain) in ABAQUS to represent the inelastic portion of the stress-strain curve.

Since the material model in ABAQUS is based upon monotonic loading, any unloading is handled through elastic unloading and elastic reloading up to the point where the previous loading stopped and unloaded. This type of response is acceptable for this study since the slabs in the experimental data base were usually loaded monotonically to failure.

B.4. Inelastic Concrete Properties

B.4.1. Tension Stiffening

Although the primary purpose of inputting the uniaxial stress-strain curve in ABAQUS is to define concrete inelastic behavior, it does not provide a complete picture of the inelastic behavior of concrete during biaxial loading and cracking. First of all, ABAQUS does not consider the effects of bond slip or dowel action since it assumes the concrete is perfectly bonded to the rebar, but it does allow the concrete model to include cracking. Cracking is probably the most important behavior in a concrete model and the action is provided through damaged elasticity or softening at the crack plane. Cracking occurs once the strain reaches the defined tensile failure surface defined through the Failure Ratios. When an actual structure initially cracks, strain gages have noted the transfer of tensile forces by the concrete between cracks, normally through the rebar. As the cracks increase in depth, width, and number, the amount of load transfer decreases until the rebar is carrying all the tensile forces.

"Tension Stiffening" in the ABAQUS code simulates load transfer across cracks through rebar to represent the post cracking behavior (Figure B.14). ABAQUS smears the cracking over a finite volume associated with each integration point which was also used by Norman (1990) in his model for concrete behavior. This alleviates the sensitivity of crack prediction with mesh refinement. The continuous strain field of the finite element is not affected by the crack, which is similar to FINITE at the University of Illinois. The subroutine defines the retained tensile stress normal to a crack as a function of the strain or deformation in the direction normal to the crack. ABAQUS noted that Crisfeld (1986), echoed also by Norman, defined the behavior as a linear loss of strength after cracking failure until the volume carries no tensile stress beyond a limiting total strain (Figure B.15). The strain softening after cracking reduces the stress linearly to zero at a total strain of approximately 10 times the strain at initiation of cracking which is normally defined as 10^{-4} for tensile cracks in concrete (Vecchio and Collins (1986), Saadeghvaziri (1988)). FINITE at the University of Illinois defines the total strain as 20 times the strain at failure. Therefore, the total strain for no remaining tensile capacity once the concrete cracks will be defined as 10^{-3}.

Actual tension stiffening is a function of the density of reinforcement, quality of bond, and size of aggregate versus the rebar location and mesh in the model. Opened cracks represent the loss of elastic stiffness, but the ABAQUS model neglects permanent strain associated with cracking since the cracks will close completely if the stress across them becomes compressive. This will not be an issue since the loading procedure within the research plan will be monotonic. For concrete structures with little to no reinforcement (i.e., dams), the loss of tensile capacity can be defined by ABAQUS as the displacement normal to crack (i.e., $2x10^{-3}$ to $3x10^{-3}$ inches) to prevent mesh sensitivity.

B.4.2. Shear Retention

ABAQUS' default for the shear stiffness is no reduction in shear modulus in the plane of the cracks once they form. This assumption provides for a more efficient numerical solution and is

mostly accurate for the normal range of problems (i.e., small deflections developing relatively small strains at points of large shear forces). If a softening of the shear stiffness is required, the reduction is a function of the opening strain across the crack. The user needs to define the maximum strain where shear resistance drops to zero. If a crack closes, the shear modulus can also be reduced by defining the remaining percentage of shear stiffness.

According to Hegemier et. al. (1985), aggregate interlock is the key mechanism that has the greatest impact on the shear stiffness. Of course, concrete-steel bond and dowel action complete the true picture associated with shear transfer once a crack forms. By limiting the problem to monotonic loading and assuming adequate rebar embedment and cover, the primary method of shear transfer is aggregate interlock and/or the forming of a steel-concrete truss mechanism. Based on the performance of the concrete model and its handling of cracking, the aggregate interlock function is the key to defining the shear stiffness. Hegemier et. al. summarizes the results of interface shear transfer tests conducted by Fenwick and Paulay (1968), Paulay and Loeber (1974), Houde and Mirza (1974), and White and Holly (1972) where the shear displacement or slip was measured as the crack widths were increased (Figures B.16 to B.21). The aggregate interlock is a function of the aggregate type and properties such as angular or rounded, water/cement ratio, curing, crack width, and axial force for a few. With some extrapolation on the figures, it appears that a crack width of between 0.035 to 0.05 inches will effectively reduce the shear stiffness to zero. Since ABAQUS only provides the option of defining the crack opening in terms of strain, the maximum crack width must be divided by the distance between the crack initiators in these experiments which was approximately six inches. Therefore, the maximum strain across a crack defining the point where the shear stiffness reduces to zero is (0.05 in) /(6 in) = 0.00833. The percentage of shear stiffness available when a crack closes will be 0.5 (Saadeghvaziri, 1988).

B.4.3. Failure Ratios

The stress conditions resulting from the monotonic loading conditions for the slab strips being studied are at most biaxial. ABAQUS provides a fairly recognized biaxial failure surface (Figures B.22-B.23) which can be adjusted based on varying any of the four ratios. Biaxial failure surfaces have provided good analysis results in the past while studying the behavior of slab strips (Park and Paulay (1975), Hibbitt et. al. (1996), Neville (1996)). When eventually analyzing some of the support conditions, the state of stress could resemble a triaxial state of stress. However, there is really no highly praised encoded triaxial failure surface for reinforced concrete and using a biaxial failure surface in which a two dimensional state of stress dominates with the three biaxial combinations provides sufficient accuracy for most triaxial state of stress loading conditions.

ABAQUS provides a biaxial failure surface which has an isotropically hardening yield surface that is active when the stress is primarily compressive, an independent "crack detection surface" which determines if a point fails by cracking, and oriented damage to the elasticity to model the reversible part of the material response. The shape of the biaxial failure surface is defined through four ratios: the ratio of the ultimate biaxial compressive stress to the ultimate uniaxial compressive stress [default = 1.16]; the absolute value of the ratio of the uniaxial tensile stress at failure to the uniaxial compressive stress at failure [default = 0.09]; the ratio of the magnitude of the principal component of plastic strain at ultimate stress in biaxial compression to the plastic strain at ultimate stress in uniaxial compression [default = 1.28]; and the ratio of the tensile principal stress at cracking, in plane stress, when the other non-zero principal stress component is at the ultimate compressive stress value, to the tensile cracking stress under uniaxial tension [default = 0.333].

These default values seem to be reasonable average values, but some researchers have provided relationships to better define these ratios. The first ratio of concern is the ratio of the ultimate biaxial compressive stress to the uniaxial compressive stress. The default is 1.16 which is the same as the one provided by Park and Paulay (1975) for equal biaxial compressive stress. They do note that a larger ratio (1.27) is possible when the biaxial stresses are not equal (Figure

B.23). Gerstle et. al. (1980) provides charts to interpret average values of equal biaxial and uniaxial ultimate stresses (1.26). Kupfer et. al. (1969) reported ratios between 1.16 to 1.27. Hegemier et. al. (1985) noted biaxial strengths up to 1.3 times f'_c. Neville (1996) observed that at any particular biaxial stress combination, the strength decreases as the uniaxial compressive strength increases. Based on the perception that a state of equal biaxial stresses will be fairly limited in the model, a gradually decreasing ratio value will be used: 1.27 at 3000 psi to 1.16 at 20,000 psi (Table B.1).

The absolute value of the ratio of uniaxial tensile stress at failure to the uniaxial compressive stress at failure can be determined using either the rupture modulus or tensile splitting equations which are normally a function of the uniaxial compressive stress. Park and Paulay (1975) report the following:

$$f_r = K\sqrt{f'_c}\ (\text{psi})\ ,\ K=7 \text{ to } 13 \qquad \text{EQN B.9.}$$

They recommend K = 7.5 which is less than the ACI Committee 363 (1992) recommendation of K = 11.7 (3000 psi < f'_c < 12,000) for the rupture tensile strength. ACI Committee 363 recommends K = 7.4 for their splitting tensile strength. Chinn and Zimmerman (1965) recommend the following equation for the rupture modulus:

$$f_r = (f'_c)^{0.702} \qquad \text{EQN B.10.}$$

Neville (1996) states that the ACI splitting tensile strength equation over-estimates tensile strength in flexure at low compressive strengths (3000 psi) and greatly under-estimates tensile strength at high compressive strengths (20,000 psi). He recommends using either Raphael's (1984) equation:

$$f_t = 1.7(f'_c)^{2/3} \qquad \text{EQN B.11}$$

or Oluokun's (1991) equation:

$$f_t = 1.4(f'_c)^{.7} \qquad \text{EQN B.12}$$

developed from tensile testing of concrete cylinders. Every equation mentioned above provides a large variation in the tensile to compressive ratio as the compressive strength varies and are a function of the testing procedures. Since the tensile failure behavior in flexure (beams) is somewhere between the failure in the tensile test and the rupture test, an average value of the ACI

363 rupture strength, Raphael and Oluokun's equations will be used to develop the uniaxial tensile to uniaxial compressive ratio (Table B.1).

The graphs and charts provided by Gerstle et. al. (1980) and Kupfer et. al. (1969) (Figures B.24 and B.25) were used to define the ratio of the magnitude of the principal component of plastic strain at ultimate stress in biaxial compression to the plastic strain at ultimate stress in uniaxial compression. The ratio varies from 1.3 to 1.6 whether the ends of the specimen was confined or on a frictionless boundary. Based on the data available, the ratio for all compressive strengths will be 1.33 (Table B.1).

Very little direct information could be found on the ratio of the tensile principal stress at cracking in plane stress when the other non-zero principal stress component is at the ultimate compressive stress value compared to the pure tensile cracking stress under uniaxial tension. Gerstle et. al. (1980) pointed out in his report that biaxial stress creates 1.5 to 2 times the strain in the unloaded direction in comparison with uniaxial stress conditions. However, this ratio is a condition where the stresses are of opposite signs. Kupfer et. al. (1969) provided biaxial-tension and biaxial compression-tension results (Figures B.24 and B.25) that clearly showed that less compressive strength was available as the tensile stress was increased. This makes sense if one is inclined to believe that a compressive failure, which leads to crushing or explosive pop outs of concrete in uniaxial and biaxial stress states, is preceded by cracking that weakens through decreasing the thickness of the concrete resisting the compressive stresses. Failure during uniaxial compressive testing is most likely the result of tensile cracking due to the tensile strain in the unloaded directions. It would take very little tensile stress in a perpendicular direction to cause cracking when the loading in the other principal stress component is approaching peak compressive strength. When comparing an estimated tensile stress associated with at least a 95 percent peak compressive stress in the opposite direction (Figure B.24) with the stress from a uniaxial tension test (Figure B.25), the resulting ratio could be anywhere from 0.2 to 0.3. It is obvious that the amount of tensile stress combined with compressive biaxial stress would be much less to cause cracking than with uniaxial tension alone. A constant ratio of 0.25 will be used for all compressive

strengths since the other failure ratios capture the variations in strength increases due to changes in uniaxial compressive strengths.

B.5. Rebar

The items discussed above define the concrete model within ABAQUS. The missing piece in order to properly define reinforced concrete is how the rebar is input into the model. There are three techniques: defining numerous single bars, defining a layer of bars or smearing within an element, or defining truss elements which are attached at the nodes. A comparison completed during the verification phase showed no appreciable difference between any of the three techniques, especially when numerous small bars were modeled. The comparison of a single large bar versus a layer creates large variation in strength as would be expected in an actual structural member. The layering technique appears to provide the most efficient modeling and input technique, and will be used during this research effort.

In ABAQUS, an elastic, perfectly-plastic material model will define the uniaxial rebar reinforcement behavior. Once the yield stress is reached during elastic strain, the steel will deform infinitely with no strength loss and no rupturing. This fact requires tracking of the total strain within the rebar to ensure no excessive deformations skew the results. When defining the rebar as a single bar or a layer within a concrete element, the steel and concrete layers are modeled at an instant of time as a superposed continua constrained to have the same deformation gradient at the same spatial points. However, the concrete and rebar behavior are considered independently.

Table B.1 ABAQUS Input Parameters

f'c (psi)	E (psi)	ν	Peak ε_o	Elastic Limit σ (ksi)	Failure Ratios σ_{cb}/σ_c	$/\sigma_t/\sigma_c/$	$\varepsilon_{cb}/\varepsilon_c$	σ_{tb}/σ_t
3000	3.19E+06	0.220	0.0019	1.5	1.270	0.127	1.33	0.25
3500	3.37E+06	0.218	0.0020	1.8	1.267	0.119	1.33	0.25
4000	3.53E+06	0.216	0.0022	2.4	1.264	0.113	1.33	0.25
4500	3.68E+06	0.214	0.0023	2.7	1.260	0.109	1.33	0.25
5000	3.83E+06	0.212	0.0024	3.5	1.257	0.104	1.33	0.25
5500	3.97E+06	0.210	0.0025	3.9	1.254	0.101	1.33	0.25
6000	4.10E+06	0.208	0.0026	4.5	1.251	0.097	1.33	0.25
6500	4.22E+06	0.206	0.0027	4.9	1.247	0.094	1.33	0.25
7000	4.35E+06	0.204	0.0028	5.3	1.244	0.092	1.33	0.25
7500	4.46E+06	0.201	0.0028	5.6	1.241	0.090	1.33	0.25
8000	4.58E+06	0.199	0.0029	6.0	1.238	0.087	1.33	0.25
8500	4.69E+06	0.197	0.0029	6.4	1.234	0.085	1.33	0.25
9000	4.79E+06	0.195	0.0030	6.8	1.231	0.084	1.33	0.25
9500	4.90E+06	0.193	0.0030	7.1	1.228	0.082	1.33	0.25
10000	5.00E+06	0.191	0.0030	7.5	1.225	0.080	1.33	0.25
10500	5.02E+06	0.189	0.0031	7.9	1.221	0.079	1.33	0.25
11000	5.05E+06	0.187	0.0032	8.8	1.218	0.078	1.33	0.25
11500	5.07E+06	0.185	0.0032	9.2	1.215	0.076	1.33	0.25
12000	5.09E+06	0.183	0.0032	9.6	1.212	0.075	1.33	0.25
12500	5.12E+06	0.181	0.0032	10.0	1.209	0.074	1.33	0.25
13000	5.15E+06	0.179	0.0032	10.4	1.205	0.073	1.33	0.25
13500	5.18E+06	0.177	0.0033	10.8	1.202	0.072	1.33	0.25
14000	5.20E+06	0.175	0.0033	11.2	1.199	0.071	1.33	0.25
14500	5.29E+06	0.173	0.0033	11.6	1.196	0.070	1.33	0.25
15000	5.38E+06	0.171	0.0033	12.0	1.192	0.069	1.33	0.25
15500	5.47E+06	0.169	0.0034	12.4	1.189	0.068	1.33	0.25
16000	5.56E+06	0.166	0.0034	12.8	1.186	0.068	1.33	0.25
16500	5.65E+06	0.164	0.0034	13.2	1.183	0.067	1.33	0.25
17000	5.73E+06	0.162	0.0035	13.6	1.179	0.066	1.33	0.25
17500	5.81E+06	0.160	0.0035	14.0	1.176	0.065	1.33	0.25
18000	5.90E+06	0.158	0.0036	14.4	1.173	0.065	1.33	0.25
18500	5.98E+06	0.156	0.0036	14.8	1.170	0.064	1.33	0.25
19000	6.06E+06	0.154	0.0036	15.2	1.166	0.063	1.33	0.25
19500	6.14E+06	0.152	0.0037	15.6	1.163	0.063	1.33	0.25
20000	6.22E+06	0.150	0.0037	16.0	1.160	0.062	1.33	0.25

Table B.2. ABAQUS Stress-Strain Input Parameters

	A	B	C	D	E	F	G	H
175	3.0		3.5		4.0		4.5	
176	1500		1750		2400		2700	
177	1691	0.00011	2249	0.00022	2788	0.00021	3312	0.00028
178	1808	0.00016	2362	0.00027	2897	0.00026	3420	0.00033
179	2065	0.00028	2608	0.00039	3136	0.00038	3652	0.00045
180	2304	0.00041	2835	0.00052	3355	0.00051	3867	0.00058
181	2554	0.00058	3073	0.00069	3585	0.00068	4091	0.00075
182	2649	0.00066	3163	0.00077	3672	0.00076	4177	0.00083
183	2862	0.00091	3367	0.00102	3869	0.00101	4370	0.00108
184	2970	0.00116	3470	0.00127	3971	0.00126	4471	0.00133
185	2996	0.00131	3496	0.00142	3996	0.00141	4496	0.00148
186	3000	0.00141	3500	0.00152	4000	0.00151	4500	0.00158
187	2996	0.00151	3496	0.00162	3996	0.00161	4496	0.00168
188	2977	0.00166	3477	0.00177	3977	0.00176	4476	0.00183
189	2918	0.00191	3418	0.00202	3917	0.00201	4415	0.00208
190	2850	0.00203	3185	0.00248	3617	0.00232	4215	0.00227
191	2660	0.00253	2952	0.00298	3262	0.00282	3815	0.00277
192	2480	0.00303	2722	0.00348	2912	0.00332	3265	0.00327
193	2310	0.00353	2502	0.00398	2572	0.00382	2560	0.00377
194	2150	0.00403	2292	0.00448	2272	0.00432	2260	0.00427
195	2000	0.00453	2092	0.00498	2082	0.00482	2070	0.00477
196	1860	0.00503	1902	0.00548	1892	0.00532	1880	0.00527
197	1730	0.00553	1722	0.00598	1712	0.00582	1700	0.00577
198	1610	0.00603	1552	0.00648	1542	0.00632	1530	0.00627
199	1495	0.00653	1392	0.00698	1382	0.00682	1370	0.00677
200	1385	0.00703	1242	0.00748	1232	0.00732	1220	0.00727
201	1280	0.00753	1102	0.00798	1092	0.00782	1080	0.00777
202	1180	0.00803	972	0.00848	962	0.00832	950	0.00827
203	1090	0.00853	852	0.00898	842	0.00882	830	0.00877
204	1000	0.00903	742	0.00948	732	0.00932	720	0.00927
205	910	0.00953	642	0.00998	632	0.00982	620	0.00977
206	820	0.01003	552	0.01048	542	0.01032	530	0.01027
207	730	0.01053	472	0.01098	462	0.01082	450	0.01077
208	645	0.01103	402	0.01148	392	0.01132	380	0.01127
209	560	0.01153	342	0.01198	332	0.01182	320	0.01177
210	475	0.01203	287	0.01248	277	0.01232	265	0.01227
211	390	0.01253	232	0.01298	222	0.01282	210	0.01277
212	305	0.01303	177	0.01348	167	0.01332	155	0.01327
213	220	0.01353	122	0.01398	112	0.01382	100	0.01377
214	135	0.01403	67	0.01448	57	0.01432	45	0.01427
215	50	0.01453						
216								

Table B.2. ABAQUS Stress-Strain Input Parameters (Cont.)

	I	J	K	L	M	N	O	P
175	5.0		5.5		6.0		6.5	
176	3500		3850		4500		4875	
177	3826	0.00022	4330	0.00026	4827	0.00023	5200	0.00015
178	3931	0.00027	4435	0.00031	4932	0.00028	5424	0.00030
179	4161	0.00039	4663	0.00043	5161	0.00040	5653	0.00042
180	4372	0.00052	4873	0.00056	5371	0.00053	5865	0.00055
181	4594	0.00069	5094	0.00073	5591	0.00070	6087	0.00072
182	4678	0.00077	5178	0.00081	5676	0.00078	6172	0.00080
183	4870	0.00102	5370	0.00106	5869	0.00103	6367	0.00105
184	4971	0.00127	5470	0.00131	5970	0.00128	6470	0.00130
185	4996	0.00142	5496	0.00146	5995	0.00143	6495	0.00145
186	5000	0.00152	5500	0.00156	6000	0.00153	6500	0.00155
187	4996	0.00162	5496	0.00166	5996	0.00163	6496	0.00165
188	4976	0.00177	5476	0.00181	5975	0.00178	6475	0.00175
189	4830	0.00202	5300	0.00203	5800	0.00190	6150	0.00205
190	4710	0.00209	4950	0.00253	5350	0.00240	5450	0.00235
191	4110	0.00259	4250	0.00303	4450	0.00290	4550	0.00285
192	3210	0.00309	3150	0.00353	3195	0.00340	3250	0.00335
193	2410	0.00359	2000	0.00403	2390	0.00390	2350	0.00385
194	1810	0.00409	1450	0.00453	2070	0.00440	2030	0.00435
195	1310	0.00459	1000	0.00503	1870	0.00490	1830	0.00485
196	910	0.00509	650	0.00553	1670	0.00540	1630	0.00535
197	610	0.00559	450	0.00603	1475	0.00590	1435	0.00585
198	410	0.00609	350	0.00653	1290	0.00640	1250	0.00635
199	310	0.00659	250	0.00703	1115	0.00690	1075	0.00685
200	210	0.00709	200	0.00753	950	0.00740	910	0.00735
201	160	0.00759	150	0.00803	795	0.00790	755	0.00785
202	120	0.00809	110	0.00853	650	0.00840	615	0.00835
203	90	0.00859	80	0.00903	505	0.00890	475	0.00885
204	70	0.00909	60	0.00953	370	0.00940	345	0.00935
205	60	0.00959	50	0.01003	245	0.00990	225	0.00985
206	55	0.01009	40	0.01053	140	0.01040	125	0.01035
207	50	0.01059	30	0.01103	45	0.01090	35	0.01085
208	45	0.01109	20	0.01153				
209	40	0.01159	10	0.01203				
210	35	0.01209						
211	30	0.01259						
212	25	0.01309						
213								

Table B.2. ABAQUS Stress-Strain Input Parameters (Cont.)

	Q	R	S	T	U	V	W	X
175	7.0		7.5		8.0		8.5	
176	5250		5625		6000		6375	
177	5650	0.00019	6284	0.00028	6760	0.00028	7231	0.00028
178	5911	0.00032	6393	0.00033	6870	0.00033	7344	0.00033
179	6142	0.00044	6628	0.00045	7110	0.00045	7588	0.00045
180	6356	0.00057	6844	0.00058	7330	0.00058	7814	0.00058
181	6581	0.00074	7073	0.00075	7563	0.00075	8052	0.00075
182	6667	0.00082	7160	0.00083	7653	0.00083	8144	0.00083
183	6864	0.00107	7361	0.00108	7858	0.00108	8354	0.00108
184	6969	0.00132	7468	0.00133	7967	0.00133	8467	0.00133
185	6995	0.00147	7495	0.00148	7995	0.00148	8495	0.00148
186	7000	0.00157	7500	0.00158	8000	0.00158	8500	0.00158
187	6996	0.00167	7496	0.00168	7995	0.00168	8495	0.00168
188	6900	0.00182	7380	0.00179	7920	0.00179	8410	0.00176
189	6700	0.00199	6100	0.00194	6200	0.00199	6700	0.00199
190	5900	0.00229	5200	0.00214	5200	0.00224	5500	0.00219
191	4800	0.00279	3200	0.00274	3000	0.00269	3000	0.00264
192	3350	0.00329	2500	0.00324	2490	0.00319	2240	0.00314
193	2250	0.00379	2050	0.00374	2040	0.00369	1680	0.00364
194	1900	0.00429	1750	0.00424	1740	0.00419	1480	0.00414
195	1600	0.00479	1550	0.00474	1540	0.00469	1280	0.00464
196	1400	0.00529	1350	0.00524	1340	0.00519	1170	0.00514
197	1220	0.00579	1200	0.00574	1190	0.00569	1060	0.00564
198	1070	0.00629	1080	0.00624	1040	0.00619	950	0.00614
199	960	0.00679	970	0.00674	930	0.00669	840	0.00664
200	870	0.00729	860	0.00724	820	0.00719	730	0.00714
201	740	0.00779	730	0.00774	710	0.00769	620	0.00764
202	600	0.00829	590	0.00824	600	0.00819	510	0.00814
203	460	0.00879	450	0.00874	490	0.00869	400	0.00864
204	330	0.00929	320	0.00924	380	0.00919	290	0.00914
205	210	0.00979	200	0.00974	270	0.00969	180	0.00964
206	110	0.01029	100	0.01024	160	0.01019	70	0.01014
207	40	0.01079	35	0.01074	50	0.01069		
208								

Table B.2. ABAQUS Stress-Strain Input Parameters (Cont.)

	Y	Z	AA	AB	AC	AD	AE	AF
175	9.0		9.5		10.0		10.5	
176	6750		7125		7500		7875	
177	7698	0.00027	8160	0.00025	8617	0.00023	9121	0.00023
178	7813	0.00032	8278	0.00030	8739	0.00028	9242	0.00028
179	8064	0.00044	8536	0.00042	9005	0.00040	9507	0.00040
180	8296	0.00057	8774	0.00055	9251	0.00053	9752	0.00053
181	8540	0.00074	9026	0.00072	9510	0.00070	10011	0.00070
182	8634	0.00082	9123	0.00080	9610	0.00078	10110	0.00078
183	8850	0.00107	9345	0.00105	9840	0.00103	10340	0.00103
184	8965	0.00132	9464	0.00130	9963	0.00128	10463	0.00128
185	8995	0.00147	9495	0.00145	9994	0.00143	10494	0.00143
186	9000	0.00157	9500	0.00155	10000	0.00153	10500	0.00153
187	8995	0.00167	9420	0.00165	9800	0.00160	10300	0.00163
188	8700	0.00179	9300	0.00175	9500	0.00172	9900	0.00173
189	7900	0.00194	8100	0.00195	8400	0.00195	8700	0.00183
190	5650	0.00219	5850	0.00215	5150	0.00210	5250	0.00203
191	2650	0.00259	2600	0.00255	2450	0.00250	2400	0.00243
192	2090	0.00309	1980	0.00305	1850	0.00300	1840	0.00293
193	1625	0.00359	1515	0.00355	1450	0.00350	1440	0.00343
194	1425	0.00409	1315	0.00405	1250	0.00400	1240	0.00393
195	1225	0.00459	1065	0.00455	1050	0.00450	1040	0.00443
196	1115	0.00509	965	0.00505	950	0.00500	940	0.00493
197	1005	0.00559	865	0.00555	850	0.00550	840	0.00543
198	895	0.00609	765	0.00605	750	0.00600	740	0.00593
199	785	0.00659	665	0.00655	650	0.00650	640	0.00643
200	675	0.00709	565	0.00705	550	0.00700	540	0.00693
201	565	0.00759	465	0.00755	450	0.00750	440	0.00743
202	455	0.00809	365	0.00805	350	0.00800	340	0.00793
203	345	0.00859	265	0.00855	250	0.00850	240	0.00843
204	235	0.00909	165	0.00905	160	0.00900	140	0.00893
205	125	0.00959	65	0.00955	60	0.00950	50	0.00943
206	15	0.01009						
207								

Table B.2. ABAQUS Stress-Strain Input Parameters (Cont.)

	AG	AH	AI	AJ	AK	AL	AM	AN
175	11.0		11.5		12.0		12.5	
176	8800		9200		9600		10000	
177	9400	0.00011	9650	0.00009	10200	0.00014	10700	0.00017
178	9734	0.00016	10227	0.00024	10714	0.00025	11190	0.00025
179	10000	0.00028	10494	0.00032	10984	0.00030	11465	0.00031
180	10246	0.00041	10741	0.00039	11233	0.00037	11718	0.00040
181	10507	0.00058	11003	0.00056	11497	0.00054	11987	0.00053
182	10607	0.00066	11104	0.00064	11599	0.00062	12091	0.00058
183	10838	0.00091	11337	0.00089	11835	0.00087	12331	0.00083
184	10963	0.00116	11462	0.00114	11962	0.00112	12461	0.00108
185	10994	0.00131	11494	0.00129	11994	0.00127	12494	0.00123
186	11000	0.00141	11500	0.00137	12000	0.00132	12500	0.00127
187	10850	0.00151	11350	0.00146	11800	0.00143	12300	0.00138
188	10400	0.00166	10800	0.00161	11200	0.00153	11600	0.00148
189	9000	0.00176	9200	0.00172	9700	0.00163	10000	0.00155
190	5240	0.00186	5230	0.00179	5200	0.00171	5155	0.00163
191	2390	0.00221	2380	0.00213	2350	0.00205	2305	0.00185
192	1830	0.00266	1820	0.00258	1790	0.00250	1745	0.00230
193	1430	0.00316	1420	0.00308	1390	0.00300	1345	0.00280
194	1230	0.00366	1220	0.00358	1190	0.00350	1145	0.00330
195	1030	0.00416	1020	0.00408	990	0.00400	945	0.00380
196	930	0.00466	920	0.00458	890	0.00450	845	0.00430
197	830	0.00516	820	0.00508	790	0.00500	745	0.00480
198	730	0.00566	720	0.00558	690	0.00550	645	0.00530
199	630	0.00616	620	0.00608	590	0.00600	545	0.00580
200	530	0.00666	520	0.00658	490	0.00650	455	0.00630
201	430	0.00716	420	0.00708	400	0.00700	375	0.00680
202	330	0.00766	320	0.00758	310	0.00750	295	0.00730
203	230	0.00816	220	0.00808	220	0.00800	215	0.00780
204	140	0.00866	130	0.00858	130	0.00850	125	0.00830
205	50	0.00916	40	0.00908	40	0.00900	35	0.00880
206								

Table B.2. ABAQUS Stress-Strain Input Parameters (Cont.)

	AO	AP	AQ	AR	AS	AT	AU	AV
175	13.0		13.5		14.0		14.5	
176	10400		10800		11200		11600	
177	11300	0.00018	12000	0.00027	12100	0.00025	12500	0.00021
178	11942	0.00031	12680	0.00042	13159	0.00048	13664	0.00044
179	12201	0.00041	12962	0.00057	13448	0.00058	13951	0.00054
180	12476	0.00051	13071	0.00067	13560	0.00065	14062	0.00061
181	12582	0.00063	13323	0.00082	13818	0.00081	14319	0.00077
182	12827	0.00079	13459	0.00106	13958	0.00094	14458	0.00096
183	12980	0.00104	13494	0.00114	13994	0.00109	14494	0.00111
184	12994	0.00113	13500	0.00119	14000	0.00115	14500	0.00111
185	13000	0.00121	13200	0.00125	13700	0.00121	14100	0.00120
186	12700	0.00128	12000	0.00131	12500	0.00126	13200	0.00124
187	11900	0.00135	10300	0.00142	10700	0.00136	11400	0.00132
188	10200	0.00148	5450	0.00150	5350	0.00143	5300	0.00140
189	5450	0.00156	2285	0.00167	2185	0.00159	2135	0.00154
190	2290	0.00176	1685	0.00212	1585	0.00204	1535	0.00199
191	1690	0.00221	1285	0.00262	1185	0.00254	1135	0.00249
192	1290	0.00271	1085	0.00312	985	0.00304	935	0.00299
193	1090	0.00321	885	0.00362	785	0.00354	785	0.00349
194	890	0.00371	785	0.00412	685	0.00404	685	0.00399
195	790	0.00421	685	0.00462	585	0.00454	585	0.00449
196	690	0.00471	585	0.00512	495	0.00504	495	0.00499
197	590	0.00521	485	0.00562	415	0.00554	415	0.00549
198	490	0.00571	395	0.00612	335	0.00604	335	0.00599
199	400	0.00621	315	0.00662	265	0.00654	265	0.00649
200	320	0.00671	235	0.00712	205	0.00704	205	0.00699
201	240	0.00721	175	0.00762	155	0.00754	155	0.00749
202	180	0.00771	115	0.00812	105	0.00804	105	0.00799
203	120	0.00821	25	0.00862	25	0.00854	25	0.00849
204	30	0.00871						
205								

Table B.2. ABAQUS Stress-Strain Input Parameters (Cont.)

	AW	AX	AY	AZ	BA	BB	BC	BD
175	15.0		15.5		16.0		16.5	
176	12000		12400		12800		13200	
177	13882	0.00036	14370	0.00036	14857	0.00038	15345	0.00038
178	14155	0.00045	14645	0.00045	15136	0.00044	15626	0.00044
179	14445	0.00050	14938	0.00053	15432	0.00052	15925	0.00052
180	14557	0.00057	15051	0.00061	15600	0.00060	16300	0.00064
181	14816	0.00073	15314	0.00069	15900	0.00080	16500	0.00076
182	14970	0.00096	15457	0.00095	15980	0.00098	16485	0.00094
183	14993	0.00102	15493	0.00103	15993	0.00110	16495	0.00104
184	15000	0.00107	15500	0.00110	16000	0.00111	16500	0.00110
185	14500	0.00116	15000	0.00118	15000	0.00120	15900	0.00117
186	13800	0.00120	13300	0.00123	13800	0.00122	14300	0.00119
187	12000	0.00128	11500	0.00127	12000	0.00126	12500	0.00123
188	5150	0.00136	5150	0.00135	5150	0.00132	6150	0.00128
189	2100	0.00150	2100	0.00145	2100	0.00142	2000	0.00137
190	1500	0.00195	1500	0.00190	1500	0.00187	1400	0.00182
191	1100	0.00245	1100	0.00240	1100	0.00237	950	0.00232
192	900	0.00295	900	0.00290	900	0.00287	750	0.00282
193	750	0.00345	750	0.00340	750	0.00337	600	0.00332
194	650	0.00395	650	0.00390	650	0.00387	500	0.00382
195	550	0.00445	550	0.00440	550	0.00437	400	0.00432
196	460	0.00495	460	0.00490	460	0.00487	310	0.00482
197	380	0.00545	380	0.00540	380	0.00537	230	0.00532
198	310	0.00595	310	0.00590	310	0.00587	160	0.00582
199	250	0.00645	250	0.00640	250	0.00637	100	0.00632
200	200	0.00695	200	0.00690	200	0.00687	50	0.00682
201	150	0.00745	150	0.00740	150	0.00737		
202	100	0.00795	100	0.00790	100	0.00787		
203	20	0.00845	20	0.00840	20	0.00837		
204								

Table B.2. ABAQUS Stress-Strain Input Parameters (Cont.)

	BE	BF	BG	BH	BI	BJ	BK	BL
175	17.0		17.5		18.0		18.5	
176	13600		14000		14400		14800	
177	15831	0.00043	16317	0.00039	16803	0.00039	17288	0.00035
178	16116	0.00048	16605	0.00044	17094	0.00044	17583	0.00040
179	16418	0.00059	16911	0.00055	17403	0.00054	17896	0.00050
180	16700	0.00073	17300	0.00069	17800	0.00070	18250	0.00066
181	16850	0.00083	17400	0.00079	17900	0.00076	18350	0.00072
182	16980	0.00094	17454	0.00093	17954	0.00092	18453	0.00091
183	16993	0.00109	17493	0.00108	17993	0.00107	18493	0.00106
184	17000	0.00111	17500	0.00109	18000	0.00114	18300	0.00113
185	16400	0.00116	16900	0.00114	17400	0.00119	17900	0.00116
186	14800	0.00119	15300	0.00117	15800	0.00123	16100	0.00118
187	10000	0.00128	9500	0.00124	9000	0.00129	9000	0.00122
188	1800	0.00156	1780	0.00151	1760	0.00156	1750	0.00149
189	950	0.00206	930	0.00201	930	0.00206	920	0.00199
190	750	0.00256	730	0.00251	730	0.00256	720	0.00249
191	600	0.00306	600	0.00301	600	0.00306	590	0.00299
192	500	0.00356	500	0.00351	500	0.00356	490	0.00349
193	400	0.00406	400	0.00401	400	0.00406	390	0.00399
194	310	0.00456	310	0.00451	310	0.00456	300	0.00449
195	230	0.00506	230	0.00501	230	0.00506	220	0.00499
196	160	0.00556	160	0.00551	160	0.00556	150	0.00549
197	100	0.00606	100	0.00601	100	0.00606	90	0.00599
198	50	0.00656	50	0.00651	50	0.00656	40	0.00649
199	20	0.00706	20	0.00701	20	0.00706	10	0.00699
200								

Table B.2. ABAQUS Stress-Strain Input Parameters (Cont.)

	BM	BN	BO	BP	BQ	BR	BS	BT
175	19.0		19.5		20.0			
176	15200		15600		16000			
177	17773	0.00034	18258	0.00036	19047	0.00053		
178	18071	0.00038	18559	0.00046	19372	0.00063		
179	18400	0.00049	18900	0.00056	19700	0.00073		
180	18800	0.00062	19004	0.00059	19900	0.00083		
181	18900	0.00074	19294	0.00071	19951	0.00093		
182	18980	0.00090	19452	0.00089	19992	0.00103		
183	18993	0.00105	19493	0.00104	19500	0.00110		
184	18500	0.00112	19300	0.00111	18700	0.00113		
185	18000	0.00115	18200	0.00114	17200	0.00117		
186	16200	0.00118	16400	0.00118	8000	0.00120		
187	9100	0.00122	9000	0.00121	1600	0.00145		
188	1700	0.00149	1680	0.00148	850	0.00195		
189	900	0.00199	880	0.00198	670	0.00245		
190	710	0.00249	690	0.00248	550	0.00295		
191	590	0.00299	570	0.00298	460	0.00345		
192	500	0.00349	480	0.00348	370	0.00395		
193	400	0.00399	380	0.00398	280	0.00445		
194	310	0.00449	290	0.00448	200	0.00495		
195	230	0.00499	210	0.00498	130	0.00545		
196	160	0.00549	140	0.00548	70	0.00595		
197	100	0.00599	80	0.00598	20	0.00645		
198	50	0.00649	30	0.00648				
199	20	0.00699						
200								

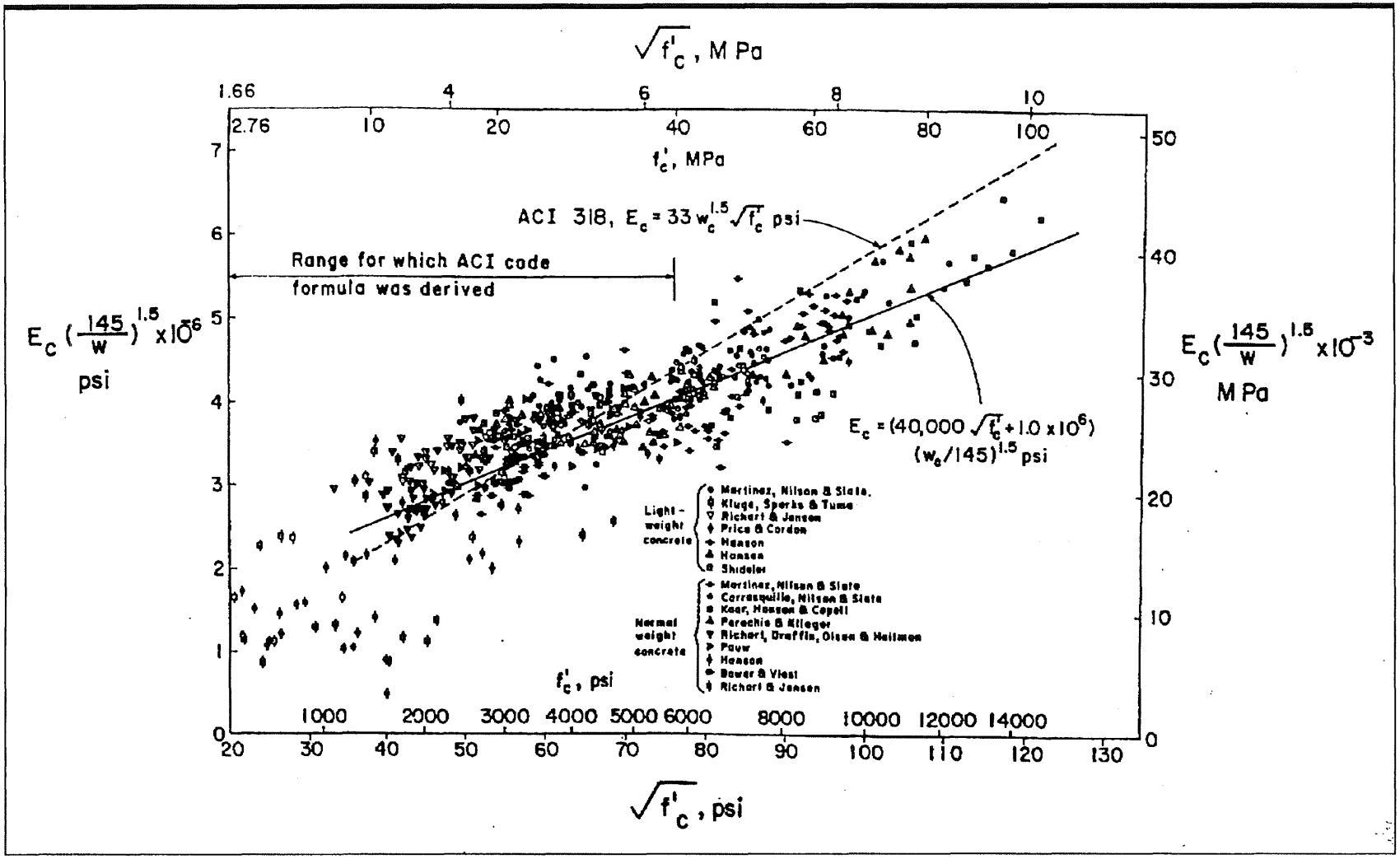

Figure B.1. Modulus of Elasticity Versus Concrete Strength (ACI 363, 1992)

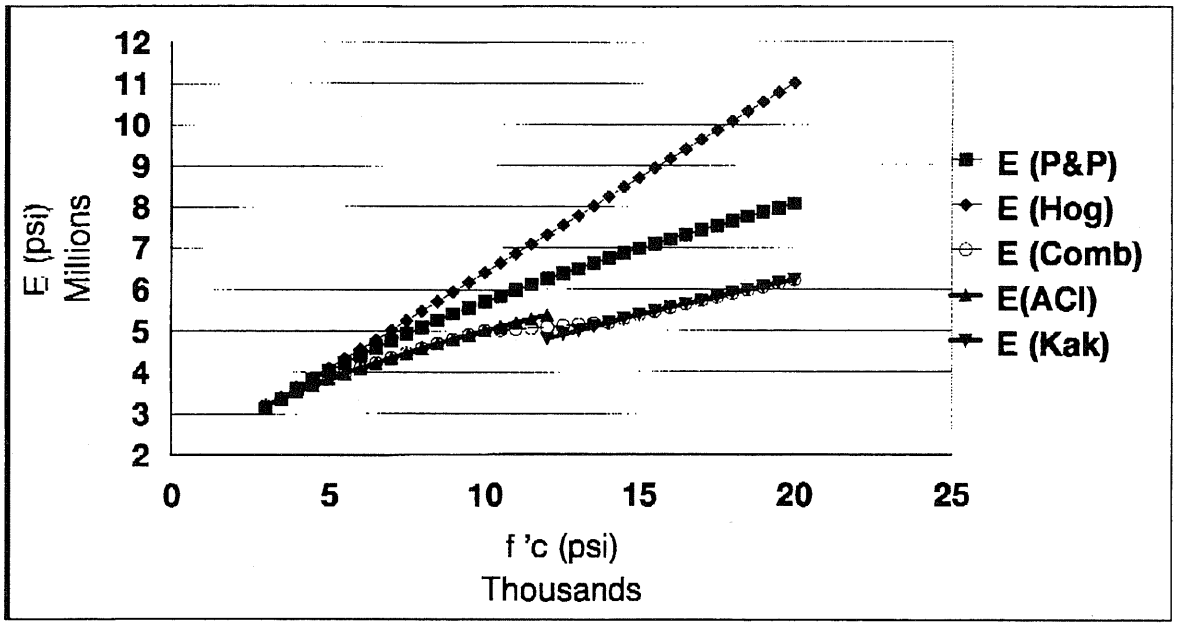

Figure B.2. Young's Modulus Versus Concrete Strength

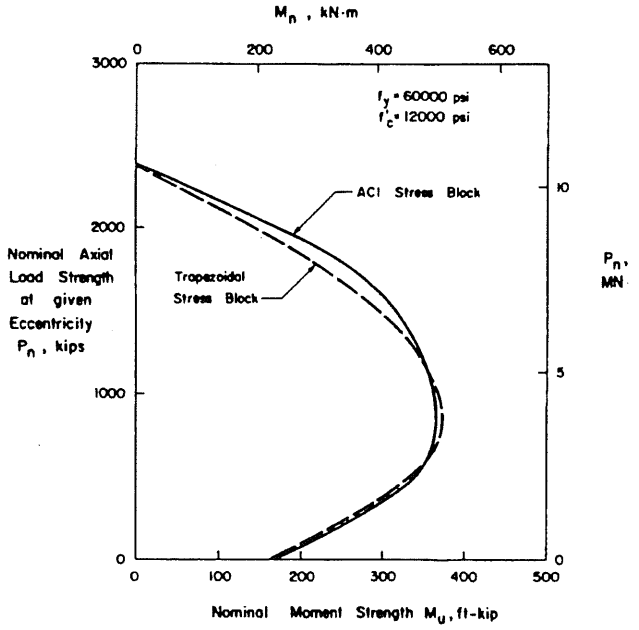

Figure B.3. Comparative Interaction Diagrams for High-Strength Concrete Column (ACI 363, 1992)

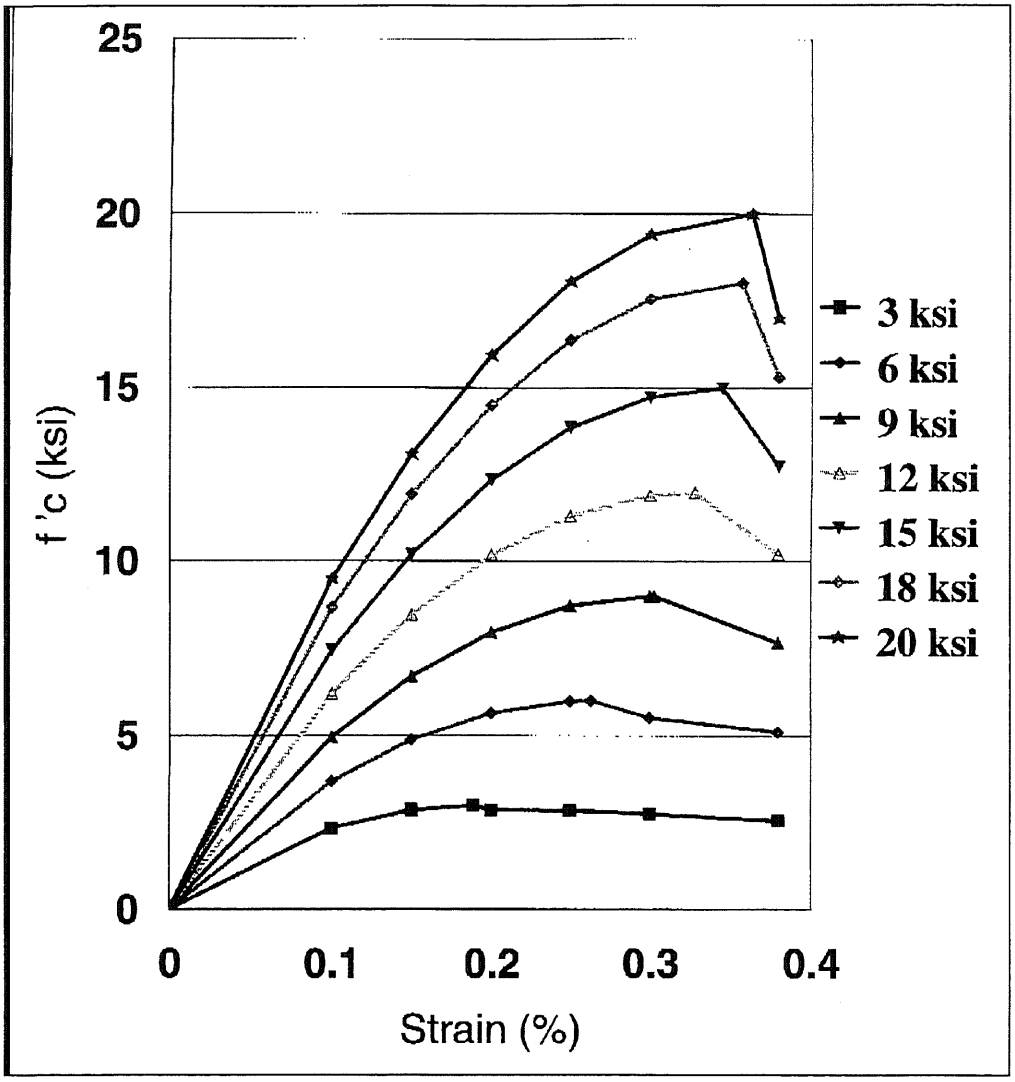

Figure B.4. Hognestad's Stress-Strain Curves

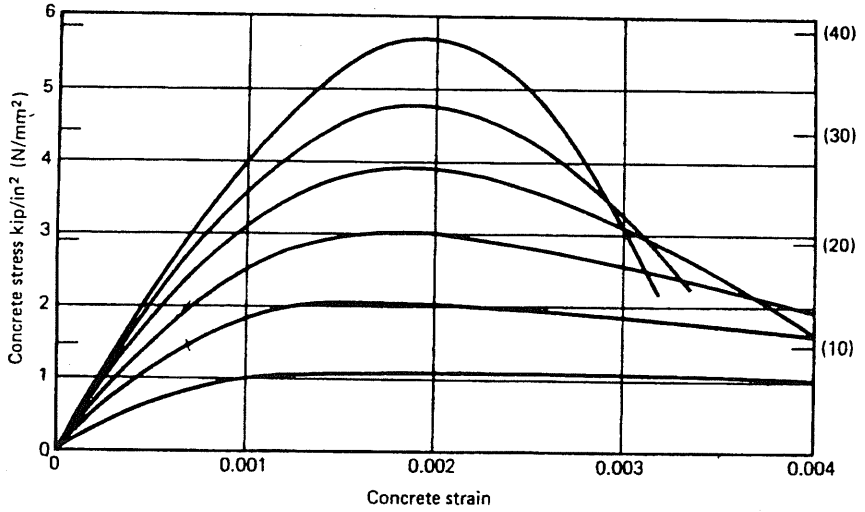

Figure B.5. Stress-Strain Curves for Concrete Cylinders Loaded in Uniaxial Compression (Park and Paulay, 1975)

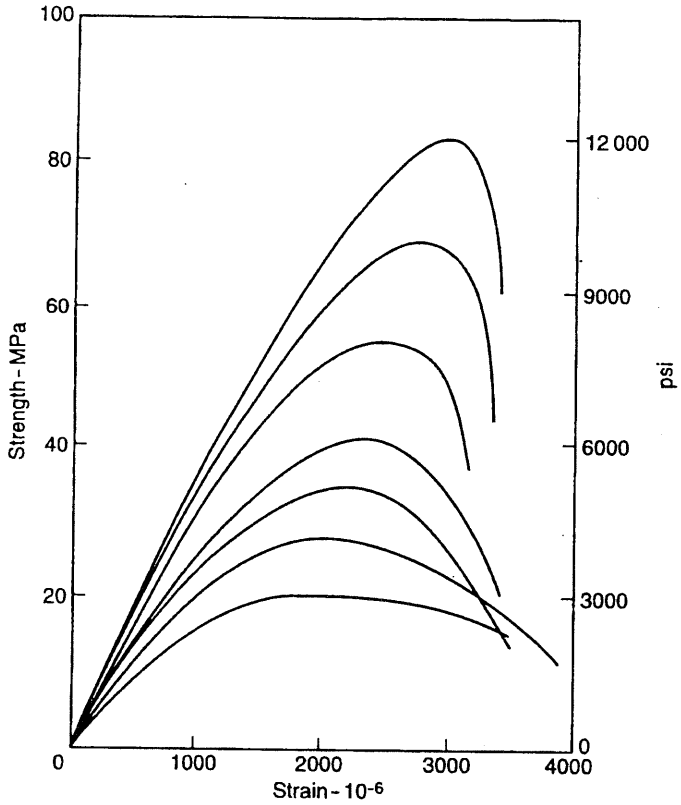

Figure B.6. Examples of Stress-Strain Relation in Compression for Concrete Cylinders With Compressive Strength up to 12,000 psi (Neville, 1996)

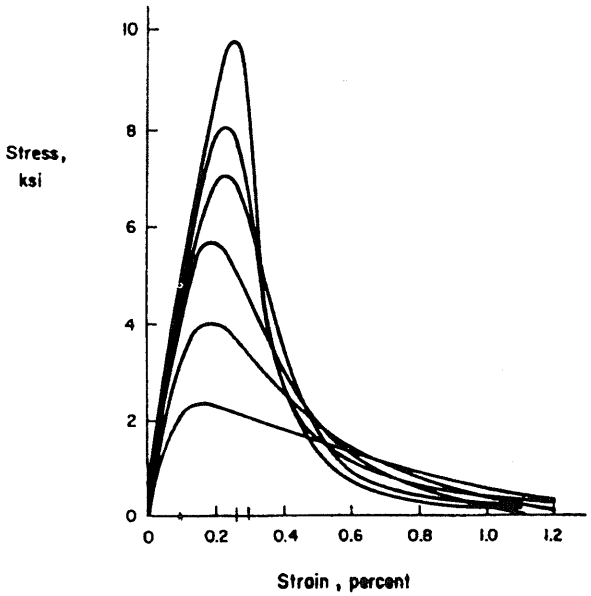

Figure B.7. Complete Compressive Stress-Strain Curves (ACI 363, 1992)

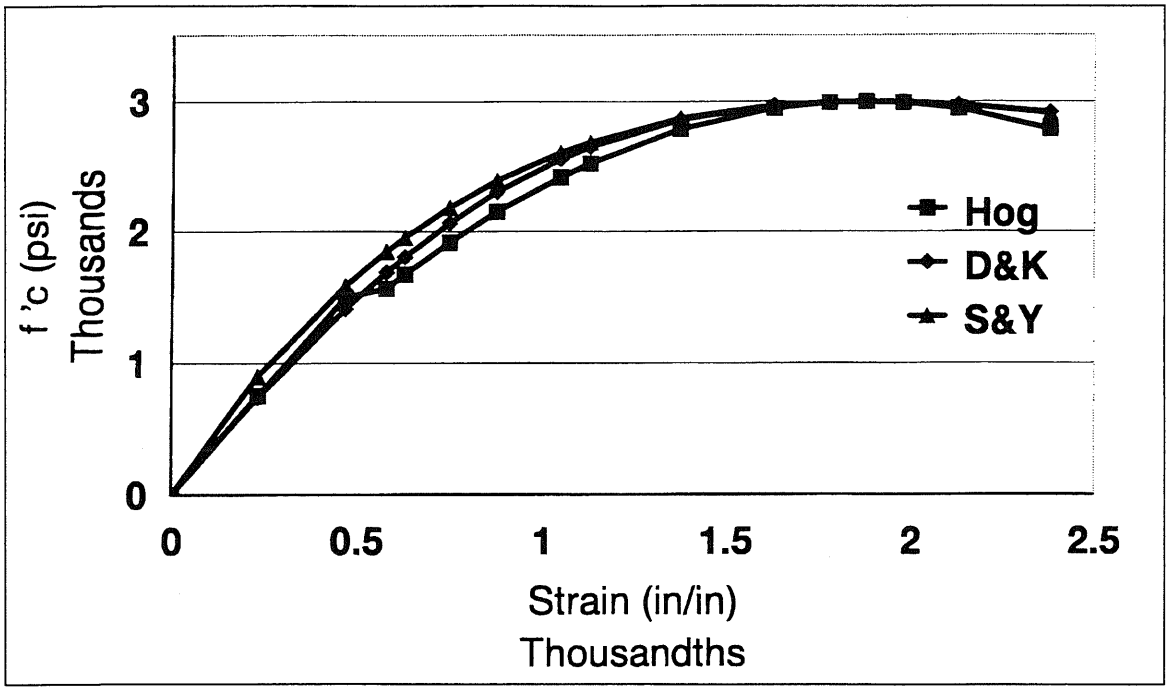

Figure B.8. Comparison of Stress-Strain Curves for Hognestad, Desayi-Krishnan, and Smith-Young for $f'_c = 3000$ psi

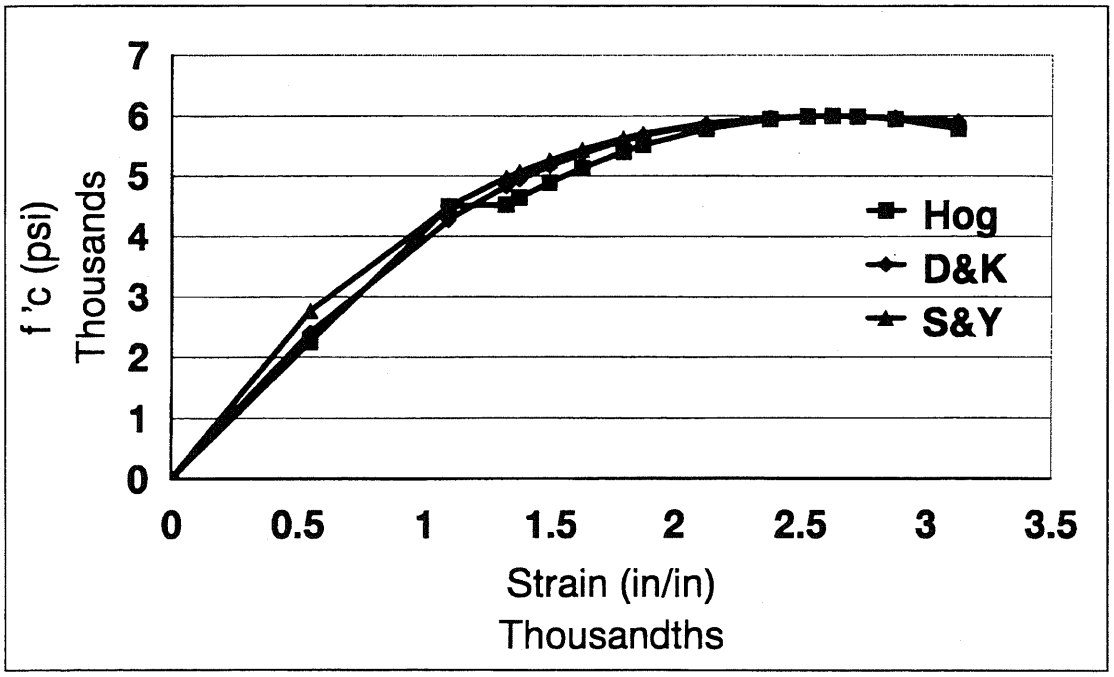

Figure B.9. Comparison of Stress-Strain Curves for Hognestad, Desayi-Krishnan, and Smith-Young for $f'_c = 6000$ psi

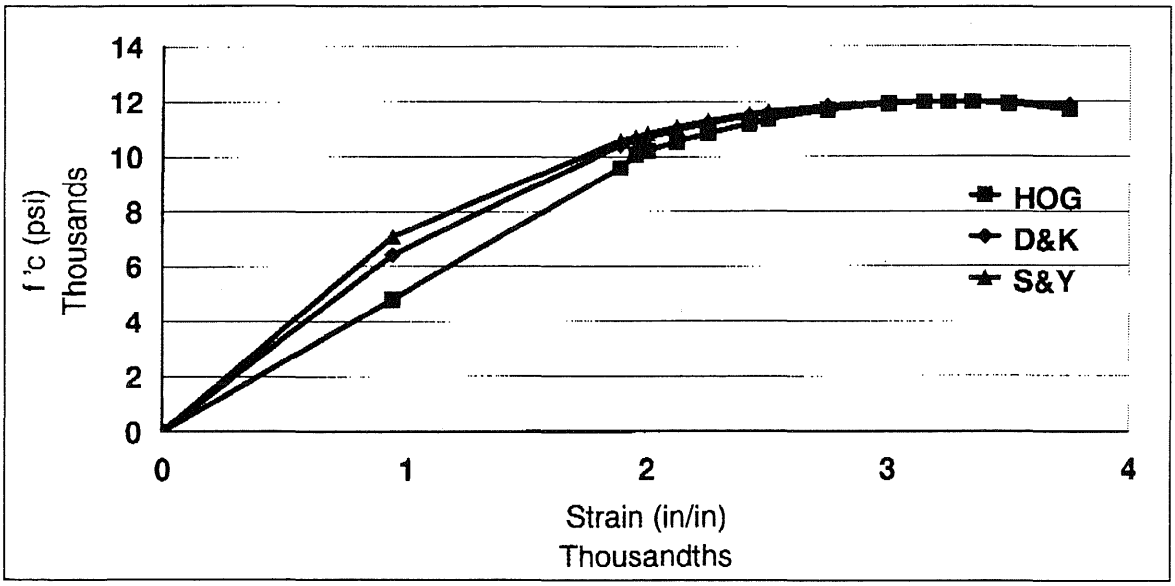

Figure B.10. Comparison of Stress-Strain Curves for Hognestad, Desayi-Krishnan, and Smith-Young for $f'_c = 12{,}000$ psi

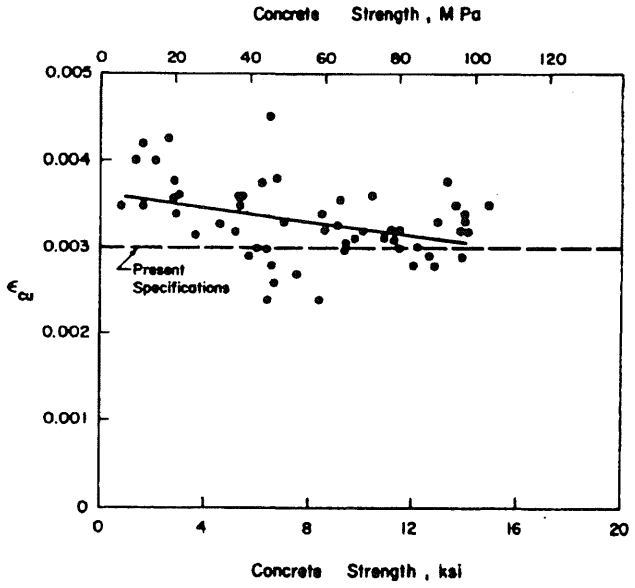

Figure B.11. Ultimate Concrete Flexural Strain ε_{cu} Versus Concrete Compressive Strength (ACI 363, 1992)

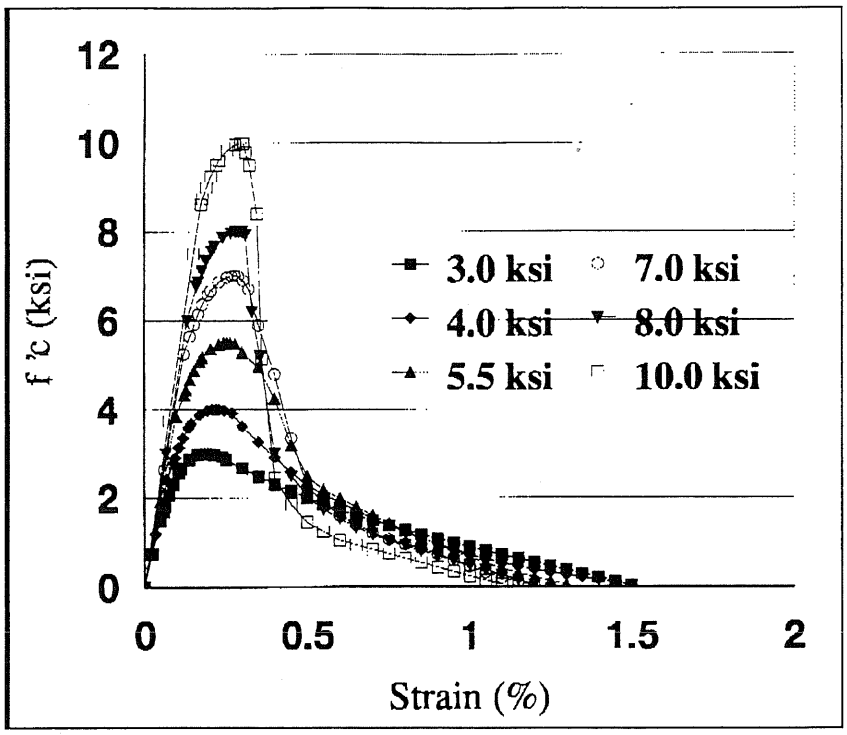

Figure B.12. Compressive Stress-Strain Curves up to $f'_c = 10{,}000$ psi

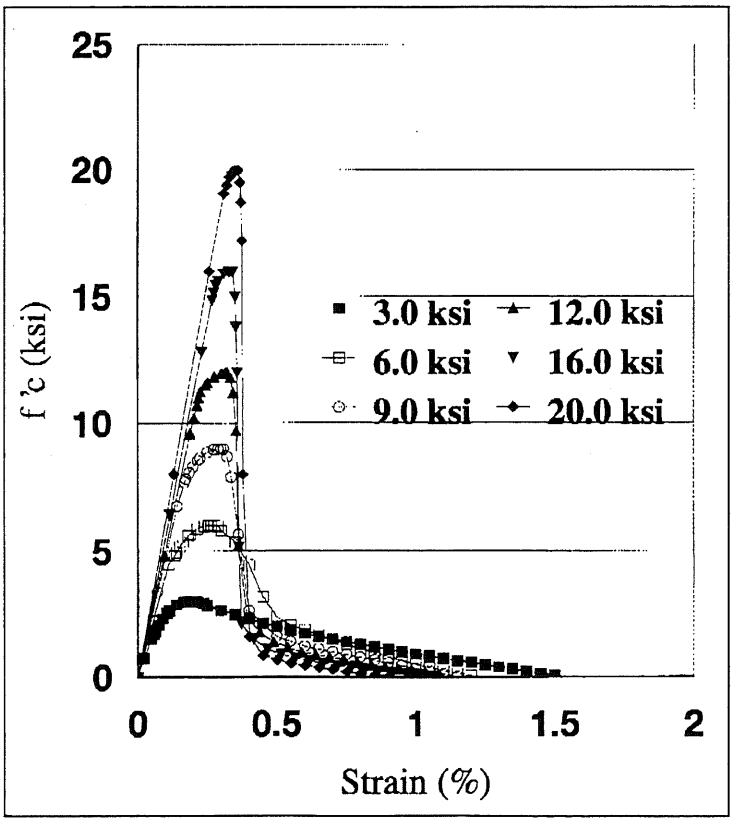

Figure B.13. Compressive Stress-Strain Curves up to $f'_c = 20{,}000$ psi

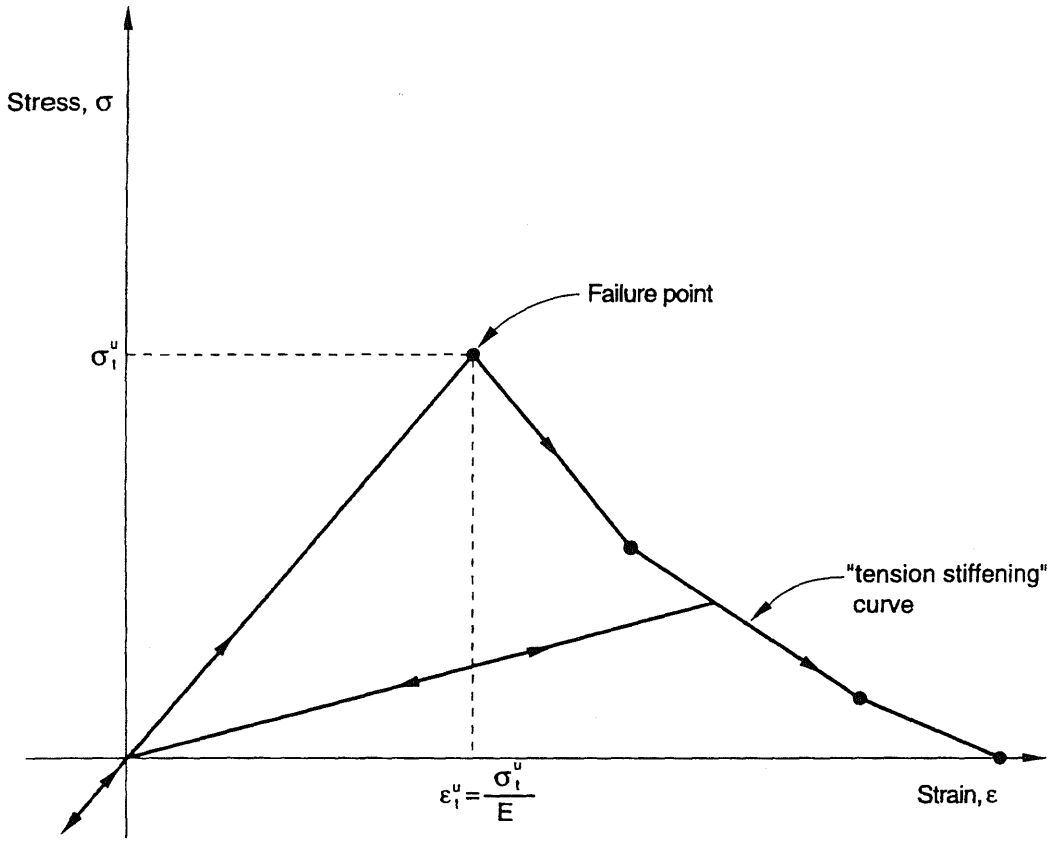

Figure B.14. "Tension Stiffening" Model (Hibbitt et. al., 1996)

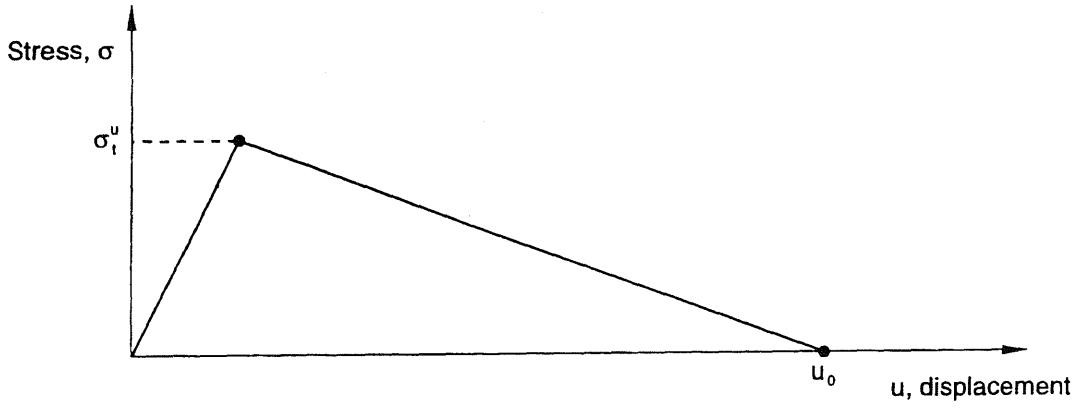

Figure B.15. Fracture Energy Cracking Model (Hibbitt et. al., 1996)

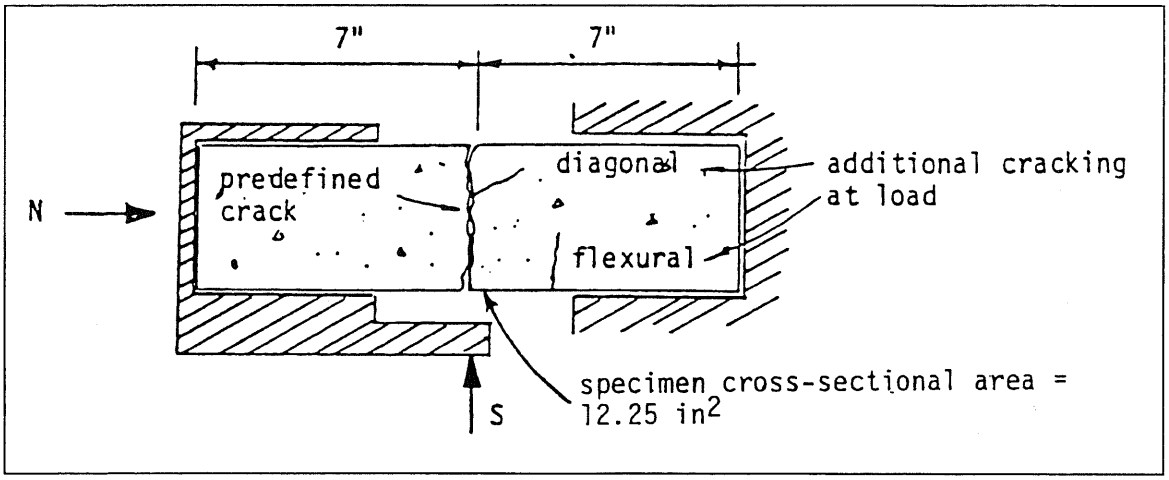

Figure B.16. Aggregate Interlock Test Specimen (Fenwick and Paulay, 1968)

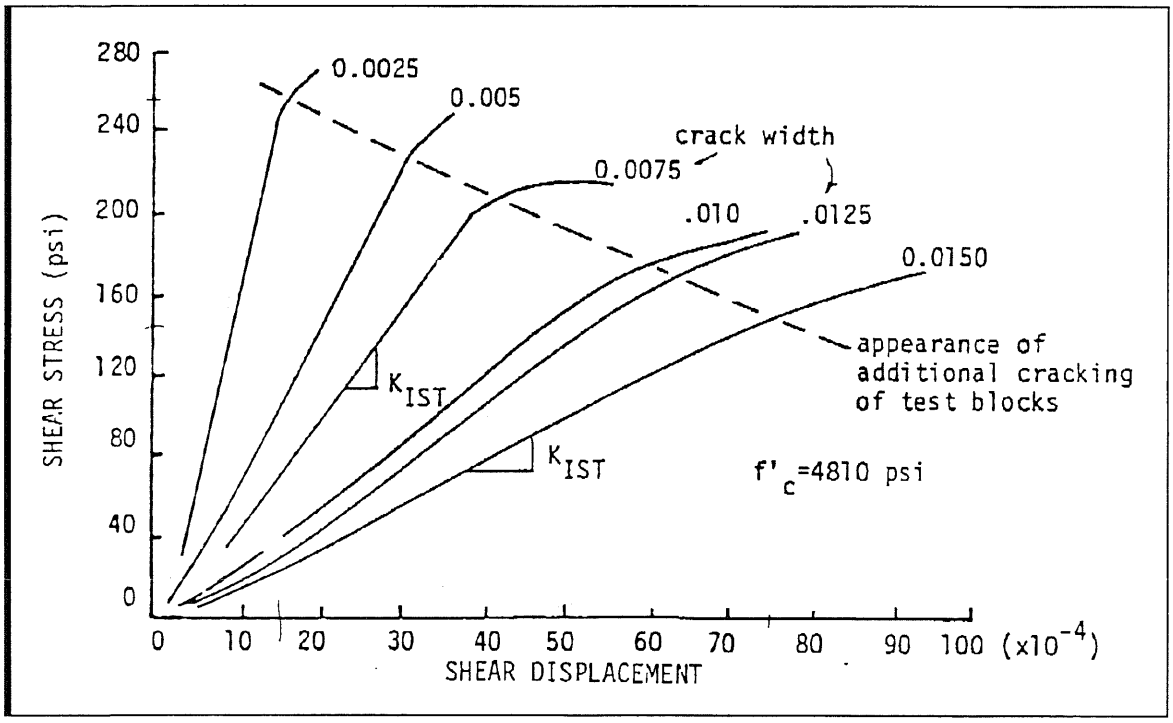

Figure B.17. Shear Stress-Displacement Curves (Fenwick and Paulay, 1968)

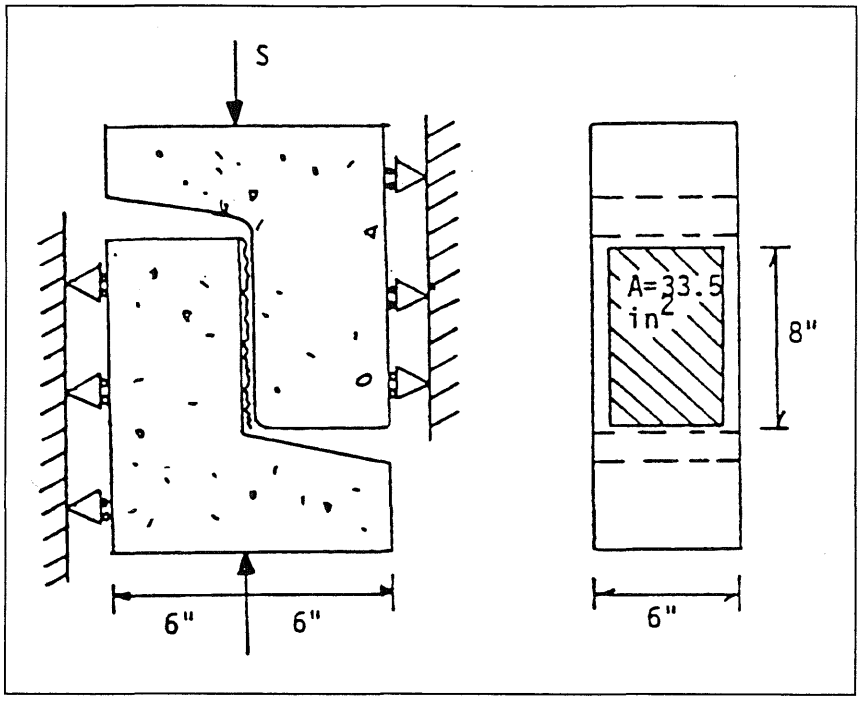

Figure B.18. Test Specimen (Paulay and Loeber, 1974)

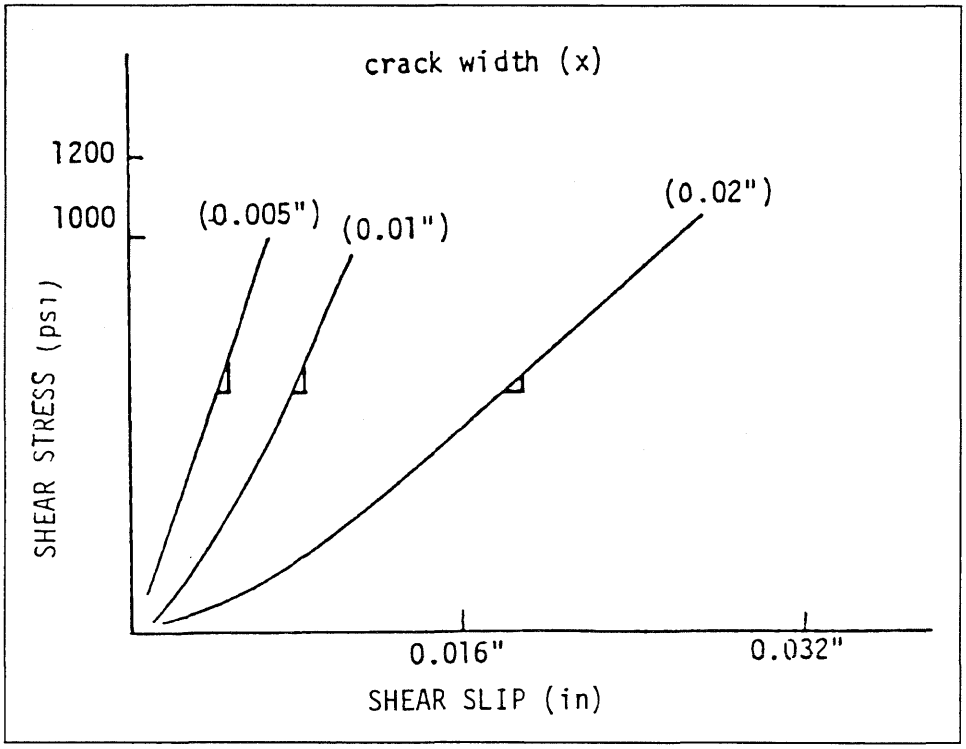

Figure B.19. Shear Stress -Shear Slip Curve (Paulay and Loeber, 1974)

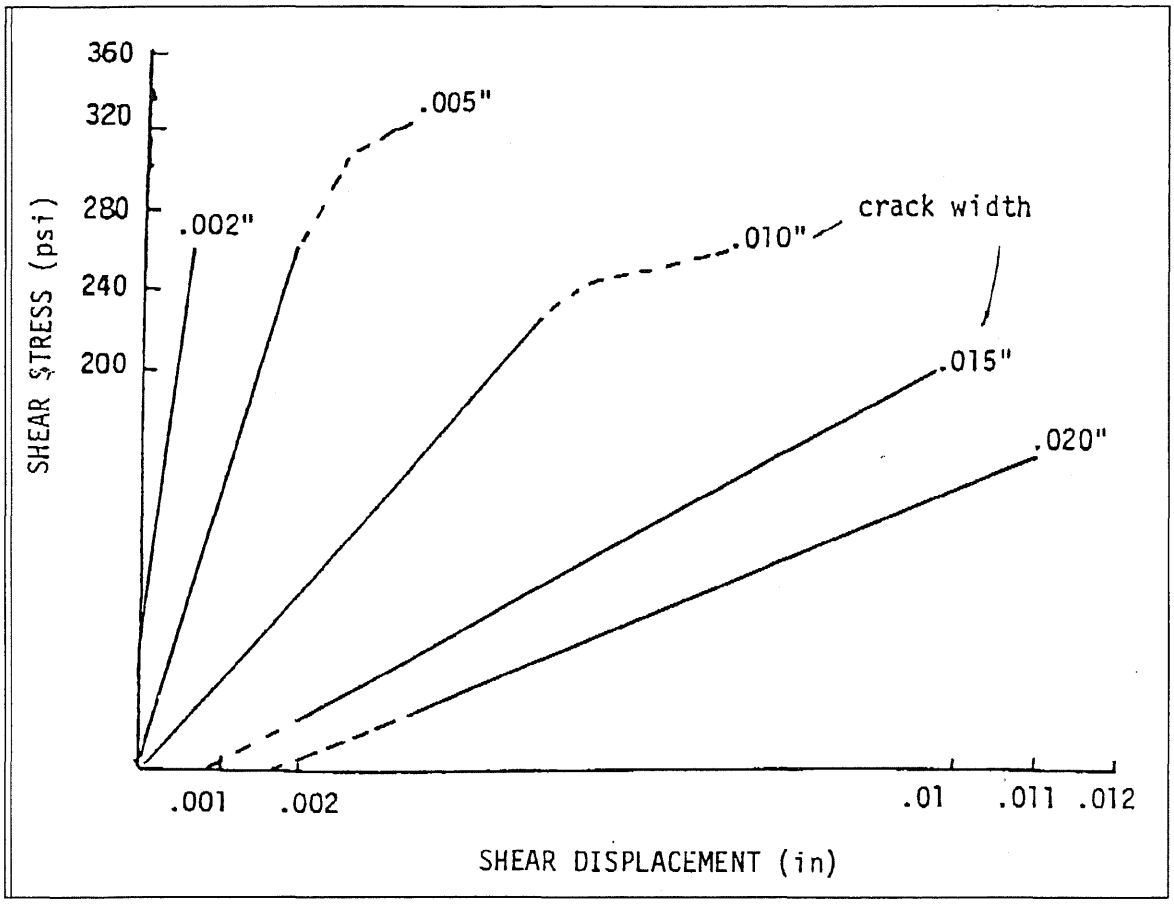

Figure B.20. Typical Displacement Curve (Houde and Mirza, 1974)

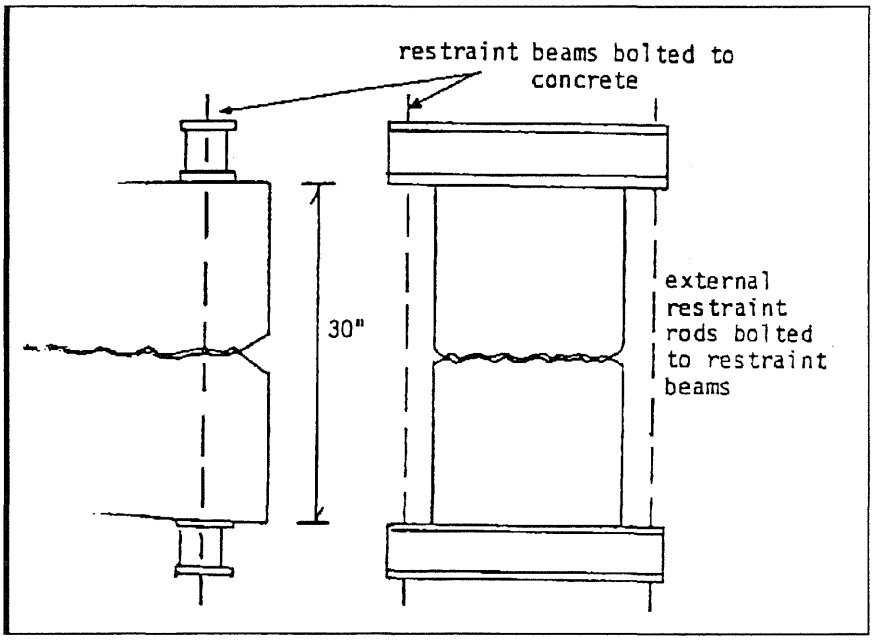

Figure B.21. Test Specimen Configuration (White and Holley, 1972)

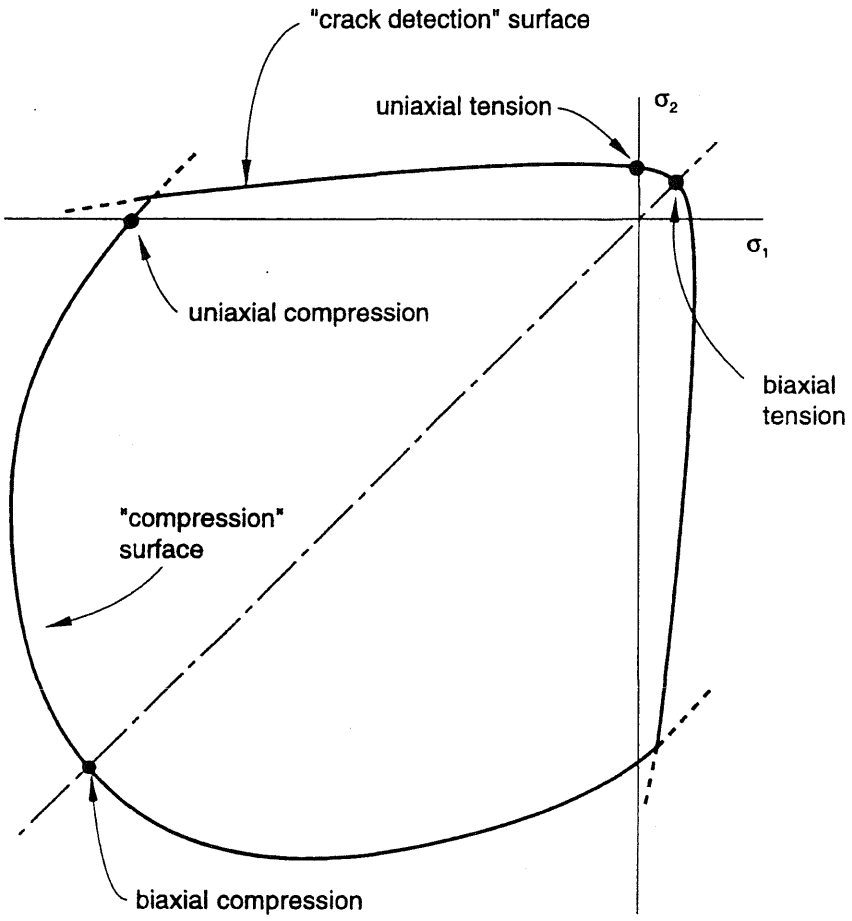

Figure B.22. Yield and Failure Surfaces in Plane Stress (Hibbitt et. al., 1996)

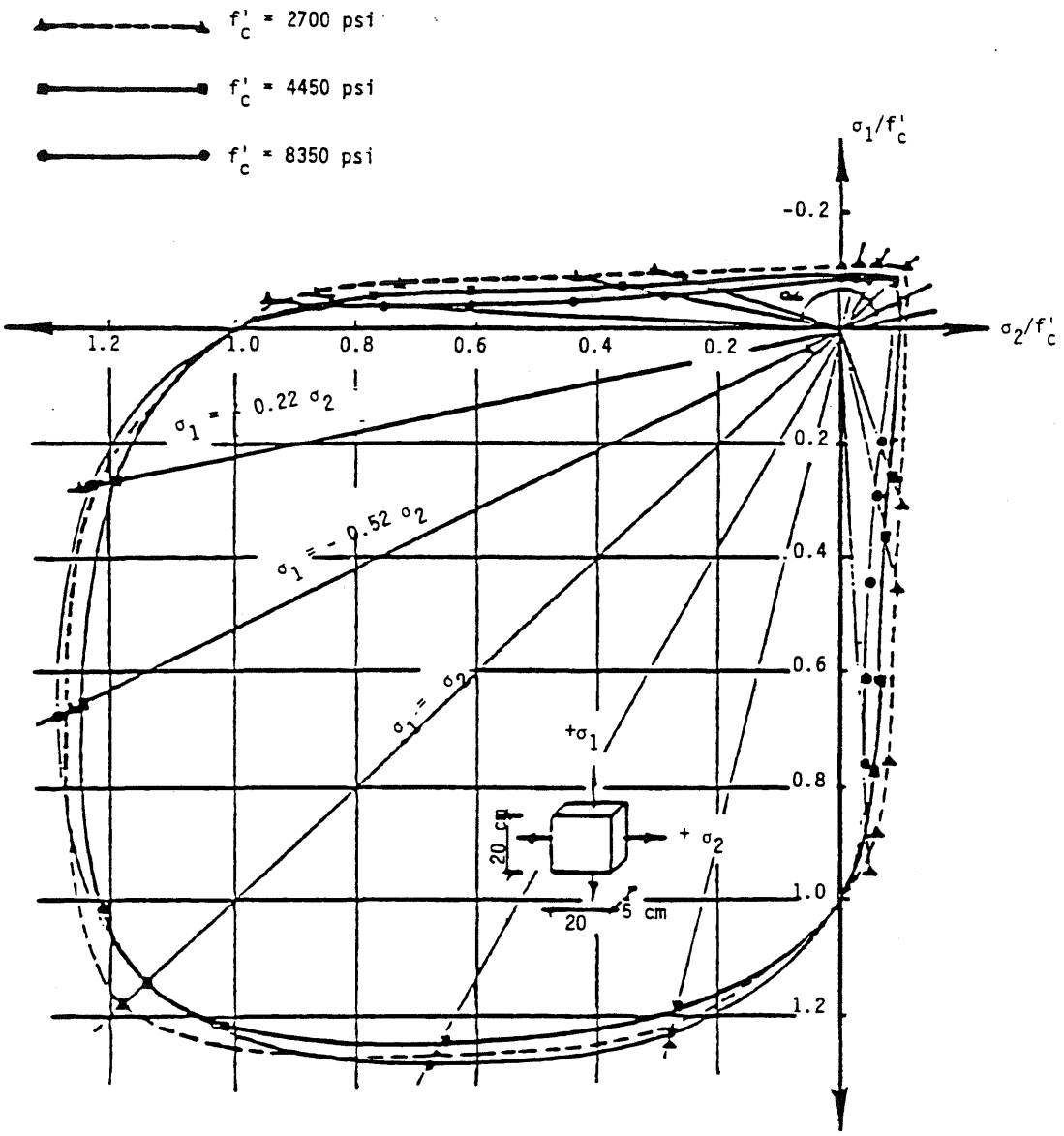

Figure B.23. Typical Biaxial Strengths of Plain Concrete (Hegemeir et. al., 1985)

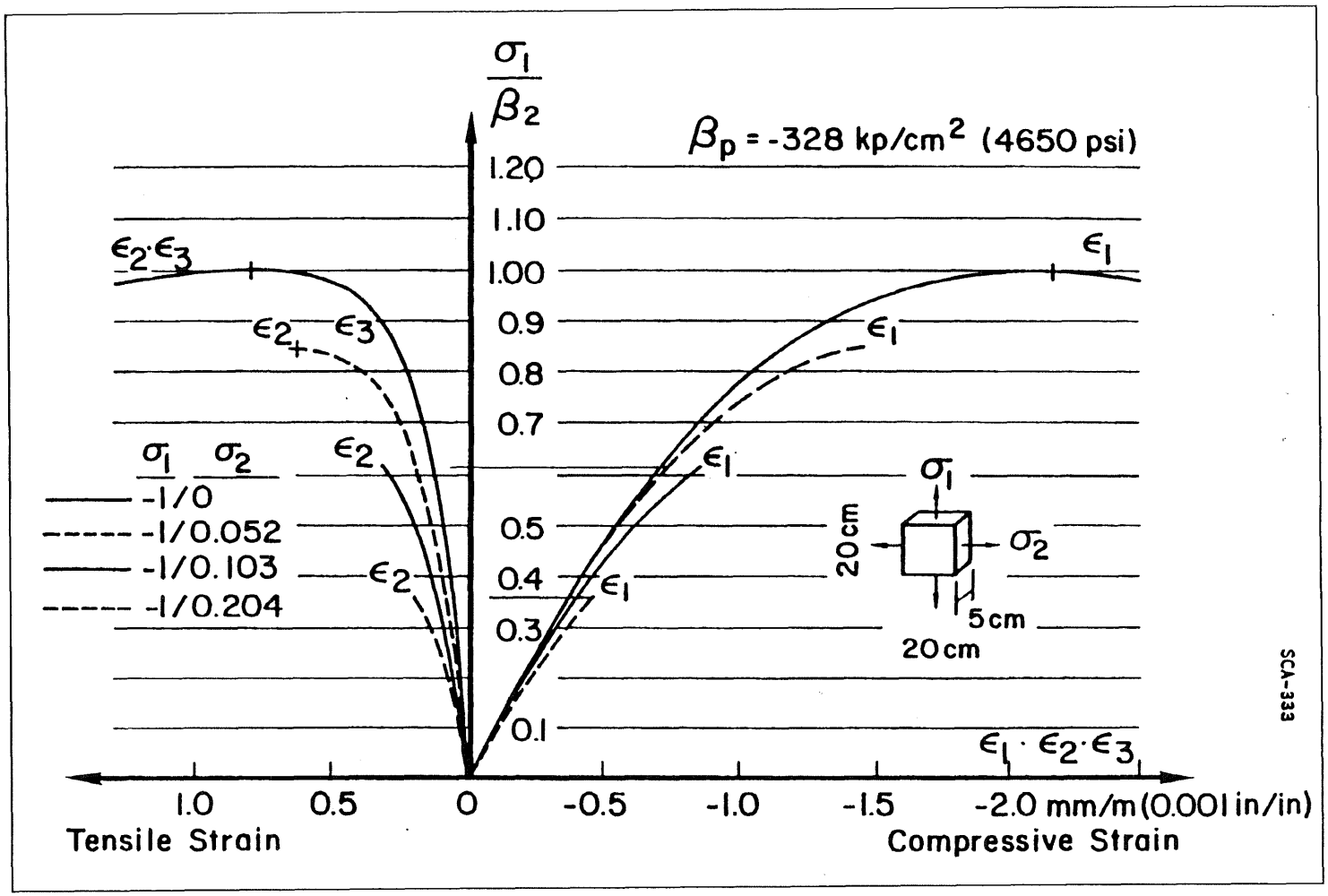

Figure B.24. Biaxial Compression-Tension Response (Kupfer et. al., 1969)

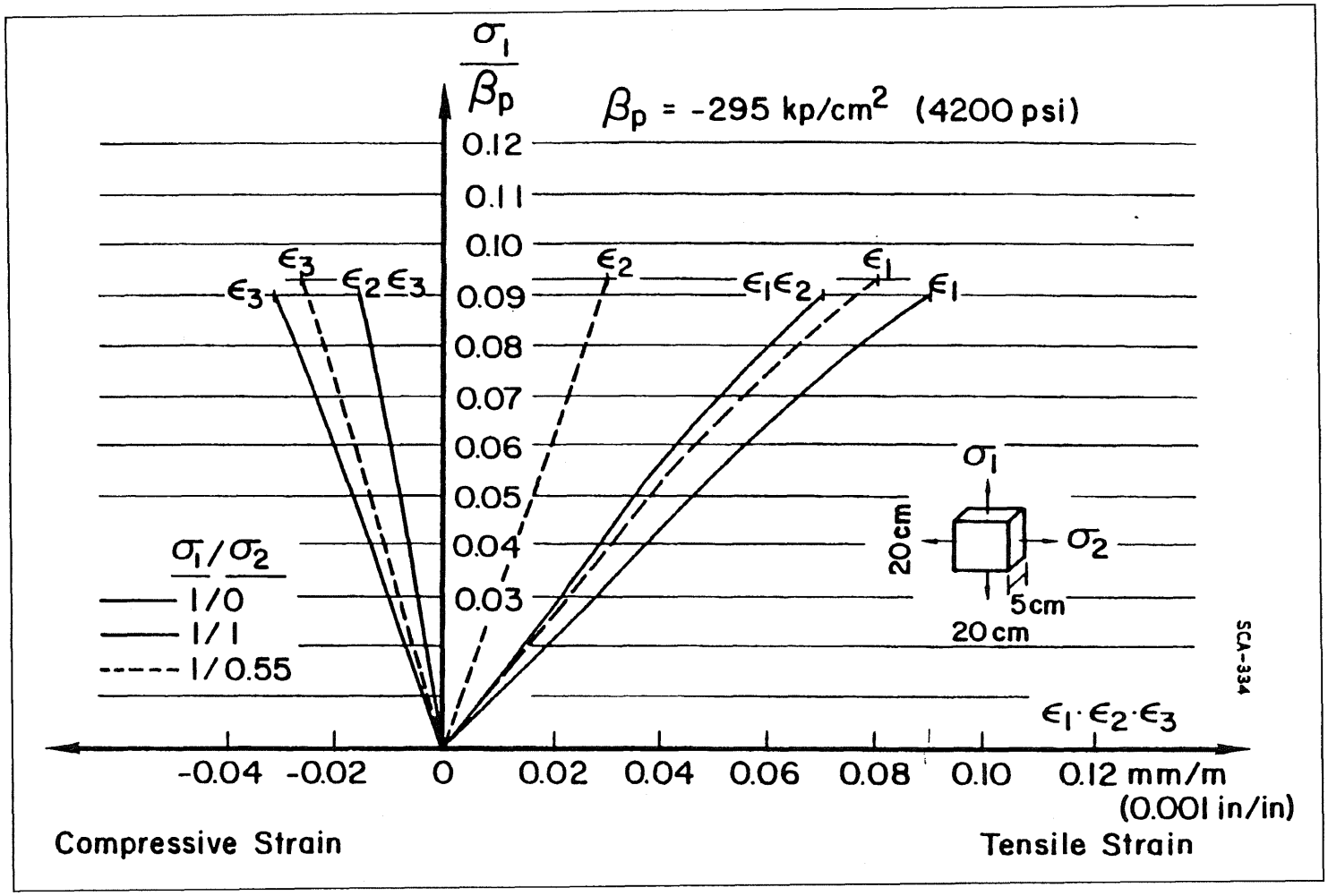

Figure B.25. Biaxial Tension Response (Kupfer et. al., 1969)

APPENDIX C

FINITE ELEMENT MODEL VERIFICATION

C.1. Introduction

A competent engineer completes numerous problem solving exercises and analysis and design projects. Through this journey, the engineer gains an appreciation for the behavior of structures and the equations associated with analyzing and designing structural elements. Usually beginning with hand calculations, the learning process quickly moves to computer programs capable of structural analysis and design. Any initial computer use is always checked against widely accepted hand calculations which are normally required by the professor. This thorough procedure provides the student with confidence in not only the structural elements, but also in the computer program itself. Now armed with this new knowledge, the engineer takes full advantage of the computers capability to perform the same predetermined steps accurately each time.

If the engineer decides to analyze a new type of problem or even use a newly developed finite element, which may be computationally more efficient or possibly more exact, he/she must verify the accuracy of the finite element and/or the entire computer program. The goal of each finite element computer program and its numerous subroutines is to allow the engineer to obtain results more efficiently and with greater accuracy. Normally new elements are developed to satisfy a certain type of loading/deformation situation or can be used in numerous structural problems such as plane stress, plane strain, axisymmetric, etc. The validity of any analysis, especially for structural issues with little or no available experimental data, depends heavily on the engineers evaluation of, and confidence in, the material, kinematic, loading, and finite element models to include program subroutines within the computer analysis package.

This current discussion begs the question: "What type of program is necessary to analyze laterally restrained reinforced concrete one-way slabs?" A large number of Direct Stiffness Method (DSM) programs which provide fairly accurate results for frame type structures have been used by engineers for quite some time, but the frame elements, consisting of beam/column

elements, do not always provide enough detail through the thickness for proper analysis of complex stress fields, especially at the supports. Additionally, these programs only instantaneous load the structure instead of allowing for gradual loading. Nor do the DSM programs allow for externally generated in-plane forces, except through the center of the element where the only node is, or through an external moment which is equivalent to an axial load with an eccentricity. These primary limitations necessitate the consideration of a finite element program with more than beam and shell elements, such that detailed meshes of stress/displacement elements, especially through the thickness, can capture possibly important stress/strain fields. The finite element program ABAQUS was chosen because of its inherent capabilities for both gradual static loading and dynamic analysis, a fairly robust concrete material model, and its availability at the University of Illinois through the National Center for Super-Computing Applications (NCSA).

C.2. The Finite Element

Numerous elements are available within ABAQUS, but based on the type of structure to be analyzed such as the slab/slab strip, the beam, shell, plane stress/strain, and continuum elements were initially considered. The beam and shell elements may not be ideal for many of the same reasons for not using a DSM program for this research effort. They have limited edge loading conditions and stress field details. However, even though these elements do not appear to provide the required detail through the thickness and are the best elements for slender beams and very thin slabs (i.e., tensile membrane action only), the beam and shell elements did provide initial results on the entire load-deformation curve including compressive and tensile membrane behavior. The available behavioral detail from these beam and shell elements will be compared with the results provided by continuum elements.

The plane stress/strain elements are not practical based on the detailed meshing and unfavorably large aspect ratios required to properly define the stress/strain fields through the depth of the slab strip at the support, and the very limited reinforcement techniques. What remains is the

extremely flexible solid continuum elements which are the standard volume elements and most comprehensive of the element libraries within ABAQUS.

The ABAQUS solid (i.e., triangular, quadratic, and brick shaped) elements can be homogeneous or layered with different materials, and used for linear and/or nonlinear analysis. However, upon closer review of each element, the 3D brick continuum element is the element of choice. The triangular and tetrahedral elements cannot be used with the rebar smearing option, are overly stiff, and exhibit slow convergence such that they require extremely fine meshes for stress analysis. Even if the rebar is modeled discretely, the number of required elements makes the placement of the rebar very difficult. As will be shown later, the finer the mesh, the greater the occurrence of element instability because of the crushing and cracking of the concrete. The quadratic (2D) elements are essentially the same as the plane stress/strain elements discussed earlier and placing rebar in the longitudinal direction would be limited to discretely placing a single rebar between elements connected at the nodes along the 2D element sides.

The hexahedral (3D bricks), or more exactly to the second-order C3D20 brick elements, capture stress concentrations more effectively and, therefore, are better in bending dominated problems. ABAQUS provides an effective comparison of linear and quadratic continuum elements in a simple bending problem, a slender cantilever (Figure C.1). The variation of the number of elements along the length and depth (Figure C.2) demonstrated the better performance of the quadratic elements, CPS8 and C3D20, during flexural behavior (Table C.1, Part 1). The linear elements, CPS4 and C3D8, performed poorly because of shear locking and hourglassing.

Since the mesh will be regularly shaped with no initially distorted elements, the reduced-integration bricks or C3D20R elements with 8 integration points can provide results that are just as accurate (Table C.1, Part 2) as the fully integrated bricks or C3D20 elements with 27 integration points for 3.5 times the computational savings in forming the element stiffness matrix. The mass matrix and distributed loading still require full integration. Additionally, second-order bricks do not have a difficulty with hourglassing or shear and volumetric locking. There are hybrid elements

to use with incompressible material behavior and incompatible mode elements to improve first-order element bending behavior in large strain problems which will be discussed later.

C.3. Verification

In ABAQUS, the user defines the concrete material model through Young's Modulus, Poisson's Ratio, the inelastic portion of the uniaxial compressive (f'_c-ε) curve, Tension Stiffening, Shear Retention, and Failure Ratios which define the biaxial failure curve (Appendix B, ABAQUS Input Parameters). Since most of these parameters vary according to f'_c, the development of the uniaxial compression curve and the element's performance defined by this stress-strain curve are crucial to obtaining plausible results. The uniaxial compressive curve is defined first, by the peak elastic stress in which the associated strain is determined using Young's Modulus, and secondly, by sequential inelastic stresses and the accumulative inelastic strain.

C.3.1. Simple Mechanics Problem

A simple mechanics problem was chosen to validate the basic tenets of the concrete model within ABAQUS. The single element block of concrete was tested in compression and tension using beam and continuum elements (beam elements performed similarly to the continuum elements).

C.3.1.1. Compression

A 10"x10"x1" homogeneous block was modeled by a single brick element (i.e., C3D8, C3D8I, C3D20, C3D20R, CPS8) and loaded in compression by a uniformly distributed load (Figure C.3). During elastic loading levels, the compressive stress/strain should be directly proportional to the load. Once the load develops a stress within the inelastic range, the increase in strain should be greater than the proportional increase in stress. The material should not develop an average stress greater than the peak compressive/tensile stress and should have a marked decrease in load carrying capacity with increasing strain once peak stress is reached.

Example problems presented in ABAQUS only show the uniaxial compressive curve being defined by the peak elastic stress and the ultimate peak stress with associated inelastic strain. The initial analysis of the simple mechanics block was analyzed using this two-step definition of the uniaxial compressive curve. The STATIC RIKS method which increments the loading was used to capture the behavior of the structure during loading. Using either the 8-node or 20-node quadrilateral/brick, the elastic behavior matched generally accepted solid mechanics equations for

$$\sigma = \frac{P}{A} \qquad \text{EQN C.1}$$

$$\varepsilon_{33} = \frac{\sigma_{33}}{E_c} \qquad \text{EQN C.2}$$

$$\varepsilon_{11 \text{ or } 22} = \upsilon\varepsilon_{33} \qquad \text{EQN C.3}$$

$$u_{33} = \varepsilon_{33} l_3 \qquad \text{EQN C.4}$$

stress (EQN C.1), strain (EQN C.2), lateral strain (EQN C.3), and displacement (EQN C.4) (Table C.2, Part 1). The loading function provided uniformly distributed loads to the element surface and the element stress at all integration points matched the distributed loading. With the onset of inelastic behavior, the increase in stress was less than the resulting increase in strain.

The 8-node brick never reached the ultimate stress before the RIKS method changed loading direction because of non-linear geometric and/or material behavior (i.e., unloaded the structure). A property of the material model that was observed during this reversal of loading was that during unloading the element correctly maintained the developed inelastic strain. Decreasing the maximum time step provided limited assistance in continued loading along the stress-strain curve. Even if the element rapidly jumped past the peak stress, the element should have continued to strain similar to the f'_c-ε curve while the stress decreased. Only the inclusion of the NLGEOM

parameter within ABAQUS or use of the C3D8I (i.e., I means incompatible mode) brick allowed for loading the structure to the ultimate inelastic stress. Once the peak stress was reached by using either the 8-node or 20-node brick, the structure continued to strain while maintaining the peak stress (Table C.2, Part 2). This behavior may be acceptable if the structure was in a triaxial state of stress or had heavy shear confinement, but it was not. Additionally, the stresses and strains in the unloaded directions did not display the appropriate values for a triaxial state of stress. It is therefore necessary to define the entire uniaxial compressive stress-strain curve for this research effort for each compressive strength out to a satisfactory strain of 0.01-.012 in/in (Table B.2, Appendix B).

Using a properly defined uniaxial compressive stress-strain curve and the NLGEOM parameter, the eight-node brick, C3D8, performed satisfactorily (Table C.2, Part 3). Using a maximum time step of 0.01 provided more detail through smaller time steps than a maximum time step of 0.05, but it required more computer time and increments to develop the same level of ultimate strain at the same ultimate stress. The C3D8I brick performed better than C3D8 brick without the NLGEOM parameter, but it required an tremendous number of time increments (i.e., >8000) to reach the desired level of peak strain. Using the NLGEOM parameter with the C3D8I element provided the same level of performance as the C3D8 brick with the NLGEOM parameter, but the stress/strain values fluctuated at the integration points once the compressive strain passed 0.004 in/in on the descending portion of the completely defined stress-strain curve.

The twenty-node brick (C3D20) also performed satisfactorily using full integration, a maximum time step of 0.05, and including the NLGEOM parameter within the analysis (similar results to Table C.2, Part 3). The stress/strain values determined at all integration points matched calculations throughout the elastic range and were identical at all the integration points during each increment of loading until the compressive strain reached 0.004 in/in, which was similar to the C3D8I element. At a compressive strain of 0.004 in/in, the accompanying lateral strain due to Poisson's effect began to develop tension stress large enough to generate cracking. Continued straining led to even greater disparity between values at the different integration points due to the

instability caused by the concrete crushing and cracking. The element behavior continued to generally follow the f'_c- ε curve until reaching an average strain of 0.009 and a load of 750 psi where the analysis stopped because of too many attempts to establish equilibrium (i.e., too much damage).

Since most concrete structures include some reinforcement, longitudinal steel areas of 0.01, 0.05 and 0.1 in^2 were added with the anticipation that it would increase the load carrying capacity and stability at increased straining levels. The reinforcement was effectively a smeared layer onto the concrete element similar to a composite layer. The load carrying capacity increased with each increase in the rebar cross sectional area, but the instability was either not affected or initiated at an earlier point along the descending portion of the stress-strain curve (Table C.2, Parts 3 through 6). The peak capacity occurred once the reinforcement yielded and the concrete was at maximum compressive strength. The element carried less load as the rebar continued to yield and the concrete continued through the descending portion of the stress-strain curve. With the initiation of fluctuations of stress and strain values at the integration points within the element, the RIKS method changed direction on the load path and unloaded the element which was noted by the decrease in displacement.

In an additional effort to increase stability, transverse steel ($A = 0.005$ in^2) was included in both lateral directions (Table C.2, Part 7). The longitudinal steel was $A_s = 0.05$ in^2. The inclusion of lateral reinforcement increased the load capacity to that of $A_s = 0.1$ in^2, but the instability continued and the behavior was similar (Table C.2, Parts 6 - 7). The 2D continuum element, CPS8 (Table C.2, Part 8), was investigated based on the performance shown in Table C.1. Its performance was comparable to the 3D continuum element with a tremendous savings in computational time, but longitudinal reinforcement could only be included discretely at the nodes between elements which results in placement of only single rebars. It will be shown later in C.3.2. Jain and Kennedy Slab that a single rebar versus a layer develops as expected a slightly different result.

C.3.1.2. Tension

To investigate pure tensile behavior, the loading was reversed on the element. The material model performed exactly as expected. At a stress defined by the ratio between peak tensile stress and peak compressive stress defined by the Failure Ratios in ABAQUS, the concrete cracked and began unloading while continuing to strain (Table C.2, Part 9). The load carried by the concrete dropped to an extremely small value while continuing to strain to 10 times the cracking strain. In this simple model, the entire structure was unloaded at this point. Looking at the fully cracked tension zones in a flexural problem, the strain continues well past 10 times the cracking strain while the concrete maintains a very small tension stress (i.e., tension stiffening). With the addition of reinforcement, the behavior was similar with the following exceptions: more tensile load capacity due to the presence of the rebar; rebound in load capacity due entirely to the rebar after the initial drop in load when the concrete cracks; and ultimate capacity determined by the yield strength of the rebar (Table C.2, Part 10).

C.3.1.3. Summary

Upon consideration of all these ABAQUS results, the concrete model in ABAQUS will perform satisfactorily during uniaxial loading when using correct analysis options such as NLGEOM, a maximum time step less than or equal to 0.05, etc. Low compressive loads produced linearly-elastic stresses, strains, and displacements. Larger compressive loads produced inelastic behavior with the stress never exceeding the peak compressive stress of the defined stress-strain curve. Once the strain exceeded the strain associated with peak stress, the stress decreased while the strain increased The sum of the reactions equaled the distributed load multiplied by the top surface area. An interesting note was that the loading initially produced an outward movement, as expected, of the roller supports. Increasing the load eventually produced inward movement of the roller supports. Fixed supports would have affected the stress field when the initially compressive and then tensile lateral stresses developed near the support areas.

It is important to completely define the stress-strain curve. If the stress-strain curve arbitrarily stops at a defined peak strain of 0.003 to 0.0038 depending on the source (Appendix B), the model in ABAQUS will maintain the associated stress while continuing to strain past the defined peak strain, which is similar to confined concrete behavior. This behavior is satisfactory if the boundary, loading or reinforcement conditions develop a triaxial state of stress for all elements.

The fact that the analysis stopped when the program completed too many equilibrium attempts is great. However, if the element would simply lose capacity to carry stress when a capability was exceeded, it would be better in some instances. It is always important to know when instability due to excessive cracking/crushing occurs in concrete. Based on the results of the compressive loading of the simple mechanics block, the model will begin to develop excessive cracking when the lateral tension stress/strain due to Poisson's effect intersects the tensile failure surface of the defined biaxial failure surface. When considering flexural behavior in reinforced concrete members with excessive cracking, the cracks could be either completely through the elements such as in flexural tension areas, or the result of actual crushing or pop outs as in flexural compression areas where there is cracking through the element due to laterally induced strain. This observation prompts the next required investigation.

C.3.2. Jain and Kennedy Slab

The Jain and Kennedy (J-K) one-way slab is an example problem in ABAQUS to present the effectiveness of tension stiffening in simulating the load transfer across cracks. Eventually the tensile force travels through the rebar after the crack fully forms. Since the example provided an excellent comparison between the ABAQUS model and the experimentally derived load-deformation curve for a one-way simply supported slab, the data and model were used initially to develop a better understanding of ABAQUS, the STATIC RIKS loading method, required input/output, all facets of the concrete material model, rebar placement, and a flexural loading comparison of beam versus continuum elements.

C.3.2.1. J-K Beam Modeled Slab

In the ABAQUS example, one-half of the slab (i.e., 15"x18"x1.5") was modeled with five beam elements, with the stress-strain curve only defined up to peak stress/strain and a single smeared rebar in the center of the cross-section (i.e., a layer over entire element width) (Figures C.4 and C.5). The STATIC RIKS command was used to capture the material/geometric non-linearity of the slab's behavior through incremental static loading, which was similar to the hydrostatic loading employed at WES. Since this ABAQUS example only desired to examine early loading behavior, the effect of only defining the stress-strain curve up to the peak stress was never an issue. A completely defined stress-strain curve (Figures B.12 and B.13, Appendix B) and compression rebar (i.e., doubly reinforced) were added to the input file to set conditions similar to future research cases. Initial comparisons were extended only to the extreme boundary conditions of simply- and fixed-supported cases using beam and continuum elements.

The beam modeled slab was analyzed first. Two conditions were set for recording results: initiation of tension steel yielding and a deflection of two times the depth or 3.0 inches for the simply-supported slab. For the fixed-supported slab, the point marking the initiation of tension membrane action was also noted. The first variation concerned the optimum number of beam elements (i.e., 2-node linear beam element) along the half length. Two through fifteen beam elements along the half-length provided aspect ratios of 2.5 to 18, respectively. The results are located in Table C.3.

The theoretical load capacities for the simply-supported case came directly from Park and Paulay. For singly and doubly lightly-reinforced sections, the load capacity should be approximately 3.5 and 3.7 psi, respectively (Figure C.6). Using two to 15 elements provided acceptable load capacity results. All capacities were close to these two values, but using three or five beam elements provides the closest results for the doubly reinforced section, 3.78 and 3.66, respectively (Table C.3, Part 1). These results compare well with the J-K experimental results of 3.9 psi (Hibbitt et. al., 1996). The deflections can only be accurately compared while the concrete behavior remains elastic.

The theoretical load capacities for the fixed-supported case are from Park and Paulay (1975) and Park and Gamble (1980). The load capacity from Park and Paulay of 7.4 psi using yield line capacity greatly under-estimates the true capacity since it ignores the enhancements due to in-plane forces (Figure C.7). Park and Gamble provides an analysis using the modified rigid-plastic method for laterally restrained slabs with the load capacity at 14.8 psi (Figure C.8). Park and others note that the method could over-estimate the true capacity if the peak capacity deflection is not used as an index with the method (i.e., 14.8 psi is the computed peak point capacity, Figure C.9). Upon comparison with the ABAQUS results for beam elements, it appears that using two to three elements may be too stiff in the fixed-supported case (Table C.3, Part 2). The results of 16.8 to 20.1 psi for 15 to 5 elements, respectively, appear to be converging to an average value of around 17 psi for fully rigid boundaries. The axial force-moment interaction diagram should provide some capability to estimate the load capacity. Using the in-plane forces generated during the ABAQUS analysis, which are less than P_{bal} (Table C.3, Part 2), in the interaction equations will provide an enhanced moment capacity (Figures C.10 and C.11). The in-plane load capacity was 16.8 to 17.7 psi when using the enhanced moment at each end for the moment capacity in the yield line equation (Figure C.7). The key to this method is the magnitude of the generated in-plane forces. When considering the aspect ratios, it appears that 10 to 15 elements provides a reasonable upper and lower limit.

The important development was the ability to observe the complete load/resistance process of fixed beams/slabs when loaded to failure. First the beam/slab resisted the load through compressive membrane behavior based on the available stiffness of the supports. This load capacity was nearly twice as large as the capacity from yield line theory. Once the peak capacity was reached, the load dropped off rapidly because of snap-through while the structure continued to strain/displace. If the available reinforcement ratio is large enough to catch the structure and the fixed supports are capable of resisting tensile forces, the load capacity will increase based on tension membrane behavior through catenary action of the reinforcement until yielding of the rebar. Since the reinforcement defined in ABAQUS will not break, the ultimate load will eventually

plateau. However, the strain must be watched to prevent excessive strain from affecting the results.

C.3.2.2. J-K Continuum Modeled Slab

The first priority was to conduct an element parameter study to further validate the ABAQUS results (C.2. The Finite Element) with the two extremes of this study: simply- and fixed-supported conditions. The elements C3D8, C3D8I, C3D20, and C3D20R were compared, while modeling one-half of the J-K Slab with a varying number of elements along the length (i.e., 1, 3, 5, 10, 15 elements), width (i.e., 1, 3, 6, 12 elements) and depth (i.e., 1, 2, 6, 15, 30 elements) (Figure C.12). The number of elements used in a model will be given by length/width/depth in the table. As a part of this effort, a study of how to best model the reinforcement was completed with the first five models using the elements C3D8, C3D8I, C3D20 and C3D20R. The reinforcement was modeled as a single bar, six bars, and a smeared layer. Similar results were determined for each element so the results for the 20 node element, C3D20, are presented in Table C.4 with the same model analyzed without any reinforcement (i.e., "n"). The "r" presented with the increment represents using the reduced integration scheme or the C3D20R element and the number in the parentheses represents the method of modeling the reinforcement (i.e., 1-one bar, L - layer, etc.). The use of six bars or a layer of reinforcement provided the same results. Efforts to use discrete modeling of the reinforcement provided the same results as the layer of reinforcement, but an extremely large number of elements was required. A very refined mesh eventually created convergence problems which is discussed next. Since the most efficient method of modeling the reinforcement is the layer option, it was the method of choice.

The results presented are only for the peak capacity or the final step provided during the analysis. In some cases the analysis stopped either because of too many attempts to establish equilibrium, or the time step required is smaller than 10^{-5}, or the analysis method began to unload due to geometric/material instability when the next increment missed the appropriate path. As will be seen in the comparison of the different elements for each finite element mesh (Table C.5), none

of the analyses using continuum elements was able to progress past the peak point, if the analysis reached that far. The termination point was close to the peak load capacity noted through analysis with beam elements (i.e., Table C.3 and C.5). Any unloading that occurred was accompanied by decreasing strain/displacement.

It appears that increasing the number of continuum elements along the longitudinal axis (i.e., decreasing the element size), decreases the distance the analysis proceeds along the load-deformation path due to equilibrium issues. In many past finite element efforts to analyze metal structures, increasing the mesh refinement normally improved the convergence of the analysis. In this case, the crushing action of the concrete creates large variations of stresses/strains at the integration points within the heavily damaged elements. Therefore, the larger the actual element, the longer it takes for most of the element to become completely damaged and the farther the analysis actually progressed. The smaller the element size, the quicker the element became damaged leading to equilibrium and stability problems.

C.4. Finite Element Analysis of a Previously Tested One-Way Slab

Roberts' (1969) RB18 slab was used to compare finite element analysis with experimental results (Appendix A). The experimentally measured peak compressive membrane capacity for slab RB18 was 15.6 psi at a deflection of 0.46 inches. The finite element results are listed in Table C.6 (beam) and Table C.7 (continuum). The best correlation for peak capacity was for 7 beam elements in the half-length, while the best correlation for deflection was for the peak thrust point using 3 beam elements. Increasing the number of beam elements in the half-length decreased the capacity and deflection at the peak point. The continuum results generated a smaller capacity with a 14.5 psi average, while the deflections were less than a third of the experimental results.

The beam element results denoted a peak point, while the continuum element results stopped before defining a peak point. The continuum elements do not display the stress and strain near the concrete surface compared to the beam elements since the integration points are at the element's quarter or third points for full or reduced integration, respectively. To obtain accurate

stress and strain values near the surface, a large number of continuum elements through the thickness would be necessary. However, decreasing the thickness of the elements by increasing the number of elements through the thickness within the heavily damaged areas where the readings are desired would further restrict the investigation since smaller elements would become fully damaged and unstable at a faster rate, and lead to earlier termination of the analysis.

C.5. Summary

ABAQUS appears to possess the sub-routines to properly analyze a laterally restrained one-way slab up to the peak compressive membrane capacity, but not into the tensile membrane zone, because of to much concrete damage associated with reaching the tensile membrane zone. The proper mesh of beam or continuum elements provides further insight through the stresses, strains, damage levels, etc. of a slab's behavior once the finite element capacity is matched with the empirical data at a known L/h ratio. To rely on finite element methods to predict structural capacity without some experimental correlation, especially at this level of extreme damage, does not appear prudent. The beam elements exhibit more stability and provided analysis farther along the load-deflection curve while normally denoting a peak capacity. However, too many beam elements also limits the analysis similar to using continuum elements.

Recently, an American Society of Civil Engineers (ASCE) paper by Famiyesin and Hossain (1998) points to acceptable finite element results using 3D degenerated layered shell elements for two-way slabs which appears similar to using beam elements for one-way slabs. They used two methods of analysis: displacement controlled (DC) or load controlled (LC). The DC method requires a previously determined load-deflection curve in which they used the results from Powell's 1956 thesis. Even though the shape of the finite element produced load-deflection curve is plausible and the peak capacity is a good match, the deflections are still off by an order of magnitude even though actual displacements were used in the analysis. The LC method also leads to realistic estimates of the peak capacity and deflection estimates that are off an order of magnitude. Additionally, there is no transition zone or decreased capacity in the LC method after

the peak capacity, which similar to only defining up the peak compressive strength and strain for the uniaxial concrete stress-strain curve in ABAQUS (i.e., triaxial stress case). Since neither method provides accurate deflection estimates, Famiyesin and Hossain used the LC method which was easier to employ and developed a displacement factor of 3.2 to increase the finite displacement results to correlate with empirical data from Powell (1956), Park (1964), and Hung and Nawy (1971).

Unfortunately, Famiyesin and Hossain's design charts only apply to very thin slabs (i.e. $L/h > 26$) which does not correlate well with the thicker slabs in this dissertation (Appendix A). If time is available at a later date, the author plans to continue to experiment with shell elements for one-way thick slabs ($L/h < 18$). The initial analysis with shell elements on thin slabs was not different from the results using beam elements.

If analyzing structures only loaded with service loads, the continuum element will provide greater flexibility and more detailed data than the beam element. Unfortunately, the structures of interest are being heavily damaged during compression membrane action and possibly loaded to rupture of reinforcement during the tensile membrane stage. Both the beam and continuum element were used to analyze slabs listed in Appendix A. Element removal, load removal, etc., were used with the continuum elements to increase the distance along the load-deflection curve afforded by the finite element analysis. However, only the results with the beam elements provided results usable within this thesis. Hopefully, in the near future mathematical algorithms will allow for an element to stop functioning (i.e., when crushing or pop-outs occur) while not stopping the entire analysis.

Table C.1. ABAQUS Continuum Element Comparison (Hibbitt et. al., 1996)

Element	Mesh Size (Depth x Length)			
	1 x 6	2 x 12	4 x 12	8 x 24
Part 1				
CPS4	0.074	0.242	0.242	0.561
CPS8	0.994	1.000	1.000	1.000
C3D8	0.077	0.248	0.243	0.563
C3D20	0.994	1.000	1.000	1.000
Part 2				
CPS4R	20.3	1.308	1.051	1.012
CPS8R	1.000	1.000	1.000	1.000
C3D8R	70.1	1.323	1.063	1.015
C3D20R	1.000	1.000	1.000	1.000

Table C.2. Mechanics Block ABAQUS Results

Inc. No.	Load (psi)	σ_{33} (psi)	ε_{33}	$\varepsilon_{11}=\varepsilon_{22}=\nu\varepsilon_{33}$	Inelastic $I\varepsilon_{33}$	Disp (in)	Remarks
Part 1							
5	50	-50	-1.567E-05	2.351E-06		-1.567E-04	
100	1000	-1000	-3.135E-04	4.702E-05		-3.135E-03	
200	2000	-2000	-6.269E-04	9.404E-05		-6.269E-03	
287	2870	-2870	-8.997E-04	1.349E-04		-8.997E-03	
288	2872	-2872	-9.032E-04	1.370E-04	-2.771E-06	-9.032E-03	
289	2873	-2873	-9.069E-04	1.396E-04	-6.370E-06	-9.069E-03	
319	2884	-2884	-1.013E-03	2.125E-04	-1.087E-04	-1.013E-02	
320	2875	-2875	-1.010E-03	2.120E-04	-1.087E-04	-1.010E-02	**Unloading**
357	2505	-2505	-8.939E-04	1.946E-04	-1.087E-04	-8.939E-03	
Part 2							
289	same	values	to this point	from above			
319	2884	-2884	-1.013E-03	2.125E-04	-1.087E-04	-1.013E-02	
601	2999	-2999	-8.890E-03	9.101E-04	-1.088E-03	-2.026E-02	
604	3000	-3000	-2.038E-03	9.176E-04	-1.098E-03	-2.036E-02	**Maintaining**
1000	3000	-3000	-3.471E-03	1.929E-03	-2.531E-03	-3.465E-02	**constant stress**
Part 3							
287	same	values	to this point	from above			
300	2877	-2877	-9.466E-04	1.669E-04	-4.474E-05	-9.466E-03	
319	2885	-2885	-1.014E-03	2.138E-04	-1.106E-04	-1.014E-02	
601	2999	-2999	-2.028E-03	9.101E-04	-1.088E-03	-2.026E-02	
604	3000	-3000	-2.038E-03	9.176E-04	-1.098E-03	-2.036E-02	**Peak**
605	2999	-2999	-2.045E-03	9.202E-04	-1.102E-03	-2.040E-02	
700	2884	-2884	-2.391E-03	1.187E-03	-1.487E-03	-2.388E-02	
850	2701	-2701	-2.942E-03	1.608E-03	-2.095E-03	-2.938E-02	
1000	2528	-2528	-3.493E-03	2.028E-03	-2.701E-03	-3.487E-02	
1500	2095	-2095	-5.324E-03	3.398E-03	-4.667E-03	-5.310E-02	
2000	813	-813	-6.821E-03	4.680E-03	-6.566E-03	-6.798E-02	
3000	541	-541	-9.693E-03	6.758E-03	-9.524E-03	-9.647E-02	
4000	439	-439	-1.258E-02	8.819E-03	-1.244E-02	-.1251	**Increments stopped**

Table C.2. Mechanics Block ABAQUS Results (cont.)

Inc. No.	Load (psi)	σ_{33} (psi)	ε_{33}	$\varepsilon_{11}=\varepsilon_{22}=\nu\varepsilon_{33}$	Inelastic $I\varepsilon_{33}$	Disp (in)	Rebar Stress	Remarks
Part 4	A_s=.05							
1000	3001	-2870	-8.999E-04	1.350E-04	-	-8.996E-03	-26095	
1217	3053	-2893	-1.100E-03	2.272E-04	-1.930E-04	-0.01090	-31900	**Yielding**
2000	3134	-2974	-1.823E-03	7.698E-04	-8.905E-04	-0.01820	-31900	**Peak**
2608	2974	-2651	-2.897E-03	1.581E-03	-2.012E-03	-0.02461	-31900	**Stop - Equil**
Part 5	A_s=.01							
2157	3032	-3000	-2.038E-03	9.174E-04	-1.098E-03	-0.02036	-31900	**Peak**
2560	2768	-2559	-2.928E-03	1.621E-03	-1.098E-03	-0.02464	-31332	**Displ drops**
Part 6	A_s=.1							
2323	3318	-3000	-2.033E-03	9.148E-04	-1.093E-03	-0.02028	-31900	**Peak**
3109	2973	-2536	-3.657E-03	2.172E-03	-2.863E-03	-0.03658	-31900	**Displ drops**
Part 7	A_s=.05							
1043	3130	-2870	-8.997E-04	1.347E-04	-	-8.992E-03	-26083	
1272	3215	-2898	-1.101E-03	2.730E-04	-1.056E-03	-0.01995	-31900	**Yielding**
2335	3327	-3007	-2.046E-03	9.201E-04	-1.099E-03	-0.02037	-31900	**Peak**
2635	2990	-2596	-2.505E-03	1.303E-04	-1.658E-03	-0.02384	-30024	**Displ drops**
Part 8	A_s=.05							
191	2868	-2866	-8.982E-04	1.347E-04	-	-8.978E-03	-	
397	3003	-3000	-2.038E-03	9.169E-04	-1.097E-03	-0.02036	-	**Peak**
653	2532	-2528	-3.494E-03	2.027E-03	-2.701E-03	-0.02384	-	**Fluctuation**
996	2096	-2059 -2127	-5.100E-03 -5.557E-03	3.558E-03	-4.432E-03 -4.912E-03	-0.05316	-	
Part 9								
93	-186	186	5.830E-05	-8.746E-06	-	5.830E-04		
94	-187.4	187.4	5.896E-05	-8.768E-06	-1.668E-20	5.896E-04		**Crack**
99	-186.1	186.1	6.229E-05	-8.768E-06	-1.668E-20	6.230E-04		**Unloading**
1000	-1.532	1.532	4.575E-04	-8.768E-06	-1.668E-20	4.577E-03		
Part 10	A_s=.05							
65	-195	186.5	5.846E-05	-8.642E-06	-	5.847E-04	1695	
66	-195.9	187.2	5.945E-05	-8.644E-06	-4.818E-11	5.949E-04	1726	**Crack**
70	-194.7	185.5	6.328E-05	-8.645E-06	-4.818E-11	6.332E-04	1835	**Unloading**
369	-130.1	79.4	3.496E-04	-8.712E-06	-4.818E-11	3.497E-03	10136	
588	-82.9	1.853	5.592E-04	-8.761E-06	-4.818E-11	5.594E-03	16214	
1154	-161.2	1.834	1.101E-03	-8.887E-06	-4.818E-11	1.101E-02	31900	**Reloading**
2000	-161.1	1.833	2.183E-03	-8.991E-06	-4.818E-04	2.254E-02	31900	**& Yielding**

Table C.3. J-K Beam Modeled Slab Results

Inc. No.	Load (psi)	σ_{11} (psi)	ε_{11}	Inelastic $I\varepsilon_{11}$	Rebar (psi)	Disp (in)	RF1 (lb)	RF3 (lb)	Remarks
Part 1	simple	spt							
2 Elem									
220	4.08	-3000	-2.041E-03	-1.101E-03	31900	-0.7681	-	1104	
854	4.22	-751	-7.322E-03	-7.086E-03	31900	-3.0	-	1125	
3 Elem									
171	3.78	-2999	-2.040E-03	-1.100E-03	31900	-0.6022	-	1030	
840	3.89	-1308	-9.485E-03	-9.310E-03	31900	-3.0	-	1050	
5 Elem									
70	3.66	-2909	-2.314E-03	-1.402E-03	31900	-0.4869	-	989	
420	3.73	-1555	-1.390E-02	-1.378E-02	31900	-3.0	-	996	
7 Elem									
104	3.59	-2980	-1.864E-03	-9.290E-04	31903	-0.3400	-	972	
395	3.69	-2821	-1.759E-02	-1.740E-02	31900	-3.0	-	983	
10 Elem									
96	3.59	-2999	-2.030E-03	-1.090E-03	31900	-0.3631	-	971	
4000	3.61	-2680	-2.007E-02	-1.999E-02	31900	-2.641	-	966	Need more
12 Elem									steps
107	3.55	-2951	-1.616E-03	-6.909E-04	31900	-0.2763	-	960	
306	3.65	-2813	-2.638E-02	-2.634E-02	31900	-3.0	-	973	
15 Elem									
70	3.52	-2913	-1.278E-03	-3.651E-04	31900	-0.2166	-	949	
342	3.68	-2893	-3.577E-03	-3.121E-03	31900	-3.0	-	981	

Table C.3. J-K Beam Modeled Slab Results (cont.)

Inc. No.	Load (psi)	σ_{11} (psi)	ε_{11}	Inelastic $I\varepsilon_{11}$	Rebar (psi)	Disp (in)	RF1 (lb)	RF3 (lb)	Remarks
Part 2	Fixed	Spt							
2 Elem									
234	35.8	-2980	-1.871E-03	-9.374E-04	31900	-0.1623	-28687	9671	Peak
2865	11.7	-324	-1.897E-02	-1.889E-02	31900	-2.186	-1436	3153	Trough
3948	18.1	-75	-1.813E-02	-1.816E-02	31900	-3.0	+11654	4858	Ultimate
3 Elem									
230	25.8	-2997	-2.184E-03	-1.259E-03	31900	-0.1627	-27753	6970	Peak
1768	8.6	-428	-1.311E-02	-1.298E-02	31900	-1.316	-6314	2323	Trough
3271	14.0	-2996	-1.562E-02	-1.551E-02	31900	-2.369	+7975	3781	Ultimate
5 Elem									
110	20.9	-2989	-2.640E-03	-1.762E-03	31900	-0.1483	-25817	5647	Peak
790	7.22	-1041	-1.570E-02	-1.559E-02	31900	-1.125	-4920	1952	Trough
2336	16.9	-2138	-3.914E-02	-3.909E-02	31900	-3.0	+9104	4563	Ultimate
7 Elem									
209	19.1	-2972	-3.020E-03	-2.180E-03	31900	-0.1363	-24065	5172	Peak
1453	6.81	-1046	-1.900E-02	-1.890E-02	31900	-1.014	-4630	1839	Trough
3063	10.9	-2992	-3.030E-02	-3.020E-02	31900	-2.014	+8313	2965	Ultimate
10 Elem									
188	17.9	-2934	-3.160E-03	-2.330E-03	31900	-0.1177	-22564	4849	Peak
728	7.72	-1676	-1.470E-02	-1.450E-02	31900	-0.4950	-18025	2085	Time
12 Elem									
186	17.49	-2925	-3.440E-03	-2.640E-03	31900	-0.1145	-22414	4723	Peak
1538	6.4	-1032	-3.051E-02	-3.050E-02	31900	-1.042	-788	1733	Trough
2584	7.8	-2387	-3.859E-02	-3.855E-02	31900	-1.54	+5225	1927	Ultimate
15 Elem									
90	16.8	-2989	-3.743E-03	-2.969E-03	31900	-0.1091	-21948	4551	Peak
290	10.8	-2167	-1.373E-02	-1.361E-02	31900	-0.2862	-20594	2934	Time

Table C.4. J-K Continuum Modeled Slab Rebar Results

Inc. No.	Load (psi)	σ_{11} (psi)	ε_{11}	Inelastic $I\varepsilon_{11}$	Rebar (psi)	Disp (in)	RF1 (lb)	RF3 (lb)	Remarks
Part 1	**1/1/1**								
129 (n)	57.4	-2308	-7.110E-04	-9.830E-06	-	-.0398	-29187	15513	
208r(n)	18.6	-1990	-6.167E-04	-4.170E-07	-	-0.1110	-26738	5025	
110(1)	51.0	-1812	-5.570E-04	-9.694E-06	10609	-0.0335	-24088	13775	
10r(1)	4.25	-201	-6.205E-06	-3.170E-07	1962	-0.0241	-300	1149	**Unloading**
110(6)	same	as	110(1)						
47r(6)	27.8	-2261	-6.998E-04	6.600E-07	23762	-0.1330	-30109	7530	
110(L)	same	as	110(1)						
226r(L)	32.6	-2665	-8.242E-04	-1.276E-06	28236	-0.1763	-35362	8813	
Part 2	**3/1/1**								
49(n)	14.7	-2715	-8.120E-04	-6.823E-06	-	-0.0829	-17747	3961	
19r(n)	all	the	reduced	integration	results	unload	at a	.003	load
49(1)	18.49	-2751	-8.231E-04	-1.147E-05	31900	-0.0773	-15902	4992	
40(6)	18.54	-2820	-8.422E-04	-8.183E-06	31900	-0.0788	-16597	5005	
45(L)	18.66	-2792	-8.341E-04	-6.134E-06	31900	-0.0762	-15853	5038	
Part 3	**5/3/1**								
61(n)	11.47	-2590	-7.738E-04	-6.375E-06	-	-0.0734	-16548	3096	
82r(n)	15.86	-3288	-1.108E-03	-1.806E-04	-	-0.1883	-41311	4281	
45(1)	13.39	-2531	-7.551E-04	-1.318E-05	31900	-0.0605	-12493	3616	
83r(1)	22.39	-3266	-1.344E-03	-4.381E-04	31900	-0.1847	-40344	6046	
50(6)	16.24	-2984	-9.158E-04	-2.866E-05	31900	-0.0737	-15672	4384	
96r(6)	22.97	-3441	-1.175E-03	-2.367E-04	31902	-0.1882	-42056	6204	
38(L)	16.22	-2988	-9.172E-04	-2.895E-05	31900	-0.0737	-15704	4379	
97r(L)	23.03	-3486	-1.244E-03	-2.904E-04	31902	-0.1942	-42433	6219	
Part 4	**5/3/2**								
46(n)	11.31	-3645	-1.166E-03	-1.201E-04	-	-0.0765	-17256	3054	
53r(n)	13.06	-3512	-1.141E-03	-1.086E-04	-	-0.0980	-23004	3525	
30(1)	10.5	-2536	-7.565E-04	-8.688E-06	25584	-0.0477	-9822	2836	
138r(1)	17.65	-3613	-1.222E-03	-1.555E-04	31900	-0.0969	-21718	4765	
61(6)	20.85	-4994	-1.944E-03	-5.624E-04	31900	-0.1159	-24684	5631	
51r(6)	17.13	-3534	-1.200E-03	-1.536E-04	31901	-0.0892	-20139	4624	
65(L)	20.97	-5026	-1.963E-03	-5.735E-04	31903	-0.1170	-24893	5662	
51r(L)	17.15	-3540	-1.204E-03	-1.562E-04	31902	-0.0894	-20170	4631	
Part 5	**5/6/2**								
33(n)	11.19	-3649	-1.169E-03	-1.012E-04	-	-0.0756	-17043	3022	
39r(n)	11.50	-3154	-9.564E-04	-1.245E-06	-	-0.0829	-18482	3105	
35(1)	11.12	-2724	-8.131E-04	-1.427E-05	27167	-0.0507	-10467	3004	
38r(1)	13.50	-2871	-8.698E-04	-1.003E-05	31903	-0.0670	-14538	3646	
61(6)	19.81	-4747	-1.801E-03	-4.790E-04	31901	-0.1056	-22878	5348	
43r(6)	16.19	-3361	-1.106E-03	-9.873E-05	31900	-0.0821	-18531	4371	
52(L)	20.01	-4798	-1.832E-03	-4.917E-04	31900	-0.1075	-23201	5404	
44r(L)	16.18	-3366	-1.109E-03	-1.010E-04	31900	-0.0819	-18556	4368	

Table C.5. J-K Continuum Modeled Slab Results

Elem Type	Load (psi)	σ_{11} (psi)	Disp (in)	RF1 (lb)	Error Message	Remarks
Part 1	**1/1/1**					
C3D8	186.3	-1809	-0.0236	-40217	Too many attempts	Rebar had no effect
C3D8I	229.5	-2154	-0.0560	-58393	Time increment smaller	"
C3D20	51.02	-1812	-0.0335	-24088	Too many attempts	"
C3D20R	32.63	-2665	-0.1763	-35362	Time increment smaller	"
Part 2	**3/1/1**					
C3D8	22.63	-690	-0.0204	-9052	Time increment smaller	Rebar had little effect
C3D8I	28.47	-2725	-0.1272	-35934	Time increment smaller	"
C3D20	18.66	-2792	-0.0760	-15853	Time increment smaller	"
C3D20R	.003	-	-	-		
Part 3	**5/3/1**					
C3D8	11.58	-513	-0.0224	-5486	Time increment smaller	Rebar had little effect
C3D8I	25.3	-3137	-0.1701	-41735	Time increment smaller	"
C3D20	16.22	-2988	-0.0737	-15704	Too many attempts	"
C3D20R	23.03	-3486	-0.1942	-42433	Time increment smaller	"
Part 4	**5/3/2**					
C3D8	14.18	-970	-0.0260	-7866	Too many attempts	
C3D8I	22.31	-3766	-0.1175	-25198	Time increment smaller	Rebar Yielding
C3D20	20.97	-5026	-0.1170	-24893	Time increment smaller	"
C3D20R	17.15	-3540	-0.0894	-20170	Time increment smaller	"
Part 5	**5/6/2**					
C3D8	13.33	-879	-0.0234	-6806	Time increment smaller	
C3D8I	21.98	-3712	-0.1136	-24599	Too many attempts	Rebar Yielding
C3D20	20.01	-4798	-0.1075	-23201	Too many attempts	"
C3D20R	16.18	-3366	-0.0821	-18556	Too many attempts	"
Part 6	**5/6/6**					
C3D8	8.36	-1209	-0.0234	-4471	Time increment smaller	
C3D8I	5.26	-1164	-0.0191	-3022	Too many attempts	Rebar Yielding
C3D20	15.55	-4156	-0.0731	-15998	Too many attempts	"
C3D20R	16.22	-4285	-0.0860	-19209	Time increment smaller	"
Part 7	**5/6/15**					
C3D8I	19.15	-3627	-0.0925	-20913	Time increment smaller	Rebar Yielding
C3D20	15.88	-4286	-0.0755	-16577	Time increment smaller	"
C3D20R	15.67	-3948	-0.0829	-18426	Time increment smaller	"
Part 8	**5/6/30**					
C3D8I	4.85	-996	-0.0170	-3251	Time increment smaller	Rebar Yielding
C3D20	15.82	-4289	-0.0751	-16484	Time increment smaller	"
C3D20R	16.08	-3876	-0.0867	-19257	Too many attempts	"
Part 9	**5/12/15**					
C3D8I	16.36	-3542	-0.0730	-16525	Time increment smaller	Rebar Yielding
C3D20	15.15	-4106	-0.0708	-15456	Time increment smaller	"
C3D20R	15.74	-3975	-0.0835	-18557	Too many attempts	"
Part 10	**10/6/15**					
C3D8I	2.84	-666	-0.0088	-1039	Time increment smaller	Rebar Yielding
C3D20	15.77	-5558	-0.0824	-18243	Time increment smaller	"
C3D20R	5.87	-1721	-0.0225	-3901	Time increment smaller	"

Table C.6. ABAQUS Results for Roberts Slab RB18 (L/h = 18.8) Using Beam Elements (B22)

# elem	Inc	σ_{11} (psi)	ε_{11}	Iε_{11}	σ_{11} (psi) rebar	Load (psi)	Δ_{mid} (in)	Thrust (lb)	Remarks
2	58	-357(s)	-1.104E-04(s)	--	1697	-3.22	-0.011	+7.45	Crk (s)
	92	-571(s)	-1.762E-04(s)	--	2596	-4.78	-0.018	-237	Crk (m)
	935	-2801(m)	-1.702E-03(m)	-8.379E-04	35000	-17.4	-0.216	-19612	Yield
	1252	-3000(m)	-2.348E-03(m)	-1.422E-03	35000	-18.7	-0.294	-23188	
	1299	-3000(s)	-2.445E-03(m)	-1.521E-03	35000	-18.8	-0.306	-23549	
	1487	-2947(s)	-2.851E-03(m)	-1.959E-03	35000	-18.9	-0.352	-24826	Pk
	1880	-2640(m)	-3.769E-03(m)	-3.007E-03	35000	-18.1	-0.452	-26102	Pk Thrust
3	51	-358(s)	-1.108E-04(s)	--	1525	-2.83	-0.009	+5.91	Crk (s)
	94	-678(s)	-2.101E-04(s)	--	2604	-4.64	-0.018	-374	Crk (m)
	1043	-2984(s)	-2.163E-03(s)	-1.239E-03	35000	-16.6	-0.229	-21186	Yield
	1122	-3000(s)	-2.346E-03(s)	-1.417E-03	35000	-16.9	-0.247	-22107	
	1263	-3000(m)	-2.712E-03(s)	-1.801E-03	35000	-17.2	-0.281	-23312	
	1463	-2915(m)	-3.227E-03(s)	-2.387E-03	35000	-17.4	-0.329	-24498	Pk
	1806	-2473(m)	-4.130E-03(m)	-3.401E-03	35000	-16.6	-0.413	-25390	Pk Thrust
5	47	-363(s)	-1.124E-04(s)	--	1418	-2.61	-0.009	+4.42	Crk (s)
	97	-822(s)	-2.454E-04(s)	--	2581	-4.53	-0.019	-512	Crk (m)
	908	-3000(s)	-2.351E-03(s)	-1.422E-03	26030	-14.5	-0.188	-19586	
	1178	-2922(m)	-3.199E-03(s)	-2.355E-03	35000	-15.8	-0.245	-22441	Yield
	1319	-3000(m)	-3.673E-03(s)	-2.889E-03	35000	-16.1	-0.276	-23797	
	1411	-2971(m)	-3.999E-03(s)	-3.254E-03	35000	-16.2	-0..297	-24450	Pk
	1585	-2701(m)	-4.769E-03(s)	-4.110E-03	35000	-15.9	-0.338	-24782	Pk Thrust
7	45	-361(s)	-1.119E-04(s)	--	1361	-2.49	-0.009	+4.45	Crk (s)
	103	-987(s)	-3.057E-04(s)	--	2566	-4.46	-0.020	-773	Crk (m)
	778	-3000(s)	-2.350E-03(s)	-1.421E-03	19411	-13.1	-0.156	-17544	
	1239	-2922(m)	-4.313E-03(s)	-3.605E-03	35000	-15.4	-0.250	-22462	Yield
	1370	-3000(m)	-4.947E-03(s)	-4.308E-03	35000	-15.50	-0.279	-23490	
	1396	-2996(m)	-5.082E-03(s)	-4.456E-03	35000	-15.51	-0.285	-23638	Pk
	1401	-2995(m)	-5.116E-03(s)	-4.494E-03	35000	-15.50	-0.286	-23640	Pk Thrust
10	44	-364(s)	-1.127E-04(s)	--	1333	-2.44	-0.008	+4.23	Crk (s)
	157	-1593(s)	-5.467E-04(s)	-5.354E-05	2355	-3.96	-0.029	-3542	Crk (m)
	663	-3000(s)	-2.326E-03(s)	-1.397E-03	15253	-11.7	-0.129	-15896	
	1275	-2898(m)	-6.197E-03(s)	-5.672E-03	35000	-14.53	-0.251	-21777	Yield
	1295	-2921(m)	-6.343E-03(s)	-5.830E-03	35000	-14.54	-0.255	-21912	Pk/Thrust
	1460	-3000(m)	-8.205E-03(s)	-7.827E-03	35000	-14.03	-0.290	-21612	
15	102	-1190(s)	-3.683E-04(s)	--	2096	-3.64	-0.017	-829	Attempts

Table C.7. ABAQUS Results for Roberts Slab RB18 (L/h = 18.8)
Using Continuum Elements (C3D20)

# elem	Inc	σ_{11} (psi)	ε_{11}	Iε_{11}	σ_{11} (psi) rebar	Load (psi)	Δ_{mid} (in)	Thrust (lb)	Remarks
7	28	-327(s)	-9.121E-05(s)	--	1521	-2.79	-0.009	-3.94	Crk (s)
	111	-690(m)	-2.158E-04(s)	--	3455	-5.87	-0.037	-3705	Crk (m)
	496	-2450(m)	-1.079E-03(m)	-3.598E-04	21291	-14.7	-0.159	-19050	Time Inc
10	27	-324(s)	-9.033E-05(s)	--	1476	-2.70	-0.009	-1.81	Crk (s)
	134	-893(s)	-2.585E-04(m)	--	3462	-5.94	-0.043	-5549	Crk (m)
	518	-2495(s)	-1.095E-03(m)	-3.702E-04	21159	-14.4	-0.163	-19696	Unloading

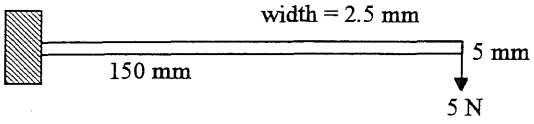

Figure C.1. Cantilever Example (Hibbitt et. al.,1996)

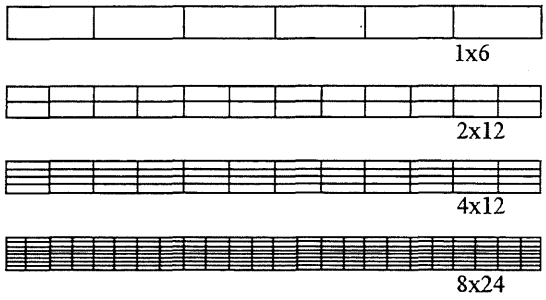

Figure C.2. Mesh Size for Cantilever (Hibbitt et. al., 1996)

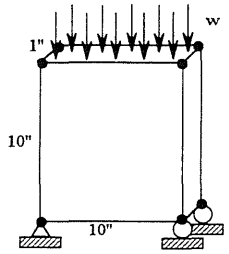

Figure C.3. Simple Mechanics Block Example

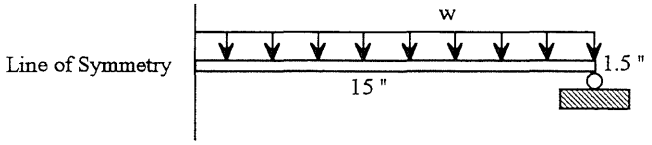

Figure C.4. Jain and Kennedy Slab

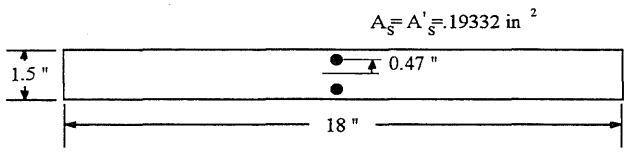

Figure C.5. J-K Slab Cross-Section

	A	B	C	D	E	F	G	H	I
1	**Simply Supported Beam/Slabstrip**								
2									Doubly
3	L=	30	in	Es=	2.9E+07	psi			Negative
4	t=h=	1.5	in	As=	0.19332	in^2			0.19331
5	b=bw=	18	in	d=	1.22	in			
6	f'c=	3000	psi	A's=	0.19331	in^2			0.19332
7	Fy=	31900	psi	d'=	0.28	in			
8	β1=	0.85		ecu=	0.003	in/in	k=	0.290541	
9	Ec=	3190000	psi	I=bh^3/12	5.0625	in^4	kd=	0.354459	
10				Icr=	0.27596	in^4 - P=0			
11				Icr=	0.630037	in^4 - including P		Icr(avg)=	0.452998
12	**Singly Reinforced Sections**				**Doubly Reinforced Sections**				
13									
14									
15									
16	w=8M/L^2 (lb/in)				w=8M/L^2 (lb/in)				
17	**w=**	**63.2**	**lb/in**		**w=**	**66.2**	**lb/in**		
18		**3.5**	**psi**			**3.7**	**psi**		
19									
20	U=5wL^4/384EI (in)				U=5wL^4/384EI (in)				
21	**U=**	**0.0413**	**in**		**U=**	**0.0433**	**in**		
22		**0.3316**	cracked w/ P			**0.3475**	cracked w/P		
23	σ=	My/I=Mc/I	(c)		σ=	My/I=Mc/I	(c)		
24	**σ=**	**221.97**	**psi**		**σ=**	**348.42**	**psi**		
25									
26	*Test failure mechanism:*				*Failure Mechanism test is the same*				
27									
28	ρ =	As/bd=	0.0088		ρ =	As/bd=	0.0088		
29					*balanced*	ρ =			
30	*balanced* ρ =				es=eu(B1d-a(bal))/a(bal)=Fy/Es				
31	es=Fy/Es				equil:	.85f'ca(bal)b=AsFy-A'sf's=(r(bal)Fy-r'f's)bd			
32	(Fy/Es)/eu =(d-c)/c				a(bal)=(r(bal)Fy-r'f's)d/.85fc				
33	c=euEsd/(euEs+Fy)				f's=eu(1-B1d')/a(bal)				
34	a=cB1				f's=euEs[1-(d'/d)((euEs+Fy)/euEs)] if >Fy, then Fy				
35	ρ =	.85f'ca/Fyd			f's=	31900			
36	ρ =	(.85f'cB1/Fy)(euEs/(euEs+Fy))			ρ =	(.85f'cB1/Fy)(euEs/euEs+Fy)+A'sF's/Fybd			
37	ρ =	0.0497			ρ =	0.0585			
38	ρ*.75=	0.0373			ρ*.75 =	0.0439			
39	**Tension Failure**				**Tension Failure**				
40									
41		**Primary Tension Failure**							
42	C=T				*Assume all steel yielding*				
43	T=AsFs				Cc=.85f'cab=Ja				
44	C=.85f'cab				J=	45900	lb/in		
45	jd=d-.5a				Cs=A'sFy				
46	Mu=Tjd=Cjd				Cs=	6166.589	lb		
47					T=AsFy				
48	C=T				T=	6166.908	lb		
49	a=(AsFy)/.85f'cb				a=(T-Cs)/J				
50	a=	0.1344	in		a=	0.000	in		
51	c=a/B1=	0.1581	in		c=a/B1=	0.000	in		
52									
53	es=eu*(d-c)/c				*yield strain*				
54	es=	0.02016			ε=	fy/E=	0.0011		
55	ey=Fy/Es	0.00110			e's=	-102.73242			
56					f's=	Not Yielding	psi		
57	Mu=	7.109E+03	in-lb		-1.5E-05	**<-- Use if Comp Steel not Yielding**			
58					0.201	=a	in	**Must Solve!!!**	
59	**Primary**	**Compression Failure**			c=	0.237	in		
60									
61	(.85f'cbd/ecuEsAs)a^2+ad-B1d^2=0				Cs=	-3073.0	lb		
62	-1.26514	**<-- Use if Comp.Failure**			es=	447.629915			
63	0	=a	in		fs=	31900	psi		
64					T=	6166.908	lb		
65	Mu=.85f'cab(d-.5a)				Cc=	9236.5			
66	Mu=	0.000E+00	in-lb		Mu=Cc(d-.5a)+Cs(d-d')				
67					Mu=	7.451E+03	in-lb		
68									
69					Dependable				
70					Mu=	7.542E+03	in-lb		

Figure C.6. Simply-Supported One-Way Slab Spreadsheet Results

	X	Y	Z	AA	AB
10	**Fixed**				
11	**Both Middle and End Are**				
12	**Doubly Reinforced Sections (M'u)**			**P = 21948**	**lb**
13	Mu=	**7.451E+03**		17010.27	
14	M'u=	**7.454E+03**		17010.27	
15					
16	w=8M/L^2 (lb/in)				
17	**w=**	**132.5**	**lb/in**	302.4	lb/in
18		**7.4**	**psi**	**16.8**	psi
19					
20	U=wL^4/384EI (in)				
21	**U=**	**0.0173**	**in**	**0.0395**	**in**
22		**0.3175**	cracked	**0.3174**	cracked w
23	σ=	My/I=Mc/I	(c)	**0.9522**	canti-w/P
24	**σ=**	**3.486E+02**	**psi**	edge	w/P =0
25		**3.484E+02**		middle	**0.7246**
26	*Failure Mechanism test is the same*				**2.1738**
27					
28	ρ =	As/bd=	0.0088		
29	*balanced*	ρ =			
30	es=eu(B1d-a(bal))/a(bal)=Fy/Es				
31	equil:	.85f'ca(bal)b=AsFy-A'sf's=(r(bal)Fy-r'f's)bd			
32	a(bal)=(r(bal)Fy-r'f's)d/.85f'c				
33	f's=eu(1-B1d')/a(bal)				
34	f's=euEs[1-(d'/d)((euEs+Fy)/euEs)]			if >Fy, then Fy	
35	f's=	31900			
36	ρ =	(.85f'cB1/Fy)(euEs/euEs+Fy)+A'sF's/Fybd			
37	ρ =	0.0585			
38	ρ*.75 =	0.0439			
39	**Tension Failure**				
40					
41	*Assume all steel yielding*				
42	Cc=.85f'cab=Ja				
43	J=	45900	lb/in		
44	Cs=A'sFy				
45	Cs=	6166.589	lb		
46	T=AsFy				
47	T=	6166.908	lb		
48	a=(T-Cs)/J				
49	a=	0.000	in		
50	c=a/B1=	0.000	in		
51	added change to ensure c never < 0				
52	*yield strain*				
53	ε=	fy/E=	0.0011		
54	e's=	-102.732423			
55	f's=	Not Yielding	psi		
56	2.1524E-06	<-- **Use if Comp Steel not Yielding**			
57	0.201	=a	in	**Must Solve!!!**	
58	c=	0.237	in		
59					
60	Cs=	-3070.3	lb		
61	es=	447.6299154			
62	fs=	31900	psi		
63	T=	6166.908	lb		
64	Cc=	9237.7			
65	Mu=Cc(d-.5a)+Cs(d-d')				
66	Mu=	7.454E+03	in-lb		

Figure C.7. Fixed-Supported One-Way Slab Spreadsheet Results

	A	B	C	D	E	F	G	H	I	J	K	L	M
1	Park Strip Method			Bottom-middle			Top-spt			Singly			
2				ρ=	0.8803	%	ρ=	0.8803	%	Wjl/8=mu=T(d-.59T/f'c)			
3	S=	3.190E+06	lb/in	T=	342.6	lb	T'=	342.6	lb	Wjl/8=	394.883	lb/in	
4	β=	0.5		Bottom-spt			Top-middle			Doubly			
5				ρ=	0.8803	%	ρ=	0.8803	%	Wjl/8=mu'+mu=T'(d-.59T'/f'c)+T(d-.59T/f'c)			
6				C's=	342.6	lb	Cs=	342.6	lb	Wjl/8=	789.7661		
7													
8		e+2t/l=nu/hEc+2nu/lS=((1/hEc+2/lS)[.85f'cB1(h/2-del/4-(T'-T-C's+Cs)/1.7f'cB1)+Cs-T])/(1+.2125f'cB1Bl^2(1/hEc+2/lS)/del)											
9		1/hEc+2/lS=		2.3E-07									
10	m'u+mu-nu(del)=(.85f'cB1h[h/2(1-B1/2)+del/4(B1-3)+Bl^2/4del(B1-1)(e+2t/l)+del^2/8h(2-B1/2)+Bl^2/4h(1-B1/2)(e+2t/l)-B1B^2l^4/16hdel^2(e+2t/l)^2])												
11		-1/3.4f'c(T'-T'+C's+Cs)^2+(C's+Cs)(h/2-d'-del/2)+(T'+T)(d-h/2+del/2)											
12	δ=		e+2t/l=	m'u+mu-nu(del)=						del/h	W/Wj(sin)	W/Wj(dou	w
13	0.02		9.7616E-05	1202	=	558	+	644		0.013	3.04	1.52	10.68
14	0.04		0.00015355	1444	=	800	+	644		0.027	3.66	1.83	12.84
15	0.06		0.00018934	1564	=	920	+	644		0.040	3.96	1.98	13.90
16	0.08		0.00021388	1626	=	982	+	644		0.053	4.12	2.06	14.45
17	0.10		0.00023149	1656	=	1012	+	644		0.067	4.19	2.10	14.72
18	0.12		0.00024453	1668	=	1024	+	644		0.080	4.22	2.11	**14.83**
19	0.14		0.0002544	1669	=	1025	+	644		0.093	4.23	2.11	14.83
20	0.16		0.00026199	1662	=	1018	+	644		0.107	4.21	2.10	14.77
21	0.18		0.00026787	1650	=	1006	+	644		0.120	4.18	2.09	14.66
22	0.20		0.00027243	1634	=	990	+	644		0.133	4.14	2.07	14.52
23	0.23		0.00027744	1606	=	962	+	644		0.153	4.07	2.03	14.27
24	**0.26**		0.00028078	1574	=	930	+	644		0.173	3.98	1.99	**13.99**
25	0.29		0.0002829	1539	=	895	+	644		0.193	3.90	1.95	13.68
26	0.32		0.00028408	1503	=	859	+	644		0.213	3.81	1.90	13.36
27	0.35		0.00028454	1467	=	823	+	644		0.233	3.71	1.86	13.04
28	0.38		0.00028441	1429	=	785	+	644		0.253	3.62	1.81	12.71

Figure C.8. Park and Gamble Modified Rigid-Plastic Spreadsheet Results

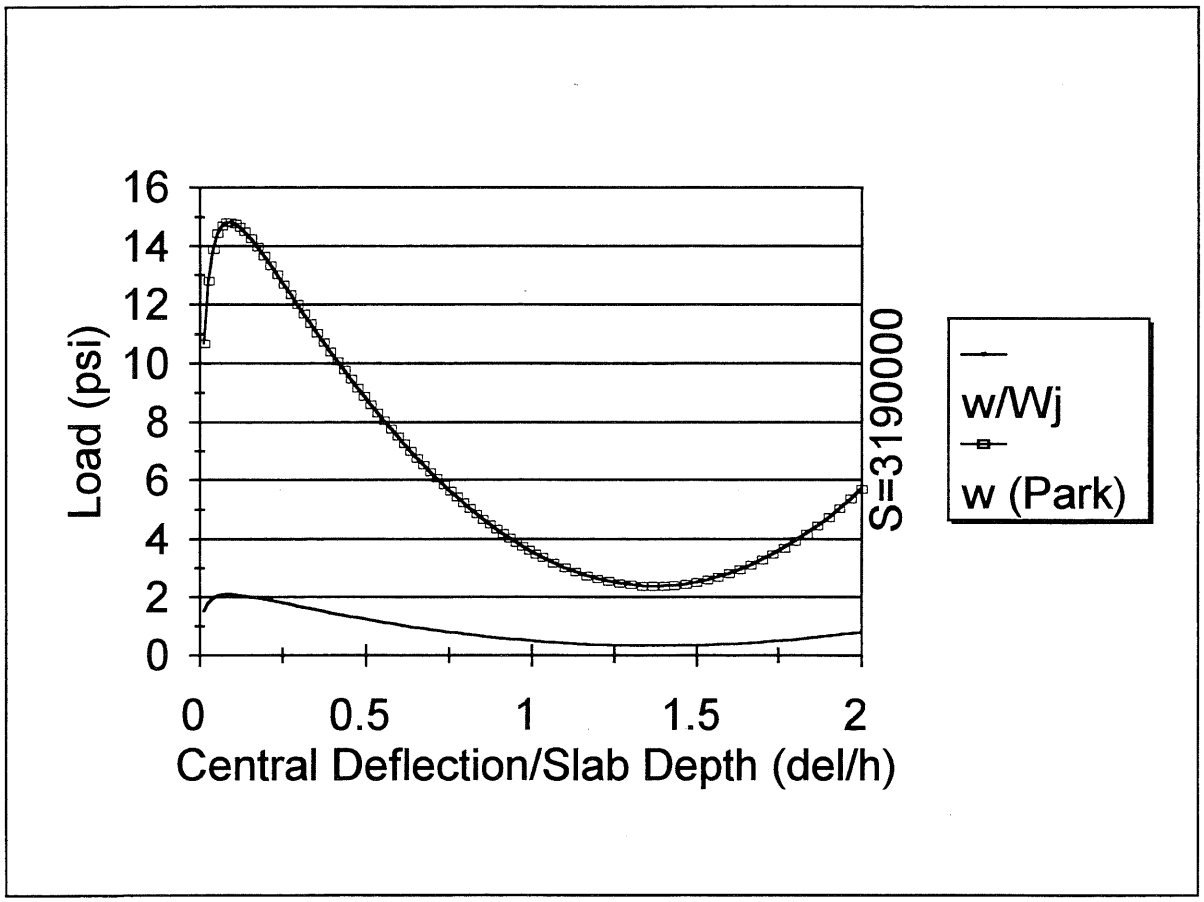

Figure C.9. Graph of Park and Gamble's Modified Rigid-Plastic Method

	A	B	C	D	E	F	G	H	I	J	K
1	**Axially Loaded Members - Interaction Diagram**										
2											
3	*Balanced Failure*						*Tension Failure*				
4							Pu=	**21948**	lb		
5	assume F's=Fy						assume Pu<Pb, Fs=Fy, F's=Fy				
6	a(bal)=B1c(bal)=euEsB1d/(Fy+euEs)						a=(Pu-A'sFy+AsFy)/.85f'cb				
7	a(bal)=	0.76	in				a=	0.48	in		
8	c(bal)=	0.89	in				c=	0.56	in		
9	e's=eu(c-d')/c>=Fy/Es						e's=eu(c-d')/c>=Fy/Es				
10	e's=	0.00206	Fy/Es=	0.00110			e's=	0.00150683	Fy/Es=	0.0011	
11	F's=	31900	psi				F's=	31900	psi		
12	Pu=.85f'ca(bal)b+A'sF's - AsFy						d"=(.85f'cbh(d-.5h)+A'sFy(d-d'))/(.85f'cbh+(As+A's)Fy)				
13	Pu=	34828	lb				d"=	0.47	in		
14	Mu=Pue=.85f'cab(d-.5a)+A'sFy(d-d')						Mu=Pe=	Pu(d-d"-.5a)+A'sFy(d-d'-d")+AsFyd"			
15	Mu=Pue=	3.507E+04		e=	1.01		Mu=Pe=	**1.701E+04**	in-lb	e=	0.78
16	.85f'cbh(d-.5h)+A'sFy(d-d')=Pod"=(.85f'cbh+(As+A's)Fy)d"										
17	d"=(.85f'cbh(d-.5h)+A'sFy(d-d'))/(.85f'cbh+(As+A's)Fy)						Pu=0				
18	d"=	0.47	in				.85f'cba^2+(A'seuEs-AsFy)a-A'seuEsB1d'=0				
19	Mu=Pe=.85f'cab(d-d"-.5a)+A'sFy(d-d'-d")+AsFyd"						-3.7E-09	**Must solve**			
20	Mu=Pe=	1.870E+04		e=	0.54		0.20	=a			
21							0.24	=c			
22							F's=	-15884.7	psi		
23							d"=	0.47	in		
24	*Compression Failure*						Mu=Pe=.85f'cab(d-d"-.5a)+A'sF's(d-d'-d")+AsFyd"				
25	Pu=	45000	lb				Mu=Pe=	7.454E+03	in-lb	e=	0.00
26	assume Pu>Pb, Fs<Fy, F's=Fy										
27	.85f'cba^2+(A'sFy+AseuEs-Pu)a-AseuEsB1d=0						Pu=tension				
28	6.1E-06	**Must solve**					Pu=-AstFy				
29	0.90	=a	e's=	0.00221			Pu=	-12333.497	lb		
30	1.06	=c	F's=	31900			Graph				
31	Fs=	13105.4	psi								
32	d"=	0.47	in								
33	Mu=Pe=.85f'cab(d-d"-.5a)+A'sFy(d-d'-d")+AsFsd"							Mu	Pu		
34	Mu=Pe=	1.647E+04	in-lb	e=	0.37		Tensile	0	-12333.5		
35							No Pu	7453.86366	0		
36	*Pure Axia*						tension	17010.271	21948		
37	Pu=.85f'cAg+AsFy+A'sFy						balanced	18704.4135	34827.71		
38	Pu=	8.118E+04	lb				compres	16473.5617	45000		
39							axial	0	81183.5		
40											

Figure C.10. Axial-Moment Interaction Spreadsheet Results

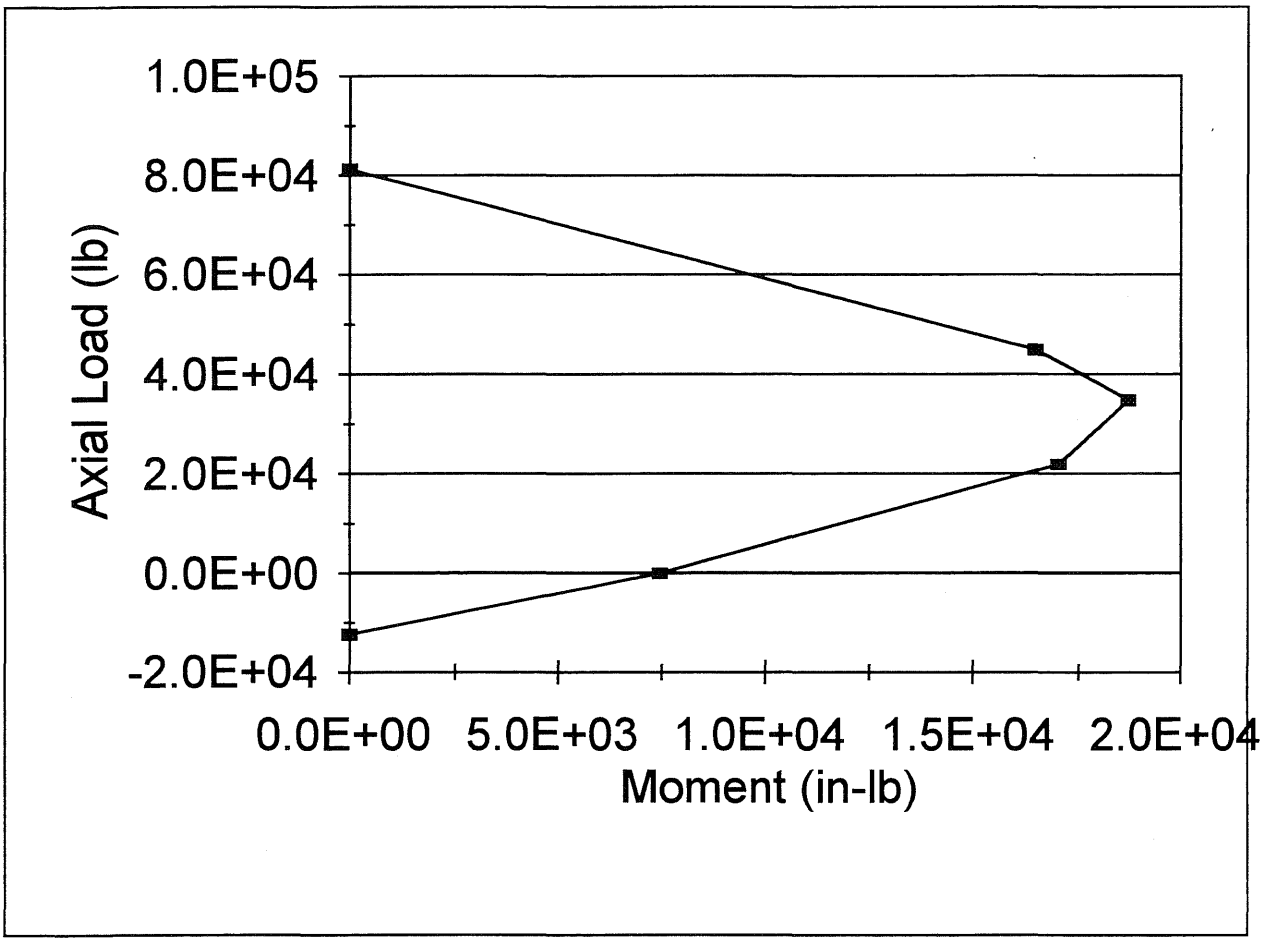

Figure C.11. Axial-Moment Interaction Graph

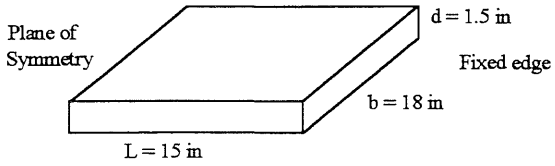

Figure C.12. 3D View of J-K Slab

APPENDIX D

MEMBRANE THEORY RESULTS

D.1. Introduction

In Chapter 4, the derivations used to predict the complete load-deflection curve for a laterally restrained reinforced concrete one-way slab are presented. The detailed results summarized in Chapter 4, especially comparisons between the modified and Park and Gamble's compressive membrane theories, are presented here for the readers more in-depth review. The improved method for estimating the peak compressive membrane capacity and the associated midspan deflection (Point B, Figure 4.1) were the primary goals for this dissertation.

D.2. Peak Compressive Membrane Capacity Results

The presented compressive membrane derivation generally follows Park and Gamble's derivation except for a modification within the equations for the geometric distance between points A and B (Figure 4.6) and the adoption of the peak thrust, rather than the peak capacity deflection, as the index for the peak capacity within the compressive membrane theory. There is a small, but appreciable, difference between the predicted peak capacity with the modified compressive membrane theory and Park and Gamble's peak capacity for slabs with low L/h's (Figure D.1). However, the thinner the slab, the greater the difference between the new theoretical curve (i.e., curve shifts upward) and Park and Gamble's theoretical curve (Figures 4.8, 4.9, and D.2). The differences in these curves were consistent whether the member was singly- or doubly-reinforced. The curves in Figures 4.8 - 4.9 and D.1 - D.2 were plotted for doubly-reinforced members.

The predicted capacities using Park and Gamble's compressive membrane theory are presented in Table D.1, while the modified compressive membrane theory predicted capacities are presented in Table D.2. In each table, the following capacities were evaluated against the experimental capacity: the yield-line capacity with simple-supports, the yield-line capacity with fixed-supports (YL), the computed peak capacity (PP or WP), the deflection indexed capacity

using experimentally measured peak capacity deflections listed in Appendix A (PDI or WDI), the peak thrust indexed capacity (PTI or WTI), and an averaged capacity between the computed and the peak thrust indexed capacities (P_{avg} or W_{avg}). The first abbreviation represents the results with Park and Gamble's compressive membrane theory, while the second abbreviation delineates the results with the modified compressive membrane theory.

The author used a spreadsheet to calculate the different capacities for each increment of the deflection (Figures D.3 - D.6). The experimental deflection, which is shaded, indexes the WDI capacity, while the shaded peak thrust indexes the WTI capacity. Notice that the value $(1-\varepsilon)(\varepsilon+2t/\ell-2\beta\varepsilon)$ is also a maximum when the thrust is a maximum. Additionally, the computed peak capacity (WP) is shaded. As shown in Figure D.3 - D.6, the experimental deflection can index a capacity that is sometimes prior to the computed peak capacity (WP), between the computed peak capacity and the peak thrust indexed capacity, or after the peak thrust indexed capacity, while the peak thrust indexed capacity is always after the computed peak capacity.

The bottom two lines of Tables D.1 and D.2 provides the average and the standard deviation for the results while considering all the slabs. The computed peak capacity (PP) followed by the average peak capacity (P_{avg}) generates the best peak capacity estimates using Park and Gamble's compressive membrane theory (Table D.1), while the peak thrust indexed capacity (WTI) and the averaged peak capacity (W_{avg}) provides the best peak capacity estimates using the modified (author's) compressive membrane theory (Table D.2). In order to further evaluate the two theories, the average and standard deviation were computed for the thick, thin and very thin slabs, separately (Table D.3). As shown in Table D.3, the peak thrust indexed peak capacity estimate (PTI and WTI) is as good of an estimate for the peak capacity as the deflection indexed peak capacity (PDI and WDI) without the need to estimate the midspan deflection first. In this comparison, the actual experimental deflections and not an estimate were used to index the peak capacity. The peak thrust indexed (WTI) capacity using the modified compressive membrane theory slightly under-estimated the peak capacity, except for the very thin slabs.

In Park and Gamble's equations, using the average peak capacity (P_{avg}) provides the best estimate while still predicting a capacity which is less than the experimental capacity. For the author's equations, the peak thrust indexed peak capacity (WTI) provides the best estimate with the smallest standard deviation for both the thick and thin slabs.

Since most of the past researchers either did not test the lateral stiffness of their support structures or did not list the lateral support stiffness used to predict the peak capacity within the compressive membrane theories, an investigation was conducted on the effect of the different support stiffness on the peak capacity. The results of the author's study are presented in Table D.4 for Park and Gamble's compressive membrane theory and Table D.5 for the modified compressive membrane theory. The peak capacity was estimated for each slab using a lateral support stiffness (lb/in) with a scalar magnitude of E_c, $0.1E_c$, and $0.01E_c$. The estimated peak capacity using a lateral support stiffness between a scalar magnitude of 0.1 and $0.01E_c$ for the thick slabs generally bracketed the experimental peak capacity. Of course, a lateral stiffness value nearly equal to a scalar magnitude of E_c was required to estimate the capacity for the thin slabs since the experimental reaction structure was known to have a lateral stiffness close to a scalar magnitude of E_c. A lateral support stiffness scalar magnitude of $0.01E_c$ generally predicted a peak capacity of 1.5 to 2.0 times the yield line capacity with fixed-supported edge conditions for all of the slabs (Tables D.4 - D.5).

In Chapter 3, the finite element results for thick slabs using fixed-supported edge conditions greatly over-estimated the peak capacity (Tables 3.3, 3.4, 3.7, 3.9). A lateral stiffness value of scalar magnitude E_c has been noted by past researchers (Chapter 2) as representing the fully fixed-supported lateral edge conditions. Therefore, a lateral support stiffness of scalar magnitude E_c in Park and Gamble's and the author's equations should generate the same results as the fully fixed-supported edge conditions in the finite element results. Upon comparison of the compressive membrane peak capacities with the average finite element (FE) peak capacities (Table D.6), the compressive membrane results were very close to the FE peak capacities. The average FE peak capacity is used to make the comparison listed in the parentheses (i.e., the compressive

membrane capacity divided by the average FE peak capacity) of Table D.6, and then averaged at the bottom of the table. The peak capacity generalities are the same as observed before. The average of the computed peak capacity and the peak thrust indexed capacity (P_{avg}) in Park and Gamble's compressive membrane theory provides the best correlation (i.e., 1.004) with the FE average peak capacity, while the peak thrust indexed capacity generates the second best correlation (i.e., 0.972). The peak thrust indexed capacity in the modified compressive membrane theory provides the best correlation (i.e., 1.043). Once again, the peak thrust indexed capacity provides the best overall peak capacity estimate for the estimated lateral support stiffness, i.e., a scalar magnitude of E_c to represent fully fixed-supported conditions.

The results in Tables D.4 - D.6 support the use of the compressive membrane theory to estimate the peak compressive membrane capacity in thick slabs. The compressive membrane theory equations matched, not only the acceptable analysis results when using finite element analysis methods for thick slabs, i.e., fixed-supported edge conditions, but also the results when the supports are not laterally fixed (i.e., the experimental results in Appendix A). Even the associated peak capacity deflections from the compressive membrane theory are more acceptable than the extremely small deflections provided through finite analysis for thick slabs. Even though the deflections are not required in estimating the peak capacity (i.e., index the peak capacity with the peak thrust), an acceptable peak capacity deflection is still required to develop the load-deflection history.

D.3. Peak Compressive Membrane Capacity Deflection Results

The use of the peak thrust to index the peak capacity does not eliminate the need for a peak capacity deflection estimate. In most dynamic analysis, especially in the blast arena, there is still the need for a complete load-deflection curve as input. The load-deflection history provides invaluable insight into the energy absorption capability of the slab. Upon close evaluation of the empirical results for the one-way slabs listed in Appendix A, the deflections range from a low of 0.03h to a high of 0.4h. Fortunately, the peak capacity deflection is a function of L/h (Figure D.7 -

D.8) and the concrete compressive strength (Figure D.9). A number of deflection estimation techniques were evaluated to include: empirically based linear relationships, deflections associated with the compressive membrane theory computed peak capacity and the peak thrust indexed capacity, general concrete deflection equations available in most textbooks, and curvature based relationships.

The peak capacity deflection estimates for the varying procedures using a strain of 0.005 in/in are listed in Tables D.7 and D.8. Some results are listed in both tables for ease in comparison with the other deflection estimates. The deflection estimates using Park and Gamble's compressive membrane theory are presented in Table D.7, while the deflection estimates using the author's compressive membrane theory are listed in Table D.8. The comparison format is similar to the comparison for peak capacity estimates in Section D.2, in that for each slab the deflection estimate is divided by the experimental peak capacity deflection. The overall accuracy of each prediction technique is further evaluated through the average and standard deviation when considering all the slabs or just the thick slabs, the thin slabs, or the very thin slabs.

Upon consideration of the general deflection estimates available in most textbooks, the best overall estimate for the peak capacity midspan deflection was through modeling the slab as simply-supported with a fully cracked moment of inertia. These deflection estimates (SS) are presented in both Tables D.7 and D.8. The last two lines of the Tables D.7 and D.8 provide the overall average and standard deviation while considering all the slabs. A more detailed breakout of averages and standard deviations using the simply-supported deflection estimate for thick ($L/h < 18$), thin ($18 < L/h < 22$), or very thin ($L/h > 22$) slabs is presented in Table D.9. The use of simply-supported edge conditions with a fully cracked moment of inertia estimated the peak capacity midspan deflection extremely well for only the thin slabs ($18 < L/h < 22$), while under-estimating the deflection for thick slabs ($L/h < 18$) and over-estimating the deflection for very thin slabs ($L/h > 22$).

The author averaged the Δ/h's for each L/h grouping in Appendix A and plotted them in Figure D.10. There was an obvious correlation between Δ/h and L/h depending on whether the

slabs were thick (L/h < 15) or thin (L/h > 18). The linear regression output for the L/h - Δ/h curves plotted in Figures D.7 and D.8 are presented in the second and third columns of Table D.10. The deflection estimates from these empirically based curves (EC) listed in the last two columns of both Tables D.7 and D.8 include estimates using the interpolation technique presented in Section 4.3.2 for the slabs with an L/h between 15 and 18. The detailed analysis of averages and standard deviations using the empirical deflection curves for thick, thin and very thin slabs is provided in Table D.9. The empirically based curves estimate the midspan peak capacity deflection exceptionally well.

Since the compressive membrane theory relates the midspan deflection to the uniform load supported by the slab, the deflection associated with either the computed peak point or the peak thrust should estimate the peak capacity midspan deflection. The deflection associated with the computed peak capacity (PP or WP) and the peak thrust indexed peak capacity (PTI or WTI) are listed in Tables D.7 (i.e., using Park and Gamble's compressive membrane theory, PP, PTI) and D.8 (i.e., using the author's compressive membrane theory, WP, WTI). The deflection associated with the computed peak capacity is nearly half of the experimental deflection except for the deep slabs (L/h < 5), where the deflection is nearly double the experimental deflection. The deflection associated with the peak thrust in the Park and Gamble's compressive membrane theory is larger than the experimental deflections for both the thick and thin slabs, while the deflection associated with the peak thrust in the modified compressive membrane theory over-estimates the deflections for thick slabs and under-estimates the deflections for thin slabs. As an interesting exercise, the associated deflections for the peak thrust from Park and Gamble's and the modified compressive membrane theories were averaged and compared with the experimental peak capacity deflections (Table D.11). The estimated deflections for all the thin slabs correlated very well with the experimental peak capacity deflections, while the estimates for the thick slabs were over-estimated due to the huge over-estimation of the deflections for the deep slabs (L/h < 5).

Mattock (1965) performed a number of experiments to develop a relationship for the rotational capacity of hinging regions in reinforced concrete beams (EQNs 4.17 and 4.18). His

goal was to determine the magnitude of the strains in the hinging regions during the redistribution of moments. The deflection estimates using Mattock's (M) equations and a strain of 0.005 in/in are presented in both Tables D.7 and D.8. The deflection estimate was lower than the experimental peak capacity deflection if an error did not occur, except for slab K2 which was considered an outlier for other deflection estimates because of the low experimental deflection.

Adjusted concrete compressive strains (ε(M), Table D.7) in Mattock's equations eventually produced deflections that matched the experimental peak capacity deflections, except for the thin slabs (L/h > 18) which did not have tension reinforcement in the negative and positive moment regions. For the thin slabs, C1 - C4, with positive and negative moment tension reinforcement, the adjusted strains were less than half of the finite element suggested value of 0.005 in/in. This low strain value for the thin slabs coincides with the low strain values determined with the curvature based deflection estimates discussed later.

Mattock's equations should only be used to predict the peak capacity deflection for thick slabs with tension reinforcement at both the positive and negative moment regions. Additional experimental results for doubly reinforced thin slabs is necessary before attempting to correlate Mattock's equations for use with thin slabs. The reinforcement ratio (ρ), the reinforcement index (q), the span length-to-thickness ratio (L/h), and the concrete compressive uniaxial strength (f'_c) were plotted against the adjusted strain values for the thick slabs. The best correlation occurred when plotting the slab's uniaxial concrete compressive strength against the adjusted strains (Figure D.11). The regression analysis results are listed in Table D.10 (f'c - ε (M)), while the comparison of estimated strain values to the adjusted strain values is presented in Table D.12 ($\varepsilon(M)_{est}/\varepsilon(M)_{adj}$). Since this technique could not estimate the peak capacity deflections for thin slabs, the comparison with other methods was stopped after comparison of strain estimates.

Keenan's (1969) curvature based deflection equations were modified to include axial shortening as defined in Park and Gamble's and the modified compressive membrane theories. The detailed results (K(P)) for a maximum concrete compressive strain of 0.005 in/in in EQN 4.21 used with Park and Gamble's compressive membrane theory are presented in Table D.7, while the

detailed results (K(W)) for a maximum concrete compressive strain of 0.005 in/in in EQN 4.22 used with the author's compressive membrane theory are listed in Table D.8. Only the deflection estimates for the deep slabs ($L/h < 5$) were even close. The ultimate concrete compressive strain (ε(K(P)) in Table D.7 and ε(K(W)) in Table D.8) was adjusted until the estimated deflection matched the experimental peak capacity deflection. There were no adjusted strain values determined for use in EQN 4.21 that provided acceptable results for the thin slabs reinforced only along the entire bottom of the slab (i.e., Roberts' slabs (RB) in Table D.7). Even though EQN 4.22 assumes that the slab is reinforced with equal amounts of tensile and compressive reinforcement at the supports and midspan, it was possible to determine an ultimate strain for the thin slabs (i.e., only bottom reinforcement) which produced a matching peak deflection (Table D.8).

The author also developed a curvature based deflection equation for use with both his and Park and Gamble's compressive membrane theories (EQN 4.24). The results (W(P)) when using a slightly adjusted form of EQN 4.24 with Park and Gamble's theory and an ε of 0.005 in/in are presented in Table D.7, while the results (W(W)) when using EQN 4.24 with the modified compressive membrane theory and an ε of 0.005 in/in are listed in Table D.8. The estimated deflections were very similar for both theories even down to the error message for thin slab deflection estimates. The strain (ε(W(P)) in Table D.7 and ε(W(W)) in Table D.8) was adjusted until the estimated deflection matched the experimental deflection. Strains much smaller than expected were necessary to remove the error message and achieve matching deflections for the thin slabs (Table D.7 and D.8).

Since Keenan's EQN 4.21 could not match the experimental peak deflection results for the thin slabs when the ultimate concrete compressive strain was varied, it was dropped from further evaluation. The reinforcement ratio (ρ) (Figure D.12), the reinforcement index (q) (Figure D.13), the length-to-thickness ratio (L/h) (Figure D.14), and the concrete compressive uniaxial strength (f'_c) (Figure D.15) were plotted against adjusted strains (i.e., ε(W(P)) in Table D.7 and ε(K(W)) and ε(W(W)) in Table D.8). The adjusted strain values plotted in Figures D.12 - D.15 were from the author's curvature based deflection equation used with his compressive membrane theory

($\varepsilon(W(W))$, Table D.8). Neither a linear nor exponential curve really fit the data in any of the graphs (Figures D.12 - D.15) as long as the strain values for the thin slabs were included. Since the adjusted strain values for the thin slabs are rather constant and below a strain value of 0.002 in/in (Table D.7 and D.8), those data points were removed, leaving the adjusted curves in Figures D.16 - D.18, D.9. The best fit of a curve to the data occurred when plotting the slab's uniaxial concrete compressive strength against the adjusted strains (Figures D.9). Similar results occurred for the data sets from Keenan's simplified deflection equation used with the author's compressive membrane theory ($\varepsilon(K(W))$) and from the author's curvature based deflection equation used with Park and Gamble's compressive membrane theory ($\varepsilon(W(P))$). The regression analysis results for the f 'c - ε curves are listed in Table D.10, while the resulting strain estimates and the comparison with the adjusted strain values for use with Keenan's simplified deflection estimate ($\varepsilon(K(W))_{est}/\varepsilon(K(W))_{adj}$), the author's deflection estimate used with Park and Gamble's compressive membrane theory ($\varepsilon(W(P))_{est}/\varepsilon(W(P))_{adj}$), and the author's deflection estimate used with the his compressive membrane theory ($\varepsilon(W(W))_{est}/\varepsilon(W(W))_{adj}$) are listed in Table D.12. The average and standard deviation for the comparison of the estimated strain values to the adjusted strain values are listed at the bottom of Table D.12. The best average and smallest standard deviation for the estimated to adjusted strains was for the estimated strain values to be used in the author's curvature based deflection equation as part of his compressive membrane theory.

For the thin slab strain values removed from consideration above, the strain values were simply averaged for use in the curvature based deflection equations. The averages and standard deviations for the thin ($18 < L/h < 22$) and the very thin ($22 < L/h < 29$) slabs are listed at the bottom of Table D.12 for use with each deflection technique. The average strain values for the thin slabs are much smaller than what the finite element results (i.e., 0.005 in/in) would predict. However, the curvature based deflection equation does assume crushing of the concrete at peak capacity which does not always occur in the thin slabs, and the averaged strain values do provide a good deflection estimate.

Even though the best correlation between estimated-to-adjusted concrete compressive strains occurred with the strain estimates for the author's curvature based deflection equation used with his compressive membrane theory, the four viable methods for predicting the peak midspan deflection for both thick and thin slabs were compared in Tables D.13 and D.14. The empirically based deflection curves (EC) are probably the simplest to use, except when evaluating a slab with an L/h within the range of $15 < L/h < 18$. However, a simple interpolation between the results provided by substituting the given L/h into both equations, 4.15 and 4.16, results in an acceptable deflection estimate. The curves point out a direct correlation between the span-to-thickness ratio and the peak capacity midspan deflection-to-thickness ratio. The curves also highlight the behavioral change at the peak capacity for thick slabs controlled by material instability and thin slabs controlled by geometric instability.

The curvature based deflection estimates shed light on the fact that the concrete compressive strength plays a major role in determining the concrete compressive strain used to estimate the peak capacity deflection. The linear curves in Table D.10 were used to estimate the strain values for the thick slabs, while the averaged adjusted strain values at the bottom of Table D.12 were used for the thin ($18 < L/h < 22$) and very thin ($22< L/h < 29$) slabs. As an example, the deflection estimate (W(W)) using the estimated strain in the author's curvature based deflection equation is indexed in Figures D.3 - D.6 by the peak thrust. The deflection estimate from the other curvature based deflection equations are also indexed by the peak thrust. Even though Keenan's simplified deflection estimate assumes equal tensile and compressive reinforcement ratios, the estimated deflections were fairly close to the experimental deflections (Table D.14). However, the author's curvature based deflection equation used with either Park and Gamble's or the author's compressive membrane equations provides the best correlation and the smallest standard deviation from the experimental deflections, without assuming equal tensile and compressive reinforcement (Table D.14). As can be seen in the bottom half of Table D.14, disregarding a few of the outliers greatly improves the accuracy and nearly cuts in half the standard deviation.

The peak thrust should be used to index the peak capacity with the author's compressive membrane theory and to index the corresponding peak capacity midspan deflection with his curvature based deflection equation.

D.4. Load-Deflection Curve Results

The load-deflection curve provides insight into the complete response of a structural element. Even though most structures are never loaded to failure, protective structures, on the other hand, are designed to resist extremely heavy loading. In dynamic analysis, engineers use numerical integration schemes and the load-deflection curve to determine the slab's energy absorption capability and overall ductility during loading. Therefore, an accurately constructed load-deflection response for a given slab design is an extremely valuable asset.

The general shape of the load-deflection curve for a laterally restrained reinforced concrete one-way slab has a parabolic rise in capacity to the peak compressive membrane capacity, a roughly parabolic decline in load capacity until the tensile membrane action catches the load, and an approximately linear increase in capacity until rupture of the reinforcement during tensile membrane resistance. The transition between compressive and tensile membrane resistance is usually smooth unless there is a shear failure.

The author proposes the use of a roughly parabolic ascending curve up to the peak capacity, a descending parabolic curve from the peak capacity until intersection with the tensile membrane curve, and a linear extension along the tensile membrane curve to represent the tensile membrane resistance. This method of developing the load-deflection curve will provide a simple, and possibly a more accurate, representation of the experimental results.

The estimated load-deflection curve is comprised of the following:

- the ascending portion of the compressive membrane resistance curve (C1, EQN 4.28) using the peak thrust indexed capacity and the strain controlled curvature based deflection to define the peak point;

- the descending portion of the compressive membrane resistance curve until intersection with the tensile resistance curve (C2, EQN 4.29) using L/h and whether support rotation occurs to determine first the appropriate yield line capacity, and then, the associated deflection from the pertinent tensile membrane curve (T1 or T2) to define the trough point; and
- the linear portion of tensile membrane resistance curve (Ten) using an L/h based incipient collapse deflection and the previously selected tensile membrane curve (T1 or T2) to construct the linear curve from the trough point to the point of reinforcement failure. In each figure, the experimental curve (Exp), the author's compressive membrane curve (CMC), and the linear tensile membrane curves (T1, only tensile reinforcement at midspan; T2, all of the reinforcement at midspan) are presented for comparison with the author's estimated load-deflection curve.

A sample of estimated load-deflection curves using the presented estimation techniques for a variety of span length-to-thickness ratios are presented in Figures D.19 - D.31. The estimated load-deflection curves are for the following slabs:

- Wood1, L/h = 2.7, Figure D.19
- Wood3, L/h = 4.4, Figure D.20
- Wood4, L/h = 8, Figure D.21
- B3, L/h = 10, Figure D.22
- W1, L/h = 10.4, Figure D.23
- G4, L/h = 14.8, Figure D.24
- C1, L/h = 17.1, Figure D.25
- RB18, L/h = 18.8, Figure D.26
- RB23, L/h = 18.8, Figure D.27
- C3, L/h = 20, Figure D.28
- C4, L/h = 24, Figure D.29
- RB25, L/h = 28.3, Figure D.30
- RB12, L/h = 28.3, Figure D.31

The experimental curves plotted in the figures are as accurate as possible since the data points were generated through hand-drawn lines on graphs provided in the literature. All peak and trough points were captured by using a small deflection increment. In general, the estimated load-deflection curves match the response of the experimental curves. For the thin slabs, the experiments were stopped shortly after the peak capacity since the edges were restrained only for outward lateral movement. The continuation of the estimated curves for thin slabs beyond the peak capacity is based on the experimental results presented in Chapter 2 for two-way slabs rigidly restrained at the edges. For the thick slabs, the averaged capacity (Table D.2) between the peak thrust indexed capacity and the computed peak capacity was used for q_u in Figures D.32 - D.37. In most cases, there was an improvement in the correlation between the experimental peak capacity and the estimated peak capacity.

D.5. Simple Estimate for the Peak Capacity Results

The thrust (Table 4.12) used in the axial force-moment interaction equations to predict the peak capacity was determined by trial and error. In most cases the experimental peak capacity could not be matched by even the balanced conditions when considering P-Δ effects, which are usually small within the elastic loading ranges for fixed-supported edge conditions. Therefore, the thrust generating the peak capacity without inclusion of the P-Δ effects was used to establish the T/P_o ratio.

The thrusts (T(A-M)) generated within the axial force-moment interaction equations were compared (Table D.15) with the peak thrusts generated through Park and Gamble's compressive membrane equations (Park), the author's compressive membrane equations (Author), the finite element analysis presented in Chapter 3 (Finite), the axial force-moment thrusts when considering P-Δ effects (T(A-M w P-Δ)), the thrust at balanced failure (P_{bal}), and the ultimate axial thrust capacity (P_o). Only slab K2 generated thrusts, in any method, that exceeded the balance thrust condition. The thrust generated through finite element analysis using fixed-supported boundary conditions compared well to the thrusts generated with either Park and Gamble's or the author's

compressive membrane equations. Generally, the thrust used in the axial force-moment interaction equations (T(A-M)) was less than the thrust generated in either Park and Gamble's equations, the author's equations, or the finite element analysis.

Table D.1. Peak Compressive Membrane Capacity Estimates (Point B, Figure 4.1) Using Park and Gamble (1980)

Slab Group	w_{exp} (psi)	Simply Spt (psi)	YL (psi)	YL/w	Computed Peak (PP)(psi)	PP/w	Defl Indexed (PDI)(psi)	PDI/ w	Thrust Indexed (PTI)(psi)	PTI/w	P_{avg} (PP+PTI)/2 (psi)	P_{avg}/w ((PP+PTI)/2)/w
Wood1	1486	486	972	0.654	1808	1.217	1708*	1.149	1630	1.097	1719	1.157
Wood2	1620	186	359	0.222	1216	0.750	1105*	0.682	1038	0.641	1127	0.696
Wood3	557	174	347	0.622	612	1.098	592*	1.063	535	0.960	573	1.029
B1	290	80.4	160.8	0.554	373	1.287	370*	1.276	316	1.088	345	1.187
Wood4	68.8	14.4	28.9	0.420	78.1	1.134	68.9	1.001	59.1	0.858	68.5	0.996
Wood5	86.0	27.8	55.7	0.647	101.4	1.179	90.2	1.049	82.4	0.958	91.9	1.068
Wood6	133	45.8	91.6	0.688	135.9	1.022	124.7	0.937	116.9	0.879	126.5	0.950
W14	126	44.1	88.0	0.698	129.4	1.027	121.2	0.962	113.5	0.900	121.5	0.964
K2	174	34.8	69.6	0.400	166.5	0.956	166.4	0.956	149.9	0.862	158.2	0.909
B2	61	18.4	36.9	0.604	72.2	1.184	71.9	1.179	56.1	0.919	64.2	1.052
B3	101	34.4	66.8	0.661	97.8	0.968	88.9	0.879	81.7	0.808	89.7	0.888
W18	68.7	22.9	46.5	0.676	77.7	1.131	70.0	1.019	63.9	0.931	70.8	1.031
W910	73.5	23.3	49.6	0.674	79.2	1.077	70.8	0.964	66.4	0.903	72.8	0.990
W1	66.0	25.9	47.7	0.722	70.0	1.061	56.5	0.856	57.3	0.868	63.6	0.964
W2	64.0	23.1	44.3	0.692	69.9	1.093	62.4	0.974	57.2	0.894	63.6	0.994
W3	68.0	29.7	40.8	0.600	64.9	0.955	46.1	0.678	52.2	0.767	58.6	0.861
W45	72.5	29.9	60.5	0.834	80.6	1.110	66.1	0.911	71.3	0.983	75.9	1.047
W6	68.0	41.1	82.2	1.208	90.3	1.327	90.2*	1.326	88.3	1.290	89.3	1.310
W713	69.0	30.5	61.0	0.880	77.6	1.124	69.7	1.010	70.9	1.027	74.2	1.076
W15	52.0	21.7	43.5	0.836	61.9	1.190	50.6	0.972	54.3	1.045	58.1	1.118
G1	52.0	14.0	26.2	0.503	62.1	1.190	50.4	0.968	50.4	0.968	56.2	1.080
G2	72.0	21.2	42.4	0.588	76.1	1.057	47.7	0.663	64.4	0.895	70.3	0.976
G3	95.0	29.6	59.2	0.623	92.5	0.973	68.5	0.721	80.7	0.850	86.6	0.912
K1	110	33.8	67.6	0.615	104.9	0.953	98.6	0.896	98.6	0.896	101.8	0.925
G4	27.5	9.2	18.3	0.665	31.1	1.130	21.8	0.793	24.5	0.891	27.8	1.011

* This capacity is located prior to the computed peak capacity.

Table D.1. Peak Compressive Membrane Capacity Estimates (Point B, Figure 4.1) Using Park and Gamble (1980) (cont.)

Slab Group	w_{exp} (psi)	Simply Spt (psi)	YL (psi)	YL/w	Computed Peak (PP)(psi)	PP/w	Defl Indexed (PDI)(psi)	PDI/ w	Thrust Indexed (PTI)(psi)	PTI/w	P_{avg} (PP+PTI)/2 (psi)	P_{avg}/w ((PP+TI)/2)/w
G5	41.0	13.8	26.7	0.651	39.5	0.963	34.6	0.843	32.9	0.802	36.2	0.882
G6	46.0	16.9	33.5	0.728	45.4	0.986	39.4	0.856	38.8	0.843	42.1	0.915
C1	16.5	4.4	8.7	0.53	16.8	1.021	16.4	0.991	14.5	0.876	15.7	0.948
C2	18.3	4.4	8.8	0.480	20.1	1.100	19.8	1.080	16.7	0.914	18.4	1.023
RB26	23.3	1.4	1.9	0.085	19.6	0.843	19.2	0.823	15.8	0.678	17.7	0.761
RB27	15.7	1.4	1.7	0.108	11.7	0.744	11.0	0.700	9.8	0.621	10.7	0.683
RB18	15.6	3.5	3.5	0.224	14.3	0.913	13.4	0.858	12.09	0.775	13.2	0.844
RB20	24.5	3.5	3.5	0.143	20.3	0.830	19.6	0.801	16.9	0.689	18.6	0.760
RB19	19.3	3.5	3.5	0.181	14.4	0.746	13.2	0.684	11.9	0.621	13.2	0.684
RB21	16.2	5.2	5.2	0.321	11.7	0.723	11.0	0.680	10.4	0.638	11.0	0.680
RB22	18.5	5.4	5.4	0.292	16.4	0.887	15.7	0.846	13.9	0.753	15.2	0.820
RB23	26.9	5.6	5.6	0.208	24.1	0.896	23.1	0.858	20.2	0.752	22.2	0.824
C3	13.3	3.7	7.3	0.549	13.5	1.018	13.1	0.982	11.6	0.871	12.6	0.944
C4	8.8	2.6	5.1	0.579	9.3	1.060	9.2	1.039	7.8	0.883	8.6	0.972
RB25	6.0	0.9	0.9	0.183	4.7	0.790	4.1	0.687	3.7	0.615	4.2	0.702
RB24	8.0	0.9	0.9	0.163	7.5	0.938	6.6	0.818	5.7	0.708	6.6	0.823
RB11	5.1	1.3	1.3	0.254	4.8	0.949	4.2	0.829	3.8	0.747	4.3	0.848
RB10	7.9	1.3	1.3	0.165	7.7	0.978	6.8	0.856	5.9	0.745	6.8	0.862
RB12	7.0	1.7	1.7	0.242	6.2	0.887	5.3	0.757	4.8	0.678	5.5	0.783
RB13	5.7	1.7	1.7	0.298	5.9	1.026	5.21	0.914	4.6	0.805	5.2	0.915
RB14	7.9	1.7	1.7	0.215	7.9	1.011	7.2	0.909	6.2	0.778	7.1	0.895
RB15	5.9	2.1	2.1	0.355	5.3	0.896	4.7	0.793	4.3	0.722	4.8	0.809
RB17	7.3	2.2	2.2	0.301	8.6	1.175	7.6	1.040	6.7	0.923	7.7	1.049
AVG:				0.490		1.012		0.907		0.846		0.929
STD	DEV:			0.244		0.142		0.152		0.138		0.137

Table D.2. Peak Compressive Membrane Capacity Estimates (Point B, Figure 4.1) With the Author's Compressive Membrane Theory

Slab Group	w_{exp} (psi)	Simply Spt (psi)	YL (psi)	YL/w	Computed Peak (WP)(psi)	WP/w	Defl Indexed (WDI)(psi)	WDI/ w	Thrust Indexed (WTI)(psi)	WTI/ w	W_{avg} (WP+WTI)/2 (psi)	W_{avg}/w ((WP+WTI)/2)/ w
Wood1	1486	486	972	0.654	1812	1.219	1713*	1.153	1631	1.097	1721	1.160
Wood2	1620	186	359	0.222	1220	0.753	1103*	0.681	1040	0.642	1130	0.697
Wood3	557	174	347	0.622	614	1.102	595*	1.068	542	0.972	578	1.037
B1	290	80.4	160.8	0.554	375	1.294	373*	1.287	316	1.089	346	1.192
Wood4	68.8	14.4	28.9	0.420	79.1	1.150	69.4	1.008	60.4	0.878	69.7	1.010
Wood5	86.0	27.8	55.7	0.647	102.5	1.192	90.6	1.053	83.7	0.973	93.1	1.083
Wood6	133	45.8	91.6	0.688	137.0	1.030	125.1	0.941	118.3	0.889	127.6	0.959
W14	126	44.1	88.0	0.698	130.4	1.035	121.6	0.965	114.5	0.908	122.4	0.972
K2	174	34.8	69.6	0.400	173.1	0.995	172.5	0.991	160.1	0.919	166.6	0.957
B2	61	18.4	36.9	0.604	73.3	1.202	72.9	1.195	57.4	0.941	65.4	1.071
B3	101	34.4	66.8	0.661	98.9	0.979	89.4	0.885	82.9	0.821	90.9	0.900
W18	68.7	22.9	46.5	0.676	78.6	1.144	70.0	1.019	65.0	0.946	71.8	1.045
W910	73.5	23.3	49.6	0.674	80.1	1.090	71.1	0.967	67.5	0.918	73.8	1.004
W1	66.0	25.9	47.7	0.722	70.9	1.074	56.5	0.856	58.3	0.883	64.6	0.978
W2	64.0	23.1	44.3	0.692	70.9	1.107	62.7	0.978	58.2	0.910	64.6	1.008
W3	68.0	29.7	40.8	0.600	65.9	0.968	46.1	0.678	53.2	0.780	59.6	0.876
W45	72.5	29.9	60.5	0.834	81.4	1.122	66.1	0.911	72.2	0.995	76.8	1.058
W6	68.0	41.1	82.2	1.208	90.6	1.330	90.6	1.330	88.1	1.295	89.3	1.313
W713	69.0	30.5	61	0.880	78.1	1.132	69.8	1.011	71.7	1.038	74.9	1.085
W15	52.0	21.7	43.5	0.836	62.6	1.203	50.6	0.972	55.1	1.058	58.8	1.131
G1	52.0	14	26.2	0.503	63.5	1.220	50.6	0.972	51.6	0.992	57.5	1.106
G2	72.0	21.2	42.4	0.588	77.5	1.076	47.6	0.661	66.6	0.925	72.1	1.000
G3	95.0	29.6	59.2	0.623	93.8	0.987	68.2	0.717	81.9	0.862	87.9	0.925
K1	110	33.8	67.6	0.615	112.9	1.026	99.6	0.905	110.8	1.007	111.8	1.016
G4	27.5	9.2	18.3	0.665	32.2	1.172	21.9	0.795	25.4	0.923	28.8	1.047

* This capacity is located prior to the computed peak capacity.

Table D.2. Peak Compressive Membrane Capacity Estimates (Point B, Figure 4.1) With the Author's Compressive Membrane Theory (cont.)

Slab Group	w_{exp} (psi)	Simply Spt (psi)	YL (psi)	YL/w	Computed Peak (WP)(psi)	WP/w	Defl Indexed (WDI)(psi)	WDI/ w	Thrust Indexed (WTI)(psi)	WTI/ w	W_{avg} (WP+WTI)/2 (psi)	W_{avg}/w ((WP+WTI)/2)/w
G5	41.0	13.8	26.7	0.651	40.6	0.989	34.9	0.851	34.5	0.841	37.5	0.916
G6	46.0	16.9	33.5	0.728	46.5	1.010	39.6	0.861	39.6	0.862	43.1	0.936
C1	16.5	4.4	8.7	0.53	17.7	1.069	16.8	1.015	15.4	0.932	16.5	1.000
C2	18.3	4.4	8.8	0.480	21.3	1.160	20.5	1.122	18.0	0.984	19.6	1.073
RB26	23.3	1.4	1.9	0.085	25.0	1.073	21.3	0.914	23.3	1.000	24.2	1.036
RB27	15.7	1.4	1.7	0.108	14.0	0.893	11.5	0.732	13.1	0.834	13.6	0.864
RB18	15.6	3.5	3.5	0.224	16.8	1.074	13.9	0.891	15.8	1.013	16.3	1.040
RB20	24.5	3.5	3.5	0.143	25.3	1.032	21.3	0.868	23.6	0.962	24.4	0.997
RB19	19.3	3.5	3.5	0.181	17.2	0.888	13.4	0.694	16.2	0.838	16.7	0.863
RB21	16.2	5.2	5.2	0.321	13.2	0.813	11.3	0.696	12.6	0.776	12.9	0.795
RB22	18.5	5.4	5.4	0.292	19.4	1.046	16.3	0.881	18.3	0.991	18.8	1.018
RB23	26.9	5.6	5.6	0.208	29.9	1.110	25.0	0.929	27.8	1.030	28.9	1.070
C3	13.3	3.7	7.3	0.549	14.3	1.074	13.4	1.009	12.4	0.933	13.4	1.004
C4	8.8	2.6	5.1	0.579	10.0	1.139	9.6	1.086	8.6	0.975	9.3	1.056
RB25	6.0	0.9	0.9	0.183	6.4	1.065	4.3	0.720	5.9	0.988	6.2	1.026
RB24	8.0	0.9	0.9	0.163	10.9	1.365	8.2	1.018	10.1	1.258	10.5	1.310
RB11	5.1	1.3	1.3	0.254	6.4	1.247	4.4	0.862	5.9	1.160	6.2	1.205
RB10	7.9	1.3	1.3	0.165	11.0	1.396	7.4	0.934	10.2	1.280	10.6	1.340
RB12	7.0	1.7	1.7	0.242	8.3	1.188	5.7	0.808	7.7	1.098	8.0	1.143
RB13	5.7	1.7	1.7	0.298	7.8	1.360	5.5	0.957	7.2	1.259	7.5	1.310
RB14	7.9	1.7	1.7	0.215	11.3	1.420	7.9	0.995	10.4	1.310	10.8	1.360
RB15	5.9	2.1	2.1	0.355	6.8	1.140	4.8	0.820	6.3	1.060	6.5	1.106
RB17	7.3	2.2	2.2	0.301	12.1	1.656	8.3	1.140	11.2	1.540	11.7	1.590
AVG:				0.490		1.121		0.933		0.991		1.056
STD	DEV:			0.244		0.159		0.153		0.159		0.156

Table D.3. Comparison of Averages/Standard Deviations for Park and Gamble's and the Author's Compressive Membrane Capacity

	YL/w [a]	PP/w [b]	PDI/w [c]	PTI/w [d]	P_{avg}/w [e]	WP/w [b]	WDI/w [c]	WTI/w [d]	W_{avg}/w [e]
Average - All:	0.490	1.012	0.907	0.846	0.929	1.121	0.933	0.991	1.056
Standard Deviation:	0.244	0.142	0.152	0.137	0.137	0.158	0.153	0.159	0.155
Average - Thick (L/h < 18):	0.644	1.078	0.954	0.918	0.999	1.098	0.960	0.941	1.019
Standard Deviation:	0.169	0.116	0.159	0.116	0.113	0.114	0.163	0.114	0.109
Average - Thin (18 < L/h < 22):	0.235	0.844	0.804	0.711	0.778	1.000	0.846	0.931	0.965
Standard Deviation:	0.133	0.091	0.094	0.079	0.084	0.100	0.106	0.087	0.092
Average - Very Thin (L/h > 22)	0.276	0.971	0.864	0.760	0.866	1.298	0.934	1.193	1.245
Standard Deviation:	0.118	0.101	0.108	0.087	0.093	0.167	0.125	0.164	0.163

[a] YL - yield line capacity with fixed-supported edge conditions.
[b] Compressive membrane theory computed peak capacity: PP - Park and Gamble; WP - Author.
[c] Compressive membrane theory experimental deflection indexed capacity: PDI - Park and Gamble; WDI - Author.
[d] Compressive membrane theory peak thrust indexed capacity: PTI - Park and Gamble; WTI - Author.
[e] Average between the computed peak capacity and the peak thrust indexed capacity: P_{avg} - Park and Gamble; W_{avg} - Author.

Table D.4. Peak Compressive Membrane Capacity Estimates (Point B, Figure 4.1) With Park and Gamble (1980) for Varying Lateral Support Stiffness

Slab Group	S [a] (lb/in)	w_{exp} (psi)	Simply Spt (SS)(psi)	YL (psi)	YL/w	Computed Peak (PP)(psi)	PP/w	Defl Indexed (PDI)(psi)	PDI /w	Thrust Indexed (PTI)(psi)	PTI /w	P_{avg} (PP+PTI)/2 (psi)	P_{avg}/w
Wood1	E_c	1486	486	972	0.654	2131	1.434	2093	1.408	2080	1.399	2105	1.416
Wood1	$0.1E_c$					2037	1.370	2036	1.370	1936	1.302	1986	1.330
Wood1	$0.01E_c$					1748	1.170	1602*	1.078	1556	1.047	1652	1.110
B1	E_c	290	80.4	160.8	0.554	488.6	1.685	452	1.558	466	1.607	477	1.646
B1	$0.1E_c$					455	1.569	441	1.521	416	1.434	436	1.502
B1	$0.01E_c$					353	1.217	345*	1.189	290.6	1.002	321.8	1.109
Wood4	E_c	68.8	14.4	28.9	0.420	107.6	1.563	72.9	1.059	98.3	1.429	102.9	1.496
Wood4	$0.1E_c$					98.9	1.437	72.7	1.056	84.5	1.228	91.7	1.333
Wood4	$0.01E_c$					69.8	1.014	65.2	0.947	50.3	0.732	60.1	0.874
B2	E_c	61	18.4	36.9	0.604	104.7	1.716	88.3	1.447	95.0	1.557	99.8	1.636
B2	$0.1E_c$					95.6	1.567	86.2	1.413	83.2	1.364	89.4	1.466
B2	$0.01E_c$					66.8	1.095	66.8	1.095	50.9	0.835	58.9	0.965
G2	E_c	72.0	21.2	42.4	0.588	90.8	1.372	46.5	0.645	83.6	1.161	87.2	1.211
G2	$0.1E_c$					85.0	1.181	46.9	0.651	75.4	1.097	80.2	1.113
G2	$0.01E_c$					65.9	0.915	48.3	0.671	53.6	0.744	59.8	0.829
G4	E_c	27.5	9.2	18.3	0.665	40.1	1.458	21.7	0.789	34.9	1.269	37.5	1.364
G4	$0.1E_c$					36.7	1.334	21.8	0.793	30.8	1.120	33.8	1.229
G4	$0.01E_c$					25.6	0.931	20.9	0.760	18.9	0.687	22.3	0.809
RB18	E_c	15.6	3.5	3.5	0.224	14.3	0.913	13.4	0.859	12.1	0.776	13.2	0.846
RB18	$0.1E_c$					13.1	0.839	12.8	0.821	10.6	0.679	11.9	0.759
RB18	$0.01E_c$					8.9	0.571	8.6*	0.551	6.3	0.404	7.6	0.487
RB13	E_c	5.7	1.7	1.7	0.298	5.8	1.017	5.2	0.912	4.6	0.807	5.2	0.912
RB13	$0.1E_c$					5.3	0.932	5.0	0.877	3.9	0.684	4.6	0.808
RB13	$0.01E_c$					3.4	0.596	3.4	0.596	2.2	0.377	2.8	0.491

* Capacity is located before the computed peak capacity.

[a] E_c portrays a magnitude only and not the units.

Table D.5. Peak Compressive Membrane Capacity Estimates (Point B, Figure 4.1) With the Author's Compressive Membrane Theory for Varying Lateral Support Stiffness

Slab Group	S [a] (lb/in)	w_{exp} (psi)	Simply Spt (SS)(psi)	YL (psi)	YL/w	Computed Peak (WP)(psi)	WP/w	Defl Indexed (WDI)(psi)	WDI /w	Thrust Indexed (WTI)(psi)	WTI /w	W_{avg} (WP+WTI)/2 (psi)	W_{avg}/w
Wood1	E_c	1486	486	972	0.654	2159	1.453	2101	1.413	2122	1.427	2140	1.440
Wood1	$0.1E_c$					2047	1.377	2044	1.375	1952	1.313	1999	1.346
Wood1	$0.01E_c$					1751	1.178	1607*	1.081	1557	1.047	1654	1.113
B1	E_c	290	80.4	160.8	0.554	507	1.748	454	1.565	494	1.701	500	1.724
B1	$0.1E_c$					463	1.596	444	1.531	428	1.476	445	1.536
B1	$0.01E_c$					354	1.221	347*	1.196	290.7	1.002	322.3	1.111
Wood4	E_c	68.8	14.4	28.9	0.420	115	1.672	72.9	1.059	110	1.599	112.5	1.635
Wood4	$0.1E_c$					102	1.482	72.9	1.059	89.6	1.302	95.8	1.392
Wood4	$0.01E_c$					70.6	1.026	65.6	0.953	51.5	0.748	61.1	0.888
B2	E_c	61	18.4	36.9	0.604	115	1.885	89.4	1.466	110.6	1.813	112.8	1.849
B2	$0.1E_c$					100	1.639	87.4	1.433	88.9	1.457	94.5	1.548
B2	$0.01E_c$					67.6	1.108	67.6	1.108	52.1	0.854	59.8	0.981
G2	E_c	72.0	21.2	42.4	0.588	97.3	1.351	46.3	0.643	94.2	1.308	95.8	1.329
G2	$0.1E_c$					87.9	1.221	46.7	0.649	79.4	1.103	83.7	1.162
G2	$0.01E_c$					66.4	0.922	48.3	0.671	54.4	0.756	60.4	0.839
G4	E_c	27.5	9.2	18.3	0.665	45.9	1.669	21.6	0.785	43.9	1.596	44.9	1.633
G4	$0.1E_c$					39.4	1.433	21.8	0.793	33.9	1.233	36.6	1.333
G4	$0.01E_c$					26.1	0.949	21.1	0.767	19.5	0.709	22.8	0.829
RB18	E_c	15.6	3.5	3.5	0.224	16.8	1.076	13.9	0.891	15.8	1.013	16.3	1.045
RB18	$0.1E_c$					14.3	0.918	13.4	0.859	12.1	0.776	13.2	0.847
RB18	$0.01E_c$					9.1	0.585	8.9*	0.568	6.5	0.417	7.8	0.501
RB13	E_c	5.7	1.7	1.7	0.298	7.8	1.366	5.5	0.965	7.2	1.263	7.5	1.316
RB13	$0.1E_c$					6.3	1.101	5.3	0.929	5.1	0.895	5.7	1.000
RB13	$0.01E_c$					3.5	0.614	3.5	0.614	2.3	0.403	2.9	0.509

* Capacity is located before the computed peak capacity.

[a] E_c portrays only the magnitude and not the units.

Table D.6. Peak Compressive Membrane Capacity Estimates (Point B, Figure 1.1) With Park and Gamble's (1980) and the Author's Compressive Membrane Theory For a Lateral Support Stiffness of Scalar Magnitude E_c Versus Finite Element Results for Fully Fixed-Supported Edge Conditions

Slab Group	S [a] (lb/in)	w_{exp} (psi)	Simply Spt (SS)(psi)	YL (psi)	Computed [b] Peak (PP)(psi)	Defl Indexed (PDI)(psi)	Thrust Indexed (PTI)(psi)	P_{avg} (PP+PTI)/2 (psi)	Peak FE [d] 5 Elements (psi)	Peak FE 7 Elements (psi)	Peak FE 10 Elements (psi)	Average FE (psi)
Wood3	E_c	557	174	347	754 (1.044)	729 (1.009)	729 (1.009)	742 (1.028)	782	684	699	722
Wood4	E_c	68.8	14.4	28.9	108 (0.987)	73 (0.669)	98 (0.902)	103 (0.944)	116	109	103	109
G1	E_c	52.0	14.0	26.2	77 (0.939)	51 (0.621)	70 (0.851)	73.4 (0.895)	86.3	81.5	77.2	82
G4	E_c	27.5	9.2	18.3	46 (1.177)	22 (0.554)	44 (1.126)	44.9 (1.151)	42.2	39.3	36.4	39
AVG:					1.037	0.713	0.972	1.004				
Slab Group	S [a] (lb/in)	w_{exp} (psi)	Simply Spt (SS)(psi)	YL (psi)	Computed [c] Peak (WP)(psi)	Defl Indexed (WDI)(psi)	Thrust Indexed (WTI)(psi)	W_{avg} (WP+WTI)/2 (psi)	Peak FE [d] 5 Elements (psi)	Peak FE 7 Elements (psi)	Peak FE 10 Elements (psi)	Average FE (psi)
Wood3	E_c	557	174	347	774 (1.072)	734 (1.017)	760 (1.053)	767 (1.062)	782	684	699	722
Wood4	E_c	68.8	14.4	28.9	115 (1.055)	73 (0.669)	110 (1.009)	113 (1.032)	116	109	103	109
G1	E_c	52.0	14.0	26.2	84 (1.024)	51 ((0.623)	81 (0.983)	82.1 (1.001)	86.3	81.5	77.2	82
G4	E_c	27.5	9.2	18.3	46 (1.177)	22 (0.554)	44 (1.126)	44.9 (1.151)	42.2	39.3	36.4	39
AVG:					1.082	0.716	1.043	1.061				

[a] E_c portrays only the magnitude and not the units.
[b] First P in abbreviation represents Park and Gamble's compressive membrane theory.
[c] W in abbreviation represents the author's compressive membrane theory.
[d] FE represents finite element.

Table D.7. Deflection Estimates (Point B, Figure 4.1) Using Park and Gamble (1980)

Slab Group	Δ_{exp} (in)	SS [a] (in)	SS /Δ	Defl PP [b] (in)	PP/ Δ	Defl PTI [c] (in)	PTI/ Δ	K(P) [d] (in)	K(P) /Δ	ε (K(P)) (adj) [e] (in/in)	M [f] (in)	M/Δ	ε (M) (adj) [g] (in/in)	W(P) [h] (in)	W(P) /Δ	ε (W(P)) (adj) [i] (in/in)	EC [j] (in)	EC/Δ
Wood1	0.41	0.053	0.130	0.89	2.17	2.30	5.61	0.387	0.94	0.00670	0.098	0.24	0.02500	0.420	1.02	0.00451	0.493	1.201
Wood2	0.39	0.027	0.069	0.89	2.28	2.30	5.89	0.389	0.99	0.00520	0.247	0.63	0.00977	0.420	1.08	0.00369	0.493	1.264
Wood3	0.41	0.082	0.200	0.71	1.73	1.75	4.27	0.424	1.03	0.00450	0.036	0.86	0.01690	0.456	1.11	0.00364	0.626	1.527
B1	0.53	0.109	0.207	0.65	1.23	1.60	3.02	0.444	0.84	0.00755	0.235	0.44	0.01350	0.476	0.89	0.00628	0.646	1.218
Wood4	0.835	0.164	0.196	0.44	0.53	1.10	1.32	0.481	0.58	0.01075	0.473	0.57	0.01220	0.504	0.60	0.00984	0.713	0.854
Wood5	0.885	0.188	0.212	0.44	0.49	1.10	1.24	0.481	0.54	0.01147	0.195	0.22	0.02645	0.504	0.57	0.01052	0.713	0.805
Wood6	0.893	0.164	0.184	0.44	0.49	1.10	1.23	0.481	0.54	0.01158	err	-	0.04050	0.504	0.56	0.01063	0.713	0.798
W14	0.8	0.165	0.207	0.41	0.51	1.04	1.30	0.471	0.59	0.01016	err	-	0.03700	0.492	0.62	0.00941	0.719	0.898
K2	0.21	0.135	0.640	0.23	1.09	0.56	2.66	0.319	1.52	0.00300	0.203	0.97	0.00510	0.320	1.52	0.00296	0.719	3.426
B2	0.50	0.247	0.494	0.44	0.88	1.07	2.14	0.618	1.24	0.00351	0.343	0.69	0.00740	0.648	1.29	0.00323	0.735	1.470
B3	0.86	0.209	0.243	0.44	0.51	1.07	1.24	0.618	0.72	0.00778	err	-	0.02900	0.648	0.75	0.00718	0.735	0.854
W18	0.813	0.233	0.286	0.41	0.50	1.01	1.24	0.131	0.16	0.04720	err	-	0.02010	0.606	0.75	0.00718	0.741	0.911
W910	0.825	0.225	0.273	0.41	0.49	0.98	1.19	0.122	0.15	0.05120	0.108	0.13	0.02640	0.599	0.73	0.00740	0.741	0.898
W1	1.0	0.272	0.272	0.38	0.38	0.98	0.98	0.592	0.59	0.00930	err	-	0.03250	0.617	0.62	0.00869	0.741	0.741
W2	0.8	0.244	0.305	0.38	0.48	0.98	1.23	0.592	0.74	0.00735	err	-	0.02315	0.616	0.77	0.00685	0.741	0.926
W3	1.2	0.277	0.230	0.38	0.32	0.98	0.82	neg	-	-	err	-	0.01546	0.952	0.79	0.00607	0.741	0.617
W45	1.1	0.251	0.228	0.38	0.35	0.89	0.81	neg	-	-	err	-	0.04850	0.669	0.61	0.00828	0.741	0.673

[a] Deflection associated with simply-supported end conditions and a fully cracked moment of inertia.
[b] Deflection associated with the computed peak capacity in Park and Gamble's compressive membrane theory.
[c] Deflection associated with the peak thrust indexed capacity in Park and Gamble's compressive membrane theory.
[d] Keenan's predicted deflection using EQN 4.21 and a strain of 0.005 in/in with Park and Gamble's compressive membrane theory.
[e] The adjusted strain which produces a deflection matching Δ_{exp} using EQN 4.21 with Park and Gamble's compressive membrane theory.
[f] Mattock's predicted capacity using a strain of 0.005 in/in.
[g] The adjusted strain in Mattock's equations which produces a deflection matching Δ_{exp}.
[h] The predicted capacity using the author's curvature based deflection equation and a strain of 0.005 in/in with Park and Gamble's compressive membrane theory.
[i] The adjusted strain in the author's curvature based deflection equation which produces a deflection matching Δ_{exp}.
[j] The predicted deflection using the empirical L/h - Δ/h curves.

Table D.7. Deflection Estimates (Point B, Figure 4.1) Using Park and Gamble (1980) (cont.)

Slab Group	Δ_{exp} (in)	SS [a] (in)	SS /Δ	Defl PP [b] (in)	PP/ Δ	Defl PTI [c] (in)	PTI /Δ	K(P) [d] (in)	K(P) /Δ	ε (K(P)) (adj) [e] (in/in)	M [f] (in)	M/Δ	ε (M) (adj) [g] (in/in)	W(P) [h] (in)	W(P) /Δ	ε (W(P)) (adj) [i] (in/in)	EC [j] (in)	EC/Δ
W6	0.25	0.307	1.229	0.29	1.16	0.56	2.24	0.429	1.72	0.00255	0.085	0.34	0.01450	0.436	1.74	0.00248	0.741	2.963
W713	0.857	0.256	0.298	0.32	0.37	0.80	0.93	0.507	0.59	0.00895	0.096	0.11	0.04379	0.522	0.61	0.00855	0.741	0.864
W15	1.0	0.277	0.277	0.32	0.32	0.83	0.83	0.516	0.52	0.01022	0.115	0.12	0.04400	0.533	0.53	0.00972	0.741	0.741
G1	0.798	0.205	0.257	0.32	0.40	0.80	1.00	0.505	0.63	0.00827	0.352	0.44	0.01530	0.512	0.64	0.00802	0.741	0.928
G2	1.335	0.223	0.167	0.32	0.24	0.80	0.59	0.503	0.38	0.01300	0.125	0.09	0.05000	0.517	0.39	0.01248	0.741	0.555
G3	1.179	0.186	0.157	0.32	0.27	0.80	0.68	0.506	0.43	0.01185	err	-	0.05120	0.519	0.44	0.01135	0.741	0.628
K1	1.00	0.532	0.532	0.38	0.38	1.00	1.00	1.309	1.31	0.00385	err	-	0.02900	1.296	1.29	0.00384	2.250	2.250
G4	0.805	0.366	0.455	0.26	0.32	0.68	0.84	0.765	0.95	0.00523	0.275	0.34	0.01345	0.783	0.97	0.00507	0.766	0.952
G5	0.601	0.293	0.486	0.26	0.43	0.68	1.13	0.765	1.27	0.00393	err	-	0.01428	0.782	1.30	0.00381	0.766	1.270
G6	0.65	0.295	0.453	0.26	0.40	0.68	1.05	0.766	1.18	0.00426	err	-	0.01880	0.783	1.21	0.00413	0.766	1.178
C1	0.65	0.722	1.110	0.41	0.63	1.07	1.65	2.040	3.13	0.00167	0.424	0.65	0.00926	2.010	3.13	0.00167	1.000	1.538
C2	0.65	0.697	1.070	0.47	0.72	1.19	1.83	2.157	3.14	0.00149	0.515	0.79	0.00705	2.132	3.28	0.00149	1.000	1.538
RB26	0.446	0.286	0.640	0.32	0.72	0.80	1.79	neg	-	-	36965	-	-	err	-	0.00110	0.517	1.160
RB27	0.441	0.382	0.867	0.23	0.52	0.65	1.47	neg	-	-	37003	-	-	err	-	0.00115	0.517	1.170
RB18	0.462	0.567	1.220	0.26	0.56	0.68	1.47	err	-	-	err	-	-	err	-	0.00104	0.517	1.120

Table D.7. Deflection Estimates (Point B, Figure 4.1) Using Park and Gamble (1980) (cont.)

Slab Group	Δ_{exp} (in)	SS [a] (in)	SS /Δ	Defl PP [b] (in)	PP/ Δ	Defl PTI [c] (in)	PTI/ Δ	K(P) [d] (in)	K(P) /Δ	ε (K(P)) (adj) [e] (in/in)	M [f] (in)	M/Δ	ε (M) (adj) [g] (in/in)	W(P) [h] (in)	W(P) /Δ	ε (W(P)) (adj) [i] (in/in)	EC [j] (in)	EC/Δ
RB20	0.474	0.439	0.926	0.32	0.68	0.77	1.63	neg	-	-	96133	-	-	err	-	0.00108	0.517	1.090
RB19	0.551	0.305	0.553	0.26	0.47	0.71	1.29	neg	-	-	96760	-	-	err	-	0.00127	0.517	0.939
RB21	0.447	0.234	0.523	0.20	0.45	0.35	0.78	neg	-	-	err	-	-	err	-	0.00071	0.517	1.150
RB22	0.45	0.695	1.544	0.26	0.58	0.71	1.57	neg	-	-	1.5E5	-	-	err	-	0.00086	0.517	1.150
RB23	0.512	0.527	1.029	0.32	0.63	0.80	1.56	neg	-	-	1.5E5	-	-	err	-	0.00109	0.517	1.010
C3	0.65	0.864	1.320	0.41	0.63	1.01	1.55	err	-	0.00136	0.448	0.69	0.00847	err	-	0.00136	0.548	0.844
C4	0.65	1.308	2.010	0.44	0.68	1.16	1.78	err	-	0.00083	0.547	0.84	0.00638	err	-	0.00083	0.762	1.172
RB25	0.50	0.708	1.416	0.23	0.46	0.62	1.24	neg	-	-	2.6E8	-	-	err	-	0.00072	0.510	1.020
RB24	0.55	0.639	1.160	0.29	0.53	0.71	1.29	neg	-	-	2.6E8	-	-	err	-	0.00079	0.510	0.928
RB11	0.506	0.883	1.744	0.23	0.45	0.62	1.23	neg	-	-	3.9E8	-	-	err	-	0.00067	0.510	1.008
RB10	0.576	1.073	1.860	0.29	0.50	0.71	1.23	neg	-	-	3.9E8	-	-	err	-	0.00079	0.510	0.886
RB12	0.545	1.192	2.186	0.26	0.48	0.68	1.25	neg	-	-	5.2E8	-	-	err	-	0.00069	0.510	0.936
RB13	0.506	0.991	1.958	0.26	0.51	0.65	1.28	neg	-	-	5.2E8	-	-	err	-	0.00062	0.510	1.008
RB14	0.536	1.110	2.070	0.29	0.54	0.71	1.32	neg	-	-	5.2E8	-	-	err	-	0.00069	0.510	0.951
RB15	0.507	1.205	2.376	0.23	0.45	0.62	1.22	neg	-	-	err	-	-	err	-	0.00054	0.510	1.006
RB17	0.562	1.174	2.089	0.29	0.52	0.71	1.26	neg	-	-	6.5E8	-	-	err	-	0.00069	0.510	0.907
AVG:			0.799		0.63		1.59		0.55			0.17			0.62			1.108
STD	DEV:		0.676		0.42		1.07		0.72			0.28			0.72			0.514

Table D.8. Deflection Estimates (Point B, Figure 4.1) Using the Author's Compressive Membrane Theory

Slab Group	Δ_{exp} (in)	SS [a] (in)	SS /Δ	Defl WP [b] (in)	WP/ Δ	Defl WTI [c] (in)	WTI /Δ	K(W) [d] (in)	K (W)/ Δ	ε (K(W)) (adj) [e] (in/in)	M [f] (in)	M/Δ	ε (M) (adj) [g] (in/in)	W(W) [h] (in)	W (W)/ Δ	ε (W(W)) (adj) [i] (in/in)	EC [j] (in)	EC/Δ
Wood1	0.41	0.053	0.130	0.89	2.17	2.30	5.61	0.382	0.93	0.00635	0.098	0.24	0.02500	0.416	1.01	0.00510	0.493	1.201
Wood2	0.39	0.027	0.069	0.89	2.28	2.30	5.89	0.382	0.98	0.00550	0.247	0.63	0.00970	0.416	1.07	0.00390	0.493	1.264
Wood3	0.41	0.082	0.200	0.68	1.66	1.70	4.15	0.417	1.02	0.00475	0.035	0.09	0.01690	0.449	1.09	0.00388	0.626	1.527
B1	0.53	0.109	0.207	0.65	1.23	1.60	3.02	0.436	0.82	0.00780	0.235	0.44	0.01350	0.468	0.88	0.00657	0.646	1.218
Wood4	0.835	0.164	0.196	0.41	0.49	1.07	1.28	0.469	0.56	0.01094	0.473	0.57	0.01220	0.493	0.59	0.01022	0.713	0.854
Wood5	0.885	0.188	0.212	0.41	0.46	1.07	1.21	0.469	0.53	0.01167	0.195	0.22	0.02645	0.493	0.56	0.01092	0.713	0.805
Wood6	0.893	0.164	0.184	0.41	0.46	1.07	1.19	0.469	0.53	0.01179	err	-	0.04050	0.493	0.55	0.01103	0.713	0.798
W14	0.8	0.165	0.207	0.38	0.47	1.01	1.26	0.459	0.57	0.01036	err	-	0.03700	0.480	0.60	0.00977	0.719	0.898
K2	0.21	0.135	0.640	0.18	0.86	0.44	2.09	0.299	1.42	0.00336	0.203	0.97	0.00510	0.301	1.43	0.00332	0.719	3.426
B2	0.50	0.247	0.494	0.44	0.88	1.04	2.08	0.602	1.20	0.00370	0.343	0.69	0.00740	0.633	1.27	0.00343	0.735	1.470
B3	0.86	0.209	0.243	0.44	0.51	1.04	1.21	0.602	0.70	0.00798	err	-	0.02900	0.633	0.74	0.00745	0.735	0.854
W18	0.813	0.233	0.286	0.38	0.47	0.98	1.21	0.591	0.73	0.00747	err	-	0.02010	0.592	0.73	0.00745	0.741	0.911
W910	0.825	0.225	0.273	0.38	0.46	0.95	1.15	0.586	0.71	0.00765	0.108	0.13	0.02640	0.586	0.71	0.00767	0.741	0.898
W1	1.0	0.272	0.272	0.38	0.38	0.95	0.95	0.576	0.58	0.00950	err	-	0.03250	0.602	0.60	0.00900	0.741	0.741
W2	0.8	0.244	0.305	0.38	0.47	0.95	1.19	0.576	0.72	0.00752	err	-	0.02315	0.602	0.75	0.00712	0.741	0.926
W3	1.2	0.277	0.230	0.38	0.32	0.95	0.79	0.576	0.48	0.01115	err	-	0.01546	0.922	0.77	0.00630	0.741	0.617
W45	1.1	0.251	0.228	0.35	0.32	0.86	0.78	0.537	0.49	0.01083	err	-	0.04850	0.654	0.59	0.00855	0.741	0.673

[a] Deflection associated with simply-supported end conditions and a fully cracked moment of inertia.
[b] Deflection associated with the computed peak capacity in the author's compressive membrane theory.
[c] Deflection associated with the peak thrust indexed capacity in the author's compressive membrane theory.
[d] Keenan's predicted deflection using EQN 4.22 and a strain of 0.005 in/in with the author's compressive membrane theory.
[e] The adjusted strain which produces a deflection matching Δ_{exp} using EQN 4.22 with the author's compressive membrane theory.
[f] Mattock's predicted capacity using a strain of 0.005 in/in.
[g] The adjusted strain in Mattock's equations which produces a deflection matching Δ_{exp}.
[h] The predicted capacity using the author's curvature based deflection equation and a strain of 0.005 in/in with the author's compressive membrane theory.
[i] The adjusted strain in the author's curvature based deflection equation which produces a deflection matching Δ_{exp}.
[j] The predicted deflection using the empirical L/h - Δ/h curves.

Table D.8. Deflection Estimates (Point B, Figure 4.1) Using the Author's Compressive Membrane Theory (cont.)

Slab Group	Δ_{exp} (in)	SS [a] (in)	SS /Δ	Defl WP [b] (in)	WP/ Δ	Defl WTI [c] (in)	WTI /Δ	K(W) [d] (in)	K (W)/ Δ	ε (K(W)) (adj) [e] (in/in)	M [f] (in)	M/Δ	ε (M)[g] (adj) (in/in)	W(W) [h] (in)	W (W)/ Δ	ε (W(W)) (adj) [i] (in/in)	EC [j] (in)	EC/Δ
W6	0.25	0.307	1.229	0.26	1.04	0.59	2.36	0.425	1.70	0.00261	0.085	0.34	0.01450	0.432	1.73	0.00255	0.741	2.963
W713	0.857	0.256	0.298	0.32	0.37	0.77	0.89	0.497	0.58	0.00908	0.096	0.11	0.04379	0.512	0.59	0.00881	0.741	0.864
W15	1.0	0.277	0.277	0.32	0.32	0.80	0.80	0.505	0.51	0.0104	0.115	0.12	0.04400	0.521	0.52	0.01010	0.741	0.741
G1	0.798	0.205	0.257	0.29	0.36	0.77	0.97	0.487	0.61	0.00860	0.352	0.44	0.01530	0.501	0.69	0.00836	0.741	0.928
G2	1.335	0.223	0.167	0.29	0.22	0.74	0.55	0.485	0.36	0.01326	0.125	0.09	0.05000	0.499	0.37	0.01301	0.741	0.555
G3	1.179	0.186	0.157	0.29	0.25	0.77	0.65	0.487	0.41	0.01210	err	-	0.05120	0.502	0.43	0.01180	0.741	0.628
K1	1.00	0.532	0.532	0.10	0.10	0.29	0.29	1.209	1.21	0.00421	err	-	0.02900	1.197	1.20	0.00421	2.250	2.250
G4	0.805	0.366	0.455	0.26	0.32	0.65	0.81	0.733	0.91	0.00543	0.275	0.34	0.01345	0.751	0.93	0.00531	0.766	0.952
G5	0.601	0.293	0.486	0.26	0.43	0.62	1.03	0.733	1.22	0.00412	err	-	0.01428	0.751	1.25	0.00403	0.766	1.270
G6	0.65	0.295	0.453	0.26	0.40	0.65	1.00	0.733	1.13	0.00446	err	-	0.01880	0.751	1.15	0.00436	0.766	1.178
C1	0.65	0.722	1.110	0.35	0.54	0.92	1.42	1.944	2.99	0.00184	0.424	0.65	0.00926	1.922	2.95	0.00184	1.000	1.538
C2	0.65	0.697	1.070	0.41	0.63	1.04	1.60	2.036	3.13	0.00168	0.515	0.79	0.00705	2.015	3.09	0.00168	1.000	1.538
RB26	0.446	0.286	0.640	0.12	0.27	0.29	0.65	2.030	4.55	0.00149	36965	-	-	2.290	5.13	0.00144	0.517	1.160
RB27	0.441	0.382	0.867	0.08	0.18	0.23	0.52	2.016	4.57	0.00140	37003	-	-	err	-	0.00139	0.517	1.170
RB18	0.462	0.567	1.220	0.08	0.17	0.23	0.49	2.010	4.33	0.00157	err	-	-	err	-	0.00130	0.517	1.120

Table D.8. Deflection Estimates (Point B, Figure 4.1) Using the Author's Compressive Membrane Theory (cont.)

Slab Group	Δ_{exp} (in)	SS [a] (in)	SS /Δ	Defl WP [b] (in)	WP/ Δ	Defl WTI [c] (in)	WTI /Δ	K(W) [d] (in)	K (W)/ Δ	ε (K(W)) (adj) [e] (in/in)	M [f] (in)	M/Δ	ε (M) (adj) [g] (in/in)	W(W) [h] (in)	W (W)/ Δ	ε (W(W)) (adj) [i] (in/in)	EC [j] (in)	EC/Δ
RB20	0.474	0.439	0.926	0.10	0.21	0.29	0.61	2.053	4.29	0.00159	96133	-	-	err	-	0.00142	0.517	1.090
RB19	0.551	0.305	0.553	0.08	0.16	0.23	0.42	2.019	3.66	0.00185	96760	-	-	err	-	0.00154	0.517	0.939
RB21	0.447	0.234	0.523	0.06	0.13	0.20	0.45	2.008	4.49	0.00153	err	-	-	err	-	0.00090	0.517	1.150
RB22	0.45	0.695	1.544	0.08	0.18	0.23	0.51	2.020	4.48	0.00153	1.5E5	-	-	err	-	0.00115	0.517	1.150
RB23	0.512	0.527	1.029	0.12	0.23	0.32	0.63	2.030	3.96	0.00170	15449	-	-	err	-	0.00143	0.517	1.010
C3	0.65	0.864	1.320	0.35	0.54	0.86	1.32	err	-	0.00151	0.448	0.69	0.00847	err	-	0.00151	0.548	0.844
C4	0.65	1.308	2.010	0.38	0.59	0.95	1.46	err	-	0.00098	0.547	0.84	0.00638	err	-	0.00098	0.762	1.172
RB25	0.50	0.708	1.416	0.06	0.12	0.18	0.36	err	-	0.00108	2.6E8	-	-	err	-	0.00095	0.510	1.020
RB24	0.55	0.639	1.160	0.01	0.18	0.23	0.42	err	-	0.00115	2.6E8	-	-	err	-	0.00108	0.510	0.928
RB11	0.506	0.883	1.744	0.06	0.12	0.18	0.36	err	-	0.00109	3.9E8	-	-	err	-	0.00089	0.510	1.008
RB10	0.576	1.073	1.860	0.10	0.17	0.23	0.39	err	-	0.00120	3.9E8	-	-	err	-	0.00108	0.510	0.886
RB12	0.545	1.192	2.186	0.06	0.11	0.20	0.37	err	-	0.00115	5.2E8	-	-	err	-	0.00094	0.510	0.936
RB13	0.506	0.991	1.958	0.06	0.12	0.20	0.39	err	-	0.00108	5.2E8	-	-	err	-	0.00087	0.510	1.008
RB14	0.536	1.110	2.070	0.08	0.15	0.23	0.43	err	-	0.00113	5.2E8	-	-	err	-	0.00098	0.510	0.951
RB15	0.507	1.205	2.376	0.06	0.12	0.18	0.36	err	-	0.00109	err	-	-	err	-	0.00075	0.510	1.006
RB17	0.562	1.174	2.089	0.10	0.18	0.23	0.41	err	-	0.00117	6.5E8	-	-	err	-	0.00098	0.510	0.907
AVG:			0.799		0.47		1.21		1.29			0.17			0.71			1.108
STD	DEV:		0.676		0.47		1.19		1.49			0.28			0.94			0.514

Table D.9. Comparison of Averages/Standard Deviations for the Deflection Estimates in Tables D.7 - D.8 Determined Through Park and Gamble's and the Author's Compressive Membrane Theories

	SS/Δ [a]	PP/Δ [b]	WP/Δ [b]	PTI/Δ [c]	WTI/Δ [c]	K(P)/Δ [d]	K(W)/Δ [d]	M/Δ [e]	W(P)/Δ [f]	W(W)/Δ [f]	EC/Δ [g]
Average - All:	0.799	0.634	0.475	1.587	1.208	0.550	1.293	0.175	0.621	0.708	1.108
Standard Deviation:	0.676	0.424	0.475	1.068	1.197	0.725	1.492	0.277	0.729	0.943	0.514
Average - Thick (L/h < 18):	0.375	0.693	0.651	1.723	1.636	0.911	0.956	0.236	1.028	0.995	1.163
Standard Deviation:	0.289	0.533	0.534	1.344	1.359	0.736	0.656	0.284	0.678	0.636	0.649
Average - Thick (no outliers):						0.746	0.800		0.867	0.845	0.944
Standard Deviation:						0.435	0.332		0.342	0.327	0.254
Average - All Thin (L/h > 18):	1.447	0.545	0.026	1.380	0.555	-	1.807	0.081	-	0.270	1.024
Standard Deviation:	0.576	0.082	0.129	0.231	0.301	-	2.128	0.236	-	1.146	0.103
Average - Thin (18 < L/h < 22):	0.958	0.581	0.229	1.457	0.623	-	3.815	0.077	-	0.570	1.070
Standard Deviation:	0.335	0.085	0.116	0.270	0.259	-	1.378	0.216	-	1.612	0.108
Average - Very Thin (L/h > 22):	1.887	0.512	0.185	1.311	0.495	-	-	0.084	-	-	0.982
Standard Deviation:	0.346	0.062	0.136	0.161	0.323	-	-	0.253	-	-	0.078

[a] Deflection estimate for simply-supported slab with a fully cracked moment of inertia.
[b] Deflection associated with the compressive membrane computed peak capacity: PP - Park and Gamble; WP - Author.
[c] Deflection associated with the compressive membrane peak thrust indexed capacity: PTI - Park and Gamble; WTI - Author.
[d] Deflection estimate using Keenan's curvature based equation within a compressive membrane theory: K(P) - Park and Gamble; K(W) - Author.
[e] Mattock's deflection estimate.
[f] Deflection estimate using the author's curvature based equation with a compressive membrane theory: W(P) - Park and Gamble; W(W) - Author.
[g] Empirical curve deflection estimate.

Table D.10. Regression Output for the Empirical Deflection Curves and the Strain Estimates

	L/h (L/h < 15) - Δ/h	L/h (L/h >18) - Δ/h	f' c –ε (M)	f' c –ε (W(P))	f'c –ε (W(W))	f' c –ε (K(W))
Constant	-0.03757	0.007527	0.071153	0.018821	0.018495	0.019664
Std Err of Y Est	0.053254	0.035505	0.011450	0.002140	0.002082	0.002365
R Squared	0.880808	0.62512	0.339619	0.493556	0.499424	0.443470
# of Observations	8	4	27	27	27	27
Degrees of Freedom	6	2	25	25	25	25
X Coefficient	0.034423	0.008764	-9.44692454E-06	-2.43088747E-06	-2.39279751E-06	-2.42940757E-06
Std Err of Coefficient	0.00517	0.004799	2.63463985E-06	4.92484641E-07	4.79110781E-07	5.44305234E-07

Table D.11. Deflection Estimates Using the Average of the Peak Thrust Indexed Capacities From Park and Gamble's and the Author's Compressive Membrane Theories

Slab Group	Δ_{exp} (in)	PTI [a] (in)	PTI /Δ	WTI [b] (in)	WTI /Δ	TI_{avg} (PTI+WTI)/2 (in)	TI_{avg} /Δ
Wood1	0.41	2.30	5.61	2.30	5.61	2.30	5.61
Wood2	0.39	2.30	5.89	2.30	5.89	2.30	5.89
Wood3	0.41	1.75	4.27	1.70	4.15	1.73	4.21
B1	0.53	1.60	3.02	1.60	3.02	1.60	3.02
Wood4	0.835	1.10	1.32	1.07	1.28	1.09	1.29
Wood5	0.885	1.10	1.24	1.07	1.21	1.09	1.22
Wood6	0.893	1.10	1.23	1.07	1.20	1.09	1.21
W14	0.8	1.04	1.30	1.01	1.26	1.03	1.28
K2	0.21	0.56	2.66	0.44	2.09	0.50	2.38
B2	0.50	1.07	2.14	1.04	2.08	1.06	2.11
B3	0.86	1.07	1.24	1.04	1.21	1.06	1.23
W18	0.813	1.01	1.24	0.98	1.21	0.99	1.22
W910	0.825	0.98	1.19	0.95	1.15	0.97	1.17
W1	1.0	0.98	0.98	0.95	0.95	0.97	0.97
W2	0.8	0.98	1.23	0.95	1.19	0.96	1.21
W3	1.2	0.98	0.82	0.95	0.79	0.97	0.80
W45	1.1	0.89	0.81	0.86	0.78	0.88	0.79
W6	0.25	0.56	2.24	0.59	2.36	0.58	2.30
W713	0.857	0.80	0.93	0.77	0.89	0.79	0.92
W15	1.0	0.83	0.83	0.80	0.80	0.82	0.82
G1	0.798	0.80	1.00	0.77	0.97	0.78	0.98
G2	1.335	0.80	0.59	0.74	0.55	0.77	0.58
G3	1.179	0.80	0.68	0.77	0.65	0.79	0.66
K1	1.00	1.00	1.00	0.29	0.29	0.65	0.65
G4	0.805	0.68	0.84	0.65	0.81	0.67	0.83

[a] The peak thrust indexed capacity using Park and Gamble's compressive membrane theory.
[b] The peak thrust indexed capacity using the author's compressive membrane theory.

Table D.11. Deflection Estimate Using the Average of the Peak Thrust Indexed Capacities From Park and Gamble's and the Author's Compressive Membrane Theories (cont.)

Slab Group	Δ_{exp} (in)	PTI [a] (in)	PTI /Δ	WTI [b] (in)	WTI /Δ	TI_{avg} (PTI+WTI)/2 (in)	TI_{avg} /Δ
G5	0.601	0.68	1.13	0.62	1.03	0.65	1.08
G6	0.65	0.68	1.05	0.65	1.00	0.67	1.02
C1	0.65	1.07	1.65	0.92	1.42	0.99	1.53
C2	0.65	1.19	1.83	1.04	1.60	1.12	1.72
RB26	0.446	0.80	1.79	0.29	0.65	0.55	1.22
RB27	0.441	0.65	1.47	0.23	0.52	0.44	0.99
RB18	0.462	0.68	1.47	0.23	0.49	0.46	0.98
RB20	0.474	0.77	1.62	0.29	0.61	0.53	1.12
RB19	0.551	0.71	1.29	0.23	0.42	0.47	0.85
RB21	0.447	0.35	0.78	0.20	0.45	0.27	0.62
RB22	0.45	0.71	1.57	0.23	0.51	0.47	1.04
RB23	0.512	0.80	1.56	0.32	0.63	0.56	1.09
C3	0.65	1.01	1.55	0.86	1.32	0.93	1.44
C4	0.65	0.65	1.78	0.95	1.46	1.06	1.62
RB25	0.50	0.62	1.24	0.18	0.36	0.40	0.80
RB24	0.55	0.71	1.29	0.23	0.42	0.47	0.86
RB11	0.506	0.62	1.22	0.18	0.36	0.40	0.79
RB10	0.576	0.71	1.23	0.23	0.40	0.47	0.82
RB12	0.545	0.68	1.25	0.20	0.37	0.44	0.81
RB13	0.506	0.65	1.28	0.20	0.39	0.43	0.84
RB14	0.536	0.71	1.32	0.23	0.43	0.47	0.88
RB15	0.507	0.62	1.22	0.18	0.36	0.40	0.79
RB17	0.562	0.71	1.26	0.23	0.41	0.47	0.84

Table D.11. Deflection Estimate Using the Average of the Peak Thrust Indexed Capacities From Park and Gamble's and the Author's Compressive Membrane Theories (cont.)

Slab Group	Δ_{exp} (in)	PTI [a] (in)	PTI /Δ	WTI [b] (in)	WTI /Δ	TI_{avg} (PTI+WTI)/2 (in)	TI_{avg} /Δ
Average - All:			1.587		1.208		1.398
Standard Deviation:			1.068		1.196		1.116
Average - Thick:			1.723		1.636		1.679
Standard Deviation:			1.344		1.359		1.349
Average - All Thin:			1.380		0.555		0.968
Standard Deviation:			0.231		0.301		0.239
Average - Thin:			1.457		0.622		1.041
Standard Deviation:			0.270		0.259		0.216
Average - Very Thin:			1.311		0.495		0.903
Standard Deviation:			0.161		0.323		0.241

Table D.12. Comparison of Computed Strains

Slab Group	ε [a] $(M)_{adj}$ (in/in)	ε [b] $(M)_{est}$ (in/in)	$\varepsilon (M)_{est}/\varepsilon (M)_{adj}$	ε [a] $(W(P))_{adj}$ (in/in)	ε [c] $(W(P)_{est}$ (in/in)	$\varepsilon (W(P)_{est}/\varepsilon (W(P))_{adj}$	ε [d] $(W(W))_{adj}$ (in/in)	ε [e] $(W(W))_{est}$ (in/in)	$\varepsilon (W(W))_{est}/\varepsilon (W(W))_{adj}$	ε [d] $(K(W))_{adj}$ (in/in)	ε [f] $(K(W)_{est}$ (in/in)	$\varepsilon (K(W)_{est}/\varepsilon (K(W))_{adj}$
Wood1	0.02500	0.01542	0.617	0.00451	0.004378	0.971	0.00510	0.004656	0.931	0.00635	0.005331	0.839
Wood2	0.00970	0.01542	1.589	0.00369	0.004378	1.186	0.00390	0.004656	1.194	0.00550	0.005331	0.969
Wood3	0.01690	0.01542	0.912	0.00364	0.004378	1.203	0.00388	0.004656	1.200	0.00475	0.005331	1.122
B1	0.01350	0.01419	1.051	0.00628	0.004067	0.647	0.00657	0.004342	0.661	0.00780	0.005015	0.643
Wood4	0.01220	0.03337	2.735	0.00984	0.008924	0.907	0.01022	0.009256	0.906	0.01094	0.009947	0.909
Wood5	0.02645	0.03337	1.262	0.01052	0.008924	0.848	0.01092	0.009256	0.848	0.01167	0.009947	0.852
Wood6	0.04050	0.03337	0.824	0.01063	0.008924	0.839	0.01103	0.009256	0.839	0.01179	0.009947	0.844
W14	0.03700	0.03752	1.014	0.00941	0.009977	1.060	0.00977	0.010321	1.056	0.01036	0.011016	1.063
K2	0.00510	0.00748	1.467	0.00296	0.002368	0.799	0.00332	0.002623	0.789	0.00336	0.003290	0.979
B2	0.00740	0.01372	1.854	0.00323	0.003947	1.222	0.00343	0.004221	1.231	0.00370	0.004894	1.323
B3	0.02900	0.01372	0.473	0.00718	0.003947	0.549	0.00745	0.004221	0.567	0.00798	0.004894	0.614
W18	0.02010	0.02416	1.202	0.00718	0.006591	0.918	0.00745	0.006895	0.926	0.00747	0.007578	1.015
W910	0.02640	0.02581	0.978	0.00740	0.007010	0.947	0.00767	0.007319	0.954	0.00765	0.008003	1.046
W1	0.03250	0.02893	0.890	0.00869	0.007799	0.897	0.00900	0.008118	0.902	0.00950	0.008805	0.927
W2	0.02315	0.02893	1.249	0.00685	0.007799	1.139	0.00712	0.008118	1.140	0.00752	0.008805	1.171
W3	0.01546	0.02893	1.871	0.00607	0.007799	1.285	0.00630	0.008118	1.288	0.01115	0.008805	0.789
W45	0.04850	0.02874	0.593	0.00828	0.007752	0.936	0.00855	0.008069	0.944	0.01083	0.008756	0.808

[a] The adjusted strains from Table D.7.

[b] The author's estimated strain for Mattock's equations using a relationship between f'_c and ε.

[c] The author's estimated strain for his curvature based deflection equation in Park and Gamble's compressive membrane theory using a relationship between f'_c and ε.

[d] The adjusted strains from Table D.8.

[e] The author's estimated strain for his curvature based deflection equation in his compressive membrane theory using a relationship between f'_c and ε.

[f] The author's estimated strain for Keenan's equations in the author's compressive membrane theory using a relationship between f'_c and ε.

Table D.12. Comparison of Computed Strains (cont.)

Slab Group	ε [a] $(M)_{adj}$ (in/in)	ε [b] $(M)_{est}$ (in/in)	$\varepsilon (M)_{est}/\varepsilon (M)_{adj}$	ε [a] $(W(P))_{adj}$ (in/in)	ε [c] $(W(P)_{est}$ (in/in)	$\varepsilon (W(P)_{est}/\varepsilon (W(P))_{adj}$	ε [d] $(W(W))_{adj}$ (in/in)	ε [e] $(W(W))_{est}$ (in/in)	$\varepsilon (W(W))_{est}/\varepsilon (W(W))_{adj}$	ε [d] $(K(W))_{adj}$ (in/in)	ε [f] $(K(W)_{est}$ (in/in)	$\varepsilon (K(W)_{est}/\varepsilon (K(W))_{adj}$
W6	0.01450	0.02874	1.982	0.00248	0.007752	3.126	0.00255	0.008069	3.164	0.00261	0.008756	3.361
W713	0.04379	0.03176	0.725	0.00855	0.008517	0.996	0.00881	0.008844	1.004	0.00908	0.009534	1.049
W15	0.04400	0.03752	0.853	0.00972	0.009907	1.026	0.01010	0.010321	1.022	0.0104	0.011016	1.059
G1	0.01530	0.03014	1.970	0.00802	0.008108	1.011	0.00836	0.008430	1.008	0.00860	0.009118	1.060
G2	0.05000	0.03084	0.617	0.01248	0.008285	0.664	0.01301	0.008609	0.662	0.01326	0.009298	0.702
G3	0.05120	0.02992	0.584	0.01135	0.008051	0.709	0.01180	0.008372	0.709	0.01210	0.009060	0.749
K1	0.02900	0.02382	0.821	0.00384	0.006507	1.695	0.00421	0.006811	1.618	0.00421	0.007493	1.779
G4	0.01345	0.02396	1.781	0.00507	0.006541	1.290	0.00531	0.006845	1.289	0.00543	0.007527	1.386
G5	0.01428	0.02407	1.686	0.00381	0.006570	1.724	0.00403	0.006874	1.707	0.00412	0.007556	1.832
G6	0.01880	0.02396	1.274	0.00381	0.006541	1.584	0.00436	0.006845	1.569	0.00446	0.007527	1.688
C1	0.00926			0.00413			0.00184			0.00184		
C2	0.00705			0.00167			0.00168			0.00168		
RB26				0.00149			0.00144			0.00149		
RB27				0.00110			0.00139			0.00140		
RB18				0.00115			0.00130			0.00157		
RB20				0.00104			0.00142			0.00159		
RB19				0.00127			0.00154			0.00185		
RB21				0.00071			0.00090			0.00153		
RB22				0.00086			0.00115			0.00153		
RB23				0.00109			0.00143			0.00170		
C3	0.00847			0.00136			0.00151			0.00151		
C4	0.00638			0.00083			0.00098			0.00098		

Table D.12. Comparison of Computed Strains (cont.)

Slab Group	ε^{a} $(M)_{adj}$ (in/in)	ε^{b} $(M)_{est}$ (in/in)	$\varepsilon (M)_{est}/\varepsilon (M)_{adj}$	ε^{a} $(W(P))_{adj}$ (in/in)	ε^{c} $(W(P)_{est}$ (in/in)	ε $(W(P)_{est}/\varepsilon (W(P))_{adj}$	ε^{d} $(W(W))_{adj}$ (in/in)	ε^{e} $(W(W))_{est}$ (in/in)	ε $(W(W))_{est}/\varepsilon (W(W))_{adj}$	ε^{d} $(K(W))_{adj}$ (in/in)	ε^{f} $(K(W)_{est}$ (in/in)	ε $(K(W)_{est}/\varepsilon (K(W))_{adj}$
RB25				0.00072			0.00095			0.00108		
RB24				0.00079			0.00108			0.00115		
RB11				0.00067			0.00089			0.00109		
RB10				0.00079			0.00108			0.00120		
RB12				0.00069			0.00094			0.00115		
RB13				0.00062			0.00087			0.00108		
RB14				0.00069			0.00098			0.00113		
RB15				0.00054			0.00075			0.00109		
RB17				0.00069			0.00098			0.00117		
AVG	(Thick):		1.218			1.118			1.116			1.133
STD	DEV:		0.548			0.489			0.489			0.537
AVG	(Thin):			0.00117			0.00142			0.00161		
STD	DEV:			0.00024			0.00024			0.00013		
AVG	(VThin):			0.00070			0.00095			0.00111		
STD	DEV:			0.00021			0.00018			0.00013		

Table D.13. Peak Capacity Deflection Estimates Generated With Strain Estimates and Empirical Deflection Curves

Slab Group	Δ_{exp} (in)	W(P) [a] (in)	W(P) /Δ	W(W) [b] (in)	W(W) /Δ	K(W) [c] (in)	K(W) /Δ	EC [d] (in)	EC/Δ
Wood1	0.41	0.4068	0.992	0.4077	0.994	0.3876	0.945	0.493	1.201
Wood2	0.39	0.4068	1.043	0.4077	1.045	0.3876	0.994	0.493	1.264
Wood3	0.41	0.4359	1.063	0.4371	1.066	0.4266	1.040	0.626	1.527
B1	0.53	0.4403	0.831	0.4419	0.834	0.4365	0.823	0.646	1.218
Wood4	0.835	0.7693	0.921	0.7689	0.921	0.7702	0.922	0.713	0.854
Wood5	0.885	0.7693	0.869	0.7689	0.869	0.7702	0.870	0.713	0.805
Wood6	0.893	0.7693	0.861	0.7689	0.861	0.7702	0.862	0.713	0.798
W14	0.8	0.8424	1.053	0.8402	1.050	0.8463	1.058	0.719	0.898
K2	0.21	0.1782	0.861	0.1726	0.822	0.2064	0.983	0.719	3.426
B2	0.50	0.5604	1.112	0.5666	1.133	0.594	1.188	0.735	1.470
B3	0.86	0.5604	0.651	0.5666	0.659	0.594	0.691	0.735	0.854
W18	0.813	0.7559	0.929	0.7607	0.936	0.8235	1.013	0.741	0.911
W910	0.825	0.7872	0.954	0.7916	0.959	0.8593	1.042	0.741	0.898
W1	1.0	0.8998	0.879	0.9032	0.903	0.9289	0.929	0.741	0.741
W2	0.8	0.8998	1.125	0.9032	1.129	0.9289	1.161	0.741	0.926
W3	1.2	1.7208*	1.434	1.7276*	1.439	0.9288	0.774	0.741	0.617
W45	1.1	1.0207	0.851	1.0291	0.936	0.8755	0.796	0.741	0.673
W6	0.25	0.6717	2.686	0.684	2.736	0.7378	2.951	0.741	2.963
W713	0.857	0.8538	0.996	0.8604	1.004	0.9028	1.053	0.741	0.864
W15	1.0	1.0215	1.022	1.0308	1.031	1.0753	1.075	0.741	0.741

* Estimated strain was too large and resulted in an error. The strain was lowered until no error occurred. The reported deflection corresponds with a strain reduction of 0.00713 in/in (0.007799 estimated).

[a] Predicted deflection using an estimated concrete compressive strain in the author's curvature based equation within Park and Gamble's compressive membrane theory.

[b] Predicted deflection using an estimated concrete compressive strain in the author's curvature based equation within his compressive membrane theory.

[c] Predicted deflection using an estimated concrete compressive strain in Keenan's simplified curvature based equation within the author's compressive membrane theory.

[d] Predicted deflection using the empirical relationship between L/h and Δ/h.

Table D.13. Peak Capacity Deflection Estimates Generated With Strain Estimates and Empirical Deflection Curves (cont.)

Slab Group	Δ_{exp} (in)	W(P) [a] (in)	W(P) /Δ	W(W) [b] (in)	W(W) /Δ	K(W) [c] (in)	K(W) /Δ	EC [d] (in)	EC/Δ
G1	0.798	0.8074	1.011	0.8052	1.009	0.8486	1.063	0.741	0.928
G2	1.335	0.8226	0.616	0.8202	0.614	0.8644	0.647	0.741	0.555
G3	1.179	0.8125	0.689	0.8002	0.679	0.8435	0.715	0.741	0.628
K1	1.00	1.7470	1.747	1.7012	1.701	1.9396	1.939	2.250	2.250
G4	0.805	1.1393	1.415	1.1487	1.427	1.3674	1.698	0.766	0.952
G5	0.601	1.1476	1.909	1.1569	1.925	1.3831	2.301	0.766	1.270
G6	0.65	1.1393	1.752	1.1487	1.767	1.3674	2.104	0.766	1.178
C1	0.65	0.4967	0.764	0.5217	0.803	0.5799	0.892	0.755	1.162
C2	0.65	0.5501	0.846	0.5692	0.876	0.628	0.966	0.755	1.162
RB26	0.446	0.4686	1.051	0.4405	0.988	0.4818	1.080	0.517	1.160
RB27	0.441	0.4472	1.014	0.4488	1.018	0.4743	1.076	0.517	1.170
RB18	0.462	0.5124	1.109	0.5100	1.104	0.4748	1.028	0.517	1.120
RB20	0.474	0.5046	1.065	0.4754	1.003	0.481	1.015	0.517	1.090
RB19	0.551	0.5112	0.928	0.5038	0.914	0.4755	0.863	0.517	0.939
RB21	0.447	0.733	1.639	0.7759	1.736	0.4715	1.055	0.517	1.150
RB22	0.45	0.5846	1.299	0.5706	1.268	0.476	1.058	0.517	1.150
RB23	0.512	0.5429	1.060	0.5079	0.992	0.4826	0.943	0.517	1.010
C3	0.65	0.5796	0.892	0.6154	0.947	0.6886	1.059	0.548	0.844
C4	0.65	0.5769	0.887	0.6318	0.972	0.7211	1.109	0.762	1.172
RB25	0.50	0.4862	0.972	0.4976	0.995	0.5188	1.038	0.510	1.020
RB24	0.55	0.4991	0.907	0.4765	0.866	0.5268	0.958	0.510	0.928
RB11	0.506	0.5257	1.039	0.5465	1.080	0.5181	1.024	0.510	1.008
RB10	0.576	0.5188	0.901	0.4972	0.863	0.5264	0.914	0.510	0.886
RB12	0.545	0.5537	1.016	0.5516	1.012	0.5215	0.957	0.510	0.936
RB13	0.506	0.561	1.109	0.5637	1.114	0.5204	1.028	0.510	1.008
RB14	0.536	0.5422	1.012	0.5203	0.971	0.5263	0.982	0.510	0.951
RB15	0.507	0.6534	1.289	0.6877	1.356	0.5179	1.021	0.510	1.006
RB17	0.562	0.5699	1.014	0.5412	0.963	0.5271	0.938	0.510	0.907

Table D.14. The Average and Standard Deviation for the Deflection Estimates Generated With Strain Estimates and the Empirically Based Deflection Curves

Slab Group	W(P) [a] (in)	W(W) [b] (in)	K(W) [c] (in)	EC [d] (in)
Average - All:	1.085	1.089	1.097	1.108
Standard Deviation:	0.356	0.364	0.415	0.514
Average - Thick:	1.121	1.128	1.172	1.163
Standard Deviation:	0.443	0.448	0.539	0.649
Average - Thin:	1.061	1.059	1.003	1.070
Standard Deviation:	0.229	0.243	0.073	0.108
Average - Very Thin:	1.015	1.019	0.997	0.982
Standard Deviation:	0.113	0.135	0.055	0.078
Average - All (No W6, K1, G5, G6):	1.003	1.004	0.985	1.016
Standard Deviation:	0.191	0.201	0.159	0.275
Average - Thick (No W6):	1.069	1.066	1.103	1.099
Standard Deviation:	0.327	0.324	0.419	0.564
Average - Thick (No W6, K1, G5, G6):	0.971	0.970	0.971	1.013
Standard Deviation:	0.190	0.197	0.211	0.349

[a] Predicted deflection using an estimated concrete compressive strain in the author's curvature based equation within Park and Gamble's compressive membrane theory.
[b] Predicted deflection using an estimated concrete compressive strain in the author's curvature based equation within his compressive membrane theory.
[c] Predicted deflection using an estimated concrete compressive strain in Keenan's simplified curvature based equation within the author's compressive membrane theory.
[d] Predicted deflection using the empirical relationship between L/h and Δ/h.

Table D.15. Thrust Comparison

Slab Group	Park [c] (lb)	Author [c] (lb)	Finite [d] (# of Elements) (lb)	T (A-M) [e] (lb)	T (A-M) [e] (w P-Δ) (lb)	P_{bal} (lb)	P_o (lb)
Wood1	300054	300901	-	160000	170000	430190	1294000
Wood2	300054	300901	-	403000	430244*	430244	1150000
Wood3	170745	171723	183390 (10)	120500	130500	258090	793900
B1	146520	147558	-	75300	85300	218802	656500
Wood4	65883	66820	68670 (10)	41700	74900	100781	261500
Wood5	65883	66820	-	44700	76700	93533	284300
Wood6	65883	66820	-	61000	86753*	86753	317100
W14	57657	58511	-	51100	85168*	85168	281200
K2	114914	119860	-	97855[b]	97855*	97855	448800
B2	61669	62871	-	38300	52000	95806	328100
B3	61669	62871	-	61700	83926*	83926	363700
W18	53475	54584	-	38400	58400[a]	95923	278900
W910	52518	53589	-	40700	58000[a]	90954	273200
W1	50550	51602	-	26300	26300[a]	73275	256300
W2	50550	51601	-	41600	70394*	70394	256200
W3	50550	51601	-	35700	42000[a]	55925	253100
W45	42816	43763	-	43000	56183*	56183	254000
W6	19349	19913	-	32567	32567*	32567	257200
W713	34492	35316	-	41200	44700[a]	50103	242100
W15	36173	36973	-	30800	49709*	49709	203500
G1	55815	57356	61486 (7)	33700	69700	90756	229000
G2	55253	56770	-	41900	61900[a]	84382	241500
G3	55995	57545	-	50900	70900[a]	85815	263600
K1	202470	232792	-	201300	253149*	253149	859600
G4	38595	40355	42784 (7)	24500	17100	52808	189200

* Balance condition not matching the experimental capacity.
[a] The large deflection decreased the capacity at any other value for P.
[b] P_{bal} required to match the experimental capacity.

Table D.15. Thrust Comparison (cont.)

Slab Group	Park [c] (lb)	Author [c] (lb)	Finite [d] (# of Elements) (lb)	T (A-M) [e] (lb)	T (A-M) [e] (w P-Δ) (lb)	P_{bal} (lb)	P_o (lb)
G5	38548	40304	-	38500	55695*	55695	205200
G6	38595	40355	-	39800	54300*	54300	217200
C1	13425	14506	-	12900	26474*	26474	62400
C2	17972	19400	-	13700	36788*	36788	84750
RB26	38169	46649	-	35500	63573*	63573	140400
RB27	22601	26837	-	34772[b]	34772*	34772	70230
RB18	23622	28170	23640 (7)	21600	28900[a]	33764	76680
RB20	36383	44433	-	35772[b]	57386*	57386	132300
RB19	24925	29875	-	36207[b]	36206*	36206	81220
RB21	16543	19211	-	18209[b]	18209*	18209	56030
RB22	26014	31315	25694 (10)	23500	35379*	35379	87980
RB23	39819	48691	-	34400	60803*	60803	157600
C3	12162	13352	-	12000	25258*	25258	61210
C4	12051	13623	-	10800	27067*	27067	64760
RB25	13534	17983	-	13300	21522	21522	48570
RB24	22043	30306	-	16300	38844*	38844	93860
RB11	12866	16948	15029 (7)	10300	19138*	19138	46730
RB10	21749	29823	-	15800	37180*	37180	92260
RB12	16465	22167	-	14300	25376*	25376	62010
RB13	15270	20485	-	11500	23035*	23035	57360
RB14	21605	29586	-	15500	35872*	35872	92000
RB15	12615	16564	15051 (10)	11900	16681*	16681	47620
RB17	22346	30771	-	11400	36614*	36614	99330

[c] Peak thrust in Park and Gamble or the author's compressive membrane theory.
[d] Peak thrust in the finite element analysis using beam elements and fixed supports.
[e] Thrust used within the axial force-moment interaction equations to match the experimental capacities (with and without consideration of P-Δ effects.

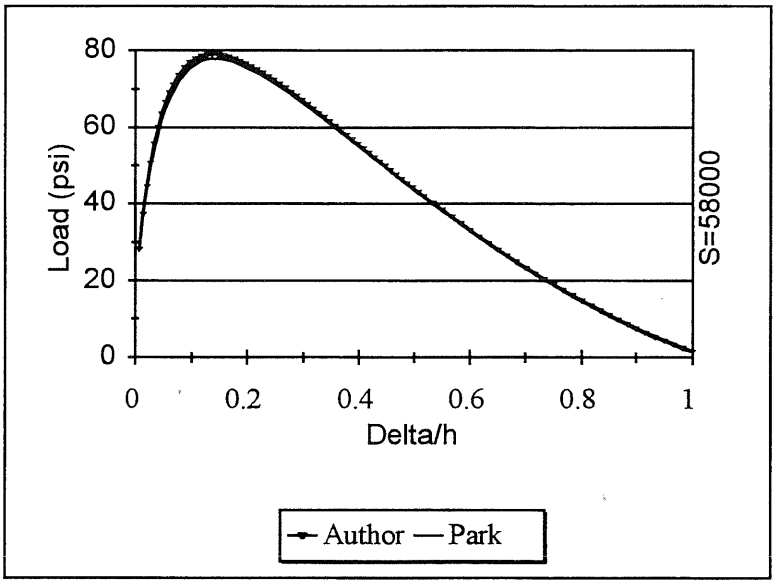

Figure D.1. Comparison of Park and Gamble's vs. the Author's Compressive Membrane Theory for a Thick Slab (Wood4, L/h = 8)

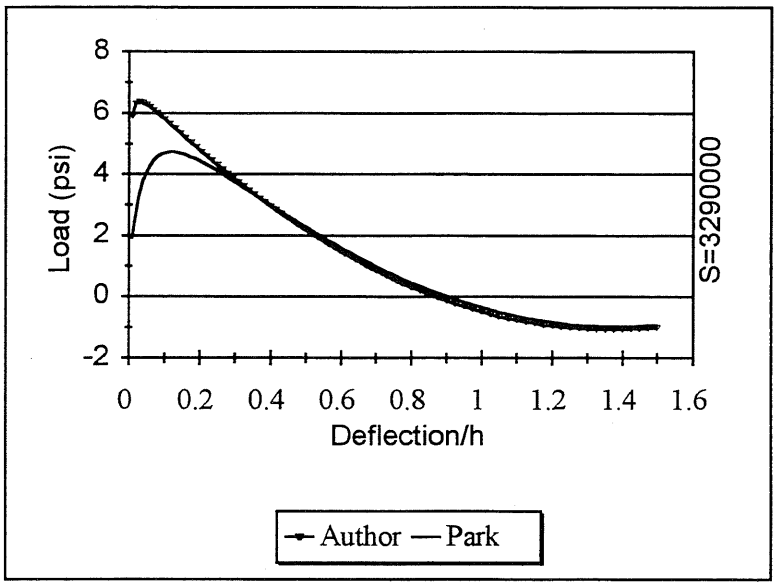

Figure D.2. Comparison of Park and Gamble's vs. the Author's Compressive Membrane Theory for a Thin Slab (RB25, L/h = 28.3)

	B	C	D	E	F	G	H	I	J	K	L	M	N	O	P
3															
4		**Wood3**													
5		Author's Compressive Membrane Theory									Singly				
6					Bottom-middle			Top-spt			Wjl/8=mu=T(d-.59T/f'c)				
7		S=	5.800E+04	lb/in	ρ=	0.955	%	ρ=	0.955	%	Wjl/8=	12445.45	lb/in		
8		β=	0.5		T=	2750.4	lb	T'=	2750.4	lb	Doubly				
9					Bottom-spt			Top-middle			Wjl/8=mu'+mu=T'(d-.59T/f'c)+T(d-.59T/f'c)				
10		fs =	60000		ρ=	0.955	%	ρ=	0.955	%	Wjl/8=	24890.9	lb/in		
11		**ecu=**	**0.004656**		C's=	2750.4	lb	Cs=	2750.4	lb					
12												Keenan(s=inf) =		0.123284	
13		support rotation allowed (yes or no) =			no			Nu(bal)=	258150	lb			del/t=	0.022415	
14															
15														Author	
16		δ=	e+2t/l-2Be=		del/h	W/Wj(sin)	W/Wj(doub)		w		Nu			Delta	
17		(in)							(psi)		(lb)			(in)	
18		0.02	0.0007258		0.004	1.98	0.99		343.02		12019.2			0.143746	
19		0.10	0.0030158		0.018	2.61	1.30		450.65		50308.7			0.212609	
20		0.20	0.0049656		0.036	3.05	1.52		526.84		82909.5			0.271956	
21		0.32	0.0065313		0.058	3.33	1.66		575.39		109087.8			0.320104	
22															
23		**0.41**	0.0073658		0.075	3.44	1.72	**WDI**	**595.24**		123040.3			0.345949	
24		**Experimental Deflection**													
25		0.50	0.0080070		0.091	3.51	1.75		606.62		133762.2			0.365899	
26															
27		0.68	0.0089047		0.124	3.55	1.78	**WP**	**614.26**		148771.0			0.393955	
28															
29		0.89	0.0095463		0.162	3.52	1.76		608.80		159499.5			0.414105	
30		1.01	0.0097882		0.184	3.48	1.74		601.95		163544.4			0.421722	
31		1.10	0.0099269		0.200	3.45	1.72		595.66		165862.9			0.426094	
32		1.22	0.0100664		0.222	3.39	1.70		586.18		168196.2			0.430497	
33		1.31	0.0101430		0.238	3.35	1.67		578.44		169477.7			0.432917	
34		1.40	0.0101997		0.255	3.30	1.65		570.31		170425.0			0.434706	
35		1.52	0.0102490		0.276	3.23	1.62		559.02		171249.8			0.436264	
36		1.60	0.0102676		0.291	3.19	1.59		551.29		171561.9			0.436854	
37															
38		1.70	0.0102773		0.309	3.13	1.57	**WTI**	**541.45**	**Pk Thrust**	**171723.0**		**W(W)**	**0.437158**	
39															
40		1.80	0.0102736		0.327	3.07	1.54		531.48		171661.9			0.437042	
41															

Figure D.3. Portion of Slab Wood3 Spreadsheet

	B	C	D	E	F	G	H	I	J	K	L	M	N	O	P
3															
4		**Wood4**													
5		Author's Compressive Membrane Theory									Singly				
6					Bottom-middle			Top-spt			Wjl/B=mu=T(d-.59T/f'c)				
7		S=	5.800E+04	lb/in	ρ=	0.26	%	ρ=	0.26	%	Wjl/B=	817.0615	lb/in		
8		β=	0.5		T=	347.9	lb	T'=	347.9	lb	Doubly				
9					Bottom-spt			Top-middle			Wjl/B=mu'+mu=T'(d-.59T'/f'c)+T(d-.59T/f'c)				
10		fs =	55750		ρ=	0.26	%	ρ=	0.26	%	Wjl/B=	1634.123			
11		ecu=	**0.009256**		C's=	347.9	lb	Cs=	347.9	lb					
12												Keenan(s=inf) =		0.483202	
13		support rotation allowed (yes or no)	=		no			Nu(bal)=	101452	lb			del/t=	0.161067	
14															
15														Author's	
16		δ=	e+2t/l-2Be=		del/h	W/Wj(sin)	W/Wj(doub)		w		Nu			Delta	
17		(in)							(psi)		(lb)			(in)	
18		0.02	0.0003894		0.007	2.49	1.24		28.25		6467.1			0.500658	
19		0.10	0.0015354		0.033	4.91	2.46		55.75		25627.4			0.582576	
20		0.20	0.0024135		0.067	6.27	3.14		71.18		40307.5			0.647268	
21		0.32	0.0030483		0.107	6.87	3.44		77.98		50919.8			0.695165	
22		0.38	0.0032650		0.127	6.96	3.48		78.99		54542.7			0.711746	
23															
24		0.41	0.0033556		0.137	6.97	3.49	**WP**	79.13		56058.1			0.718717	
25															
26		0.44	0.0034364		0.147	6.97	3.48		79.07		57408.2			0.724945	
27		0.50	0.0035727		0.167	6.92	3.46		78.48		59686.8			0.735497	
28		0.68	0.0038355		0.227	6.55	3.27		74.31		64081.0			0.755984	
29		0.80	0.0039289		0.267	6.20	3.10		70.41		65642.4			0.763308	
30															
31		**0.83**	0.0039450		0.277	6.11	3.06	**WDI**	**69.36**		65911.8			0.764574	
32		**Experimental Deflection**													
33		0.86	0.0039586		0.287	6.02	3.01		68.28		66140.2			0.765649	
34		0.98	0.0039923		0.327	5.62	2.81		63.81		66702.8			0.768296	
35		1.04	0.0039985		0.347	5.42	2.71		61.52		66806.4			0.768783	
36															
37		1.07	0.0039993		0.357	5.32	2.66	**WTI**	60.36	**PK Thrust**	66820.6		**W(W)**	**0.768849**	
38															
39		1.10	0.0039988		0.367	5.22	2.61		59.20		66811.8			0.768808	
40		1.25	0.0039784		0.417	4.70	2.35		53.38		66470.9			0.767201	
41															

Figure D.4. Portion of Slab Wood4 Spreadsheet

	B	C	D	E	F	G	H	I	J	K	L	M	N	O	P
3															
4		**W45**													
5		Author's Compressive Membrane Theory									Singly				
6					Bottom-middle			Top-spt			Wjl/8=mu=T(d-.59T/f'c)				
7		S=	5.800E+04	lb/in	ρ=	1.14	%	ρ=	1.19	%	Wjl/8=	2136.734	lb/in		
8		β=	0.5		T=	1301.7	lb	T=	1358.8	lb	Doubly				
9					Bottom-spt			Top-middle			Wjl/8=mu'+mu=T'(d-.59T'/f'c)+T(d-.59T/f'c)				
10		fs =	63000		ρ=	1.14	%	ρ=	0.4	%	Wjl/8=	4356.99			
11		ecu=	**0.008069**		C's=	1301.7	lb	Cs=	456.8	lb					
12												Keenan(s=inf) =		0.613896	
13		support rotation allowed (yes or no) =				no		Nu(bal)=	78117	lb			del/t=	0.265468	
14															
15														Author's	
16		δ=	e+2t/l-2Be=		del/h	W/Wj(sin)	W/Wj(doub)		w		Nu			Delta	
17		(in)							(psi)		(lb)			(in)	
18		0.02	0.0002639		0.009	1.97	0.97		58.55		4383.4			0.692557	
19		0.10	0.0010503		0.043	2.41	1.18		71.57		17530.3			0.794945	
20		0.20	0.0016580		0.086	2.65	1.30		78.68		27689.3			0.880119	
21		0.32	0.0020925		0.138	2.74	1.34		81.26		34953.3			0.944995	
22															
23		0.35	0.0021695		0.151	2.74	1.34	**WP**	**81.36**		36240.2			0.956886	
24															
25		0.38	0.0022371		0.164	2.74	1.34		81.32		37369.5			0.967426	
26		0.50	0.0024335		0.216	2.70	1.32		80.10		40653.9			0.998674	
27		0.62	0.0025457		0.268	2.62	1.29		77.87		42529.1			1.016933	
28		0.71	0.0025921		0.307	2.56	1.25		75.85		43305.3			1.024584	
29		0.83	0.0026181		0.359	2.46	1.20		72.91		43740.1			1.028892	
30															
31		0.86	0.0026194		0.372	2.43	1.19	**WTI**	**72.16**	**Pk Thrust**	**43763.3**		**W(W)**	**1.029122**	
32															
33		0.89	0.0026191		0.385	2.41	1.18		71.40		43757.3			1.029062	
34		0.98	0.0026087		0.424	2.33	1.14		69.10		43584.8			1.027346	
35		1.07	0.0025866		0.463	2.25	1.10		66.82		43215.1			1.023682	
36															
37		**1.10**	0.0025770		0.476	2.23	1.09	**WDI**	**66.07**		43054.5			1.022094	
38		**Experimental Deflection**													
39		1.13	0.0025664		0.489	2.20	1.08		65.32		42877.1			1.020344	
40		1.25	0.0025150		0.541	2.10	1.03		62.39		42019.4			1.011920	
41															

Figure D.5. Portion of Slab W45 Spreadsheet

	B	C	D	E	F	G	H	I	J	K	L	M	N	O	P
3															
4		**G4**													
5		Author's Compressive Membrane Theory									Singly				
6					Bottom-middle			Top-spt			Wjl/8=mu=T(d-.59T/f'c)				
7		S=	1.000E+05	lb/in	ρ=	0.58	%	ρ=	0.58	%	Wjl/8=	582.0382	lb/in		
8		β=	0.5		T=	488.1	lb	T'=	488.1	lb	Doubly				
9					Bottom-spt			Top-middle			Wjl/8=mu'+mu=T'(d-.59T'/f'c)+T(d-.59T/f'c)				
10		fs =	67330		ρ=	0.58	%	ρ=	0.58	%	Wjl/8=	1164.076			
11		ecu=	**0.006845**		C's=	488.1	lb	Cs=	488.1	lb					
12												Keenan(s=inf) =		0.570797	
13		support rotation allowed (yes or no) =				yes		Nu(bal)=	57468	lb			del/t=	0.351259	
14															
15														Author's	
16		δ=	e+2t/l-2Be=		del/h	W/Wj(sin)	W/Wj(doub)		w		Nu			Delta	
17		(in)							(psi)		(lb)			(in)	
18		0.02	0.0002043		0.012	2.12	1.06		17.11		5861.2			0.832695	
19		0.10	0.0007339		0.062	3.46	1.73		27.98		21128.0			0.953945	
20		0.20	0.0010692		0.123	3.94	1.97		31.87		30793.5			1.043638	
21		0.23	0.0011333		0.142	3.98	1.99		32.17		32640.6			1.062403	
22															
23		0.26	0.0011863		0.160	3.99	1.99	**WP**	**32.23**		34169.6			1.078424	
24															
25		0.29	0.0012304		0.178	3.97	1.99		32.11		35438.4			1.092084	
26		0.41	0.0013426		0.252	3.78	1.89		30.56		38675.2			1.128630	
27		0.50	0.0013827		0.308	3.56	1.78		28.79		39830.7			1.142345	
28		0.62	0.0014009		0.382	3.23	1.61		26.09		40354.9			1.148694	
29															
30		0.65	0.0014009		0.400	3.14	1.57	**WTI**	**25.39**	**Pk Thrust**	**40355.5**		**W(W)**	**1.148700**	
31															
32		0.68	0.0013995		0.418	3.05	1.53		24.68		40314.4			1.148198	
33		0.77	0.0013879		0.474	2.79	1.40		22.57		39980.4			1.144141	
34															
35		0.80	0.0013819		0.492	2.71	1.35	**WDI**	21.87		39809.3			1.142075	
36		**Experimental Deflection**													
37		0.83	0.0013751		0.511	2.62	1.31		21.18		39612.5			1.139712	
38		1.01	0.0013192		0.622	2.13	1.06		17.19		38001.4			1.120780	
39		1.25	0.0012171		0.769	1.55	0.77		12.49		35060.2			1.087937	
40															

Figure D.6. Portion of Slab G4 Spreadsheet

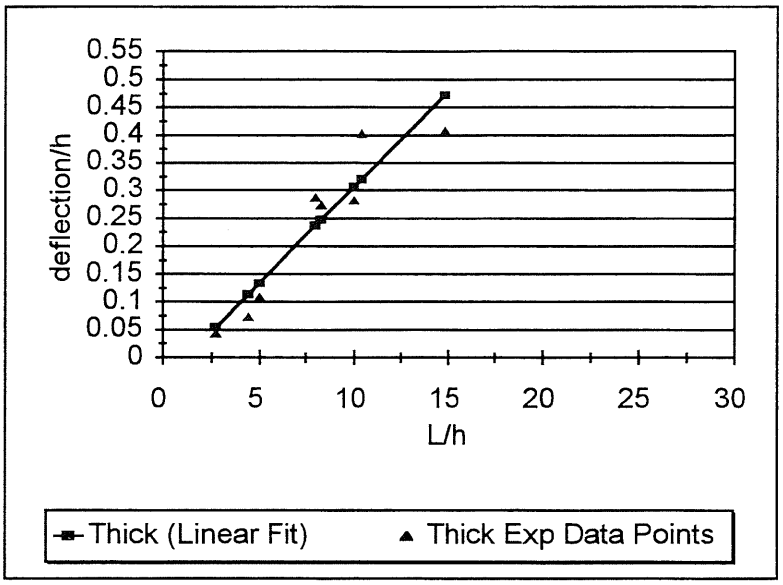

Figure D.7. Empirical Data for Span Length-to-Thickness (L/h) vs. Midspan Deflection-to-Thickness (Δ/h) for Thick Slabs

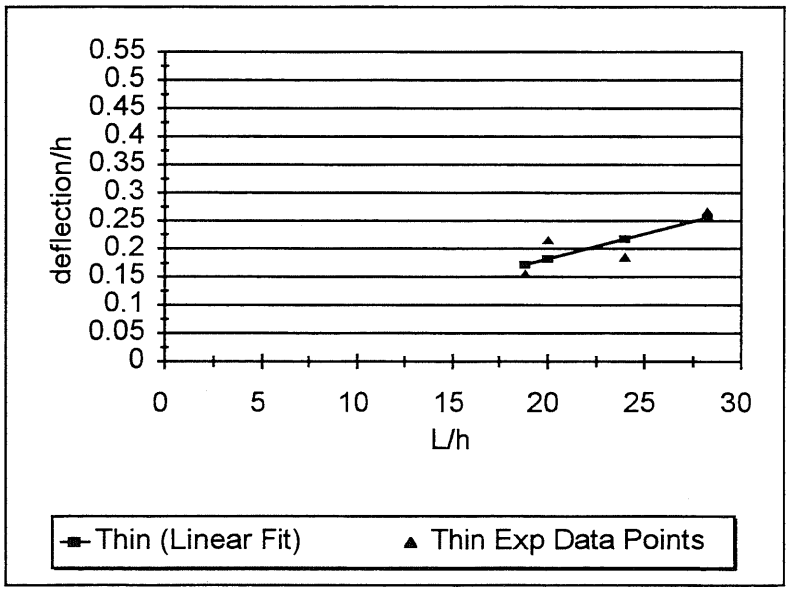

Figure D.8. Empirical Data for Span Length-to-Thickness (L/h) vs. Midspan Deflection-to-Thickness (Δ/h) for Thin Slabs

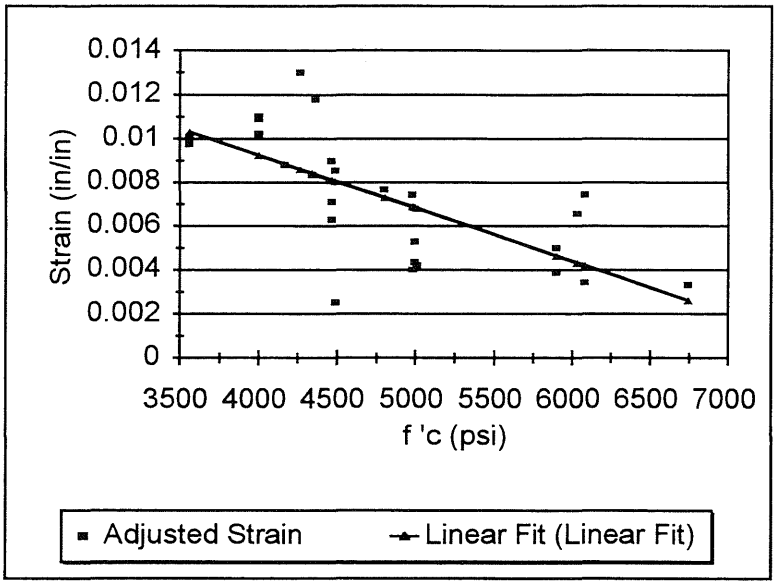

Figure D.9. Concrete Compressive Strength vs. Concrete Compressive Strain in the Author's Curvature Based Deflection Estimate for Thick Slabs

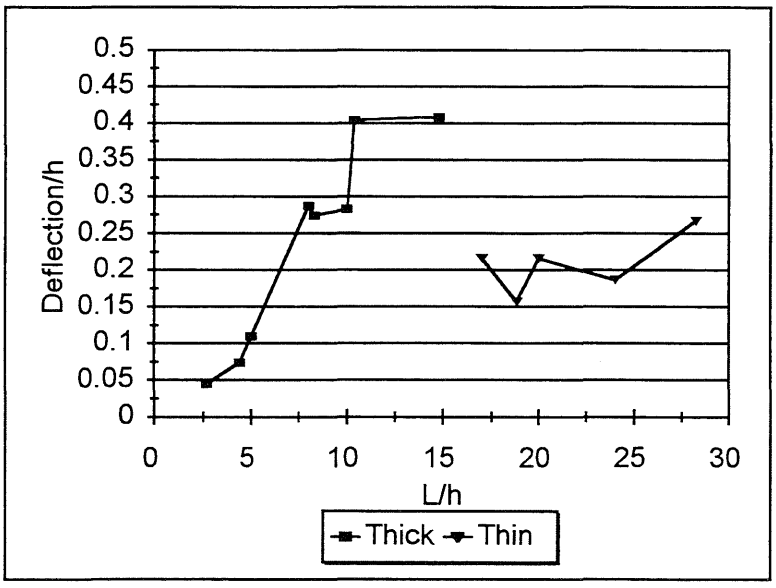

Figure D.10. Empirical Data for Span Length-to-Thickness (L/h) vs. Midspan Deflection-to-Thickness (Δ/h) for Thick and Thin Slabs

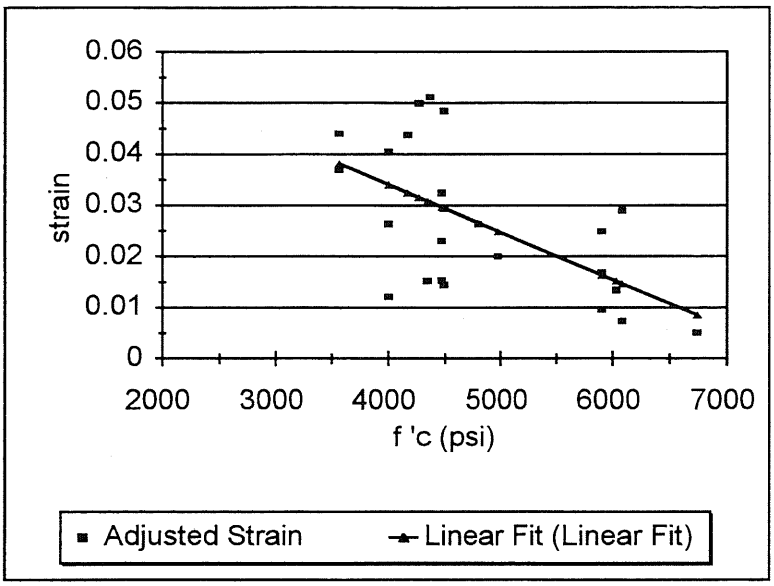

Figure D.11. Concrete Compressive Strength vs. Adjusted Concrete Compressive Strain in Mattock's Deflection Estimate for Thick Slabs

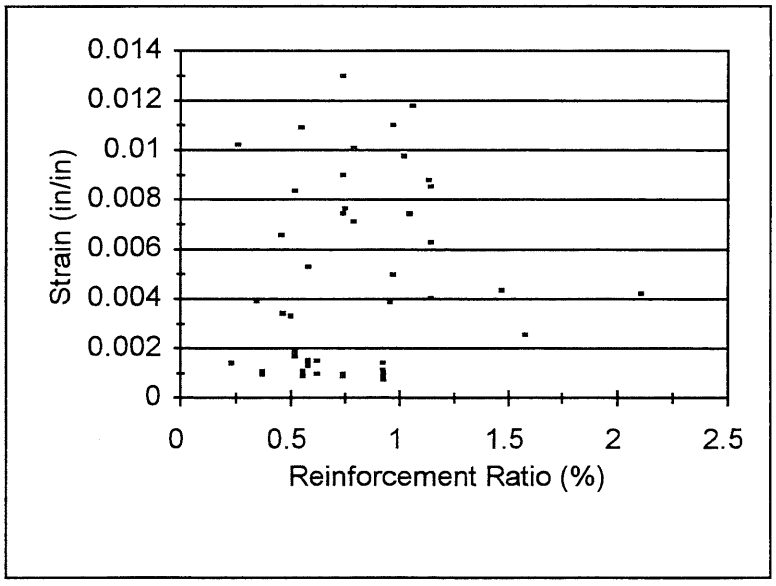

Figure D.12. Reinforcement Ratio vs. Concrete Compressive Strain in the Author's Curvature Based Deflection Estimate for Thick and Thin Slabs

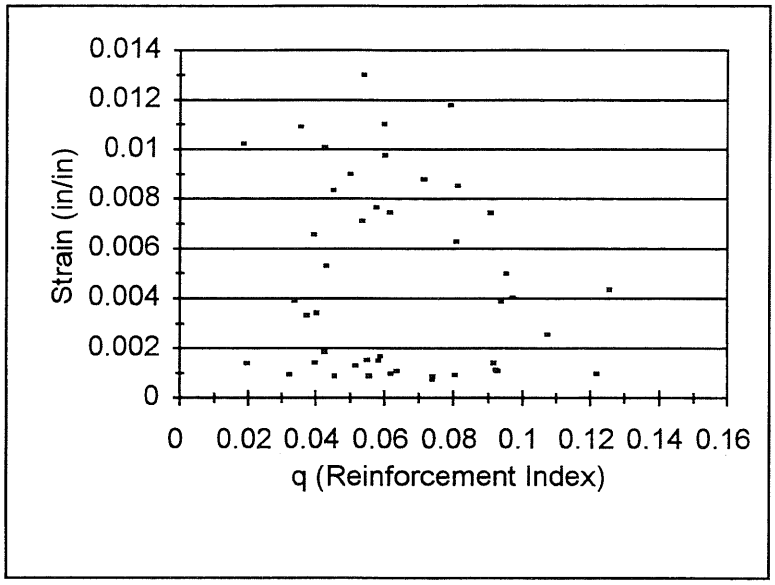

Figure D.13. Reinforcement Index vs. Concrete Compressive Strain in the Author's Curvature Based Deflection Estimate for Thick and Thin Slabs

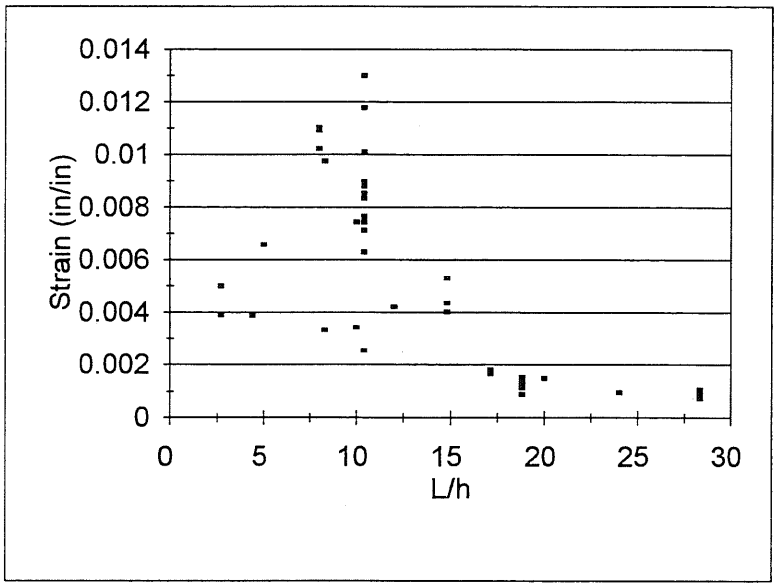

Figure D.14. Span Length-to-Thickness vs. Concrete Compressive Strain in the Author's Curvature Based Deflection Estimate for Thick and Thin Slabs

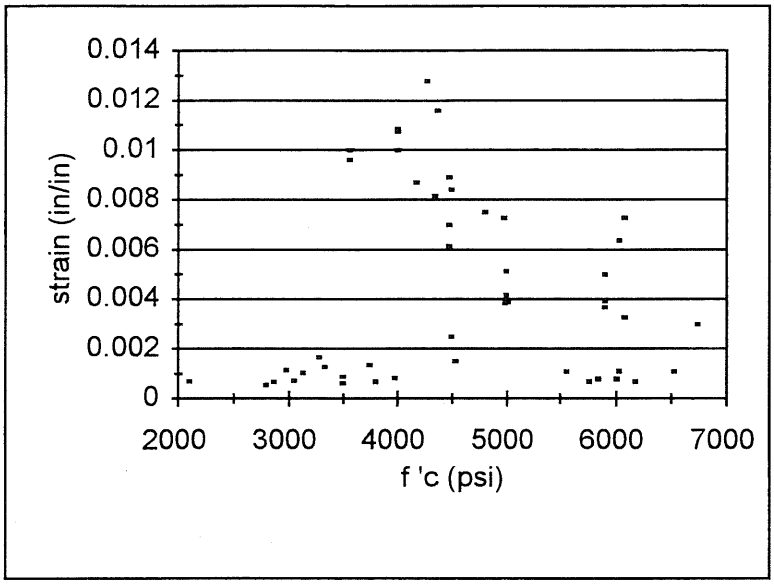

Figure D.15. Concrete Compressive Strength vs. Concrete Compressive Strain in the Author's Curvature Based Deflection Estimate for Thick and Thin Slabs

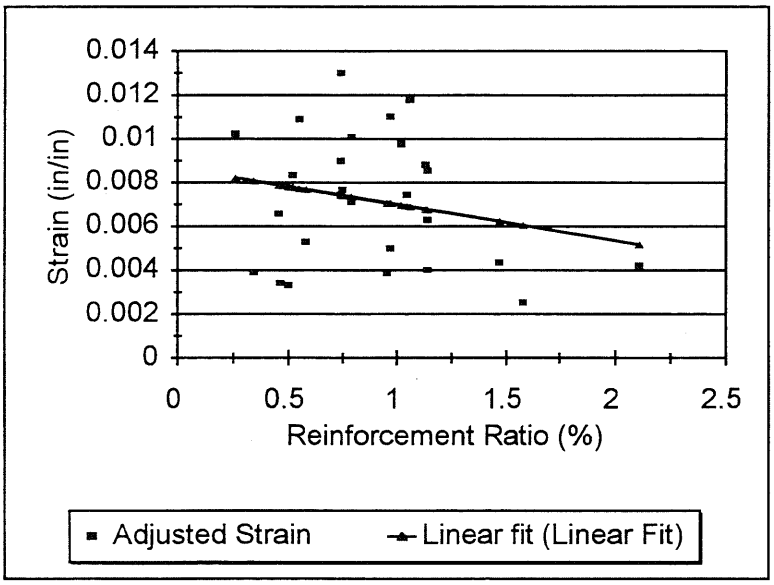

Figure D.16. Reinforcement Ratio vs. Concrete Compressive Strain in the Author's Curvature Based Deflection Estimate for Thick Slabs

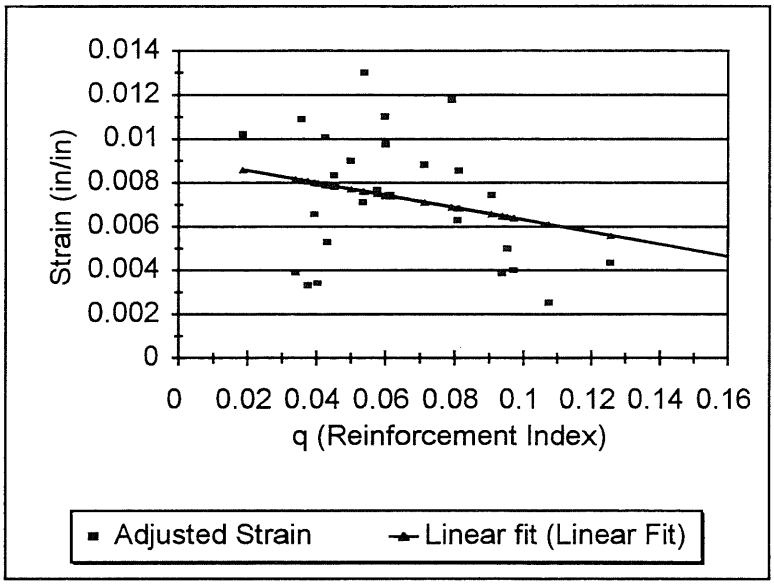

Figure D.17. Reinforcement Index vs. Concrete Compressive Strain in the Author's Curvature Based Deflection Estimate for Thick Slabs

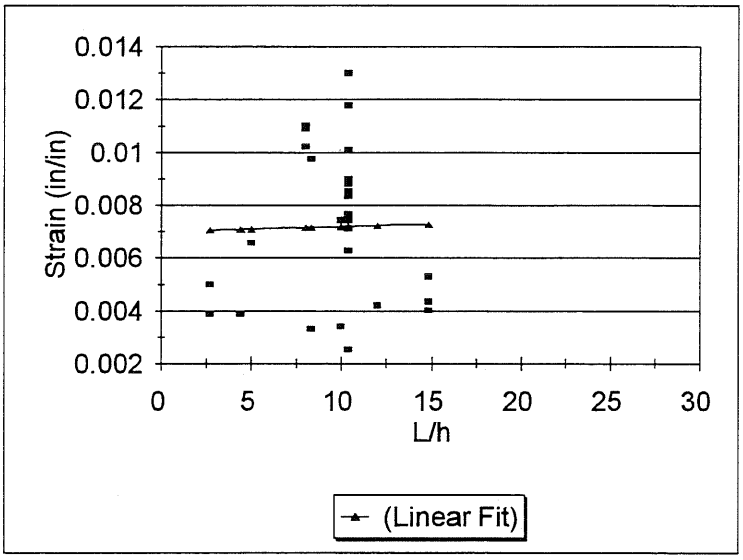

Figure D.18. Span Length-to-Thickness vs. Concrete Compressive Strain in the Author's Curvature Based Deflection Estimate for Thick Slabs

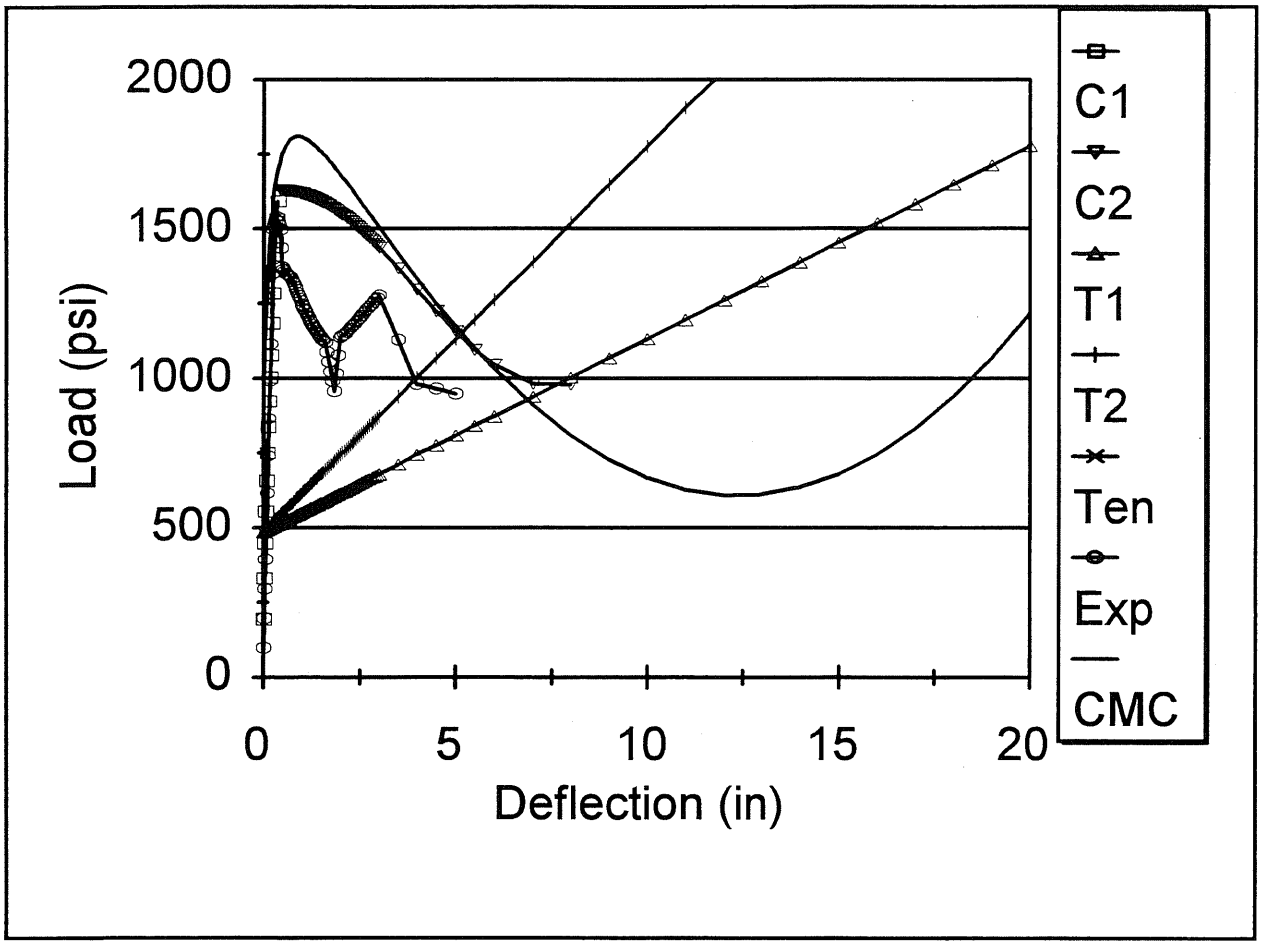

Figure D.19. Compressive Membrane Theoretical Curve, Experimental Load-Deflection Curve, and the Author's Peak Thrust Estimated Load-Deflection Curve for Woodson's Slab (Wood1, L/h = 2.7, $\rho = 0.969\%$) (1994)

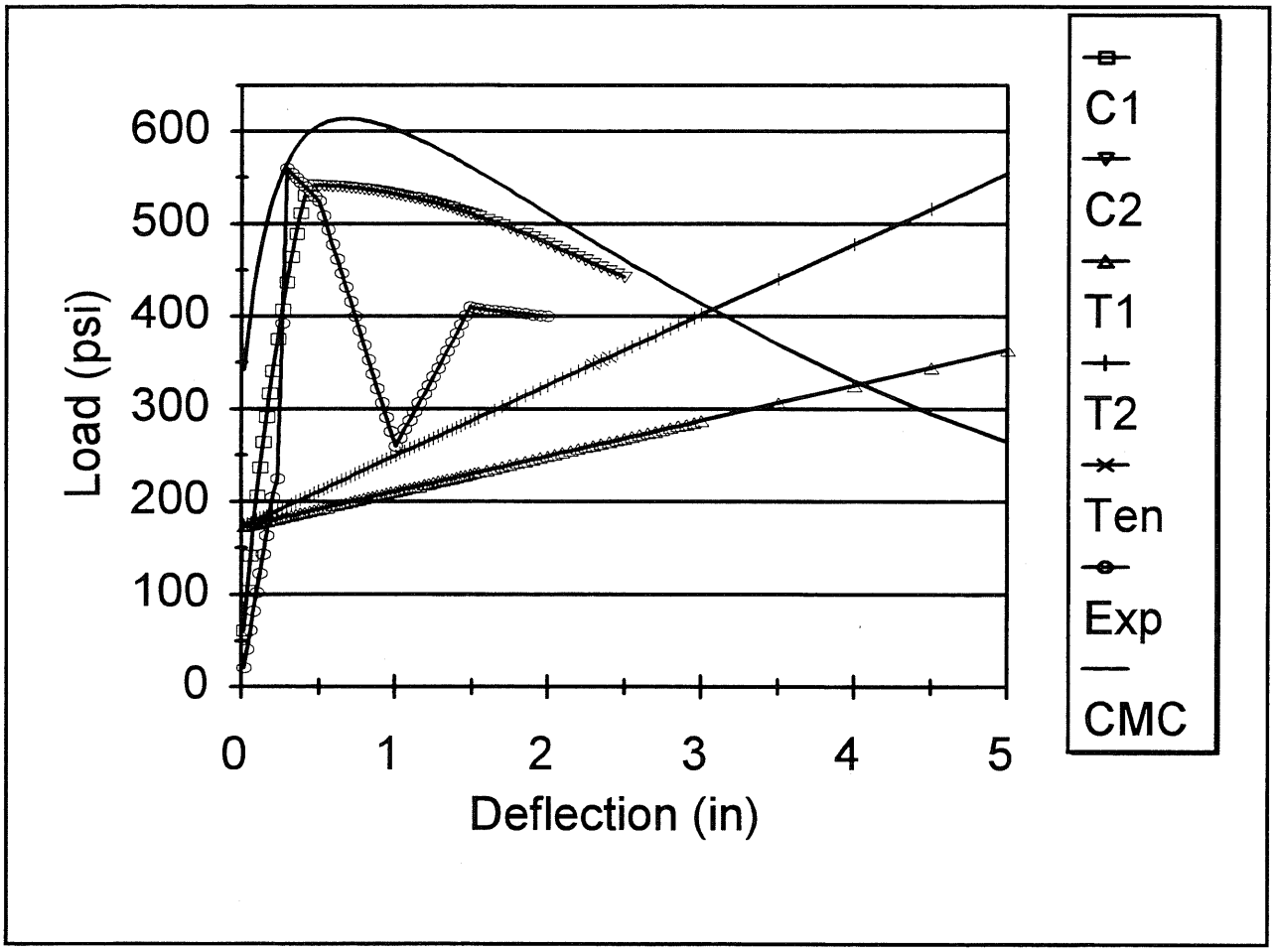

Figure D.20. Compressive Membrane Theoretical Curve, Experimental Load-Deflection Curve, and the Author's Peak Thrust Estimated Load-Deflection Curve for Woodson's Slab (Wood3, L/h = 4.4, $\rho = 0.955\%$) (1994)

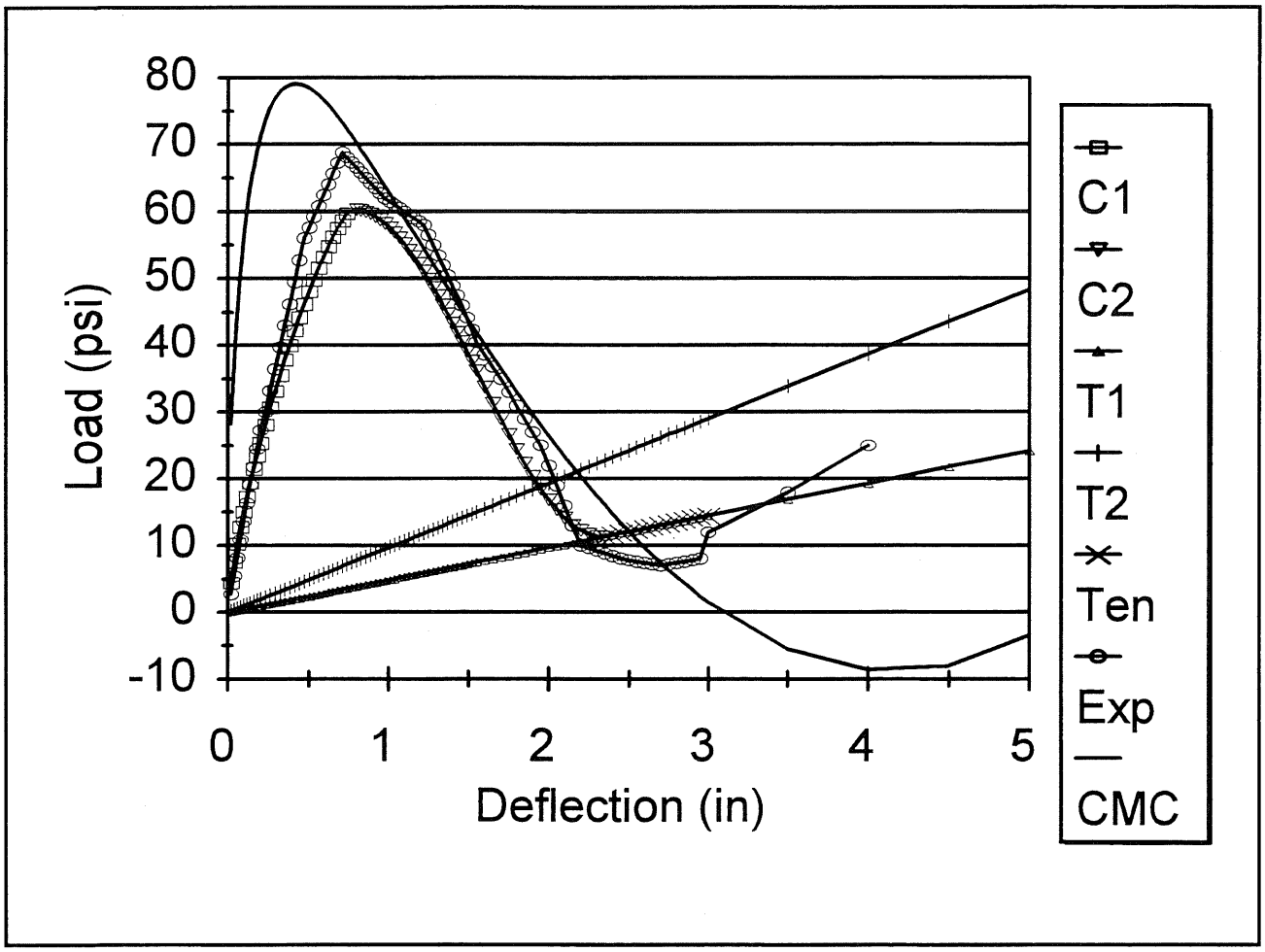

Figure D.21. Compressive Membrane Theoretical Curve, Experimental Load-Deflection Curve, and the Author's Peak Thrust Estimated Load-Deflection Curve for Woodson's Slab (Wood4, L/h = 8, $\rho = 0.26\%$) (1993)

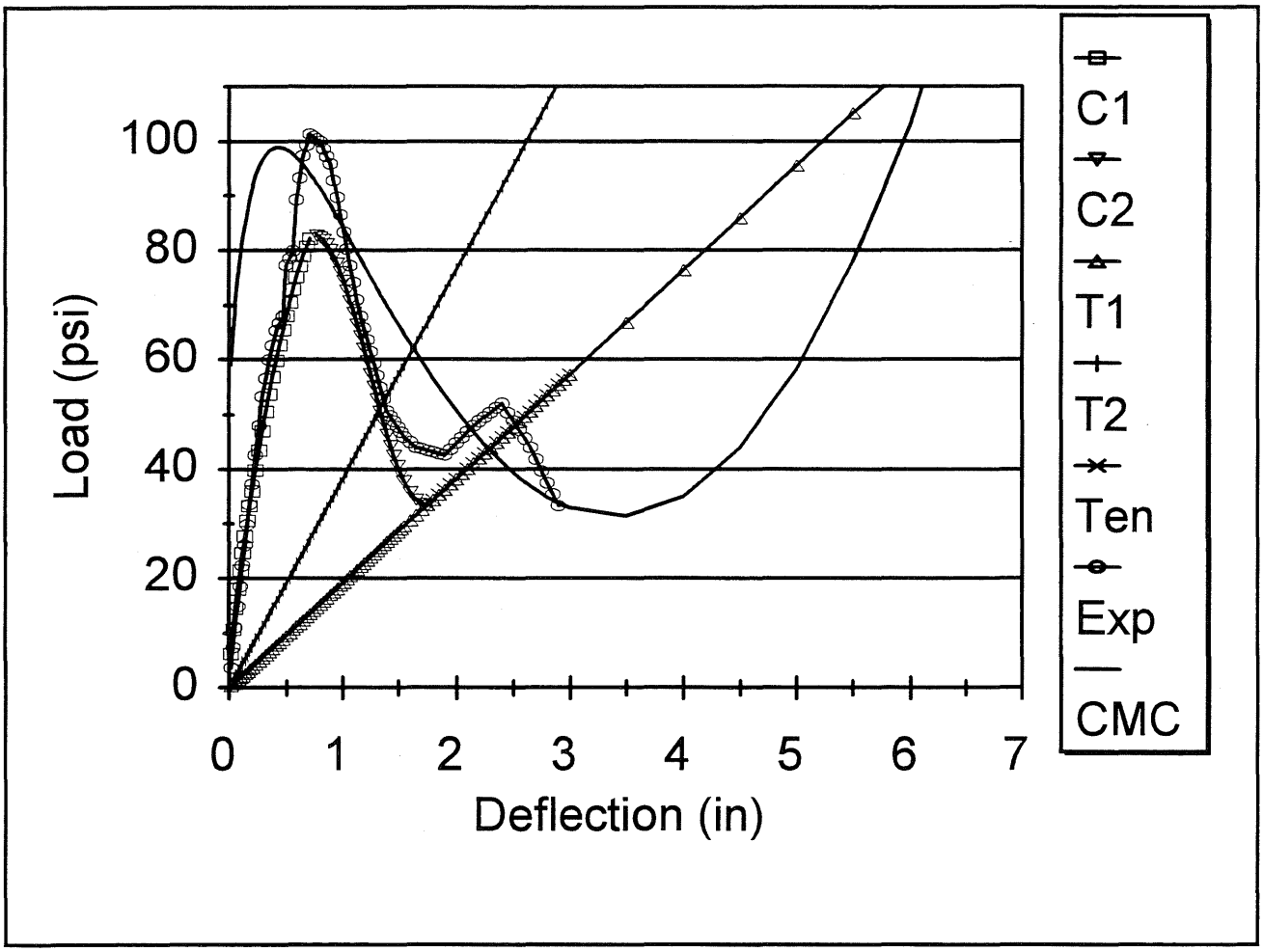

Figure D.22. Compressive Membrane Theoretical Curve, Experimental Load-Deflection Curve, and the Author's Peak Thrust Estimated Load-Deflection Curve for Baylot's Slab (B3, L/h = 10, ρ = 1.045%) (1985)

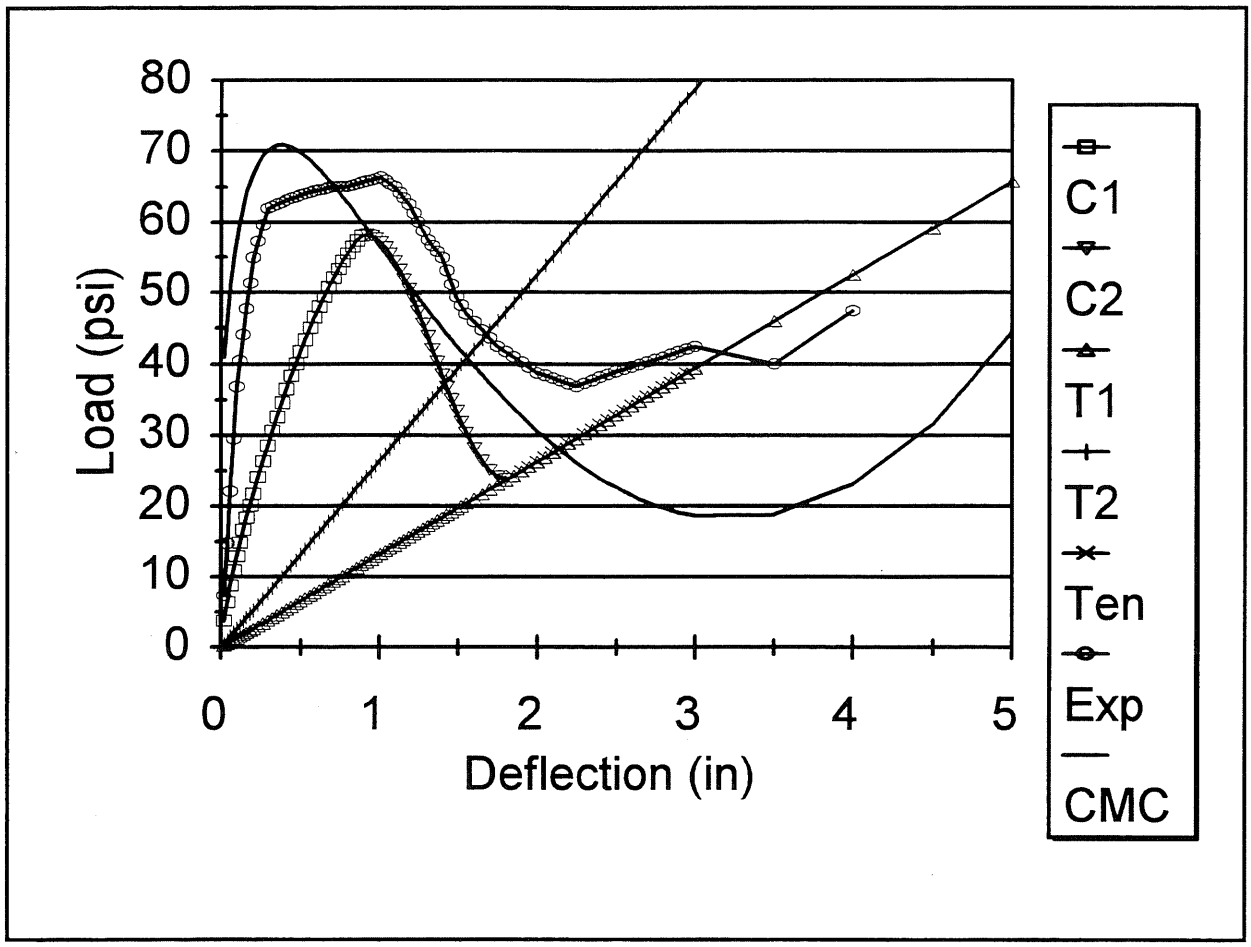

Figure D.23. Compressive Membrane Theoretical Curve, Experimental Load-Deflection Curve, and the Author's Peak Thrust Estimated Load-Deflection Curve for Woodson's Slab (W1, L/h = 10.4, $\rho = 0.74\%$) (1985)

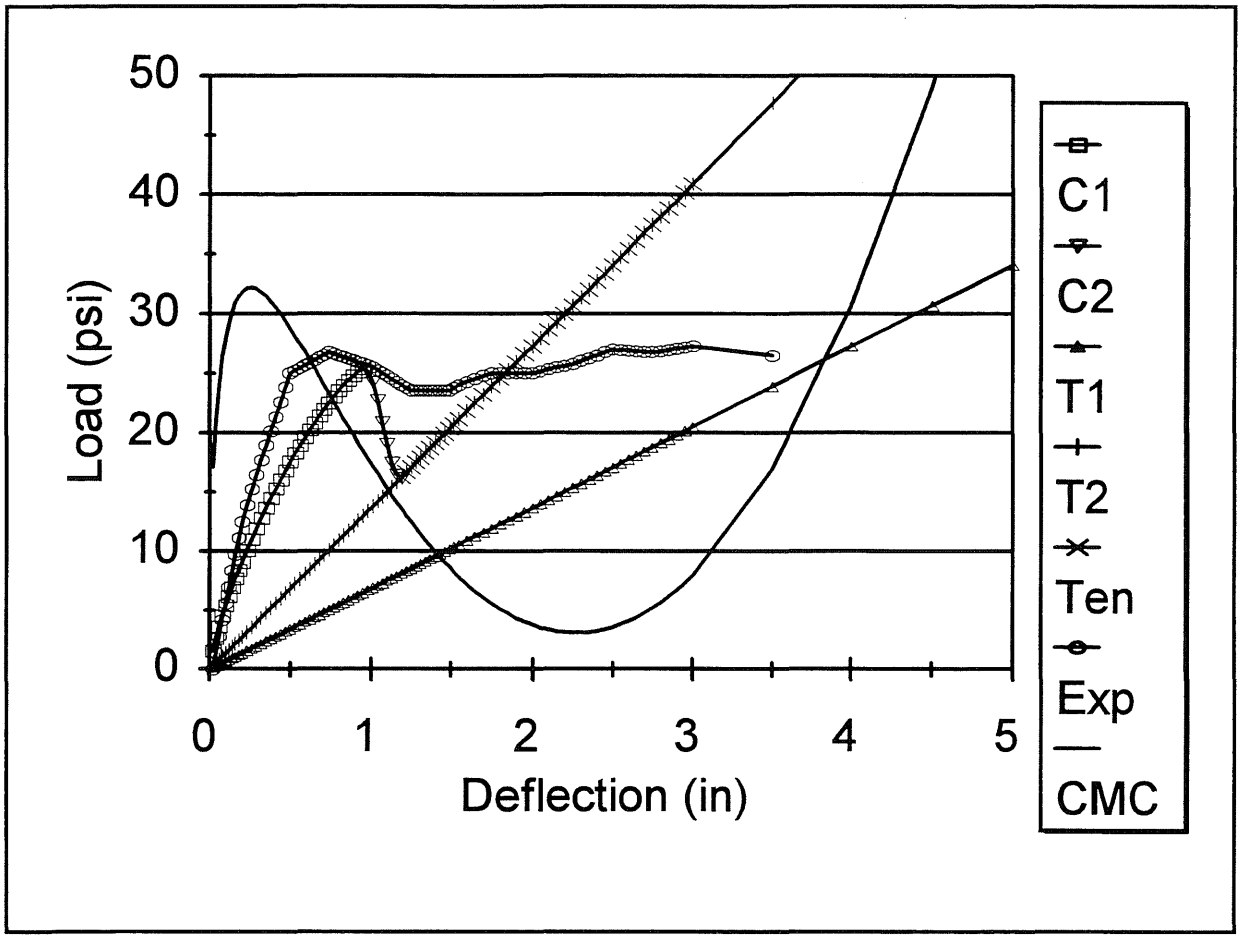

Figure D.24. Compressive Membrane Theoretical Curve, Experimental Load-Deflection Curve, and the Author's Peak Thrust Estimated Load-Deflection Curve for Guice's Slab (G4, L/h = 14.8, $\rho = 0.58\%$) (1986)

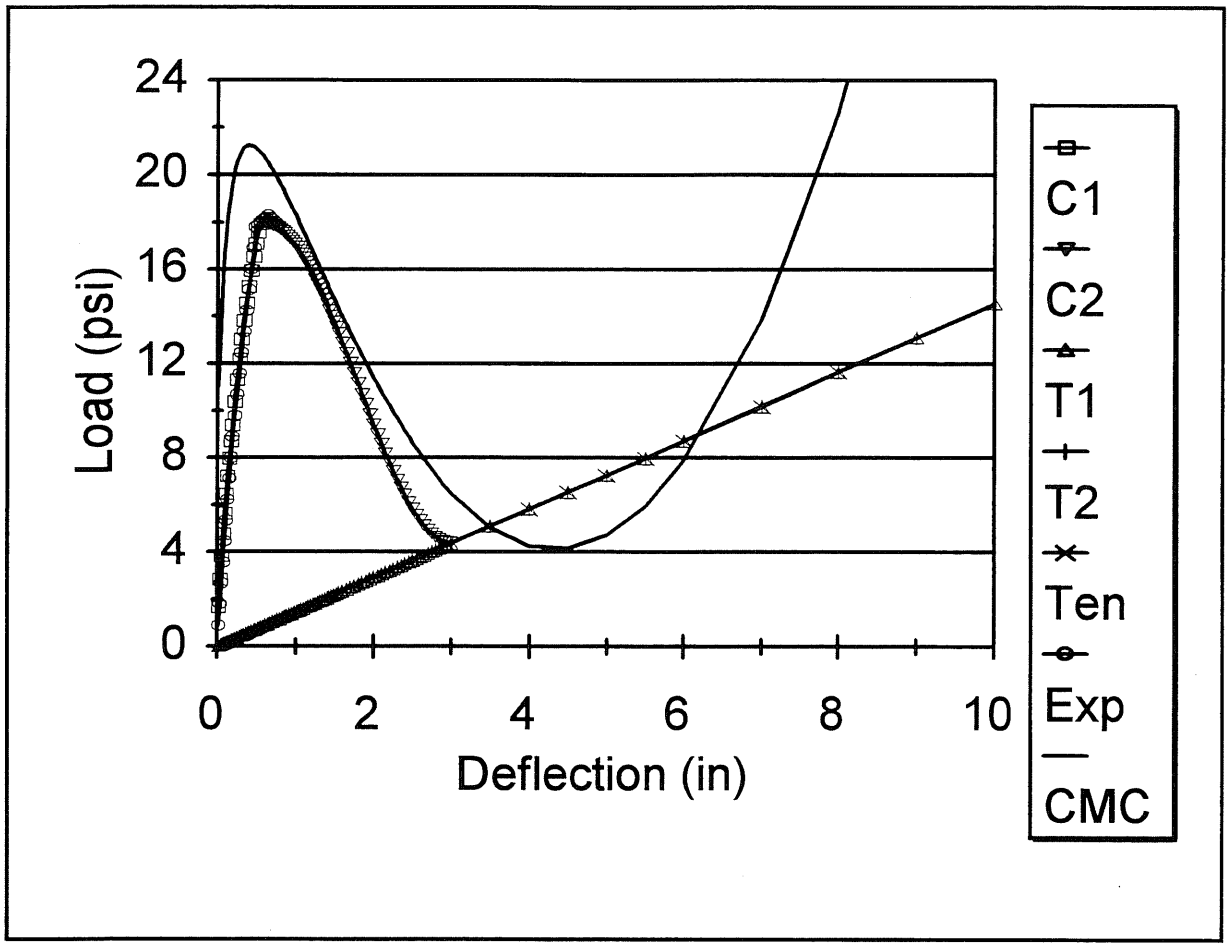

Figure D.25. Compressive Membrane Theoretical Curve, Experimental Load-Deflection Curve, and the Author's Peak Thrust Estimated Load-Deflection Curve for Christiansen's Slab (C2, L/h = 17.1, $\rho = 0.52\%$) (1963)

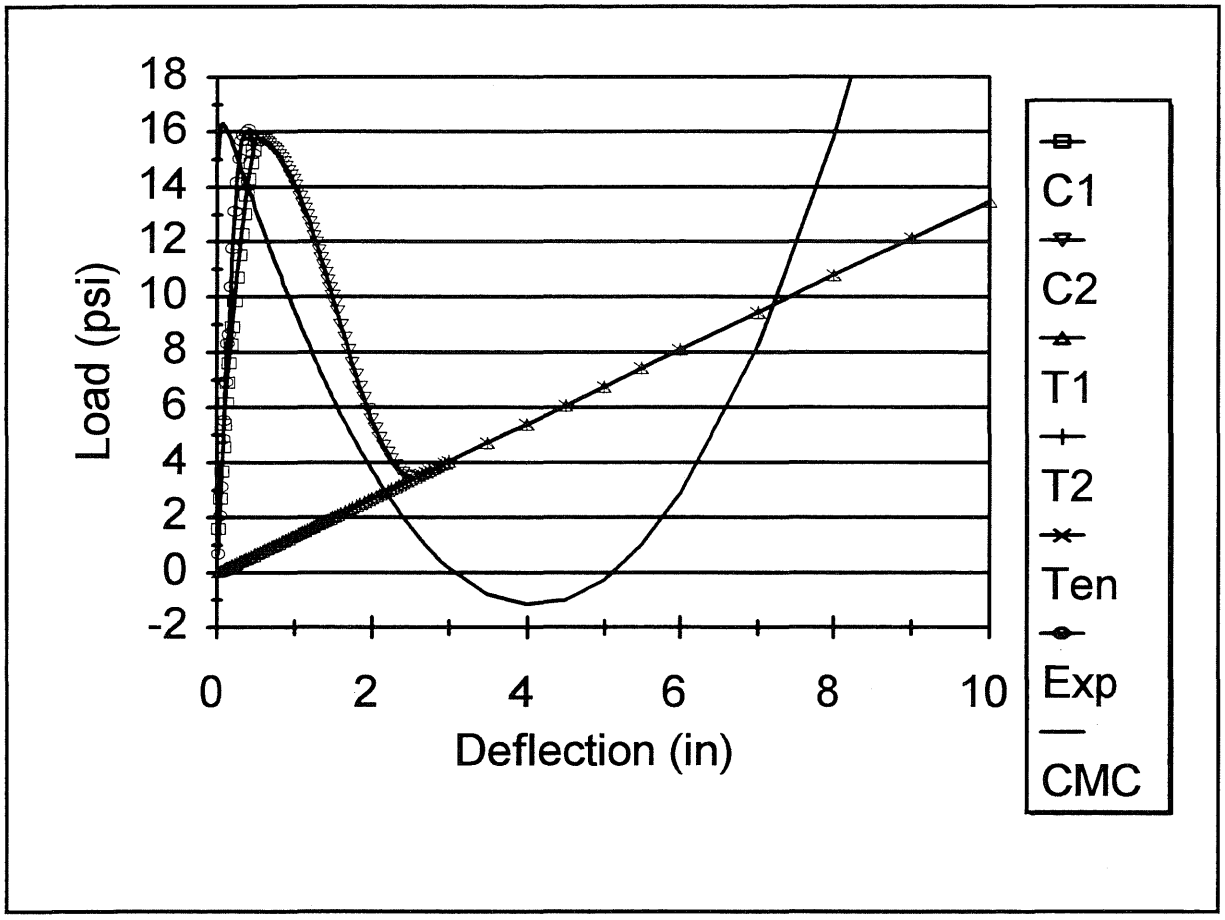

Figure D.26. Compressive Membrane Theoretical Curve, Experimental Load-Deflection Curve, and the Author's Peak Thrust Estimated Load-Deflection Curve for Roberts' Slab (RB18, L/h = 18.8, $\rho = 0.578\%$) (1969)

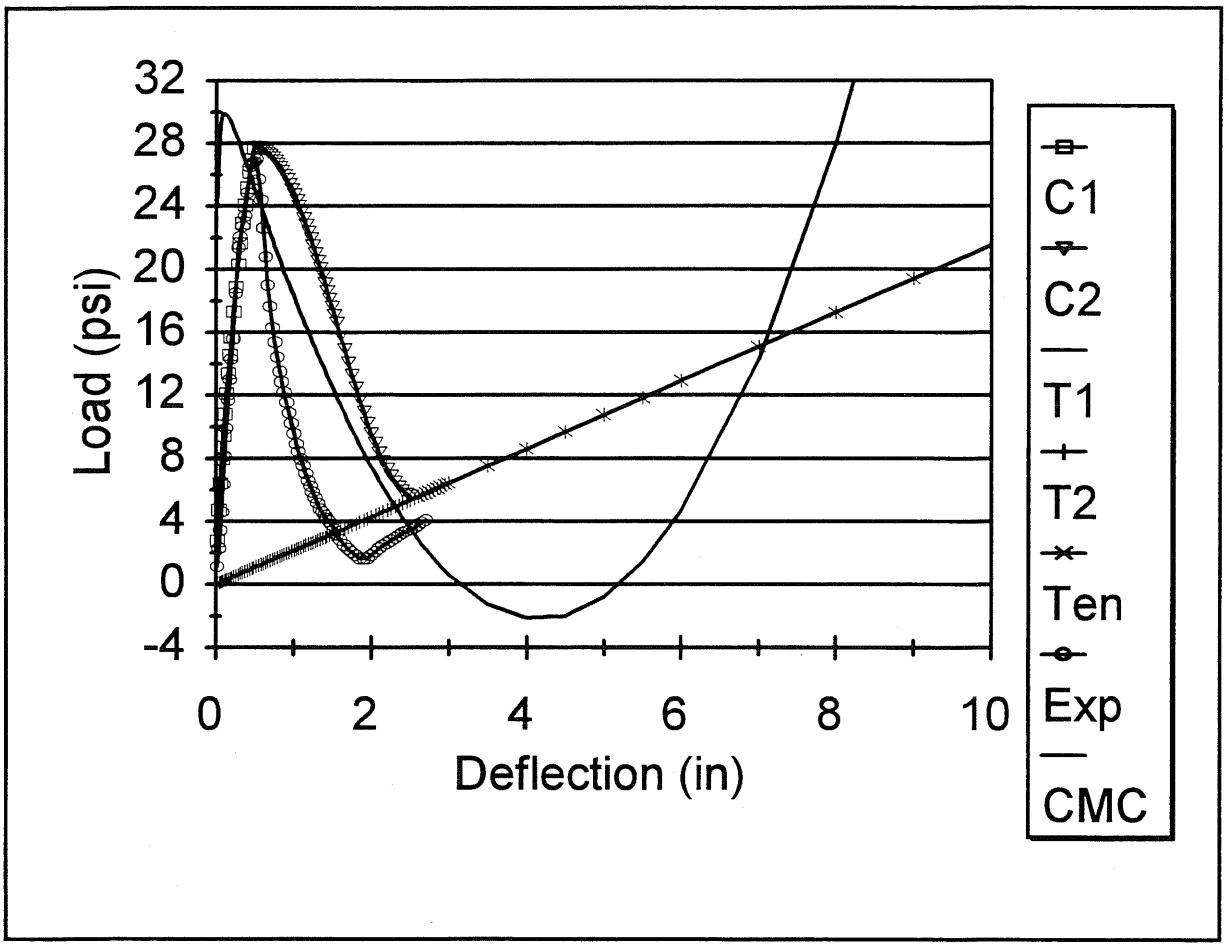

Figure D.27. Compressive Membrane Theoretical Curve, Experimental Load-Deflection Curve, and the Author's Peak Thrust Estimated Load-Deflection Curve for Roberts' Slab (RB23, L/h = 18.8, $\rho = 0.924\%$) (1969)

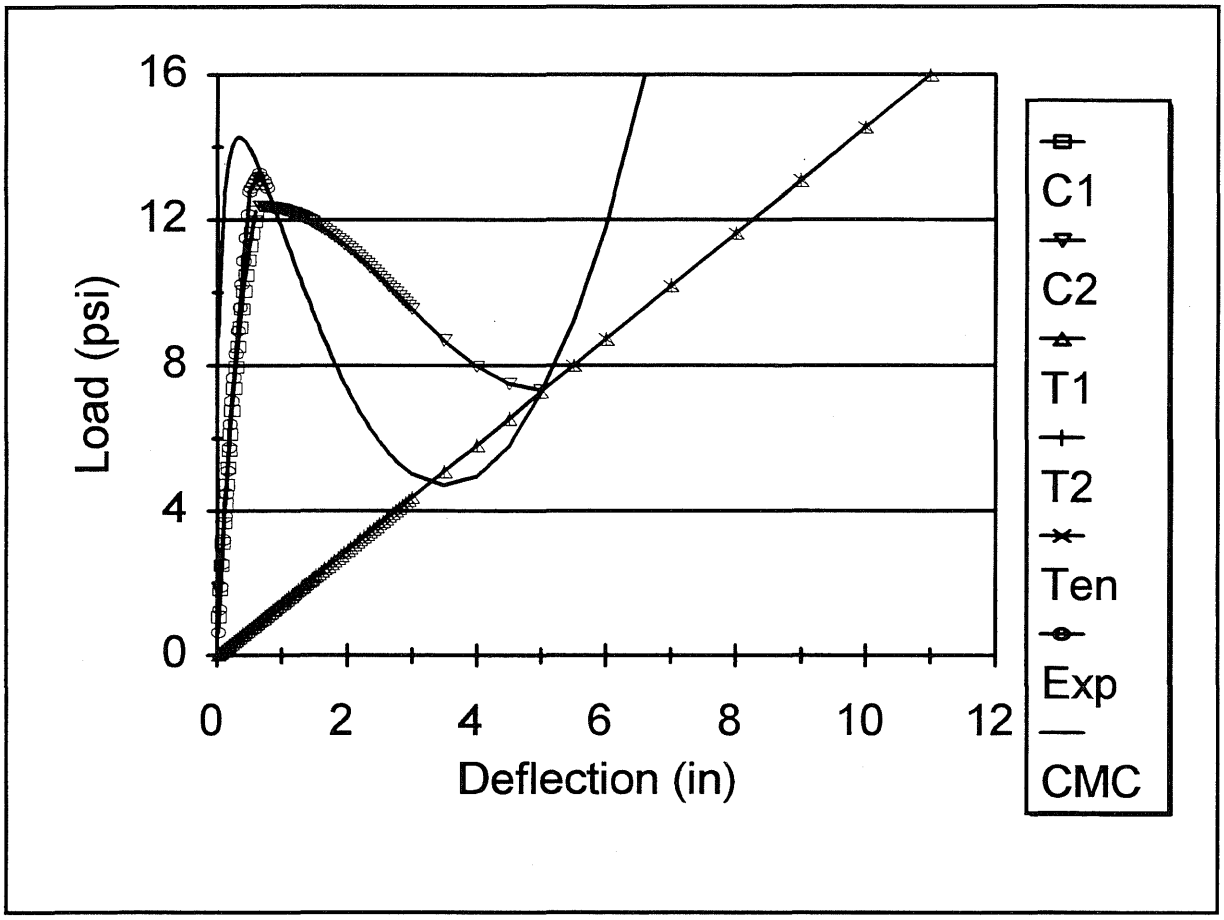

Figure D.28. Compressive Membrane Theoretical Curve, Experimental Load-Deflection Curve, and the Author's Peak Thrust Estimated Load-Deflection Curve for Christiansen's Slab (C3, L/h = 20, $\rho = 0.623\%$) (1963)

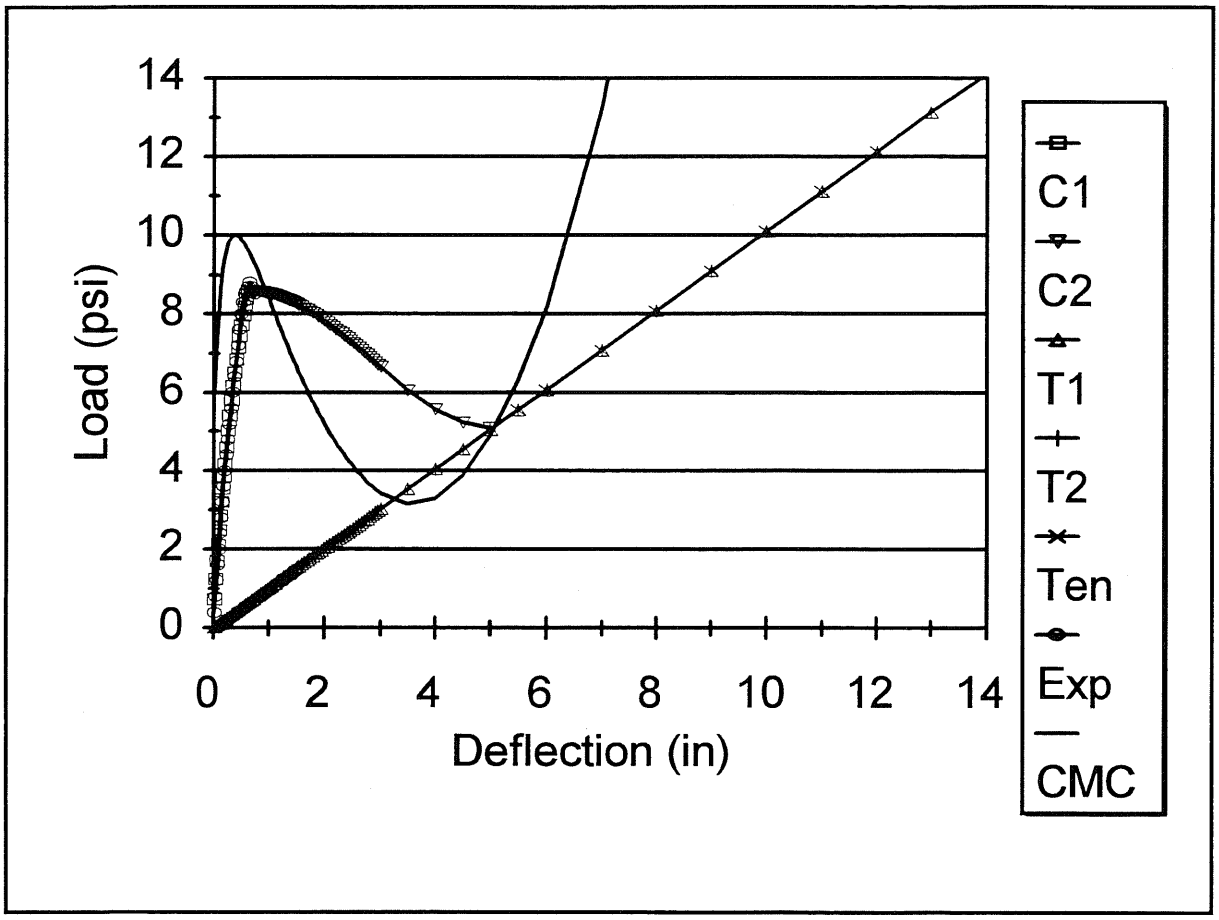

Figure D.29. Compressive Membrane Theoretical Curve, Experimental Load-Deflection Curve, and the Author's Peak Thrust Estimated Load-Deflection Curve for Christiansen's Slab (C4, L/h = 24, $\rho = 0.623\%$) (1963)

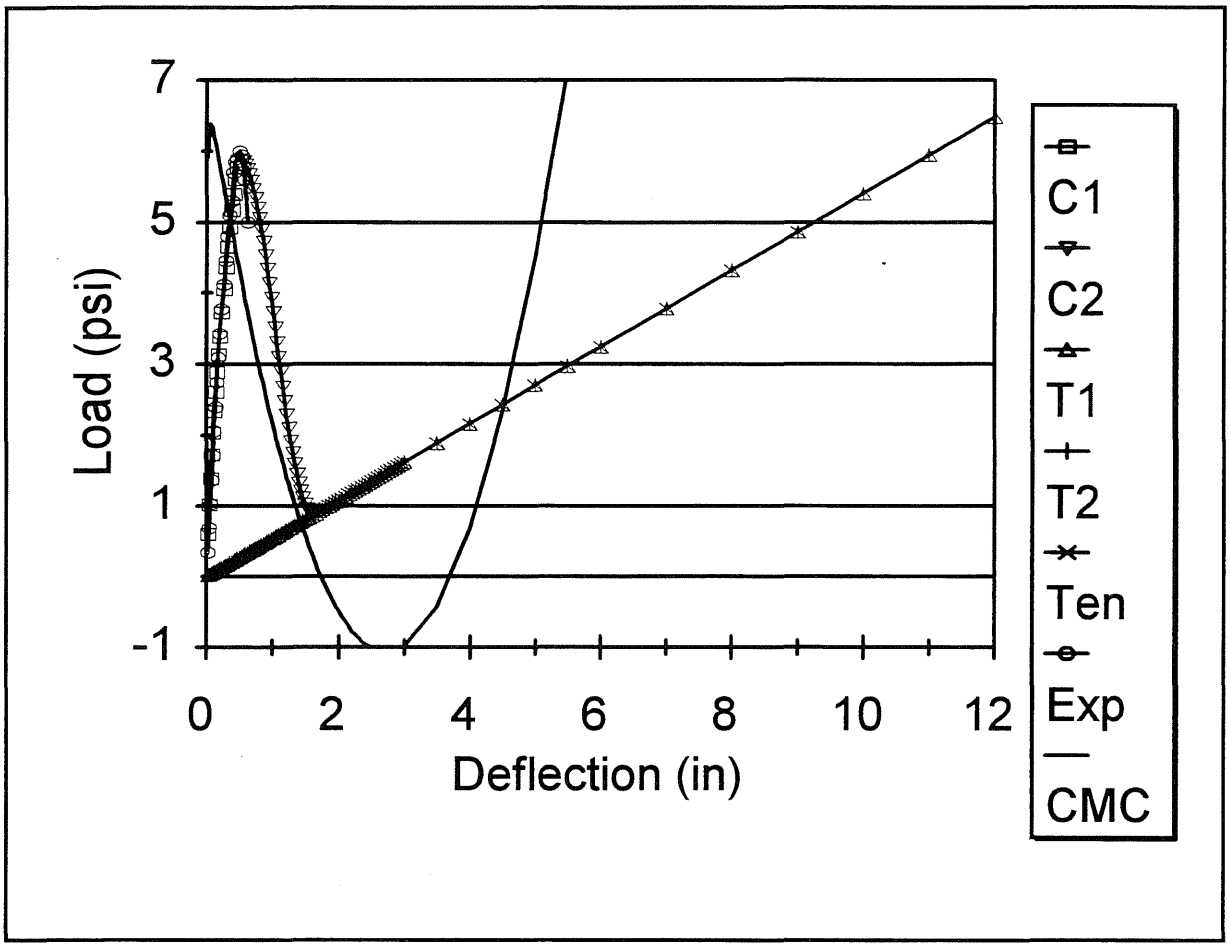

Figure D.30. Compressive Membrane Theoretical Curve, Experimental Load-Deflection Curve, and the Author's Peak Thrust Estimated Load-Deflection Curve for Roberts' Slab (RB25, L/h = 28.3, $\rho = 0.371\%$) (1969)

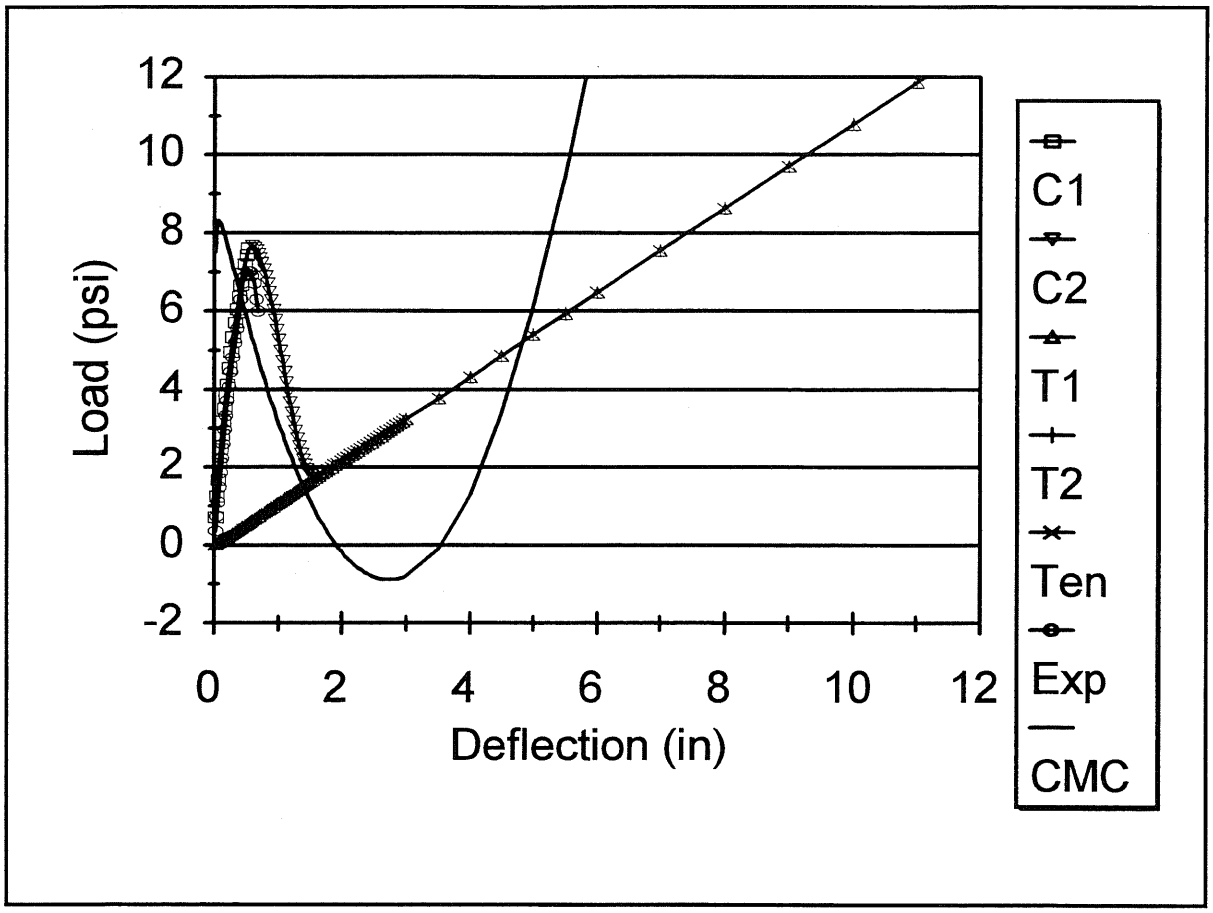

Figure D.31. Compressive Membrane Theoretical Curve, Experimental Load-Deflection Curve, and the Author's Peak Thrust Estimated Load-Deflection Curve for Roberts' Slab (RB12, L/h = 28.3, $\rho = 0.741\%$) (1969)

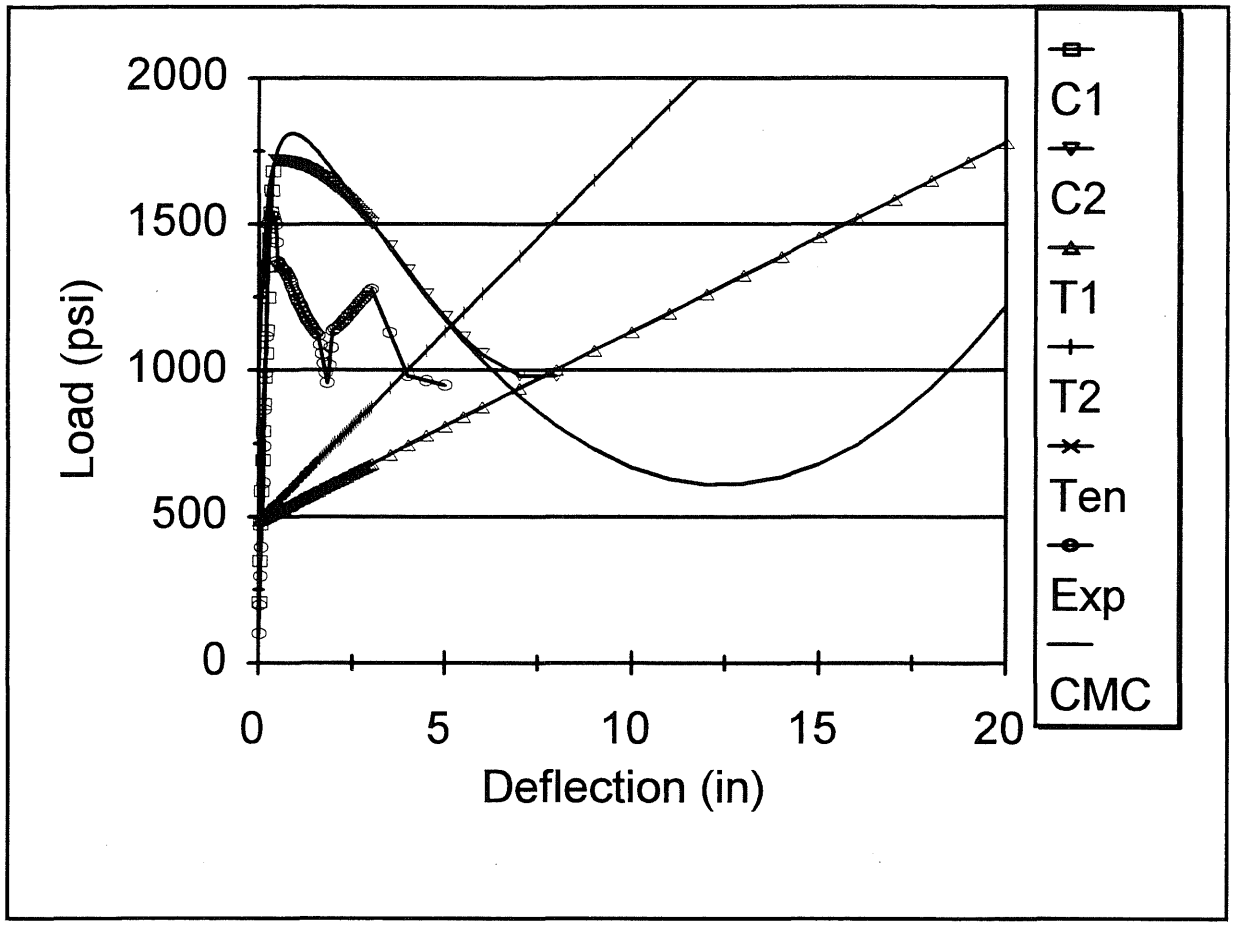

Figure D.32. Compressive Membrane Theoretical Curve, Experimental Load-Deflection Curve, and the Author's Averaged Peak Thrust and Computed Peak Capacity Estimated Load-Deflection Curve for Woodson's Slab (Wood1, L/h = 2.7, $\rho = 0.969\%$) (1994)

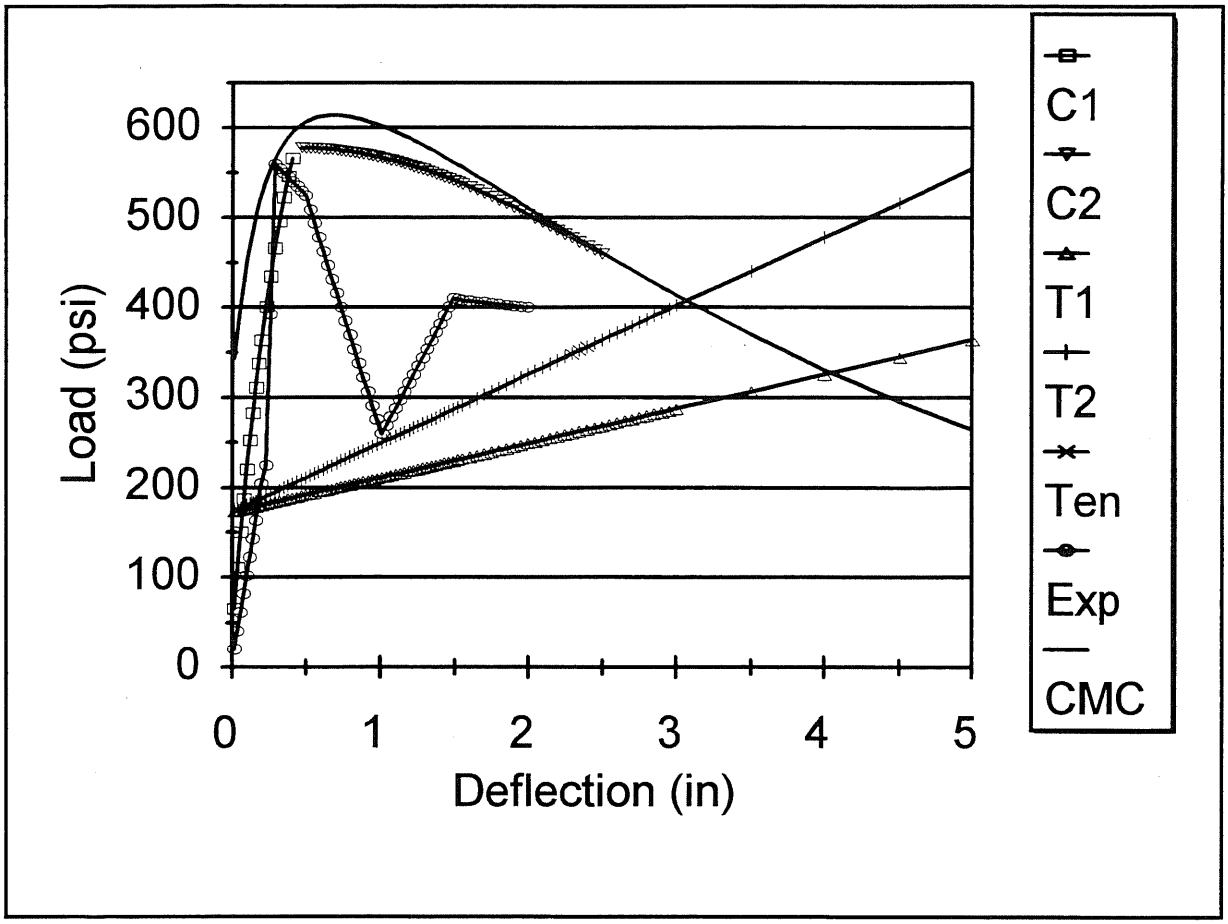

Figure D.33. Compressive Membrane Theoretical Curve, Experimental Load-Deflection Curve, and the Author's Averaged Peak Thrust and Computed Peak Capacity Estimated Load-Deflection Curve for Woodson's Slab (Wood3, L/h = 4.4, $\rho = 0.955\%$) (1994)

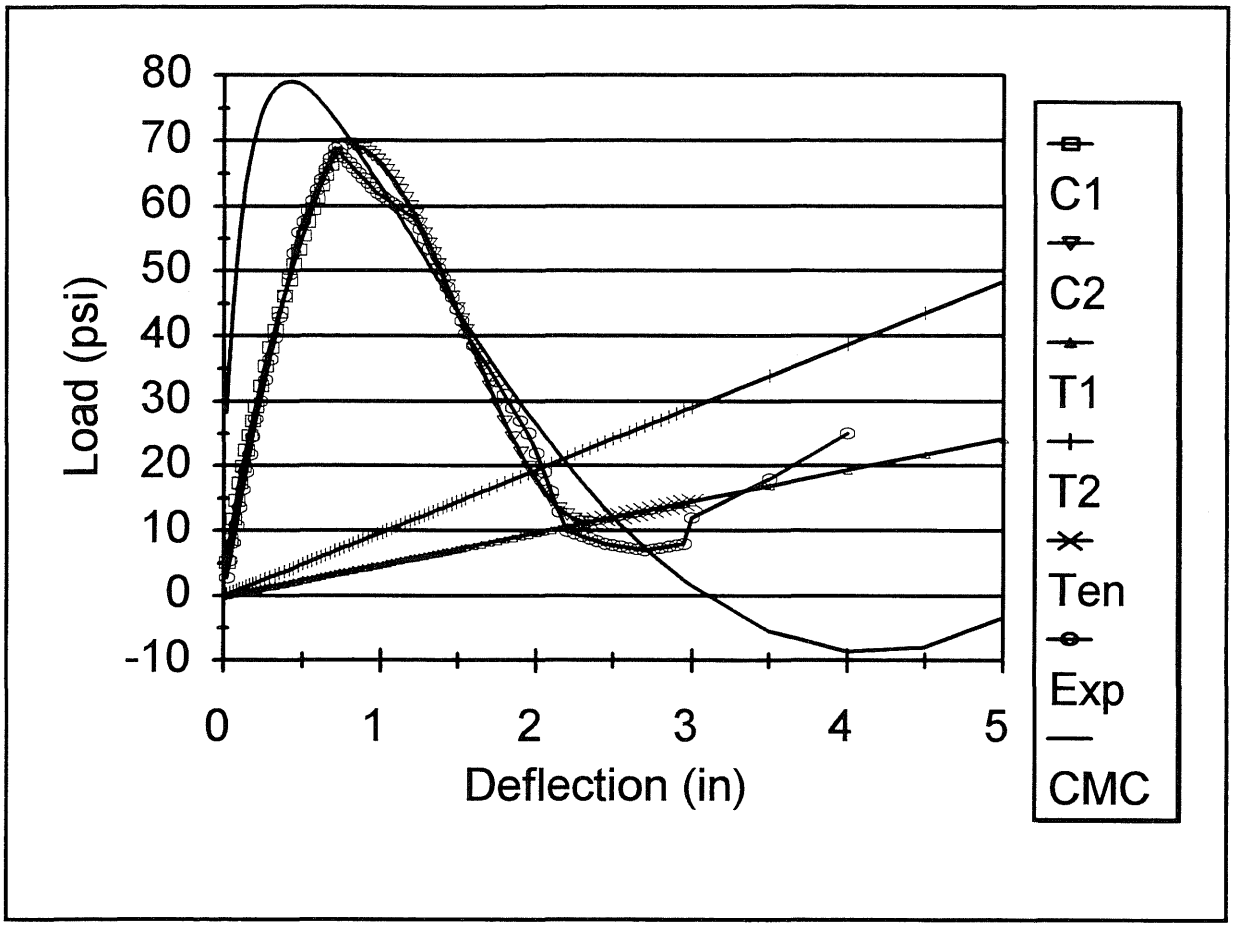

Figure D.34. Compressive Membrane Theoretical Curve, Experimental Load-Deflection Curve, and the Author's Averaged Peak Thrust and Computed Peak Capacity Estimated Load-Deflection Curve for Woodson's Slab (Wood4, L/h = 8, $\rho = 0.26\%$) (1993)

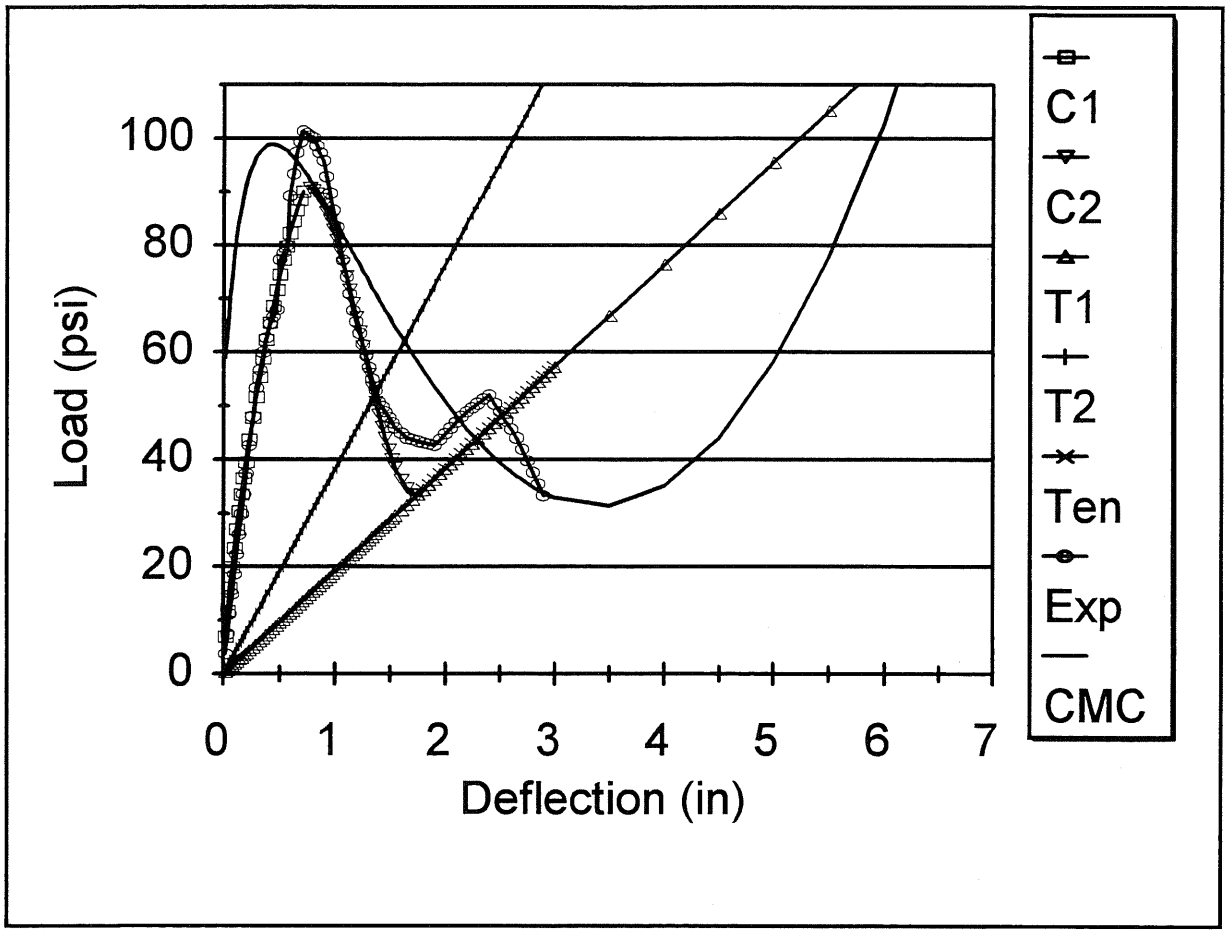

Figure D.35. Compressive Membrane Theoretical Curve, Experimental Load-Deflection Curve, and the Author's Averaged Peak Thrust and Computed Peak Capacity Estimated Load-Deflection Curve for Baylot's Slab (B3, L/h = 10, ρ = 1.045%) (1985)

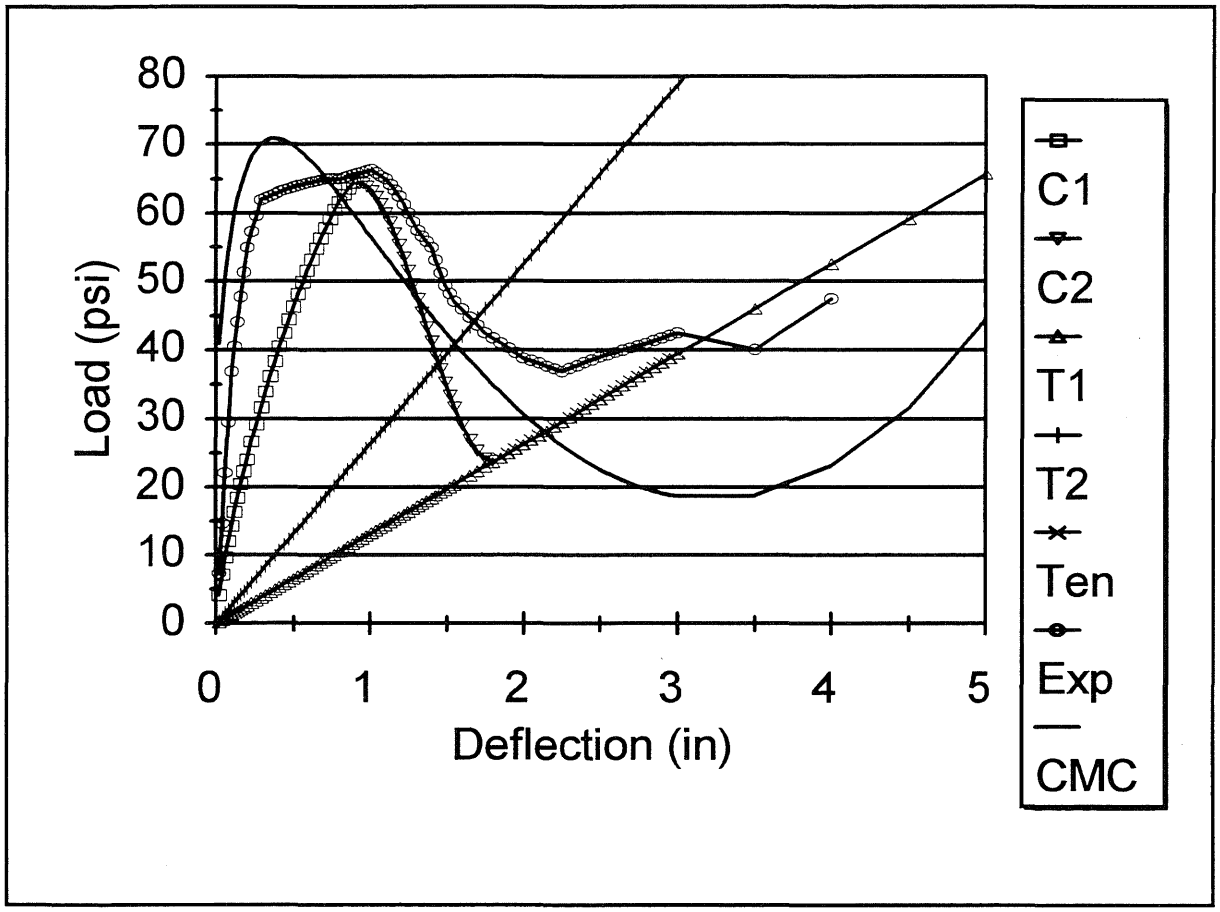

Figure D.36. Compressive Membrane Theoretical Curve, Experimental Load-Deflection Curve, and the Author's Averaged Peak Thrust and Computed Peak Capacity Estimated Load-Deflection Curve for Woodson's Slab (W1, L/h = 10.4, $\rho = 0.74\%$) (1985)

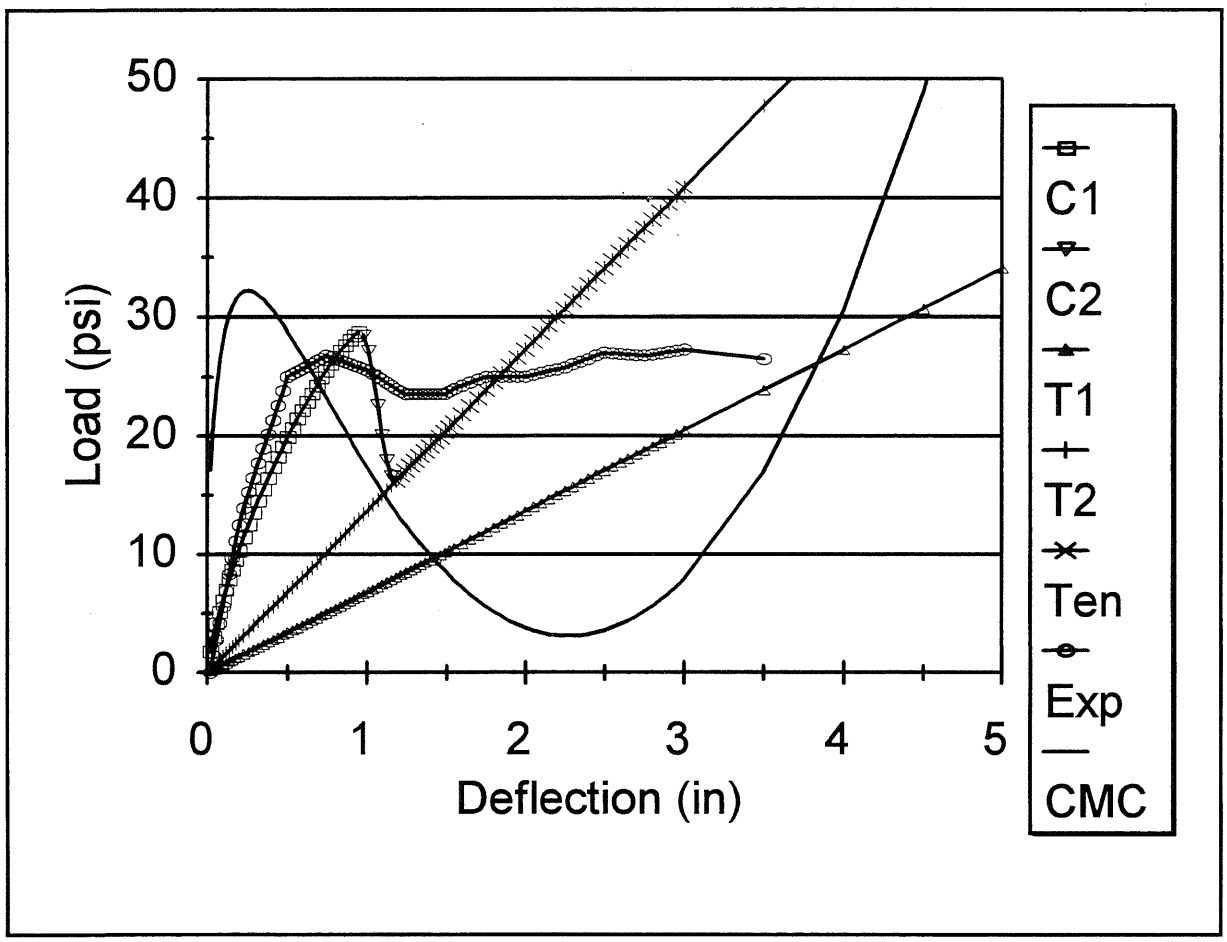

Figure D.37. Compressive Membrane Theoretical Curve, Experimental Load-Deflection Curve, and the Author's Averaged Peak Thrust and Computed Peak Capacity Estimated Load-Deflection Curve for Guice's Slab (G4, L/h = 14.8, $\rho = 0.58\%$) (1986)